# The Magnetospheric Cusps: Structure and Dynamics

*Edited by*

Theodore A. Fritz

Shing F. Fung

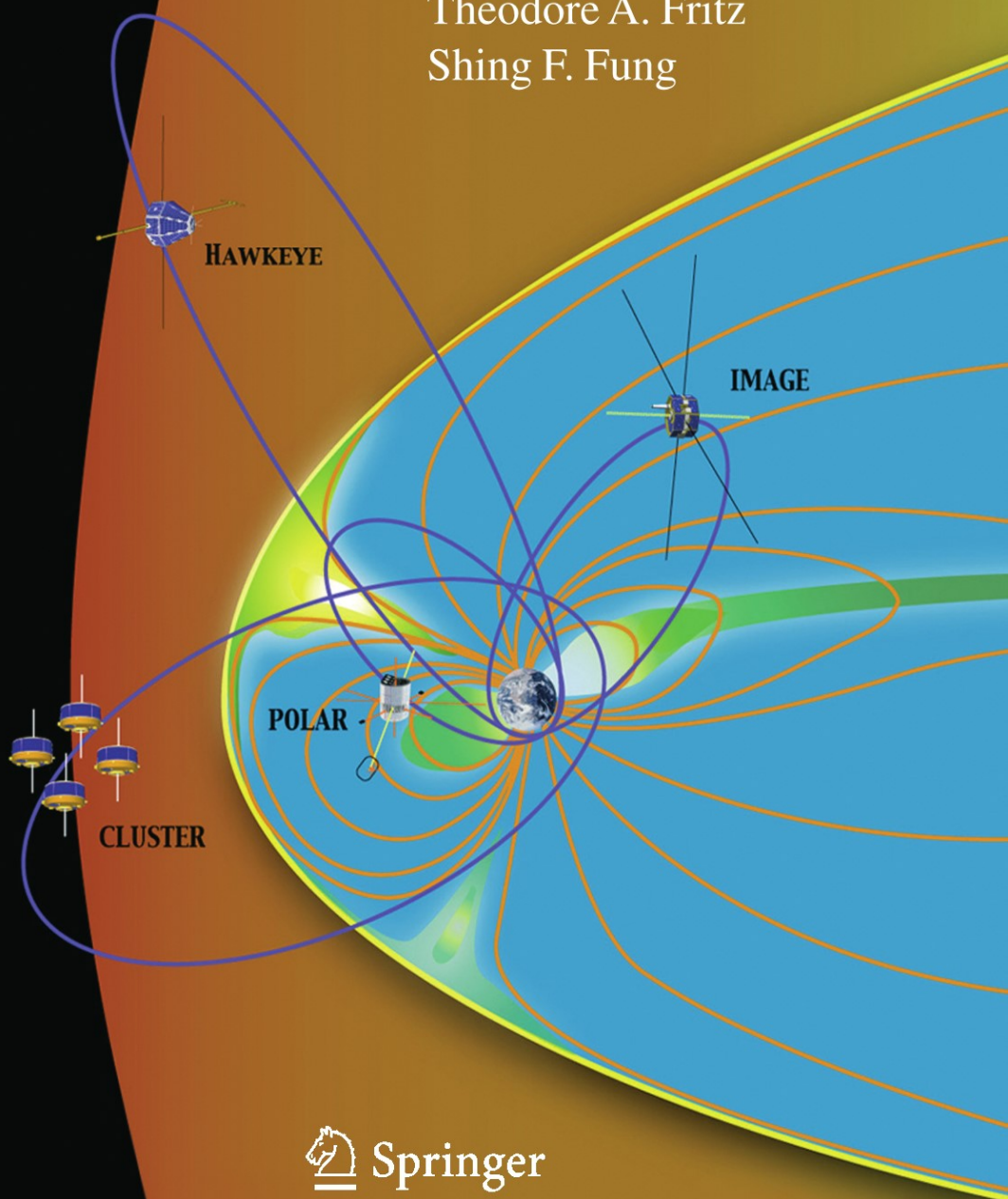


Springer

The Magnetospheric Cusps: Structure and Dynamics

# The Magnetospheric Cusps: Structure and Dynamics

Edited by
THEODORE A. FRITZ and SHING F. FUNG

Reprinted from *Surveys in Geophysics,* Volume 26(1–3), 2005

Springer

**A C.I.P catalogue record for this book is available from the Library of Congress**

ISBN 1-4020-3438-5 (HB)
ISBN 1-4020-3605-1 (e-book)
ISBN 9781402034381 (HB)
ISBN 9781402036057 (e-book)

Published by Springer,
P.O. Box 17, 3300 AA Dordrecht, The Netherlands

Sold and distributed in North, Central and South America
By Springer,
101 Philip Drive, Norwell, MA 02061, USA

In all other countries, sold and distributed
By Springer,
P.O. Box 322, 3300 AH Dordrecht, The Netherlands

*Printed on acid-free paper*

All Rights Reserved
© 2005 Springer
No part of the material protected by this copyright notice may be reproduced or utilized in any form or by any means, electric or mechanical, including photocopying, recording or by any information storage and retrieval system, without written permission from the copyright owner.

Printed in the Netherlands

## Table of contents


**Preface** 1–3

**Cluster Observations of the Cusp: Magnetic Structure and Dynamics**
M.W. Dunlop, B. Lavraud, P. Cargill, M.G.G.T. Taylor, A. Balogh, H. Réme, P. Decreau, K.-H. Glassmeier, R.C. Elphic, J.-M. Bosqued, A.N. Fazakerley, I. Dandouras, C. P. Escoubet, H. Laakso and A. Marchaudon 5–55

**Magion-4 High-Altitude Cusp Study**
J. Merka, J. Šafrnkov, Z. Nmeek and J. Šimnek 57–69

**High-Altitude Cusp: The Extremely Dynamic Region in Geospace**
Jiasheng Chen and Theodore A. Fritz 71–93

**Magnetosheath Interaction with the High Latitude Magnetopause**
S. Savin, A. Skalsky, L. Zelenyi, L. Avanov, N. Borodkova, S. Klimov, V. Lutsenko, E. Panov, S. Romanov, V. Smirnovy, U. Yermolaev, P. Song, E. Amata, G. Consolini, T. A. Fritz, J. Buechner, B. Nikutowski, J. Blecki, C. Farrugia, N. Maynard, J. Pickett, J. A. Sauvaud, J. L. Rauch, J. G. Trotignon, Y. Khotyaintsev and K. Stasiewicz 95–133

**Cluster Observes the High-Altitude Cusp Region**
B. Lavraud, H. Rme, M.W. Dunlop, J.-M. Bosqued, I. Dandouras, J.-A. Sauvaud, A. Keiling, T.D. Phan, R. Lundin, P.J. Cargill, C.P. Escoubet, C.W. Carlson, J.P. McFadden, G.K. Parks, E. Moebius, L.M. Kistler, E. Amata, M.-B. Bavassano-Cattaneo, A. Korth, B. Klecker and A. Balogh 135–174

**Low-Frequency Plasma Waves in the Outer Polar Cusp: A Review of Observations from Prognoz 8, Interball 1, Magion 4, and Cluster**
J. Blecki, R. Wronowski, S. Savin, N. Cornilleau-Wehrlin, M. Parrot, Z. Nemecek, J. Safrankova, O. Santolik, K. Kudela and J.-A. Sauvaud 175–189

**Multiple Flux Rope Events at the High-Latitude Magnetopause: Cluster/Rapid Observation on 26 January, 2001**
Z.Y. Pu, Q.-G. Zong, T.A. Fritz, C.J. Xiao, Z.Y. Huang, S.Y. Fu, Q.Q. Shi, M.W. Dunlop, K.-H. Glassmeier, A. Balogh, P. Daly, H. Reme, J. Dandouras, J.B. Cao, Z.X. Liu, C. Shen and J.K. Shi 191–212

**Energetic Electrons as a Field Line Topology Tracer in the High Latitude Boundary/Cusp Region: Cluster Rapid Observations**
Q.G. Zong, T.A. Fritz, A. Korth, P.W. Daly, M. Dunlop, A. Balogh, J.F. Fennell, J.D. Sullivan, R.W.H. Friedel and H. Reme 213–238

**Energetic Particles Observed in the Cusp Region During a Storm Recovery Phase**
S.Y. Fu, Q.G. Zong, Z.Y. Pu, C.J. Xiao, A. Korth, P. Daly and H. Reme 239–252

**Coupling the Solar-Wind/IMF to the Ionosphere through the High Latitude Cusps**
Nelson C. Maynard 253–278

**Spatial and Temporal Cusp Structures observed by Multiple Spacecraft and Ground based Observations**
K.J. Trattner, S.A. Fuselier, T.K. Yeoman, C. Carlson, W.K. Peterson, A. Korth, H. Reme, J.A. Sauvaud and N. Dubouloz 279–303

**Observations of a Unique Cusp Signature at Low and Mid Altitudes**
W.R. Keith, J.D. Winningham, M.L. Goldstein, M. Wilber, A.N. Fazakerley, H. Reme, T.A. Fritz, A. Balogh, N. Cornilleau-Wehrlin and M. Maksimovic 305–337

**Cusp Modeling and Observations at Low Altitude**
S. Wing, P.T. Newell and C.-I Meng 339–365

**Simulation Studies of High-Latitude Magnetospheric Boundary Dynamics**
Q.Q. Shi, Z.Y. Pu, H. Zhang, S.Y. Fu, C.J. Xiao, Q.-G. Zong, T.A. Fritz and Z.X. Liu 367–384

**Cusp Geometry in MHD Simulations**
George Siscoe, Nancy Crooker, Keith Siebert, Nelson Maynard, Daniel Weimer and Willard White 385–405

**The Magnetospheric cusps: A Summary**
T.A. Fritz and Q.G. Zong 407–412

Surveys in Geophysics (2005) 26: 1–3
DOI 10.1007/s10712-005-1870-8 © Springer 2005

# PREFACE

The cusps have traditionally been described as narrow funnel-shaped regions that provide a focus of the Chapman–Ferraro currents that flow on the magnetopause, a boundary between the cavity dominated by the geomagnetic field (i.e., the magnetosphere) and the external region of the interplanetary medium. From low-altitude satellite and ground-based measurements the cusps appear to behave in much the manner predicted for the responses of the narrow funnel-shaped structures to changes in the upstream interplanetary medium. Measurements at higher altitudes have been reported by past and recent missions such as the Russian Interball satellites, the US/NASA Hawkeye, Polar, and IMAGE satellites, and the joint European Space Agency/NASA Cluster suite of four satellites, all in mid- to high-altitude polar orbits. From these measurements, it has become clear that the cusps are no longer confined to narrow regions near local noon but appear to encompass a large portion of the dayside high-latitude magnetosphere. An unexpected result is that the cusps appear to be a major source region of energetic charged particles for the magnetosphere.

We try in this collection of papers to address the question "What is the Cusp?" We consider what is its role in coupling the solar wind to the magnetosphere as well as its role in charged particle transport and energization within the magnetosphere. In the literature we have had the cusp known by many names. These names appear again in papers of this Special Issue.

Boundary Cusp [BL]
Cusp Throat [CT]
Exterior Cusp [ET]
Stagnant Exterior Cusp [SEC]
Turbulent Boundary Layer [TBL]
Cusp Proper [CP]
Double Cusp
Sash
True Cusp [TC]

The cusp has been reported as a single region but also as a double region each with unique properties. Multiple simultaneous cusps are discussed as well. Within the cusp there are features that have been called the following:

Cusp Diamagnetic Cavity [CDC]
Diamagnetic Bubble [DB]
Outer Throat [OT]/Inner Throat [IT]

Temporal and/or Spatial Energy Steps
Cusp Energetic Particle events [CEP]
Outer Cusp [OC]/Inner Cusp [IC]
Plasma Ball [PB]

The Turbulent Boundary Layer [TBL] has been further divided into an outer TBL zone [OZ], middle TBL zone [MZ], and inner TBL zone [IZ].

Do these many names mean that we understand the cusp and its underlying physical principles or do they indicate a lack of understanding? In this collection of papers arguments are advanced, based on observations and theory, that cusp features are entirely produced and driven by the incoming solar wind and interplanetary magnetic field structure while other papers argue that much of the turbulence, structure, and resulting particle acceleration are produced locally within the cusp. In one of the papers the cusp is depicted as a very narrow region connected to the subsolar merging site and associated with the last closed field line, whereas a couple of statistical studies reported here present evidence demonstrating that the cusp is a vast dayside region of shocked solar wind plasma existing inside the magnetopause. The reader will encounter a paper that argues that most or all of the features of the low altitude particle signatures associated with the cusp are produced by temporal changes while the authors of another paper argue that these same features are spatial and frozen in time. To assist the readers of these papers the editors have encouraged each author to define early in their paper what distinguishes their cusp from other surrounding regions of the dayside high-latitude magnetosphere. The title of this special issue is ''The Magnetospheric Cusps: Structure and Dynamics''. The guest editors for this Special Issue of Surveys in Geophysics are Professor Theodore A. Fritz of Boston University, Boston, MA, USA and Dr. Shing F. Fung of the NASA Goddard Space Flight Center, Greenbelt, MD, USA. As editors of this special issue our main goal has been to provide a comprehensive set of overview papers that focus on the properties of the cusp as a function of altitude and the effects of the adjoining magnetopause boundary layer. A number of topical papers of high interest have also been included in this volume. The core papers for this issue have been drawn from a special session held at the spring meeting of the American Geophysical Union in May 2002. The session was entitled ''Turbulence and Dynamics at the High Altitude Cusp and Dayside Magnetopause Boundary Layer'' and the convenors were Dr. Jiasheng Chen and Professor Theodore A. Fritz. The editors would like to acknowledge and express their appreciation to the following individuals who devoted their time and effort to reviewing the papers in this collection: James L. Burch, Jiasheng Chen, Nancy U. Crooker, Timothy E. Eastman, Joseph F. Fennell, Richard C. Elphic, Charles C. Goodrich, Patrick T. Newell, Nelson C. Maynard, Richard W. McEntire, Douglas Menietti, Barbara Popielawska, Patricia H.

Reiff, David G. Sibeck, George L. Siscoe, J. David Winningham, Joachim Woch, Masatoshi Yamauchi, Andrew W. Yau, and Qiugang Zong

The editors of this special issue express deep gratitude to the Managing Editor of Surveys in Geophysics, Dr. Michael Rycroft, for his support during the project, which was "above and beyond the call of duty", and for his careful reading and his insightful comments on each of the papers published in this issue.

*Guest Editors*

THEODORE A. FRITZ
*Center for Space Physics*
*Boston University*
*Boston, MA 02215*
*USA*

SHING F. FUNG
*Space Physics Data Facility*
*NASA Goddard Space Flight Center*
*Greenbelt, MD 20771*
*USA*

Surveys in Geophysics (2005) 26: 5–55
DOI 10.1007/s10712-005-1871-7
© Springer 2005

# CLUSTER OBSERVATIONS OF THE CUSP: MAGNETIC STRUCTURE AND DYNAMICS

M. W. DUNLOP[1], B. LAVRAUD[2], P. CARGILL[3], M. G. G. T. TAYLOR[4], A. BALOGH[3], H. RÉME[2], P. DECREAU[5], K.-H. GLASSMEIER[6], R. C. ELPHIC[4], J.-M. BOSQUED[2], A. N. FAZAKERLEY[7], I. DANDOURAS[2], C. P. ESCOUBET[8], H. LAAKSO[8] and A. MARCHAUDON[9]

[1]*SSTD, Rutherford Appleton Laboratory, Chilton, Didcot, Oxon, OX11 0QX, UK*
*E-mail: m.dunlop@rl.ac.uk;*
[2]*CESR, 9 ave Colonel Roche, 31028, Toulouse Cedex 4, France;*
[3]*Imperial College, Exhibition Road, London, SW7 2BW, UK;*
[4]*Los Alamos National Laboratory, Los Alamos, NM 87545, USA;*
[5]*LPCE/CNRS and Université d'Orléans, F-45071, Orléans, France;*
[6]*Institut für Geophysik und Meteorologie, TUBS, Braunschweig, Germany;*
[7]*Mullard Space Science Laboratory, University College London, UK;*
[8]*ESA/ESTEC RSSD, Keplerlaan 1, 2200 AG, Noordwijk, The Netherlands;*
[9]*CETP, 4 avenue de Neptune, F-94107, Saint-Maur-des-Fossés Cedex, France*

(Received 27 March 2003; Accepted 30 April 2004)

**Abstract.** This paper reviews Cluster observations of the high altitude and exterior (outer) cusp, and adjacent regions in terms of new multi-spacecraft analysis and the geometry of the surrounding boundary layers. Several crossings are described in terms of the regions sampled, the boundary dynamics and the electric current signatures observed. A companion paper in this issue focuses on the detailed plasma distributions of the boundary layers. The polar Cluster orbits take the four spacecraft in a changing formation out of the magnetosphere, on the northern leg, and into the magnetosphere, on the southern leg, of the orbits. During February to April the orbits are centred on a few hours of local noon and, on the northern leg, generally pass consecutively through the northern lobe and the cusp at mid- to high-altitudes. Depending upon conditions, the spacecraft often sample the outer cusp region, near the magnetopause, and the dayside and tail boundary layer regions adjacent to the central cusp. On the southern, inbound leg the sequence is reversed. Cluster has therefore sampled the boundaries around the high altitude cusp and nearby magnetopause under a variety of conditions. The instruments onboard provide unprecedented resolution of the plasma and field properties of the region, and the simultaneous, four-spacecraft coverage achieved by Cluster is unique. The spacecraft array forms a nearly regular tetrahedral configuration in the cusp and already the mission has covered this region on multiple spatial scales (100–2000 km). This multi-spacecraft coverage allows spatial and temporal features to be distinguished to a large degree and, in particular, enables the macroscopic properties of the boundary layers to be identified: the orientation, motion and thickness, and the associated current layers. We review the results of this analysis for a number of selected crossings from both the North and South cusp regions. Several key results have been found or have confirmed earlier work: (1) evidence for magnetically defined boundaries at both the outer cusp/magnetosheath interface and the inner cusp/lobe or cusp/dayside magnetosphere interface, as would support the existence

of a distinct exterior cusp region; (2) evidence for an associated indentation region on the magnetopause across the outer cusp; (3) well defined plasma boundaries at the edges of the mid- to high-altitude cusp "throat", and well defined magnetic boundaries in the high-altitude "throat", consistent with a funnel geometry; (4) direct control of the cusp position, and its extent, by the IMF, both in the dawn/dusk and North/South directions. The exterior cusp, in particular, is highly dependent on the external conditions prevailing. The magnetic field geometry is sometimes complex, but often the current layer has a well defined thickness ranging from a few hundred (for the inner cusp boundaries) to 1000 km. Motion of the inner cusp boundaries can occur at speeds up to 60 km/s, but typically 10–20 km/s. These speeds appear to represent global motion of the cusp in some cases, but also could arise from expansion or narrowing in others. The mid- to high-altitude cusp usually contains enhanced ULF wave activity, and the exterior cusp usually is associated with a substantial reduction in field magnitude.

**Keywords:** boundary dynamics, clustermagnetospheric cusps

**Abbreviations:** ACE – advanced composition explorer; GSE – geocentric solar ecliptic; GSM – geocentric solar magnetic; IMF – interplanetary magnetic field; LT – local time; MVA – minimum variation analysis; $R_E$ – earth's radius; ULF – ultra-low frequency; UT – universal time

## 1. Introduction

The region associated with the Earth's magnetospheric cusps is one of the most complex in the magnetosphere, in terms of both its morphology and the processes operating. The cusps are believed to be the main places of transport of plasma into the magnetosphere and therefore contain (modified) magnetosheath plasma (e.g. Frank, 1971; Newell and Meng, 1988). Their extent and location are known to respond to the IMF and solar wind pressure (Newell et al., 1989; Woch and Lundin, 1992; Newell and Meng, 1994; Yamauchi and Lundin, 1994; Yamauchi et al., 1996; Savin et al., 1998; Fedorov et al., 2000; Dubinin et al., 2002). The cusps, however, have an often complex magnetic topology, whose direct relation to processes occurring elsewhere on the magnetopause and in the adjacent magnetosheath is not fully understood. There is often a combination of processes operating, having both local and remote effects. Adding to this complexity are the facts that the region is of large (many $R_E$) spatial extent, containing a variety of distinct structures having both plasma and field specific characteristics, but is highly dynamic and often with changes in magnetic topology. This makes measurements of the region extremely difficult to interpret. The magnetic and plasma structures surrounding the cusps often depend on prevailing conditions. The boundaries surrounding the region have therefore not been well characterised. In particular, the relation between a possible, distinct exterior cusp, as part of the high altitude cusp region, and an indentation on the magnetopause (Spreiter et al., 1968; Haerendel et al., 1978; Vasyliunas et al.,

1979) is not well formulated. A more comprehensive review of these earlier studies can be found in a companion paper in this issue (Lavraud et al., 2003).

The four-spacecraft Cluster mission is currently returning co-ordinated, multi-point information on the region of the cusps at unprecedented detail. It has the potential to resolve cusp structure, first investigated during the early Hawkeye and HEOS missions (e.g., see Paschmann et al., 1976; Haerendel et al., 1978; Farrell and Van Allen, 1990; Kessel et al., 1996; Dunlop et al., 2000; Eastman et al., 2000) over 30 years ago, and more recently re-explored with the Polar mission (e.g. Grande et al., 1997; Russell, 2000; Scudder et al., 2002, Fritz et al., 2003) as well as the Interball mission (Savin et al., 1998; Fedorov et al., 2000; Dubinin et al., 2002). The orbital dynamics is designed so as to place the spacecraft array into a nearly regular tetrahedral configuration in the location of the cusps. Both the high capabilities of the onboard instruments and the tetrahedral spacecraft configuration permit very accurate and precise determination of the physical particle and wave phenomena and small-scale dynamical analysis. Many cusp crossings have been recorded by Cluster, during 2001 and 2002, covering a variety of ambient conditions, and these have sampled the cusp region with a range of spatial scales (100–2000 km). Nevertheless, the analysis of Cluster data requires particular interpretation, currently at a phenomenological level. A number of four-spacecraft techniques have been devised to combine the multi-point dataset (see Paschmann and Daly, 1988). These techniques can determine such properties as thin boundary layers, their orientation and motion, and the nature of associated current layers, and are in development to explore further applications. Two techniques in particular are described below, the Curlometer (Dunlop and Balogh, 1993; Robert and Roux, 1993; Robert et al., 1998) and Discontinuity Analyser (DA) (Dunlop et al., 1997; Dunlop and Woodward, 1998, 1999). The application of these techniques is defined by the comparative spatial and temporal scales.

During the mission, the spacecraft are maintained in a closely separated array formation (at mean distances which, over the mission, have ranged between 100 and 6000 km), having a repeating evolution every orbit. Manoeuvres are performed at six-monthly to yearly intervals. The orbit is shown, for example, in Figure 2 (described in Section 3), for a typical dayside orientation of the line of apsides, in comparison with the T89 (Tsyganenko, 1989) model field, shown for guidance. Different dipole orientations occur with respect to the orbit for other passes. The orbits are inertial, having identical periods for all spacecraft and a polar orientation, with a rising argument of perigee. Perigee and apogee are at 4 and 19.6 $R_E$, respectively. Cluster therefore samples the cusp at both high and mid altitudes during different phases of the orbit. In the plot, the configuration formed by the relative locations of each spacecraft, at different times around the orbit, is shown scaled up by a factor of 20. Not only does this spacecraft configura-

tion distort dramatically around the orbit, but its scale size varies also. Therefore, the array of four spacecraft samples the magnetic field in very different ways at different positions. This has the consequence that some combinations of the four-point measurements are more fruitful than others, depending upon the structures present. It is critical to know, for instance, what are the comparative inter-spacecraft separations with respect to the characteristic scale size of the structures present. Usually the analysis will involve crude estimates of scale (degree of stationarity or relative size, large or small-scale structures), inferred from the measured, time series variations. Fortunately, different magnetospheric phenomena often produce anisotropic structures that can be described in terms of similar global frames of reference, for example, corresponding to a flow, field, or boundary aligned co-ordinate system (Dunlop et al., 1993). The multi-spacecraft methods generally give better results than single spacecraft methods, and they give much better defined local systems of reference.

This paper reviews the analysis of a few comparative events taken from the data set, concentrating primarily on the dynamics and magnetic structure of the boundaries. A companion paper (Lavraud et al., 2003) deals with the plasma characteristics observed within key regions of the cusp, partly in the context of the magnetic boundaries. Section 2, below, summarises the four spacecraft techniques used to order the data; Section 3 then introduces each event, describing their basic properties and the solar wind/magnetosheath context, and Section 4 discusses their characteristics, interpreted from the four-spacecraft locations. Section 3 concentrates on the sampling context to characterise each event, using multi-spacecraft crossings where appropriate, whereas Section 4 discusses how well this character may be quantified by the four-spacecraft analysis, and understood in terms of the response of the region to the external conditions. In Section 5, this interpretation is summarised.

## 2. Measurements and techniques

### 2.1. Cluster instrumentation

The data used in this paper have been taken by the magnetometer and plasma instruments residing onboard the Cluster spacecraft. Although the analysis presented here depends primarily on the magnetic field measurements, the plasma data are shown for context. The fluxgate magnetometer (FGM) experiment is providing high time resolution magnetic field measurements from the primary sensors on all four spacecraft (Balogh et al., 2001). The experiment consists of two sensors on each spacecraft, mounted near the middle and end of a rigid 5-m boom, together with their onboard data processing units. Currently, the primary sensor is the outboard sensor, providing magnetic field measurements at 22.4 Hz (normal mode) or 67 Hz (burst mode). The instruments are

operating continuously and the data have been filtered and re-sampled onboard from an internal sampling rate of 202 Hz. The data are believed to be inter-calibrated to at least 0.1 nT accuracy overall. Here, we employ both spin resolution and high time resolution data where appropriate, which have been re-calibrated to higher accuracy where necessary.

The Cluster Ion Spectrometer (CIS) is fully described by Réme et al. (2001) and is capable of obtaining full three-dimensional ion distribution functions down to a time resolution of 4 s. The CIS experiment is composed of two complementary sensors: the COmposition and DIstribution Function analyser sensor (CODIF), which utilises a Time of Flight system in order to resolve ion masses, and the Hot Ion Analyser (HIA) that does not separate ion species but has a better angular resolution. The CIS experiment is currently providing data from both sensors on two spacecraft (1 and 3) and from CODIF only on spacecraft 4. We present data from both instruments in the present paper. The Plasma Electron And Current Experiment (PEACE, Johnstone et al., 1997) is providing low- and mid-energy electron data from all four spacecraft. It consists of two sensors, the High Energy Electron Analyser (HEEA) and the Low Energy Electron Analyser (LEEA), mounted on diametrically opposite sides of the spacecraft. They are designed to measure, in combination, the three dimensional velocity distributions of electrons in the range 0.6 eV to 26 keV. The HEEA normally measures the range 35 eV to 26 keV and the LEEA the range 0.6 eV to 1 keV, although either can be set to cover any subset of the energy range. Thus, the overlap energy range (measured by both sensors) effectively has 2-s resolution or can be used to cross calibrate the sensors. Data presented in this paper are derived using preliminary calibrations.

### 2.2. The discontinuity analyser (DA)

This technique characterises the macroscopic properties of boundaries or discontinuities, and determines parameters that describe the motion, geometry and orientation of these structures. The first application of this technique to Cluster data has been reported by Dunlop et al. (2002a) and here we use it only in the case of stationary, planar boundaries. The basic algorithm uses single spacecraft methods, such as Minimum Variance Analysis (Sonnerup and Cahill, 1967) or co-planarity, to determine the normals to the boundary at each spacecraft crossing point, independently. The boundary orientation and motion can then be calculated by combining the boundary crossing times, at each spacecraft, with spacecraft separation vectors and the boundary normals as determined above. Figure 1a shows the idealised case of a planar discontinuity. Boundary normals are envisaged as having been determined to be nearly parallel at each of the four spacecraft (s/c 1, 2, 3, 4). Because the normals are determined independently, parallel normals directly

imply a planar geometry over the spacecraft array and allow the boundary motion (velocity $\mathbf{v_n}$, and acceleration $\mathbf{a_n}$), to be determined from

$$\mathbf{r_n} = \mathbf{v_n^0} t + \frac{1}{2}\mathbf{a_n} t^2 \tag{1}$$

where $\mathbf{r_n} = \Delta\mathbf{r_{ij}} \bullet \mathbf{n}$, etc., and $t = t_{ij}$.

If the motion is constant over the spacecraft array ($\mathbf{a_n}$ is found to be small), equation 1 can be used to compute $\mathbf{n}/v_n^0$ (Russell et al., 1983). This computation of $\mathbf{n}$ and $v_n^0$, under an assumption of constant velocity, is referred to below as a timing analysis, since the results only depend on the timing of the crossings at each spacecraft. When the results of the DA suggest

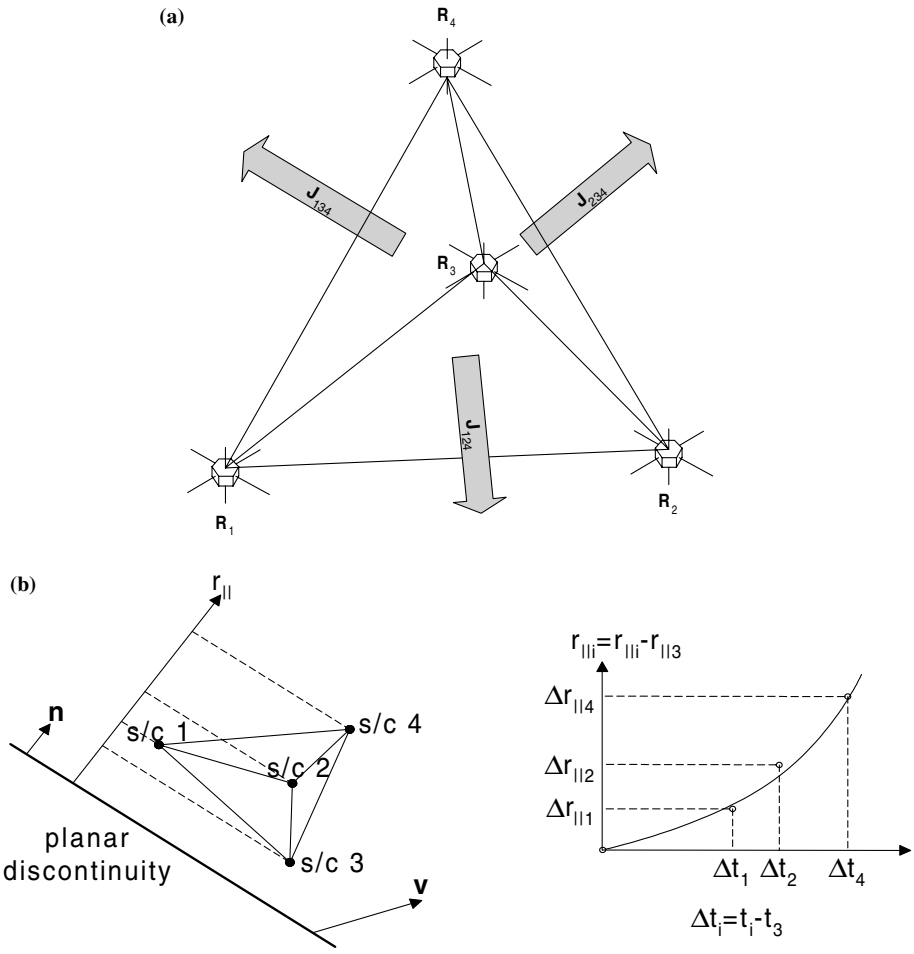


*Figure 1.* (a) The application of the DA to a planar discontinuity (after Dunlop et al. (2002a)), and (b) The curlometer concept (after Dunlop et al. (2002b)).

that the motion is indeed almost constant, these values can provide a consistency check for the planar-DA, either of the normals, or of the estimates of the motion. If the acceleration of the boundary is changing rapidly, $\mathbf{a_n}$ may not well represent the boundary reversals.

Even with this simple form of the technique, Equation (1) rests on the determination of the inter-spacecraft time differences between the boundary crossings at each of the spacecraft, together with the assumption that the structure does not evolve over the time intervals. In practice, this requires that identifiable features in the time series data are stationary (can be interpreted as convected stable structures). These, often sharp (short duration), features are usually best viewed by the change in the maximum variance component of the magnetic field, following transformation to MVA co-ordinates (or in the field intensity where there is low field rotation). Typically, for magnetic discontinuities and other plasma boundaries, stationarity is only valid near these sharp boundaries. Particularly for the case of well-defined current sheets, the maximum variance component will suggest a magnetic field rotation over some finite time interval. These intervals correspond to the traversal times through the current sheet (time intervals to cross the current sheet, as represented by the shear in the magnetic field).

In the results analysed below we quote the mean normals, obtained from the individual spacecraft normals, where only planar crossings have been analysed. The mean normals, of course, will give better estimates of the boundary orientation than the spacecraft normals. We also quote the computed velocity between each independent spacecraft pair in order to identify the relative motion of the boundary, as determined from the DA. Once any change of this velocity over the spacecraft array has been found, this motion can be used to scale each traversal time through the current layer (at each spacecraft) to a boundary thickness. These estimates of boundary thickness are also quoted.

### 2.3. The curlometer

The description of the curlometer and its development has been referenced in the Introduction, and first application of the technique has been reported recently by Dunlop et al. (2002b). The technique directly combines simultaneous data across the different spacecraft with the position information of the spacecraft to calculate the curl of the magnetic field from Ampére's law as an estimate of the average current density through the spacecraft configuration, using the difference approximation

$$\mu_0 \mathbf{J} \bullet (\Delta \mathbf{r_i} \times \Delta \mathbf{r_j}) = \Delta B_i \bullet \Delta \mathbf{r_j} - \Delta B_j \bullet \Delta \mathbf{r_i}$$

representing: $\mu_0 \int \mathbf{J} \bullet ds = \oint \mathbf{B} \bullet d\mathbf{l}$

with $\Delta\mathbf{r_i} = \mathbf{r_i} - \mathbf{r_l}$, and similarly $\Delta\mathbf{B_i} = \mathbf{B_i} - \mathbf{B_l}$ (see Dunlop et al., 2002b). This effectively estimates the average current normal to the face ($l$, $i$, $j$) of the tetrahedron (see Figure 1b). Since the vector defining the face is known by $\Delta\mathbf{r_i} \times \Delta\mathbf{r_j}$, the currents normal to three faces can easily be re-projected into a Cartesian co-ordinate system. Generally, this approximation requires that the spacecraft separation is much less than the scale lengths on which the current density varies. If this assumption does not hold, the estimate of **J** becomes inaccurate (but may still reflect real effects). Some check on the linearity of the spatial magnetic field gradients is therefore desirable, and it is also possible to calculate an estimate for div(**B**) from

$$div(\mathbf{B})|\Delta\mathbf{r_i} \bullet \mathbf{r_j} \times \Delta\mathbf{r_k}| = |\Sigma_{\text{cyclic}}\ \Delta\mathbf{B_i} \bullet \Delta\mathbf{r_j} \times \Delta\mathbf{r_k}|$$

The calculation of div(**B**) produces non-zero values as a consequence of non-linear spatial gradients neglected in its estimate (as well as containing the effect of timing and measurement errors). It therefore usefully measures the combined effect of the linear approximation for those diagonal terms in the dyadic $\Delta\mathbf{B}$, and both quantities are monitored routinely. The information from div(**B**), however, only indirectly refers to the estimate of the error in **J**. In particular, the use of div(**B**) as an indicator is less valid at extreme distortions of the spacecraft tetrahedron and these configurations are avoided. The ratio |div(**B**)|/|curl(**B**)| is actually used to monitor a dimensionless quantity, expressed as a percentage deviation from zero. The effect of measurement errors (uncertainties) in the determination of **r** and **B** (and time) is very critical for the calculation of **J**, since it involves differences in the quantities. Their contribution to the error in **J** is also highly sensitive to both the spacecraft configuration and the magnetic structure. In the analysis below we comment on the curlometer calculation only briefly, but have checked that these qualifications on the estimate give consistent results for the analysis performed.

## 3. Events

We summarise here the description of particular cusp traversals, which have been covered by Cluster at mean spatial separations of 600 km (from the dayside pass in 2001) and 100 km (from the dayside pass in 2002). In the first case, the spacecraft configurations are scaled up by a factor of × 20 and, in the second, by a factor of ×100. Three primary events are described in some

detail, with the small separation events being presented for comparison, together with a quiet time event to show the underlying gross features of each region of the cusp. The events have been chosen to show both the extreme changes in character of the regions surrounding the cusp which have been observed and some of the different sampling configurations which have been covered by the Cluster spacecraft. We describe the properties of the events fully below, including their four-spacecraft context. The significance of the multi-point analysis is then discussed further in Section 4.

### 3.1. Event of 17 march 2001

Figure 2 shows a northern cusp crossing, which occurred during quiet external conditions, and during essentially northward IMF-$B_Z$. The crossing occurred during the exit of the spacecraft from the magnetosphere on the outbound, northern leg of the Cluster orbits. In Figure 2, the spacecraft orbit and the configuration at intervals along the orbit are shown projected into the $X,Z_{GSM}$ plane (with the inset being the corresponding $X,Y_{GSM}$ projection). The dots on the orbit are hours of the day from zero UT at the perigee end of the segment shown. The plane of the orbit lies almost at magnetic noon, just on the dawn-side for the whole pass until the final magnetopause exit at 09:20 UT (confirmed by the magnetic field and ion data shown in Figures 3 and 4).

Figure 3 shows the magnetic field data compared with the Tsyganenko model field (T89, for $Kp = 1$). The underlying trends in $B_Z$ and $B_Y$ follow the model closely until the spacecraft are near the magnetopause. The magnetic field is directed down (South) and slightly duskward, as required for this location, and defines the "throat" of the cusp as field aligned. [Note that for convenience of description, we will refer to the mid- to high-altitude region (say between 5 and 10 $R_E$ radial distance, if the sub-solar magnetopause is placed at 11 $R_E$) as the cusp throat and the outer, high-latitude region (the "mouth" of the cusp) as the exterior cusp. We recognise here that other authors, referred to above, have introduced a variety of definitions, and we will try to build a consistent plasma and field description around these geometrical terms as we proceed]. After about 08:00 UT, the field turns from southward to northward, corresponding to the passage through dayside field lines. During this period, the model deviates significantly from the $B_X$ component, the component expected to be most sensitive to the precise conditions near the magnetopause boundary. The observed deviation simply means that near the external cusp region the field points less northward than predicted by this model. This is plausibly explained as an effect of the high-altitude cusp structure on surrounding magnetic field lines (in both the lobe and closed dayside regions), which is not included in the earlier T89 model and which has been addressed by Tsyganenko and Russell (1999).

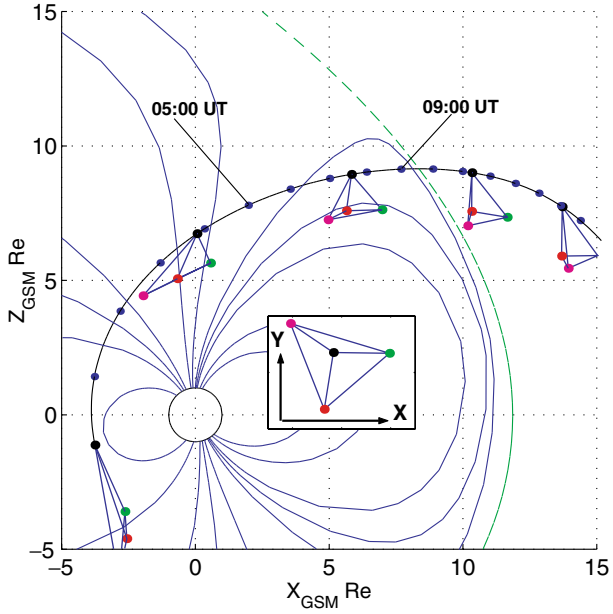


*Figure 2.* The event of 17 March 2001, which corresponds to a northern cusp crossing during the outbound leg of the orbits. This dayside orientation of the Cluster orbits is projected into the Z, $X_{GSM}$ plane on the main axes. The spatial configurations of the spacecraft are shown at a sequence of times around the orbit and scaled (enlarged) by a factor of 20. The inset shows the corresponding X, $Y_{GSM}$ projection of the configuration between the labelled times. The spacecraft are colour coded as follows: s/c1 (black), s/c2 (red), s/c3 (green), s/c4 (magenta); with spacecraft 1 corresponding to the orbit shown. Blue dots around the orbit correspond to hourly intervals starting from 00:00 UT. Also shown are model field lines, taken from the Tsyganenko model (Tsyganenko, 1989). The magnetopause position (Sibeck et al., 1991) for the conditions observed by ACE is also shown, so that the spacecraft are expected to exit into the magnetosheath at around 09:30 UT (as predicted on the plot).

In addition to the DC trend seen in Figure 3, there are a number of features. Entry into the cusp throat at 05:05 UT (5 $R_E$) is seen as an increase in ULF fluctuations on all spacecraft traces. The character of these fluctuations in fact changes as the passage proceeds through the region (Cargill et al; private communication), particularly after about 06:25 UT. The spacecraft configurations in Figure 2 show that they are arranged with spacecraft 1 and 3 outermost along the throat and spacecraft 2 and 4 innermost. Close inspection of the individual traces in |B| (best seen on the plot in $B_Z$), for example, reveals that spacecraft 1 sees the weakest field, spacecraft 3 a stronger field, spacecraft 2 the next strongest, and spacecraft 4 the strongest. This trend is followed though the throat into the dayside region, as expected from the model field and these spacecraft locations.

Figure 4 shows the ion spectrograms and the density and velocity moments, measured by the CIS-HIA instrument, together with the FGM

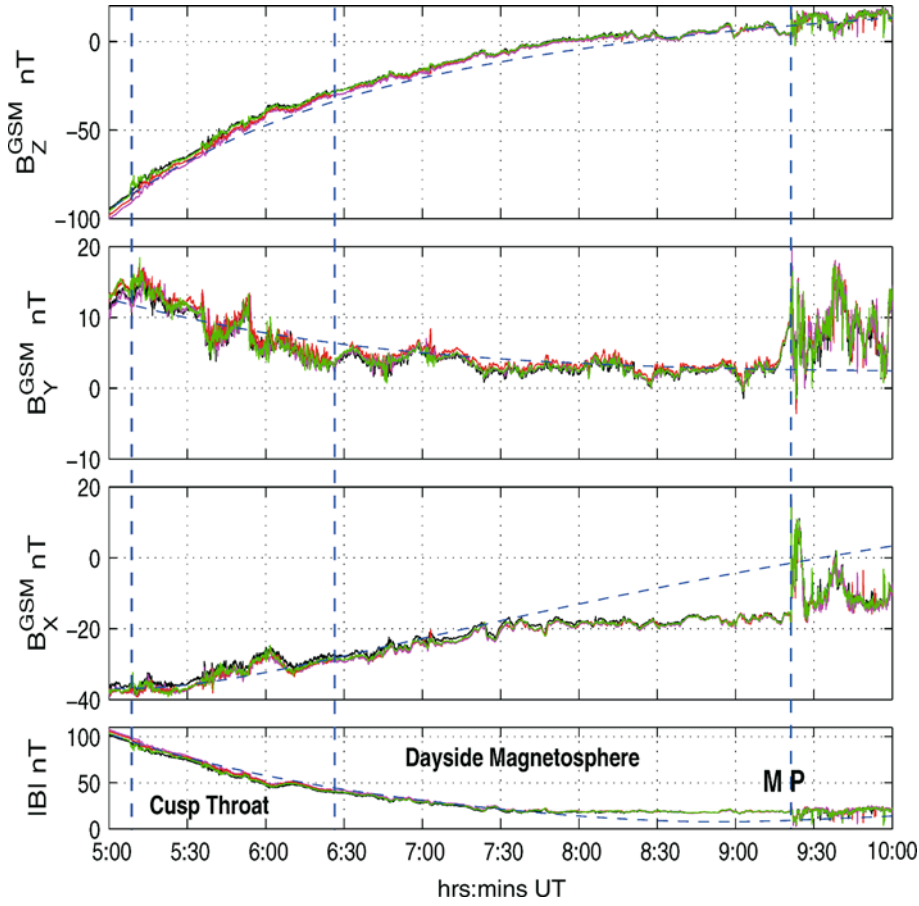


*Figure 3*. The corresponding multi-spacecraft, vector magnetic field plot for the event in Figure 2 is plotted with the four spacecraft traces overlain. The colours for each superimposed trace correspond to the spacecraft colours defined in Figure 2. At high field the traces separate in the order described in the text and the vertical dashed blue lines refer to the boundaries described in the text, separating the regions indicated. The dashed blue lines are the T89 model field values along the orbits (only s/c 1 is shown) and have been calculated for low magnetic activity.

magnetic field, from spacecraft 1. Also shown is the ACE-IMF, suitably lagged for solar wind convection (Lepping et al., 1995), as taken from the observed bulk velocity (not shown). The lag times are all given in the figure captions. The plasma data mainly show an entry into and through the cusp throat and then dayside plasma sheet (closed magnetosphere) and out into the magnetosheath, confirming the interpretation from the magnetic field data. After about 05:05 UT and before 06:25 UT, the ions show a broadband signature at magnetosheath energies (top panel). We interpret this as corresponding to passage through the cusp throat. The band fades through a

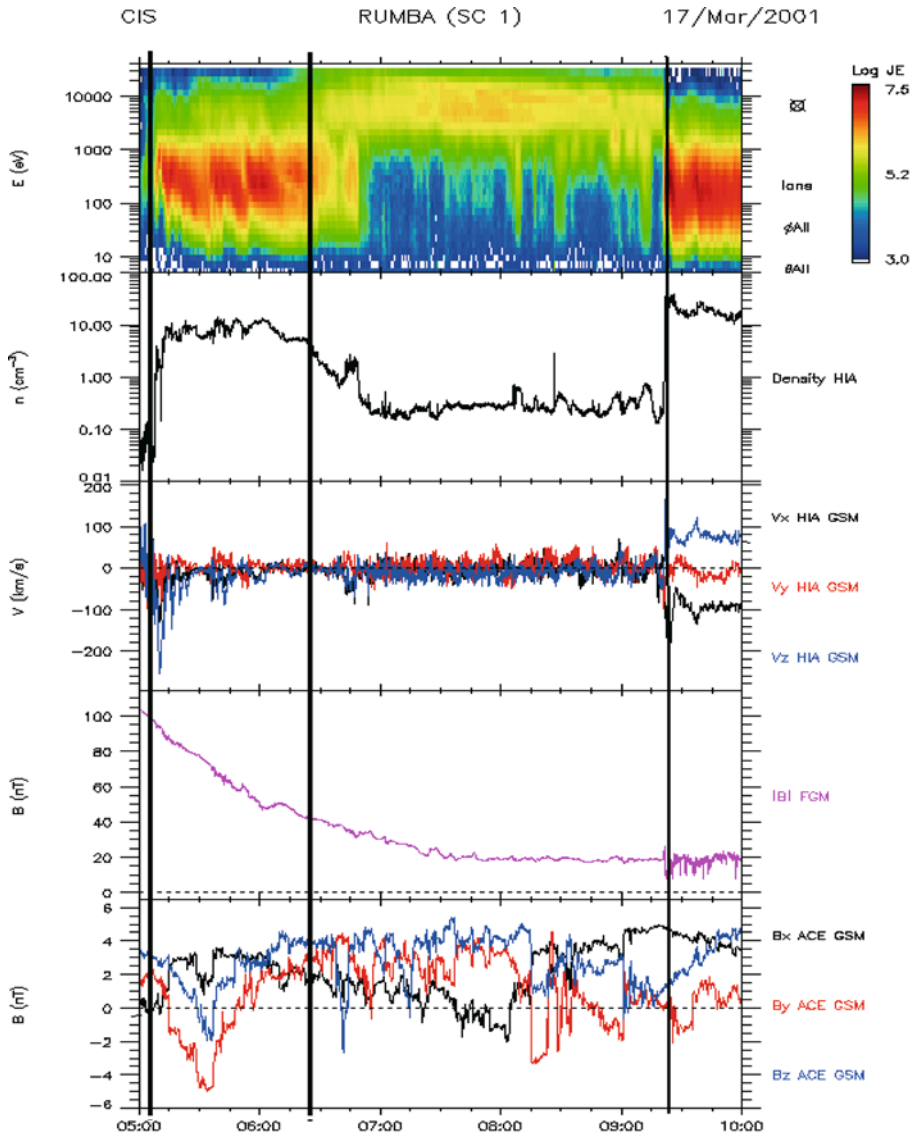


*Figure 4*. Multi-panel plot of the plasma and field information from Cluster and ACE, with vertical dashed lines indicating the corresponding features to those in Figure 3. From top to bottom these are: the ion energy spectrogram, density, velocity and magnetic field from Cluster, and the lagged ACE magnetic field representing the IMF. The lag time is computed as a simple convection time, using the ACE solar wind velocity, and is 82 min in this case.

boundary region, starting from about 06 UT, where the density begins to fall from 10 $cm^{-3}$ to the low densities expected for the dayside plasma sheet (0.2–0.3 $cm^{-3}$). During this transition, there is an onset of a high-energy band

of ions (between 5 and 10 keV). The spacecraft therefore appear to traverse the dayside region after about 06:25 UT, which is filled with trapped plasma sheet ions on closed field lines (not shown, see the companion paper by Lavraud et al., 2003). After 07 UT and until the magnetopause exit at 09:20 UT the ion density remains low with no significant bulk flow (during this period the GSM magnetic field turns from southward to northward). These gross features are characteristic of the regions traversed in all the events shown in this paper.

Within the interval through the throat (between 05:15 and 06:15 UT) there are a number of additional transient signatures. Some of these relate to dispersive signatures in the plasma data (Vontrat-Reberac et al., 2003) and some to transient, impulsive signatures, which can be correlated with plasma flows in the ionosphere (Marchaudon et al., 2003). The latter are associated with brief, southward (and dawnward) turnings of the IMF during the pass. On one occasion (06:40 UT) the spacecraft appear to be taken back into the throat region from the dayside (plasma sheet). Such an occurrence would be expected for a southward (or sunward) motion of the equatorward edge of the cusp, perhaps due to erosion of the dayside magnetopause. Such transient motions also appear more dramatically in the other events discussed below. The event here, however, has few clear boundary crossings within the cusp structure to confirm such motions or to confirm spatial as opposed to temporal effects. Nevertheless, the spacecraft sequence through a number of features in the time series data gives timing information, which confirms the expected order in passing from one region into another. For example, spacecraft 3 (green) exits first from the cusp throat, followed by 2, then 1 and 4 together, as implied by the orientation of the spacecraft configuration with respect to the cusp throat. Again, observation of these trends is useful in developing the interpretations below.

This event therefore corresponds to a traversal across the mid- to high-altitude throat region, followed by a passage through magnetospheric field lines near the dayside boundary, before a final exit into the magnetosheath. The event is chosen, and described first, because these quiet, external conditions produce a classic pass through the region, where the cusp location appears to be close to that predicted by the Tsyganenko model and the slow change in magnetic field topology can clearly be seen. The spacecraft pass out into the magnetosheath almost as indicated in Figure 2, drawn relative to the model field lines, which apparently change orientation from the southward/tailward throat alignment to the northward, dayside alignment, along the orbit. The event thus serves as a good template for the other events, some of which occurred during more dynamic conditions, often with repeated large-scale cusp motion, which adds to the observed signature. The pass is similar to that described in Section 3.3 below, in particular, but appears to be deeper within the dayside region.

### 3.2. Events of 13 and 20 February 2001 and 4 April 2001

Figure 5 shows the orbit and spacecraft configurations for two inbound traversals through the southern cusp regions for different IMF conditions. The first of these events has been briefly studied by Cargill et al. (2001), from the point of view of the magnetic field measurements, and both have been comparatively studied by Cargill et al. (2003) in combination with PEACE and CIS data. The crossings occurred during the entry of the spacecraft into the magnetosphere on the inbound, southern leg of the Cluster orbits. During the period of entry into the magnetosphere, the IMF was varying in some components. In the first case the field was more variable, but predominantly southward. In the second case it was dawnward and had turned southwards before entry into the cusp region and magnetosphere (at 23:00 UT, see Figure 7). The magnetic field magnitude (as measured by the FGM instru-

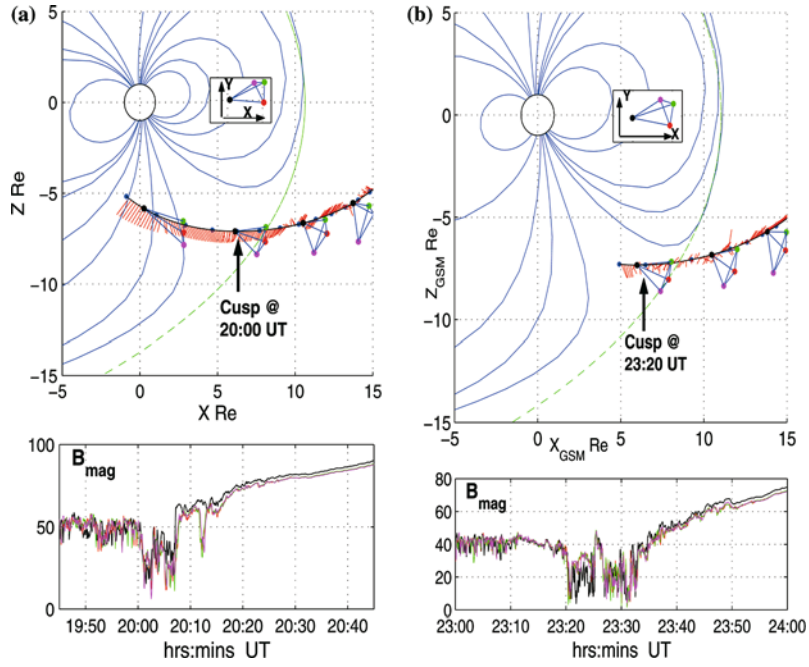


*Figure 5.* (a) The event of 13 February 2001, which corresponds to a southern cusp crossing, during an inbound leg of the orbit, ending at 24:00 UT. The orbit and spacecraft configurations (top panel) are drawn in the same format as for Figure 2, together with insets showing the $X,Y_{GSM}$ projection of the configuration at cusp entry. Projected magnetic field vectors, as measured by FGM, are also shown around the orbit. The bottom panel shows the corresponding measured magnetic field magnitude for all spacecraft traces overlain with the same colour coding. The presumed, exterior cusp entry is indicated on the orbit track. (b) The event of 20 February 2001, which corresponds to a southern cusp crossing during an inbound leg of the orbit in the same format as for (a).

ment) for a 1-h interval around the cusp traversals is shown in the bottom panels of Figure 5 and the projected field direction is added along the orbit tracks in the top panels. In each case, entry into what we define as an ''exterior'' cusp region appears to be directly from the magnetosheath and is identified here by both a depression in the magnetic field magnitude and an increase in the magnetic field fluctuations. These features are clearly visible in both events. The approximate position of the initial cusp entry in each case is indicated on the orbit.

Figure 5a, for example, shows that on 13 February the spacecraft entered the cusp from the magnetosheath (or boundary layer) at about 20:00:30 UT. Figure 5b shows that on 20 February the spacecraft entered the cusp from the magnetosheath (or boundary layer) at about 23:20:30 UT (these times refer to the end of the transition, seen as a decrease in $|B|$). One of the projected spacecraft configurations is drawn for these times in the top panels of each Figure. The main exits from the low field region (into the magnetosphere) occurred at 20:07 UT for 13 February 2001 and at 23:33 UT for 20 February 2001. These are both interpreted as an exit from the rear of the cusp-throat region into the plasma mantle, and subsequently into the tail lobe. These exits appear to be directly from a low field (diamagnetic) region. The insets in the figures show the projected spacecraft configurations into the $X,Y_{GSM}$ plane for both events. From these and the main projections in Figure 5, it is apparent that both events have very similar nominal locations with respect to the magnetosphere: in fact, both lie slightly duskwards of noon. The four spacecraft, vector magnetic field data from both events (on an expanded scale focussing on the cusp entry and exit) are shown in Figure 6 (showing entry and exits by the dashed vertical lines).

As mentioned, the crossings through the exterior cusp region are characterised by a reduced field magnitude, but it is also apparent from Figure 6 that large magnetic shears (changes in the field direction: second and third panels from the bottom) are also present, particularly for 20 February 2001. In the case of 20 February 2001, the traversal is complicated by a brief exit back into the magnetosheath or an adjacent boundary region at 23:25 UT, but with a cusp re-entry at 23:26:30 UT. In both cases, just prior to the initial cusp entry, the magnetosheath field is dawnward, but is consistently southwards (in line with the IMF) only in the case of 13 February 2001 (see Figure 7). For 20 February 2001, the orientation turns southwards before the first entry, but remains predominantly dawnward at the re-entry (just before 23:26:30 UT). Thus, differences between the observed IMF and local magnetosheath conditions at these latitudes can be significant. In both events, the final exit appears to be into the tailward magnetosphere (mantle region), showing a duskward as well as a southward field, implying an exit into the duskside mantle region.

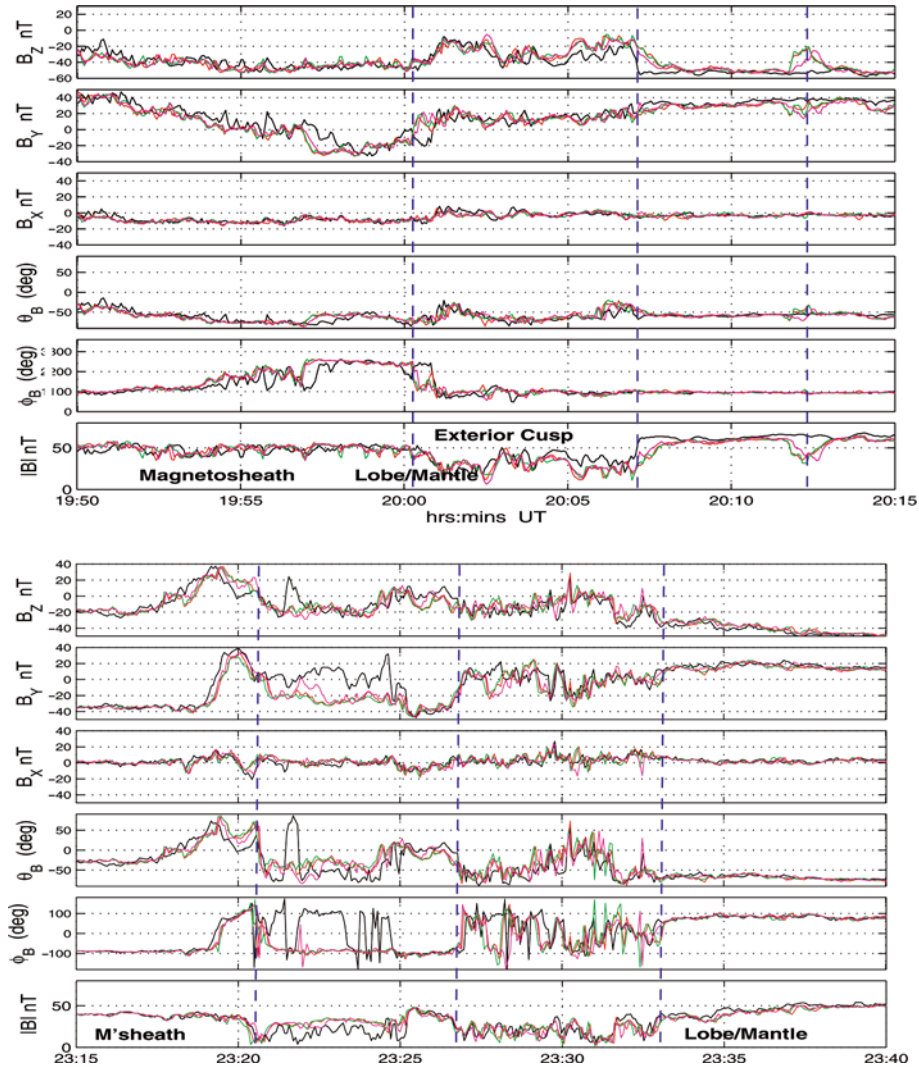


*Figure 6*. The four spacecraft vector magnetic fields in GSM co-ordinates, as measured by FGM, showing the angular variations also, for the interval around the cusp crossings for 13 February 2001 (top panel) and 20 February 2001 (bottom panel). The key boundaries and regions (discussed in the text) are indicated by vertical dashed lines.

Figure 7 shows the ion spectrograms and the density and velocity moments measured by the CIS-HIA instrument, together with the FGM magnetic field, from spacecraft 3 for 13 February 2001 and 20 February 2001. Also shown is the ACE-IMF, already mentioned above, suitably lagged for solar wind convection (note the correlation with the magnetosheath trend seen at Cluster before cusp entry) as for the 17 March 2001 event. From these figures it is seen that the plasma ion distributions show a more extended

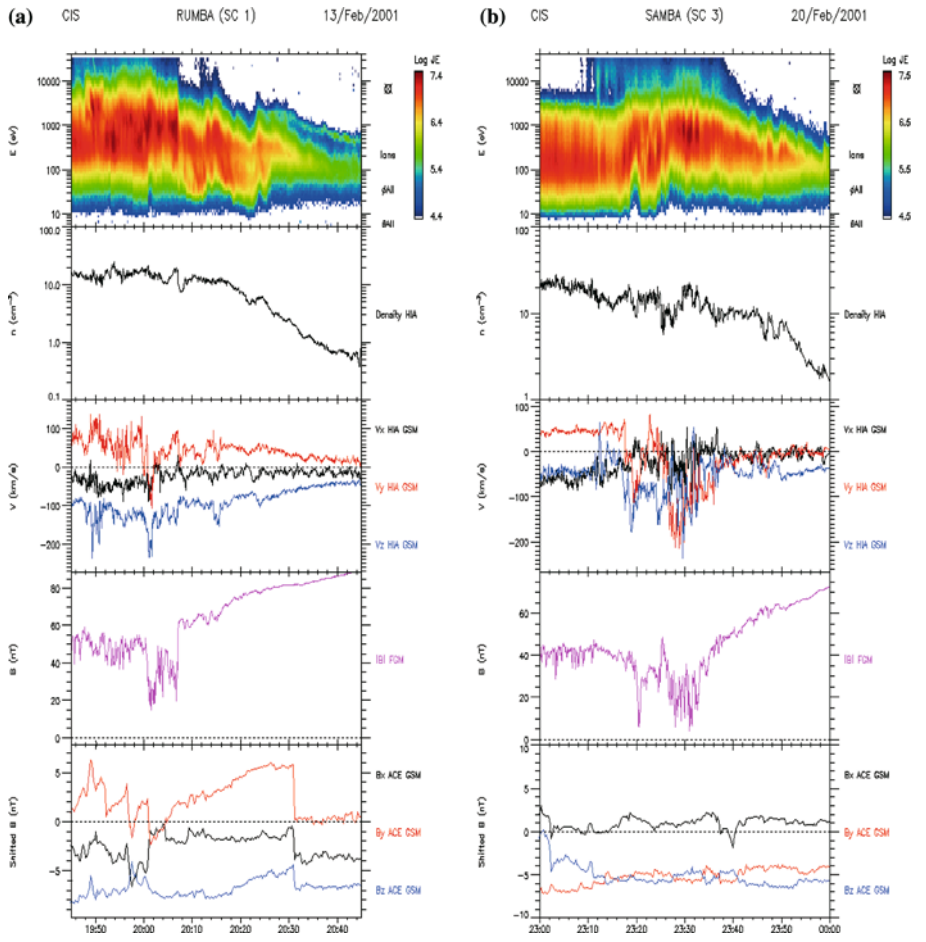


*Figure 7.* Plots of the Cluster ion spectra and moments and magnetic field, together with lagged ACE-IMF data in the same format as Figure 4, (a) for 13 February 2001 and (b) for 20 February 2001. The lag times used for the ACE magnetic field are: 53 min 20 s, for 13 February 2001, and 73 min 20 s for 20 February 2001.

structure than the magnetic field. It is also clear that the plasma moments show no evidence of the ''stagnant'' regions observed in the events discussed by Lavraud et al. (2002, 2003). In both cases, however, the southward and dawnward directed IMF (and magnetosheath field) is likely to result in significant and perhaps continual magnetic reconnection across the dayside magnetopause, and the result of such field line merging is likely to be that field lines are continually swept tailward across the cusp. In the case of 13 February 2001, the ion velocity data show a continual southward component, which in the magnetosheath is consistent with the southward location and flow around the magnetopause, and in the cusp is consistent with the

convection of reconnected field lines persisting into the plasma mantle. In the case of 20 February 2001, however, the IMF and magnetosheath field had a dominating dawnward component (more so in GSE coordinates), so that we expect this convection of reconnected field and flow to have a significant dawnward component, as observed. On entry to and exit from the cusp region there are clear deflections in the velocity, particularly at the cusp entry from the magnetosheath, which shows a strong deflection into $-Y_{GSE}$. The electron spectrograms (not shown), measured by the PEACE instrument, for the cusp entries also show no sharp signatures. There is, however, a drop in the flux of the high-energy band (above 100 eV) on entry (possibly representing lower temperature), and an increase in energy of the low-energy band on exit before a slow transition into the mantle. Although overall there is only a slow change electron and ion distribution, the sharp exit from the cusp into the mantle region, seen by the magnetic field, is well visible (in the case of 13 February 2001). For example, the ion density changes by a factor of 2 on spacecraft 3.

Although entry to, and exit from, the low field cusp region appear to be clear from these data signatures, close inspection of the full magnetic shear reveals that the spacecraft crossing order does not imply a simple outward motion of the boundaries across the spacecraft array. This is particularly so in the case on entry. For instance, the spacecraft configurations for both days (Figures 5 to 7) show that spacecraft 1 (black) is leading (and innermost), with the other spacecraft lying in a plane which is oriented close to the nominal magnetopause. Taking a model magnetopause boundary orientation, therefore, and simple outward motion of the boundary, it would be expected that spacecraft 1 enters and exits the cusp region first, with the order of the other spacecraft depending upon the actual boundary orientation and relative motions. It is fairly clear (Figure 6) that spacecraft 1 appears to be the first to exit the low $|\mathbf{B}|$ region of the exterior cusp into the magnetospheric lobes (mantle) at 20:07 UT (13 February 2001) and 23:33 UT (20 February 2001). In fact, the spacecraft crossing order in both events (spacecraft: 1, 4, 3/2) implies the cusp-throat motion is both northwards (outwards) and dawnwards across the spacecraft array. This motion is possibly consistent with a stress-induced motion arising from the dawnwards directed magnetosheath field (and consistent with the IMF orientation upstream), for instance. The entry to the cusp from the magnetosheath, however, is obscured by changes in the magnetic field direction so that the implication of the crossing order of the spacecraft is somewhat more confused. Even the assumption that the dawnwards directed magnetosheath field also results in a significant dawnwards motion of the cusp, on entry, is insufficient to explain the crossing order. It is possible, however, that an indentation in the cusp/magnetosheath boundary could suitably affect the spacecraft crossing order (see Section 4).

Further analysis of the boundary dynamics of the whole traversal, together with a possible narrowing or expansion of the cusp region, are discussed in Section 4. The details of the magnetic fluctuations and other magnetic structure throughout the traversal are not discussed here, but are dealt with by Cargill et al. (2003). We comment here, however, that the 20 February 2001 event does not correspond to clearly southward IMF conditions, and shows a more turbulent and twisted magnetic field configuration within the cusp. A third southern cusp traversal, corresponding to 4 April 2001, is shown in Figure 8 in the same format as the previous examples. Here, entry from the magnetosheath occurred at around 19:44 UT, with final exit into the mantle at around 20:28 UT (timings from spacecraft 1). This event shows a more extended signature than for either of the previous two, but has very similar character; we do not discuss it in detail. There is a brief exit back into the magnetosheath at 20:08 UT (similar to that seen on 20 February 2001). At the inner cusp boundary, on exit into the tail lobe, spacecraft 1 exits the

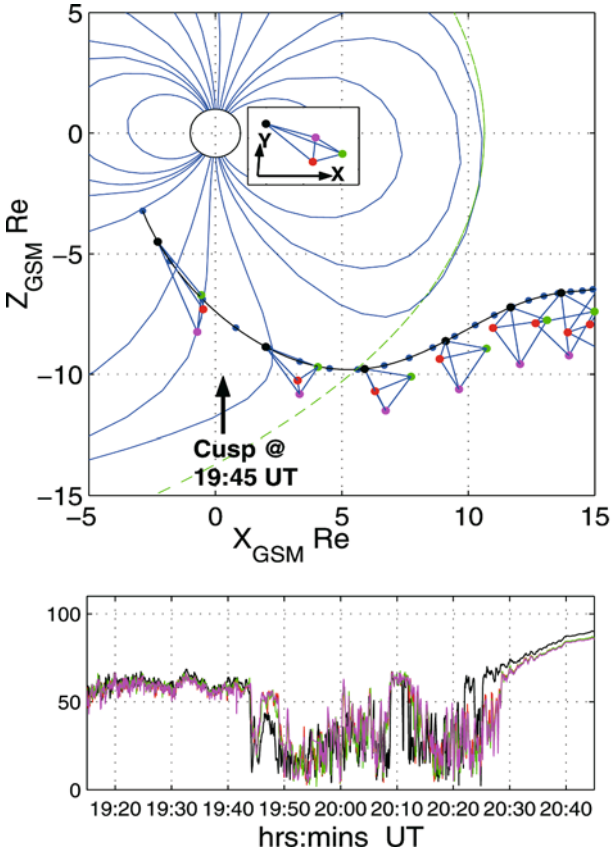


*Figure 8*. The event of 4 April 2001, which corresponds to a southern cusp crossing during and inbound leg of the orbit in the same format as for Figure 5.

cusp on a couple of occasions before all spacecraft finally exit into the lobe. The magnetic field again shows a rapidly changing orientation throughout this long encounter (see Figure 9). This event is of interest since the spacecraft crossing order appears to be clearer than for the previous events, and fits a simple traversal through the cusp region during an outward motion of the magnetopause, overall (the brief exit at 20:08 UT shows a nested signature consistent with a simple reversal in this motion of the boundary). For instance, spacecraft 1 enters each region first, followed by the others in the expected order (i.e. spacecraft two and three together and four trailing on the cusp entry) for a boundary nominally aligned with the magnetopause. The possibility that the more confused crossing order, seen during the previous two events, is due to dawnward motion (arising from the apparent $B_Y$ induced stress) is therefore given more credence by this counter example.

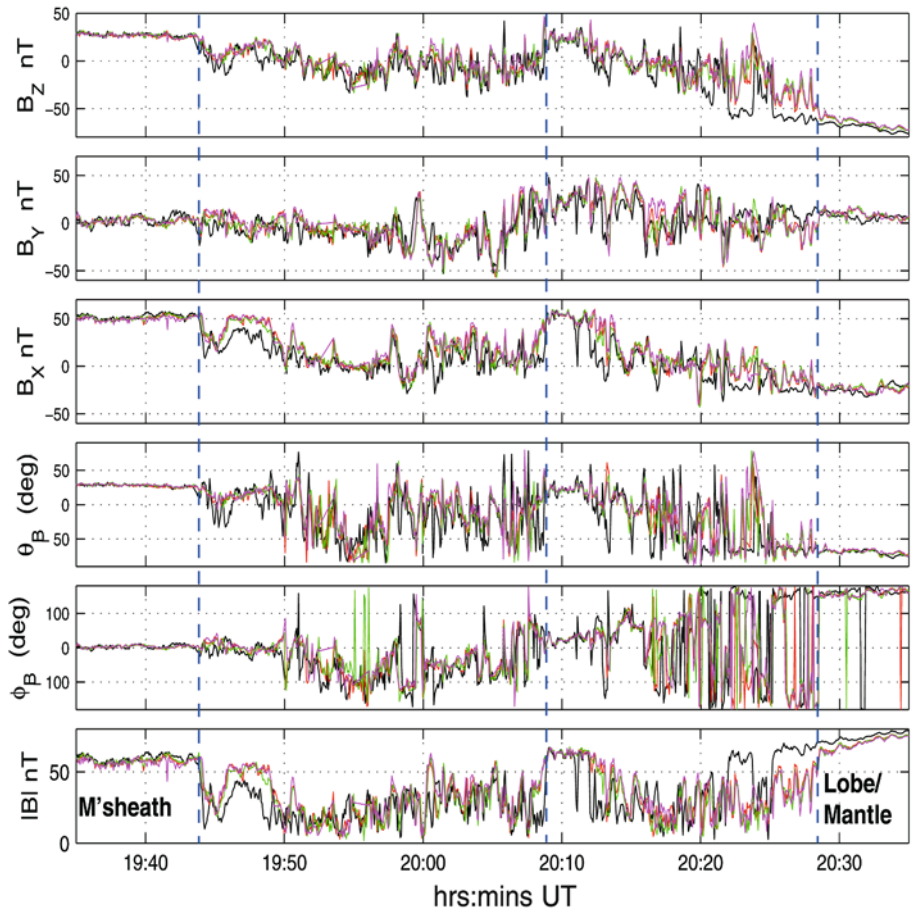


*Figure 9*. The four spacecraft vector magnetic field in GSM co-ordinates for 4 April 2001, showing the key regions discussed in the text.

### 3.3. Event of 26 February 2001

Figure 10 shows the orbit and spacecraft configuration for a traversal, which occurred during more dynamic conditions, corresponding to a southward IMF ($-B_Z$), but also fairly radial (i.e. strong $B_X$) component. These conditions produced a complex series of boundary crossings through the different regions adjacent to the cusp. The event occurred during an outbound, northern exit of the spacecraft from the magnetosphere, as shown in the top panel of Figure 10. The cusp traversal separates into a passage through two distinct plasma regions. The first appears to correspond to a mid- to high-altitude (i.e. within the "throat" of the cusp) traversal. The second corresponds to a dynamic interval during which several entries to and exits from the high-altitude (or an exterior) cusp and dayside magnetosphere occur before the exit into the magnetosheath (also via multiple crossings). During the traversal the cusp boundaries appear to undergo some reconfiguration in the form of possible erosion (and recovery) of the equatorward boundary and large-scale motion of the whole high-altitude region. In Section 4 we concentrate on summarising the analysis of the time interval after 05:30 UT,

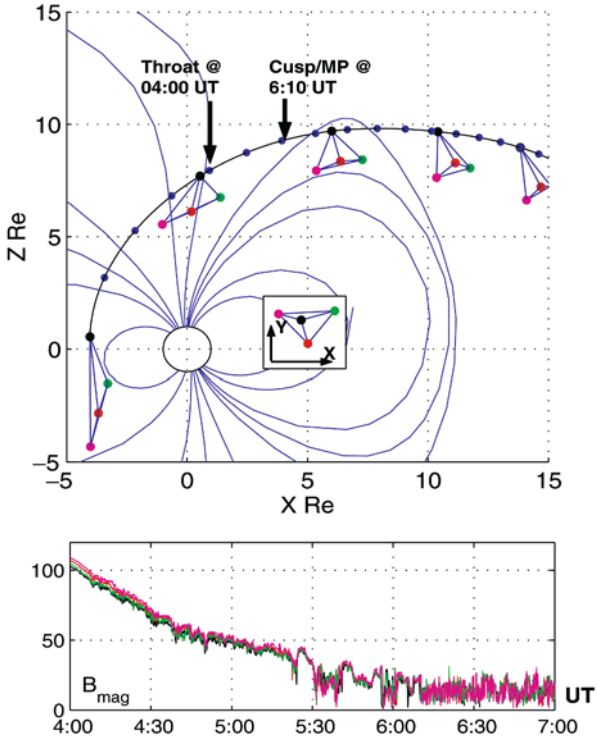


*Figure 10*. The event of the 26th February 2001, which corresponds to a northern cusp crossing during an outbound leg of the orbit in the same format as for Figure 5.

when repeated motion of high-altitude cusp resulted in the spacecraft encountering the dayside magnetospheric boundary, and then magnetosheath.

The spacecraft entered the cusp throat at around 04:08 UT, as suggested by increased ULF wave activity, apparent as increased fluctuations in |B| in the lower panel of Figure 10. The spacecraft traversed the throat during the next hour, and appeared to move to higher altitudes during this time in a manner almost as inferred by the model field lines and orbit track, shown in the top panel of Figure 10. In consequence, the field magnitude slowly falls on all spacecraft during this time, as expected for a slow movement up the throat. The spacecraft configuration near 04 UT (top panel) indeed shows that the spacecraft form a sequence in order of relative position outward along the cusp throat: 4(magenta), 2(red), 3(green), 1(black) from the lowest (highest field) to highest (lowest field) position. The multi-spacecraft traces separate, in terms of decreasing field magnitude, according to the same sequence (4,2,3,1). They follow this trend until about 05:20 UT, when the magnetic field configuration changes. After this time, the sequence of crossings in and out of the cusp can be seen as changes in the magnetic fluctuations.

Figure 11 shows the ion data in conjunction with the magnetic field data from spacecraft 1 and the (lagged) IMF measured by ACE in the same format as Figure 7. The key difficulty with interpreting this event is that the IMF($-B_Z$) is variable, but often southward, and $B_X$ is often strongly negative, giving an almost radially aligned field during the passage through the cusp. The orbit naturally moves from dawn to dusk (remaining within an hour of local noon) during the exit from the magnetosphere, but is almost at magnetic noon at 05:00 UT. The actual spacecraft location will therefore be sensitive to any dawn–dusk motion of the cusp as well as to any North–South motion. In combination, these facts make any correlation with IMF conditions very hazardous, and the high variability evident in this pass probably results from the IMF configuration in the solar wind. Nevertheless, both the CIS data shown in Figure 11 and the PEACE data (Figure 13, see later) indicate that the spacecraft pass through distinct plasma boundaries at 05:12 and 05:21 UT.

The ion energy time spectrogram shown in the top panel of Figure 11, for example, suggests that the Cluster spacecraft enter a distinct region (adjacent to the cusp) after about 05:12 UT, presumably on the equatorward edge of the throat. After this time, they appear to exit into a region made up of high energy, bi-directional electrons and high-energy trapped (loss cone in the distribution functions) ions, and therefore we interpret it as the dayside magnetosphere (or plasma sheet). The bulk density falls slowly during the approach to this boundary (presumably within the cusp throat) and then falls dramatically on exit into the dayside region. The

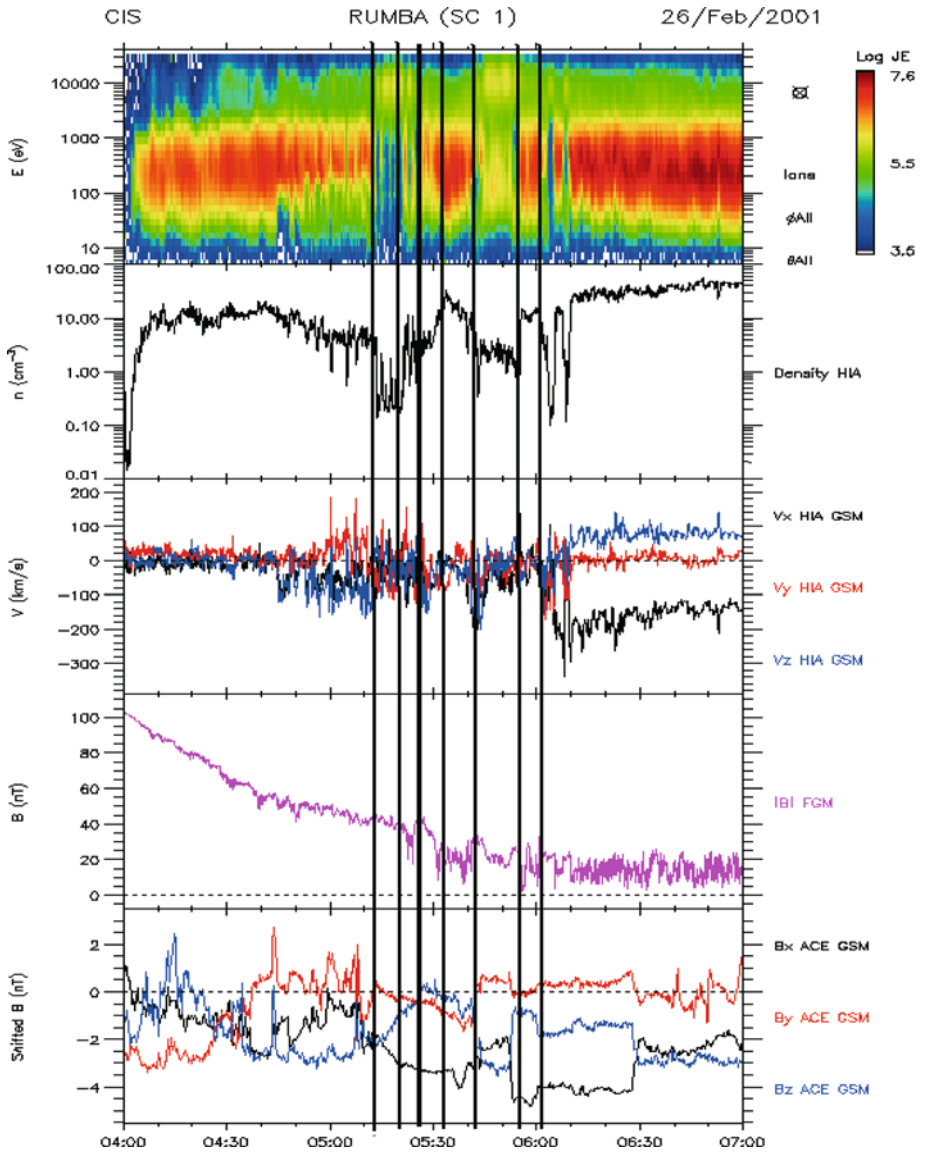


*Figure 11.* Plots of the Cluster ion spectra and moments and magnetic field, together with lagged ACE-IMF data in the same format as Figure 4 for the event of 26 February 2001. The lag time used is 85 min. Vertical dashed lines indicate the boundaries discussed in the text.

energy spectrum (top panel) shows a high-energy band (centred on 10 keV), consistent with a magnetospheric population. In addition, the interval between 05:12 and 05:21 UT contains a number of transient structures, which therefore appear to be near the equatorward edge of the cusp throat. These were also reported by Lundin et al. (2003), who interpreted them as

PTE signatures. We do not discuss these transient features further here, since they are the subject of future work (Taylor et al. (2003), private communication). The magnetic field at Cluster (lower panel in Figure 12) shows all negative components for this interval, which is consistent with an exit on the dusk-dayside of the cusp throat, but also arising from significant northward motion of the throat. At the start of this interval (05:12 UT) the ACE magnetic field turns from being predominantly southward, until $B_Z$ is nearly zero at 05:21 UT, while at the same time the $B_X$ component increases to dominate the field orientation and $B_Y$ remains slightly negative. It is therefore possible that the exit of the spacecraft from the cusp throat into the dayside arises as a result of a narrowing of the cusp, possibly following the switch-off of dayside merging, which is likely to result in the equatorward edge of the cusp moving tailward.

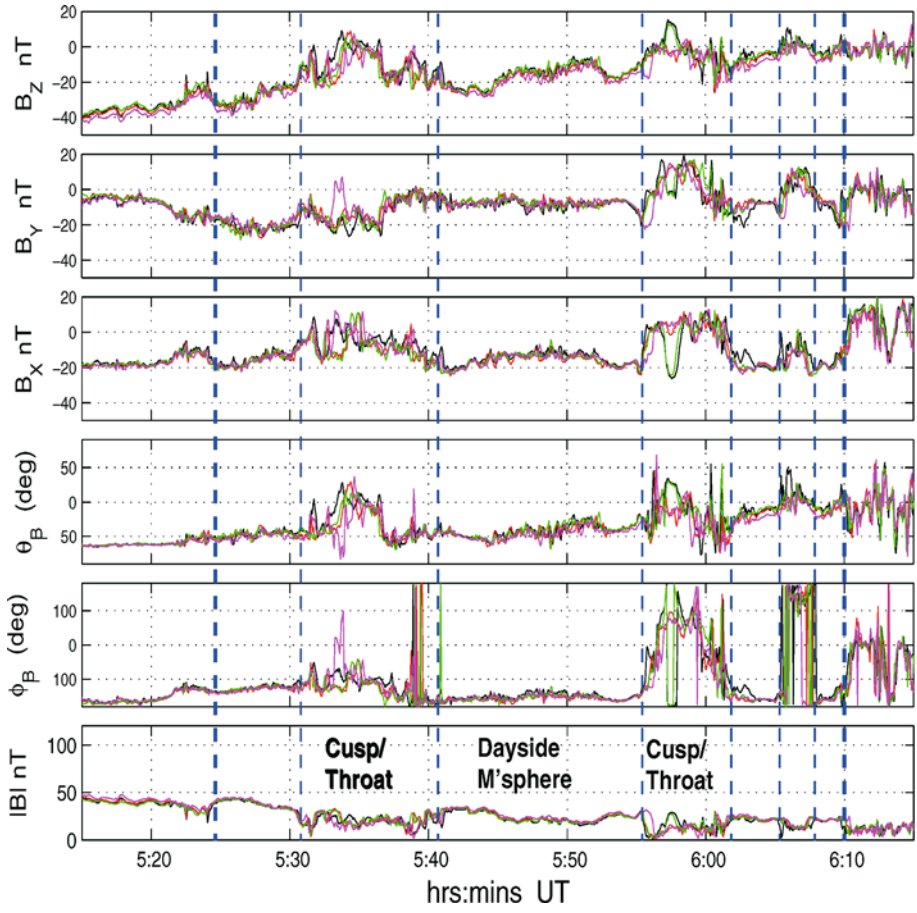


*Figure 12.* The four spacecraft vector magnetic field for 26 February 2001. Vertical dashed lines indicate the boundaries discussed in the text and as also shown on Figure 11.

The ion distribution just after re-entry to the cusp throat at 05:21 UT shows a number of rapid changes. It appears that the cusp structure undergoes a reconfiguration at this time, taking the spacecraft back to the tailward side of the throat, possibly through the cusp. The $B_Y$ component on all Cluster spacecraft remains negative during this time, suggesting that the spacecraft remain on the dusk-side of the cusp. This reconfiguration is harder to correlate with any upstream changes. Figure 12 shows that between 05:25 and 06:10 UT the field configuration increasingly changes during the transit through the cusp. This is interpreted as representing repeated entries into the different regions surrounding the duskside, equatorward edge of the cusp. At the same time, the spacecraft move to higher altitudes, further into both the outer cusp region and adjacent dayside plasma sheet at alternate crossings as we describe below.

Between 05:31 and 05:41 UT, for instance, the spacecraft appear to pass completely through the cusp throat (on the duskside) from the tail lobe (mantle) into the dayside magnetosphere (or entry layer) and the spacecraft crossing sequence appears to suggest a northward (tailward) motion of the cusp boundaries. Between these times (i.e. within the cusp) the magnetic field is depressed, its fluctuations are enhanced and the ion data show very low net flows. The spacecraft appear to return into the outer (exterior) cusp region (perhaps through the dayside entry layer) at 05:56:30 UT, during what appears to be an equatorward motion of the equatorward cusp boundary (or cusp throat). They then exit back to the dayside entry layer at 06:02 UT, during a reverse motion of the boundary, tailwards (all implied by the spacecraft crossing sequences). Between these times the magnetic field is again depressed, shows enhanced fluctuations and does not take the local magnetosheath orientation. The ion data show no net flows. This motion (or else a dawn/dusk motion) is repeated at the later crossings at 06:05 and 06:08 UT, but then the spacecraft appear to enter a more magnetosheath-like plasma population (the ion velocity moments show a magnetosheath-like velocity). This suggests that the spacecraft have now moved to the extreme edge of the cusp region and may pass directly through the magnetopause (MP). The crossing at 06:10 UT, for example, appears to be a direct MP exit into the magnetosheath. Immediately after 06:02 UT and before 05:56:30 UT, the magnetic field remains oriented along a funnel-like geometry consistent with a location on the dusk and equatorward edge of the cusp, but then progressively tilts less southward and takes a wholly dawnward direction surrounding the 06:05–06:08 crossings. This implies that the spacecraft move through the edge of the magnetospheric field lines as drawn in the top panel of Figure 10 (note that the orbit passes through this region in the plot at later times 07–09 UT).

The ion signature (and also the electron signature) for this interval therefore broadly supports this sequence of crossings, with a clear entry into

the dayside regions, showing the re-appearance of a high-energy (above 5 keV) band (top panel, Figure 11), between 05:41 and 05:56 UT. There is, however, some doubt regarding the later crossings from 05:56:30 UT. In boundary orientation, they appear to be at the extreme edge of the outer cusp region. Nevertheless, overall the boundary normals define the geometry discussed here, being significantly tilted with respect to the nominal magnetopause boundary, suggesting the presence of an indented region.

A tailward motion of the whole cusp region during the interval (05:31–05:41 UT) is not inconsistent with the fact that the IMF($-B_Z$) remains close to zero until 05:42 UT. The computed lag used here places a sudden southward turning of the IMF at that time, which lasts until 05:52 UT. Although the latter time is just before the entry into the exterior cusp region at 05:56 UT it is possible that this entry is a result of erosion of the dayside boundary, which moves the equatorward edge equatorward (southward). After 05:56 UT, the IMF($-B_Z$) remains close to zero until just after 06:00 UT. It is at least plausible that the equatorward edge moves northward again as a result of reduced dayside merging. The spacecraft are seen to re-enter the dayside region at 06:02 UT. After this time the IMF($-B_Z$) again turns more southward, possibly inducing the second (short) excursion into the exterior cusp region. The IMF direction does not appear to support the repeated sequence (06:05–06:08 UT) very well, however, since the timing of each turning differs by a few minutes, probably a result of poor estimates of the actual convection times. It is likely that the variable conditions during this event require a variable time lag to be applied to the ACE data for correct correlation. However, the main deficiency is that the radial magnetic field conditions (large $B_X$(GSM) component) mean that the correlation with solar wind conditions is likely to be poor at best. The above sequence in fact does not account for the apparent dawn-dusk motion of the high-latitude cusp region, which seems to be the dominant motion, judging by the change in magnetic field orientation at Cluster through the last two cusp excursions (see also the DA results below). Perhaps the location of the cusp is very sensitive to small changes in $B_Y$ during radial field conditions. Such sensitivity could be explained by the fact that the crossing lies very close to local noon.

Figure 13 shows the electron data measured by PEACE for the same interval as for Figure 12. The main features through the interval correspond with those already seen in the magnetic field and ion data. In particular, the throat crossings and exit to/from the dayside plasma sheet and the throat can all be distinguished (and are indicated by dashed vertical lines on the plot). Cusp electrons show a broadband distribution rather like that seen in the ion signature. In addition, these four-spacecraft plots reveal key differences between the spacecraft, particularly in the case

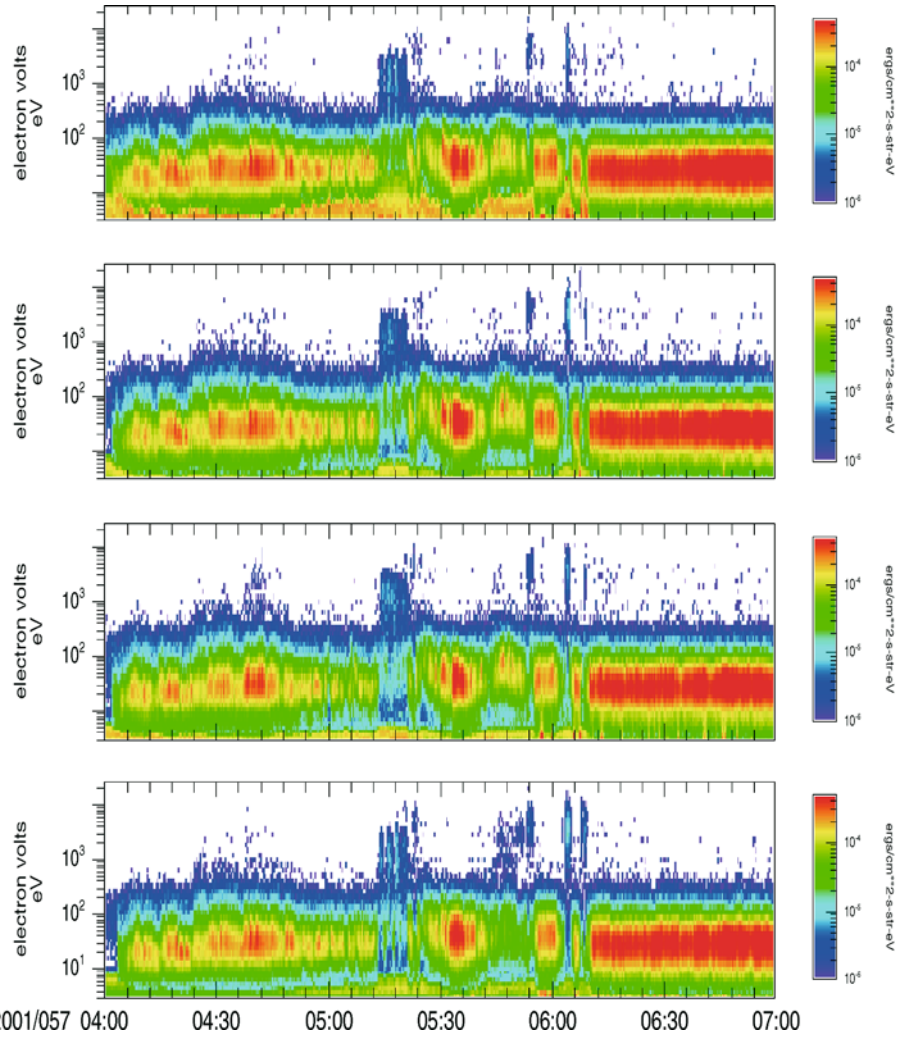


*Figure 13.* Stacked four spacecraft electron energy spectrograms for the event of 26 February 2001, with the data from spacecraft 1 at the top. Vertical dashed lines indicate the boundaries discussed in the text and as also shown on Figure 11.

of the dayside interval from 05:42–05:55 UT, where all but spacecraft 4 see short (transient) signatures within the dayside interval. This is similar to the occurrence seen during the earlier interval (05:12–05:21 UT). The plot in the top panel of Figure 12 shows that spacecraft 4 is the furthest away from the cusp on the dusk-side (following the interpretation that the cusp-throat moves dawn-ward at 05:41 UT to take the spacecraft into the adjacent dayside region). This would imply that the transient signatures are cusp related (nearby the cusp).

### 3.4. Events of 25 February and 2 March 2002

The following events are taken from the 2002 dayside passes of Cluster with small spacecraft separations (100 km). They are considered here to provide a comparative coverage with the events from 2001. The event of 25 February 2002 corresponds most closely in character with that of 26 February 2001 and that of March 2002 with that of 17 March 2001, although with additional crossings of the dayside cusp boundary layer. The orbital configurations of the spacecraft for both events are shown in Figure 14. It should be noted that now the spacecraft constellations are enlarged by a factor of 100. In both cases the orbits lay close to magnetic local noon. Figure 15 shows the plasma and field information in a similar format to that in Figure 7, and Figure 16 shows the four spacecraft magnetic field data in the same format as Figure 3, for both events.

For 2 March 2002 the Cluster orbits lie about an hour dawnwards of noon and for 25 February 2002 they lie about an hour duskwards of noon. In both cases, however, crossings appear to be dominated by North–South spacecraft motions, rather than any charges of relative dawn-dusk orientation. In both cases the orbits appear to graze dayside fieldlines after a traversal across the high-altitude throat. In fact the event of 2 March 2002 appears to pass deeper into the dayside region (or entry layer) than does the 25 February 2002 one. The crossings through the cusp boundaries appear to follow the simple spacecraft ordering implied by the configurations shown in Figure 14, i.e. on exit from the throat region, spacecraft 4 is just ahead of spacecraft 2 and these two lead spacecraft 1 and 3. Additionally spacecraft 1, 2 and 4 lie almost parallel to the nominal magnetopause orientation, with spacecraft 3

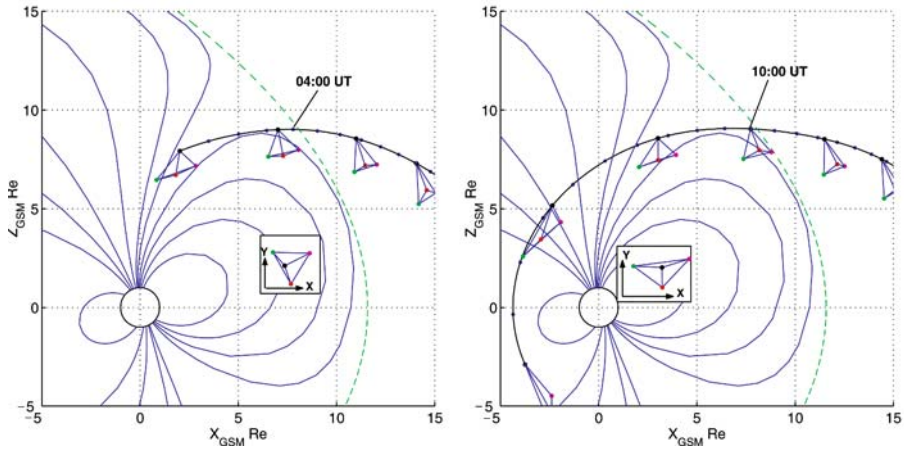


*Figure 14.* The events of 2 March 2002 (left) and 25 February 2002 (right), which correspond to northern cusp crossings during and outbound leg of the orbit in the same format as for Figure 2.

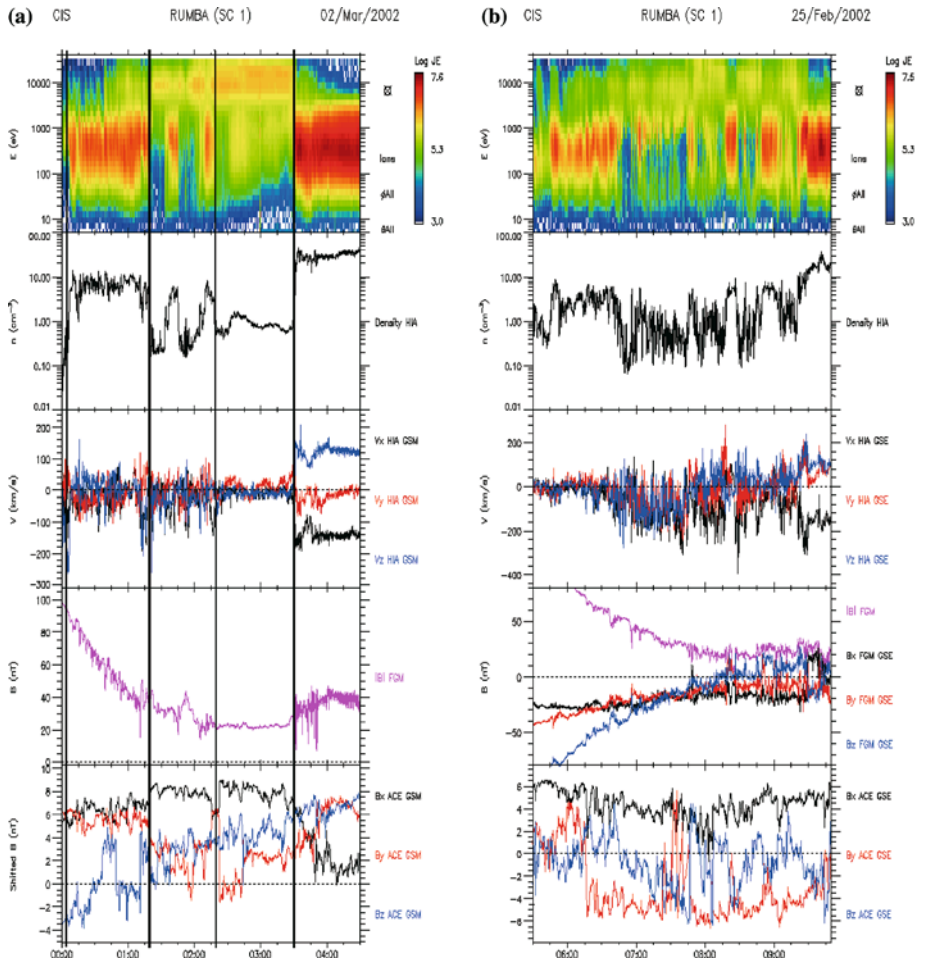


*Figure 15*. Plots of the Cluster ion spectra and moments and magnetic field, together with lagged ACE-IMF data in the same format as Figure 4, (a) for the event of 2 March 2002 (left panel), and (b) for 25 February 2002 (right panel). The lag time used is 70 min. Vertical dashed lines indicate the boundaries discussed in the text.

innermost with respect to the magnetopause. This order is confirmed, for the 2 March 2002 event, by the final exit into the magnetosheath at 03:30 UT.

Figure 15 shows the Cluster ion and magnetic field data for both events. For the event of 2 March 2002 the spacecraft enter into the cusp throat just before 00:07 UT, and for 25 February 2002 they skim along the equatorward cusp edge. For 2 March 2002 the ion spectra shows a magnetosheath-like plasma distribution during this throat traversal until a sharp cut off at 01:19 UT. This cut off is interpreted as a crossing of the equatorward edge of the cusp into the dayside plasma sheet (closed magnetospheric fieldline region), since the ion distributions show similar characteristics as those in Figure 4.

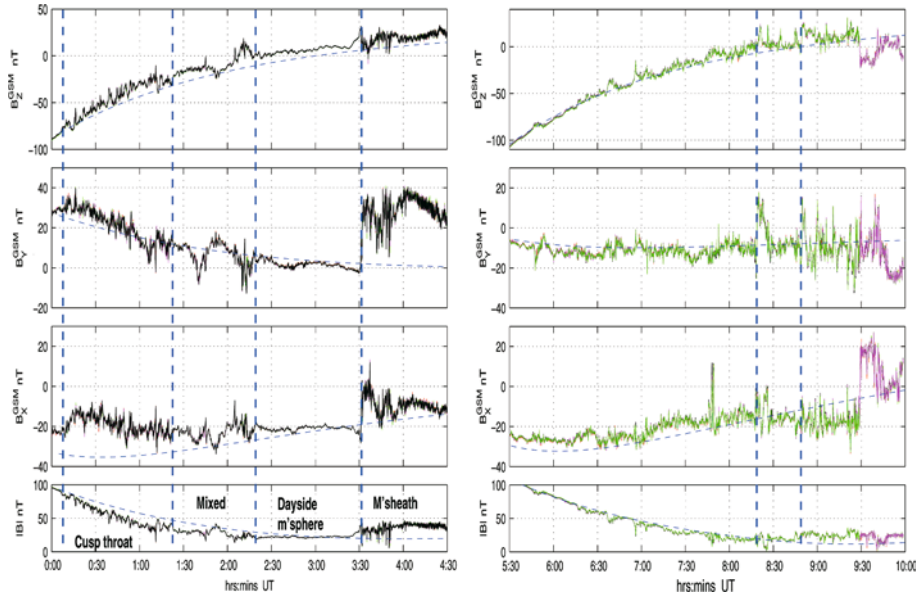


*Figure 16*. The four spacecraft vector magnetic field for the interval around the cusp crossings for 2 March 2002 (left panel) and 25 February 2002 (right panel) in the same format as for Figure 3. The vertical dashed lines indicate the boundaries discussed in the text and as also shown in Figure 15.

The magnetic field contains ULF fluctuations during this period (as shown in the top panel of Figure 16) in which the spacecraft slowly move up the throat and towards the equatorward edge. The total magnetic field magnitude falls smoothly during this time (following the model magnetic field), with only a small $B_Y$ component, in line with the orbital location near local noon. After 01:19 UT the spacecraft appear to enter into the dayside magnetosphere, but with two excursions back into the cusp throat ending at 01:45 and 02:16 UT; these are discussed further in Section 4 below. During this period (01:19–02:16 UT) the magnetic field shows additional variability along with some gross changes in orientation, reflecting the changing location with respect to the cusp structure. After 02:12 UT the spacecraft appear to remain in the dayside plasma sheet. The magnetic field orientation is stable and $B_Z$ turns slightly positive, confirming that the spacecraft are traversing the dayside region during this time until the magnetopause crossing at 03:30 UT. The IMF measured by ACE shows an unstable configuration with the IMF $B_Z$ turning northward from about 01:30 UT and having a duskward orientation. A northward movement or narrowing of the cusp throat is therefore expected overall, with the short excursions back into the throat corresponding to periods where the IMF $B_Z$ lies closer to zero. Nevertheless, there is a strong radial component to the IMF making correlations with Cluster hazardous, as for the 26 February 2001 event.

For 25 February 2002, the IMF is again very changeable, with a predominantly dawn-ward orientation and multiple northward turnings through the pass. The ion data (not shown) have a correspondingly highly variable signature right up to the final exit into the magnetosheath (at 09:30 UT), with alternating dayside cusp boundary and cusp throat signatures. This event is therefore interpreted as a traversal up the cusp throat, skimming its equatorward edge, so that the spacecraft repeatedly cross back and forth between the dayside boundary layer and the cusp throat. Figure 16 shows the multi-spacecraft vector magnetic field plot for both events; at these small spacecraft separations the traces do not deviate significantly from one another very often. The changing character in the magnetic signature during the traversals is apparent. Also plotted is the Tsyganenko T89 model (as in Figure 3), chosen to correspond closely to the conditions during each pass. Deviations from the nominal magnetospheric geometry, which would result from global displacement of the cusp, for example, or induced currents, are highlighted by this model field guideline. The local magnetosheath orientation, in particular, can be seen to be northward on exit from the magnetosphere on 2 March 2002, and excursions into and out of the cusp throat are also apparent (for both events). For example, for 2 March 2002 (top panel) the interval separates into four distinct regions: the throat passage until 01:20 UT; the period containing entry into and out of the dayside boundary layer until 02:20 UT; the full crossing into the dayside plasma sheet until 03:30 UT, and the dayside exit into the magnetosheath. These traversals have been discussed above.

On the other hand, for the 25 February 2002 event, the ULF activity remains at about the same amplitude throughout the throat passage and different regions are more difficult to distinguish. There are two notable excursions back into the throat, however, at 08:19 and 08:49 UT, which give clear boundary crossings, discussed below in Section 4. These plausibly correspond to turnings of the IMF, suggesting a widening of the cusp region as a result of increased dayside merging. Additionally, the ACE plasma data (not shown) show that the solar wind ram pressure slowly increases from a low value during the pass. During the traversal, the magnetospheric $B_Z$ turns northward at 08:20 UT (top right panel of Figure 16), as the spacecraft move towards the magnetopause along the equatorward edge of the cusp. However, $B_Y$ remains negative, implying that the cusp remains dawnwards of the spacecraft.

The conclusion from this preliminary description is that, for the first event, the spacecraft cross the cusp throat fully into the dayside region, whereas for the second event the spacecraft move slowly up the cusp throat, skimming either side of the equatorward edge, as the cusp moves North/South.

## 4. Four-spacecraft analysis

We now turn to the multi-spacecraft analysis of the above events, which have been carried out using the techniques described in Section 2. The curlometer, for example, provides only limited results since the various magnetic structures often appear to be complex (discussed below). Some analysis of the simpler boundaries, surrounding the (exterior) cusp region, is shown below. Those boundaries in this high-altitude cusp region also lend themselves readily to the dynamic analysis of the DA. Deeper into the mid- to high-altitude throat region, however, often the magnetic structure at the plasma boundaries is not clear enough for full analysis of the magnetic time series. Table I summarises the DA for all of the boundaries discussed in Section 3. The full DA analyses, as well as the computed ''timing'' normals (under the assumption of constant velocity), both described in Section 2, are quoted for comparison. The magnetosheath/cusp (magnetosheath/closed region) interface is labelled ''MP'' (''mp'') and the inner cusp/tail or cusp/closed region boundary is labelled ''cusp''. Crossings through (across) the deeper throat are labelled ''th''.

Columns in the table refer (from left to right) to: the date, time and local time (LT) of each crossing, the eigenvalue ratio for the MVA analysis and

TABLE I

Summarises the DA for all of the boundaries. 'In' and 'out' refers to entry and exit from the cusp region respectively. Vn refers to componenet along the normal directions quoted

| Date | UT | MP | LT | 2/3 | $n_{GSM}$ | | | $n_{timing}$ | | | $V_{timing}$ | t3_1 | t3_2 | t3_4 | $V_n(1)$ | $V_n(2)$ | $V_n(4)$ | $\langle V_n \rangle$ | $D_1$ | $D_2$ | $D_3$ | $D_4$ |
|---|---|---|---|---|---|---|---|---|---|---|---|---|---|---|---|---|---|---|---|---|---|---|
| 13/02/01 | 20:01:00 | MP | 11:7 | 11.2 | 0.96 | -0.22 | -0.15 | 0.94 | 0.30 | 0.14 | 58.00 | -7.7 | 2.4 | 4.3 | 72.4 | 35.6 | -15.6 | 30.8 | 1601.1 | 1862.9 | 2056.8 | 2099.9 |
| 13/02/01 | 20:07:00 | cusp | 11:7 | 10.0 | 1.00 | -0.07 | -0.03 | 0.98 | -0.16 | 0.14 | 24.00 | -20.6 | 2.9 | -6.7 | 29.9 | 5.4 | 23.9 | 19.7 | 750.2 | 816.9 | 857.8 | 913.6 |
| 20/02/01 | 23:20:00 | MP-in | 10:39 | 5.0 | 0.89 | 0.00 | -0.43 | 0.52 | 0.09 | 0.85 | -30.00 | 6.2 | 12.8 | 16.2 | -98.0 | -0.6 | -0.4 | -33.0 | | | | |
| 20/02/01 | 23:27:00 | MP-in | 10:37 | 4.0 | 0.98 | 0.01 | 0.18 | 0.76 | 0.64 | 0.06 | -126.00 | 4.0 | 2.2 | 2.2 | -161.4 | -35.2 | -127.1 | -107.9 | | | | |
| 20/02/01 | 23:32:00 | cusp | 10:34 | 4.5 | 0.78 | -0.42 | 0.46 | 0.78 | -0.42 | 0.46 | 41.00 | -10.7 | -3.0 | -7.3 | 64.7 | 43.6 | 31.9 | 46.7 | 802.5 | 955.5 | 902.6 | 677.1 |
| 04/04/01 | 19:44:00 | MP | 7:40 | 5.0 | 0.55 | -0.13 | -0.83 | 0.50 | 0.15 | -0.85 | 66.00 | -4.8 | -1.0 | 3.3 | 95.0 | 41.8 | 61.4 | 66.0 | | | | |
| 04/04/01 | 20:28:00 | cusp | 7:14 | 10.0 | 0.92 | -0.17 | -0.35 | 0.68 | 0.41 | -0.61 | 46.00 | -12.2 | -3.0 | -2.3 | 58.6 | 124.8 | 23.1 | 68.8 | | | | |
| 26/02/01 | 05:31:00 | th | 15:11 | 9.2 | 0.56 | 0.68 | -0.47 | 0.65 | 0.27 | -0.71 | -27.00 | 15.9 | 6.3 | 10.8 | -28.7 | -48.7 | -25.3 | -34.2 | 1246.5 | 1472.5 | 1531.7 | 1354.1 |
| 26/02/01 | 05:41:30 | th | 15:4 | 8.1 | 0.73 | 0.17 | -0.67 | 0.76 | 0.07 | -0.64 | -47.00 | 19.1 | 5.3 | 13.7 | -26.1 | -34.8 | -25.8 | -28.9 | 841.4 | 970.4 | 865.4 | 934.9 |
| 26/02/01 | 05:56:00 | in | 14:54 | 3.5 | 0.24 | 0.45 | -0.86 | -0.37 | 0.60 | -0.71 | 17.00 | -12.1 | -2.8 | 24.8 | 36.7 | 28.5 | 1.0 | 22.1 | 1810.7 | 1669.4 | 1557.3 | 2176.7 |
| 26/02/01 | 06:02:00 | out | 14:54 | 2.5 | 0.36 | -0.59 | 0.73 | 0.11 | -0.35 | 0.93 | 25.00 | 14.4 | -2.0 | -8.6 | 14.4 | 24.4 | 47.2 | 28.7 | 1190.4 | 1312.7 | 1356.6 | 1360.4 |
| 26/02/01 | 06:05:30 | in | 14:48 | 4.3 | 0.18 | -0.85 | 0.49 | -0.06 | -0.94 | 0.35 | -19.00 | -16.3 | -14.3 | 6.2 | -15.6 | -10.6 | -37.2 | -21.1 | 707.7 | 941.1 | 821.9 | 988.9 |
| 26/02/01 | 06:08:00 | out | 14:48 | 4.1 | 0.25 | 0.27 | -0.93 | -0.13 | 0.11 | -0.98 | -21.00 | 15.8 | -6.2 | -13.4 | -28.1 | 3.4 | -1.6 | -8.8 | 1231.1 | 1056.5 | 1043.2 | 1183.4 |
| 02/03/02 | 01:45:00 | th | 14:19 | 6.8 | 0.71 | -0.08 | -0.69 | 0.41 | -0.51 | -0.75 | -15.60 | 2.4 | -2.0 | -2.0 | -8.5 | -19.9 | -30.5 | -19.6 | 667.4 | 1264.5 | 440.0 | 1550.6 |
| 02/03/02 | 02:12:00 | cusp | 14:7 | 4.5 | 0.40 | 0.65 | 0.64 | 0.27 | 0.71 | 0.66 | -20.30 | -2.2 | 1.6 | -2.0 | -23.1 | -12.3 | -29.2 | -21.5 | 248.0 | 240.9 | 262.2 | 323.8 |
| 02/03/02 | 03:30:00 | mp | 12:45 | 9.5 | 0.74 | -0.05 | 0.67 | 0.77 | 0.25 | 0.59 | -57.40 | -2.5 | -2.1 | -1.6 | -33.7 | -36.4 | -39.3 | -36.5 | 462.7 | 448.7 | 416.5 | 409.0 |
| 25/02/02 | 08:19:00 | th | 14:18 | 2.0 | 0.18 | -0.31 | 0.93 | 0.06 | -0.41 | 0.91 | -24.00 | -3.8 | -2.2 | -1.5 | -24.9 | -23.5 | -26.5 | -25.0 | 774.5 | 730.9 | 803.6 | 784.4 |
| 25/02/02 | 08:49:00 | th | 14:10 | 2.0 | 0.66 | -0.62 | 0.43 | 0.61 | -0.57 | 0.55 | -24.00 | -3.3 | -3.7 | -2.7 | -21.0 | -24.4 | -26.4 | -24.0 | 365.5 | 372.8 | 366.3 | 396.8 |

MVA boundary normals, averaged over spacecraft, the timing normals and corresponding (constant) speed along the normal, the inter-spacecraft differences in the crossing times for three independent spacecraft pairs, the corresponding speed of the boundary between each spacecraft pair and the mean value of these speeds, and finally the estimated boundary thickness at each spacecraft (calculated from traversal times through the current layer and the relative speed at each spacecraft in turn). Velocity information is defined so as to refer to motion of the boundary along the boundary normal quoted, so that positive motion usually corresponds to outwards motion. The observed variation in speed between each pair of spacecraft suggests the sense of any acceleration, although that may be inaccurate, as discussed below. Although the cusp structure is often complex, however, the selected crossings discussed do give reasonably consistent results. Usually, problems only arise when the normal analysis is somewhat unstable, resulting in poor determination of the velocity profile, and we note these cases.

Although the implied, overall cusp geometry corresponds to large differences in the orientations of the different boundaries, together with implied curvature on the scale of the whole region, we believe that this does not overly affect the assumption that each boundary is locally planar on the scale of the Cluster array. Deviations in the "timing" normals, with respect to the mean DA boundary normals, are predominantly related to the effect of acceleration, which is significant for some crossings. This latter point is reinforced by the results for the boundary thickness using the calculated velocity at each spacecraft. We show below that nearly all crossings give a more constant thickness at each spacecraft when this scaling is used (and when stable normals exist). Furthermore, it appears that often the cusp region itself shows no clear curlometer signature at either separation scale, but does show significant current at the high-altitude cusp boundaries.

We start with the southern cusp events, since the first event described in Section 3.1 was introduced only as a template for the others. As described in Section 3.2, for the case of the southern cusp crossings (13 February 2001 and 20 February 2001), the spacecraft appear to enter into the cusp from the magnetosheath. Cusp entry appears to be the result of an expansion of the magnetosphere (outward motion of the magnetopause) in combination with a dawnwards motion of the exterior cusp region. The subsequent exit from the cusp into the magnetosphere appears to be from the rear of the cusp throat into the lobe or the mantle, on the duskside of the cusp region in both cases. Although the outer cusp/magnetosheath interface could be interpreted as the effective magnetopause crossing, the entry into the magnetospheric lobe region crosses a more clearly magnetopause-like boundary in terms of the current layer. In fact the outer boundary appears to be a rotational discontinuity (RD) in both cases. The field fluctuations are Alfvéic, with a highly satisfied Walen relation, whereas the inner boundary is a targential

discontinuity in both cases (see below). The crossing profiles of the spacecraft are most clear on this (inner) boundary.

For the 13 February 2001 event, for example, the DA analysis results in a mean boundary normal, $\mathbf{n} = (0.95, -0.2, -0.15)$, having a direction tilted into $-Y_{GSE}$ and with a small $Z_{GSE}$ component, which is significantly skewed with respect to the nominal magnetopause direction (Sibeck et al. (1991) model) at this location: $\mathbf{n} = (0.75, 0.15, -0.65)$. Although our interpretation is that this represents an outer boundary of the cusp, this result is nevertheless consistent with an entry into an indented region on the magnetopause, and places the spacecraft on the duskward and southern edge of this indentation. The geometry is represented schematically in Figure 17, in the GSM (X,Y) and (X,Z) planes, where the implied boundary normals are drawn in the direction of motion of the boundary (from Table I, see discussion below in Section 5). As the cusp is traversed, the magnetic field tilts duskward and southward in line with an implied cusp topology on the duskside of the throat (southern hemisphere). Moreover, the (variable) dawnward directed magnetosheath field could be responsible for a dawnward motion of the cusp as well as outward motion along the normal.

The results of the DA analysis suggest a strong deceleration of the boundary from an initial outward speed of 70 km/s. The crossing order of the spacecraft, taken from the profiles in the magnetic field components, is not consistent with those taken from the field magnitude (crossing times in Table I are taken from the drop in magnitude on cusp entry), and this prevents an unambiguous interpretation of the crossings. In fact, the velocity profile across the spacecraft array reverses direction at the last crossing (spacecraft 4), indicating that the motion is not a simple acceleration. This may in turn suggest that the cusp reconfigures during the cusp entry. An expansion of the cusp region during the crossing, for example, could confuse the analysis of the crossing motion. It is also consistent with ongoing

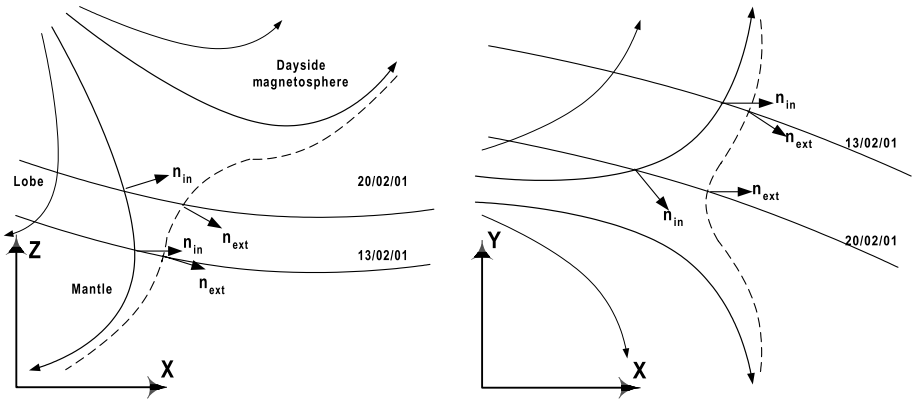


*Figure 17.* Schematic of the cusp crossings: southern geometry.

reconnection (erosion of the magnetospheric field) at the dayside magnetopause result from the southward magnetosheath field. As a result of applying the DA, the thickness of the current sheet can be calculated to be 1500–2000 km. The value is somewhat unstable, however, implying that the velocity change does contain a large error, or perhaps the existence of an extended boundary layer. In support of this interpretation (and as indicated above), the MVA results are suggestive of a RD, although the field component normal to the boundary is small ($<2nT$), and the Walen test across the boundary is satisfied to a high degree (Cargill et al., 2003). Lavraud et al. (2002, 2003) show the character of the outer boundary to be suggestive of a RD, in the case of the event of 4 February 2001, and they discuss the significance of this (see also Onsager et al., 2001, for comparative events).

The exit to the mantle produces a more stable and unambiguous result, giving an inner boundary orientation (consistent with the outermost part of the rear cusp throat) of $\mathbf{n} = (1, 0, 0)$. The motion resulting from the DA produces a smooth velocity profile, which suggests a slowing of the boundary across the spacecraft array from 30–5 km/s. This deceleration can clearly be seen in the crossing profiles near 20:07 UT in the middle panel of Figure 7. The calculated boundary thickness in the Table gives almost constant values and is estimated as 800–900 km (but note that this represents only the current layer). The nature of the boundary (obtained from MVA) is consistent with a simple, tangential discontinuity (TD), and comparison with the ion data shows a poorly satisfied Walen relation (analysis not shown).

For the second event, on 20 February 2001, the analysis is superficially similar, although in this case only the final exit from the cusp into the magnetospheric mantle gives stable velocity results. The two cusp entries give $\mathbf{n} = (0.9, 0, -0.4)$ and $(1, 0, 0.2)$ so that, again, these normals are significantly skewed from the model magnetopause normal. In the case of any indentation on the magnetopause (at the cusp/magnetosheath boundary), these normals would imply that the two crossings are central in $Y_{GSM}$, but to the southern edge, with the second entry being further South than the first. This is shown schematically by the implied trajectory in Figure 17. For both of these crossings, however, the crossing order of the spacecraft at the cusp/magnetosheath interface is not consistent with outward motion of the boundary. The analysis produces unstable results, but implies an inward motion. The current sheet thickness is therefore not computed in this case and is not quoted in the Table. Because it is clear that the spacecraft must traverse the cusp in order eventually to exit into the lobe region of the magnetosphere, it is probable that this boundary is a complex structure, perhaps non-stationary and evolving, so that the DA results are confused. It is certainly true that the boundary normal analysis is not very stable for this crossing. Another possibility is that the spacecraft enter the cusp region via a grazing cut through dayside field lines (or entry layer) initially on the dusk-side of the cusp,

resulting from combined North/South and dawn-dusk motion of the whole region.

This interpretation could be related to the fact that the magnetosheath field rotates from South to North, from 23:16 to 23:19 UT. This is followed by a further, sharper, field rotation from the prevailing dawnward magnetosheath field to a duskward orientation, at 23:19 UT. This later rotation possibly represents an initial (partial or grazing) magnetopause crossing and has the correct spacecraft ordering for a simple initial expansion of the magnetopause. This would take the spacecraft into the edge of the external cusp before subsequent motion within this region takes the spacecraft back through the external interface (for example, an initial dawnward and southward deviation in the trajectory shown in Figure 17, followed by a return motion). The subsequent field rotations (as opposed to the change in field magnitude) themselves are indications that the boundary in this case is rather complex and dynamic, perhaps controlled by rapid changes in the magnetosheath field orientation which continue during the crossings. A similar scenario could be envisaged for the second cusp/magnetosheath interface.

On exit, the cusp/mantle crossing is again clear and stable, and results in a boundary $\mathbf{n} = (0.8, -0.4, 0.5)$. This suggests a similar exit to that of the other event, but perhaps deeper into the cusp throat, which would correspond to the $+Z$ direction of the normal. This orientation is also consistent with an exit into the duskside mantle and lobe, and a dawnward motion of the cusp, as would be implied by the strong $B_Y$ magnetosheath component. The duskward pointing lobe field is consistent with this interpretation. The current sheet thickness is 700–900 km for this inner boundary. Before this exit from the cusp each spacecraft often shows different field orientations, implying a very turbulent region and, perhaps, that the spacecraft remain within the outer cusp/magnetosheath interface; this would also be consistent with the double entry observed and the proposed grazing incidence.

The third southern cusp event gave a much more directly observable ordering to the spacecraft crossings implying a simple outward motion of the magnetopause. For example, the magnetic field trace for spacecraft 1 always leads the entry and exit through the cusp region (see Figure 9). The stability in the DA results shown in Table I confirms this and gives $\mathbf{n} = (0.55, -0.15, -0.8)$ on cusp entry, which is close to the model magnetopause orientation, and $\mathbf{n} = (0.9, -0.15, -0.35)$ on exit into the mantle. The traversal could have occurred near the centre of the exterior cusp region, but the inner normal (with a $-Z_{GSM}$ component) suggests an entry on the southern edge of the cusp region. Thus, this event, at least, which appears to correspond to the northward magnetosheath conditions, provides a counter example to the appearance of an indented exterior cusp/magnetosheath interface. No evidence for an outer indented region was observed during the 4 February 2001 event either (Lavraud et al., 2003), which also occurred under northward

magnetosheath (and northward IMF) conditions. It is clear from this crossing that, although the field topology inside the cusp region is complex, the boundary crossings are nevertheless simple in the absence of a dawn/dusk directed magnetic stress transmitted from the magnetosheath. We do not include a full analysis here for this event, but comment that the magnetic profiles provide smooth transitions across each boundary, giving stable velocity and thickness estimates.

The curlometer calculation (top panel) for 13 February 2001 is shown in Figure 18 (the calculation for 20 February 2001 does not give a clear current signature, and so it is not shown). The bottom panel of Figure 18 (see also Cargill et al. (2003)) shows the ion density, ion temperature and the ion velocity for spacecraft 1 and 3. The $V_Y$ component of the flow shows a large deflection through (just after) the cusp entry, but not at the cusp exit (inner boundary). For the three times, where significant current bursts are seen, vertical dashed lines are drawn in the upper panel of Figure 18. The last refers to a transient, convecting structure at 20:12 UT, discussed by Cargill et al. (2003). The first two correspond to the cusp entry and exit, respectively. The curlometer suggests that there is a significant current layer in both cusp boundaries, exterior and interior. These currents are all directed in the same sense, dawnward and northward, and have a magnitude of 50–80 n $\mathrm{Am}^{-2}$. It turns out that the magnetic stress $J \times B$ lies predominantly along the dawn direction on cusp entry, and this is the sense of the ion flow deflection seen just after this time (bottom panel of Figure 18). This stress is, however, much less for the exit at 20:07 UT, since the magnetic field direction is then tilted into dusk, so that no strong flow deflection is seen at this interface.

The fact that the current estimates can plausibly explain the observed ion jets at these boundaries gives some confidence that the calculation is justified in this region. It would seem that a reconnection geometry, in which the magnetosheath field has a major Y component, is consistent with such plasma jets. It is also apparent that the main ion flow burst occurs at the outer boundary (on entry into the cusp), so that significant stress is transferred here (Cargill et al., 2003). It is an open question as to the nature of each boundary and particularly whether it is more correct to refer to the cusp/magnetosheath interface, or the cusp/mantle boundary, as the magnetopause transition. (This question has also been addressed, at least in part, by Vasyliunas (1995), Russell (2000) and Onsager et al. (2001)). The question is, however, related to the definition of the outer region of the cusp as an "exterior" cusp, and the issue is discussed at more length in Lavraud et al. (2003). It appears that the nature of the outer boundary is affected by the direction of the local magnetosheath field at least; Lavraud et al. (2003) discuss the case of northward IMF and magnetosheath field in particular.

We now turn to the northern cusp crossing presented in Section 3.3, occurring on 26 February 2001, which clearly represents a more actively

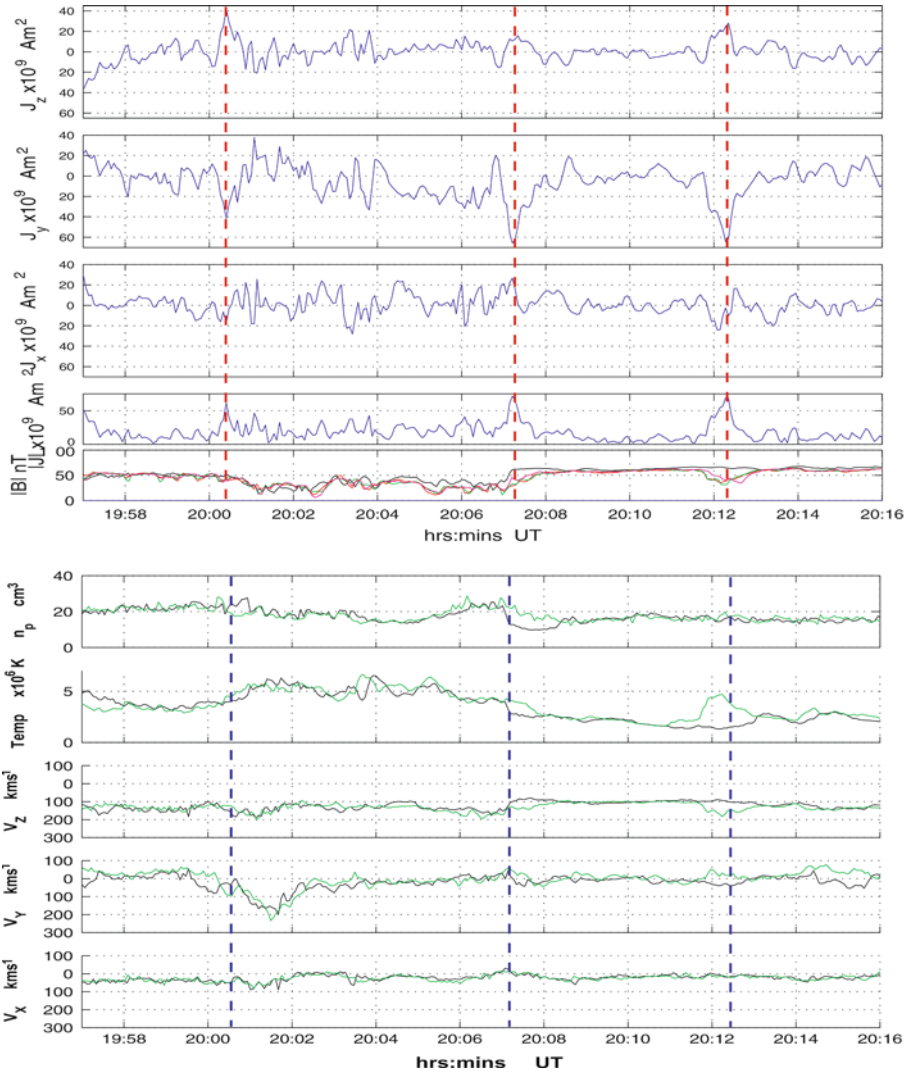


*Figure 18*. The top panel plots the curlometer calculation for 13 February 2001, showing the GSM components of **J** and the field magnitudes. The vertical dashed lines refer to the entry and exit to/from the cusp region and the transient signature at 20:12 UT. The bottom panel shows the ion moments of velocity (in boundary normal coordinates) and density (spacecraft 1 and 3), with the magnetic field from spacecraft 1 for guidance.

dynamic encounter, with several large-scale motions of the cusp. Some of these can be related to changes in IMF orientation, as already discussed in Section 3.3. After the early crossing of the cusp throat (04:08 to 05:12 UT), there appears to be an initial brief exit into the dayside boundary adjacent to the duskside, equatorward edge of the throat (05:12 to 05:21 UT). Both the analysis of the magnetic field data and the timing sequence for the

four-spacecraft electron data shown in Figure 13 give boundary normals which are consistent with the scenario discussed in Section 3.3. For instance, on exit into the dayside region, $\mathbf{n}_{GSM} = (0.6, 0.3, -0.7)$, and on re-entry through the cusp, $\mathbf{n}_{GSM} = (0.75, 0.6, -0.3)$). The second normal, in particular, is consistent with a re-entry from the region duskward and slightly South of the cusp throat (given a funnel-like geometry). The implied motion at the first boundary (i.e. northward or tailward along the normal), from the DA and timing analysis (not shown explicitly here), are also consistent with the sense of an exit into the dayside region, duskward of the cusp throat. At the second boundary (at 05:21 UT), the motion implied by the DA and timing analysis supports the view that the cusp structure reverses to move southward, since it shows a rapidly accelerating motion (equatorward) along the normal and the spacecraft appear to reenter the throat.

Subsequently, during 05:31–05:41 UT, the spacecraft appear to recross the throat, again from the duskside, back into the dayside magnetosphere. The DA results shown in Table I for these two crossings confirm that the cusp boundary moves tailward (negative velocity along the normals, here quoted in GSM components). The computed motion is fairly constant and stable at both crossings. The geometry is depicted in the left panel of Figure 19. The normals listed in Table I give an orientation of $\mathbf{n}_{GSM} = (0.55, 0.7, -0.5)$, at 05:31 UT, and $\mathbf{n}_{GSM} = (0.7, 0.2, -0.7)$, at 05:41 UT. These are suggestive of passage through a funnel boundary in the manner illustrated in the left panel of Figure 19 (discussed further in Section 5). In the Figure, the arrows represent the motion of the boundary at the first ($\mathbf{n}_1$) and second crossing ($\mathbf{n}_2$), and the cusp funnel is represented by an oval cut at the assumed height of the Cluster orbits. The field orientation shown in the lower panel in Figure 12 remains fairly well aligned to the implied axis of this funnel, except for some brief excursions on spacecraft 4.

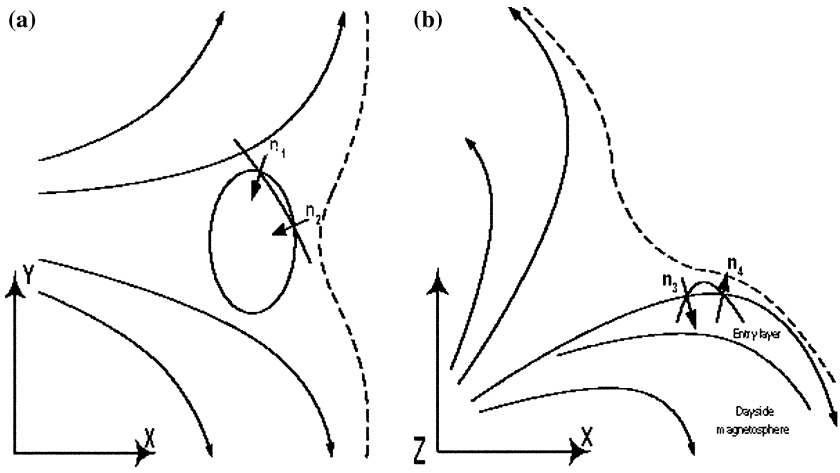


*Figure 19.* Schematic of the cusp crossings: northern geometry.

The DA analysis also suggests that the funnel boundary is slightly thinner on the equatorward edge, and is 1000 km overall.

A second entry, between 05:56 and 06:02 UT, represents a reversal in and out of what could possibly be the exterior cusp region (at least sampling at higher altitudes than the throat crossings). The spacecraft are again originally equatorward and on the duskside of the cusp. A crossing at higher altitude is also suggested by the larger $Z_{GSM}$ component of the normal at 05:56 UT (entry into the cusp), $\mathbf{n}_{GSM} = (0.25, 0.45, -0.85)$. At 06:02 UT, the tilt of the normal, $\mathbf{n}_{GSM} = (-0.35, 0.6, -0.7)$, appears to correspond to the extreme edge of the cusp (and corresponds in orientation to an indented magnetopause). These crossings (labelled $\mathbf{n}_3$, $\mathbf{n}_4$) are schematically represented in the right panel of Figure 19 (but note that the spacecraft appear to lie on the duskside of the cusp to be consistent with the substantial $Y_{GSM}$ component of the normals in each case). Again, on Figure 19, the arrows on the boundary normals are drawn in the implied direction of motion of the boundary. It is noteworthy that the magnetic field orientation inside the cusp is now twisted from the well-ordered, throat-aligned configuration seen during the earlier passage through the cusp (see the magnetic field angles in the lower panel of Figure 12). This twist in the field into $B_Y$ positive is suggestive of a duskward motion of the cusp, taking the spacecraft across the cusp cross-section and then back to the duskside on exit, when the motion reverses. The motion resulting from the DA analysis confirms this view with a clearly slowing velocity profile along the normal on cusp entry (duskward motion), and a slowing velocity along the normal, dawnwards, on cusp exit. The velocity profile on cusp exit at 06:02 UT gives a particular well scaled estimate for the boundary thickness of 1300 km. The cusp entry gives a slightly higher thickness of 1700 km, but is more unstable.

At 06:05 and 06:08 UT a second excursion from the magnetosphere occurs in a similar manner to those at 05:56 and 06:02 UT, but perhaps now directly into the magnetosheath. Again the velocity clearly reverses from dusk-ward to dawn-ward motion, although the acceleration is not so stable (see Table I). The differing normal directions from entry to exit imply that there is also a degree of cusp expansion during the two crossings. The boundary thickness appears to remain between 800 and 1100 km. The magnetic field again twists in orientation confirming the dawn/dusk motion of the cusp across the spacecraft. We note at this point that the plasma signatures for this last pair of crossings are only marginally different from the signatures in the adjacent magnetosheath, after 06:10 UT. We suppose that this implies that the region sampled is at least a modified magnetosheath plasma distribution, or else simply an indented region on the magnetopause. The outer cusp/magnetosheath interface, seen during the southern cusp encounters discussed above, appears not to be sampled in this event, since the final magnetopause exit appears to be through the dayside magnetopause.

It is apparent that this traversal through the high altitude cusp suggests that a funnel-like geometry is the most appropriate description for the cusp throat, as inferred by the discussion above for the earlier crossings. Moreover, the regions surrounding the cusp (boundary of the dayside magnetosphere, or extension of the entry layer, on the equatorward side and lobe or mantle region on the tailward side) appear to be well recognisable. These lend further credence to the view given for the spacecraft locations and motion through the cusp itself.

We now turn to the magnetic currents observed during this event. Figure 20 shows the curlometer calculation for the interval 05:00–06:20 UT (top panel), together with the ion moments from spacecraft 1 and 3 from the CIS instrument for the corresponding interval. In the figure, the vertical dashed lines refer to each of the boundaries discussed above, drawn in this case on the ion data plot. There are bursts of ion flow just outside the funnel boundaries at 05:31 and 05:41 UT, and the ion density is clearly enhanced inside the funnel. The main current signature, however, lies inside the funnel and appears to be, to a large degree, field aligned. Therefore it does not provide a significant $J \times B$ force. At the next (exterior) cusp boundaries there is a large current signature where the field twists in the centre of the cusp region. Figure 21 shows the balance between the ion and magnetic pressures for the set of crossings discussed here. It is quite apparent that the magnetic and plasma pressures anti-correlate rather well through the whole interval shown. Their fluctuations are precisely in anti-phase within the cusp regions. A possible explanation for this is that the cusp boundary is a standing slow mode shock, producing an anti-correlation between the plasma density and the magnetic field intensity. More generally, however, the overall pressure balance suggests that the crossings result predominantly from simple dynamic motions, rather than from a more complex evolution of reconfigurations in the cusp region. This view is consistent with the stable results found for this event and shown in Table I. We find here that the ion pressure scales in proportion to the magnetic pressure better than the density does.

For comparison with the results discussed above, we now turn to the two events at small spacecraft separation scales, introduced in Section 3.4, which have been analysed with both the DA and curlometer. Sharp boundaries exist through the central interval 01:00–02:20 UT, as seen in the left panel of Figure 16, for 2 March 2002. The results from two of these are quoted in Table I, along with the magnetopause exit at 03:30 UT. The first crossing, labelled "throat" crossing, is interpreted as the second clear entry into the dayside boundary region (as discussed in Section 3) from the cusp throat. The boundary normal is found to be $\mathbf{n}_{GSM} = (0.7, -0.1, -0.7)$, which is consistent for the implied central location at the equatorward edge of the cusp, given a funnel-like geometry. The timing normal deviates significantly from this boundary orientation and we believe that it is unreliable in this case. The

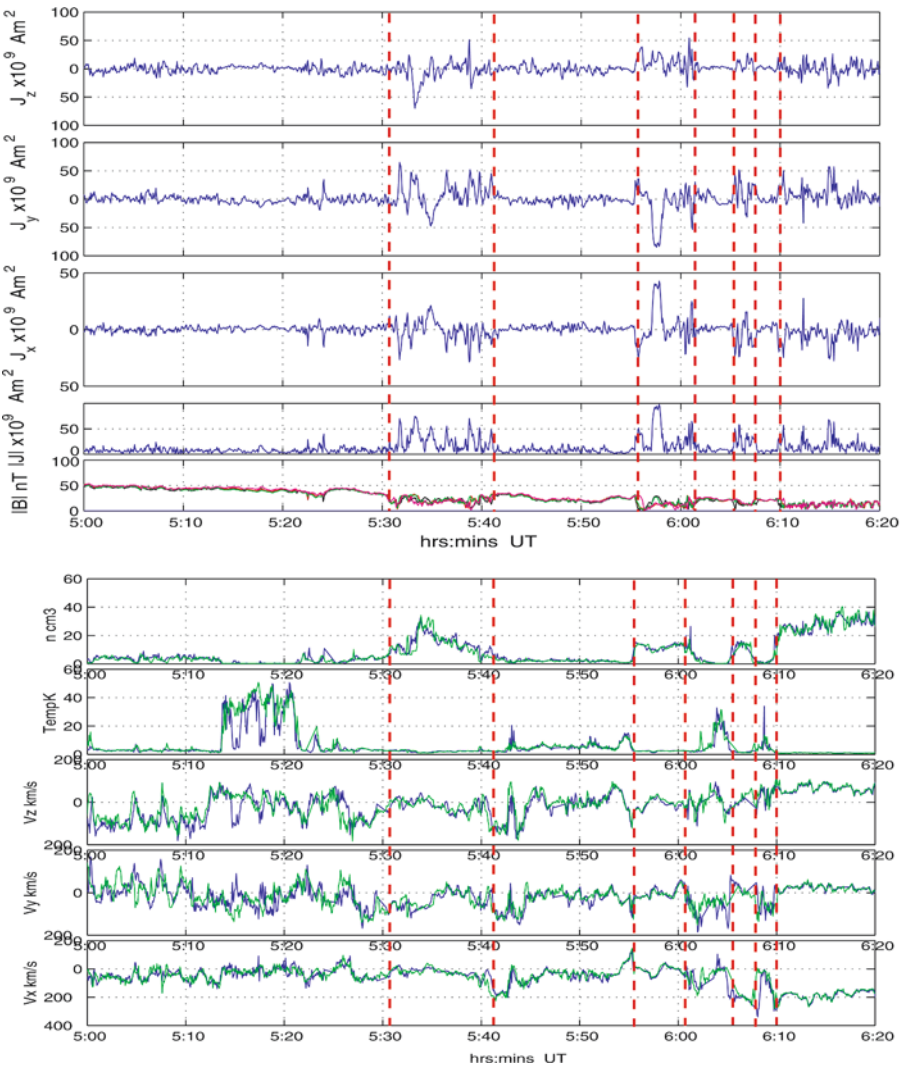


*Figure 20*. The top panel plots the curlometer calculation for 26 February 2001 observations, showing the GSM components of **J** and the field magnitudes. The vertical dashed lines refer to the entry to and exit from the cusp region as discussed in the text. The bottom panel shows the corresponding ion moments of velocity temperature and density (spacecraft 1 and 3) for the same interval.

analysis confirms the possible northward motion (with respect to the normal), or narrowing, of the cusp throat at this time taking the spacecraft into the dayside boundary region, and is consistent with the northward turning of the IMF seen at ACE. The second crossing gives $\mathbf{n}_{GSM} = (0.4, 0.65, 0.65)$ and is labelled ''cusp'' since it appears to be consistent with a crossing into the (indented) exterior cusp region from the dayside magnetosphere. The tilt in

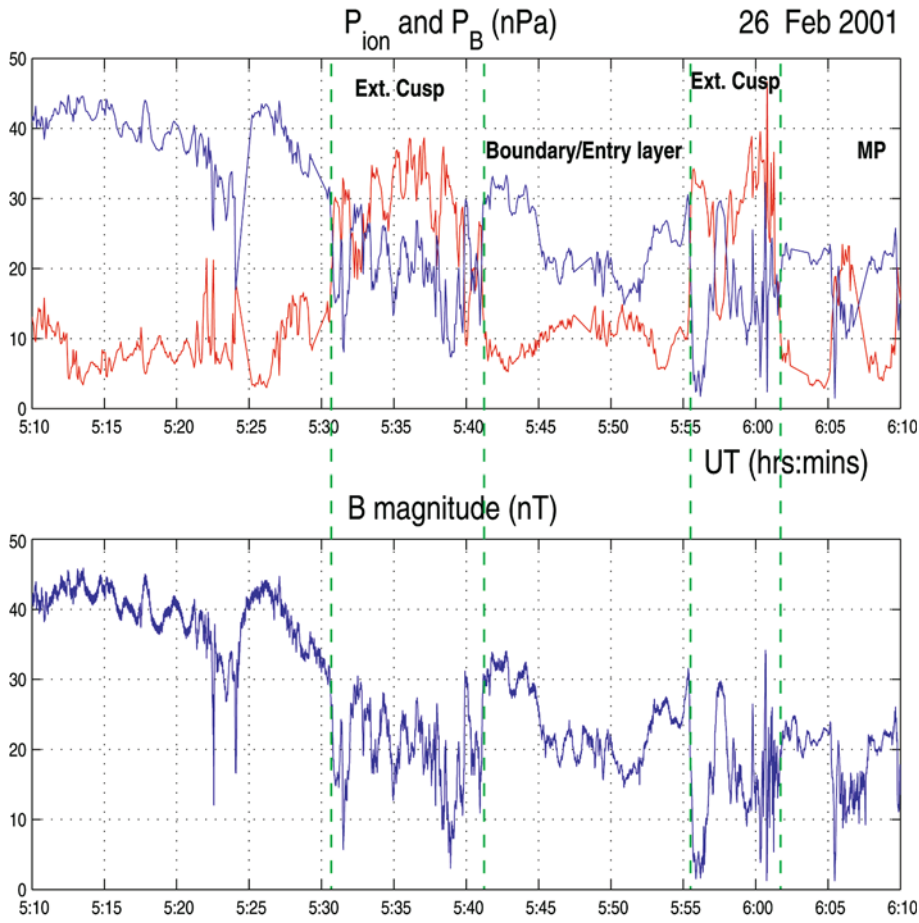


*Figure 21.* Comparison of ion (red) and magnetic (black) pressures showing the anti-correlation in the exterior and high-latitude cusp regions. The field magnitude is drawn for guidance in the bottom plot.

$Y_{GSM}$ together with a turning into positive $B_Y$ supports a location on the dawnside of the cusp. The velocity along this normal confirms a southward motion or widening of the cusp region (perhaps associated with erosion of the magnetopause), corresponding to a brief period of the IMF-$B_Z$ returning to zero before turning northward again at 02:20 UT (when the spacecraft move back into the dayside magnetosphere).

It is worth remembering here that the quoted normals represent the mean boundary normal for the four spacecraft, and the analysis presented here is performed for boundaries for which it can be demonstrated that the individual spacecraft crossings show co-linear normals within MVA statistical accuracy. For the larger spacecraft separations, it is the case that most crossings show planar boundaries in this sense, where the results are stable.

At these smaller scales the individual normals show no more significant alignment within the statistical deviations, thus providing indirect support that the implication of planar geometry at the larger separations is correct. Moreover, at these small separations we expect that the effect of any acceleration is very small over the spacecraft array, so that the velocity ought to remain almost constant except for an unusually large acceleration. For the second of these crossings, an approximately constant velocity is indeed found with the velocity profile showing only an apparent small reduction of velocity. The timing analysis and the DA give similar normals in this case. These normals have an orientation which implies that the spacecraft are sampling very near the exterior region or in the indentation region of the exterior cusp or magnetopause. The velocity profile for the first crossing appears to indicate a stronger change in velocity across the array. In this case, however, the normal is somewhat unstable implying that part of this acceleration is not real. The smaller separations, therefore, can emphasise the effect of unstable results when the velocity profiles are inconsistent. This also reinforces the result that the DA analysis is usually self-checking in the sense that inconsistencies are easily revealed.

This last point is reinforced by the fact that the analysis of the first crossing (01:45 UT) gives an unstable value for the boundary thickness (interpreted as being due to the false velocity change over the array). Thus, the implied acceleration would also have been questionable in the light of the variation obtained for the thickness. The second crossing gives a much more consistent value of thickness at each spacecraft, however, again justifying the interpretation given above. Nevertheless, it is apparent that both crossings result in reasonable estimates for the boundary thickness across the throat of between 1000 and 300 km. The final magnetopause exit (at 03:30 UT) is also quoted here for completeness and shows a stable boundary normal having the nominal magnetopause orientation. A very smooth, and small, velocity change through the array is found which gives a remarkably constant estimate for the magnetopause boundary layer of 450 km. Both the DA and timing normals agree very well in this case also.

There are two clear throat crossings at 08:19 and 08:49 UT on 25 February 2002, where both are apparent as deviations from the model field in the right panel in Figure 16. Both are reentries into the high-altitude throat during southward motion of the cusp, with a recovery in between these times when the cusp motion reverses. The difference from the 2 March 2002 traversal, however, is that the spacecraft appear never to pass deeply into the dayside region. This interpretation is confirmed by the DA analysis shown in Table I. This gives a boundary orientation of $\mathbf{n}_{GSM} = (0.2, -0.3, 0.9)$ for the first crossing and $\mathbf{n}_{GSM} = (0.7, -0.6, 0.4)$ for the second, implying that the spacecraft exit into the exterior cusp region or within the indentation region. For both crossings the velocity confirms a southward motion. The tilt of the

normals into $-Y_{GSM}$ suggest an exit on the dusk-side of the cusp, which is expected from the negative $B_Y$ component of the magnetospheric field through the traversal. Both of these excursions into the cusp throat coincide with southward turnings of the lagged ACE-IMF, and so could result from erosion of the equator-ward cusp boundary. The velocity profiles for these two throat crossings are particularly smooth and constant, and agree well with the result of the timing estimates. They produce estimates of boundary thickness of 750 and 400 km, respectively.

## 5. Conclusions

The geometry of the high-latitude cusp has been discussed since the early missions referred to in the Introduction. The concept of an exterior cusp region, for example, was introduced following analysis of data from the HEOS missions (Haerendel et al., 1978; Vasyliunas et al., 1979). Furthermore, the possibility of an associated cusp indentation on the magnetopause has been discussed recently in terms of Hawkeye (Zhou and Russell, 1997; Eastman et al., 2000) and HEOS-2 (Dunlop et al., 2000) data, although the detail of the enclosed region was unresolved. The existence of separate cusp interfaces has been unconfirmed until now and the extent of any region exterior to the magnetopause, and its connection to the deeper cusp funnel, is therefore not well understood. To explore the geometry, dynamical properties and connectivity of these regions, this paper has reviewed a number of North and South cusp passes, made by the Cluster array of spacecraft at a range of spatial separation scales. For the first time use is made of four spacecraft co-ordinated measurements to identify key properties of the regions covered by the spacecraft orbits.

For the northern cusps, for example, the four-spacecraft pass consecutively through the northern lobe and cusp throat at mid- to high-altitudes. The spacecraft then either sample the exterior cusp region near the magnetopause or the dayside boundary region adjacent to the central cusp region (dayside entry layer), depending upon conditions. On the southern, inbound leg the sequence is reversed. This multi-spacecraft coverage has allowed spatial and temporal features to be distinguished and, in particular, has identified macroscopic properties of the boundary layers – the orientation, motion and thickness. The feasibility of particular multi-spacecraft techniques has been demonstrated and, in some cases, the associated current layers have been quantified. Typical magnetic and plasma characteristics of each region traversed have also been discussed. These are sensitive to external conditions in the magnetosheath and upstream solar wind, and give some context for the boundary crossings identified. In all cases studied here the overall magnetic topology observed gives a consistent picture as to location

relative to the cusp and surrounding regions, in agreement with that inferred from the motional analysis and boundary orientations.

It is apparent that the discontinuity analysis (DA) gives plausible results for the passage through the cusp. These results (those for the southern cusps of 13 and 20 February, in particular) support an interpretation in which there often is an outer, indented (with respect to the nominal magnetopause), magnetosheath/cusp interface. For other events (as for 4 April 2001, and the event discussed by Lavraud et al. (2003)), indentation of the outer interface does not appear to be present, or else these events correspond to central exits through the exterior cusp/magnetosheath interface. Within this boundary (Earthward side) a region exists, which may be loosely termed the exterior cusp in the sense that inner boundaries exist. These define the interface between the cusp and the magnetospheric lobe or mantle region, on the tailward side, and between the cusp and the dayside boundary region, on the equatorward side. Within the exterior cusp the field magnitude is usually depressed; the vector field contains enhanced fluctuations and often shows a complex (twisted) structure on spatial scales smaller than the spacecraft separation scales. The nature of the region appears to be most sensitive to external conditions in the magnetosheath and upstream solar wind. It is highly dynamic so that both North/South and dawn/dusk bulk motions of the region are observed. Although the inner boundary crossing into the lobe region gave clear, stable results, the crossing of the magnetosheath interface was less clear, reflecting an evolving structure. In fact, not all crossings were stable and there were some problems associated with the spacecraft ordering in the case of the 20 February event, in particular.

Lavraud et al. (2003) confirm the existence of an inner and outer boundary containing an "exterior" cusp region. In one of the events studied there (4 February 2001), particularly stable, northward IMF and magnetosheath conditions resulted in a stagnant (omni-directional plasma flows), extremely low field region. The boundary analysis for the event (Lavraud et al., 2002) gave a similar geometry to that shown in Figure 17, but for the northern context and with no implied indentation as mentioned above. The spacecraft passed out into the magnetosheath in a manner depicted by the spacecraft track for the 20 February 2001 event. The outer boundary, in the case for 4 February 2001, showed a much better ordered exit, following the expected spacecraft sequence for the spatial configuration. In addition, a brief North/South motion of the cusp took the spacecraft across the inner cusp/dayside boundary. It also seemed the spacecraft travelled from further down the cusp throat, so that the magnetic field and plasma signatures changed only slowly into the characteristics of the low field stagnant exterior cusp region.

This interpretation that the field depressed high-latitude region is the exterior cusp raises the issue of whether the outer or inner boundaries represent the

extension of the magnetopause. It is certainly true that the outer boundary shows stress-induced deflections of the magnetosheath plasma, but the boundary does not always have properties which can simply be interpreted in terms of a RD (Lavraud et al., 2003). The inner boundary, on the other hand, also shows magnetopause-like properties in that there is always a clear magnetic transition representing a current sheet form. The nature of this inner boundary, however, depends on location up the cusp throat, and is not magnetically well defined deeper into mid-altitudes because of the relative diamagnetic effect.

In a sense, the combined four-spacecraft boundary analysis is primarily a geometrical interpretation. Figure 17 summarises this geometry for the southern cusp crossings and Figure 19 summarises the geometry for the northern crossings. The first case depicts the exterior cusp traversals, where the exit is from the cusp region into the magnetosheath. The second case depicts a cut through the throat at lower altitudes (top panel) as occurred during the northern crossing introduced in Section 3.3, 26 February 2001. That event therefore added to the geometrical view, by the additional passage through the cusp throat (suggesting a funnel-like geometry). The nature of the boundary crossings through this funnel depends critically on how deeply in the throat the spacecraft pass through. As the cusp funnel is crossed deeper into the magnetosphere (at lower altitude), for example, the decrease in the ration of plasma pressure to magnetic pressure results in the magnetic boundaries being less well defined and therefore harder to analyse. The mid- to high-altitude cusp throat usually contains enhanced ULF activity but the degree to which the magnetic field magnitude is also depressed depends on altitude. Nevertheless, the plasma signatures do show well-defined boundaries and the throat normally appears to have a well-defined extent, even at mid-altitudes. The external region, sampled later in the pass shows a particularly distinct character in line with the overall geometry defined. Furthermore, there is a strong anti-correlation in magnetic and ion pressures.

The event of 26 February 2001 shows particularly dynamic conditions, which induce multiple boundary crossings, often demonstrably as a result of changing IMF orientation. There are some problems of interpretation, however, regarding the cusp response to the IMF and solar wind conditions and in the detail of the plasma distribution, and this will be the subject of further work. Some of the changes in IMF orientation are well correlated to cusp response, but not all. It was suggested there that certain temporal effects are required in order to resolve these problems, or else a dramatic distortion of the funnel geometry. Alternatively, a more detailed calculation of convection lag is needed in view of the nearly radial IMF orientation. However, some of the boundary crossings show complex plasma distributions and confuse the global (geometric) view of the dynamic response. The short period between 05:21 and 05:25 UT is a notable example of a com-

plicated cusp re-configuration, where the interpretation of global motions from the local cluster sampling of the boundaries is somewhat confused. We have included here only those boundary crossings which give reasonably stable and clear results.

There appears to be direct control of both the cusp position and its extent by the IMF, however, both in the dawn/dusk and North/South directions. The magnetic field geometry is sometimes complex, but often the current layer has a well defined thickness ranging from a few hundred (for the inner cusp boundaries) to 1000 km. The motion of the inner cusp boundaries can occur at speeds up to 60 km/s, but typically 10–20 km/s. These speeds could represent either global motion of the cusp or expansion/narrowing of the region. The events taken from the 2002 data set primarily provide a check on the interpretation of the results from the four-spacecraft techniques, rather than new physical insight. These events provide further evidence, however, that changes in the IMF induce motions of the cusp.

## Acknowledgement

This work has been carried out with the support of PPARC.

## References

Balogh, A., Carr, C. M., Acuña, M. H., Dunlop, M. W., Beek, T. J., Brown, P., Fornacon, K.-H., Georgescu, E., Glassmeier, K.-H., Harris, J., Musmann, G., Oddy, T., and Schwingenschuh, K.: 2001, 'The Cluster Magnetic Field Investigation: Overview of in-flight Performance and Initial Results', *Ann. Geophys.* **19**, 1207–1217.

Cargill, P. J., Dunlop, M. W., Balogh, A., and the FGM Team: 2001, 'First Cluster Results of the Magnetic Field Structure of the Medium and High-altitude Cusps', *Ann. Geophys.* **19**, 1533–1543.

Cargill, P. J., Dunlop, M. W., Lavraud, B., Elphic, R.C., Holland, D. L., Nykyri, K., Balogh, A., Danouras, I., and Réme, H.: 2003, 'CLUSTER Encounters with the High Altitude Cusp: Boundary Structure and Magnetic Field Depletions', submitted to *Ann. Geophys.*

Dubinin, E., Skalsky, A., Song, P., Savin, S., Kozyra, J., Moore, T. E., Russell, C. T., Chandler, M. O., Fedorov, A., Avanov, L., Sauvaud, J.-A., and Friedel, R. H. W.: 2002, 'Polar Interball Co-ordinated Observations of Plasma and Magnetic Field Characteristics in the Regions of the Northern and Southern Distant Cusps', *J. Geophys. Res.* **107** (A5), Art. No. 1053.

Dunlop, M. W., Southwood, D. J., and Balogh, A.: 1993, 'The Cluster Configuration and the Directional Dependence of Coherence Lengths in the Magnetosheath', in *Proceedings of Spatio-Temporal Analysis for Resolving Plasma Turbulence (START)*, Aussois, France, ESA WPP-47, pp. 295–299.

Dunlop, M. W., and Balogh, A.: 1993, 'On the Analysis and Interpretation of Four Spacecraft Magnetic Field Measurements in Terms of Small Scale Plasma Processes', in *Spatio-temporal Analysis for Resolving Plasma Turbulence (START)* ESA WPP-047, pp. 223–231.

Dunlop, M. W., Woodward, T. I., Southwood, D. J., Glassmeier, K.-H., and Elphic, R. C.: 1997, 'Merging 4 Spacecraft Data: Concepts Used for Analysing Discontinuities', *Adv. Space Res.* **20**, 1101–1106.

Dunlop, M. W., and Woodward, T. I.: 1998, 'Discontinuity Analysis: Orientation and Motion', *ISSI Scientific Report SR-001*, Kluwer Academic Publishers, pp. 271–305.

Dunlop, M. W., and Woodward, T. I.: 1999, 'Analysis of Thick, Non-planar Boundaries Using the Discontinuity Analyser', *Ann Geophys.* **17**, 984–995.

Dunlop, M. W., Cargill, P., Stubbs, T., and Woolliams, P.: 2000, 'The High Altitude Cusps: HEOS-2', *J. Geophys. Res.* **105**, 27509–27517.

Dunlop, M. W., Balogh, A., and Glassmeier, K.-H.: 2002a, 'Four-Point Cluster Application Of Magnetic Field Analysis Tools: The Discontinuity Analyser', in press, *J. Geophys. Res.* **107**(A11), Art. No. 1385.

Dunlop, M. W., Balogh, A., Glassmeier, K.-H., and Robert, P.: 2002b, 'Four-Point Cluster Application of Magnetic Field Analysis Tools: The Curlometer', in press, *J. Geophys. Res.* **107**(A11), Art. No. 1384.

Eastman, T. E., Boardsen, S. A., Chen, S-H., and Fung, S. F.: 2000, 'Configuration of High-latitude and High-altitude Boundary Layers', *J. Geophys. Res.* **105**, 23193–23238.

Farrell, W. M., and Allen, J. A.Van: 1990, 'Observations of the Earth's Polar Cleft at Large Radial Distances with the Hawkeye 1 Satellite', *J. Geophys. Res.* **95**, 20945–20958.

Fedorov, A., Dubinin, E., Song, P., Budnick, E., Larson, P., and Sauvaud, J.-A.: 2000, 'Characteristics of the Exterior Cusp for Steady Southward Interplanetary Magnetic Field: Interball Observations', *J. Geophys. Res.* **105**, 15945–15957.

Frank, L. A.: 1971, 'Plasma in the Earth's Polar Magnetosphere', *J. Geophys. Res.* **76**, 5202–5219.

Fritz, T. A., Chen, J., and Siscoe, G. L.: 2003, 'Energetic Ions, Large Diamagnetic Cavities, and Chapman-Ferraro Cusp', *J. Geophys. Res.* **108**, (A1): Art. No. 1028.

Grande, M., Fennell, J., Livi, S., Kellett, B., Perry, C. H., Anderson, P., Roeder, J., Spence, H., Fritz, T., and Wilken, B.: 1997, 'First Polar and 1995–034 Observations of the Mid-altitude Cusp During a Persistent Northward IMF Condition', *Geophys. Res. Lett.* **24**, 1475–1478.

Haerendel, G., Paschmann, G., Sckopke, N., and Rosenbauer, H.: 1978, 'The Frontside Boundary Layer of the Magnetosphere and the Problem of Reconnection', *J. Geophys. Res.* **83**, 3195–3216.

Johnstone, A. D., Alsop, C., Burge, S., Carter, P. J., Coates, A. J., Coker, A. J., Fazakerley, A. N., Grande, M., Gowen, R. A., Gurgiolo, C., Hancock, B. K., Narheim, B., Preece, A., Sheather, P. H., Winningham, J. D., and Woodliffe, R. D.: 1997, 'Peace: A Plasma Electron and Current Experiment', *Space Sci. Rev.* **79**, 351–398.

Kessel, R. L., Chen, S.-H., Green, J. L., Fung, S. F., Boardsen, S. A., Tan, L. C., Eastman, T. E., Craven, J. D., and Frank, L. A.: 1996, 'Evidence of High-latitude Reconnection during Northward IMF: Hawkeye Observations', *Geophys. Res. Lett.* **23**, 583–586.

Lavraud, B., Dunlop, M. W., Phan, T. D., Reme, H., Bosqued, J. M., Dandouras, I., Sauvaud, J. A., Lundin, R., Taylor, M. G. G. T., Cargill, P. J., Mazelle, C., Escoubet, C. P., Carlson, C. W., McFadden, J. P., Parks, G. K., Moebius, E., Kistler, L. M., Bavassano-Cattaneo, M. B., Korth, A., Klecker, B., and Balogh, A.: 2002, 'Cluster Observations of the Exterior Cusp and its Surrounding Boundaries under Northward IMF', *Geophys. Res. Lett.* **29**(20), 56–63.

Lavraud, B., Réme, H., Dunlop, M. W., Bosqued, J.-M., Dandouras, I., Sauvaud, J.-A., Keiling, A., Phan, T. D., Lundin, R., Cargill, P., Escoubet, C. P., Carlson, C. W.,

McFadden, J. P., Parks, G. K., Moebius, E., Kistler, L., Amata, E., Bavassano-Cattaneo, M.-B., Korth, A., Klecker, B., and Balogh, A.: 2003, 'Cluster Observes the High Altitude/Exterior Cusp Regions'. This issue.

Lepping, R. P., Acuna, M., Burlaga, L., Farrell, W., Slavin, J., Schatten, K., Mariani, F., Ness, N., Newbauer, F., Whang, Y. C., Byrnes, J., Kennon, R., Panetta, P., Scheifele, J., and Worleyet, E.: 1995, 'The WIND Magnetic Field Investigation', *Space Sci. Revs.* **71**, 207–229.

Lundin, R., Sauvaud, J.-A., Réme, H., Balogh, A., Dandouras, I., Bosqued, J. M., Carlson, C., Parks, G. K., Moebius, E., Kistler, L. M., Klecker, B., Amata, E., Formisano, V., Dunlop, M. W., Eliasson, L., Korth, A., Lavraud, B., and McCarthy, M.: 2003, 'Evidence for Impulsive Solar Wind Plasma Penetration through the Dayside Magnetopause', *Ann. Geophys.* **21**, 457–472.

Marchaudon, A., Cerisier, J.-C., Bosqued, J.-M., Dunlop, M. W., Wild, J. A., Dècrèau, P. M. E., Förster, M., Fontaine, D., and Laakso, H.: 2003, 'Transient Plasma Injections in the Dayside Magnetosphere: One-to-one Correlated Observations by Cluster and $B_Y$ SuperDARN'. In press, *Ann. Geophys.*

Newell, P. T., and Meng, C. I.: 1988, 'The Cusp and the Cleft/LLBL: Low Altitude Identification and Statistical Local Time Variation', *J. Geophys. Res.* **93**, 14549–14556.

Newell, P. T., Meng, C. I., Sibeck, D. G., and Lepping, P.: 1989, 'Some Low-altitude Cusp Dependencies on the Interplanetary Magnetic Field', *J. Geophys. Res.* **94**, 8921–8927.

Newell, P. T., and Meng, C. I.: 1994, 'Ionospheric Projections of Magnetospheric Regions under Low and High Solar Wind Pressure Conditions', *J. Geophys. Res.* **99**, 273–286.

Ogilvie, K. W., Chornay, D. J., Fritzenreiter, R. J., Hunsaker, F., Lobell, J., Miller, G., Scudder, J. D., Sittler, E. C. Jr., Tobert, R., Bodet, D., Needell, G., Lazarus, A. J., Steinberg, J. T., Tappan, J. H., Marretic, A., Keller, J., and Gergin, E.: 1995, 'SWE: A Comprehensive Plasma Instrument for the WIND Spacecraft', *Space Sci. Revs.* **71**, 55–77 .

Onsager, T. G., Scudder, J. D., Lockwood, M., and Russell, C. T.: 2001, 'Reconnection at the High-Latitude Magnetopause during Northward Interplanetary Magnetic Field Conditions', *J. Geophys. Res.* **106**, 25467–25488.

Paschmann, G., Haerendel, G., Sckopke, N., and Rosenbauer, H.: 1976, 'Plasma and Magnetic Field Characteristics of the Distant Polar Cusp Near Local Noon: The Entry Layer', *J. Geophys. Res.* **81**, 2883–2899.

Paschmann, G., and Daley, P. (eds): 1988, *Analysis Methods for Multispacecraft Data*. ISSI Scientific Report SR-001, Kluwer Academic Publishers, pp. 271–284.

Réme, H., Aoustin, C., Bosqued, M., Dandouras, I., Lavraud, B., Sauvaud, J.-A., Barthe, A., Bouyssou, J., Camus, T., Coeur-Joly, O., Cros, A., Cuvilo, J., Ducay, F., Garbarowitz, Y., Medale, J. L., Penou, E., Perrier, H., Romefort, D., Rouzaud, J., Vallat, C., Alcayde, D., Jacquey, C., Mazelle, C., d'Uston, C., Mobius, E., Kistler, L. M., Crocker, K., Granoff, M., Mouikis, C., Popecki, M., Vosbury, M., Klecker, B., Hovestadt, D., Kucharek, H., Kuenneth, E., Paschmann, G., Scholer, M., Sckopke, N., Seidenschwang, E., Carlson, C. W., Curtis, D. W., Ingraham, C., Lin, R. P., McFadden, J. P., Parks, G. K., Phan, T., Formisano, V., Amata, E., Bavassano-Cattaneo, M. B., Baldetti, P., Bruno, R., Chionchio, G., Di Lellis, A., Marcucci, M. F., Pallocchia, G., Korth, A., Daly, P. W., Graeve, B., Rosenbauer, H., Vasyliunas, V., McCarthy, M., Wilber, M., Eliasson, L., Lundin, R., Olsen, S., Shelley, E. G., Fuselier, S., Ghielmetti, A. G., Lennartsson, W., Escoubet, C. P., Balsiger, H., Friedel, R., Cao, J. B., Kovrazhkin, R. A., Papamastorakis, I., Pellat, R., Schudder, J., and Sonnerup, B.: 2001, 'First Multispacecraft Ion Measurements in and Near the Earth's Magnetosphere with the Identical Cluster Ion Spectrometry (CIS) Experiment', *Ann. Geophys.* **19**, 1303–1354.

Robert, P., and Roux A.: 1993, 'Dependance of the Shape of the Tetrahedron on the Accuracy of the Estimate of the Current Density', in *Spatio-temporal Analysis for Resolving Plasma Turbulence (START)*, ESA WPP-047, pp. 289–302.

Robert, P., Dunlop, M.W., Roux, A., and Chanteur, G.: 1998, 'Accuracy of Current Density Determination, in Analysis Methods for Multispacecraft Data', ISSI Science Report, SR-001, Kluwer Academic Publishers, pp. 395–418.

Russell, C. T., Melliot, M. M., Smith, E. J., and King, J. H.: 1983, 'Multiple Spacecraft Observations of Interplanetary Shocks: Four Spacecraft Determinations of Shock Normals', *J. Geophys. Res.* **88**, 4739–4748.

Russell, C.T.: 2000, 'POLAR Eyes in the Cusp, Proc. of the Cluster II workshop: Multiscale/Multi-oint Plasma Measurements', ESA SP-449, pp. 47–55.

Savin, S. P., Romanov, S. A., Fedorov, A. O., Zelenyi, L., Klimov, S. I., Yermolaev, Yu. I, Budnik, E. Yu, Nikolaeva, N. S., Russell, C. T., Zhou, X.-W., Urquhart, A. L., and Reiff, P. H.: 1998, 'The Cusp/Magnetosheath Interface on May 29, 1996: Interball 1 and Polar Observations', *Geophys. Res. Lett.* **25**, 2963–2966.

Scudder, J. D., Mozer, F. S., Maynard, N. C., and Russell, C. T.: 2002, 'Fingerprints of Collisionless Reconnection at the Separator, I, Ambipolar-Hall Signatures', *J. Geophys. Res.* **107**(A10), Art. No. 1294.

Sibeck, D. G., Lopez, R. E., and Roelof, E. C.: 1991, 'Solar Wind Control of the Magnetopause Shape Location and Motion', *J. Geophys. Res.* **96**, 5489–5495.

Sonnerup, B. U. O., and Cahill, L. J.: 1967, 'Magnetopause Structure and Attitude from Explorer 12 Observations', *J. Geophys. Res.* **72**, 171–183.

Spreiter, J. R., Alksne, A. Y., and Summers, A. L..: 1968. 'External Aerodynamics of the Magnetosphere', in R. L. Carovillano, J. F.. McClay, and H. R.. Radoski (eds.), *Physics of the Magnetosphere*, D. Reidel, Hingham, Mass, pp. 301–375.

Tsyganenko, N. A.: 1989, 'A Magnetospheric Field Model with a Warped Tail Current Sheet', *Planet. Space Sci.* **37**, 5–20.

Tsyganenko, N. A., and Russell, C. T.: 1999, 'Magnetic Signatures of the Distant Polar Cusps: Observations $B_Y$ Polar and Quantitative Modeling', *J. Geophys. Res* **104**, 24939–24955.

Vasyliunas, V. M., Skopke, N., and Rosenbauer, H.: 1979, 'Structure of the Polar Magnetosheath as Observed $B_Y$ HEOS 2', *EOS Trans. AGU* **58**, 1206–1215.

Vasyliunas, V. M.: 1995, 'Multiple-Branch Model of the Open Magnetopause', *Geophys. Res. Lett.* **22**, 1145–1147.

Vontrat-Reberac, A., Bosqued, J. M., Taylor, M. G., Lavraud, B., Fontaine, D., Dunlop, M. W., Laakso, H., Cornilleau-Werhlin, N., Canu, P., and Fazarkerley, A.: 2003, 'Cluster Observations of the High-altitude Cusp for Northward Interplanetary Magnetic Field: A Case Study', *J. Geophys. Res.*, **108**(A9), Art. No. 1346.

Woch, J., and Lundin, R.: 1992, 'Magnetosheath Plasma Precipitation in the Polar Cusp and its Control $B_Y$ the Interplanetary Magnetic Field', *J. Geophys. Res.* **97**, 1421–1430.

Yamauchi, M., and Lundin, R.: 1994, 'Classification of Large-scale and Meso-scale Ion Dispersion Patterns Observed $B_Y$ Viking over the Cusp-mantle Region', in J. A. Holtet, and A. Egeland (eds.), *Physical Signatures of Magnetospheric Boundary Layer Process*, Kluwer Academic Publishers, pp. 99–109.

Yamauchi, M., Nilsson, H., Eliasson, L., Norberg, O., Boehm, M., Clemmons, J. H., Lepping, R. P., Blomberg, L., Ohtani, S.-I., Yamamoto, T., Mukai, T., Terasawa, T., and Kokubun, S.: 1996, 'Dynamic Response of the Cusp Morphology to the Solar Wind: A Case Study during Passage of the Solar Wind Plasma Cloud on February 21, 1994', *J. Geophys. Res.* **101**, 24675–24687.

Zhou, X.-W., and Russell, C. T.: 1997, 'The Location of the High-latitude Polar Cusp and the Shape of the Surrounding Magnetopause', *J. Geophys. Res.* **102**, 105–110.

Surveys in Geophysics (2005) 26: 57–69
DOI 10.1007/s10712-005-1872-6 © Springer 2005

# MAGION-4 HIGH-ALTITUDE CUSP STUDY

J. MERKA[1], J. ŠAFRÁNKOVÁ[2], Z. NĚMEČEK[2] and J. ŠIMŮNEK[3]
[1]*L-3 Communications Government Services, Inc, Vienna, Virginia, USA*
*E-mail: jan.merka@gsfc.nasa.gov;*
[2]*Faculty of Mathematics and Physics, Charles University, Prague, Czech Republic;*
[3]*Institute of Atmospheric Physics, Prague, Czech Republic*

(Received 18 October 2002; Accepted 30 April 2004)

**Abstract.** The polar cusps have traditionally been described as narrow funnel-shaped regions of magnetospheric magnetic field lines directly connected to magnetosheath ones, allowing the magnetosheath plasma to precipitate into the ionosphere. However, recent middle- to high-altitude observations (i.e., the Interball, Hawkeye, Polar, Image, and Cluster spacecraft) reported the cusps to encompass a broad area near local noon. The present paper focuses on a statistical study of the high-altitude cusp and surrounding magnetosheath regions as well as on some peculiarities of the cusp-magnetosheath transition. For a comparison of high- and low-altitude cusp determination, we present a mapping of two-year Magion-4 (a part of the Interball project) observations of cusp-like plasma along model magnetic field lines (according to the Tsyganenko 96 model) down to the Earth's surface. The footprint positions show a substantial latitudinal dependence on the dipole tilt angle. The dependence can be fitted by a line with a slope of 0.14° MLAT per 1° of tilt. In contrary to previously reported IMF or solar wind influences on the cusp shape or location, some differences exist: (1) a possible IMF $B_X$ dependence of the cusp location, (2) a split cusp for $B_Y \neq 0$, and (3) a smaller cusp during periods of higher solar wind dynamic pressure. The conclusions following from the statistical analysis are confirmed by case studies which reveal the physical mechanisms leading to the observed phenomena. Results have shown that (1) reconnection near the cusp does not necessarily lead to observable precipitation, (2) the cusp precipitation in one hemisphere can be supplied from the conjugate hemisphere, and (3) the cusp geometry at a certain time depends on the IMF history.

**Keywords:** cusp-like plasma, dipole tilt angle, high-altitude cusp, magnetopause, magnetosheath, reconnection

## 1. Introduction

In this paper, recent results from MAGION-4 regarding the high-altitude cusp region are reviewed. The paper is also complemented by two-point observations provided by the INTERBALL-1 and MAGION-4 spacecraft because two-point measurements are especially suitable for a study of the topology and dynamics of the high-altitude cusp and its vicinity under changing IMF and solar wind conditions.

The INTERBALL-1/MAGION-4 satellite/subsatellite pair, called project INTERBALL-Tail, was launched into a highly elliptical orbit with 63° inclination, with apogee at 200 000 km (or $31R_E$) and perigee at 750 km. During the years 1995–1997, they performed two-point measurements in the high-altitude cusp reaching altitudes above those of the apogee of Polar ($9R_E$). The two satellites could remain in the cusp region for periods of more than 2 h and scanned the vertical profile of the cusp from altitude $\sim 3R_E$ up to the magnetosheath. The INTERBALL-1 and MAGION-4 spacecraft were equipped with a comprehensive set of instruments for plasma and magnetic field investigations (Klimov et al., 1997; Němeček et al., 1997; Šafránková et al., 1997).

In the first part of this review, MAGION-4 data used for extensive studies of the position and shape of the high-altitude cusp will be discussed. Then a review of two-point INTERBALL-1/MAGION-4 observations of the cusp-magnetosheath transition will follow. Finally, some directions and possibilities for future research will be outlined.

## 2. Statistical properties of the high-altitude cusp

The traditional image of the cusp is a narrow funnel-shaped region where magnetosheath plasma enters into the magnetosphere (Haerendel et al., 1978). However, at low altitudes, a DMSP satellite has observed that the cusp's local magnetic time extent can reach 3.7 h of MLT (Maynard et al., 1997). On the other hand, the low- and mid-altitude cusp is quite narrow in latitude, only about 1–2° (Newell and Meng, 1989; Aparicio et al., 1991; Potemra et al., 1992). Both the cusp's position and size depend on many solar wind/IMF and magnetospheric parameters of which the most important role is played by the orientation of the Earth's dipole axis, the dynamic pressure of the solar wind, and the IMF orientation (Newell and Meng, 1987, 1989, 1994; Farrell and Allen, 1990; Weiss et al., 1995; Zhou et al., 1999, 2000; Němeček et al., 2000; Merka et al., 2002). Therefore, the influence of the afore-mentioned parameters must be taken into account in order to estimate the cusp's dimensions.

At high altitudes, the cusp-like plasma is observed over a wide range of magnetic latitudes. Figure 1 depicts, in Solar Magnetic (SM) coordinates, all parts of the MAGION-4's orbits on which cusp-like plasma was detected. The cusp region is clearly much wider than narrow funnel-shaped region of entry of magnetosheath plasma (Haerendel et al., 1978). As discussed in the previous paragraph, the cusp location changes in response to magnetospheric, solar wind and IMF conditions and these effects certainly contribute to the cusp width as displayed in Figure 1.

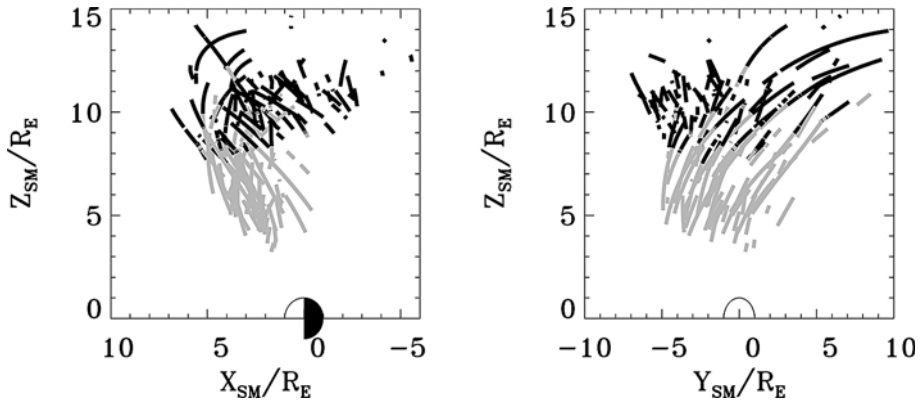


*Figure 1.* Cusp crossings observed by MAGION-4 during 1995–1997 years plotted in Solar Magnetic (SM) coordinates. Different colors distinguish measurements made closer or farther than $3R_E$ from the magnetopause (the T96 model). Adopted from Merka et al. (2002).

The orientation of the Earth's dipole axis has a significant effect on the cusp's latitudinal position (Newell and Meng, 1989; Zhou et al., 1999; Němeček et al., 2000). The analysis of the MAGION-4 data revealed that the cusp's footprint position shifts by 0.14° MLAT per 1° of tilt (Němeček et al., 2000; Merka et al., 2002). Furthermore, Němeček suggested a slightly higher (by 0.01° MLAT per 1° of tilt) cusp shift within $3R_E$ of the model magnetopause. Moreover, they found the slope of the tilt angle dependence higher by 0.04° for negative $B_Z$ than for positive $B_Z$. In summary, the dependence of the cusp location on the tilt angle increases with altitude, from 0.06° MLAT/1° of tilt at 835 km (Newell and Meng, 1989), through 0.07° MLAT/1° of tilt for altitudes ~5–10$R_E$ (Zhou et al., 1999), up to 0.14° MLAT/1° of tilt near the magnetopause (Němeček et al., 2000; Merka et al., 2002). The dipole tilt angle effect has been recently demonstrated by Savin et al. (2002) even for the turbulent boundary layer (TBL) which is located just outside and/or at the near-cusp magnetopause. Due to the magnitude of the dipole tilt effect, the projected cusp positions have to be corrected before further analysis (Merka et al., 2002).

The high-altitude cusp as seen from MAGION-4 covers much larger area than reported by the low-altitude observations (Newell and Meng, 1992, 1994; Merka et al., 2002). Figure 2 presents footprints of all parts of the MAGION-4 orbits which lay below the magnetopause and on which the cusp-like plasma was detected. The different colors represent the number of minutes that the satellite spent in a particular bin of 0.5 h × 1° (MLT × MLAT). Note that the latitude of each footprint has been corrected for the tilt angle dependence. Figure 2 shows that the cusp-like plasma is observed over a large interval in both MLAT and MLT: ~70°–85° MLAT and 6.5–16.5 h MLT. However, Merka et al. (2002) argued that the cusp is narrower and that its displacement, caused by the different factors (i.e., the

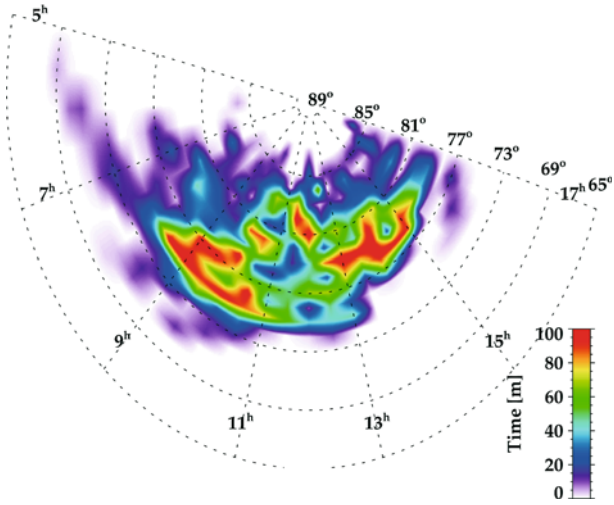


*Figure 2.* The number of minutes of cusp-like plasma observations in 0.5 h × 1° bins (MLT × MLAT) mapped along the model field lines toward the Earth's surface. The positions have been corrected for the dipole tilt dependence (Merka et al., 2002).

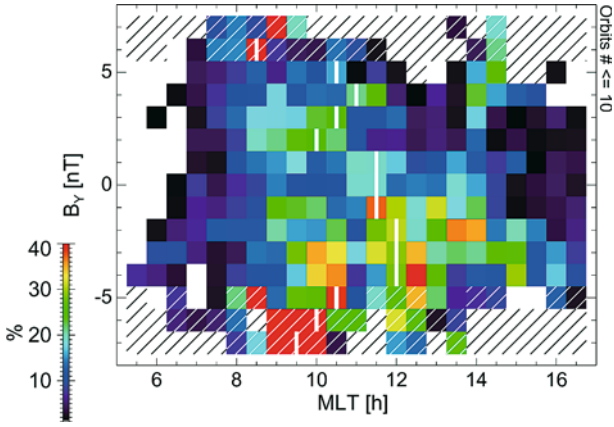


*Figure 3.* The cusp longitudinal (MLT) location as a function of the IMF $B_Y$ component (Merka et al., 2002).

solar wind dynamic pressure and IMF orientation effects), is greater than the cusp width itself. Based on this interpretation, they estimated the cusp latitudinal width to be ~5°–6° MLAT. In order to improve this estimate, we can rescale the observed positions to "nominal conditions" or employ multiple spacecraft dispersed in latitude. The first approach, however, requires a knowledge of the scaling factors for various solar wind or magnetospheric parameters, and their effects on the high-altitude cusp. The scaling factors are often either unknown or known only very approximately.

The MAGION-4 results (Merka et al., 1999, 2002) on cusp shift with IMF $B_Z$ are generally consistent with results obtained from DMSP at low altitudes (Newell et al., 1989), Viking at middle altitudes (Woch and Lundin, 1992), and Hawkeye and Polar at high altitudes (Eastman et al., 2000; Zhou et al., 2000). Analysis of the MAGION-4 data (Merka et al., 2002) showed that, for IMF $B_Z < 0$ nT, if IMF is more negative, the cusp moves equatorward (by $\sim 0.5°$ per 1 nT) but, when IMF $B_Z > 0$ nT, the cusp latitude is approximately constant.

Merka et al. (2002) reported that the high-altitude cusp observations of MAGION-4 indicate the presence of two separate statistical cusp populations for $B_Y > 0$ nT (Figure 3). According to Zhou et al. (2000), the center of the reconnection site moves duskward in the northern hemisphere and dawnward in the southern hemisphere for positive $B_Y$. Since each reconnection site is connected to both northern and southern hemispheres, this mechanism was suggested by Merka et al. (2002) to split the cusp and to move the two parts away from noon. A precise study of the probability of cusp observations in their paper has shown that the observation of two sources of the cusp precipitation, attributed to reconnection in conjugate hemispheres, is a common feature at high altitudes (see Figure 3). These two sources are projected onto different MLT and their separation seems to be controlled by the IMF $B_Y$ component. However, the peaks of the probability are less than 50% and thus it is not clear whether these two cusps would be observed simultaneously. This problem will be discussed later.

Contrary to other observations, from the MAGION-4 data it follows that the cusp position depends on the IMF $B_X$ component (Merka et al., 1999, 2002). A possible explanation was suggested in Cowley, but the shift could be an artificial effect of the magnetospheric magnetic field model T96 (Tsyganenko and Stern, 1996), used for the field line tracing in the MAGION-4 data analysis, which is not parameterized by IMF $B_X$.

The low-altitude observations show a broader cusp during periods of enhanced solar wind dynamic pressure $P_{SW}$ (Farrell and Allen, 1990; Newell and Meng, 1994; Zhou et al., 2000). In the analysis of the MAGION-4 data, the statistical cusp seems to shrink with increasing solar wind pressure, $P_{SW}$ (Merka et al., 2002). In fact, the cusp position varies rather more for lower than higher values of $P_{SW}$. We should note that this result can be influenced by the low number of cusp-like plasma measurements for $P_{SW} > 3$ nPa in the MAGION-4 data set.

## 3. The cusp-magnetosheath transition

Several sources of cusp plasma have been suggested over the course of time. However, it is understood now that the dominant (if not the only) source is reconnection of IMF with magnetospheric field lines. Reconnection produces

accelerated plasma populations which excite different kinds of plasma waves. As a result, the region adjacent to the magnetopause is highly turbulent and occupied by heated, magnetosheath-like plasma with a low drift velocity. This region called the turbulent boundary layer, the stagnation region or the exterior cusp in different papers (Haerendel et al., 1978; Paschmann et al., 1978) seems to be the proper source of the cusp precipitation. The turbulent boundary layer has been extensively studied using INTERBALL-Tail data (Savin et al., 2002; Sandahl, 2002 and references therein).

The reconnection occurs between magnetic field lines of opposite polarity: for southward IMF, the magnetosheath and magnetospheric field lines connect near the subsolar magnetopause (Dungey 1961, 1963); for northward IMF, anti-parallel reconnection occurs at high-latitudes poleward of the Earth's magnetic cusps (Kessel et al., 1996; Russell et al., 1998; Šafránková et al., 1998; Savin et al., 1998; Fuselier et al., 2000; Merka et al., 2000). For southward IMF, the so-called normal ion dispersion (i.e., the ion energy decreases with increasing invariant latitude) is observed in the cusp region (Onsager et al., 1993). The so-called reverse ion dispersion (observed ion energy decreases with decreasing invariant latitude) is found in the cusp for northward IMF conditions (Woch and Lundin, 1992; Russell et al., 1998; Fuselier et al., 2000; Merka et al., 2000; Le et al., 2001). The reverse ion dispersion is a direct result of the time-of-flight or velocity filter effects produced by reconnection and subsequent sunward convection of the newly connected field line. Fedorov et al. (2002) studied high-latitude reconnection in INTERBALL-1 data when the IMF was dominated by the $B_Y$ component. Their observations were consistent with the magnetopause topology based on the antiparallel merging hypothesis (Crooker, 1979).

In contrast to the low- and middle-altitude studies, the main problem is the separation of the cusp-like region and magnetosheath at high altitudes. Merka et al. (2000) analyzed a structure of the cusp-magnetosheath transition for two different orientations of the IMF $B_Z$ component. They found a stable structure similar to that inferred earlier from low-altitude observations for a northward oriented IMF. This structure exhibits a clear reversal of the plasma flow caused by reconnection tailward of the cusp (Figure 4a) which turns a part of the magnetosheath plasma into the cusp.

For northward IMF orientation, two-point observations reveal that reconnection is steady (Šafránková et al., 2002). Small changes of the IMF direction modulate the observed plasma density but do not stop precipitation. The ions entering the magnetosphere are spatially dispersed (Šafránková et al., 2002), probably due to the $\mathbf{E} \times \mathbf{B}$ drift, resulting in an increase of the energy of precipitating particles with latitude. This effect is often observed at low altitudes for positive IMF $B_Z$ (Woch and Lundin, 1992).

The MAGION-4 and INTERBALL-1 observations unveiled the presence of a vortex-like cavity filled by slow-moving heated plasma in the outer cusp

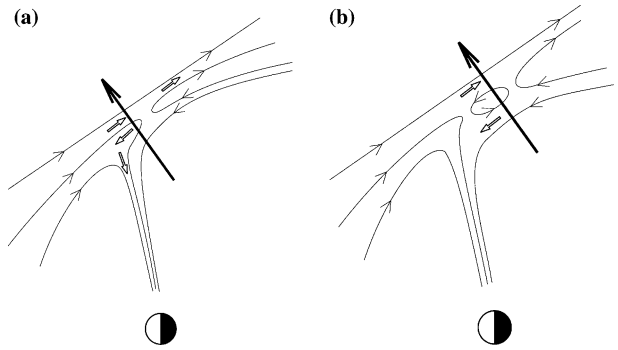


*Figure 4*. Magnetic field geometry formed by reconnection tailward of the cusp: (a) standard geometry, and (b) illustration of the INTERBALL-1 observation of a vortex-like structure in the outer cusp. The open arrows show the direction of plasma flow; the heavy arrow shows the spacecraft trajectory.

during periods of positive IMF $B_Z$ (Šafránková et al., 2002). The observations correspond to the configuration shown in Figure 4b. The rotation of the magnetic field observed by INTERBALL-1 is shown in Figure 5. Note the decrease of the magnetic field strength connected with the presence of hot plasma inside the vortex. The same structure was observed about 20 min later by MAGION-4. Since this time delay corresponded well to the separation of the two spacecraft, Šafránková et al. (2002) concluded that the region was steady and thus converted the temporal scale of Figure 5 into a spatial scale. The diameter of the observed vortex derived from measurements at the two spacecraft was ~2000 km. Šafránková et al. (2002) argue

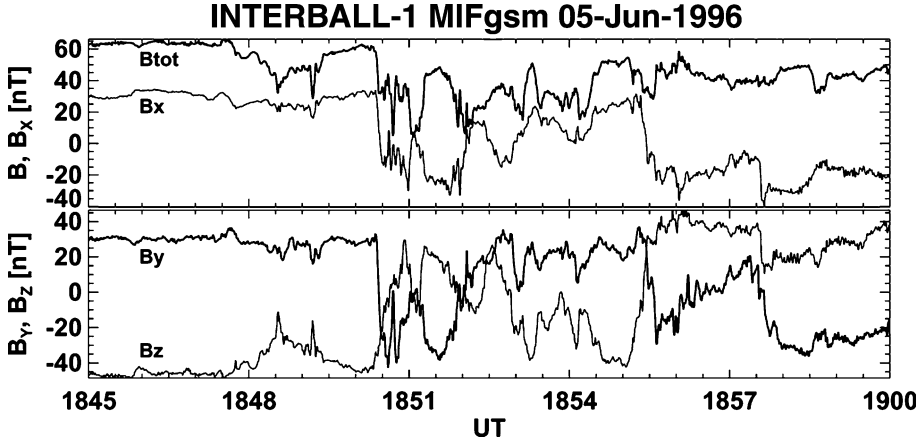


*Figure 5*. The magnetic field as measured by INTERBALL-1 during a crossing of the cusp-magnetosheath boundary. Note a rotation of all three components, indicating a vortex inside the boundary layer.

that this relatively small structure would not be observed too often even if it were a regular feature of the high-altitude cusp.

When the IMF pointed southward, a configuration like that shown in Figure 6a has been found (Fedorov et al., 2000; Merka et al., 2000). Merka et al. 2000 pointed out that the magnetopause in the cusp region is not well defined under such conditions. This is true especially at the poleward edge of the cusp because all parameters change gradually during the crossing. In contrast to the common belief that the cusp region is highly variable, stable precipitation patterns were observed for several hours by MAGION-4. The intensity of observed precipitation was only weakly modulated by magnetosheath density fluctuations observed simultaneously by GEOTAIL (Merka et al., 2000). Fedorov et al. (2000) studied the particle distributions from the INTERBALL-1 CORALL particle instrument during steady southward IMF. They presented evidence that during steady southward IMF the exterior cusp contains open magnetic field lines.

Under still not well understood conditions, the INTERBALL-1 and MAGION-4 spacecraft observed a region of dense stationary plasma adjacent to the magnetopause (Šimůnek et al., 2003), as shown in Figure 6b. This feature was observed during periods of negative IMF $B_Z$ when the shear across the magnetopause in the cusp region is low; therefore, the transitions from the cusp into a stagnant region and then into the magnetosheath were not accomplished with a notable change of the magnetic field. Even the two-point observations were not sufficient for a decision on whether this region lay on magnetospheric or on magnetosheath field lines.

However, Šimůnek et al. (2003) further examined the observations under changing IMF direction. The IMF was pointing generally tailward and southward and then it turned to a northward direction for ~6 min. Due to this change, both INTERBALL-1 and MAGION-4 underwent an excursion from the cusp to the magnetosheath. The magnitudes of the magnetic field

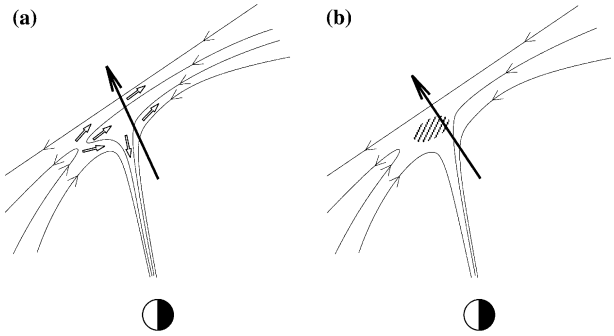


*Figure 6.* Cusp geometry during intervals of southward IMF: (a) standard geometry, and (b) location of the *stagnant* region.

before and after the excursion were the same, but the new direction was different, and only slowly returned to the original orientation. Furthermore, the plasma density was about 10 times lower and only gradually increased. The rotation of the magnetic field can be seen in Figure 7 which depicts the magnetic field vector evolution along the spacecraft orbit. Until the IMF turn (point A), the measured magnetic field roughly corresponds to the T96 model field. Then it turns toward a new orientation and, in course of the next 15 min, gradually returns to the orientation close to the model (point B). The direction measured after this point is highly variable because the satellite entered the turbulent boundary layer.

Šimůnek et al. (2003) suggested that the principal difference in the magnetospheric response to the North–South and South–North IMF turning was connected with the location of the reconnection sites. When the IMF $B_Z$ was negative, the particles entered the subsolar region and proceeded toward the ionosphere. Some of them were reflected and then these particles were observed on mantle field lines at high altitudes near the magnetopause. This path was about 20 $R_E$ long and, assuming 100 km/s as a mean velocity, the particles needed about 20 min to be observed in the mantle region. When the IMF turned northward at the subsolar region, reconnection was stopped there but the magnetosheath magnetic field tailward of the cusp still pointed southward; thus, there was no source of cusp plasma for several minutes. However, the cusp was full of particles which were able to supply the mantle population. When the IMF turned northward above the cusp, mantle field lines, formed during the previous interval of southward IMF, connected to become cusp field lines and were supplied with plasma from both sides until a new equilibrium state was reached. The mantle plasma disappeared as one would expect for the IMF pointing northward. On the other hand, when the

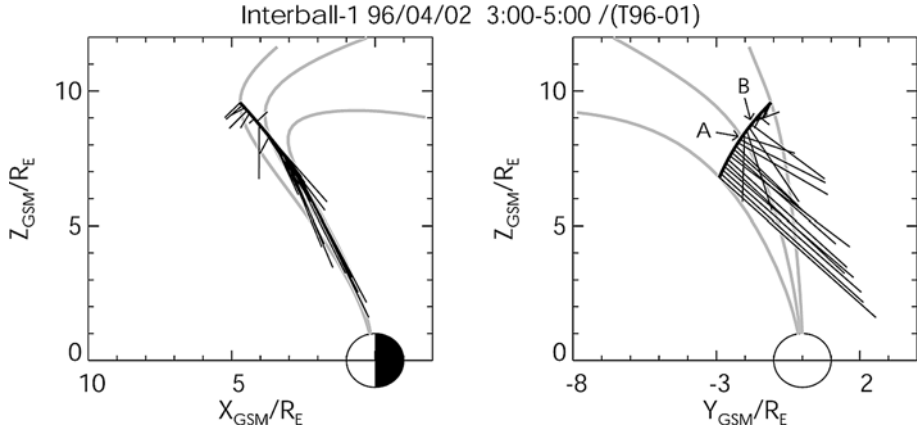


*Figure 7.* Illustration of a gradual recovery of the cusp magnetic field after an IMF rotation (Šimůnek et al., 2003). The magnetic field vectors shown are observed 5 min apart.

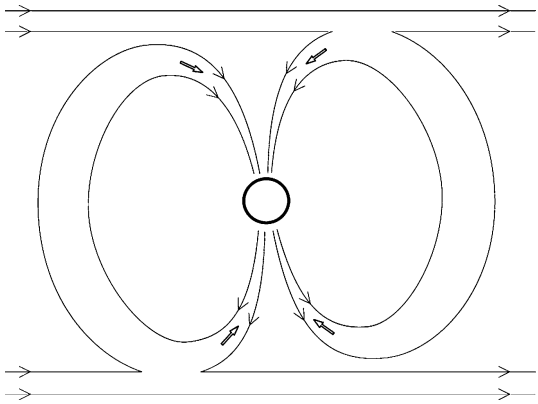

*Figure 8*. Location of possible sources of the cusp plasma during intervals of westward IMF.

IMF turned from North to South, subsolar reconnection started before the high-latitude reconnection terminated. As the magnetosheath plasma propagated much faster and had a much shorter path to the mantle region than the cusp plasma, this turn would result in the empty mantle field lines for several minutes.

A very extensive study of the high-altitude cusp transition formed by a $B_Y$ -oriented magnetosheath magnetic field [Němeček et al. 2003] confirms the earlier hypothesis that the cusp can be supplied from the conjugate hemisphere. The location of possible sources of the cusp-like plasma is shown in Figure 8. However, the study reveals an important role of the magnetosheath velocity at the reconnection site for the cusp precipitation. If this velocity exceeds the Alfvén velocity, the acceleration caused by the reconnection of field lines is not able to turn the bulk of the plasma into the cusp, and only a small part of suprathermal ions can precipitate. At lower altitudes, electrons exhibit features of cusp precipitation, whereas the ion precipitation is weak and sporadic. Such precipitation is then classified as from the cleft or boundary layer (Němeček et al., 2003). According to a model of magnetosheath flow (Spreiter et al., 1966), this situation frequently occurs above the winter cusp; thus, the tilt angle is a parameter determining which reconnection site will be the source of the cusp precipitation.

## 4. Summary and possible future directions

The magnetospheric cusp is a key region for solar wind plasma entry into the deep magnetosphere. In spite of intense *in situ* observations of the cusp for almost two decades, the dynamics of the cusp are not fully understood up to now. From the statistical point of view, at high altitudes, we find a much wider cusp than expected or than is observed at lower altitudes. This

discrepancy has initiated a further study of the cusp topology and dynamics. According to the analysis of the MAGION-4 data, there are two principal factors influencing the structure of the high-altitude cusp and the amount of the plasma penetrating into the magnetosphere: (1) the direction of magnetosheath magnetic field, and (2) the plasma velocity in the cusp region. The tilt angle of the Earth's dipole can be considered as a factor of second order because it influences the cusp precipitation through a change of the magnetospheric magnetic field direction with respect to the solar wind flow, and through a change of the magnetosheath velocity in the cusp region (this velocity is generally lower above the summer than above the winter cusp).

In summary, while we have learned much about the high-altitude cusp from the MAGION-4 and INTERBALL-1 observations, there is much more left to do. Projects consisting of more satellites (e.g., CLUSTER or the planned Magnetospheric Constellation) with separations ranging from hundreds of kilometers up to several $R_E$ would provide data with a better time/space resolution. For example, a spacecraft configuration consisting of a satellite pair/cluster separated by up to 2000 km and one or more additional probes/clusters 1–2 $R_E$ apart would allow the study of both the small- and large-scale cusp features simultaneously. Appropriate processing of such data together with new MHD and/or particle models will be able to further enhance our understanding of both the physics of the solar wind-magnetosphere interaction and the plasma transport within the Earth's magnetosphere.

## Acknowledgements

This work was performed while J. Merka held a National Research Council Research Associateship Award at NASA/GSFC. The authors from Charles University acknowledge the support of Research Project, MSM 113200004, and Czech Grant Agency grant, 205/02/0947.

## References

Aparicio, B., Thelin, B., and Lundin, R.: 1991. 'The Polar Cusp from a Particle Point of View: A Statistical Study based on Viking data', *J. Geophys. Res.* **96**(A8), 14023–14031.

Cowley, S.W.H.: 1981. 'Asymmetry Effects Associated with the X-Component of the IMF in a Magnetically Open Magnetosphere', *Planet. Space Sci.* **29**(8), 809–818.

Crooker, N. U.: 1979. 'Dayside Merging and Cusp Geometry', *J. Geophys. Res.* **84**(NA3), 951–959.

Dungey, J. W.: 1961. 'Interplanetary Field and Auroral Zones', *Phys. Rev. Lett.* **6**(2), 47.

Dungey, J. W.: 1963, *Geophysics: The Earth's Environment, Chapt. The structure of the exosphere or adventures in velocity space*, Gordon and Breach, New York 526.

Eastman, T. E., Boardsen, S. A., Chen, S.-H., Fung, S. F., and Kessel, R. L.: 2000. 'Configuration of High-latitude and High-altitude Boundary Layers', *J. Geophys. Res.* **105**(A10), 23221–23238.

Farrell, W. M., and Allen, J. A. V.: 1990. 'Observations of the Earth's Polar Cleft at Large Radial Distances with the Hawkeye 1 Magnetometer', *J. Geophys. Res.* **95**(A12), 20945–20958.

Fedorov, A., Budnik, E., and Sauvaud, J.-A.: 2002. 'On the Origin of the High-latitude Boundary Layer', *Adv. Space Res.* **30**(12), 2763–2770.

Fedorov, A., Dubinin, E., Song, P., Budnick, E., Larson, P., and Sauvaud, J. -A.: 2000. 'Characteristics of the Exterior Cusp for Steady Southward Interplanetary Magnetic Field: Interball Observations', *J. Geophys. Res.* **105**(A7), 15945–15957.

Fuselier, S. A., Petrinec, S. M., and Trattner, K. J.: 2000. 'Stability of the High-latitude Reconnection Site for Steady Northward IMF', *Geophys Res. Lett.* **27**(4), 473–476.

Haerendel, G., Paschmann, G., Sckopke, N., and Rosenbauer, H.: 1978. 'The Frontside Boundary Layer of the Magnetosphere and the Problem of Reconnection', *J. Geophys. Res.* **83**(NA7), 3195–3216.

Kessel, R. L., Chen, S. H., Green, J. L., Fung, S. F., Boardsen, S. A., Tan, L. C., Eastman, T. E., Craven, J. D., and Frank, L. A.: 1996. 'Evidence of High-latitude Reconnecting during Northward IMF: Hawkeye Observations', *Geophys. Res. Lett.* **23**(5), 583–586.

Klimov, S., Romanov, S., Amata, E., Blecki, J., Buchner, J., Juchniewicz, J., Rustenbach, J., Triska, P., Woolliscroft, L. J. C., Savin, S., Afanasyev, Y., deAngelis, U., Auster, U., Bellucci, G., Best, A., Farnik, F., Formisano, V., Gough, P., Grard, R., Grushin, V., Haerendel, G., Ivchenko, V., Korepanov, V., Lehmann, H., Nikutowski, B., Nozdrachev, M., Orsini, S., Parrot, M., Petrukovich, A., Rauch, J. L., Sauer, K., Skalsky, A., Slominski, J., Trotignon, J. G., Vojta, J., and Wronowski, R.: 1997. 'ASPI Experiment: Measurements of Fields and Waves Onboard the Interball-1 Spacecraft', *Ann. Geophys.* **15**(5), 514–527.

Le, G., Raeder, G., Russell, J., Lu, C. T., Petrinec, S. M., and Mozer, F. S.: 2001. 'Polar Cusp and Vicinity Under Strongly Northward Interplanetary Magnetic Field on April 11, 1997: Observations and MHD Simulations', *J. Geophys. Res.* **106**(A10), 21083–21093.

Maynard, N. C., Weber, E. J., Weimer, D. R., Moen, J., Onsager, T., Heelis, R. A., and Egeland, A.: 1997. 'How Wide in Magnetic Local Time is the Cusp? An Event Study', *J. Geophys. Res.* **102**(A3), 4765–4776.

Merka, J., Šafránková, J., and Němeček, Z.: 1999. 'Interball Observations of the High-altitude Cusp-like Plasma: A Statistical Study', *Czech. J. Phys.* **49**(4a), 695–709.

Merka, J., Šafránková, J., and Němeček, Z.: 2002. 'Cusp-like Plasma in High Altitudes: A Statistical Study of the Width and Location of the Cusp from Magion-4', *Ann. Geophys.* **20**, 311–320.

Merka, J., Šafránková, J., Němeček, Z., Savin, S., and Skalsky, A.: 2000. 'High-altitude Cusp: INTERBALL Observation', *Adv. Space Res.* **25**(7/8), 1425–1434.

Newell, P. T., and Meng, C.-I.: 1987. 'Cusp Width and Bz: Observations and Conceptual Model', *J. Geophys. Res.* **92**(A12), 13673–13678.

Newell, P. T., and Meng, C.-I.: 1989. 'Dipole Tilt Angle Effects on the Latitude of the Cusp and Cleft/Low-latitude Boundary Layer', *J. Geophys. Res.* **94**(A6), 6949–6953.

Newell, P. T., and Meng, C.-I.: 1992. 'Mapping the Dayside Ionosphere to the Magnetosphere according to Particle Precipitation Characteristics', *Geophys. Res. Lett.* **19**(6), 609–612.

Newell, P. T., and Meng, C.-I.: 1994. 'Ionospheric Projections of Magnetospheric Regions under Low and High Solar Wind Pressure Conditions', *J. Geophys. Res.* **99**(A1), 273–286.

Newell, P. T., Meng, C.-I., Sibeck, D. G., and Lepping, R.: 1989. 'Some Low-altitude Cusp Dependencies on the Interplanetary Magnetic Field', *J. Geophys. Res.* **94**(A7), 8921–8927.

Němeček, Z., Fedorov, A., Šafránková, J., and Zastenker, G.: 1997. 'Structure of the Low-latitude Magnetopause: MAGION-4 Observation', *Ann. Geophys.* **15**(5), 553–561.

Němeček, Z., Měrka, J., and Šafránková, J: 2000. 'The Tilt Angle Control of the Outer Cusp Position', *Geophys. Res. Lett.* **27**(1), 77–80.

Němeček, Z., Šafránková, J., Přech, L., Šimůnek, J., Sauvaud, J.-A., Fedorov, A., Stenuit, H., Fuselier, S. A., Savin, S., Zelenyi, L., and Berchem, J.: 2003, 'Structure of the Outer Cusp and Sources of the Cusp Precipitation during Intervals of a Horizontal IMF'. *J. Geophys. Res.* **108**(A12), 1420, doi: 10.1029/2003JA009916.

Onsager, T. G., Kletzing, C. A., Austin, J. B., and MacKiernan, H.: 1993. 'Model of Magnetosheath Plasma in the Magnetosphere: Cusp and Mantle Particles at Low Altitudes.', *Geophys. Res. Lett.* **20**(6), 479–482.

Paschmann, G., Haerendel, G., Sckopke, N., and Rosenbauer, H.: 1978. 'The Entry Layer', *J. Atmos. Terr. Phys.* **40**(3), 257–259.

Potemra, T. A., Erlandson, R. E., Zanetti, L. J., Arnoldy, R. L., Woch, J., and Friis-Christensen, E.: 1992. 'The Dynamic Cusp', *J. Geophys. Res.* **97**(A3), 2835–2844.

Russell, C. T., Fedder, J. A., Slinker, S. P., Zhou, X.-W., Lee, G., Luhmann, J. G., Fenrich, F., Chandler, M. O., Moore, T. E., and Fuselier, S. A.: 1998. 'Entry of the POLAR Spacecraft into the Polar Cusp under Northward IMF Conditions', *Geophys. Res. Lett.* **25**(15), 3015–3018.

Šafránková, J., Merka, J., and Němeček, Z.: 2002. 'Plasma Flow Across the Cusp-Magnetosheath Boundary under Northward IMF', *Adv. Space Res.* **30**(12), 2787–2792.

Šafránková, J., Němeček, Z., Sibeck, D. G., Přech, L., Merka, J., and Santolík, O.: 1998. 'Two Point Observation of High-latitude Reconnection', *Geophys. Res. Lett.* **25**(23), 4301–4304.

Šafránková, J., Zastenker, G., Němeček, Z., Fedorov, A., Simerský, M., and Přech, L.: 1997. 'Small Scale Observation of the Magnetopause Motion: Preliminary Results of the INTERBALL Project', *Ann. Geophys.* **15**(5), 562–569.

Sandahl, I.: 2002. 'Recent Cusp and Cleft Results from Interball', *Adv. Space Res.* **30**(7), 1711–1722.

Savin, S. P., Romanov, S. A., Fedorov, A. O., Zelenyi, L., Klimov, S. I., Yermolaev, Y. I., Budnik, E. Y., Nikolaeva, N. S., Russell, C. T., Zhou, X. -W., Urquhart, A. L., and Reiff, P. H.: 1998. 'The Cusp/Magnetosheath Interface on May 29, 1996: Interball-1 and Polar Observations', *Geophys. Res. Lett.* **25**(15), 2963–2966.

Savin, S. P., Zelenyi, L., Maynard, N., Sandahl, I., Kawano, H., Russell, C. T., Romanov, S., Amata, E., Avanov, L., Blecki, J., Buechner, J., Consolini, G., Gustafsson, G., Klimov, S., Marcucci, F., Němeček, Z., Nikutowski, B., Pickett, J., Rauch, J. L., Šafránková, J., Skalsky, A., Smirnov, V., Stasiewicz, K., Song, P., Trotignon, J. G., and Yermolaev, Y.: 2002. 'Multi-spacecraft Tracing of Turbulent Boundary Layer', *Adv. Space Res.* **30**(12), 2821–2830.

Spreiter, J. R., Summers, A. L., and Alksne, A. Y.: 1966. 'Hydromagnetic Flow Around the Magnetosphere', *Planet. Space Sci.* **14**, 223–253.

Tsyganenko, N. A., and Stern, D. P.: 1996. 'A New-generation Global Magnetosphere Field Model based on Spacecraft Magnetometer Data', *ISTP Newsletter* **6**, 1–21.

Šimůnek, J., Němeček, Z., and Šafránková, J.: 2003. 'Configuration of the Outer Cusp after an IMF Rotation', *Adv. Space Res.* **31**(5), 1395–1400.

Weiss, L. A., Reiff, P. H., Weber, E. J., Carlson, H. C., Lockwood, M., and Peterson, W. K.: 1995. 'Flow-aligned Jets in the Magnetoshperic Cusp: Results from the Geospace Environment Modeling Pilot Program', *J. Geophys. Res.* **100**(A5), 7649–7659.

Woch, J., and Lundin, R.: 1992. 'Signatures of Transient Boundary Layer Processes Observed with Viking', *J. Geophys. Res.* **97**(A2), 1431–1447.

Zhou, X.-W., Russell, C. T., and Le, G.: 2000. 'Solar Wind Control of the Polar Cusp at High Altitude', *J. Geophys. Res.* **105**(A1), 245–251.

Zhou, X.-W., Russell, C. T., Le, G., Fuselier, S. A., and Scudder, J. D.: 1999. 'The Polar Cusp Location and its Dependence on Dipole Tilt', *Geophys. Res. Lett.* **26**(3), 429–432.

Surveys in Geophysics (2005) 26: 71–93
DOI 10.1007/s10712-005-1873-5 © Springer 2005

# HIGH-ALTITUDE CUSP: THE EXTREMELY DYNAMIC REGION IN GEOSPACE

JIASHENG CHEN and THEODORE A. FRITZ
*Center for Space Physics, Boston University, 725 Commonwealth Avenue, Boston, MA, 02215 USA*
*E-mail: jschen@bu.edu*

(Received 22 November 2002; Accepted 2 July 2004)

**Abstract.** The high-altitude dayside cusps (both northern and southern) are extremely dynamic regions in geospace. Large diamagnetic cavities with significant fluctuations of the local magnetic field strength have been observed there. These cusp diamagnetic cavities are always there day after day and are as large as 6 $R_E$. Associated with these cavities are charged particles with energies from 20 keV up to 10 MeV. The intensities of the cusp energetic ions have been observed to increase by as much as four orders of the magnitude when compared with regions adjacent to the cusp which includes the magnetosheath. Their seed populations are a mixture of ionospheric and solar wind particles. The measured energetic ion fluxes in the high-altitude cusp are higher than that in both the regions upstream and downstream from the bow shock. Turbulent electric fields with an amplitude of about 10 mV/m are also present in the cusp, and a cusp resonant acceleration mechanism is suggested. The observations indicate that the dayside high-altitude cusp is a key region for transferring the solar wind mass, momentum, and energy into the Earth's magnetosphere.

**Keywords:** cusp, energetic particles, magnetosphere, space physics

## 1. Introduction

Since the discovery of the Earth's radiation belt by Van Allen and his colleagues in 1958 (Van Allen and Frank, 1959; Yoshida et al., 1960), the origin of the energetic particles in the ring current and in the upstream ion events has been a long-standing and significant problem. Recently, a new magnetospheric phenomenon called the Cusp Energetic Particle (CEP) event has been observed by the POLAR spacecraft (Chen et al., 1997, 1998). Observationally, the CEP event is defined as follows: (1) a decrease in magnetic field magnitude in the dayside cusp, (2) a more than one order of magnitude increase in intensity for the 1–10 keV ions, and (3) a more than three sigma increase above background for $>40$ keV ion (dominated by proton) intensity. The CEP events have been shedding light on the long-standing unsolved fundamental issue about the origins of the energetic particles in the magne-

tosphere (Fritz and Chen, 1999a; Fritz et al., 2000, 2003a, b; Eccles and Fritz, 2002) and in the upstream ion events (Chen and Fritz, 1998, 2000, 2002a, b). They may hold the key to understanding how the solar wind mass, momentum, and energy transfer into the Earth's magnetosphere (Fritz et al., 2003c).

The cusps were once viewed as either focal points with near zero magnetic field magnitude for the shielding currents confining the magnetosphere (Chapman and Ferraro, 1931) or small funnel-shaped volumes between field lines that map to the dayside and nightside of the magnetopause surface (e.g., Roederer, 1970). Later, the cusps were viewed as open funnels for direct entry of magnetosheath plasma into the magnetosphere because of dayside magnetic merging (e.g., Reiff et al., 1977; Crooker, 1977, 1979; Reiff, 1979; Meng, 1982; Newell and Meng, 1987, 1991; Marklund et al., 1990). Recent cusp observations have shown that, in addition to the magnetosheath plasma, large intensities of energetic (40 keV up to 8 MeV) charged particles (CEPs) were also present there (Chen et al., 1997, 1998; Chen and Fritz, 1998; Sheldon et al., 1998). Because of the solar wind pressure, a geomagnetic field minimum at the equator may move to higher latitude (both North and South) and become two off-equatorial field minima in the high-altitude dayside cusps to trap charged particles (Mead, 1964; Shabansky and Antonova, 1968; Shabansky, 1971; Antonova and Shabansky, 1975).

The interpretation of the CEP events has lead to a wide and active debate on the origin of CEPs in the community. Chen et al. (1997, 1998) and Sheldon et al. (1998) suggested that these CEPs were energized locally in the high-altitude cusp – a novel acceleration region. Chen and Fritz (1998) further found that the integrated power of the cusp turbulent magnetic spectra over the ULF ranges is correlated with the intensity of the cusp MeV helium flux and suggested a resonant acceleration mechanism to energize these cusp charged particles. Some research groups have also reported particle acceleration signatures locally in the cusps (Kremser et al., 1995; Pfaff et al., 1998; Pissarenko et al., 2001; Yamauchi et al., 2001; Savin et al., 2002). On the other hand, through numerical simulations, Delcourt and Sauvaud (1999), Blake (1999), and Antonova et al. (2000) suggested a ring current source of the CEPs. This source has the particles being energized by processes in the geomagnetic tail associated with substorms. Ions energized in this manner can drift westward to form the ring current. Some of these charged particles may drift into the cusp by following the bifurcating field minima. Chen and Fritz (2001) have performed a test on such a suggestion about the ring current source by using observational data and found that the observed amplitude of the magnetic moment spectrum of the energetic $O^+$ of ionospheric origin is higher in the CEP event than in the peak of the ring current, indicating that substorm processes (via the ring current) are not the main source of the CEPs. Another possibility for the source of the CEP fluxes was

presented by Chang et al. (1998, 2001) and Trattner et al. (1999, 2001) who suggested a bow shock source for the CEPs, in which the particles were energized at the quasi-parallel bow shock and subsequently were transported into the cusp. The debate between the two groups (the bow shock source vs. the cusp source) can be found in three sets of companion papers: A Comment paper by Trattner et al. (1999) and Reply by Fritz and Chen (1999b) and two recent Comment papers (Chen et al., 2003; Sheldon et al., 2003) and Replys (Chang et al., 2003; Trattner et al., 2003).

The cusp magnetic signatures observed by POLAR from 1996 to 1998 have been reported by Tsyganenko and Russell (1999). Recent MHD simulations predicted that, for a duskward interplanetary magnetic field (IMF) component, the cusp is located on the afternoonside in the northern hemisphere and is located on the morningside in the southern hemisphere (Crooker et al., 1998; White et al., 1998).

The high-altitude cusps always feature diamagnetic cavities that are caused by the solar wind plasma in the high-altitude dayside cusp regions when the "frozen-in" magnetic field condition (Alfvén, 1950) is broken, and are identified by a combination of low magnetic field strength and high solar wind plasma intensity (Fung et al., 1997; Chen et al., 1998). New *in situ* satellite observations show that the sizes of the cusp diamagnetic cavities (CDCs) are extremely large and are always there day after day. Associated with these cavities are charged particles with energies from 20 keV up to 10 MeV. The intensities of the cusp energetic ions were observed to increase by as much as four orders of the magnitude. Turbulent electric fields with an amplitude of about 10 mV/m were also observed in the cusp. These observational facts reveal that the high-altitude dayside cusps are extremely dynamic regions in geospace.

## 2. Large cusp and CEP events observed by POLAR

On 13 May 1999, the POLAR spacecraft observed an extremely large diamagnetic cavity in the high-altitude northern cusp region in the morningside (Figure 1). From 14 to 23:20 UT, the local magnetic field strength was depressed compared with adjacent regions and displayed strong field turbulence (bottom panel of Figure 1), with the measured field strength reaching to near null values in many cases. The middle panel is the plot of the time profiles of the intensity of lower energy (1–10 keV/e) $O^{6+}$ (dotted line) and (1–18 keV/e) $He^{2+}$ (solid line), while the top panel is of the intensity of higher energy (55–200 keV/e) $He^{2+}$. These two panels exhibit significant enhancements of the ion intensities in this region identified as the cusp. It is noted that the POLAR spacecraft has an orbit period of about 18 h. Figure 1 shows that, on 13 May 1999, POLAR was in the CDC during half of its orbit period, indicating that this CDC was extremely large. In fact, this CDC has a

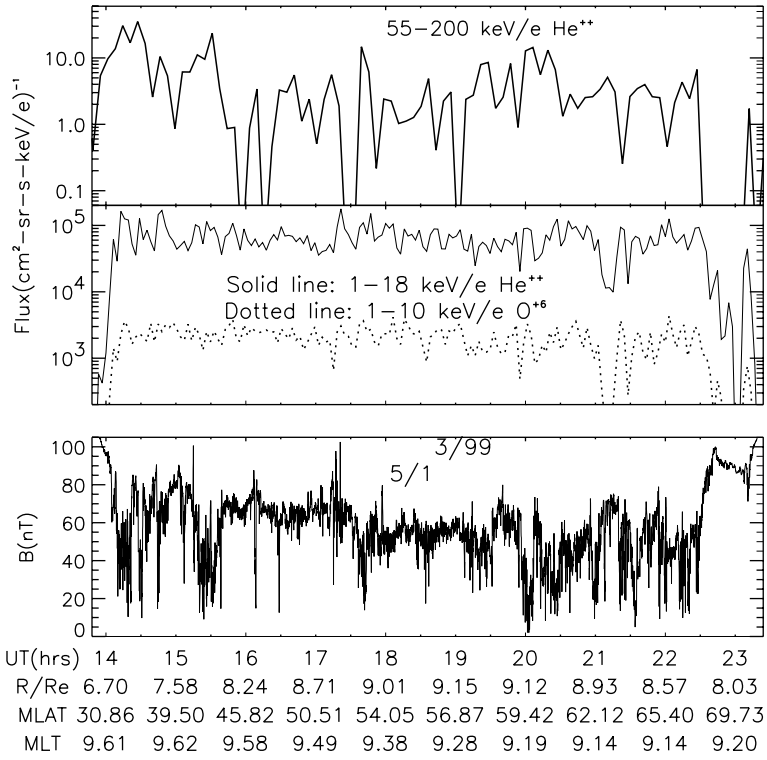


*Figure 1.* The CDCs observed by POLAR on 13 May 1999. The panels show the variation of the 55–200 keV/e $He^{2+}$ flux (top panel), the 1–18 keV/e $He^{2+}$ (solid line) and 1–10 keV/e $O^{6+}$ (dotted line) fluxes (middle), and the magnetic field (bottom) vs. time, respectively. The distance of POLAR from the Earth (in $R_E$), the magnetic latitude (MLAT), and the magnetic local time (MLT) are shown at the bottom.

size of about 6 $R_E$ in the latitudinal and/or radial directions, and this is much larger than expected from prior descriptions of the cusp noted in the Section 1. The energetic particles found in the cusp have been called CEP (cusp energetic particle) events (Chen et al., 1998; Fritz et al., 1999a).

Figure 2 compares the cusp magnetic field strength (bottom panel) observed by POLAR with the two IMF components in GSE coordinates (top two panels) measured by both the ACE (dotted line) and the WIND (solid line) spacecraft on 25 April 1999, where the corrections for the solar wind time delay from ACE (64 min) and WIND (9 min) to POLAR have been made. A large CDC was observed at about 19–24 UT on 25 April 1999. No obvious correlations of the CDC with the IMF are found. One interesting point of Figure 2 is that the IMF $B_y$ component was positive, while the CDC was observed in the morningside in the northern hemisphere (see bottom of Figure 2). As mentioned in Section 1, according to the prediction of current

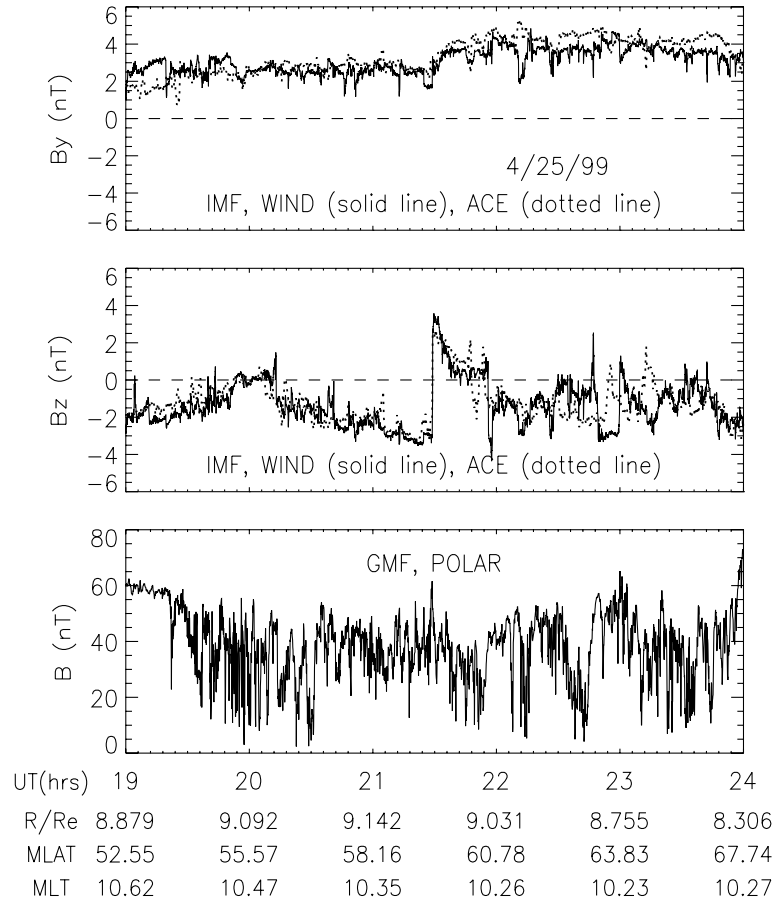


*Figure 2.* Comparison of the CDCs observed by POLAR (bottom panel) with the two IMF components measured by both WIND (solid line) and ACE (dotted line) (top two panels) on 25 April 1999. Corrections have been made for the propagation time from WIND and ACE to POLAR. The distance of POLAR from the Earth (in $R_E$), the MLAT, and the MLT are shown at the bottom.

MHD models a positive IMF $B_y$ would move the dayside northern cusp duskward into afternoonside (Crooker et al., 1998; White et al., 1998; Maynard et al., 2001). Now, assuming that the prediction of present MHD models is correct, one would expect that the northern CDC should also exist in the afternoonside at 19–24 UT on 25 April 1999. This suggests from another point of view a large CDC along the longitudinal direction.

Around solar minimum at POLAR launch through the end of 1997, there were about 300 cusp crossings, of which 279 (or 93%) of the crossings were identified as CEP events (Fritz et al., 1999b). In April 1999 when closer to solar maximum, there were 40 cusp crossings and all of them were identified

as CEP events (Fritz et al., 2003a); in May 1999, there were 35 cusp crossings and again all of them were CEP events, indicating that the CEP events are very common in the high-altitude dayside cusp regions and are always there day after day.

## 3. CEPs observed by CLUSTER

The CEP events were not only observed by POLAR as mentioned above, but are also observed by CLUSTER. Figure 3 displays the 5 March 2001 CEP event observed by the CLUSTER spacecraft (C3), when this spacecraft was crossing through the dayside high-altitude northern cusp region. The position of the CLUSTER in GSE coordinates is labeled at the bottom of Figure 3. The shaded area represents a data gap. A large CDC (bottom panel) was

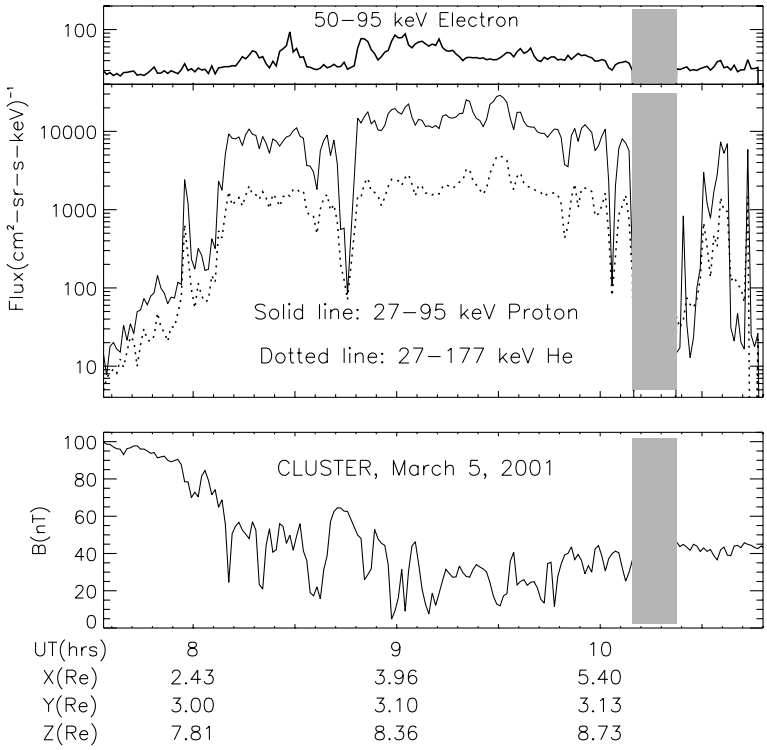


*Figure 3*. The CEP event observed by CLUSTER on 5 March 2001. The panels show the variation of the 50–95 keV electron flux (top panel), the 27–95 keV proton (solid line) and 27–177 keV helium (dotted line) fluxes (middle), and the magnetic field (bottom) vs. time, respectively. The distance of CLUSTER from the Earth (in $R_E$) is shown at the bottom in GSE coordinates.

observed by CLUSTER at 7:35–10:45 UT, corresponding to a significant increase of the energetic ion fluxes (middle panel) and an enhancement of the energetic electron flux (top panel). Note that at 8:50–10:00 UT the 27–95 keV proton flux was about three to four orders of magnitude higher than that after 10:45 UT when CLUSTER went into the magnetosheath.

The CEP events are not only observed in the northern cusp, but also measured in the southern cusp. One example is shown in Figure 4 for 3 April 2002 during 16:10–20:30 UT in which CLUSTER traveled from the magnetosheath through the high-altitude southern cusp region and measured large enhancements of both the energetic ion intensities (middle panel) and the energetic electron flux (top panel) together with a large CDC. Figures 3 and 4 further show that the enhancements of the cusp energetic electron fluxes are much less than those of the cusp energetic ion fluxes. This result is the same as that observed by POLAR (Chen et al., 1998; Chen and Fritz, 2000, 2002b). It suggests an energization process that distinguishes ions from electrons.

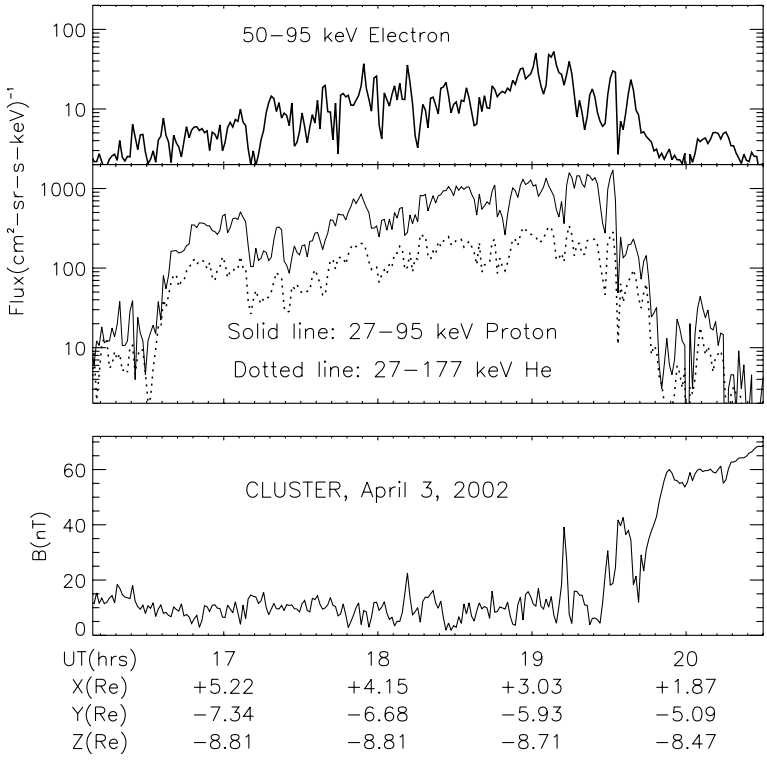


*Figure 4*. Similar plot as in Figure 3, but for the 3 April 2002 CEP event observed CLUSTER.

## 4. Seed populations of CEPs

The ion charge states can be used to determine the seed populations of the energetic ions in the high-altitude dayside cusp regions. Figure 5 is another example of the CEPs (Chen and Fritz, 2002b). On 20 April 1999, when POLAR was crossing through the dayside high-altitude cusp regions, it observed three basic features: (1) the large diamagnetic cavities with strong field turbulence (bottom panel of Figure 5), (2) enhanced intensities of the lower energy (1–10 keV/e) $O^{6+}$ of solar wind origin (middle panel), and (3) high and variable fluxes of the higher energy particles (top panel). Of particular interest is the top panel, in which an unexpected energetic $O^{+}$ (70–200 keV/e) population (solid line) was observed in the high-altitude dayside cusp. Since the $O^{+}$ ions were of ionospheric origin and the $O^{6+}$ and $He^{2+}$ ions were of solar origin (Gloeckler et al., 1986), Figure 5 reveals that the

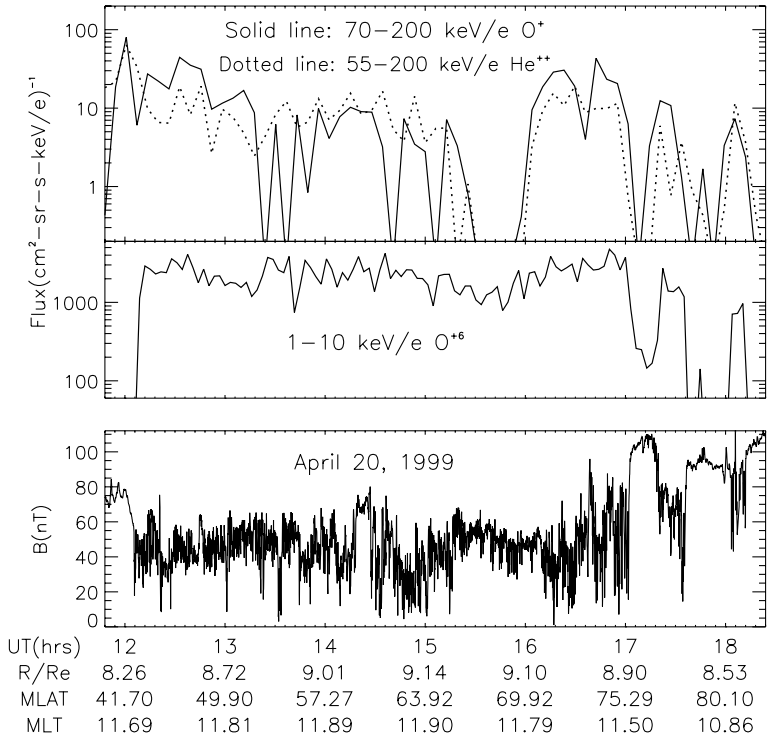


*Figure 5.* The CEP event observed by POLAR on 20 April 1999. The panels show the variation of the 70–200 keV/e $O^{+}$ (solid line) and the 55–200 keV/e $He^{2+}$ (dotted line) fluxes (top panel), the 1–10 keV/e $O^{6+}$ flux (middle), and the local magnetic field (bottom) vs. time, respectively. The distance of POLAR from the Earth (in $R_E$), the MLAT and the MLT are shown at the bottom.

seed populations of the energetic ions in the high-altitude dayside cusps were a mixture of ionospheric and solar wind particles (Chen and Fritz, 2001, 2002b).

It is noticed that the cusp ion time profiles at higher energies (55–200 keV/e) (top panel) are different from those at lower energies (1–10 keV/e) (middle panel); just as ring current and radiation belts occupy distinct and overlapping regions of the dipole trap, so 1 keV/e and 55 keV/e ions occupy distinct and overlapping regions of the cusp. It is further noticed that the time profiles of the energetic (55–200 keV/e) cusp $He^{2+}$ are similar to those of the energetic (70–200 keV/e) $O^{+}$. The key point here is that since the seed population of the cusp energetic $O^{+}$ is of ionospheric origin, and since the seed population of the cusp energetic $He^{2+}$ is solar wind plasma, the similarity of their time-intensity profiles suggests that both seed populations have been energized by a common acceleration mechanism.

## 5. Evidence of local acceleration in the cusp

Leading up to the large geomagnetic storm of 4 May 1998, the solar wind, measured by the ACE spacecraft SWICS instrument (Gloeckler et al., 1999), was observed to display an average charge state of iron (Fe) ions that varied with time over the course of a 24-h period from 16 UT on May 2nd to 16 UT on May 3rd. The value of the average charge state varied from +16 at the beginning of this period to +6 at the end. Perry et al. (2000) examined the response of the POLAR CAMMICE MICS sensor in the high altitude cusp inside the magnetosphere and found that the plasma encountered by POLAR contained Fe ions whose average charge state varied in an identical manner when corrected for the solar wind propagation delay from ACE to the subsolar magnetopause. Perry et al. (2000) concluded that the solar wind had direct and immediate access to the magnetosphere through the cusps. Fritz et al. (2003c) used the same measurements to compare the phase space density of the solar wind plasma measured by ACE and by POLAR for plasma with the same average Fe charge state. One of the periods compared by Fritz et al. (2003c) was at 2300 UT on 2 May 1998 when the average Fe charge state of both plasma populations was +10 and this comparison is presented in Figure 6. The phase space densities were dominated by protons and the ACE spectrum displayed indicates that the solar wind had a sharp peak between one and two keV/e that became thermalized, presumably by passage through the bow shock prior to being observed by POLAR. At energies greater than 2 keV/e the spectrum measure by POLAR assumed a quasi-power-law form [$E^{/\mathrm{gamma}}$] for over three orders of magnitude in energy with $\gamma \sim 3.6$. The actual change in energy at constant phase space density is less than an order of magnitude but for a sensor with a fixed energy threshold

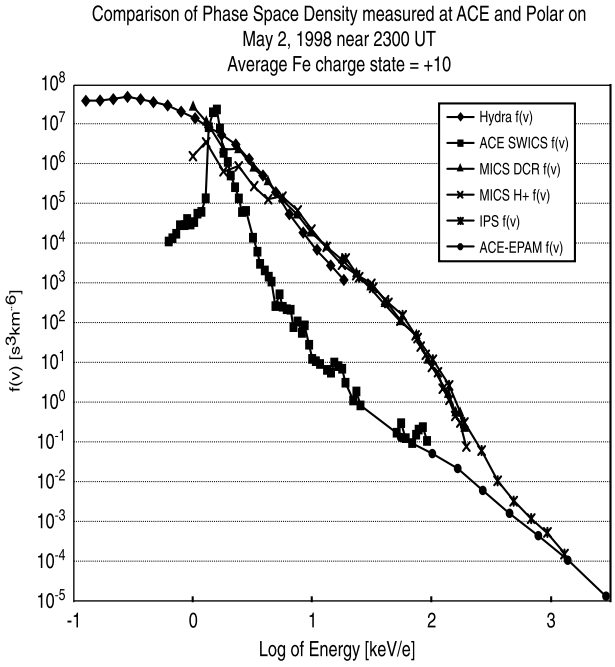


*Figure 6*. The phase space density of the total ion population determined by the SWICS and EPAM instruments at ACE and by the HYDRA, MICS, and IPS instruments on Polar as a function of energy/charge. The two populations correspond to a plasma with an average Fe charge state of +10 recorded just before 2300 UT on 2 May 1998 at ACE and just after 2300 UT at Polar.

the measured increase in intensity at 50 keV, for example, will be three orders of magnitude. The differences in the spectrum measured at POLAR and at ACE above a few keV reflect an increase as a function of energy that is characteristic of the Earth's ring current energy distribution reported by Williams (1983). For the spectrum presented in Figure 6, Fritz et al. (2003c) pointed out that the phase space densities of the solar wind measured at ACE were probably not fully capable of supplying the necessary number of particles to produce the phase space densities measured by POLAR.

When the composition of the fluxes measured by POLAR were determined it was found that there were charge states of oxygen of both high, $O^{6+}$, of solar wind origin and low, $O^{+}$ and/or $O^{2+}$, of ionospheric origin in about equal intensities and spectral slope. This observation is presented in Figure 7 and indicates that the energization which had obviously occurred by the time POLAR made the measurements at 2300 UT had used a source population that was a combination of ions from the solar wind and from the ionosphere.

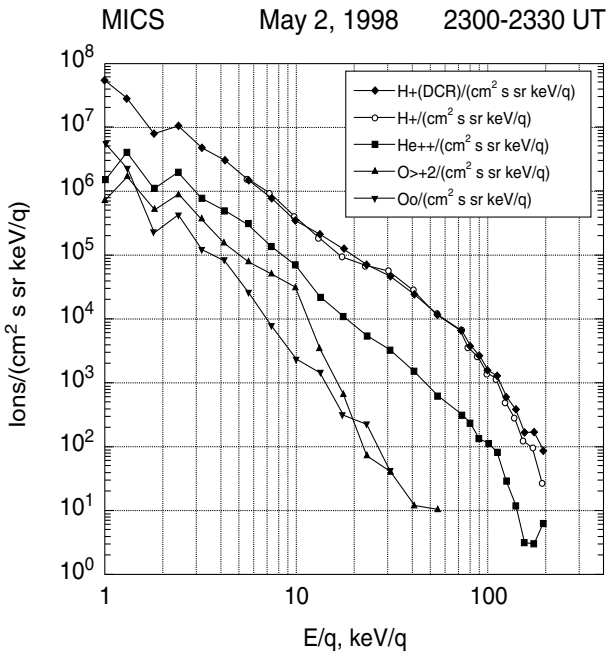


*Figure 7.* The energy spectrum of flux vs. energy/charge of the major ion species determined for the interval from 2300 UT to 2330 UT on 2 May 1998.

## 6. CEPs in geomagnetic storm time

Figure 8 plots one case in which the CEPs were observed within the 4 May 1998 major geomagnetic storm period (maximum negative $D_{st} = -205$ nT at 6 UT). The bottom panel of Figure 8 indicates that the local magnetic field strength decreased from a value of about 200 nT at 6:43 UT to near 0 nT at 6:56 UT. Such a change is about twice that shown in Figure 1 where the local field strength decreased from about 100 nT at 14 UT to 10 nT at 14:20 UT with a maximum negative $D_{st}$ value of −49 nT at 15 UT on 13 May 1999. It is noted that, compared with Figure 1, the 1–18 keV/e $He^{2+}$ peak flux (middle panel) in Figure 8 is one order of magnitude higher, while the 55–200 keV/e $He^{2+}$ peak flux (top panel) in Figure 8 is two orders of magnitude larger. Figure 8 indicates that the 55–200 keV/e $He^{2+}$ has a peak flux value of about 3000 particles/($cm^2$-sr-s-keV/e) in the high-altitude cusp, which is four orders of magnitude higher than that in the mantle.

Figure 9 is the ion (dominated by proton) energy spectrum of the 4 May 1998 CEP event, where the IPS and HIT are two ion sensors onboard POLAR. It shows that the cusp energetic ions are present with energies up to 10 MeV.

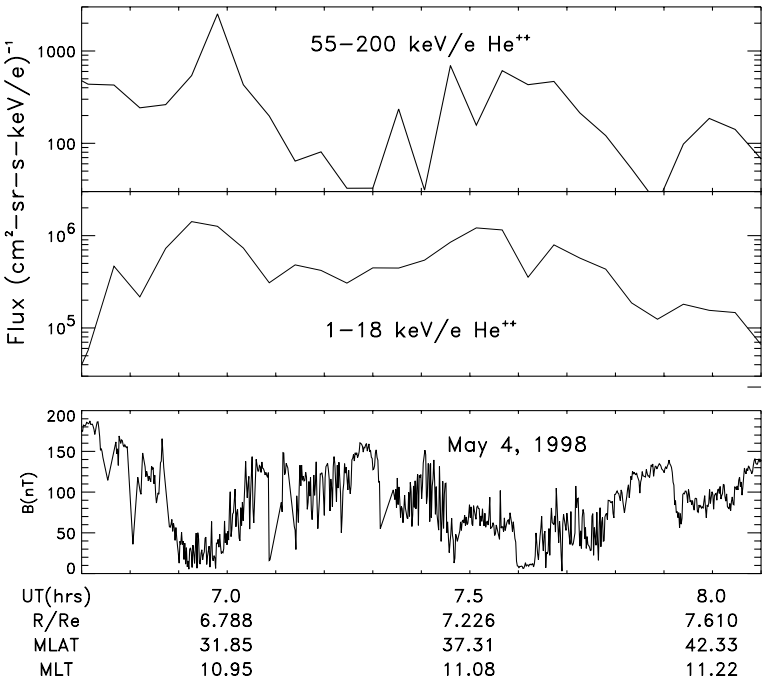


*Figure 8*. The CEP event observed by POLAR during a major geomagnetic storm time on 4 May 1998. The panels from top to bottom are the time-profiles of the 55–200 keV/e $He^{2+}$ flux, the 1–18 keV/e $He^{2+}$ flux, and the local magnetic field, respectively. The distance of POLAR from the Earth (in $R_E$), the MLAT, and the magnetic local time (MLT) are shown at the bottom.

## 7. Comparison of CEPs with downstream and upstream energetic ions

The POLAR spacecraft has a $1.8 \times 9$ $R_E$ polar orbit. Usually, POLAR was well inside the magnetosphere; occasionally, when the solar wind pressure was high, POLAR might pass through the dayside magnetopause into the magnetosheath. On 18 May 1999, when POLAR traveled outbound from the outer ring current toward higher altitudes in the northern hemisphere, it detected an increase of the lower energy solar wind $He^{2+}$ (1–18 keV/e, solid line) and $O^{6+}$ (1–10 keV/e, dotted line) fluxes at 2:00 UT (panel 3 from the top of Figure 10). Measurements of energetic $He^{2+}$ (55–200 keV/e) and $O^{+}$ (70–200 keV/e) at that time are shown in panel 2 from the top of Figure 10. The region of the measured 1–18 keV/e $He^{2+}$ flux extended to 10:50 UT, but a more than two orders of magnitude decrease of energetic $He^{2+}$ (or $O^{+}$) flux was observed by POLAR from about 2:30 to 5:10 UT (panel 2 from top) when the WIND spacecraft detected a higher solar wind pressure (top panel of Figure 10). POLAR was apparently in the low-latitude boundary layer (LLBL) at about 2–3 UT and 4–5 UT. From 3 to 4 UT, the solar wind

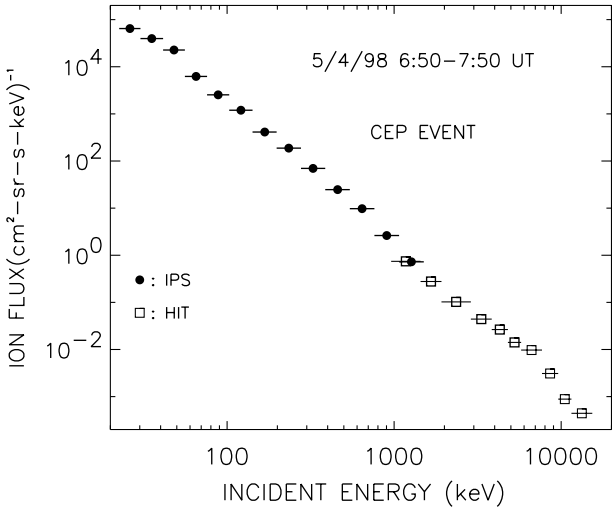


*Figure 9.* The measured storm time CEP ion energy spectrum, at 6:50–7:50 UT on 4 May 1998, where the IPS and HIT are two sensors onboard POLAR.

pressure was significantly higher than at other times as shown in the top panel of Figure 10, and the local magnetic field strength although very turbulent had a minimum value of about 50 nT (bottom panel) instead of fluctuations approaching values of zero (characteristic of the cusp), which suggest that POLAR was in the magnetosheath at the time. Figure 11 is another example which suggests that POLAR was in the morningside high-altitude cusp from 22:45 UT on 12 May 1999 to 0:10 UT on 13 May 1999 and from 3:48 UT to 5:06 UT on 13 May 1999, and was in the morningside high-altitude magnetosheath from 0:10 UT to 3:48 UT on 13 May 1999.

Both Figures 10 and 11 show that, compared with the CEP fluxes, the magnetosheath energetic ion fluxes ($He^{2+}$ and $O^{+}$) were negligible (top panels). In other words, Figures 10 and 11 show a negative energetic ion intensity gradient from the cusp to the neighboring magnetosheath.

The energetic ion intensity in the dayside high-altitude cusp is not only higher than that in the region downstream from the bow shock in the magnetosheath but also higher than that in the upstream region from the bow shock as well. On 11 September 1996 at 22:06–22:30 UT, under normal IMF conditions, GEOTAIL was in the upstream region (9.9 $R_E$, −27.5 $R_E$, −3.5 $R_E$) (in GSE) from the bow shock, where a harder energy spectrum was expected (Anagnostopoulos et al., 1986; Paschalidis et al., 1994), and POLAR was in the high-altitude cusp. Figure 12 compares the $>60$ keV ion flux observed by the GEOTAIL (open squares) with that observed by the POLAR (solid circles) during this period. It shows that the ion flux in the CEP event at 100 keV was more than four orders of magnitudes higher than that in the upstream region, and that the shape of the ion energy spectra in

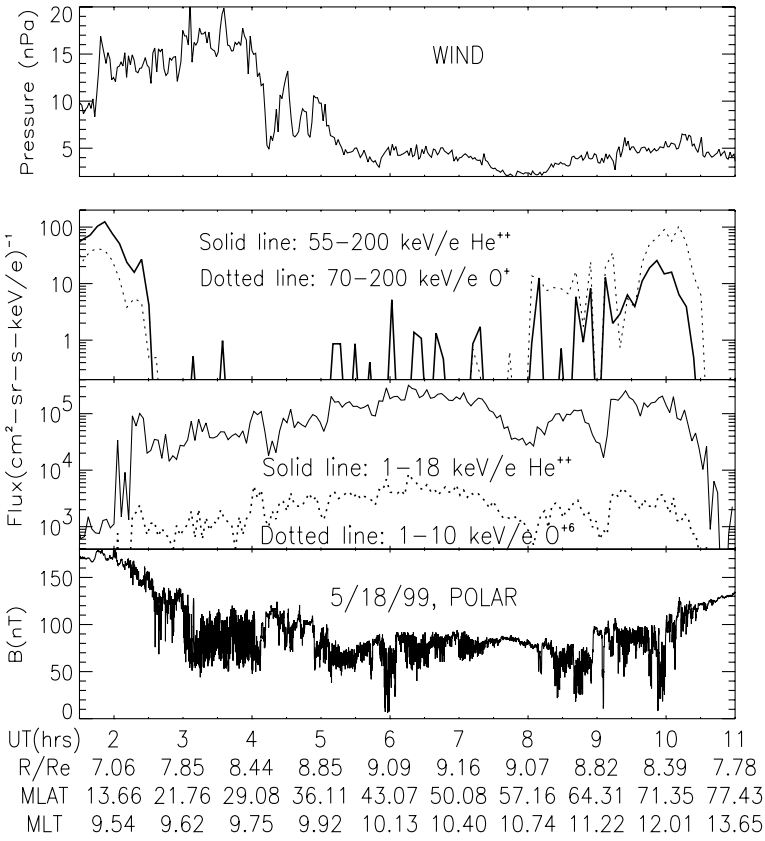


*Figure 10*. POLAR observations of the 70–200 keV/e $O^+$ (dotted line) and the 55–200 keV/e $He^{2+}$ (solid line) fluxes (panel 2 from top), the 1–18 keV/e $He^{2+}$ (solid line) and 1–10 keV/e $O^{6+}$ (dotted line) fluxes (panel 3 from top), and the local magnetic field (bottom panel), together with WIND measurements of the solar wind pressure (top panel) at 1:30–11:00 UT on 18 May 1999. The distance of POLAR from the Earth (in $R_E$), the MLAT and the MLT are shown at the bottom of the figure. Corrections have been made for the solar wind propagation time from WIND to POLAR.

the CEP events was different from that in the upstream region from the bow shock. Other examples have been reported by Chen and Fritz (1999) and Chen et al. (2003), which show that, even if the spacecraft was magnetically connected to the quasi-parallel bow shock, the detected ion flux near the bow shock was significantly lower than that near the cusp.

## 8. Cusp turbulent electric field

Figure 13 plots the CEP event on 6 May 1999. Just like other CEP events, this CEP event was also found in the high-altitude dayside cusps and

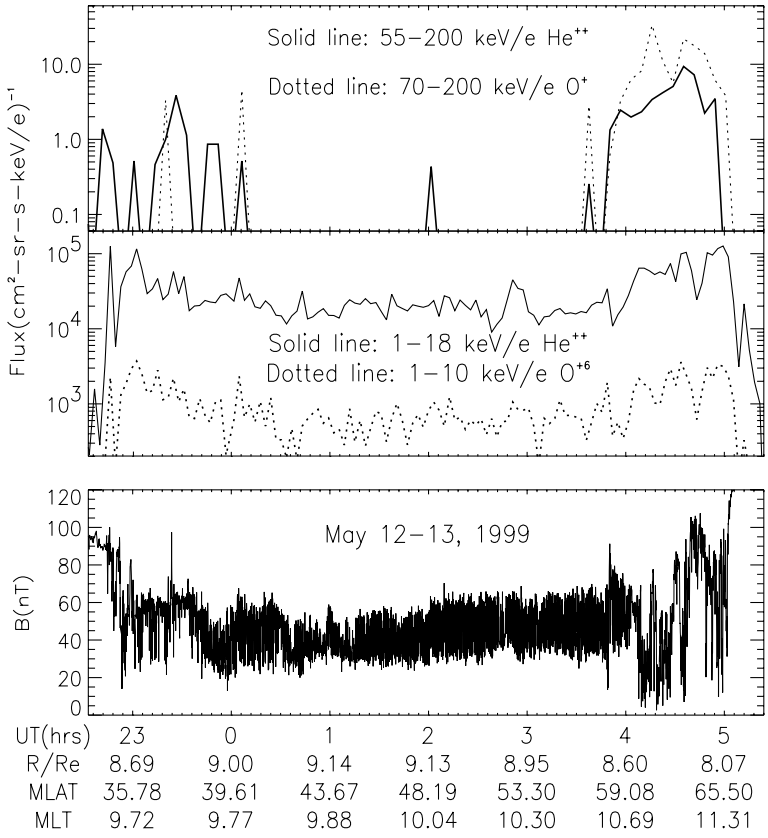


*Figure 11.* POLAR observations of the 70–200 keV/e $O^+$ (dotted line) and the 55–200 keV/e $He^{2+}$ (solid line) fluxes (top panel), the 1–18 keV/e $He^{2+}$ (solid line) and 1–10 keV/e $O^{6+}$ (dotted line) fluxes (middle panel), and the local magnetic field (bottom panel) from 22:30 UT on 12 May 1999 to 5:24 UT on 13 May 1999. The distance of POLAR from the Earth (in $R_E$), the MLAT, and the MLT are shown at the bottom of the figure.

shows three basic features as well: (1) there was a more than one order of magnitude increase of the low-energy solar wind plasma (1–5 keV/e $H^+$ in this case, panel 2 from the top of Figure 13), (2) the energetic ion intensities increased greatly (both energetic oxygen of ionospheric origin and energetic helium of solar wind origin, top panel), and (3) the local magnetic field magnitude decreased, with large fluctuations (bottom panel). Panel 3 of Figure 13 reveals that a turbulent electric field is also present in the high-altitude dayside cusp region. This electric field was measured in the POLAR spin plane, and Figure 13 shows that for this CEP event the local cusp electric field had a maximum amplitude of about 14 mV/m = 14 V/km.

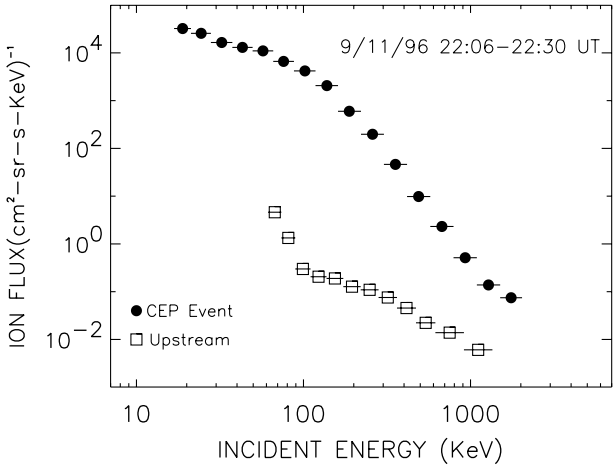


*Figure 12.* Ion energy spectra observed by the GEOTAIL ($9.9R_E$, $-27.5R_E$, $-3.5R_E$) (in GSE) upstream from the bow shock (open squares) and by the POLAR in the cusp (solid circles) at 22:06–22:30 UT on 11 September 1996.

## 9. Discussion

Arising from the high-altitude dayside cusp observations reported herein, a fundamental scientific issue remains. How are the CEPs energized? The similar time-intensity profiles of the cusp energetic oxygen ions of ionospheric origin and helium ions of solar wind origin, shown in Figures 5, 10, 11 and 13, suggest that these two species may be energized by the same mechanism. Since the energetic $O^+$ should not be accelerated by the bow shock, one would expect that the energetic $He^{2+}$ should not also be energized by the bow shock if both species were energized by the same mechanism. Four observational facts about the CEPs demonstrate that bow shock acceleration is not the main source of these CEPs. These are (1) the CEPs have energies up to 10 MeV (Figure 9), (2) the presence of the energetic $O^+$ of ionospheric origin in the high-altitude dayside cusp regions (Figures 5, 10, 11 and 13), (3) the absence of energetic $He^{2+}$ ions in the magnetosheath (Figures 10 and 11), and (4) energetic ion fluxes in the solar wind being orders of magnitude less than those in the cusp (Figures 6 and 12).

As mentioned before, the CEPs are always there in the high-altitude dayside cusp regions and are independent of substorm timing. Recently, Chen and Fritz (1999, 2001) reported three observational facts that (i) no energy dispersion signatures are observed in the CEP events, (ii) the amplitude of the magnetic moment spectrum of the energetic $O^+$ is higher in the cusp than in the peak of the ring current and (iii) the flux (or phase space density) of energetic ($>18$ keV/e) $He^{2+}$ is higher in the cusp than in the peak

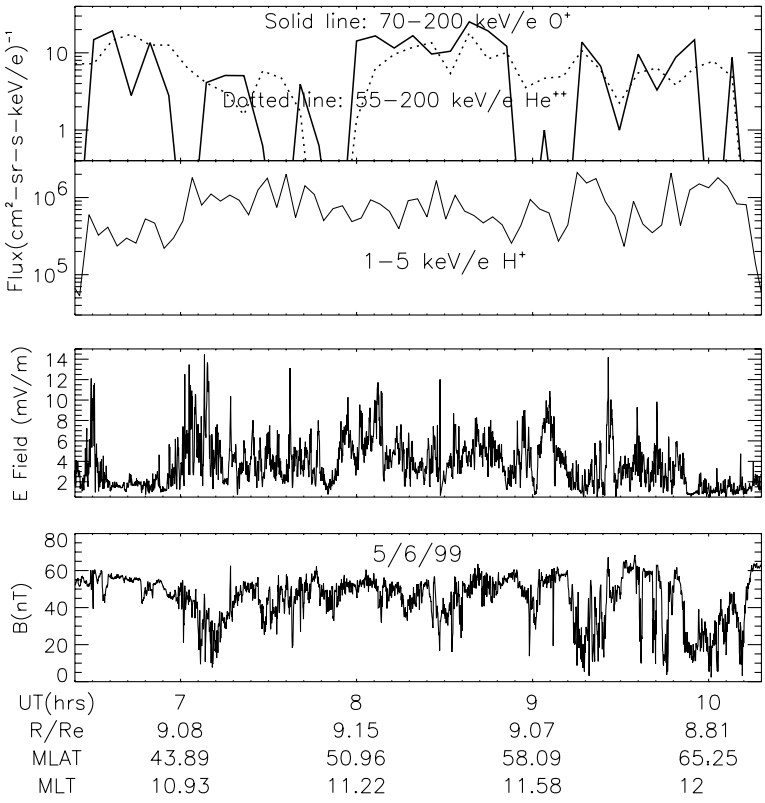


*Figure 13*. The CEP events observed by POLAR on 6 May 1999. The panels show the variation of the 70–200 keV/e $O^+$ (solid line) and the 55–200 keV/e $He^{2+}$ (dotted line) fluxes (top panel), the 1–5 keV/e proton flux (panel 2 from top), the local electric field in spin plane (panel 3), and the local magnetic field (bottom) vs. time, respectively. The distance of POLAR from the Earth (in $R_E$), the MLAT and the MLT are shown at the bottom.

ring current at a given magnetic moment. These facts argue against the substorm (via the ring current) as the main energization source for the CEPs.

One possibility for producing the enhanced CEP fluxes is locally in the cusps. Sheldon et al. (1998) reported that the charged particles could drift on a closed path in the high-altitude dayside cusp without crossing the dawn–dusk plane. In such an orbit, the charged particles are shown mirroring around the minimum magnetic field near the cusp center, and drifting in closed drift shells around the cusp. The cusp has a locally outward magnetic gradient in contrast to the typical inward gradient in the radiation belts. POLAR measurements reveal that the local magnetic field in the CEP events is very turbulent, and the high-altitude cusp is probably a dynamic trapping region that can only temporarily confine charged particles (Chen et al., 1997).

The charged particles could be energized in such a dynamic trapping region by the resonant interactions of these particles with the turbulent ultra-low frequency (ULF) electromagnetic power (Chen and Fritz, 1998). The turbulent magnetic energy will produce the inductive turbulent electric field to interact resonantly with the cusp charged particles – a physical mechanism that converts electromagnetic energy into ion energy.

The proton gyro-frequency in the CEP events has a value of about 1 Hz, while the electron gyro-frequency in the CEP events is about 2000 Hz. Chen et al. (1998) reported that the power density of magnetic plasma waves at 2000 Hz is more than three orders of magnitudes lower than that at 6 Hz. If resonant acceleration is the mechanism that energized the charged particles in the high-altitude dayside cusps, then it predicts that the enhancement of the energetic electron flux should be much less than that of the energetic ion flux, and that the number of electron CEP events should be less than the number of the ion CEP events. These two predictions have been confirmed by both the POLAR (Chen et al., 1998; Chen and Fritz, 2000, 2002b) and the CLUSTER observations (Figures 3 and 4). Local acceleration signatures in the cusps have also reported by other research groups (Kremser et al., 1995; Pfaff et al., 1998; Pissarenko et al., 2001; Yamauchi et al., 2001; Savin et al., 2002).

As shown in panel 3 of Figure 13, the local turbulent electric field for the 6 May 1999 CEP event has a maximum amplitude of about 14 V/km. For discussion purpose, if it is assumed that the cusp perpendicular electric field has a left-hand circular polarization at proton cyclotron frequency with a given amplitude, then the energy per second obtained by a cusp proton will be proportional to the square-root of its perpendicular kinetic energy. For example, if the given amplitude is 10 V/km, a 1 keV proton with 90° pitch angle will obtain about 27 keV within 1 s, while a 10 and 100 keV proton will obtain about 87 and 270 keV within 1 s, respectively. If this is true, then cusp energization is the most efficient acceleration mechanism in geospace, which may explain why the CEPs are observed so suddenly, with no obvious time delay as measured by POLAR (Chen and Fritz, 1999, 2001). Especially when compared with bow shock acceleration, the efficiency of cusp acceleration must be more significant. In order to be accelerated at a quasi-parallel bow shock, the ions need to interact with the bow shock many times and to stay there for an extended period. The higher the energy obtained, the longer the time required. By analyzing 33 diffuse ion events upstream from bow shock, Ipavich et al. (1981) found an inverse velocity dispersion in every event and found that the average delay time between the maximum intensity of 30 keV protons and that of 130 keV protons was about 40 min. Therefore, the ratio of the acceleration efficiency in the cusp to that in the quasi-parallel bow shock is about 2400. A follow-on paper focussing on the local cusp acceleration mechanism is planned.

## 10. Summary

Extremely large diamagnetic cavities have been observed in the dayside high-altitude cusp regions in both northern and southern hemispheres.

These diamagnetic cavities were associated with strong local magnetic field turbulence. Our principal results are the following:

(1) The CDCs are very large, seen in both hemispheres and continuously present, having a size of up to 6 $R_E$.
(2) Associated with these cavities are 20 keV up to 10 MeV ions that are more typical of the trapped ring current and radiation belt populations.
(3) The intensities of the cusp energetic ions were observed to increase by as much as four orders of the magnitude.
(4) The charge state distribution of these CEPs was indicative of their seed populations being a mixture of ionospheric and the solar wind particles.
(5) The energetic ion fluxes in the high-altitude cusp were higher than that in both the neighbouring magnetosheath and upstream from the bow shock.
(6) Turbulent electric fields with an amplitude of about 10 mV/m were also measured in the cusp; a cusp resonant acceleration mechanism is suggested.
(7) The significant increase of the energetic ion fluxes and the large field turbulence in the CDCs suggest that the high-altitude cusp is an extremely dynamic region of geospace.

## Acknowledgements

We are grateful to J.W. Bieber, N.U. Crooker, G.M. Erickson, C.- I. Meng, H.E. Petschek, Z. Pu, C.T. Russell, R.B. Sheldon, G.L. Siscoe, H.E. Spence, and Q.-G. Zong for useful discussions. We want to acknowledge the contribution of B. Laubscher, R. Hedges, R. Vigil, and G. Lujan on the CAMMICE sensor system at the Los Alamos National Laboratory; S. Livi, H. Sommer, and H. Steinmetz at the Max Planck Institute for Aeronomy in Germany; M. Grande and colleagues at the Rutherford Appleton Laboratory in Great Britian; J. Fennell, R. Koga, P. Lew, N. Katz, J. Roeder, and B. Crain on the data processing units at the Aerospace Corporation; and the administrative support and interest provided by D.D. Cobb at the Los Alamos National Laboratory. We thank C.T. Russell for providing the POLAR MFE data, F.S. Mozer for the POLAR EFI data, N. Ness for the ACE MFI data, R. Lepping for the WIND IMF data, K. Ogilvie for the WIND solar wind plasma data, A. Balogh for the CLUSTER FGM data, and D.J. Williams for the GEOTAIL ion data. This reseaxch was supported

by NASA grants NAG5-2578, NAG5-7677, NAG5-7841, NAG5-9562, and NAG5-11397.

## References

Alfvén, H.: 1950, *Cosmical Electrodynamics*, Clarendon Press, Oxford.

Anagnostopoulos, G. C., Sarris,E. T., and Krimigis,S. M.: 1986, 'Magnetospheric Origin of Energetic ($E > 50$ keV) Ions Upstream of the Bow Shock: The October 31, 1977, Event', *J. Geophys. Res.* **91**, 3020–3028.

Antonova, A. E., and Shabansky,V. P.: 1975, 'Particle and Magnetic Field in the Outer Dayside Geomagnetosphere', *Geomangn. Aeron.* **15**(2), 297–302.

Antonova, A. E., Gubar,Yu. I., and Kropotlin,A. P.: 2000, 'Energetic Particle Population in the High-Latitude Geomagnetosphere', *Phys. Chem. Earth (C)* **25**(1–2), 47–50.

Blake, J. B.: 1999, Comment on 'Cusp: A new Acceleration Region of the Magnetosphere' by Jiasheng Chen et al., *Czech. J. Phys.* **49**(4a), 675–677..

Chang, S.-W., Scudder,J. D., Fuselier,S. A., Fennell,J. F., Trattner,K. J., Pickett,J. S., Spence, H. E., Menietti,J. D., Peterson,W. K., Lepping,R. P., and Friedel,R.: 1998, 'Cusp Energetic Ions: A Bow Shock Source', *Geophys. Res. Lett.* **25**, 3729–3732.

Chang, S.-W., Scudder,J. D., Kudela,K., Spence,H. E., Fennell,J. F., Lepping,R. P., Lin,R. P., and Russell,C. T.: 2001, 'MeV Magnetosheath Ions Energized at the Bow Shock', *J. Geophys. Res.* **106**, 19101–19115.

Chang, S.-W., Scudder, J. D., Kudela, K., Spence, H. E., Fennell, J. F., Lepping, R. P., Lin, R. P. and Russell, C. T.: 2003, Reply to Comment on 'MeV Magnetosheath Ions Energized at the Bow Shock' by J. Chen, T. A. Fritz and R. B. Sheldon, *J. Geophys. Res.* **108**(A8), 1312..

Chapman, S., and Ferraro,V. C. A.: 1931, 'A New Theory of Magnetic Storms', *J. Geophys. Res.* **36**, 171 .

Chen, J., and Fritz,T. A.: 1998, 'Correlation of Cusp MeV Helium with Turbulent ULF Power Spectra and its Implications', *Geophys. Res. Lett.* **25**, 4113–4116.

Chen, J., and Fritz,T. A.: 1999, 'May 4, 1998 Storm: Observations of Energetic Ion Composition by POLAR', *Geophys. Res. Lett.* **26**, 2921–2924.

Chen, J., and Fritz,T. A.: 2000, 'Origins of Energetic Ions in CEP Events and their Implications', *Int. J. Geomagn. Aeron.* **2**, 31–44.

Chen, J., and Fritz,T. A.: 2001, 'Energetic Oxygen Ions of Ionospheric Origin Observed in the Cusp', *Geophys. Res. Lett.* **28**, 1459–1462.

Chen, J., and Fritz,T. A.: 2002a, 'Multiple Spacecraft Observations of Energetic Ions during a Major Geomagnetic Storm', *Adv. Space Res.* **30**(7), 1749–1756.

Chen, J. and Fritz, T. A.: 2002b, 'The Global Significance of the CEP Events', in H. N. Wang and R. L. Xu (eds.), *Solar-Terrestrial Magnetic Activity and Space Environment*, COSPAR Colloquia Series 14, pp. 239–249..

Chen, J., Fritz, T. A. and Sheldon, R. B.: 2003, Comment on 'MeV Magnetosheath Ions Energized at the Bow Shock' by S.-W. Chang et al., *J. Geophys. Res.* **108**(A8), 1311..

Chen, J., Fritz,T. A., Sheldon,R. B., Spence,H. E., Spjeldvik,W. N., Fennell,J. F., and Livi,S.: 1997, 'A New, Temporarily Confined Population in the Polar Cap During the August 27, 1996 Geomagnetic Field Distortion Period', *Geophys. Res. Lett.* **24**, 1447–1450.

Chen, J., Fritz,T. A., Sheldon,R. B., Spence,H. E., Spjeldvik,W. N., Fennell,J. F., Livi,S., Russell, C. T., Pickett,J. S., and Gurnett,D. A.: 1998, 'Cusp Energetic Particle Events: Implications for a Major Acceleration Region of the Magnetosphere', *J. Geophys. Res.* **103**, 69–78.

Crooker, N. U.: 1977, 'The Magnetospheric Boundary Layers: A Geometrically Explicit Model', *J. Geophys. Res.* **82**, 3629–3633.

Crooker, N. U.: 1979, 'Dayside Merging and Cusp Geometry', *J. Geophys. Res.* **84**, 951–959.

Crooker, N. U., Lyon,J. G., and Fedder,J. A.: 1998, 'MHD Model Merging with IMF By: Lobe Cells, Sunward Polar Cap Convection, and Overdraped Lobes', *J. Geophys. Res.* **103**, 9143–9152.

Delcourt, D. C., and Sauvaud,J.-A.: 1999, 'Populating of the Cusp and Boundary Layers by Energetic (Hundreds of keV) Equatorial Particles', *J. Geophys. Res.* **104**, 22635 .

Eccles, A. A., and Fritz,T. A.: 2002, 'Energetic Particle Observations at the Subsolar Magnetopause', *Ann. Geophys.* **20**, 445–460.

Fritz, T. A., and Chen,J.: 1999a, 'The cusp as a source of magnetospheric particles', *Radiat. Measurement* **30**(5), 599–608.

Fritz, T. A., and Chen,J.: 1999b, 'Reply', *Geophys. Res. Lett.* **26**, 1363–1364.

Fritz, T. A., Chen,J., and Sheldon,R. B.: 2000, 'The Role of the Cusp as a Source for Magnetospheric Particles: A New Paradigm?', *Adv. Space Res.* **25**(7–8), 1445–1457.

Fritz, T. A., Chen,J., Sheldon,R. B., Spence,H. E., Fennell,J. F., Livi,S., Russell,C. T., and Pickett, J. S.: 1999a, 'Cusp Energetic Particle Events Measured by POLAR Spacecraft', *Phys. Chem. Earth (C)* **24**(1–3), 135–140.

Fritz, T. A., Karra,M., Finkerneyer,B., and Chen,J.: 1999b, 'Statistical Studies with Polar of Energetic Particles near the Dayside Cusp', *EOS Trans. AGU* **80**(46), F862 .

Fritz, T. A., Chen,J., and Siscoe,G. L.: 2003a, 'Energetic Ions, Large Diamagnetic Cavities, and Chapman-Ferraro Cusp', *J. Geophys. Res.* **108**(Al), 1028–1036.

Fritz, T. A., Alothman,M., Bhattacharjya,J., Matthews,D., and Chen,J.: 2003b, 'Butterfly Pitch Angle Distributions Observed by ISEE-1', *Planet. Space Sci.* **51**, 205–219.

Fritz, T. A., Zurbuchen,T. H., Gloeckler,G., Hefti,S., and Chen,J.: 2003c, 'The Use of Iron Charge State Changes as a Tracer for Solar Wind Entry and Energization within the Magnetosphere', *Ann. Geophys.* **21**, 2155–2164.

Fung, S. F., Eastman,T. E., Boardsen,S. A., and Chen,S.-H.: 1997, 'High-Altitude Cusp Positions Sampled by the Hawkeye Satellite', *Phys. Chem. Earth* **22**, 653–662.

Gloeckler, G., : 1986, 'Solar Wind Carbon, Nitrogen and Oxygen Abundances Measured in the Earth's Magnetosheath with AMPTE/CCE', *Geophys. Res. Lett.* **13**, 793–796.

Gloeckler, G., Hefti,S., Zurbuchen,T. H., Schwadron,N. A., Fisk,L. A., Ipavich,F. M., Geiss, J., Bochsler,P., and Wimmer,R.: 1999, 'Unusual Composition of the Solar Wind in the 2–3 May 1998 CME Observed With SWICS on ACE', *Geophys. Res. Lett.* **26**, 157–160.

Ipavich, F. M., Galvin,A. B., Gloeckler,G., Scholer,M., and Hovestadt,D.: 1981, 'A Statistical Survey of Ions Observed Upstream of the Earth's Bow Shock: Energy Spectra, Composition, and Spatial Variation', *J. Geophys. Res.* **86**, 4337–4342.

Kremser, G., Woch,J., Mursula,K., Tanskanen,P., Wilken,B., and Lundin,R.: 1995, 'Origin of Energetic Ions in the Polar Cusp Inferred from Ion Composition Measurements by the Viking Satellite', *Ann. Geophys.* **13**, 595–607.

Marklund, G. T., Blomberg,L. G., Fäthammar,C.-G., Erlandson,R. E., and Potemra,T. A.: 1990, 'Signatures of the High-Altitude Polar Cusp and Dayside Auroral Regions as seen by the Viking Electric Field Experiment', *J. Geophys. Res.* **95**, 5767–5780.

Maynard, N. C., Savin,S., Erickson,G. M., Kawano,H., Němeček,Z., Peterson,W. K., šafránoková, J., Sandahl,I., Scudder,J. D., Siscoe,G. L., Sonnerup,B. U. Ö., Weimer,D. R., White,W. W., and Wilson,G. R.: 2001, 'Observation of the Magnetospheric "Sash" and its Implications Relative to Solar-Wind/Magnetospheric Coupling: A Multisatellite Event Analysis', *J. Geophys. Res.* **106**, 6097–6122.

Mead, G. D.: 1964, 'Deformation of Geomagnetic Field by the Solar Wind', *J. Geophys. Res.* **69**, 1181–1195.

Meng, C.-I.: 1982, 'Latitudinal Variation of the Polar Cusp during a Geomagnetic Storm', *Geophys. Res. Lett.* **9**, 60–63.

Newell, P. T., and Meng,C.-I.: 1987, 'Cusp Width and $B_z$: Observations and Conceptual Model', *J. Geophys. Res.* **92**, 13673–13678.

Newell, P. T., and Meng,C.-I.: 1991, 'Ion Acceleration at the Equatorward Edge of the Cusp: Low Altitude Observations of Patchy Merging', *Geophys. Res. Lett.* **18**, 1829–1832.

Paschalidis, N. P., Sarris,E. T., Krimigis,S. M., McEntire,R. W., Levine,M. D., Daglis,I. A., and Anagnostopoulos,G. C.: 1994, 'Energetic Ion Distributions on Both Sides of the Earth's Magnetopause', *J. Geophys. Res.* **99**, 8687–8703.

Perry, C. H., Grande,M., Zurbuchen,T. H., Hefti,S., Gloeckler,G., Fennell,J. F., Wilken,B., and Ritz,T. A.: 2000, 'Use of Fe Charge States as a Tracer for Solar Wind Entry to the Magnetosphere', *Geophys. Res. Lett.* **27**, 2441–2444.

Pfaff, R. F., Clemmons,J. H., Carlson,C. W., Ergun,R. E., McFadden,J. P., Mozer,F. S., Temerin, M., and Klumpar,D. M.: 1998, 'Initial FAST Satellite Observations of Acceleration Processes in the Cusp', *Geophys. Res. Lett.* **25**, 2037–2040.

Pissarenko, N. E., Kirpichev,I. P., Lutsenko,V. N., Savin,S. P., Budnick,E.Yu., Moszhukina, A. R., Morozova,E. I., Antonova,A. E., and Sandahl,I.: 2001, 'Cusp Energetic Particles Observed by INTERBALL-Tail Probe in 1996', *Phys. Chem. Earth (C)* **26**(1–3), 241–245.

Reiff, P. H.: 1979, 'Low-Altitude Signatures of the Boundary Layers', in *Magnetospheric Boundary Layers*, pp. 167–173, Eur. Space Agency Spec. Publ., ESA SP-148..

Reiff, P. H., Hill,T. W., and Burch,J. L.: 1977, 'Solar Wind Plasma Injection at the Dayside Magnetospheric Cusp', *J. Geophys. Res.* **82**, 479–491.

Roederer, J. G.: 1970, *Dynamics of Geomagnetically Trapped Radiation*, Springer, New York.

Savin, S., Blecki,J., Pissarenko,N., Lutsenko,V., Kirpichev,I., Budnik,E., Borod-kova,N., Nozdrachev, M., Zelenyi,L., Romanov,V., Sandahl,I., Sauvaud,J.-A., Buechner,J., Nikutowski, B., Gustafsson,G., Stasiewicz,K., and Korepanov,V.: 2002, 'Accelerated Particles from Turbulent Boundary Layer', *Adv. Space Res.* **30**(7), 1723–1730.

Shabansky, V. P.: 1971, 'Some Processes in the Magnetosphere', *Space Sci. Rev.* **12**, 299–418.

Shabansky, V. P., and Antonova,A. E.: 1968, 'Topology of Particle Drift Shells in the Earth's Magnetosphere', *Geomangn. Aeron., Engl. Transl.* **8**, 844 .

Sheldon, R. B., Chen, J. and Fritz, T. A.: 2003, Comment on 'Origins of Energetic Ions in the Cusp' by K. J.Trattner et al., *J. Geophys. Res.* **108**(A7), 1302..

Sheldon, R. B., Spence,H. E., Sullivan,J. D., Fritz,T. A., and Chen,J.: 1998, 'The Discovery of Trapped Energetic Electrons in the Outer Cusp', *Geophys. Res. Lett.* **25**, 1825–1828.

Trattner, K. J., Fuselier, S. A., Peterson, W. K. Chang, S.-W.: 1999, Comment on 'Correlation of Cusp MeV Helium with Turbulent ULF Power Spectra and its Implications' by J. Chen and T. A. Feitz, *Geophys. Res. Lett.* **26**, 1361..

Trattner, K. J., Fuselies,S. A., Peterson,W. K., S.-W.,Chang, Riedel,R., and Aellig,M. R.: 2001, 'Origins of Energetic Ions in the Cusp', *Geophys. J. Res.* **106**, 5967–5976.

Trattner, K. J., Fuselies, S. A., Peterson, W. K., Chang, S.-W., Friedel, R. and Aellig, M. R.: 2003, Reply to comment on 'Origins of Energetic Ions in the Cusp' by R. Sheldon, I. Chen and T. A. Fritz *J. Geophys. Res.* **108**(A7), 1303..

Tsyganenko, N. A., and Russell,C. T.: 1999, 'Magnetic Signatures of the Distant Polar Cusps: Observations by Polar and Quantitative Modeling', *J. Geophys. Res.* **104**, 24939–24955.

Van Allen, J. A., and Frank,L. A.: 1959, 'Radiation Around the Earth to a Radial Distance of 107,400 km', *Nature* **183**, 430 .

White, W. W., Siscoe,G. L., Erickson,G. M., Kaymaz,Z., Maynard,N. C., Siebert,K. D., Sonnerup, B. U. Ö., and Weimer,D. R.: 1998, 'The Magnetospheric Sash and the Cross-Tail S', *Geophys. Res. Lett.* **25**, 1605–1608.

Williams, D. J.: 1983, 'The Earth's Ring Current: Causes, Generation, and Decay', *Space Sci. Rev.* **34**, 223–234.

Yamauchi, M., Andersson,L., Lindqvist,P.-A., Ohtani,S., Clemmons,J., Wahlund,J.-E., Eliasson, L., and Lundin,R.: 2001, 'Acceleration Signatures in the Dayside Boundary Layer and the Cusp', *Phys. Chem. Earth (C)* **26**(1–3), 195–200.

Yoshida, S., Ludwig,G. H., and VanAllen, J. A.: 1960, 'Distribution of Trapped Radiation in the Geomagnetic Field', *J. Geophys. Res.* **65**, 807.

Surveys in Geophysics (2005) 26: 95–133
DOI 10.1007/s10712-005-1874-4 © Springer 2005

# MAGNETOSHEATH INTERACTION WITH THE HIGH LATITUDE MAGNETOPAUSE

S. SAVIN[1], A. SKALSKY[1], L. ZELENYI[1], L. AVANOV[1], N. BORODKOVA[1], S. KLIMOV[1], V. LUTSENKO[1], E. PANOV[1], S. ROMANOV[1], V. SMIRNOV[1], YU. YERMOLAEV[1], P. SONG[2], E. AMATA[3], G. CONSOLINI[3], T. A. FRITZ[4], J. BUECHNER[5], B. NIKUTOWSKI[5], J. BLECKI[6], C. FARRUGIA[7], N. MAYNARD[8], J. PICKETT[9], J. A. SAUVAUD[10], J. L. RAUCH[11], J. G. TROTIGNON[11], Y. KHOTYAINTSEV[12] and K. STASIEWICZ[12]

[1]*Space Research Institute, Profsoyuznaya 84/32, Moscow, 117810, Russia*
*E-mail: ssavin@iki.rssi.ru;*
[2]*University of Massachusetts, Lowell, MA, USA;*
[3]*Interplanetary Space Physics Institute, CNR, Roma, Italy;*
[4]*Boston University, Boston, MA, USA;*
[5]*Max-Planck Inst, Aeronomie, Katlenburg-Lindau, Germany;*
[6]*Space Research Center, Warsaw, Poland;*
[7]*University of New Hampshire, Durham, NH, USA;*
[8]*Mission Research Corporation, Nashua, NH, USA;*
[9]*University of Iowa, Iowa City, IA, USA;*
[10]*CESR, Toulouse, France;*
[11]*LPCE, Orleans, France;*
[12]*IRF-U, Uppsala, Sweden*

(Received 9 February 2003; Accepted 30 April 2004)

**Abstract.** We present both statistical and case studies of magnetosheath interaction with the high-latitude magnetopause on the basis of Interball-1 and other ISTP spacecraft data. We discuss those data along with recently published results on the topology of cusp-magnetosheath transition and the roles of nonlinear disturbances in mass and energy transfer across the high-latitude magnetopause. For sunward dipole tilts, a cusp throat is magnetically open for direct interaction with the incident flow that results in the creation of a turbulent boundary layer (TBL) over an indented magnetopause and downstream of the cusp. For antisunward tilts, the cusp throat is closed by a smooth magnetopause; demagnetized 'plasma balls' (with scale ~ few $R_E$, an occurrence rate of ~25% and trapped energetic particles) present a major magnetosheath plasma channel just inside the cusp. The flow interacts with the 'plasma balls' via reflected waves, which trigger a chaotization of up to 40% of the upstream kinetic energy. These waves propagate upstream of the TBL and initiate amplification of the existing magnetosheath waves and their cascade-like decays during downstream passage throughout the TBL. The most striking feature of the nonlinear interaction is the appearance of magnetosonic jets, accelerated up to an Alfvenic Mach number of 3. The characteristic impulsive local momentum loss is followed by decelerated Alfvenic flows and modulated by the TBL waves; momentum balance is conserved only on time scales of the Alfvenic flows ($1/f_A$~12 min). Wave trains at $f_A$~1.3 mHz are capable of synchronizing interactions throughout the outer and inner boundary layers. The sonic/Alfvenic flows, bounded by current sheets, control the TBL

spectral shape and result in non-Gaussian statistical characteristics of the disturbances, indicating the fluctuation intermittency. We suggest that the multi-scale TBL processes play at least a comparable role to that of macro-reconnection (remote from or in the cusp) in solar wind energy transformation and population of the magnetosphere by the magnetosheath plasma. Secondary micro-reconnection constitutes a necessary chain at the small-scale (~ion gyroradius) edge of the TBL cascades. The thick TBL transforms the flow energy, including deceleration and heating of the flow in the open throat, 'plasma ball' and the region downstream of the cusp.

**Keywords:** boundary layer, cusp, magnetopause, magnetosheath

**Abbreviations:** BL – Boundary Layer; FOV – Field Of View; MP – Magnetopause; GSM – Geocentric Solar Magnetic; MSH – Magnetosheath; SW – Solar Wind; ULF – Ultra-Low Frequency; UT – Universal Time; MLT – Magnetic Local Time; HEOS – Highly Eccentric Orbiting Satellite; ISEE – International Sun-Earth Explorers; GDCF – Gas Dynamic Convected Field model; FOV – Field Of View; GSE – Geocentric Solar Ecliptic

## 1. Introduction

Early single spacecraft observations with Heos-2 and later Prognoz-7, 8, 10 have shown that the magnetopause (MP) position and magnetosheath plasma flow structures are quite variable near the cusp, a magnetospheric region that is crucial for magnetosheath plasma entry (Haerendel and Paschmann, 1975; Paschmann et al., 1976; Klimov et al., 1986; Savin, 1994). Haerendel (1978) first introduced the turbulent boundary layer (TBL) to cusp physics in a discussion on the interaction of the magnetosheath flow with the magnetopause at the flank of the tail lobe. We reproduce his TBL sketch in Figure 1a: a laminar hydrodynamic flow interacts with an obstacle by generation of a TBL both in front of the obstacle (marked by "1") and behind it (marked by "2"). The zone "1" corresponds to the funnel-shaped cusp throat in Figure 1b; the obstacle is presented by uprising magnetic field tubes at the tailward cusp wall. The downstream zone "2" has been poorly studied (see Savin et al., 2004, and references therein). Because of differences in characteristics, researchers have divided the high altitude cusp into a number of layers and regions. Since full agreement in terminology is not yet achieved, we provide our definitions of the regions discussed in this paper. These regions, as shown in Figure 1b, are the outer and inner cusps, the open throat (OT) of the outer cusp, and the turbulent boundary layer. We will demonstrate, however, that the interaction pattern in Figure 1 should be further modified for winter cusp crossings.

In Figure 1b, the OT (slant-line shaded region) is outside the MP, the outer cusp (gray) is just inside the MP, and the inner cusp (black) is deeper in the magnetosphere. We identify the MP (inner white line) as the innermost current sheet where the magnetic field turns from Earth-controlled to magnetosheath-controlled (Haerendel and Paschmann, 1975). The outer cusp (OC) is a region with three different particle populations: newly injected

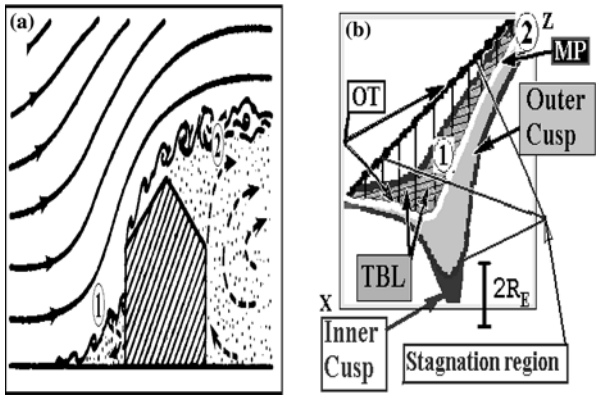


*Figure 1.* (a) Generation of a turbulent boundary layer in the process of interaction of hydrodynamic flow with an obstacle (from Haerendel, 1978). "1" – marks open cusp throat, "2" – stands for high latitude boundary layer downstream of the cusp. (b) Sketch for MSH/cusp interface in the noon-midnight plane from (Savin et al., 2002a). The boundaries and subregions are described in the text.

MSH ions, MSH ions reflected from the ionosphere, and quasi-perpendicular ions trapped in the local magnetic field minimum near the cusp (Savin et al., 1998b; Sandahl et al., 2002). There are also electrons accelerated along the field lines. The newly injected and quasi-perpendicular ions dominate over those that are reflected. This is one of the characteristics distinguishing the outer cusp from the inner cusp and from the distant mantle. The outer cusp is also characterized by moderate magnetic noise, while in the inner cusp (IC) there is a similar type of noise observed primarily only at the boundaries (Pottelette at al., 1990). The outer cusp consists of the entry layer and the portion of the plasma mantle adjoining the entry layer (Paschmann et al., 1976). According to the work of Yamauchi and Lundin (1997) the entry layer and mantle that are parts of the outer cusp form one continuous region.

At the cusp the magnetopause can be indented. This indentation was first predicted by Spreiter and Briggs (1962) and then detected by HEOS-2 (Paschmann et al., 1976), ISEE (Petrinec and Russell, 1995), and Hawkeye-1 (S. Chen et al., 1997). Interball-1 early statistics show that the indentation is on the average about 2 $R_E$ deep (Savin et al., 1998b). We call this part of the exterior cusp the OT. The plasma in the OT is highly disturbed and/or stagnant MSH plasma. The turbulent boundary layer (TBL) is a region dominated by irregular magnetic fields and plasma flows. It is located just outside and/or at the near cusp magnetopause and has recently been found to be a permanent feature (Savin et al., 1997, 1998b, 2002a; Sandahl et al., 2002). Here the energy density of the ultra low frequency (ULF) fluctuations is comparable to the ion kinetic, thermal, and DC magnetic field densities. The ULF power is usually several times larger than that in the MSH, and one

or two orders of magnitude larger than that inside the magnetopause. As recent studies conclude (see, e.g., Belmont and Rezeau, 2001, and references therein), the strong ULF fluctuations that occur just outside of or at the magnetopause can independently result in micro-reconnection and local plasma penetration all along the magnetopause surface, even without the presence of quasi-stationary global reconnection. Examples of highly turbulent magnetic and electric fields in the exterior cusp have been reported by Paschmann et al. (1976) from Heos-2, by Klimov et al. (1986) from Prognoz-10, by Savin (1994) and Blecki et al. (1998) from Prognoz-8 and by S. Chen et al. (1997) from Hawkeye-1 data.

The main goal of this paper is to survey achievements in this area and explore solutions to the problems associated with the TBL and exterior cusp physics in the Interball era. The recent baseline case studies are described in detail in Savin et al. (2001, 2002a, b, 2004). An Interball-Polar case on 19 June 1998 is utilized to display the characteristic TBL features. It demonstrates the asymmetry of boundary layers for positive (sunward) Earth magnetic dipole tilts in summer and that of the negative (anti-sunward) tilts in winter. We reproduce the most interesting results from the previous studies and analyze detailed dynamics of the ion energy and of Poynting flux to clarify the pattern of nonlinear interactions in the upstream TBL. The wave packets, going from MP upstream in a subsonic MSH flow, occur to stimulate partial randomization of the flow far in front of the MP, while the SW driver plays a minor role. The interaction with the upstream going waves launches downstream-accelerated jets at about sonic speed. The jets break up the homogeneous equilibrium streamlining by carrying down-flow up to half of the flow momentum density. That signifies the cascade-like non-linear energy transformation in the TBL, proposed by Savin et al. (2001).

We present, for the first time, a full statistical review of the high level ULF magnetic turbulence (i.e. of the TBL) from the Interball-1 data, concentrating on the MP asymmetry for the summer and winter hemispheres. The permanent plasma heating in the TBL is regarded as a result of transformation of MSH flow energy into the random and thermal energies in the process of the MSH flow interaction with the outer cusp throat. We exhibit de-magnetized large-scale 'plasma balls' inside the winter MP and study their statistics versus that of stagnant MSH plasma outside the NP in summer. We also present 3D maps of the TBL dependence on the fluctuation power and on the dipole tilt and study the 'plasma ball' occurrence that depends on the tilt, magnetic shear and interplanetary magnetic field. Finally, we discuss the presented and published Interball-1 data in relation to the MSH plasma penetration and acceleration both due to plasma percolation and turbulent heating and due to multi-scale reconnection of anti-parallel magnetic fields. We address the practically unexplored interaction of MSH flow with stagnant high-beta 'plasma ball' via the highly super-Alfvenic jets and decelerated

Alfven flows embedded into the coherent pattern of cascade-like interactions in the upstream TBL.

## 2. Turbulent boundary layer and "plasma ball" on 19 June 1998

Data from 19 June 1998 (Figure 2) illustrate the recent findings at the MSH/cusp interface. Geotail provided high-resolution SW magnetic field and synchronization with WIND plasma data, Polar traced the northern (summer) stagnation region, and Interball-1 entered the southern cusp from the MSH. The Gas Dynamic Convection model (GDCF), which is described in detail by Song et al. (1999a, b) and Dubinin et al. (2002), links the multipoint observations. While several recent papers describe some features of this event (Savin et al., 2002a, b, 2004), we report new, valuable findings in the interaction pattern.

### 2.1. Inbound magnetopause crossing

We present a sketch in Figure 3 (turned upside down for easy comparison with Figure 1b) to provide a guide for a different topology on 19 June 1998 compared with that in Figure 1. The southern hemisphere MP here has no indentation. The disturbances of the ion flow in the XZ plane ('outer BL') start in the upstream (relative to MP) flow and result in the appearance of the accelerated jets first at ~09 UT and then in front of the MP in the tailward stream (upstream TBL). The criteria fulfilling the definition of the TBL (see Section 3) are marked by gray bars on the bottom.

In the TBL map in Figure 2.A1 this case appears as a 20 min interval, centered at ~09 UT, with the interval at 09:20–10:40 UT colored according to the Df magnitude (black curve in Figure 2.A6i, see discussion below). The MP transition is thick and imbedded into the TBL, which terminates in a 'plasma ball' (PB, see Savin et al., 2002a). The PB is a high-beta (in this case up to 15) large-scale (few $R_E$) sub-region of the OC (Figure 3). As Savin et al. (1998b) and Kirpichev et al. (1999) have shown, the general OC (and PB) feature trapped MSH-origin ions – are often seen in low-beta and small-scale regions (i.e. the PB occurrence is much smaller than that of the OC, see Section 4). In the PB the magnetic field is reduced, marking the boundary between the dayside and mantle/polar cap magnetic field lines. The PB average position should tend to shift towards the anti-parallel magnetic field through the MP that corresponds to the place of minimal $B^2/2\mu_0$, predicted by the fields' vector sum (cf. Spreiter and Briggs, 1962). We will refer hereafter to the OT only in the case of the configuration of Figure 1b, which seems to be characteristic for positive tilts (see Figure 2.A2–2.A4 and related discussions in Sections 3 and 4).

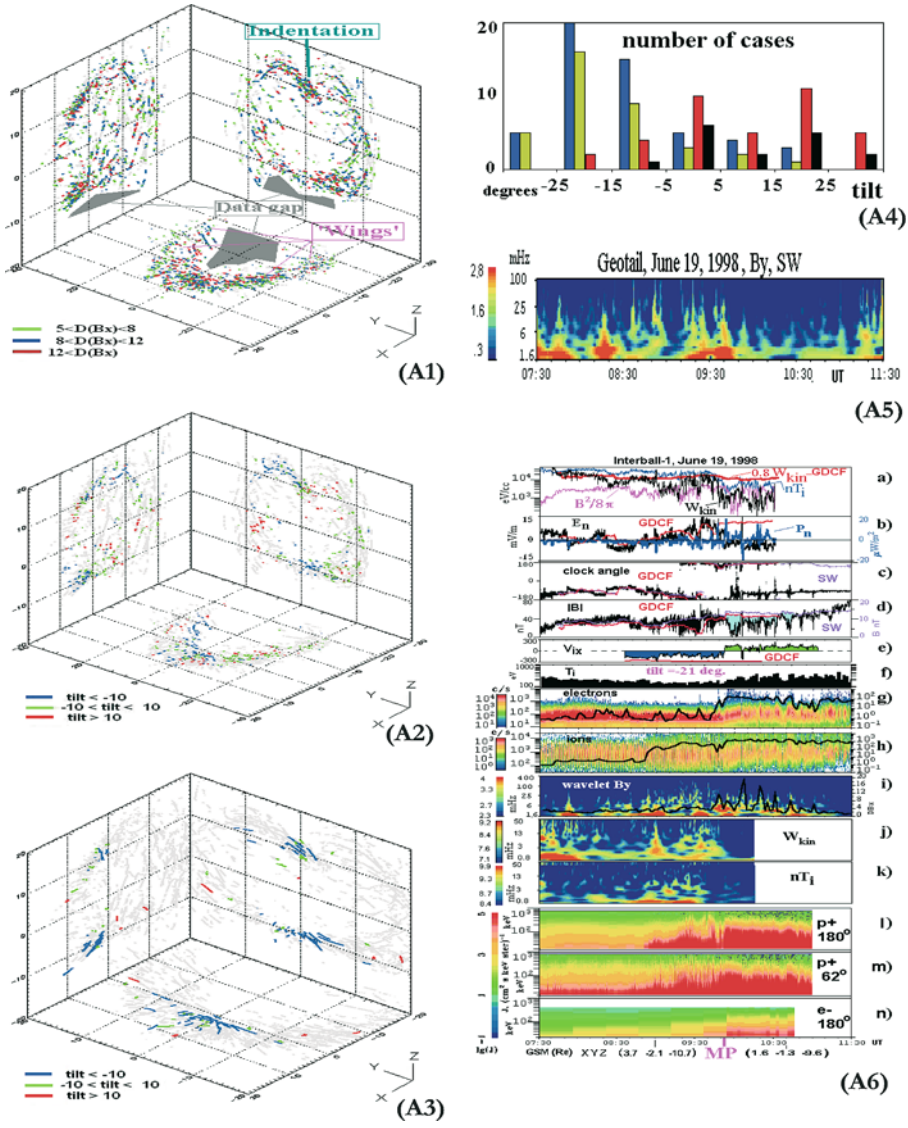


*Figure 2.* (A1) TBL level map ($nT$) in 3 GSM planes (gray color – D($B_x$) > 3 $nT$). (A2) TBL tilt dependence for D($B_x$) > 8 $nT$. (A3) PB tilt (degrees) dependence (gray color – TBL). (A4) Tilt dependence of PB (blue, green) and open OT. (A5) SW $B_y$ spectrogram (Geotail) on 19 June 1998. (A6) TBL and PB on 19 June 1998. (a) energy densities; (b) normal electric field and Poynting vector; (c) magnetic clock angle; (d) $|B|$; (e) ion $V_x$ velocity; (f) ion temperature; (g) electron spectrogram and intensity ( > 30 keV); (h) ion spectrogram and intensity ( > 30 keV); (i) magnetic $B_y$ – spectrogram and $B_x$ -variation; (j) ion kinetic energy spectrogram; (k) ion thermal energy spectrogram; (l–n) energetic ions (FOV 180 and 62 deg. from Sun) and electrons (FOV 180°. from Sun).

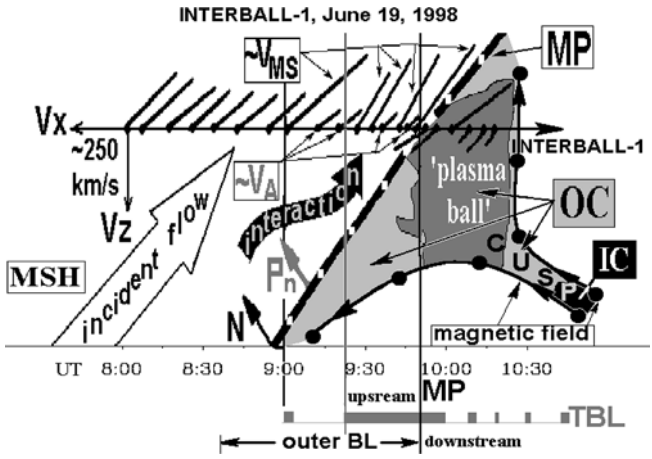


*Figure 3.* Sketch for the interaction pattern of MSH plasma flow with outer cusp on 19 June 1998; spacecraft orbit (Interball-1 moves from left to right), with characteristic ion velocity vectors in the *XZ* GSE plane; $\vec{N}$- normal to MP in GSE frame ~(0.7, 0.07, −0.71); $P_n$-projection of Poynting vector on $\vec{N}$; $V_{MS}$, $V_A$-magnetosonic and Alfven speeds, see also Figure 4; MP is shown by the thick broken curve; OC, IC – see Figure 1 and related discussions.

In Figure 3 the cusp throat is closed by the smooth MP at a larger distance, when compared with Figure 1b. A principal problem is distinguishing dynamic interactions of the SW with the MP from local disturbances. For this purpose in Figure 2.A5 a wavelet spectrogram (see details in Savin et al., 2002b) of the IMF GSE $B_y$-component from Geotail is shown for 1.6–100 mHz range (octave-based frequency scale in Hz and color scale for logarithrm of the wave power in $[nT^2/\text{Hz}]$ are shown on the left side). We compare the Geotail data with those of Interball-1, given in panel i in Figure 2.A6, where a black line represents the $B_x$-variation for 2-min intervals from 4 Hz-sampling of the magnetic field (Df, scale on right side in $[nT/\text{Hz}^{1/2}]$). The MP crossing (from MSH to OC, see Figure 3) is marked at the bottom of Figure 2.A6, along with the Interball-1 position in the GSM frame at two points. In panel a of Figure 2.A6 we display energy densities in eV/cc; ion thermal $nT_i$ (n and $T_i$-ion density and temperature) – blue line; DC magnetic $B^2/2\mu_0$-violet line; kinetic energy $W_{\text{kin}}$-black line; the red curve presents GDCF predictions for $W_{\text{kin}}$, multiplied by a factor of 0.8 to adjust the measured value in the middle MSH (following Savin et al., 2004). The time lag is chosen for best fit at 08:40–09:50 UT, while it is certainly different for 07:30–08:30 UT (see Dubinin et al. (2002) and Figure 4 below).

Panel b of Figure 2.A5 shows the electric field ($E_n$, black line), calculated from the vector product of ion velocity and magnetic field, along the MP normal (N ~ (0.7, 0.07, −0.71) in the GSE frame (see Savin et al. 2002a, b), and that of the Poynting vector $P_n$ at 5–50 mHz (blue line), also in the N

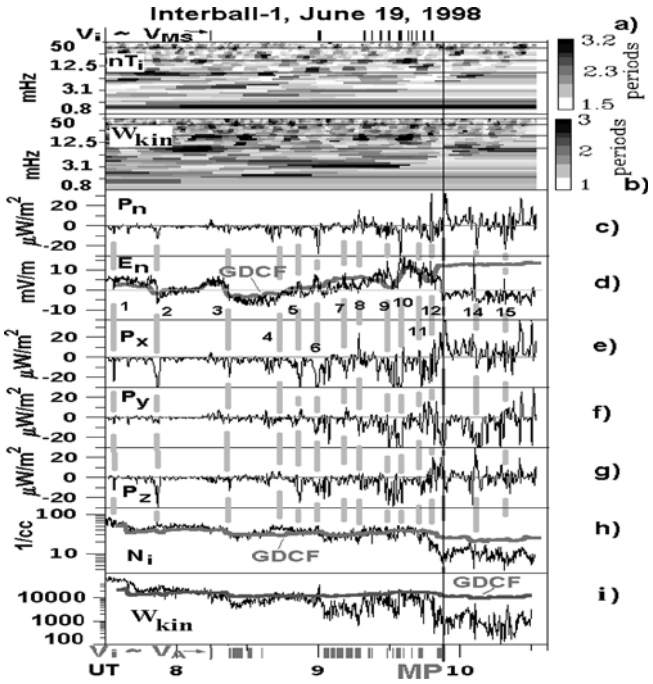


*Figure 4.* Tracing of disturbances in TBL on 19 June 1998; black vertical line – approximate MP crossing. (a) and (b) wavelet correlation time for ion thermal and kinetic energy densities, left – octave frequency scale in mHz, right – gray scale in periods of coherent signal at every frequency, black horizontal lines – 1st, 2nd and 4th spacecraft spin harmonics; (c) Poynting flux along MP normal ($P_n$, see Figure 2.A6 and related discussions) for 2–50 mHz; (d) electric field along MP normal and its GDCF prediction (thick gray line), the time lag at 08:30–10:30 UT is the same as in Figure 2.A6, the lag at 07:30–08:30 UT is 7.5 min less (numbers mark events discussed in the text); (e–g) Poynting flux along GSE $X$, $Y$ and $Z$ for 2–50 mHz; (h) ion density and its GDCF prediction (thick gray line). Top – black bars mark flows with ~ magnetosonic speed $V_{MS}$, bottom – gray bars mark flows with ~ Alfven speed $V_A$ .

direction. The GDCF proxy for $E_n$ is represented by the red color, and shifted by an extra 1 mV/m for better adjustment with the experimental data. In panel c the magnetic field clock angle is presented in degrees: the black line is for the Interball-1 data, and the violet line shows SW monitoring by Geotail shifted in time to adjust to the average Interball-1 data at 09:30–10:00 UT. Predictions of GDCF at the Interball location are represented by the red line.

All three curves correlate at ~08:40–09:50 UT, proving an MSH encounter. Panel d of Figure 2.A6 displays $|B|$ in the same format (scale for SW in $nT$ on the right side).

Systematic discrepancies between the data and SW proxy, which we call 'plasma balls', are shaded blue (cf. Figure 3). Note that at ~09:33 UT a similar field depression at Interball is predicted by GDCF. Only the appli-

cation of the model can provide a reliable tool to determine this crossing of the low-shear MP (at ~ 09:53 UT), which is imbedded in the TBL. The change of the sign of the ion velocity (± signs are marked by green/blue) in panel e ($V_{ix}$, GDCF – red line, scale in km/s) confirms the identification of the MP encounter. In panel f, the ion temperature $T_i$ slightly reduces prior to the MP and then rises by a factor of 1.5–2. This reduction reflects a diminishing effective temperature of the core MSH ions as the $T_i$ is fitted to the 3D Maxwellian ion distribution. The $T_i$ does not account correctly for the input from higher-energy protons, clearly seen in panel h from 08:53 UT on. A similar remark is also applicable for the absolute value of $nT_i$ in panel a.

In panels g and h of Figure 2.A6, electron and ion color-coded (scales for counts per second on the left side) energy spectrograms are presented, with the energy-per-charge scales in eV depicted on the left. Black lines give count rates of the ions and electrons with energies > 30 keV, which flow generally towards the Sun (count rate scales on the right vertical axes). Panel j of Figure 2.A6 depicts a wavelet spectrogram of the ion kinetic energy density, and panel k that of the thermal ion energy (vertical frequency scales are octave-based, i.e. logarithmic, cf. Figure 2.A5 and Figure 2.A6i). In panels 1–*n* we present color-coded (see the logarithmic scale on the left side in $cm^{-2}$ $keV^{-1}$ $ster^{-1}$ $s^{-1}$) spectrograms of energetic ions flowing towards the Sun (FOV 180° from the Sun, cf. black line in panel h), from the Sun (rotating FOV at 62° from the spacecraft spin axis, pointed to the Sun) and sunward flowing electrons (panel n, FOV 180°, cf. black line in panel g).

Returning to a comparison of the $B_y$-spectra from Geotail and Interball-1 (Figure 2.A5, 2.A6i), the time lag between Geotail and Interball−1 should be 5–15 min (Savin et al., 2002a). Within those lags a SW disturbance at ~07:52 UT on Interball-1 is quite similar to that at Geotail. In the middle of the MSH at ~ 08:30 UT another disturbance practically coincides with that of the SW, with the low-frequency part being strengthened in the MSH. At 09:00–10:50 UT in the MP vicinity, wide-band Interball-1 fluctuations are seen; most of them have no counterparts in the SW, and vice-versa. This implies that driving by the SW is not dominant for the near-MP period analyzed; note multiple spectral maxima in this region (TBL, see Figure 3), which are related in a complicated manner. At frequencies > 0.7 mHz the disturbances in the TBL have higher intensity levels and different frequency dependencies, as compared with the MSH; therefore we think that the MSH is also not the major source for the fluctuations in the TBL.

This is in agreement with the cross-correlation of $B_y$ at 07:30–10:10 UT being < 0.5; at 09:30–10 UT the cross-correlation is 0.23, with a time lag for Geotail of 12 min, with Geotail $V_x = -478$ km/s. Considering possible different tilts for SW disturbances (Maynard, 2003) would hardly improve the correlation substantially. Greater resolution of these variations is presented in Figure 4, which will be discussed in detail in Section 2. After implementing

different lags in Figure 4d, we can see that in events 2, 3 and 10 the GDCF (i.e. SW) disturbances produce clear responses in the Interball data, while the TBL perturbations of a comparable magnitude in events 5–7, 9 and 11 have no counterparts in the SW (cf. also Figure 2.A6, panel c). Strong differences in the magnetic spectral shapes in the Interball-1 and Geotail data are also in agreement with the local nature of the TBL turbulence (Savin et al., 2002a).

Just inside the MP, energetic electrons have a high count rate (Figure 2.A6, panel g) that marks the boundary of closed magnetospheric field lines. This provides extra support for locating the PB inside the MP. Waves in the 2–50 mHz range (panels i–k) correlate with the intensity of energetic protons (black line in panel h and panels l, m) upstream of the MP, starting from ~08:53 UT. The main wave bursts have counterparts in the energetic electrons (panel g). The low-shear MP (~80°) and PB encounters take place at a tilt ~−21° (i.e. the Southern dipole axis being turned from the Sun towards the tail). The IMF $B_z$ turned to positive values about 10 min prior to the MP. The ion plasma beta at 09:56–10:03 UT reached 15; in the rest of the blue-shaded sites it exceeds 2. Similar PB encounters occur on one previous and two following Interball-1 orbits, on 15–27 June 1998 (Savin et al., 2005, submitted).

## 2.2. Direct interaction of the magnetosheath flow with a 'plasma ball'

After this discussion of the general TBL and MP features on 19 June 1998, we embark on a detailed investigation of the TBL properties. The main physical problem to address is how the practically demagnetized PB is interacting with the incident MSH flow in the collisionless plasma. Due to the high beta both in the MSH and the PB, the magnetic forces are small, and only local electric fields and waves can provide the MSH flow deflection and/or dissipation. The electric field $E_n$ near the MP can be supported by a surface charge at the MP-related current sheet (s), and it can deflect the incident MSH plasma to flow along the MP, while it cannot stop the normal flow in the absence of wave-induced effective collisions. The 'local' $E_n$, should be seen as a regular difference between the measured and SW-induced field (i.e. GDCF one). The MP transition at −09:53 UT is manifested in the different sign as compared with the GDCF one. Figure 2.A6b shows that the difference is mostly wave-like; the only systematic difference upstream of MP is visible at 09:48–09:53 UT. Such a negative $E_n$ (relative to the GDCF one) might contribute to the flow turning, but it should accelerate the incident particles towards the MP (instead of stopping them) if the measured high-amplitude waves provide an effective perpendicular conductivity. Thus, the waves constitute the major means for the boundary and the MSH plasma interaction in the case under study.

In Figure 4a–b we display wavelet correlation times (see Savin, 2002b, 2003a, for details) for the thermal and kinetic ion energy densities, which indicate for how many periods (at each frequency) the signal is coherent. Usually a signal conserving coherence for more than 2 periods at several consecutive analysis intervals can be regarded as a regular or coherent one. Panels c, e–g display the Poynting vector normal to the MP and its GSE components in the frequency band 2–50 mHz. In Figure 2.A6, the latter serves to outline the weak sunward moving disturbances (i.e. with positive $P_n$). In panel d we present $E_n$ with different time lags at 07:30–08:30 and 08:30–10:30 UT. In Figure 4 h and i, the measured and GDCF ion densities and ion kinetic energy density are depictured with the same time lags. Thick gray vertical lines with interruptions mark characteristic disturbances to be discussed; they are numbered in panels d and e. At 07:30–08:20 UT strong post-shock activity is well seen in Figure 2.A6, (cf. Savin et al., 2002b). Both the spectral and correlation time maximums at 1–2 mHz are recognizable throughout MSH (Figure 2.A6j and Figure 4a–b). Savin et al. (2002a, b) outlined similar maxima in magnetic spectra on Interball and Polar at these times, but they couldn't detect continuous or coherent signals.

We draw attention to events 2 and 3 (Figure 4), where the measured $E_n$ on average reproduces that of the GDCE. Thus, these events represent SW disturbances moving in the downstream MSH far from the disturbed TBL. Accordingly, all Poynting flux components are negative in these events (cf. Figure 3 and Interball-1 GSM position in Figure 2.A6 at 09 UT). The same is, most probably, valid for events 1, 4 and for the low-frequency $E_n$ trends between events 9–10 and 11–12. So, moderate SW disturbances provide a validation for our Poynting flux measurements in the MSH. At 08:35–08:53 UT a weak activity in panels i–k (Figure 2.A6) resembles that of Figure 2.A5 and thus is driven by the SW. The respective maximum at ~4–5 mHz in correlation time (Figure 4b) could be traced from the post-shock region at 07:50–08:50 UT. The region at 08:50–09:50 UT is characterized by strong disturbances, which are not SW-driven ones (cf. Figure 2.A5 and panels a–e and i–k in Figure 2.A6). Soft energetic ions are registered there (panels h, 1, m, Figure 2.A6) that correlate with the strong energy fluctuations and with the drop in the MSH kinetic energy. The latter drop is well seen after 09 UT in Figure 2.A6a and Figure 4i as a systematic difference between the black and thick red traces. Figure 2.A6e also demonstrates the larger departure of $V_{ix}$ from the model after that time. Figure 2.A6e also demonstrates the larger departure of $V_{ix}$ from the model after that time.

We check the density correspondence to the model in Figure 4h; the average measured density follows the GDCF proxy rather well until the diffuse MP encounter, with two exceptions at ~07:50 and 08:45 UT. The first density departure can be affected by a partial shock crossing, while in the second one the ion momentum ($\sim nV_{ix}$) is close to the GDCF prediction, but

it departs from GDCF after 09 UT. The general agreement confirms the reliable $n_i$ measurements and, thus, the local dramatic $W_{kin}$ decrease (Figure 4i). Note that the average MSH flow is subsonic ($W_{kin} < nT_i$, see Figure 2.A5a) and super-Alfvenic ($W_{kin} > B^2/2\mu_0$). On the top of Figure 4, black bars mark flows with nearly the magnetosonic speed, $V_{MS}$ ; on the bottom gray bars mark flows with nearly the Alfven speed, $V_{MS}$ . This is also shown schematically by thin arrows in Figure 3. Besides the accelerated MS-jet at 09 UT, there are a number of smaller MS-jets in the upstream TBL.

The decrease in $W_{kin}$ mentioned above after 09 UT corresponds to a decelerated Alfvenic flow. In the upstream TBL those flows are mixed with the MS-jets. In the MSH upstream of the TBL at 08:40–08:50 UT the standard deviations of ion energy densities are: $\delta W_{kin}$~ 22%, $\delta nT_i$~ 10%. Figure 2.A6k shows that at 08:53–09:35 UT $nT_i$ fluctuates, at 09:03–09:15 UT the $nT_i$-disturbances dominate over those of $W_{kin}$ : $\delta W_{kin}$ ~ 49%, $\delta nT_i$ ~ 20%, $\delta W_{kin}/\delta nT_i$ ~ 0.48. In the middle of the upstream TBL both the kinetic and thermal ion energies are quite disturbed (09:15–09:35 UT): $\delta W_{kin}$ ~ 71%, $\delta\ nT_i$ ~ 25%, $\delta\ W_{kin}\ /\delta nT_i$ ~ 0.996. Relative to the unperturbed MSH the standard deviations in the TBL center are: $\delta\ W_{kin}$ ~ 45%, $\delta nT_i$ ~ 17%. The lower limit for the energy conversion into the irregular fluctuations in the TBL (i.e. the difference of standard deviations) is 23% of MSH kinetic energy and 7% of its thermal. As the TBL spectra in Figure 2.A6j and k are quite different from the upstream MSH ones, we would like to accept the higher limits for the MSH energy chaotization: $\delta W_{kin}$ ~ 30–40% and $\delta nT_i$ ~ 10–15%.

A strong deficit of the average $W_{kin}$ at 09:03–09:15 UT (and of the ion momentum) is displayed even in the sum of $W_{kin} + \delta W_{kin}$, which constitutes only 47% of the average upstream kinetic energy. The only candidate to carry off the momentum and kinetic energy excess is the strong impulse in the $W_{kin}$ and $V_{ix}$ in Figure 2.A6 and Figure 4 at ~09 UT. The respective hodogram of the ion speed vector tip in the plane of GSE ($V_x$, $V_y$) is shown in Figure 5a. The average speed in the depicted interval 08:59:11– 09:00:08 UT is (−252, −45, −88) km/s, and the possible inferred vortex component (i.e. the loop in the hodogram) has a radius of ~50 km/s (~4% of its average $W_{kin}$). Those estimates are given in the spacecraft frame (which is close to the MP frame), while in the frame of the unperturbed MSH the vortex kinetic energy is ~0.3 $W_{kin}$ . Since the magnitude of the $W_{kin}$-pulse reaches the local value of $nT_i$ (Figure 2.A6a), that means a nearly magnetosonic (MS) speed of the jet ($V_{MS} \sim (2T_i/M_i)^{1/2}$ in the high-beta plasma ($M_i$ – proton mass, $T_i$ – in energy units)). A magnetic loop at this time has been found at half this frequency.

This plasma jet is in the middle of a current sheet (bi-polar disturbance in the clock angle, Figure 2.A6c), bounded by $|B|$ drops down to a few $nT$ ('diamagnetic bubbles') and a bi-polar $E_n$ - spike (~5 mV/m), which can be

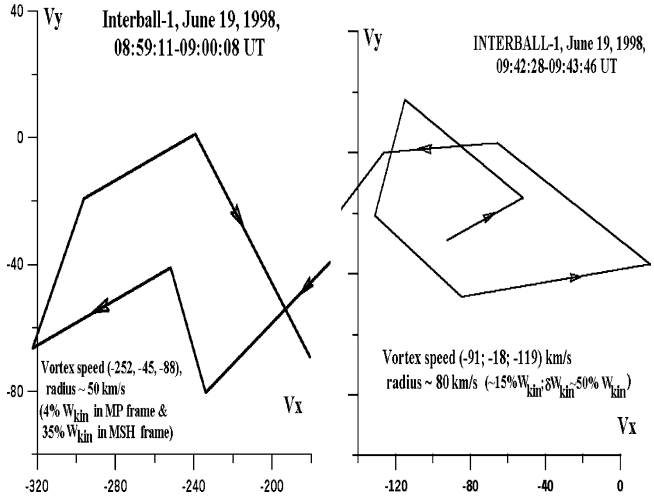


*Figure 5*. Left: Hodogram of ion $V_x$, $V_y$ at 08:59:11–09:00:08 UT, 19 June 1998. Right: Hodogram of ion $V_x$, $V_y$ 09:42:28–09:43:46 UT, 19 June 1998.

accounted by surface charges at the current sheet. In Figure 4 it is event 6 that contains the impulsive density rise. The negative spike of the Poynting flux in all components (for 5–50 mHz GSE vector being (−20, −6, −5) $\mu$W/m$^2$, i.e. at ~24° to the model speed (−247, −6, −157) km/s, departing from the model flow towards the −X and −Y directions) in event 6 conforms to the energy being pushed downstream by this strong nonlinear structure. The value of $P_n \sim -10\mu$ W/m$^2$ indicates the approach of the disturbance to the MP (see Figure 3). The latter excludes a near-MP reconnection as a mechanism for the jet acceleration: (a) any MP-related disturbance should move outward from the MP (i.e. $P_n > 0$); (b) the distance from the MP is too large (in ~1 h prior to its crossing); the GDCF does not predict any substantial outward MP movement in this period; and (c) negligible $|B|$ just inside the MP and in its vicinity (the magnetic energy density is about an order of magnitude less than that of the $W_{\rm kin}$ spike in event 6) can hardly result in such a strong plasma flow acceleration of up to an Alfvenic Mach number ~3.1 in the MS-Jet.

Between the event 4 and the MP we can see strong enhancement in the appearance of the negative (downstream) $P_x$, $P_y$ and $P_z$ -spikes (events 5–7 and 9), which correspond to local TBL disturbances without correlative feature in SW (cf. Figure 2.A5 and 2.A6). Similar to event 6, the events 5, 7, 9 have related clock angles and electric field spikes, while the plasma jetting is unique for event 6.

There is another group of perturbations with positive $P_n$ -spikes, i.e. moving from the MP towards the outer TBL border that are numbered 8, 10–12 and MP (see also Figure 2.A6b). The $P_n$ -positive events dominate

there, and event 12 has positive $P_y$ and $P_z$ moving upstream along the MP. The MP-related perturbation moves in the positive $X$ and $Z$ directions but strongly in the negative $Y$ direction. Event 14 inside the MP resembles a short double MP crossing, but generally moves from the MP (negative $P_n$), as does event 15. Between events 6 and 7 weak positive $P_n$ -spikes of short duration can be seen.

The ion velocity hodogram in the GSE plane ($V_x$, $V_y$) for the trailing part of event 11 with negative components of the Poynting vector is depicted in Figure 5b. The average speed in the interval 09:42:28–09:43:46 UT is (−91, −18, −119) km/s, and the inferred vortex component has a radius of ~80 km/s (i.e. 15% of its average $W_{\rm kin}$). Thus, the vortex energy is big enough for a non-linear wave, since it contains $>33\%$ of the chaotic kinetic energy. No obvious vortex-like magnetic loops have been detected around event 11. Correlation times in Figure 4 provide information on the coherence of the disturbances. $W_{\rm kin}$ 'synchronization' at ~5 mHz (09:15–09:45 UT) corresponds to the appearance of the positive $P_n$ – spikes in the TBL center. The reflected (sunward going) wave packets provoke interactions in the upstream region closest to the MP. At 08:45–09:35 UT (events 4–10) the strong maximum at ~3 mHz in the $W_{\rm kin}$ correlation time most probably results from regular launching of tailward wave packets from the outer TBL boundary. The maximum at 3 mHz is also seen in Figure 4a. Inside the MP the quasi-coherent signals are at ~7 mHz, and that corresponds to Pc4 pulsations.

To give more details for the TBL interactions upstream of the MP, we zoom in on the interval 08:30–10:00 UT in Figure 6.B1 and 6.B2, showing wavelet spectrograms for the ion density and velocity $V_{ix}$, respectively. The former is similar in its main features to the panel k in Figure 2.A6. The latter is quite compatible with panel j in Figure 2.A6 and provides the direct comparison with a bi-spectrum in Figure 6.B3. Figure 6.B1 demonstrates the strengthening of the low-frequency (~1.3 mHz) maximum just upstream of the plasma jet for event 6 (09 UT). The coherent signal at 4–5 mHz (panels a, b, Figure 4) can be related with a weak maximum at ~4.2 mHz. Referring to the Poynting flux in Figure 2.A6 and Figure 4, we conclude that the weak waves at ~4.2 mHz propagated upstream and triggered amplification of the down-going low-frequency waves. The weak maximum at 4.2 mHz is visible at 08:48–08:55 UT in Figure 6.B2 along with the stronger one with a rising tone from ~1.5 to 2 mHz. The latter grows further in magnitude and frequency (~2.3 mHz) until 09 UT (event 6, i.e. launching of the plasma jet), where it bifurcates into rising- and falling-frequency tones, which evolve toward about 1.3 and 2.7–3.5 mHz bands (cf. correlation time maxima in panels a, b in Figure 4). At ~09 UT maxima at about 5 and 12 mHz are also visible. In the upstream TBL at 09:00–09:45 UT the kinetic energy drops mentioned above result not only in plasma jetting but also in amplification of

the low-frequency pulsations (~1.3 mHz), three periods (~10–15 min) of which cover almost the whole upstream TBL. Those fluctuations correspond to maximums at 3–10 mHz at ~09:00, 09:15, 09:30 and 09:45 UT. A macro-equilibrium can be achieved in the outer BL (Figure 3) during a few of these periods. This is in agreement with a 'thick' TBL transition invoked by Savin et al. (2001) versus a 'thin' shock-like one.

To check if the nonlinear processes in the outer TBL are really synchronized, we analyze the wavelet bi-spectrum (bicoherence) for the velocity $V_{ix}$ in Figure 6.B3, which corresponds to a frequency sum rule for the 3-wave process, $f_s = f_l + f_k$ . The bicoherence has a substantial value only if those three processes are phase-coupled (cf. Savin et al., 2002b); the modulus of the product of the 3 complex wavelet amplitudes is normalized by the modulus of the amplitude of the three signals at their respective frequencies. This corresponds to decays (or a junction), which require a third-order non-linearity in the system. The weaker, higher-order nonlinear effects, which might also contribute to the TBL physics, are beyond the scope of this paper. In Figure 6.B3 we display the bicoherence of $V_{ix}$ at 08:42:57–09:12:51 UT for $f_k$ ~ 1.5–8.5 mHz (the larger frequency in the sum) and $f_l$ ~ 1.5-5 mHz. The horizontal and vertical lines indicate processes with nearly constant $f_l$ and $f_k$, respectively, and the negatively inclined line marks processes with $f_s = f_l + f_k$ ~ constant. We show only processes with the relative amplitude $> 0.5$ (50% of the triple product absolute value), i.e. all colors, except the dark blue background, mark signals whose bicoherence is certainly above the noise level (cf. maximum bi-spectral amplitudes are ~50% in Savin et al. 2001, 2002b, 2004).

Neglecting the frequency drifts near the bifurcation point at 09 UT in Figure 6B.2, we can distill the processes in Figure 6.B3 at several frequencies: $f_l$ ~ 1.5 mHz, lower horizontal maximum, cf. ~1.3 mHz in Figure 6.B2 and in Figure 4; $f_l$ ~ 2.2 mHz, upper weak horizontal maximum, compatible with the general upstream maximum at 08:50–09:00 UT in Figure 6.B2; $f_s = f_l + f_k$ ~ 4.5 mHz (the lower inclined line), which is close to the upper downstream maxima at 09:10–09:40 UT in Figure 6.B2 and to that of upstream maxima in Figure 6.B1, 6.B2 and Figure 4; $f_k$~ 2.2–2.6 mHz, strong vertical maximum (cf. panel b in Figure 4 and Figure 6.B1, 6.B2) with the largest amplitude at its top. The latter red spot corresponds to the second harmonic generation: (cf. Savin et al., 2002b), visible at 09 UT at ~5 mHz in Figure 6.B2 (MS-jet). Another red-spot maximum would suggest wave pumping at $(f_l, f_k)$ ~ (1.5,3) mHz with further nonlinear cascading at $f_s = f_l + f_k$ ~ 4.5 mHz (lower inclined line) and at $f_l$ ~ 1.5 mHz (see the lowest horizontal maximum up to 6 mHz (Savin et al., 2001, 2002b)). We assume that the cascade signatures (e.g., in the case of the horizontal-spread maximum, when at the sum frequency, $f = f_1 + f_2$, the bicoherence has a comparable value with that at the starting point $(f_1, f_2)$), implies that the wave

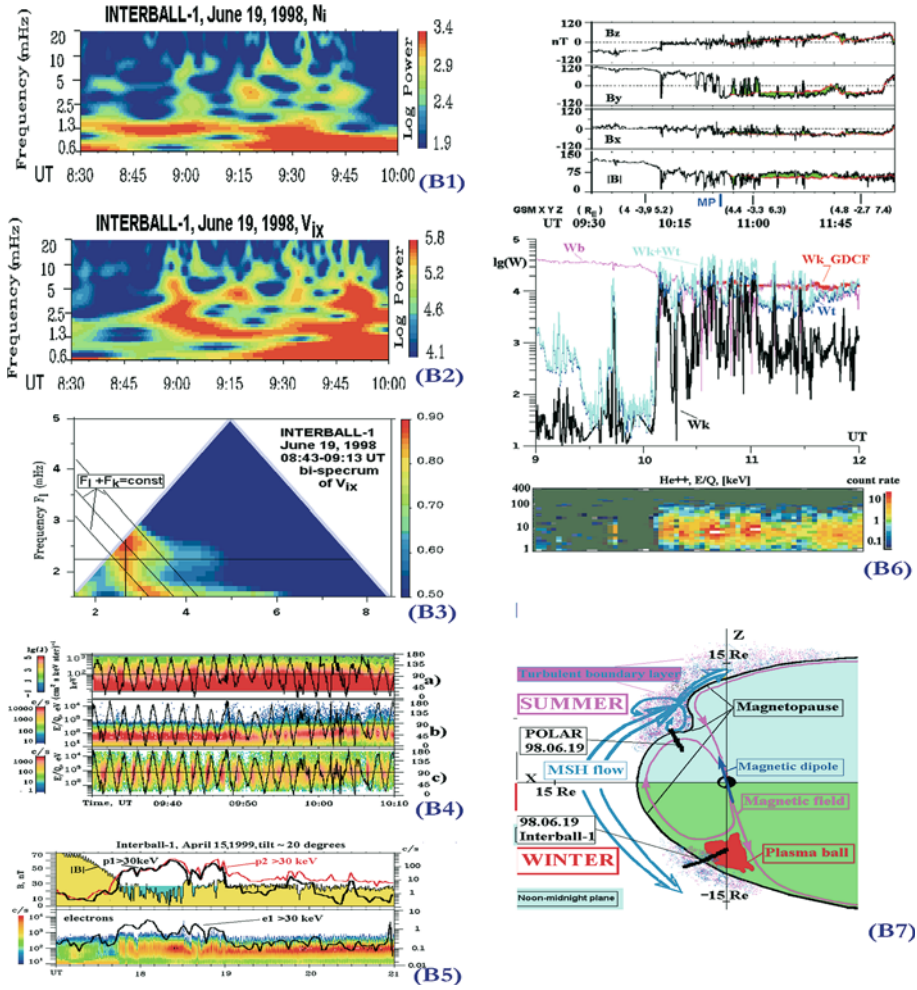


*Figure 6.* (B1) Spectrogram of ion density, 19 June 1998. (B2) Spectrogram of velocity $V_{ix}$, 19 June 1998. (B3) Bi-spectrum of velocity $V_{ix}$, 08:43–09:13 UT. (B4) Ion (a, c) and electron (b) spectrograms and pitch-angles (right scale), Interball-1, 09:30–10:10 UT, 19 June 1998. B5: Open OT, 15 April 1999. Top: $|B|$ (yellow-marked) and protons ( > 30 keV, p2 (red)- from Sun, pl- towards Sun). Bottom: electron spectrogram and intensity ( > 30 keV, towards Sun). (B6) TBL crossing by Polar, 19 June 1998. Top: GSM magnetic field versus GDCF (red line). Middle: Magnetic (violet line), thermal (blue) and ion kinetic (GDCF – red line) energy densities and their sum (light blue). Bottom: $He^{++}$ spectrogram. (B7) Sketch for MSH interaction with cusps.

at the sum frequency interacts in turn with the same initial wave at frequency $f_1$ in the following 3-wave process: $f_3 = f_1 + f$, etc. Note also horizontal and vertical cascading at the frequencies of 2.2 and 2.6 mHz mentioned above. The linkage between the spectrogram maxima represents a feature of cascade-like processes in Figures 2.A6, 6.B1 and 6.B2. Thus the bi-spectrum

provides strong support for the decay-like phase coupling of the low-frequency fluctuations in the upstream TBL.

We have also checked the wavelet spectra and bi-spectra for ion density, kinetic and thermal energies and observed a highlighting of similar processes up to about 20 Hz. The 3-wave nonlinear wave-coupling persists also in the TBL central and inner zones (not shown). Similar to the magnetic spectra in Figure 2.A6, the simultaneous magnetic bi-spectra (not shown) differ in detail from those of Figure 6.B3. First of all, the magnetic bi-spectra have lower maximum magnitudes (up to 0.6 instead of 0.9 in Figure 6.B3). Thus, in the high-beta plasma the energy-dominated ion moments are the most representative ones for understanding the nonlinear interactions.

### 2.3. Comparison with polar data on 19 june 1998

Let us briefly compare the Interball-1 data on 19 June 1998 with the simultaneous Polar data in the northern hemisphere (tilt ~20°). Referring for details to Dubinin et al. (2002), Savin et al. (2002a, b), we present the Polar outbound crossing in Figure 6.B6. The magnetic field at the top of Figure 6.B6 highlights the MSH encounter in $B_y$, changing from positive magnetospheric values to negative MSH ones, which conforms to the GDCF predictions (shown by the red line; the difference from the measured field is highlighted by the green color). We mark MP (separating average MSH and magnetospheric fields) for traverses of the magnetopause current sheet, which may be multiple. Note that the MP is at GSM Z ~6 $R_E$ versus −10 $R_E$ for Interball-1. The respective orbit traces are given by thick black lines in Figure 6.B7. In the middle panel of Figure 6.B6, we display energy densities similar to Figure 2.A6. The spiky bursts of the kinetic energy density (black line) have been attributed by Dubinin et al. (2002) and Savin et al., 2002a, 2002b) to reconnection bulges. We can see from a comparison with the model kinetic energy and between the measured and model magnetic fields that the bulges' appearance is controlled mostly by the local TBL processes (i.e. no SW driving is proved by GDCF). The micro-reconnection in the bulges should be modulated by the upstream TBL fluctuations (see previous Section), since the spectral features of the magnetic fluctuations (in the band of the repeated reconnection bursts) in the transition region at 10–11 UT are quite similar to those measured by Interball-1 in the upstream TBL (see Savin et al., 2002a). So, the current sheets at ~10:50–11:05 UT are attributed to the TBL.

Another point that we would like to make is that the kinetic energy in the 'reconnection bulges' at 10–11: 20 UT exceeds the GDCF model predictions (red thick line on the middle panel) by 1.5–2 times. Even inside the MP the magnetic field energy density has a smaller magnitude than that of ion total

energy (light blue curve) in the jets. We compare the magnetic field energy with the total ion energy because, with reconnection, the transformation of stored magnetic energy from the MSH flow to magnetosphere should go in kinetic and then partially into thermal ion energy of the bulge-related streams of the plasma. The accelerated jet at the outer TBL border (see event 6 in Figure 4 and Figure 2.A6) has similar characteristics to the spiky bursts in Figure 6.B6, which makes it a good candidate source for the regular plasma jets registered by Polar (Figure 6.6).

## 2.4. Accelerated particles

Recent multi-satellite observations demonstrate that the cusp is a region of accelerated plasma. There is evidence that the cusp is a substantial source of energetic particles (Q. Chen et al., 1997, Fritz et al., 2000). The energization mechanism is related to the strong turbulence observed in the cusp (Chen and Fritz, 1997, Blecki et al, 1998, Savin et al., 2002c), and recently mapped by Interball-1 (see Section 3). Ions with energies over 7 keV on 19 June 1998 are seen after 08:50 UT on the spectrograms in Figure 2.A6h. As mentioned above, waves in 2–50 mHz range (panels i–k, Figure 2.A6) correlate with the intensity of energetic protons upstream of MP.

Turning now to the spectrograms in panels 1–m (Figure 2.A6), we see that the upstream ions correlate best with the $W_{\mathrm{kin}}$ -fluctuations (panel j), the yellow-colored fluxes at high energies at 09:20–09:50 UT exceed those of the trapped particles inside the MP. The maximum intensity of the energetic ions occurred just inside the MP (i.e. in the PB) with the ion intensity decreasing farther inside the magnetosphere (better seen in panel m). The higher energy ions, correlating with the upstream TBL fluctuations, suggest local acceleration. The electron spectra in panel n of Figure 2.A6 upstream of the MP also generally correspond to the intensification of fluctuations in $W_{\mathrm{kin}}$, with electrons up to 50 keV appearing. In Figure 6.B4 we zoom in the electron and ion energy spectrograms from Figure 2.B6 at 09:30–10:10 UT, adding respective pitch-angles (scales in degrees on the right side). Before 09:47 UT (i.e. in the MSH) electrons (panel b) and ions at 7–25 keV (panel c) tend to have a minimum flux in the field-aligned direction. This excludes reconnection as a source for the higher energy ions, as in the southern hemisphere the magnetospheric field is pointed away from the Earth, thus particles, escaping from magnetosphere, should flow parallel to the reconnected lines (cf. Savin et al., 1998b, 2004). The only higher energy electron burst, at 09:48 UT, also demonstrates a domination of the anti-parallel flow. The main MSH ion maximum upstream of the MP occurs at pitch angles ~90° and spreads up to 25 keV (panel c), and this

strongly infers a local source for the most dense suprathermal ions. At 09:55–10:05 UT the ions at 7–25 keV are peaked at ~90° along with the most MSH-like ones. Their fluxes along the field are smaller than the perpendicular fluxes, but they exceed the anti-parallel fluxes. The latter might imply either a minor amount of the plasma-sheet-like (PS, energies 7–25 keV) ions along the field lines from the inner magnetosphere or represent a loss-cone towards the nearest (southern) ionosphere.

In Figure 6.B4a we zoom in on panel m of Figure 2.A6 and superimpose the respective pitch angle. Around 09:40 UT soft ions with energies $< 50$ keV display a minimum along the magnetic field, similar to that in panel c. This gives an estimate for the upper limit of supra-thermal ions of MSH origin. At higher energy (up to 400 keV) the parallel ion flows dominate, and this conforms to their leaking from the PB along effectively reconnected field lines. Further support for that can found in bottom panel of Figure 7; both the intensity and slope of the average ion energy spectra at energies $> 200$ keV almost coincide for the PB (curve 3) and TBL (curve 2). An instant spectrum of the field-aligned ions in the TBL (i.e. leaking along the field line from PB, shown in curve b) from the time interval 09:40:37–09:42:02 UT reproduces the average shape of the PB spectrum (curve 3), but with a slightly smaller intensity.

Coming back to panel a in Figure 6.B4, around 09:40 UT there are also narrow perpendicular spikes at the higher energy levels, which constitute the third population of energetic particles in the upstream TBL. Having practically no parallel speed, these ions can result, for example, from local perpendicular ion-cyclotron acceleration. To justify an alternative magnetospheric origin of those ions we should explain their loss of parallel energy; such ions are not seen in the OC, and to be able to reach the outer BL from distant regions along the MP they should have a parallel velocity comparable with their perpendicular velocity. In Figure 7 the respective characteristic energy spectra are marked by 'a' and 'b' in the top panel and by 'a' in the bottom panel. A difference between the maximum spectra ('a') and that of the PB spectra (curve 3) is highlighted by shading, and reaches a factor 3. The spectral shape is representative on the top panel (this channel does not rotate and has nearly constant pitch angle during the exposition of spectrum 'a'). Comparison with panel a in Figure 6.B4 suggests that the highlighted spectral difference is a systematic one. Even the average spectrum in the TBL ('2', top panel in Figure 7) is slightly larger than that of the PB at energies $> 250$ keV. Panel a in Figure 6.B4 in PB at 09:53–10:05 UT demonstrates loss-cones in the anti-parallel magnetic field direction (cf. panel c). The energetic particle culminating in the PB just under the MP can result both from the local cascading of chaotic kinetic energy and from loss of parallel momentum by magnetospherically trapped particles undergoing a wave-particle interaction. This is also necessary to trap the locally-born accelerated

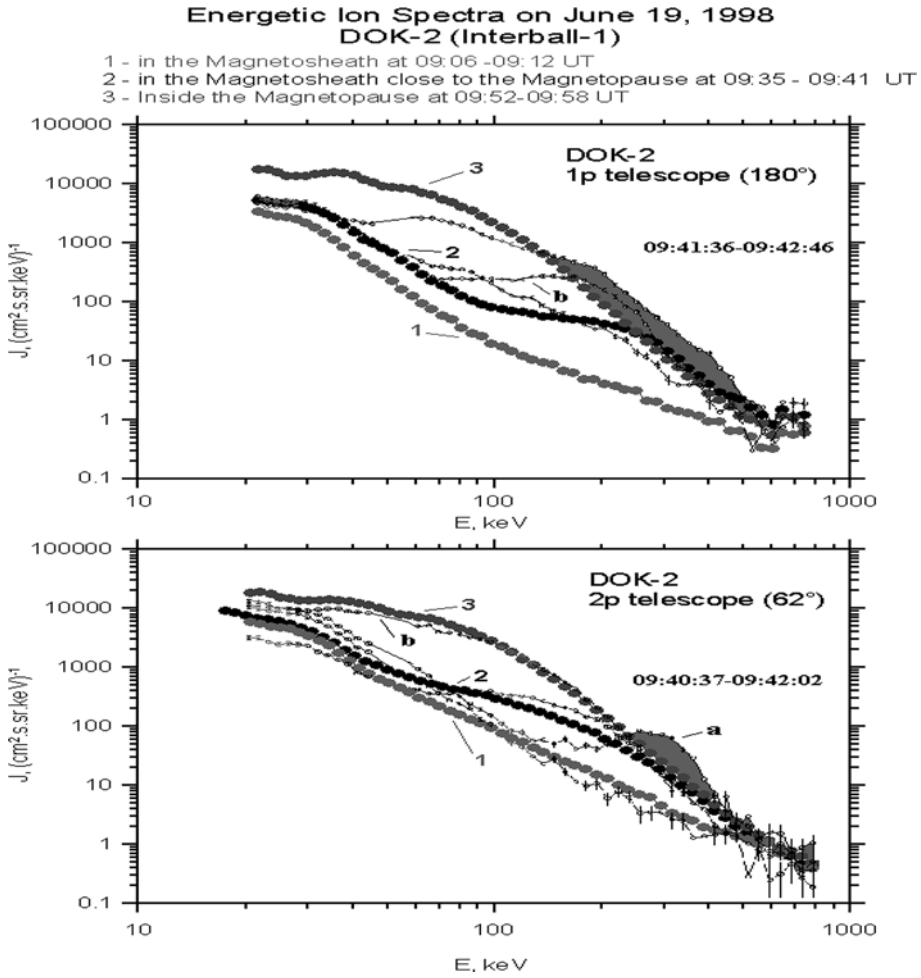


*Figure 7.* Energy spectra on 19 June 1998 for sunward (top, FOV 180° from Sun) and tailward (bottom, FOV 62° from Sun) flowing energetic ions; thick circles: 1 –MSH 09:06–09:12 UT, 2 – TBL 09:35–09:41 UT, 3 – PB 09:52–09:58 UT. Small thin circles: top – 09:41:36–09:42:46 UT, bottom – 09:40:37–09:42:02 UT. Shading marks the difference between PB ('3') and TBL perpendicular spectra denoted by 'a'.

particles in the PB, for example, the soft energetic ions $< 150$ keV (curves labeled '3' in Figure 7) can leak from the magnetosphere (curve 'b' on bottom panel) due to diffusion by the strong waves (cf. Savin et al., 1998b, 2002c).

On the bottom panel in Figure 6.B6 we present a color-coded (see color bar for the logarithmic count rate on right side) spectrogram of energy per charge (logarithmic scale in keV/e is shown on the left vertical axis) for the unique MSH constituent $He^{++}$. This clearly demonstrates the local acceleration of $He^{++}$ up to 100 keV/e in the region of numerous plasma jets and

MP-like transitions at 10–11 UT (see the upper panels and discussion above). Another peculiarity is a much greater intensity as compared with the MSH stagnation region after 11:30 UT.

As for more energetic particles (not shown), the acceleration of ions up to several hundreds of keV and of electrons up to several tens of keV is seen in the TBL, with a maximum at the multiple $B_y$ transitions (10:20–11:10 UT). Note also the difference with the Interball data: no enhanced energetic particle fluxes inside MP are registered by Polar. A similar case in the OT on 21 April 1996 from Interball-1 data has been described by Savin et al. (2002c). The electrons with energies up to 10 keV can be accelerated by whistler-mode fluctuations of about 1 Hz (see Savin et al., 1998b). Another case of the OT is presented in Figure 6.B5. Top panel depicts $|B|$ (yellow shaded, scale in $nT$ on left axis) and energetic ions (>30 keV, logarithmic scale for counts/s on right side) from the same channels as shown in panels 1–m in Figure 2.A6 (the 180° channel is marked by a black line) during an outbound MP crossing on 15 April 1999 (at ~17:45 UT). The large-scale $|B|$ reduction is shaded green, and looks similar to the PB in Figure 2.A6, but in this case the energetic ion intensities comply with the particle source being the MSH rather than the magnetosphere. The anti-sunward flowing ions (red line) have a greater flux in the MSH than inside the MP and dominate the sunward flux. Therefore, similar to Figure 6.B6, we attribute the magnetic field reduction at tilt ~20° to the OT. Both energetic ions and electrons (bottom panel) have strong clear maxima in the OT and just upstream of it, which represent a feature of local particle origin and/or accumulation.

## 3. Turbulent boundary layer encounters by Interball-1 (1995–2000)

To complement the TBL encounters on 19 June 1998, we present a survey of encounters with the TBL by Interball-1 made during 1995–2000. The Interball-1 orbit evolution provided an opportunity to cross the near-cusp MP along with the boundary between the mantle and LLBL in the near tail twice per orbit (excluding the late October – late December period). For this study we use the routinely calculated dispersion of the $B_x$ raw magnetic field waveform with a sampling rate of 4 Hz over 2-min intervals (i.e. for 0.0085–2 Hz). We multiply the $B_x$ dispersion by a factor of 3 for comparison with Df in a statistical sense (i.e. we suggest equality of the ULF average power for all 3 magnetic components). We give the AC magnetic pressure (Df) in eV/cc for comparison with the other energy densities. Similar to Savin et al. (2002a), we define the background TBL when in a time interval of $<20$ min the $B_x$-variation during 2-min intervals exceeds, at least at two points, the threshold 3 $nT$ (~5.2 $nT$ for full variation or ~67 eV/cc). This is 1.5 times higher than that of the nearby MSH. This is shown by gray-colored orbit

pieces in Figures 2.A1, 2.A2 and 2.A4. Note that in previous TBL statistical studies (Savin et al., 1999, 2002a, 2003a) a shorter time period of 1–3 years and a variation interval of 20 s have been used.

We have checked for several characteristic TBL cases that the 2-min variation interval is rather representative as Df starts to saturate with an increase of the variation interval. We have found 651 TBL events on about 400 MP crossings; thus, most MP crossings have multiple TBL encounters according to the above definition. In Figure 2.A1 we display in 3 GSM planes the color-coded distribution of the events with high magnetic variance, as function of the $B_x$-variation magnitude ($D(B_x)$), with the colors for the respective variation intervals depicted in the left lower corner. We limit our study to the region outside the magnetosphere by requiring that one of the minimum of two values is satisfied: (a) half the distance between the point most distant from the Earth's MP and the point closest to the Earth's bow shock (BS) in the same orbit, and (b) 5 $R_E$ beyond the most distant MP. We exclude single spikes in the $B_x$-variation, which clearly correspond to the main magnetic field changes at the MP itself. The gray-colored TBL background serves mostly to mark the near-MP coverage by the Interball-1 orbits. Note the data gap for $Z < -14$ $R_E$ and $|X|, |Y| < 7$ $R_E$ (which is due to the Interball-1 re-entry in October 2000). The tail MP around midnight is not covered by Interball-1 (the shaded data gap area in the center of $XY$-plane), while the dayside one is.

In Figure 2.A1 all events concentrate at high latitudes ($|Z| > 4$ $R_E$) near the OT and downstream from it, and are especially well seen for variations $> 8nT$ (blue and red colors). Those events are associated with the TBL per se. In the $YZ$-plane at low latitudes we can also recognize groups of intensive events (for both positive and negative $Y$), while the projection $XZ$-plane demonstrates that most of them are encountered in the tail. The latter corresponds to the 'sash' of a prediction (Maynard et al., 2001). The northern (upper) TBL is indented in the $YZ$-plane, corresponding to the MT indentation (cf. Savin et al., 1998a, b and Figure 1). In the southern hemisphere no indentation can be inferred. To prove that this is not an effect of an absence of coverage at large negative $Z$, we compare the appearance of events along directions $Z = 10$ $R_E$ and $Z = -10$ $R_E$: in the former case there is a clear maximum in the vicinity of $Y \sim 0$, while in the latter case there is a minimum in the event occurrence (shifted to positive $Y$). The peculiarities mentioned above are even better seen in Figure 2.A2, where the gray-scaled background events are given in the same format, while the rest of the color-coded ones are shown only for $B_x$-variations $> 8nT$ (see the discussion of tilt dependence below). In Figures 2.A1 and 2.A2 we mention the TBL 'wings' in the $XY$ and $XZ$ planes, ranging from the near-cusp TBL into the tail down to $X \sim -20$ $R_E$ . The higher-latitude 'wings' are in the vicinity of the boundary between semi-open mantle lines and closed LLBL lines. The local minimum in the total

magnetic field and the associated currents, which provide the field rotation from the open to closed lines are anticipated there. In the TBL, compressional magnetic field disturbances are also present.

While they are not dominant in the TBL power, the spiky magnetic field decreases, 'diamagnetic bubbles' (DB, see Savin et al., 1998b) provide a mechanism for plasma heating in the TBL. It has been demonstrated in a number of case studies (see Savin et al., 2004, and, references therein) that the DB differ from mirror waves by an absence of perpendicular ion energy dominance. For the DB statistics Savin et al. (1999) used the maximum depths of the spiky total field ($|B|$) drops to calculate the diamagnetic effect of the heated MSH plasma inside the DB. The DB distribution (not shown, but see, e.g., Romanov et al., 1999) is generally the same as the TBL events shown in Figures 2.A1 and 2.A2. The averaged maximum plasma pressure excess in the DB is $\delta(nT) = 2160$ eV/cc. The magnetic field inside the 'bubble' is about 8.3 times weaker than outside. Taking the plasma density in the TBL to be 5–10/cc, we observe plasma heating to 216–430 eV inside the DB, i.e. heating of 1.5–3 times the temperature of the MSH ions. This is in good correspondence with the predictions of Haerendel (1978). Most events with $Df > (15nT)^2$ and $8(nT) > 3100$ eV/cc at $|Z| > 4\ R_E$, with a prominent maximum above the cusp. Intensive heating in the high latitude tail 'wings' is seen only to $X = -6\ R_E$ .

Merka et al. (2000) concluded that the most prominent dependence of the cusp position is the dependence on dipole tilt angle. Their study was restricted to the northern hemisphere, where the tilt was positive for the majority of MP encounters by Interball-1/Magion-4. Their definition of the exterior cusp includes the TBL as a part. In Figure 2.A2 we present a map of TBL events, color-coded by the magnetic dipole tilt angle (see the colors and corresponding tilt ranges in the bottom left corner). For the analysis we have chosen only strong TBL-like events with the $B_x$-variation $> 8nT$ (480 eV/cc). In the northern indentation, the events with positive and zero tilts dominate for $Z < 10\ R_E$ . This agrees with the direct interactions of the open cusp throat with the incident MSH flows (marked "1" in Figure 1). The indentation in the TBL/MP does not represent a characteristic feature of the winter hemisphere; the events with negative tilts strongly dominate near $Y \sim 0$ at negative $Z$ in the $YZ$-plane. This asymmetry suggests that the interaction of the MSH flow can be different for negative and positive tilts.

## 4. Statistics for plasma balls and open cusp throats

We now return to the largest scale nonlinear sites in the outer cusp, which we call 'plasma balls'. Figures 2.A6 and 6.B6 demonstrate that at sunward and anti-sunward tilts (i.e. from Polar and Interball-1 data) the MSH flow

interaction includes similar features, e.g., accelerated plasma jets and stagnant heated MSH plasma at the MSH-cusp transition. The general difference is that for positive (sunward) tilts this stagnant plasma is located outside the MP (as Figure 1 and Figure 6.B6 infer), while the PB in Figure 3 and Figure 2.A6 is certainly inside it (see also Savin et al., 2002a). This means that the cusp throat can be open for direct interaction with MSH flows (OT) or closed by the MP, depending (presumably) on the tilt sign. Thus, streamlines of the MSH flow around the cusps can be asymmetric, as shown in Figure 6.B7 (where Interball-1 and Polar traces from Figures 2.A6 and 6.B6 are marked by thick black lines).

In the summer (positive tilt) hemisphere, the MSH TBL is located in the MP indentation over the cusp. In the winter (bottom), the TBL is located both upstream of the MP and at the outer PB border; while the MP indentation might exist it is not so deep as the summer one (cf. Figure 2.A1, A2). We use the same full Interball-1 database shown in Figure 2.A1, A2 to explore how characteristic such occurrences of PB are. In most high-shear cases and when energetic particles mark a clear trapped boundary, as in Figure 2.A6, we recognize the PB from key parameters and from energy-time spectrograms of the thermal particles, using the characteristic features discussed above.

For ~30% of more complicated cases (from 52 PB in Figure 2.A3, A4 and from 37 magnetic field cavities with heated plasma in the open OT in Figure 2.A4) we have analyzed the pitch-angle distributions (cf. Figure 6.B4) or detailed IMF data. We have set the lower duration limit for the large-scale PB at 10 min, the smaller 'diamagnetic bubbles' have been studied earlier using only high-resolution magnetic field (Savin et al., 1998; Romanov et al., 1999, 2002a). In Figure 2.A3 we present the distribution of PB in three GSM projections. Gray-colored marks demonstrate rather dense Interball-1 coverage of the near-MP region (see Figure 2.A1, A2 and discussions above). Most of the PB are concentrated over the cusp throats at negative tilts (blue lines). They tend to occur at the outer TBL border (farther than ~8 $R_E$, and better seen in the northern hemisphere) and have maximum spread in the $Y$ direction. Some of them are registered in the near tail, including most of those at positive tilts (red lines). The spread in the $X$ direction is presumably due to different SW dynamic pressures; for example, the blue line at $X > 10$ $R_E$ closest to the Sun corresponds to the case on 11 May 1999, when the SW almost disappeared, and its size of ~2.5 $R_E$ provides a proxy for the upper PB size limit in the $X$ direction.

A reasonable estimate for the average PB size from Figure 2.A3 would be 1–4 $R_E$, and the $Y$-size could be over 5 $R_E$ . The PB width, inferred by Savin et al. (2002a) for 19 June 1998, is close to the upper limit. For 18–19 February 1997, with very stable SW conditions (Romanov et al., 1999), an estimate for the PB spread along the orbit from the satellite-subsatellite time lag is over 2

$R_E$ . Taking into account an average MP speed of ~20 km/s (versus 1.5 km/s for the spacecraft speed), we can accept the average PB scale to be closer to the upper limit of its geometrical size in Figure 2.A3.

The PB has been identified as $|B|$ large-scale decreases with newly heated plasma inside the MP (Savin et al., 2002a). Before applying the GDCF, the PB had been thought to be located outside the MP similar to the stagnation region registered at the beginning of Interball-1 operation (Savin et al., 1998b). We have found 37 cases of the latter type, which resemble Figure 6.B5, having clear magnetic field, energetic particle behavior or particle pitch-angle features of the MSH (cf. Figure 6.B4 at ~09:40 UT). The general difference of these cases from those of the PB is that the MP, while being embedded into strong perturbations, effectively isolates the MSH electrons and most of the ions from the magnetosphere.

Another difference is that at the PB outer border the fluctuations, generated in the process of the MSH kinetic energy dissipation (see Figure 2.A6 and respective discussion above), are combined with dissipation at the MP *per se* (separated in the case of OT). This enlarges the fluctuation level and, consequently, enforces turbulent transport processes. The tilt dependence of the occurrence of PB and OT is presented in Figure 2.A4. Blue bars mark the number of PB in a dipole tilt interval, while the red bars mark the stagnant MSH outside the MP – the OT having large-scale $|B|$ reductions. The green bars denote the number of PB, for which their being inside the MP is clearly supported by the energetic particle data (see Figure 2.A6 and related discussion above); black bars depict the number of the external $|B|$-reductions with clearly dominating soft energetic particles from the MSH. We note that in ~15% cases the soft-energetic particle data were absent and that, if the trapped energetic particles were seen just inside the MP, their intensity usually exceeded that in the MHS. Fewer energetic particles in the OT could be due to particle leakage into the downflowing MSH, while in the PB they are back-scattered by the stronger TBL at the PB outer border.

All in all, Figure 2.4 shows the OT being encountered for positive tilts and the PB at negative tilts. Specifically, the maximum of 20 PB cases occurs for tilts between −15° and −25°, and 77% of the PB are registered at tilts $< -5$; 6 OT cases are seen at negative tilts and 21 cases at positive tilts ($>|5|°$). The energetic particle data prove that the PB occurs on closed magnetic field lines in a majority of cases (e.g., in 63% for tilts between −15° and −25°). No clear dependence of PB occurrence on magnetic shear across the MP has been found, while for $>65\%$ cases the IMF $B_z > 0$.

As mentioned in the discussion of Figure 3, the high-beta (2–15) plasma and direct interaction with the incident MSH flows are distinct differences of the PB from the rest of the outer cusp. Generally in the OC, quasi-

perpendicular MSH ions are strongly guided by the magnetic field (Kirpichev et al., 1999). The domination of PB during IMF $B_z > 0$ can be accounted for as follows: (i) during southern IMF the minimum $|B|$ in the OC is shifted equatorward (cf. Spreiter and Briggs, 1962, Maynard, 2003), and that favors penetration of the MSH flows into the cusp throat; (ii) drifts, caused by the inductive electric field from the MSH, move plasma from the PB towards the plasma sheet for IMF $B_z < 0$, and from the tail boundary layer towards the PB for $B_z > 0$. Quasi-perpendicular ions, evident up to the upper energy limit in Figure 6.B4c, and electrons are trapped in the diamagnetic cavity.

We infer their local heating by the strong turbulence (see, e.g., Savin et al., 1998b) both from continuous ion distributions (from MSH energies up to soft energetic particle energies) and from their absence outside the PB deeper in magnetosphere. Particles from the plasma sheet can also contribute to the trapped population (Shabansky and Antonova, 1968), but, for that to happen, they should lose their parallel momentum excess by wave-particle interactions in the TBL (i.e. be back-scattered into the PB by nonlinear waves in the TBL).

## 5. Discussion

After presentation of data for the characteristic case of 19 June 1998 from Interball-1 and Polar, and a statistical study of perturbations near the high-latitude MP, we discuss the data presented earlier. Savin et al. (1998b, 2001, 2002a, b, 2004) and Maynard (2003) provide relevant references and results.

### 5.1. Turbulent boundary layer and multiscale reconnection

An inspection of the TBL crossings observed by Interball-1 (Figure 2.A1–2.A3) shows that on 19 June 1998 the TBL is registered at a rather typical position (see Sections 2–3). The TBL is concentrated at high latitudes ($|Z| > 4$ $R_E$) over the cusp and downstream of it. Savin et al. (2002a) demonstrated that a substantial part of the events in the tail 'wings' at the higher latitudes is independent on the IMF $B_y$, which contradicts the 'sash' predictions (Maynard et al., 2001). Approximately another half of the 'wing' events follows the 'sash' $B_y$-dependence. Another possible 'wing' source is the TBL downstream of the cusps (see Figure 1, and Savin et al., 2004). The presence of TBL 'wings' for any IMF $B_y$ is in agreement with the MSH plasma penetration not only in the cusp-shaped dayside and 'sash' regions, but on the tail flanks (cf. Haerendel, 1978). The TBL is present in $>80\%$ of the high-latitude MP crossings. The most intense events could be approximated by effective disk with diameter of ~6 $R_E$ above the dayside cusps, with an average maximum

RMS of about $22nT$ (see Savin et al., 1999). At low latitudes the intense events are encountered mostly in the tail.

For positive tilts, the TBL is indented in the $YZ$-plane (Figure 2.2). This agrees with the direct interaction of the open cusp throat with the incident MSH flows (Figure 1). The indentation in the TBL/MP does not represent a characteristic feature of the winter hemisphere (Figure 2.2). This asymmetry suggests that the interaction of the MSH flow is different for negative and positive tilts (see Figure 6.B7). No such crucial dependence has been found for the IMF direction, while specific shifts have been outlined, for example by Merka et al. (2000).

Essential MSH plasma heating (~300 eV) occurs in 82% of the cases within the TBL 'diamagnetic bubbles' (Savin et al., 1999). The correlation of soft energetic particles with strong turbulence has been confirmed by the Interball-1 and Polar data on 19 June 1998 (see Section 2.4 and Chen and Fritz, 1997, Blecki et al., 1998, Savin et al., 2002c). The presence or lack of energetic particles also helps in placing of the PB and OT inside or outside the MP (see also Section 5.2 below). Detailed pitch-angle distributions and energy cuts point to three different populations of energetic particles in the disturbed TBL outside the MT: (i) dense, heated MSH particles ($< 50$ keV), which constitute a source for the soft energetic ions in PB (see panel a in Figure 6.B4, Figure 7 and related discussions in Section 2.4); (ii) intermediate energy particles escaping from PB; (iii) bursty higher energy perpendicular ions, presumably locally accelerated by the wide-band turbulence. In the PB the loss-cones in ion distributions with energies of 7–25 keV directed towards the nearest (southern) ionosphere conform to the PB as a source for precipitating particles into the dayside cusp ionosphere. On 19 June 1998, the data display typical TBL features (Figure 2.A6 and 6.A6): these are (i) wideband intensive nonlinear fluctuations (with energy density up to 40% of kinetic plasma energy density in flowing MSH); (ii) 'diamagnetic bubbles' with $|B|$ drops from ~$75nT$ down to few $nT$ (Figure 6.B6), and (iii) plasma heating and field-aligned jets, etc. (cf. Savin et al., 1998b, 2002a, b, Sandahl et al., 2002). The latter has been accounted for by reconnection bulges at the border of the outer cusp (Dubinin et al., 2002, Savin et al., 2002a, 2002b, 2004).

To combine these with well-known reconnection for northward IMF downstream of the cusp for a smooth MP, we propose the scheme depicted in Figure 8. On the indented MT in the open cusp throat (cf. Figures 1b and 6.B7) there are at least two places with anti-parallel magnetic fields on the MP. The upper reconnection site is the 'standard' large-scale (few $R_E$) tail reconnection, the lower one is inside the OT, superimposed on the TBL fluctuations. The original magnetospheric field lines are marked by the lines with arrows and those of the IMF by lines with circles. Reconnection pulses inside the OT can be recognized in Figure 6.B6: the local magnetic field is

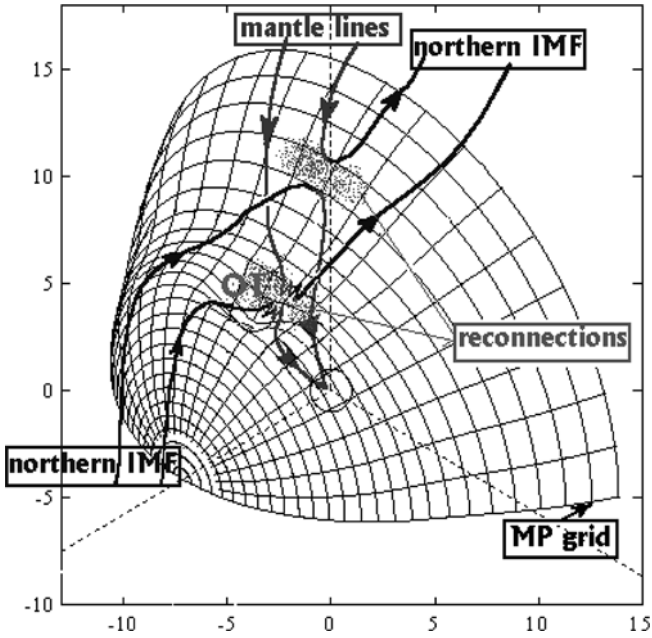


*Figure 8*. Sketch for multiple reconnection sites at the indented MP for a northern IMF.

practically anti-parallel (see changes in $B_y$), and the dominant positive $V_y$-burst direction corresponds to magnetic stress (Dubinin et al., 2002). However, the comparison with the SW data from Geotail via GDCF obviously demonstrates no evidence for the SW driving of the plasma jets. Instead, the jets' repetition conforms to TBL-driving (see Figure 2.A5, A6 and related discussions in Section 2). Savin et al. (2002a) accounted for the difference of the power for Polar and Interball spectra of about one order of magnitude by the average magnetic field annihilation in a patchy reconnection (cf. Maynard, 2003). Similar reasoning for 29 May 1996 has been proposed by Savin et al. (2004).

Simultaneously, Figure 6.B6 demonstrates the dominance of the jet ion energy over the magnetic energy, that invokes triggering of the reconnection by the accelerated plasma jets that originated in the upstream TBL (see Figure 2.6, Figure 4 and related discussions). This bursty reconnection corresponds to smaller (middle) scales. Later on we refer to this as 'primary cusp reconnection'. Its characteristic scale is estimated as a few thousand km. The primary cusp reconnection differs from that at low latitudes, where the MSH dynamic pressure results first in a compression of the static magnetic field and then a release of the magnetic energy through the (large-scale) reconnection into plasma acceleration and heating. At high latitudes the TBL-triggered bursty reconnection plays the role of a 'shutter', which provides the local

transformation of the MSH kinetic energy directly into that of deflected/accelerated flows. Savin et al., (2002a) give the respective picture for the southern IMF, which is confirmed by the sunward/vertical flows measured in the cusp vicinity by Magion 4. Maynard et al. (2003a,b) provides further evidence for most of the merging being at high latitudes and being unsteady; multiple sites can be operative at once and active for 30 s to a few minutes. In a sense, merging is continuously happening, but not continuously at most sites.

Savin et al. (2004) demonstrate parallel operation of the primary cusp reconnection and remote laminar reconnection tailward the cusp on 29 May 1996 for the dominant IMF $B_z > 0$. Belmont and Rezeau (2001) show that strong ULF fluctuations near the MP can independently result in micro-reconnection all along the MP. Another possibility is that the secondary reconnection of the fluctuating fields in the TBL can provide the plasma inflow even for a quasi-parallel magnetic field (cf. Chandler et al., 1999). The micro-reconnection scales range down to an ion gyroradius. The fluctuations (including micro-reconnection) create the specific structure of the MP current sheet (s) with magnetic islands, which results in plasma percolation through the nonlinear boundary network (Kuznetsova and Zelenyi, 1990). An estimate shows that this stochastic plasma transfer through the TBL/cusp walls can populate both the cusp and low latitude boundary layer; the diffusion coefficient $D_p$~(5–10) $10^9$ m/s for typical MP parameters results in a particle influx of (1–2) $10^{27}$ particles/s (Savin et al., 1999). Primary cusp reconnection should certainly amplify the plasma inflow.

Comparison with the kinetic simulation of thin current sheets (Savin et al., 2002b) demonstrates that the general spectral and bi-spectral properties of the TBL fluctuations can be reproduced by the modeling. For example, the registered quasi-coherent structures can be regarded as residuals of the nonlinear evolution of current sheets; the 'diamagnetic bubble' presence supports this suggestion as the field depletions in the middle of equilibrium current sheets is reproduced by a number of modeling results of the nonlinear current states (see, e.g., Buechner et al., 1999 and La Belle-Hamer et al., 1995). As a result of the multi-scale reconnection, field lines are connected through the TBL in a statistical sense, without an opportunity to trace individual field lines in the inhomogeneous non-equilibrium 2-phase medium, one phase being the frozen-in 'MHD' plasma and another represented by the unmagnetized 'diamagnetic bubbles' embedded in the nonlinear current sheets and vortices. The latter 'phase' (in the statistical sense) provides the power-law spectra with slope ~−1 (Savin et al., 2002b), which implies a special type of translation symmetry of the fluctuations. The quasi-coherent wave-packets are breaking the Gaussian statistics, most probably due to TBL intermittency.

### 5.2. Perturbation of magnetosheath flows by the outer cusp throat

We now address another primary mechanism for energy and mass transfer at the MSH/cusp interface: direct interaction of the MSH flow with the outer cusp. From Figure 1, 2, 2.A1–2.A3, 2.A6 and 6.B6–6.B7, we can see that the cusp throat might present a substantial obstacle to the plasma flow streaming around the MP. In the zero approximation the magnetic barrier can be regarded as a rigid local obstacle, the large-scale laminar reconnection being inferred as a primary mechanism for the mass and energy transfer inside the MP (see, e.g., Russell (1995), Maynard (2003), and references therein). The interaction with the barrier occurs at low latitudes and in region "1" in Figure 1 (at positive tilts). In the plasma–plasma interaction in the high-beta case over the cusp throat (at negative tilts, see Figure 3) only high-amplitude waves and, probably, surface charge at the MP can constitute the means for interactions in a self-consistent regime with pre-existed high-beta stagnant plasma (see Section 5.3 and Lavraud et al., 2002). The local plasma–plasma interaction occurs also at the interface of the OT and MSH, but its intensity should be smaller as the turbulence has its maximum magnitude deeper in the throat at the OT/OC transition.

Multi-point data on 27 January 1997 permit the TBL depth in the near tail to be evaluated as being ~2 $R_E$ from the satellite–subsatellite measurement comparisons (Savin et al., 2004). The high-latitude interactions result in the substantial MSH kinetic energy transformation into thermal energy of the particles: the ratio $W_{kin}$ /$nT_i$ rises from 20 to 50%. The schematic representation of the resulting picture is marked by "2" in Figure 1a. The sound Mach number in the unperturbed MSH ($M_s$~2) drops to $M_s$~1 downstream of the cusp obstacle. In the two cases described in Savin et al. (1998b), the MSH/OT transition in going through thin magnetic barriers has $B^2/2\mu_0 \sim nT_i + W_{kin}$ in both the MSH and OT. The latter does not resemble intermediate/slow shock solutions (see, e.g., Karimabadi et al., 1995).

$M_s$~2 is also seen in the Interball-1 data just outside the MP on 29 May 1996 (Savin et al., 1998a, 2004). Savin et al. (2001) compared the maximum ion heating in the TBL on 2 April 1996 with the Rankine–Hugoniot predictions for shock transitions using a magnetosonic Mach number ($M_m$~1.2) in the MSH, an Alfvenic Mach number for the normal ion speed ($M_{An}$~1.2) upstream of the OT, and a full Alfvenic Mach number ($M_A$~3.5): $T_i/T_{MSH} \sim 1 + \gamma - 1)M^2 \sim 1.6$ and ~5, respectively, for the Alfvenic Mach numbers of 1.2 and 3.5; we take $\gamma \sim 5/3$, and take into account that $nT_i >> W_{kin}$ in the OT. The experimental ion temperature gain on those days of ~2.2 is higher than it should be at the inclined shock transition, but it is still much less than the maximum heating at the perpendicular shock. Thus Savin et al. (2001) concluded that the energy transformation in the TBL significantly differs from a thin shock transition.

Similarly, the disturbed region at 09:45–10:00 UT (Figure 2.6) should be treated as a unique 'thick' region with both remotely operated ion velocity and pressure cascades and local discontinuities (e.g., MP and a boundary at ~09 UT). The presence of the bursty super-Alfvenic flows in the upstream TBL and PB (see discussion of the jet at 09 UT in Section 2.2) obviously contradicts the MHD descriptions of thin shocks. We would like to point out also that the TBL provides secondary magnetic flux reconnection at any magnetic shear. The magnetic flux, reconnected at small scales, on average, is capable of driving magnetospheric convection (Haerendel, 1978).

At this point we touch an open critical problem of the SW/magnetosphere interaction: where are the geomagnetic field lines being opened? Our current understanding is that this process is both a multi-point and a multiscale one. We believe that the MSH/cusp interface plays the dominant role in the opening of flux tubes, at least during quasi-steady conditions. The tilt angle dependence of the cusp position both at high and low altitudes (Merka et al., 2000) has a natural explanation if the TBL is a general source of plasma for the cusps: (a) the higher the tilt (i.e. the closer the dipole axis points to the Sun), the more open the OT becomes to the external MSH flow (i.e. the OT tailward wall represents a steeper obstacle for the MSH flow); (b) the higher the shift/penetrations at the OT tailward wall, the deeper the MSH plasma will be seen on the tail field lines; and (c) the deeper the plasma penetration (and/or tailward field line deflection), the more tailward it will be projected into the polar cap (i.e. the cusp is at higher invariant latitudes). Note that the tilt-related cusp shift has no explanation in the 'traditional' global-reconnection approach. At anti-sunward dipole tilts Interball detects demagnetized heated plasma of MSH origin in 'plasma balls', which have scales of a few $R_E$, on the Earthward side of the MP. The thick multilayered structure implies a type of interconnected non-equilibrium boundary, and the PB represents a local obstacle (partially absorbing) for the incident MSH flow. The observed high-amplitude waves constitute the means for their interaction.

The large-scale PB can have substantial impact on the MSH/magnetosphere interactions as a storage of MSH plasma, which in turn becomes a source of the MSH plasma to the magnetosphere. A sunward tilt opens the OT for direct interaction with the MSH flow. The asymmetric streamlining of the MSH flow around cusps is shown in Figure 6.B7: in summer, the MSH flow produces a TBL over the outer cusp, whereas in winter the TBL is located both upstream of the MP and at the outer PB border. The general difference of the OT with the $|B|$ reductions (Figure 6.B5) from a PB is that the MP, while being imbedded into strong perturbations, effectively isolates the MSH electrons and most of ions from the magnetosphere in the OT case. The energetic particle data prove the PB closed topology in a majority of the cases. The probability of crossing the PB at GSM $|Z| > 4$

$R_E$ at tilts $< -5°$ is ~25%. Thus, the PB are present rather regularly in the outer cusp at the negative tilts, and they could provide a valuable contribution in the populating of the magnetosphere by MSH plasma. They could also store soft energetic particles in the minimum-$|B|$ configuration (cf. Sections 2.5, 5.1 and Shabansky and Antonova, 1968). MHD modeling (Maynard et al., 2003b) demonstrates that low-$|B|$ regions occur at negative tilts in the cusp vicinity inside the dayside MP, thus confirming that the PB are a necessary element of global equilibrium at the magnetospheric boundary.

### 5.3. Turbulence sources and properties

Following Haerendel (1978), we suppose that first of all the TBL results from the turbulent mixing driven by the regular MSH flow interaction with the near-cusp magnetopause. The disturbed flows, accelerated in a region remote from the cusp reconnection site, can contribute to the TBL generation as well. The large-scale 'remote' reconnection sites (see Section 5.1) also regulate the TBL position by shifting the MP indentation according to the SW parameters. Away from the plasma stagnation region in the OT center, the Kelvin–Helmholtz plasma vortices with secondary reconnections should provide a mechanism for plasma heating/transport (cf. Q. Chen et al., 1997). The fluctuation level in the MSH, especially downstream of quasi-parallel bow shocks, is believed to stimulate the generation of ULF turbulence in the TBL.

Savin et al. (2004) reported that the correlation for time intervals of ~5–15 min in the post-BS region, middle MSH and OT reaches 0.6–0.7, and is a manifestation of the TBL/MP reactions to the SW/MSH transients. Thus, the transient current sheets and density gradients generated by dynamic SW interactions with the MP should contribute to turbulence in the TBL. However, simultaneous Geotail spectra and correlation analysis suggest the local character of the main TBL disturbances (Figure 2.A5–2.A6 and 6.B6). As a whole, the TBL collects, transforms and generates the plasma flow and magnetic field disturbances simultaneously from several sources. Its status depends on the short-term time history of the SW/magnetosphere interactions, influencing, in turn, the interaction of the magnetosphere with newly-arriving disturbances at each particular moment.

Simultaneous Interball/Polar data demonstrate the presence of a maximum at 1–2 mHz throughout the TBL in both hemispheres. The spectra of $W_{kin}$ and $nT_i$ (Figure 2.A6, Figure 4) allow this disturbance to be traced throughout the MSH. Besides the transient/dynamic reactions of the TBL to external disturbances, the TBL appears to have well-defined inherent properties, which have been traced at different points of the MSH and MP boundary layers during the favorable period of relatively steady SW

parameters. The modern wavelet technique provides us with strong evidence that the spectral characteristics of the TBL in the different hemispheres on 19 June 1998 are well defined. The most pronounced TBL waves at 0.003–0.5 Hz have characteristic kinked shapes and slopes (Savin et al., 2002a). We have checked the waves in the TBL on 26 August 1995, 29 May 1996, and 23 June 1998 and found that the kinked shape with slopes of 1–1.5 and 2–2.6 are characteristic for the TBL. The higher value of the slope in the TBL of ~2 is close to that characteristic for the developed self-consistent kinetic turbulence in the geomagnetic tail (see, e.g., Zelenyi and Milovanov, 1998, and references therein).

Comparison with the simulation of thin current sheets provides evidence that the random current sheets with features of coherent wave-packet can result in slopes of ~−1 in the magnetic power spectra (see Section 5.1 and Savin et al., 2002b). Savin et al. (2001) have proposed the following self-consistent concept of TBL interactions. Cascade-like wavelet and bicoherence spectrograms and the wavelet correlation time suggest a coherent, most probably 3-wave, interaction between wave trains, while the disturbances seem to be random in waveforms.

The local wave trains originate from the interaction of the disturbed MSH flows with the MP; their dispersion is indicative of kinetic Alfven waves (KAW, see Stasiewicz et al., 2001, and Savin et al., 2004). Johnson and Cheng (1997) proposed excitation of the transverse KAW at the MP by the interaction of compressible MSH waves with the current sheet; the wave properties discussed above are in satisfactory agreement with their predictions. Later Belmont and Rezeau (2001) demonstrated the growth of the trapped large-amplitude KAW inside the non-uniform current sheets. Our new finding here from the ion fluctuations is the global (over the MSH) synchronization at ~1.3 mHz. The MSH synchronization is seen mostly in the density (MS) fluctuations, which are transformed into velocity (KAW) fluctuations in the upstream TBL (Figure 6.B1–6.B3). Turning back to the TBL interaction scheme, while linear KAW resonances (i.e. singularities in the equations of Belmont and Rezeau, 2001) are absent, we suggest that the coherent large-scale structures can originate from the reverse KAW cascades, focused by the concave MP and/or cusp walls in the outer cusp vicinity (cf. Figure 2.A6, 6.B1–6.B4 and Savin et al., 2001, 2004). At the nonlinear stage the Alfvenic disturbances in the TBL modulate the incident MSH flow in a self-consistent manner, being globally synchronized by phase coupling with the large-scale variations (at ~3–5 mHz, see Figure 2.A6, Figure 4 and Savin et al., 2003a).

Thus, the chain is closed: the TBL seems to be a 'thick' multi-scale self-organized system of interacting nonlinear waves. This suggests a qualitative difference from the traditional approach when the MSH/cusp interaction is regarded as a linear superposition of magnetospheric responses to SW or MSH disturbances. Note also that the long-term correlation is sug-

gestive of systems out of equilibrium near the critical point (cf. Consolini and Lui, 2000). The kinked TBL spectra with characteristic slopes remarkably resemble those in the near-Earth neutral sheet in the state of self-organized criticality (see, e.g., Zelenyi and Milovanov, 1998). Using $f_1 + f_2 \sim f_3 = 4.5$ mHz$\sim \vec{k}\vec{V}/2\pi$ (see Figure 6.3B in Section 4.2 and related discussions) as a proxy for evaluation of the characteristic scale, we obtain $L \sim V_{MSH} / f_3 \sim 5$–$7$ $R_E$. This is comparable with the TBL span along the MP in the indentation or with that of a 'plasma ball' (Figure 6.B7). On the other hand, the spectral maximum seen in the MSH, through the TBL and into the outer cusp (see Figure 6.B1 and 6.B2) demonstrates the global character of the phenomenon. Such long waves can pass through the MP (see Figure 6.B2) and might resonate with the dayside flux tubes in the Pc 4–5 range or at higher harmonics (cf. Pilipenko et al., 1999).

The general scheme presented above has been defined concretely in Section 2.2 for the low-shear MP in front of the PB. As mentioned above it is valuable both because of different types of plasma–plasma interaction (versus a plasma–magnetic barrier interaction at the low-latitude MP) and because the resulting PB inside the MP represents a great MSH plasma reservoir for the inner magnetosphere. The main mechanism for the plasma–plasma (i.e. MSH flow with PB) interaction is via the nonlinear waves in the TBL upstream of the MP in the flowing MSH, but has been poorly studied at high latitudes. The main physical problem is that the practically demagnetized PB (ion beta ~15) cannot interact with the flow via magnetic forces this constitutes the principal difference with the dayside low-latitude MP which is generally a magnetic barrier.

We have analyzed the detailed dynamics of the ion energy and of the Poynting flux to clarify further the pattern of interactions in the upstream TBL. The wave packets, propagating upstream from the MP, stimulate partial randomization of the flow far in front of MP (>1 h). The interaction of fluctuations in the incident flow with the upstream-propagating waves launches transient perturbations downstream, which both result in magnetosonic jets (Figure 2 and 3) and trigger the cascade-like nonlinear energy transformation in the TBL. This causes the MSH kinetic energy to drop by up to 40%, while the jets transport the ion momentum excess downstream. The drop of kinetic energy results also in the amplification of low-frequency pulsations (at ~1.3 mHz). These fluctuations are phase-coupled with the spectral maxima at 3–10 mHz at ~09:00, 09:15, 09:30 and 09:45 UT in Figures 2.A6, 6.B 1, and 6.B2. A macro-equilibrium cannot be achieved in the outer BL until several characteristic periods have elapsed, which correspond to the time scales of patchy merging in ionosphere (Maynard, 2003). The strong upstream fluctuations plasma density and velocity can be visible at the lower latitudes (cf. 'slow mode transitions', Song et al., 1992).

### 5.4. Concluding remarks

The results of our data analysis strongly indicate that the TBL fluctuations, instead of being random, are phase-coupled and 'organized' into cascades of nonlinear (presumably 3-wave) interactions. The coherent waves described above control the spectral shape, and result in non-Gaussian statistical characteristics of the disturbances that conforms to the fluctuation intermittency (Savin et al., 2002b).

We suggest that, in the SW energy transformation to the magnetosphere, multi-scale TBL processes play at least a comparable role to those of large-scale reconnection, which generally occurs far from the cusp. Turbulent diffusion and percolation are capable of populating the magnetosphere with MSH plasma. The TBL transforms the MSH flow energy, including deceleration and heating of the flow downstream from the high latitude cusp. Patchy time-varying reconnection provides the means for energy conversion and plasma transport in the small-scale portion of the TBL energy cascade.

The plasma–plasma interaction over the closed cusp throat operates via reflected waves, which provoke the chaotization of ~40% of the upstream kinetic energy. The characteristic flow decay into magnetosonic/Alfvenic streams also launches TBL nonlinear cascades. This represents the non-stationary non-MHD mechanism for the momentum loss via TBL vortex streets, which diminish the effective plasma–plasma friction similar to that in plasma–plasma hydrodynamics (cf. Haerendel, 1978). The magnetosonic jets carry the flow momentum 'excess' downsteam, permitting deceleration of the rest of the boundary layer plasma.

## Acknowledgements

We thank K. W. Ogilvie and the SWE team for providing WIND solar wind dynamic pressure data, R. Lepping for providing WIND magnetic field data, J. Scudder for providing the HYDRA data and S. Lamey for help in preparation of the paper. We thank the GEOTAIL/MGF team, especially H. Matsui, for providing high-resolution magnetic field data used in this paper. This work was partially supported by International Space Science Institute, European Commission Research Training Network HPRN-CT-2001-00314, and by grants KBN 4 T12 016 28, INTAS 03-50-4872, RFFR 02-02-17160 and 03-02-16967, Science School 1739 2003 2.

## References

Belmont, G., and Rezeau, L.: 2001. "Magnetopause Reconnection Induced by Hall-NIED Fluctuations", *J. Geophys. Res.* **106**(A6), 10,751–10,760.

Blecki, J., Rothkaehl, H., Kossacki, K., Wronowski, R., Klos, Z., Juchniewicz, J., Savin, S., Romanov, S., Klimov, S., Triska, P., Smilauer, J., Simunek, J., Kudela, K., and Forster, M.: 1998. ''ULF-ELF-VLF-HF Plasma Wave Observations in the Polar Cusp Onboard High and Low Altitude Satelites'', *Phys. Scripta* **75**, 259–263.

Büchner, J.: 1999. ''Reconnection: Space Plasma Simulations for Multi-Spacecraft Satellite Observations in the ISTP era'', *Phys. Chem. Earth* **24**, 179–187.

Chandler, M. O., Fuselier, S. A., Lockwood, M., and Moore, T. E.: 1999. ''Evidence of Component Merging Equatorward of the Cusp'', *J. Geophys. Res.* **104**, 22,623–22,633.

Chen, J., Fritz, T. A., Sheldon, R. B., Spence, H. E., Spjeldvik, W. N., Fennell, J. F., Livi, S., Russell, C. T., Pickett, J. S., and Gurnett, D. A.: 1998. ''Cusp Energetic Particle Events: Implications for a Major Acceleration Region of the Magnetosphere'', *J. Geophys. Res* **103**, 69–78 .

Chen, J., and Fritz, T. A.: 1998. ''Correlation of Cusp MeV Helium with Turbulent ULF Power Spectra and its Implications'', *Geophys. Res. Lett.* **25**, 4113–4116 .

Chen, Q., Otto, A., and Lee, L. C.: 1997. ''Tearing instability, Kelvin–Helmholtz Instability and Magnetic Reconnection'', *J. Geophys. Res.* **102**((A1), 151–161 .

Chen, S.-H., Boardsen, S. A., Fung, S.F, Green, J. L., Kessel, R. L., Tan, L. C., Eastman, T. E., and Craven, J. D.: 1997. ''Exterior and Interior Polar Cusps: Observations from Hawkeye'', *J. Geophys. Res.* **102**(A6), 11,335–11,347.

Consolini, G., and Lui, A. T..: 2000. ''Symmetry Breaking and Nonlinear Wave–Wave Interaction in Current Disruption: Possible Evidence for a Phase Transition'', in R.. Fujii, M.. Hesse, R.. Lysak, and S.. Ohtani (eds.), *Magnetospheric Current Systems, Geophysical Monograph 118*, American Geophysical Union, Washington D.C., pp. 395–401.

Dublihin, E., Skalsky, A., Song, P., Savin, S., Kozyra, J., Moore, T. E., Russell, C. T., Chandler, M. O., Fedorov, A., Avanov, L., Sauvaud, J. A., and Friedel, R. H. W.: 2002. ''Polar-Interball Coordinated Observations of Plasma Characteristics in the Region of the Northen and Southern Distant Cusps'', *J. Geophys Res.* **107**((A5), 1010.29/2001 JA900068.

Fritz, T. A., Chen, J., and Sheldon, R. B.: 1997. ''The Role of the Cusp as a Source for Magnetospheric Particles: A New Paradigm?'', *Adv. Space Res.* **25**, 1445–1457 .

Haerendel, G., and Paschmann, G..: 1975. ''Entry of Solar Wind Plasma into the Magnetosphere'', in B.. Hultqvist, and L.. Stenfl (eds.), */em Physics of the Hot Plasma in the Magnetosphere*, Plenum, NY, pp. 23.

Haerendel, G.: 1978. ''Microscopic Plasma Processes Related to Reconnection'', *J. Atmos. Terr. Phys.* **40**, 343–353.

Johnson, J. R., and Cheng, C. Z.: 1997. ''Kinetic Alfven Waves and Plasma Transport at the Magnetopause'', *Geophys. Res. Lett.* **24**, 1423–1426.

Kirpichev, I., Fedorov, A., Grigoryev, A., Budnick, E., and Dubinin, E.: 1999. ''Quasi-trapping of the Charged Particles in the Local Minimum of Magnetic Field in Exterior Cusp'', *Cosmic Res. (Russia)* **37**((6), 638–643.

Klimov, S. I., Nozdrachev, M. N., Triska, P., Voita, Ia., and Galeev, A. A.: 1986. ''Investigation of Plasma Waves by Combined Wave Diagnostic Device BUD-WAR PROGNOZ-10-INTERCOSMOS'', *Cosmic Research (Transl. from Russian)* **24**, 177–184.

Kuznetsova, M. M. and Zelenyi, L. M.: 1990, ''The Theory of FTE: Stochastic Percolation Model''. in C. T. Russell, E. R. Priest and L. C. Lee (eds), *Physics of Magnetic Flux Ropes*, pp 473–488 American Geophysical Union..

La Belle-Hamer, A. L., Otto, A., and Lee, L. C.: 1995. ''Magnetic Reconnection in the Presence of Sheared Flow and Density Asymmetry: Application to the Earth's Magnetopause'', *J. Geophys. Res.* **100**, 11,875–11,889.

Lavraud, B., Dunlop, M. W., Phan, T. D., Reme, H., Bosqued, J. M., Dandouras, I., Sauvaud, J. A., Lundin, R., Taylor, M. G. G. T., Cargill, P J., Mazelle, C., Escoubet, C. P., Carlson, C. W., McFadden, J. P., Parks, G. K., Moebius, E., Kistler, L. M., Bavassano-Cattaneo, M. B., Korth, A., Klecker, B. and Balogh, A.: 2002, "Cluster Observations of the Exterior Cusp and its Surrounding Boundaries Under Northward IMF". *Geophys. Res. Let*. **29**(20), Art.No. (1995) Oct. 15.

Maynard, N. C., Savin, S., Erickson, G. M., Kawano, H., Nemecek, Z., Peterson, W. K., Safranokova, J., Sandahl, I., Scudder, J. D., Siscoe, G. L., Sonnerup, B. U. O., Weimer, D. R., White, W. W., and Wilson, G. R.: 2001. "Observation of the Magnetospheric 'sash' and it Simplications Relative to Solar-Wind/Magnetospheric Coupling: A Multisatellite Event Analysis", *J.Geophys. Res*. **106**, 6097–6122.

Maynard, N. C.: 2003, "Coupling of the Solar-Wind/IMF to the Ionosphere Through the High Latitude Cusps" *Surveys in Geophysics* 25, this issue.

Merka, J., Safrankova, J., Nemecek, Z., Fedorov, A., Borodkova, N., Savin, S., and Skalsky, A.: 2000. "High Altitude Cusp: INTERBALL Observations", *Adv. Space Res*. **25**(7/8), 1425–1434.

Paschmann, G., Haerendel, G., Sckopke, N., Rosenbauer, H., and Hedgecock, P. C.: 1976. "Plasma and Magnetic Field Characteristics of the Distant Polar Cusp Near Local Noon: The Entry Layer", *J. Geophys. Res*. **81**, 2883–2899.

Petrinec, S. M., and Russell, C. T.: 1995. "An Examination of the Effect of Dipole Tilt Angle and Cusp Regions on the Shape of the Dayside Magnetopause", *J. Geophys. Res*. **100**, 9559–9566.

Pilipenko, V., Fedorov, E., Mazur, N., Engebretson, M. J., and Hughes, W. J.: 1999. "Magnetohydrodynamic Waveguide/Resonator for Pc3 ULF Pulsations at Cusp Latitudes", *Earth Planets Space* **51**, 441–448.

Pottelette, R., Malingre, M., Dulouloz, N., Apanicio, B., Lundin, R., Holmgren, G., and Mark-lund, G: 1990. "High Frequency Waves in the Cusp/Cleft Regions", *J. Geophys. Res*. **95**, 5957–5971.

Romanov, V., Savin, S., Klimov, S., Romanov, S., Yermolaev, Yu., Blecki, J., and Wronowski, R.: 1999. "Magnetic Turbulence at the Magnetopause: Plasma Penetration", *J. Tech. Phys. (Poland)* **40**(1), 329–332.

Russell, C. T.: 1995, "The Structure of the Magnetopause", in: P. Song, B. U. O. Sonnerup and M. F. Thomsen (eds), *Physics of the Magnetopause*, American Geophysical Union, pp 81–98.

Sandahl, I.: 2002. "Recent Cusp and Cleft Results from Interball", *Adv. Space Res*. **30**((7), 1711–1723.

Savin, S. R.: 1994 "ELF Waves Near the High Latitude Magnetopause". In: *Abstracts of AGU Chapman Conference on Physics of the Magnelopause*, March 14–18, 41.

Savin, S. P., Balan, O., Borodkova, N., Budnik, E., Nikolaeva, N., Prokhorenko, V., Pulkkinen, T., Rybjeva, N., Safrankova, J., Sandahl, I., Amata, E., Auster, U., Bellucci, G., Blagau, A., Blecki, J., Buchner, J., Ciobanu, M., Dubinin, E., Yermolaev, Y, Echim, M., Fedorov, A., Formisano, V., Grard, R., Ivchenko, V., Jiricek, F., Juchniewicz, J., Klimov, S., Ko-repanov, V., Koskinen, H., Kudela, K., Lundin, R., Lutsenko, V., Marghitu, O., Nemecek, Z., Nikutowski, B., Nozdrachev, M., Orsini, S., Parrot, M., Petrukovich, A., Pissarenko, N., Romanov, S., Rauch, J., Rustenbach, J., Sauvaud, J. A., Sarris, E. T., Skalsky, A., Smilauer, J., Triska, P., Trotignon, J. G., Vojta, J., Zastenker, G., Zelenyi, L., Agafonov, Y., Grushin, V., Khrapchenkov, V., Prech, L., and Santolik, O.: 1997. "Interball Magnetotail Boundary Case Studies", *Adv. Space Res*. **19**, 993–1015.

Savin, S. P., Romanov, S. A., Fedorov, A. O., Zelenyi, L., Klimov, S. I., Yerinolaev, Y. I., Budnik, E. Y., Nikolaeva, N. S., Russell, C. T., Zhou, X. W., Urquhart, A. L., and Reiff,

P. H.: 1998a. "The Cusp/Magnetosheath Interface on May 29, 1996: Interball-1 and Polar Observations", *Geoph. Res. Lett.* **25**, 2963–2966.

Savin, S. P., Borodkova, N. L., Budnik, E.Yu., Fedorov, A. O., Klimov, S. I., Nozdrachev, M. N., Morozova, E. I., Nikolaeva, N. S., Petrukovich, A. A., Pissarenko, N. F., Prokhorenko, V. I., Romanov, S. A., Skalsky, A. A., Yermolaev, Yu.I., Zastenker, G. N., Zelenyi, L. M., Triska, P., Amata, E., Blecki, J., Juchniewicz, J., Buchner, J., Ciobanu, M., Grard, R., Haerendel, G., Korepanov, V. E., Lundin, R., Sandahl, I., Eklund, U., Nemecek, Z., Safrankova, J., Sauvaud, J. A., Rustenbach, J., and Rauch, J. L..: 1998b. "Interball Tail Probe Measurements in Outer Cusp and Boundary Layers", in J. L.. Horwitz, D. L.. Gallagher, and W. K.. Peterson (eds.), *Geospace Mass and Energy Flow: Results from the International Solar–Terrestrial Physics Program,* Geophysical Monograph 104. American Geophysical Union, Washington D.C., pp. 25–44.

Savin, S., Zelenyi, L., Budnik, L., Borodkova, N., Fedorov, A., Nikolaeva, N., Nozdrachev, M., Romanov, S., Petrukovich, A., Yermolaev, Yu., Mukai, T., Kawano, H., Kokubun, S., Lundin, R., Sandahl, L, Russell, C. T., Maynard, N., Parks, G., Amata, E., Safrankova, J., Nemecek, Z., Blecki, J., Buchner, J., and Nikutowski, B..: 1998c. "Manifestations of Boundary Layer Dynamics in Substorm Activity, MultiSpacecraft-Study", in S. Kokubun, and. Y. Kamide (eds.), *SUBSTORM-4, International Conference on Substorms-4', Lake Hamana, Japan: March 9–13, 1998*, Terra Scientific Publ. Co., Tokyo, pp. 125–30 .

Savin, S., Budnik, E., Nozdrachev, M., Romanov, V., Yermolaev, Y., Zelenyi, L., Blecki, J., Buechner, J., and Nikutowski, B.: 1999. "On the Plasma Turbulence and Transport at the Polar Cusp Outer Border", *Checkhoslovak J. Phys.* **49**(4a), 679–693.

Savin, S.P, Zelenyi, L. M., Romanov, S. A., Klimov, S. I., Skalsky, A. A., Galeev, A. A., Smirnov, V. N., Nozdrachev, M. N., Yermolaev, Y. I., Avanov, L. A., Amata, E., Blecki, J., Buchner, J., Nikutowski, B., Dubinin, E. M., Nemecek, Z., Safrankova, J., Pedersen, A., Rauch, J. L., Rustenbach, J., Sauvaud, J. A., Song, P., and Stasiewicz, K.: 2001. "Turbulent Boundary Layer at the Border of Geomagnetic Trap", *JETP Lett.* **74**(11), 547–551.

Savin, S., Zelenyi, L., Maynard, N., Sandahl, L., Kawano, H., Russell, C. T., Romanov, S., Amata, E., Avanov, L., Blecki, J., Buchner, J., Consolini, G., Gustafsson, G., Klimov, S., Marcucci, F., Nemecek, Z., Nikutowski, B., Pickett, J., Rauch, J. L., Safrankova, J., Skalsky, A., Smirnov, V., Stasiewicz, K., Song, P., Trotignon, J. G., and Yermolaev, Y.: 2002a. "Multi-Spacecraft Tracing of Turbulent Boundary Layer", *Adv. Space Res.* **30**((12), 2821–2830.

Savin, S., Buchner, J., Consolini, G., Nikutowski, B., Zelenyi, L., Amata, E., Auster, H. U., Blecki, J., Dubinin, E., Fornacon, K. H., Kawano, H., Klimov, S., Marcucci, F., Nemecek, Z., Pedersen, A., Rauch, J. L., Romanov, S., Safrankova, J., Sauvaud, J. A., Skalsky, A., Song, P., and Yermolaev, Y.: 2002b. "On the Properties of Turbulent Boundary Layer Over Polar Cusps", *Nonlinear Processes in Geophysics* **9**, 443–451.

Savin, S., Blecki, J., Pissarenko, N., Lutsenko, V., Kirpichev, L., Budnik, E., Borodkova, N., Nozdrachev, M., Zelenyi, L., Romanov, V., Sandahl, I., Sauvaud, J. A., Buchner, J., Nikutowski, B., Gustafsson, G., Stasiewicz, K., and Korepanov, V.: 2002c. "Accelerated Particles from Turbulent Boundary Layer", *Adv. Space Res.* **30**(7), 1723–1730.

Savin, S., Zelenyi, L., Romanov, S., Sandahl, I., Pickett, J., Amata, E., Avanov, L., Blecki, J., Budnik, E., Büchner, J., Cattell, C., Consolini, G., Fedder, J., Fuselier, S., Kawano, H., Klimov, S., Korepanov, V., Lagoutte, D., Marcucci, F., Mogilevsky, M., Nemecek, Z., Nikutowski, B., Nozdrachev, M., Parrot, M., Rauch, J., Romanov, V., Romantsova, T., Russell, C., Safrankova, J., Sauvaud, J., Skalsky, A., Smirnov, V., Stasiewicz, K.,

Trotignon, J., and Yermolaev, Yu.: 2004. "Magnetosheath – Cusp Interface", *Ann. Geophys.* **22**((1), 183–212.

Shabansky, V. P., and Antonova, A. E.: 1968. "Topology of Particle Drift Shells in the Earth's Magnetosphere", *Geomagnetism and Aeronomy* **8**, 844–859.

Song, P., Russell, C. T., and Thomsen, M. F.: 1992. "Slow Mode Transition in the Frontside Slow Mode Transition in the Magnetosheath", *J. Geophys. Res.* **97**, 8295–8305.

Song, P., Russell, C. T., Gombosi, T. I., Spreiter, J. R., Stahara, S. S., and Zhang, X. X.: 1999a. "On the Processes in the Terrestrial Magnetosheath, 1: Scheme Development", *J. Geophys. Res.* **104**, 22,345–22,355.

Song, P., Russell, C. T., Zhang, X. X., Gombosi, T. I., Stahara, S. S., and Spreiter, J. R.: 1999b. "On the Processes in the Terrestrial Magnetosheath, 2: Case Study", *J. Geophys. Res.* **104**, 22,357–22,373.

Spreiter, J. R., and Briggs, B. R.: 1962. "Theoretical Determination of the Form of the Boundary of the Solar Corpuscular Stream Produced by Interaction with the Magnetic Dipole Field of the Earth", *J. Geophys. Res.* **67**, 37–51.

Stasiewicz, K., Seyler, C. E., Gustafsson, G., Pickett, J., and Popielawska, B.: 1997. "Magnetic Bubbles and Kinetic Alfven Waves in the High-Latitude Magnetopause Boundary", *J.Geophys. Res.* **106**, 29,503–29,514 .

Yamauchi, M., and Lundin, R.: 1997. "The Wave-Assisted Cups Model: Comparison to Low-Latitude Observations", *Phys. Chem. Earth* **22**, 729–734.

Zelenyi, L. M., and Milovanov, A. V..: 1998. "Multiscale Magnetic Structure of the Distant Tail: Self-Consistent Fractal Approach", in A.. Nishida, and D. N.. Baker (eds.), *New Perspectives on the Earth Magnetotail*, Geophysical Monograph 105, AGU, Washington D.C., pp. 321–338.

Surveys in Geophysics (2005) 26: 135–175
DOI 10.1007/s10712-005-1875-3 © Springer 2005

# CLUSTER OBSERVES THE HIGH-ALTITUDE CUSP REGION

B. LAVRAUD[1], H. RÈME[1], M. W. DUNLOP[2], J.-M. BOSQUED[1], I. DANDOURAS[1], J.-A. SAUVAUD[1], A. KEILING[1], T. D. PHAN[3], R. LUNDIN[4], P. J. CARGILL[5], C. P. ESCOUBET[6], C. W. CARLSON[3], J. P. McFADDEN[3], G. K. PARKS[3], E. MOEBIUS[7], L. M. KISTLER[7], E. AMATA[8], M. -B. BAVASSANO-CATTANEO[8], A. KORTH[9], B. KLECKER[10] and A. BALOGH[5]

[1]*Centre d'*Etude Spatiale des Rayonnements*, 9 ave Colonel Roche, 31028, Toulouse, cedex 4, France*
*E-mail: lavraud@lanl.gov;*
[2]*Rutherford Appleton Laboratory, Chilton, Didcot, Oxon, OX11 0QXUK, UK;*
[3]*Space Science Laboratory, UC Berkeley, CA 94530, USA;*
[4]*Swedish Institute of Space Physics, Box 812 SE-981 28, Kiruna, Sweden;*
[5]*Imperial College, Exhibition Road, London, SW7 2AZ, UK;*
[6]*ESA/ESTEC RSSD, Keplerlaan 1, 2200 AG, Noordwijk, the Netherlands;*
[7]*University of New Hampshire, Durham, NH 03824, USA;*
[8]*Instituto di Fisica dello Spazio Interplanetario, Via del Fosso del Cavaliere, 00133, Roma, Italy;*
[9]*Max-Planck-Institut Fur Aeronomie, Max-Planck-Str. 2, 37191, Katlenburg-Lindau, Germany;*
[10]*Max-Planck-Institut Fur Extraterrestrische Physik, Postfach 1312, 85741, Garching, Germany*

(Received 1 January 2003; Accepted 30 April 2004)

**Abstract.** This paper gives an overview of Cluster observations in the high-altitude cusp region of the magnetosphere. The low and mid-altitude cusps have been extensively studied previously with a number of low-altitude satellites, but only little is known about the distant part of the magnetospheric cusps. During the spring-time, the trajectory of the Cluster fleet is well placed for dayside, high-altitude magnetosphere investigations due to its highly eccentric polar orbit. Wide coverage of the region has resulted and, depending on the magnetic dipole tilt and the solar wind conditions, the spacecraft are susceptible to encounter: the plasma mantle, the high-altitude cusp, the dayside magnetosphere (i.e. dayside plasma sheet) and the distant exterior cusp diamagnetic cavity. The spacecraft either exit into the magnetosheath through the dayside magnetopause or through the exterior cusp–magnetosheath interface. This paper is based on Cluster observations made during three high-altitude passes. These were chosen because they occurred during different solar wind conditions and different inter-spacecraft separations. In addition, the dynamic nature of the cusp allowed all the aforementioned regions to be sampled with different order, duration and characteristics. The analysis deals with observations of: (1) both spatial and temporal structures at high-altitudes in the cusp and plasma mantle, (2) signatures of possible steady reconnection, flux transfer events (FTE) and plasma transfer events (PTE), (3) intermittent cold ($< 100$ eV) plasma acceleration associated with both plasma penetration and boundary motions, (4) energetic ions (5–40 keV) in the exterior cusp diamagnetic cavity and (5) the global structure of the exterior cusp and its direct interface with the magnetosheath. The analysis is primarily focused on ion and magnetic field measurements. By use of these recent multi-spacecraft Cluster

observations we illustrate the current topics under debate pertaining to the solar wind–magnetosphere interaction, for which this region is known to be of major importance.

**Keywords:** cusp, boundary layer, magnetopause, plasma acceleration

**Abbreviations:** DMSP – Defense Meterological Satellite Program; GSE – Geocentric Solar Ecliptic; GSM – Geocentric Solar Magnetic; HEOS – Highly Eccentric Orbiting Satellite; ACE – Advanced Composition Explorer; IMF – Interplanetary Magnetic Field; MLT – Magnetic Local Time; TD – Tangential Discontinuity; RD – Rotational Discontinuity; MVA – Minimum Variance Analysis; UT – Universal Time; FGM – Fluxgate Magnetometer; FTE – Flux Transfer Event

## 1. Introduction

The magnetospheric cusps are known to be the location of magnetosheath plasma and momentum entry into the magnetosphere (Frank, 1971; Heikkila and Winningham, 1971). These regions were early evidenced in the model of Chapman and Ferraro (1931). A large number of low-altitude polar orbiting satellites have since allowed their precise characterization in terms of plasma properties and global motional behavior. The cusp plasma is made of low energy ions and electrons of magnetosheath origin (Newell and Meng, 1988). It is located near magnetic noon and extends 1–2° in latitude and 1–2 h in local time. Early statistics from the DMSP satellites have shown it moves equatorward (poleward) in response to solar wind pressure increase (decrease), as a result of its global expansion (Newell and Meng, 1994; Yamauchi et al. 1996). For southward (northward) IMF orientation it moves equatorward (poleward) and for dawnward (duskward) IMF orientations it is displaced towards dawn (dusk) (Newell et al., 1989). Depending on these conditions the cusp region can be found in the range (73°–80°) in magnetic latitude and (10:30–13:30) in MLT. Surrounding the cusp, the cleft is a broader region, characterized by substantially lower magnetosheath ion fluxes, that probably maps to the low latitude boundary layers (LLBL) at higher altitudes (Newell and Meng, 1988).

The ions entering the cusp are submitted to a large-scale convection electric field. It kinetically results in large-scale ''velocity filter'' effect and energy-time dispersion features (Reiff et al., 1977). The plasma mantle, at the poleward edge of the cusp, constitutes the tail of the dispersed cusp. It therefore contains mainly tailward up-flowing plasma. The large-scale dispersed cusp often contains smaller scale structures. Such structures appear as purely time dependent when observed isolated in the surrounding of the cusp (Carlson and Torbert, 1980). Transient structures were also reported in the cusp boundary layers at the dayside magnetosphere. Because of their short duration, such transients are characterized

by pitch angle dispersion (Woch and Lundin, 1992). Under strongly northward IMF, reversed large-scale convection is often measured in the cusp and similar short-lived injections may be observed within the global structure of the cusp. Because the pitch angle and energy time dispersions of these short transients are not reversed, while the convection is reversed, it was concluded that they are purely time dependent (Vontrat-Reberac et al., 2003). Ground based observations have permitted the corroboration of such observations (Lockwood et al., 2001a). Also, Escoubet et al. (1992) have reported "staircase ion signatures" within the low-altitude cusp structure, which correspond to the "cusp ion steps" reported by Lockwood and Smith (1992). These were interpreted in terms of time varying magnetosheath plasma injection and modeling of these features has reinforced this interpretation (Lockwood and Davis, 1995). Recent observations, however, have also highlighted the plausible spatial nature of such structures (Ohtani et al., 1995; Trattner et al., 1999, 2003).

Low and mid-altitude satellites have provided major advances in the understanding of the role and characteristics of the cusp, but such spacecraft only remotely sense the solar wind interaction with the cusp which actually occurs at higher altitudes. The early evidence for the existence of a slow flow region of magnetosheath plasma outside of a probable magnetopause indentation were outlined by Paschmann et al. (1976), Vasyliunas et al. (1977) and Haerendel et al. (1978), using the HEOS-2 data. While Vasyliunas (1977) referred to it as the "exterior cusp", Paschmann et al. (1976) and Haerendel et al. (1978) proposed the existence of a "stagnation region", and of an adjacent "entry layer", which could permit plasma and momentum entry into the magnetosphere through Eddy diffusion at their boundary (see also Haerendel (1978)). Their cusp picture was therefore close to an aerodynamic view, and the characteristics of the "stagnation region" compared with those inferred from the model of Spreiter and Summers (1967) for this high-altitude region. Although the term "stagnant" is often used in the literature since these early studies, plasma stagnation is qualitatively not obvious to occur in such a dynamic region, as noticed by Vasyliunas (1995).

Only recently, the Interball spacecraft (Fedorov et al., 2000; Merka et al., 2000) and the Polar spacecraft (Fuselier et al., 2000; Russell, 2000) observed the high-altitude regions of the dayside magnetosphere with high data sampling rates. The Interball spacecraft predominantly passed at very high latitudes and altitudes in the cusp and plasma mantle region but did not sample the most central part of the exterior cusp. On the other hand, the Polar spacecraft has an apogee of 9 Re (towards the cusp) and only rarely had access to the magnetosheath. Thus it did not permit extensive study of the very distant exterior cusp and its interface with the magnetosheath.

The cusp magnetic topology was recently shown to be compatible with expectations from steady reconnection, consistent both with anti-parallel and component merging (Fedorov et al., 2000; Fuselier et al., 2000; Russell et al., 2000; Onsager et al., 2001). However, concepts involving gas dynamics (Haerendel et al., 1978; Haerendel, 1978), kinetic effects (Lemaire and Roth, 1977; Lundin et al., 2003) or waves and turbulence (Kuznetsova and Zelenyi, 1990; Belmont and Rezeau, 2001) may need be taken into account to explain the cusp properties. For instance, Walters (1966) proposed early the existence of a shock at the cusp–magnetosheath interface (see also Cargill (1999) and Taylor and Cargill (2001)) while more recent studies favor its generation via merging processes (Russell et al., 2001; Onsager et al., 2001; Lavraud et al., 2002). In this paper, we define the exterior cusp as characterized by depressed magnetic field ($< 30$ nT) and generally low and possibly variable ion velocities, and it is thought to be (probably) part of the more global high-altitude cusp region. The exterior cusp diamagnetic cavity appears indented in accordance with a funnel shaped topology (Russell, 2000; Lavraud et al., 2002). This region is subject to interaction with the interplanetary medium through the exterior cusp–magnetosheath boundary (Lavraud et al., 2002). The existence and exact role of magnetic field merging are not yet established. The magnetopause definition and location will be addressed in this paper (Onsager et al., 2001; Russell, 2000). We present typical Cluster observations during three outbound crossings of the high-altitude cusp (19/02/2001, 04/02/2001 and 18/05/2001).

The paper is focused on ion and magnetic field measurements permitting a presentation of plasma and field characteristics within a location of the magnetosphere that is still poorly known. The magnetospheric cusps were indeed anticipated to be suitable key targets for Cluster investigations. The three orbits have been chosen since their combined observations cover most of the topics mentioned below in the context of the high-altitude cusp.

In this paper, we deal with observations of "stepped" cusp structures detected in the high-altitude cusp and plasma mantle. Whether they are spatial or temporal in nature is of importance in understanding their origin. We present the observations of transient small-scale phenomena that may relate to reconnection (flux transfer events (FTEs) (Russel and Elphic, 1978)) and impulsive penetration (Lemaire and Roth, 1978). The possible occurrence of cold plasma ($< 100$ eV) acceleration was recently examined in Cluster observations at the flank magnetopause (Sauvaud et al., 2001). We will show that such a population is also intermittently observed at the cusp boundaries. They may be linked to sporadic boundary motions or plasma penetration and the plausible source regions are still unknown (Sauvaud et al., 2001; Lundin et al., 2003). Also, the permanent presence of high-energy ion populations (from 5 keV to MeV ions) within the exterior cusp diamagnetic cavity is an intriguing feature (Delcourt and Sauvaud, 1998, 1999;

Chen and Fritz, 2001; Fritz et al., 2003; Chang et al., 2000; Trattner et al., 2001). It is of particular interest in order to understand the role of the magnetospheric cusps for high-energy particle circulation in the magnetosphere. Finally, the global exterior cusp structure and the nature of its interface with the magnetosheath (Onsager et al., 2001; Russell et al., 2001; Lavraud et al., 2002) will be discussed. It is a prime location of the solar wind–magnetosphere interaction.

## 2. Instrumentation, event selection and orbit

### 2.1. Cluster instrumentation and solar wind data

The high capabilities of the onboard instruments and the tetrahedral spacecraft configuration of the Cluster fleet both permit very accurate and precise determination of the physical particle and wave phenomena and small-scale dynamical analysis. The ion data used in this paper come from the Cluster Ion Spectrometry (CIS) experiment, which is described by Rème et al. (2001). The CIS package is capable of obtaining full three-dimensional ion distribution functions with a good time resolution (down to 1 spin resolution ~4 s) and it also permits extensive onboard data processing. CIS is composed of two complementary sensors, the COmposition and DIstribution Function

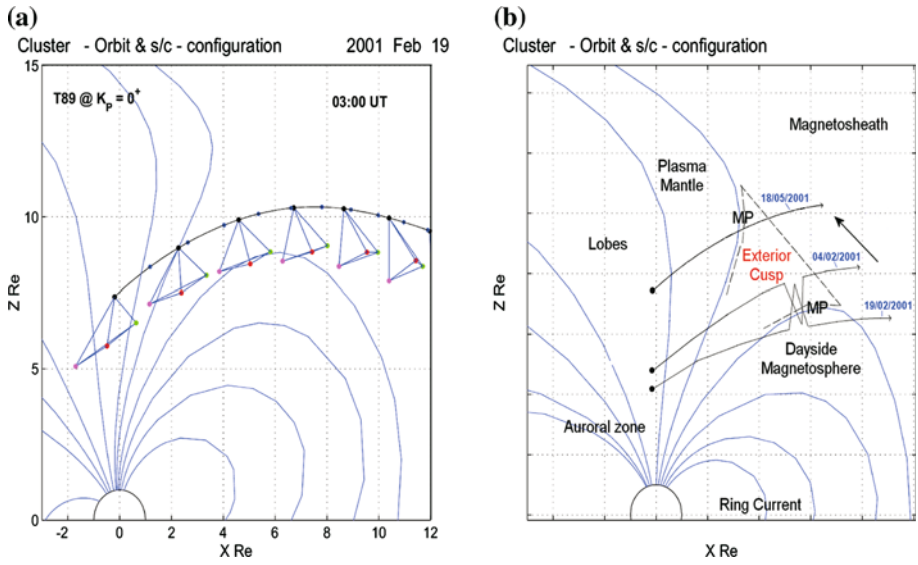


*Figure 1.* (a) Cluster satellites orbit on 19/02/2001. The fleet is flying outbound from the inner magnetosphere, crossing the high-altitude cusp, the dayside magnetosphere (plasma sheet) and towards the magnetosheath. Details are given in the text of Section 2.3. (b) Schematic view of the satellites actual paths through the high-altitude dayside regions for the three events selected here.

analyser (CODIF) sensor which handles a Time of Flight system in order to resolve ion masses, and the Hot Ion Analyser (HIA) that does not separate ion species but has a better angular resolution. The data in the present paper

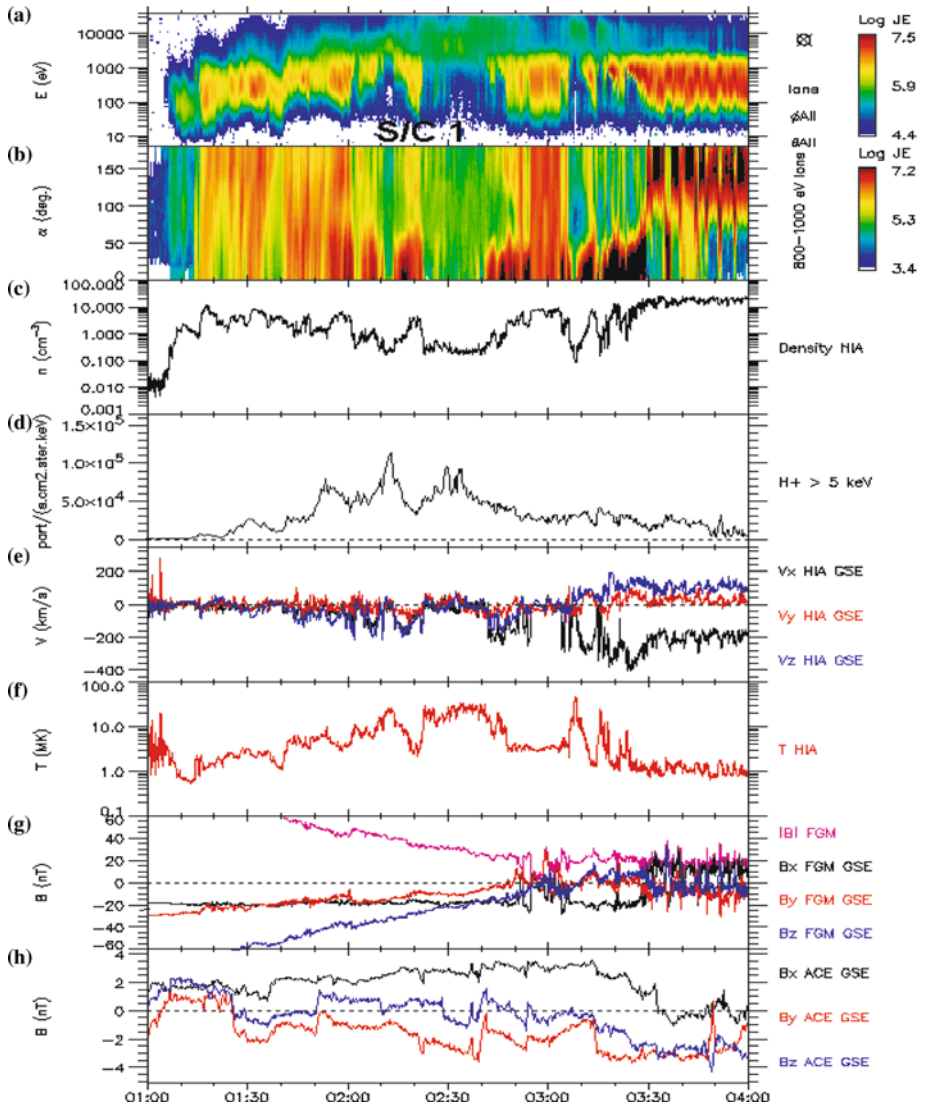


*Figure 2.* Overview of the combined CIS, FGM and ACE data for the 19/02/2001 event from spacecraft 1. The first spectrogram (panel a) presents HIA ion fluxes as a function of energy and time. The second spectrogram displays the pitch angle from HIA in the spacecraft frame (panel b). The ion density, the GSE velocity and the temperature of the ions from HIA are shown respectively in panels c, e and f. Panel d shows the $H^+$ fluxes from CODIF above 5 keV. Panel g presents the FGM magnetic field measurements while panel h displays the lagged IMF from ACE, both in GSE.

come from both instruments. The magnetic field data used was provided by the fluxgate magnetometer experiment (FGM) (Balogh et al., 2001). The instrument can produce high-time resolution (67 and 22.4 Hz) data at high absolute accuracy ( $< 0.1$ nT). The FGM data used in this study, however, are predominantly spin averaged data to match time resolution with the plasma measurements. The ACE data are used to monitor the solar wind conditions. In Figures 2, 4 and 6, the time series of IMF have been lagged to take into account the solar wind convection from the ACE location. This was performed by direct calculation from the intrinsic characteristics of the solar wind and confirmed by correlation with FGM data when the spacecraft were in the magnetosheath.

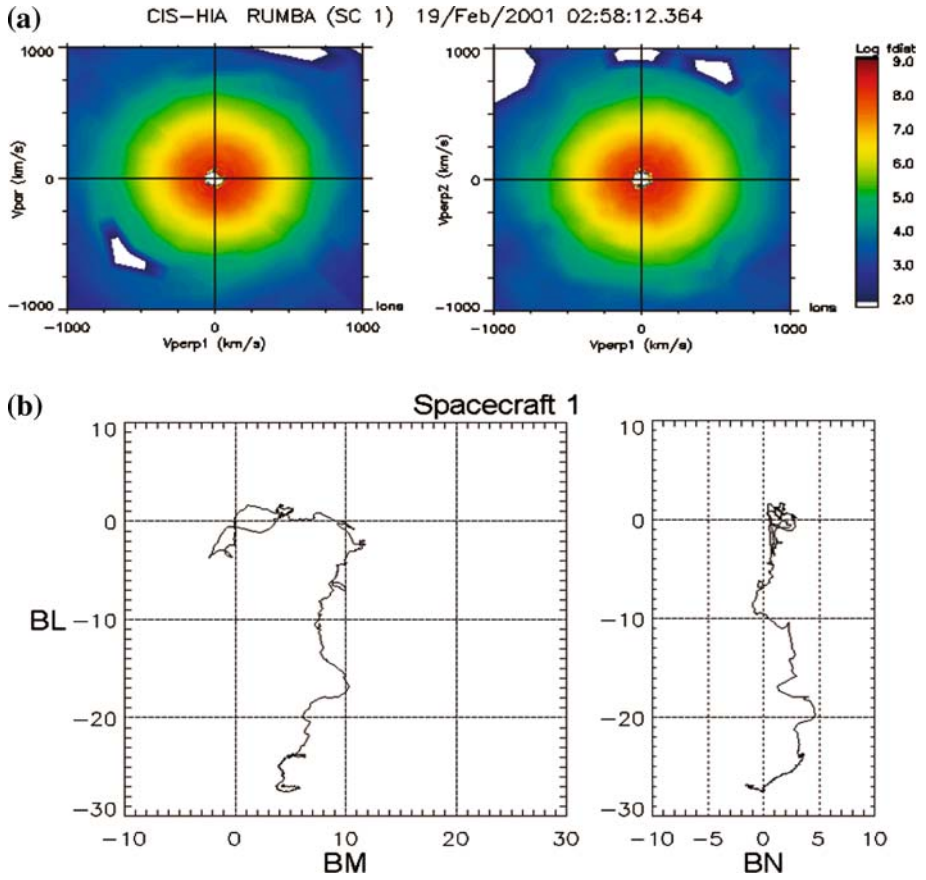


*Figure 3.* (a) Two-dimensional cuts of the ions distribution function in the ($V_{||}$, $V_{\perp}$) and (V-1, V-2) planes, in number flux (from HIA), and according to the magnetic field ($V_{||}$) and convection velocity (V-1) direction. It is sampled during the stagnant part of the exterior cusp at 02:58 UT onboard spacecraft 1. (b) Hodogram of the exterior cusp-dayside magnetosphere (boundary layer) discontinuity at ~02:55 UT (spacecraft 1). The LMN coordinate system directly arises from the application of the MVA techniques.

## 2.2. Cluster event selection

This paper is based on the observations and analysis of three Cluster events, which occurred on 19/02/2001, 04/02/2001 and 18/05/2001. The Cluster spacecraft have an elliptical and polar orbit ($19.6 \times 4$ $R_E$). During the springtime, they are outbound from the inner magnetosphere and towards

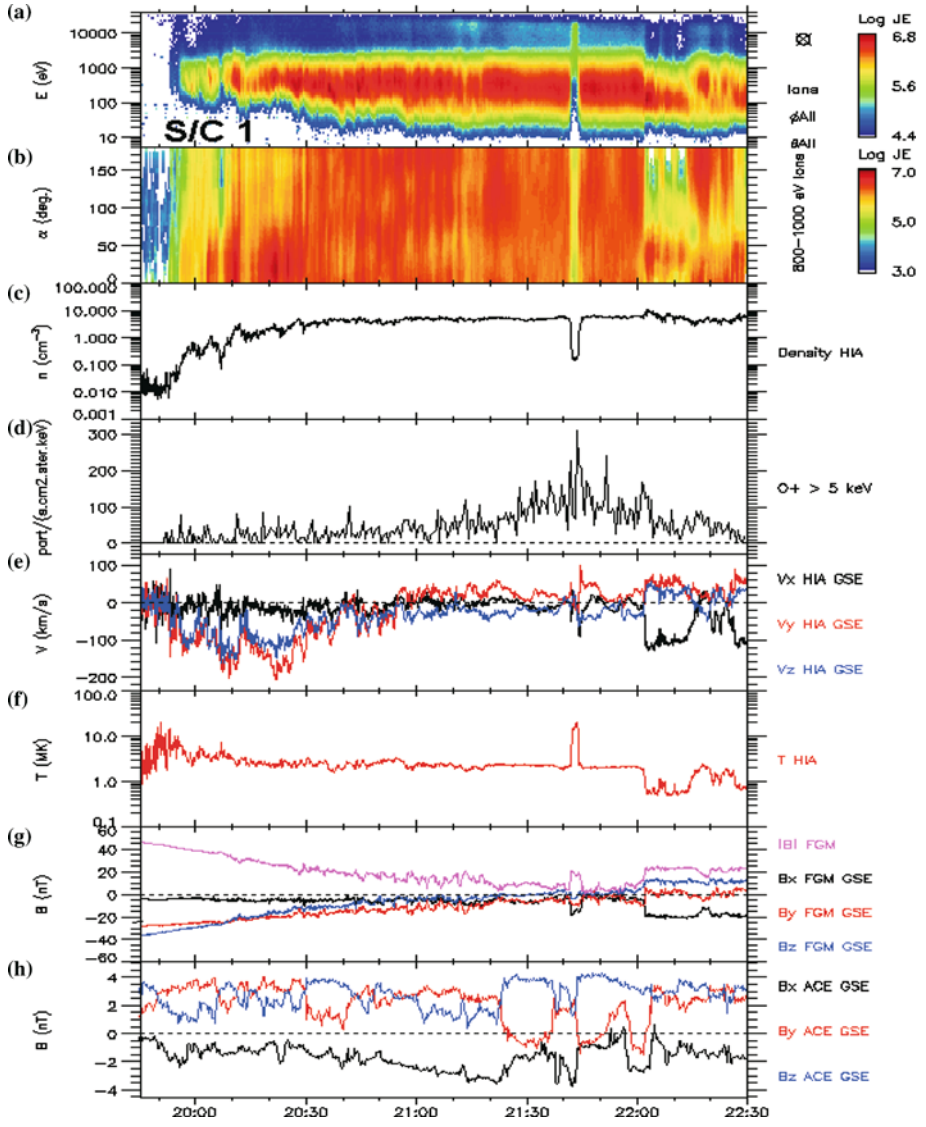


*Figure 4*. Overview of the combined CIS, FGM and ACE data for the 04/02/2001 event onboard spacecraft 1. The panels are similar to Figure 4, except that panel d shows the $O^+$ fluxes (instead of $H^+$) from CODIF above 5 keV.

the sun in the northern hemisphere. They pass through the northern lobe, plasma mantle, cusp (exterior cusp), or dayside closed magnetosphere (i.e. dayside plasma sheet) and the magnetosheath. Primarily depending on the magnetic dipole tilt angle, the solar wind conditions and the cusp global dynamics, the Cluster spacecraft are susceptible to sample these various regions with different orders and durations during similar paths on successive orbits. The 19/02/2001 and 04/02/2001 events exhibited the crossing of the exterior cusp region and its surrounding boundaries in such different ways (see later). The former event occurred under IMF $B_z \geq 0$ nT) while the latter occurred under northward IMF. During these two events the inter-spacecraft separation was ~600 km. Such a configuration allows Cluster to resolve the boundary dynamics with unprecedented accuracy (Dunlop et al., this issue).

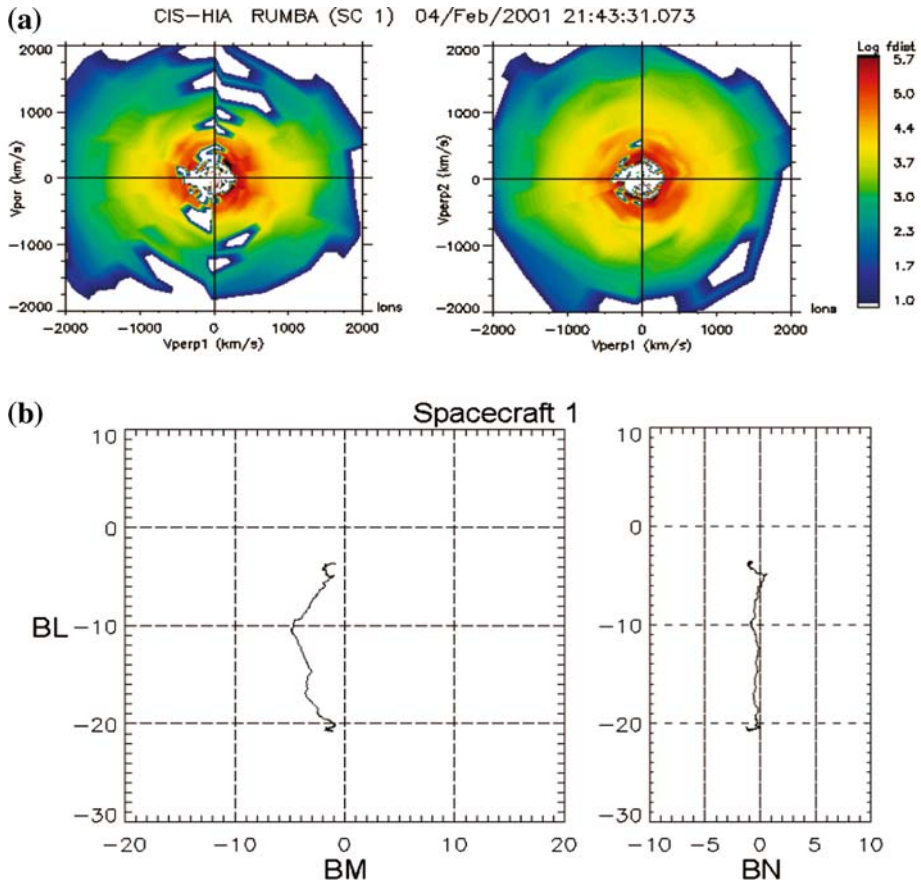


*Figure 5.* (a) Similar distribution functions as in Figure 3a, but the axes are extended to 2000 km/s. It is sampled in the trapped region of the dayside plasma sheet at 21:43 UT onboard spacecraft 1. (b) Similar hodogram to that of Figure 3b, from spacecraft 1 data at ~21:41 UT.

During the whole Cluster mission, this distance is changed once or twice a year depending on the anticipated scientific objectives. On 18/05/2001 the Cluster fleet mainly crossed the high-altitude plasma mantle region before

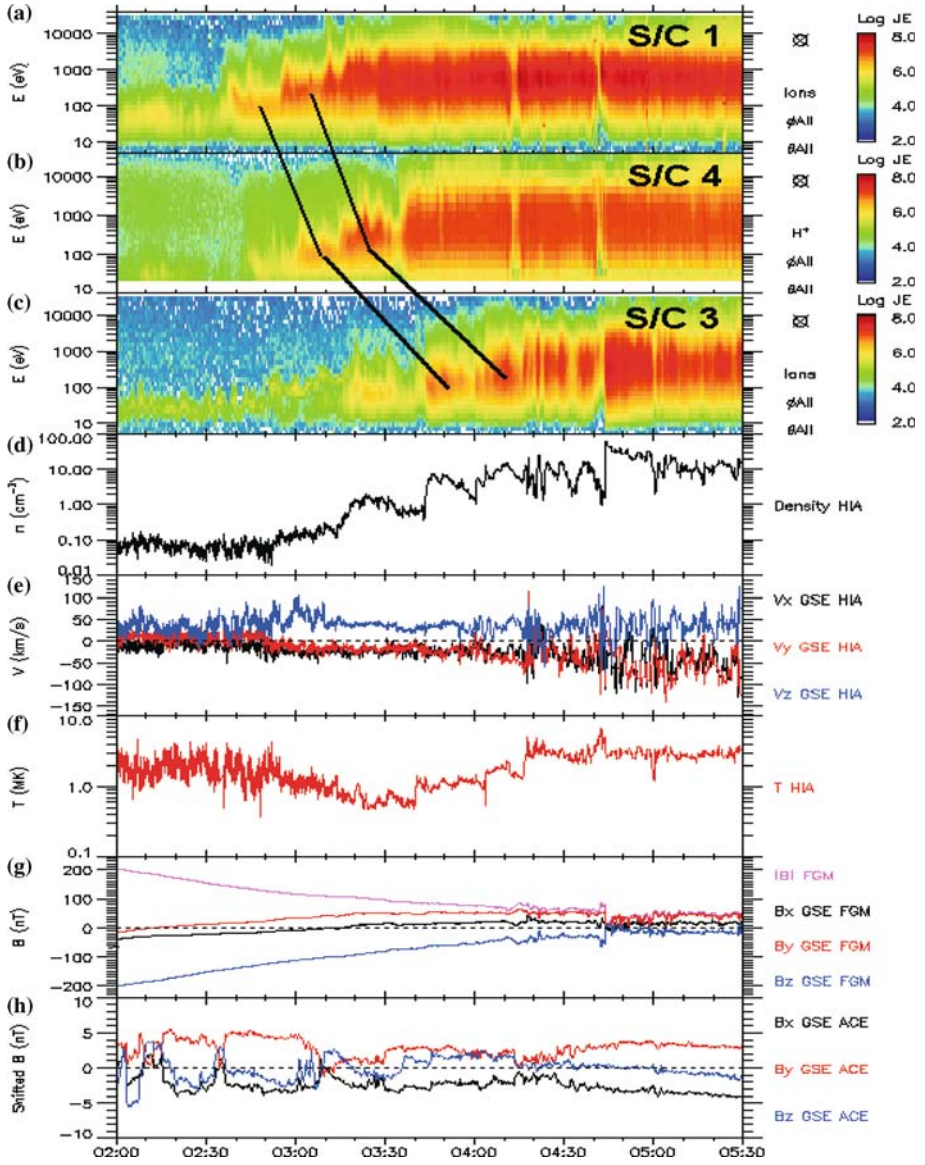


*Figure 6*. Overview of the combined CIS, FGM and ACE data for the 18/05/2001 event. The first panel is the spectrogram from HIA (all ions) onboard spacecraft 1, panel b is that of CODIF ($H^+$) onboard spacecraft 4 and panel c shows HIA ions from spacecraft 3. The ion density, the GSE velocity and the temperature of the ions from HIA onboard spacecraft 3 are shown respectively in panels d, e and f. Panel g presents the FGM magnetic field measurements (spacecraft 3) while panel h displays the lagged IMF from ACE, both in GSE.

their exited into the magnetosheath. This event is used to highlight the large-scale spatial and temporal structures often observed in the cusp and plasma mantle regions. The inter-spacecraft distance was large ($\sim$1 $R_E$) during this pass which is appropriate for large-scale structures investigations.

### 2.3. The cluster orbits

Figure 1a shows the projection of the Cluster orbit (lying within 00:30 hrs of 12:00 MLT) in the $X,Z_{GSM}$ plane for the segment between 00:00 UT and 10:00 UT on 19/02/2001. The hour intervals are marked as blue dots, increasing from 00:00 UT at the left-hand side. Superimposed with spacecraft 1 (black) attached to the orbit, are the shapes of the tetrahedra (scale factor of 20) for six arbitrary different times. The other spacecraft are color coded as: 2 (red), 3 (green) and 4 (magenta). The drawn field lines have been computed using the Tsyganenko (T89) model (Tsyganenko, 1989) with a Kp index of 0+.

The exact Cluster orbit plots are not shown for the two other events. Rather, we display a schematic of the apparent satellites'' path through the

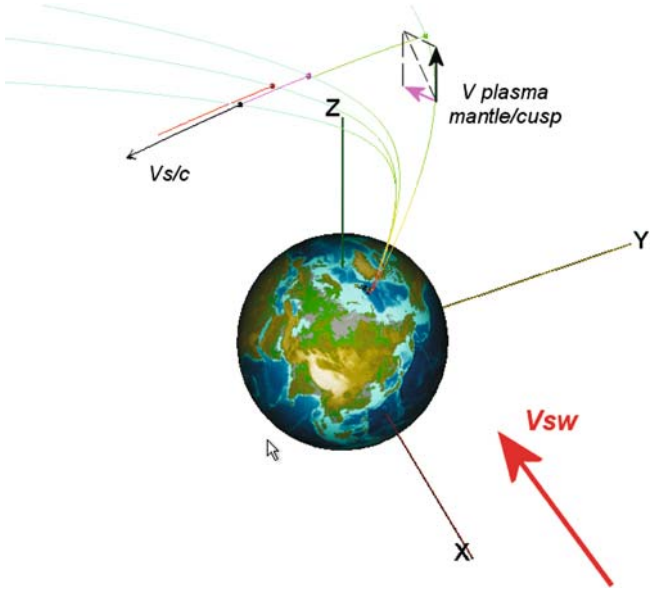


*Figure 7.* Perspective view of the orbit path of the four Cluster spacecraft for the 18/05/2001 event using the Orbit Visualization Tool (OVT). Spacecraft 1 trajectory is in black and the arrow shows its direction. Similarly spacecraft 2 is in red, spacecraft 3 is in green and spacecraft 4 is in magenta. The X, Y and Z axis are in GSE. The solar wind thus comes from the X direction. The plasma velocity orientation in the plasma mantle (see Figure 6e) is pictured through its parallel (black) and perpendicular (magenta) components, displayed as arrows.

high-altitude cusp and its surrounding regions for the three events in Figure 1b. They are deduced from the observations presented in the next section. For 19/02/2001 an observed brief exit into the exterior cusp cavity is sketched as part of the trajectory. For 04/02/2001, an observed exit in opposite sense, from the exterior cusp into the dayside plasma sheet, is shown. Finally, the satellite path on 18/05/2001 is shown occurring at high-altitudes and latitudes. It must be stressed, however, that the spacecraft crossed the plasma mantle and magnetopause on the dawn edge of the exterior cusp and that the trajectory was mainly directed dawnward. Because this is a purely schematic view, the axes of Figure 1b have no particular units. Note that a perspective view of the 18/05/2001 Cluster trajectory is shown in Figure 7 (described later).

## 3. Overview of three Cluster high-altitude cusp passes

### 3.1. 19/02/2001: A WEAKLY SOUTHWARD IMF CUSP CROSSING

Figure 2 shows the Cluster data from spacecraft 1 for the interval of interest on 19/02/2001. At 01:00 UT, the Cluster satellites were in the northern lobes, the ion density was very low, $n \sim 0.01$ cm$^{-3}$ (panel c). The interval 01:05 UT to 02:20 UT is identified as a pass through the northern mantle and high-altitude cusp. Here, the HIA experiment measured both up and down-flowing ions as seen by populations over all pitch angles (panel b). The bulk velocity was low due to these oppositely directed flows (panel e). The plasma mantle was observed first (roughly between 01:05 UT and 01:30 UT). The bulk ion velocity was characterized by a slightly positive (near zero) Vz component that gradually decreased down to −200 km/s (panel e). It indicates that more and more down-flowing particles were detected until 02:20 UT. It was also accompanied by a gradual increase in the particle mean energy. An energy-time dispersion feature is clearly observed in the spectrogram of panel a, which also reveals a stepped and saw-tooth like global pattern. The pitch angle spectrogram shows that multiple short injections occurred at small time scales. They are characterized by field aligned ($0^\circ$ pitch angle) particles being detected first. Their pitch angles then increase. The particles may ultimately become anti-field aligned ($180^\circ$) once they have mirrored at low-altitudes (for instance at 01:20 and 01:30 UT). Note that the pitch angles are computed in the spacecraft frame and for the energy range between 800 and 1000 eV.

A first short encounter with the dayside plasma sheet occurred at 02:10 UT, there the density decreased and the ion velocity became very low. The temperature and the high-energy proton fluxes were high (panels c, d, e and f). The Cluster spacecraft appear to return to the dayside plasma sheet at 02:20 UT. The HIA measurements showed a clearly trapped high-energy (all

above 1 keV) ion population at this time (distribution function not shown, a similar one is shown for the next event). Near the dayside plasma sheet-cusp boundary, the CIS instruments detected multiple transient features that appeared to contain magnetosheath like plasma. Such transients were seen at 02:30 UT in panel a, for example. They are further examined in Section 4.2.

The Cluster spacecraft thus appeared to successively cross the plasma mantle, the high-altitude cusp and the dayside plasma sheet. According to the Cluster orbits, it could have been expected that the spacecraft would then cross the dayside magnetopause. The four spacecraft appear to encounter the exterior cusp diamagnetic cavity (low field and velocity around 03:00 UT), however, and experienced a number of encounters with boundary layers at the edges of this cavity (between 02:40 and 02:55 UT for instance). The boundary layers are characterized by a mixture of populations, arising from both the magnetosheath and the dayside plasma sheet. The magnetic field shows no particular transition between the dayside plasma sheet and these boundary layers, where it thus has a typical magnetospheric orientation and strength (panel g). Sharp magnetic boundaries are delimiting these boundary layers (and subsequently the dayside plasma sheet) from the low magnetic field cavity. They were encountered at 02:55 UT on entry and 03:03 UT on exit. This diamagnetic cavity is interpreted as the exterior cusp (Russell, 2000). The magnetic field data from the 02:55 UT crossing are shown in the hodogram of Figure 3b. This boundary looks like a tangential discontinuity (TD) since Bn is $\sim$0 nT on average during the crossing. The normal direction derived from the Minimum Variance Analysis (MVA) technique (Sonnerup and Cahill, 1967) yields $\mathbf{n}$ = (−0.20; 0.81; 0.54) in GSE. The exit at 03:03 UT gave an $\mathbf{n}$ = (0.39; −0.77; −0.49) in GSE consistent with the entry. This boundary also looks like a TD (not shown). The intermediate-to-minimum eigenvalue ratio is around 2.5 for both crossings, but the normals are stable to variation of the computation interval. The application of the Planar Discontinuity Analysis (Planar DA) on the magnetic field time series (Dunlop et al., 1997) gives average normal speeds of $\sim$30 km/s for the two crossings. Moreover, the consistency of the normal derived from MVA with the delays in the Cluster four spacecraft time series is well established (see for example Dunlop et al., this issue). The multi-spacecraft time series data reveal a nested feature (not shown), suggesting the spacecraft have gone back and forth into a region rather than that they have sampled a transient structure passing by. Inside the exterior cusp (diamagnetic cavity) both the magnetic field and the plasma flow were very low as compared to the surrounding boundary layers and dayside plasma sheet regions (panels d and f). The plasma can even be shown to be quasi-isotropic and stagnant as seen in the pitch angle spectrogram (panel b). This is further revealed by the distribution function displayed in Figure 3a.

Panel d displays the $H^+$ fluxes from CODIF above 5 keV. At the beginning of the interval, no flux was observed in the lobes, but gradually increased in the high-altitude cusp. The fluxes increased further in the dayside plasma sheet (where only this high-energy component is observed). Detection of large fluxes first occurred at 02:10 UT during the first short encounter and again after 02:20 UT. The fluxes gradually decreased throughout the boundary layers and the exterior cusp cavity, from 02:40 to 02:55 UT. The presence of this high-energy component is also seen above 5 keV in the spectrogram of panel a. The fluxes consistently appear lower in the exterior cusp and boundary layers than in the dayside plasma sheet. The fluxes in panel d keep low after 03:00 UT and finally gradually decayed when the spacecraft were in the magnetosheath. The fluxes nearly vanish at 03:50 UT. Note that the $O^+$ fluxes above 5 keV show a similar behavior, but with lower fluxes (not shown).

The dayside magnetopause encounter occurred at ~03:30 UT. This magnetopause crossing was typical in the sense that the spacecraft did not exit into the magnetosheath directly from the exterior cusp (Lavraud et al., 2002). For this boundary, MVA gives a normal $\mathbf{n}$ = (0.41; 0.45; 0.78). However, the eigenvalue ratio is quite low (~2) and the possible TD or RD nature can not be inferred from the hodogram signature (not shown). In line with this, the planar DA gives not very consistent results. Applying a geometrical method as in Harvey (1998) yields a normal $\mathbf{n}$ = (0.60; 0.78; 0.17) and a rough inward normal speed of ~65 km/s, for this boundary. In the magnetosheath, the ion density was ~20 $cm^{-3}$ and the measured FGM magnetic field pointed mainly sunward and southward, as can be seen in panel g. For that time (03:10 UT) the ACE spacecraft had monitored a mainly southward IMF (panel h). The large Bx component in FGM data at that time may arise from draping effect. Some transient variations of the magnetic field were however observed during this magnetosheath period. They were correlated with somewhat enhanced flows (they are discussed in section 4.2). From 01:30 to 03:10 UT the $B_z$ component of the IMF was varying around zero. However, the Bx component was large and positive so that the expected magnetosheath field at the magnetopause should have an anti-parallel orientation with respect to the dayside magnetospheric field. From then on, the IMF was clearly southward.

### 3.2. 04/02/2001: A NORTHWARD IMF CUSP CROSSING

This event was already discussed by Lavraud et al. (2002). We review however the Cluster observations to the extent needed for the present paper. The overview of Cluster data for this event is displayed in Figure 4 for spacecraft 1. Until 19:55 UT the Cluster fleet was in the northern lobes, where the density is very low, after which they entered the high-altitude cusp.

It was characterized by down-flowing magnetosheath like plasma. On a large-scale, the cusp looked different from the previous event. First, no plasma mantle was observed at all on the poleward side of this cusp traversal (panels a and c). High energy, hot magnetosheath like plasma was encountered first with large downward velocities on the polewardmost field lines. In contrast also, the mean energy of the ions was gradually decreasing while there was a clear gradual change in ion velocity and temperature from 19:55 UT to 21:20 UT roughly (panels a, e and f). This behavior is characteristic of a reversed time dispersion that is consistent with the sunward plasma convection (not shown) measured in the flows. Also, on small-scales within the cusp structure (for instance just at 20:00 and 20:10 UT), short plasma injections are observed. The particles are mainly field aligned ($0^\circ$ pitch angle) at first, but within few minutes the particle pitch angle evolves and more up flowing ions ($180^\circ$ in pitch angle) were detected. Pitch angles are computed in the spacecraft frame for the range (800, 1000) eV.

After these cusp plasma flow signatures, instead of passing through the dayside plasma sheet as for the previous 19/02/2001 event, the spacecraft remained inside the cusp until a direct exit into the magnetosheath (apart from a very brief dayside plasma sheet encounter, discussed next). The cusp throat was filled with magnetosheath plasma, that appeared to be the more isotropic the further out the spacecraft were on their orbit path. Simultaneously, the magnetic field was continuously decreasing (from 19:55 UT until 21:20 UT). Those characteristics are displayed in the pitch angle spectrogram of panel b and in panel g for the magnetic field data. After 21:20 UT the magnetic field was constantly very low while the ion distribution functions were very isotropic. The distribution functions resembled the one shown in Figure 3a for the previous 19/02/2001 event (but not shown here). These properties led Lavraud et al. (2002) to use the descriptive term of Stagnant Exterior Cusp (SEC) for the region observed from 21:20 to 22:02 UT.

The spacecraft had a short encounter with the dayside plasma sheet at $\sim$21:43 UT, showing high fluxes of high-energy particles (all above 1 keV) and high temperatures (panels a and f). A typically trapped distribution function taken during this encounter is shown in Figure 5a (note that the axis scale is larger than in Figure 3a). In both the aligned and anti-aligned direction, the lower phase space density of the high-energy ions (as compared to the perpendicular directions) marks the loss cone effect. The spacecraft appear to enter the dayside plasma sheet but quickly return into the exterior cusp. This back and forth motion is evidenced in the nested nature of magnetic field data time series, which opposes to a lagged nature which would characterize a convected structure (see panel b in Figure 14 introduced later). The hodogram of the first boundary encounter (arising from the MVA), between the exterior cusp and the dayside plasma sheet, is shown in Figure 5b to look like a TD since the Bn component is particularly low

across the boundary. It resembles the one analyzed for the previous 19/02/2001 event, between the exterior cusp and the dayside plasma sheet (or rather the boundary layers, see previous section). The normals derived from MVA at the entrance and exit are in good accordance with expectations from a funnel shaped cusp topology. The entry and exit have respective normal orientations $\mathbf{n} = (-0.43, 0.57, 0.71)$ and $\mathbf{n} = (-0.10, -0.13, 0.99)$ in GSE coordinates. Both crossings show boundary normal velocities of $\sim$10 km/s by use of the planar DA and with good time delay consistency.

The whole exterior cusp was also filled with high-energy particles ($>5$ keV) with fluxes, however, which were lower than in the dayside plasma sheet (see panel a). This high-energy population was primarily made of $H^+$ ions (as for the previous 19/02/2001 event), but an $O^+$ component was also detected. We display the high energy $O^+$ fluxes above 5 keV during the whole event in panel d. It highlights that those ions were most present in the dayside plasma sheet and that the fluxes gradually decayed each side of the exterior cusp-dayside plasma sheet boundary. After 22:02 UT the spacecraft were in the magnetosheath and the fluxes decreased. The $H^+$ component above 5 keV behaved similarly to $O^+$ during the interval (but with well higher fluxes) (not shown). Apart from the small enhancement around 22:20 UT, the fluxes of both high-energy $O^+$ and $H^+$ became very low further out in the magnetosheath.

The spacecraft exited from the exterior cusp into the magnetosheath at 22:02 UT through a very sharp discontinuity that displayed huge plasma and field parameter jumps. Lavraud et al. (2002) found it to be rotational ($Bn \sim -3$ nT). They showed that clear plasma inflow occurred at the boundary, which was consistent with the Bn sense. Their Walen test succeeded, indicating that the tangential stress balance at the discontinuity is apparently compatible with a RD. The boundary was also shown to be spatially stable since it was similarly sampled on all four spacecraft. Its normal, derived from MVA, was pointing outwards and upwards $\mathbf{n} = (0.65, 0.45, 0.61)$. Planar DA revealed a normal boundary speed of $\sim$8 km/s inwards and showed a good consistency with the four spacecraft timings. The de Hoffmann–Teller frame at the RD was found to be (4, 31, −32) km/s in GSE, thus slowly moving sunward. As can be inferred from the pitch angle spectrogram in panel b, the distribution functions are very isotropic from 21:20 UT until the final exit into the magnetosheath. The magnetosheath is merely convecting.

### 3.3. 18/05/2001: A HIGH-ALTITUDE PLASMA MANTLE AND CUSP CROSSING

The overview of Cluster data for this event is displayed in Figure 6. While the first three panels show the spectrograms for spacecraft 1, 4 and 3, the displayed moments only come from spacecraft 3. A perspective view of the

Cluster orbit is shown in Figure 7 for the interval 03:00–04:00 UT. It shows that the three spacecraft (s/c1 in black, s/c3 in green and s/c4 in magenta) nearly follow each other on their orbit path, having a main dawnward direction. The arrows aim to give an idea of the plasma flow direction in the plasma mantle region and in the solar wind.

Until ~03:20 UT spacecraft 3 was in the northern lobes. It then entered the plasma mantle, which was characterized by upward and tailward flowing magnetosheath like plasma (panel e in Figure 6). In the plasma mantle, the convection (perpendicular component) velocity is ~20 km/s and almost exclusively in the −X GSE direction (not shown). On all spacecraft a global increase, on large scales, of the ion mean energy is seen during the interval before each of them finally exit into the magnetosheath. This can be expected, together with the density and temperature evolution, from time of flight effect (panels d and f). However, this dispersion feature is interrupted by several sudden energy increases that may be referred to as "steps" (Lockwood and Smith, 1992). There are two major steps that are similarly sampled, but delayed, on all three operating CIS instrument onboard spacecraft 1, 4 and 3. Their lag time between spacecraft 1 and 4 is 20 min while it is 68 min between spacecraft 1 and 3. These coherent structures are indicated by the black lines on Figure 6. The structures are identified in terms of their highly concordant ion mean energy, spectral width and time duration on each spacecraft. Therefore they are thought to be possibly the same structures. It may be noted that sampling several, such similar steps over a long time period is rare, adding much interest to this event. Although alternate interpretations may be kept in mind, we will deal in the discussion Section 4.1 with their probable spatial nature.

The magnetopause was encountered at 04:45 UT on spacecraft 3, as seen in the magnetic field of panel g. The MVA derived normal is $\mathbf{n} = (0.40; 0.62; 0.67)$ (hodogram not shown). The TD or RD nature is unclear. The intermediate to minimum eigenvalue ratio is quite low (~2) and the normal is not stable under variation of the computation interval. This means the computed normal may be wrong. Because of the large inter spacecraft separation, geometrical analysis cannot be performed for this crossing. It may already be noted that the magnetopause characteristics are not of prime importance for the analysis of this event. Nevertheless, taking into account the spacecraft location and the normal derived from MVA, it might be inferred that the spacecraft were near the high-altitude cusp indentation. But no cusp-like feature (penetrating plasma) was detected on spacecraft 3. After the magnetopause crossing, the Cluster fleet was in a perturbed magnetosheath. The velocities and the magnetic field were characteristic for the region but quite variable as seen in panel e. On spacecraft 1 (panel a) the magnetopause was encountered at 03:30 UT, and for this event an exterior cusp pass was observed for few tens of minutes before the exit into a disturbed magnetosheath. It was

characterized by a rather turbulent region showing downward flowing ions (not shown). Spacecraft 4 (panel b) was in the plasma mantle and also entered the exterior cusp region at ~03:40 UT. A clear plasma and magnetic boundary was observed at 04:45 UT and the spacecraft then sampled a perturbed magnetosheath (not shown). Each spacecraft thus did not sample the exterior cusp and its surrounding in the same manner, but the stepped structures that are of concern here are all detected in the plasma mantle region. At 04:45 UT, the magnetopause was crossed by spacecraft 3, but at the same time the two other spacecraft also had a short encounter with the magnetopause, as may be observed on the spectrograms of panels a and b, while they were already in the magnetosheath. Such a transient encounter with the magnetopause also occurred before, at 04:15 UT, but only for spacecraft 1 and 4. While plasma mantle structures were seen with a time delay, these magnetopause crossings occurred simultaneously. From the available ACE and WIND data, no clear IMF changes were correlated with these transient encounters (panel h). The solar wind pressure was high (4 nPa) but seems to stay constant over this interval. The features of most interest here, however, are the stepped structures observed similarly on the spacecraft in the plasma mantle region, at very different times. During most of this event the ACE spacecraft monitored a low and variable IMF $B_z$ component while a positive $B_y$ and negative $B_x$ IMF components were dominating (panel h).

## 4. Discussions

We now discuss more specific topics that constitute the main, but non-exhaustive, current scientific debates concerning the high-altitude cusp region of the magnetosphere. We place our discussion in the context of each phenomenon that we aim to describe through these three cusp passes. We highlight the new insights coming from both the recent studies referenced herein and the additional information arising from the present analysis.

First, the present observations show that the high-altitude cusp region is filled with magnetosheath plasma of solar wind origin. Both precipitating and mirrored components are often observed. On the other hand, the dayside plasma sheet is mainly populated with ions of magnetospheric origin. Another permanent difference between the dayside plasma sheet and the cusp (and magnetosheath) is the mean energy of the ions which is of few hundreds eV in the cusp while ions in the dayside plasma sheet have energies of the order of 10 keV. The plasma mantle region is located tailward of the cusp. It is composed of ions originating from the cusp, that have mirrored at low-altitude and convected tailward. Note that the plasma mantle forms a boundary layer and there also often exist boundary layer regions adjacent to the equatorward side of the cusp. They show a mixture of plasma from

different origins and usually present typical dayside magnetospheric field orientation and strength. Such boundary layers are seen on 19/02/2001 on each side of the exterior cusp diamagnetic cavity. The processes driving their formation are still unclear.

### 4.1. The spatial and temporal structures in the high-altitude cusp and mantle

A great deal of knowledge on the cusp structure has come from mid and low-altitude satellite observations, as early reported by Newell and Meng (1988), Newell et al. (1989), Woch and Lundin (1992) and Yamauchi and Lundin (1994). For instance, the large-scale energy dispersed patterns observed in the high-altitude cusp for all three events, increasing for the southward IMF on 18/05/2001 and the weak IMF $B_z$ event on 19/02/2001, and slightly decreasing for the 04/02/2001 northward IMF event, are common cusp features. These dispersions are suggestive of the differential convectional flows in the region depending on the IMF orientation (Lockwood and Smith, 1992). The plasma mantle also shows the energy latitudinal dispersion for the 19/02/2001 and 18/05/2001. In this region the plasma bulk flow is mainly directed upward and tailward. It constitutes the natural continuation of the cusp precipitation when the cusp large-scale convection is tailward. The plasma mantle thus may not form under northward IMF conditions and possible sunward cusp convection. Its absence on 04/02/2001 is strong evidence, as first reported by Sckopke et al. (1976). Of course, the presence or absence of this region strongly depends on the steady or variable nature of the IMF and the subsequent large-scale convection in the cusp.

As explained by Lockwood and Smith (1992), the combination of pulsed reconnection events and tailward field line convection possibly induces the "Cusp Ion Step" like structure observed in the low and mid-altitude cusp region (see also Escoubet et al., 1992). When taking into account the differential plasma convection velocity and spacecraft velocity in the cusp, and when assuming purely time dependent plasma injection into the cusp, such stepped structures may appear (Lockwood and Davis, 1995). Note, however that this combined convection/velocity filter effect may equally take place by considering other injection processes. A nearly equivalent behavior is expected, but within a reversed dispersion, for steady northward IMF.

The step features appear to be composed of smaller scale events, showing pitch angle evolution from down-flowing field aligned to up-flowing anti field aligned. Such short time-pitch angle dispersions are common in the cusp region. They were presented as small-scale structures in the observation section for the 19/02/2001 and 04/02/2001 events. They display the different travel time of ions in injection events depending on their individual pitch angle. This is suggestive of the temporal nature of particle injections which

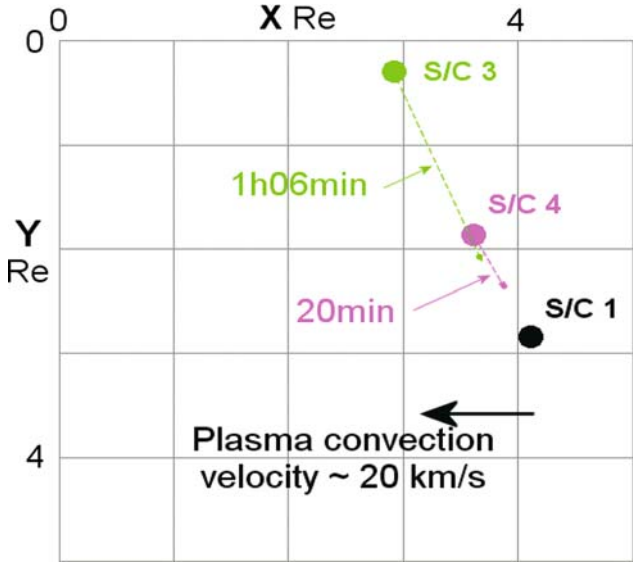


*Figure 8*. Schematic view showing the location of each spacecraft (filled circles) on 18/05/2001 at ~02:55 UT when spacecraft 1 sampled a particular structure in the plasma mantle. The two arrows show the (respective) spacecraft spatial motion of spacecraft 3 and 4 until they sample the same structure as spacecraft 1. Rough plasma convection (perpendicular velocity) at that time is shown as a black arrow.

are ultimately mirroring at lower altitude (Reiff et al., 1977; Vontrat-Reberac et al., 2003).

The temporal variability of the cusp was also pointed out, and established, in conjunction with ground observations of poleward moving auroral forms (Lockwood et al., 2001a). Such combined signatures are of major importance in discriminating between spatial and temporal interpretations. Assuming a unique time dependence, any large-scale structure in the cusp should convect as a whole poleward (equatorward) for southward (northward) IMF. However, based on dual spacecraft measurements in the mid-altitude cusp, Trattner et al. (2002) emphasized that stepped cusp structures are sometimes sampled at the same magnetic latitudes for largely different times, suggesting a spatial nature. Those structures have been interpreted in terms of possible different plasma characteristics between adjacent convection cells as well as in terms of multiple reconnection (Newell and Meng, 1991; Trattner et al., 1999, 2002; Vontrat-Reberac et al., 2003).

The 18/05/2001 event was chosen to illustrate the possible appearance of spatial structures in the high-altitude plasma mantle region. The multi-spacecraft Cluster mission is adequate for such investigations. During the period presented in Figure 6 the inter-spacecraft separation was ~1 $R_E$, in a quasi-string-of-pearl configuration. Figure 8 shows Cluster spacecraft locations (1, 3 and 4 as color-coded filled circles) at 02:55 UT (GSE), the

time when s/c 1 detected the second step feature (second black line in Figure 6). The green and magenta arrows show the respective motions of spacecraft 3 and 4 until they sampled the same feature. The time delays are respectively 68 and 20 min. The velocity computed from the delays and the spatial separation between each spacecraft at the sample time of this step yield a X component that is less than 1 km/s. The analysis shows a similar result for the first structure (first black line in Figure 6). This rough velocity estimate for the structures strongly differs from the ~20 km/s plasma convection velocity measured by CIS in the region, that is predominantly in −X GSE direction. The possible appearance of similar structures at the same locations after huge time delays, and under large-scale tailward convection, is thus evidenced here. At large inter-spacecraft separations, the Cluster fleet has been able to confirm the presence of apparently spatial structures in the plasma mantle at high-altitudes. The reasons for their existence are unclear and deserve further investigations.

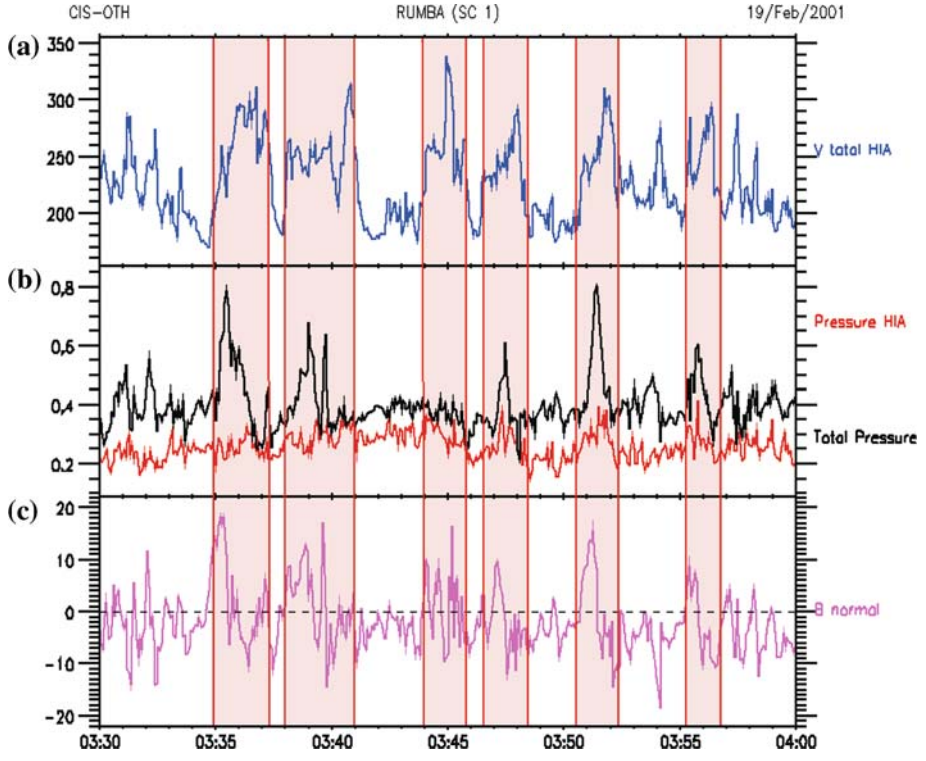


*Figure 9.* This plate displays Cluster measurements for a magnetosheath pass on 19/02/2001 that shows FTE like signatures. The magnitude of the HIA (all ions) velocity is shown in panel a. The ion pressure from HIA ($Nk_BT$) and the total pressure (ion plus magnetic pressure, from FGM) are displayed in panel b. The magnetic field component in the normal (to the magnetopause) direction is presented in panel c.

Whether such structures may imply a merging process is uncertain. A key in understanding the cusp and plasma mantle structures may remain the exact characterization of the processes which drive plasma intrusion into the magnetosphere. The occurrence of spatially steady structures more particularly in the high-altitude plasma mantle region may shed new lights on their origin.

### 4.2. Reconnection, FTEs and PTEs

As observed on 04/02/2002, the magnetic field shows no boundary normal component at the exterior cusp-dayside plasma sheet boundary (21:43 UT). On the other hand, the outer discontinuity with the magnetosheath is apparently rotational. The normal magnetic field had a negative sign, as compared to the outward pointing normal. This is compatible with lobe reconnection occurring above the spacecraft location. The de Hoffmann–Teller analysis and the Walén test success shown by Lavraud et al. (2002) are also in agreement with this interpretation. The discontinuity characteristics were further shown to be stable over the four Cluster spacecraft. Finally, large plasma flows were continuously detected at the poleward edge of the high-altitude cusp. These flows have a negative $V_y$ component, thus opposite to the IMF $B_y$ at that time (Figure 4e and h). All these arguments are suggestive of a possibly steady reconnection site.

The occurrence of sporadic, patchy reconnection events, however, is thought to be important since the first observational evidence of Russell and Elphic (1978). Such events are called flux transfer events (FTEs). During the 19/02/2001 event we presented, such signatures possibly occur after the magnetopause crossing. Several plasma accelerations, that are well correlated with magnetic field disturbances in all three components, are seen between 03:30 and 04:00 UT in Figure 2e and g. The upward and tailward velocities are consistent with the southward IMF (Figure 2h), as monitored by ACE. The feature thus appears to be compatible with possible dayside reconnection. Figure 9 shows time series of HIA and FGM measurements zoomed in this interval. Panel a displays the magnitude of ions bulk velocity. Total (ion plus magnetic) and ion ($Nk_BT$) pressures are shown in panel b, while the magnetic field component normal to the magnetopause is shown in panel c. The FTE like events are bounded between the red vertical lines and are shaded. These transients show a bipolar signature of the Bn component as well as an enhanced bulk velocity. Panel b displays a quasi-continuous ion pressure while an excess magnetic pressure is measured at each event. These observations highlight the main characteristics of such transient structures, which supposedly are FTEs. Unfortunately, the inter-spacecraft separation of $\sim$600 km is small (FTEs are often $\sim$1 $R_E$) and does not allow to study the spatial behavior of the ionic structure through the spacecraft array. It may be

noted that a similar pass through FTE signatures is fully discussed in a recent paper using Cluster data by Bosqued et al. (2001). These authors provided convincing evidence for the probable prominent role of transient reconnection.

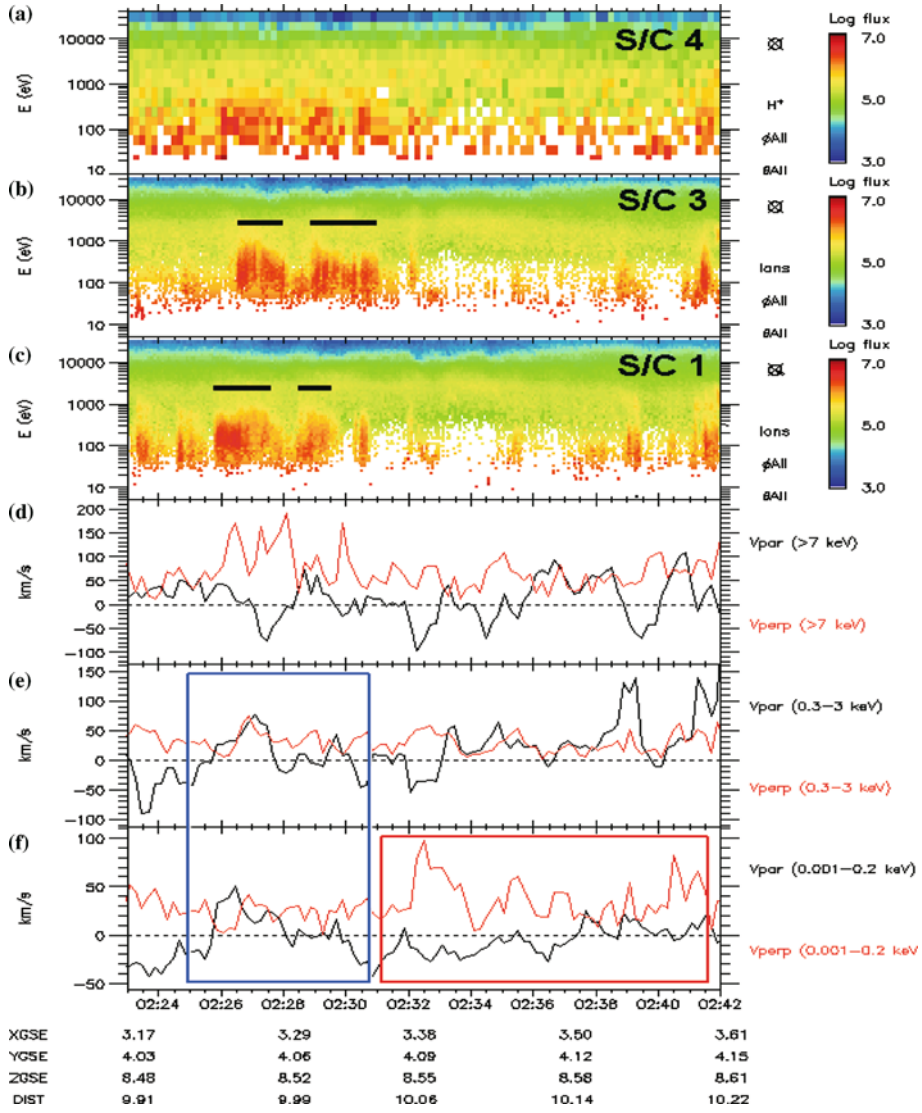


*Figure 10*. This plate presents the observations of possible evanescent PTEs (during the surrounded blue part) as well as intermittently accelerated cold plasma (during the surrounded red part). The first panel is the spectrogram from CODIF $H^+$ onboard spacecraft 4, panel b is that of HIA (all ions) onboard spacecraft 3 and panel c shows the HIA spectrogram for spacecraft 1. The parallel velocity and the magnitude of the perpendicular velocity computed from HIA measurements onboard spacecraft 1 are shown for three different energy ranges in panels d, e and f. Energy ranges are respectively: $>7$ keV, 0.3–3 keV and $<0.2$ keV.

The possibility of plasma protrusion through the magnetopause without necessity of magnetic merging was early proposed by Lemaire and Roth (1978) (see also Roth (1992)). This process is an alternative to the reconnection model. We therefore want to highlight typical observations of such possible plasma transfer events (PTEs) (Lundin et al., 2003).

Figure 10 displays a zoom in of the 02:24–02:35 UT interval during the 19/02/2001 event. It shows transient detection of magnetosheath like plasma on apparently dayside magnetospheric field lines, that are mixed with high-energy ions of plasma sheet origin. The two main transients, observed between 02:26 and 02:32 UT, are composed of $H^+$ and $He^{2+}$ ions mainly (not shown) within the energy range 0.3–3 keV, revealing they are most probably of magnetosheath (solar wind) origin. Panels a , b and c respectively show the spectrograms from spacecraft 4 (CODIF), 3 (HIA) and 1 (HIA). We used several energy ranges in computing the velocity moment for spacecraft 1 (only) in panels d, e and f. These energy ranges have been chosen to fit the three different populations observed during the interval. Energy $>7$ keV shows the behavior of the most energetic plasma sheet ions. The 0.3–3 keV range highlights that of the magnetosheath like plasma while the $<0.2$ keV range is representative of the coldest populations intermittently observed (discussed in the next subsection).

The PTE signatures presented in Figure 10 between 02:25 and 02:32 UT show nearly fully mixed populations. Here we focus on the most intense signature at 02:26–02:28 UT. It is characterized by rather low flows (see the surrounded part in blue of panels e and f) with equivalent parallel and perpendicular magnitudes in both the medium and low energy ranges. Panel d shows, however, that the perpendicular velocity of the high-energy ions is very different from those of the low and medium energy components. For high-energy ions the gradient/anisotropy, due to their large gyroradii, has strong influence on the perpendicular velocity while lower energy ions are mostly drifting in the ExB sense. In accordance with the characteristics given by Lundin et al. (2003), this particular case shows rather "evanescent" PTE signatures. Indeed, according to these authors the "active" PTEs have important drift velocities and show little (magnetosheath and plasma sheet) plasma mixing while their drift velocities are decreased (braking) and plasma mixing is large when "evanescent". These authors therefore suppose that "evanescent" PTEs should have reached the most inward magnetospheric field lines, such as is probable in the case presented in Figure 10.

The Cluster spacecraft observed PTE like events on 14/01/2001. Lockwood et al. (2001b) interpreted them as LLBL encounters. These observations revealed a clear nested feature in the time series. This favors the interpretation of LLBL being permanently attached to the cusp (and magnetopause) boundaries, and possibly due to ongoing dayside, sub-solar reconnection. However, because the PTEs are supposedly detached small

plasma blobs convected within the magnetosphere, their signatures in the time series should be lagged, and not nested. The events presented by Lundin et al. (2003) apparently presented such characteristics. In Figure 10, spacecraft 1 and 3 (panel c and b respectively) detected such two successive transients (shown with black lines). Spacecraft 4 data had low resolution during this event and did not permit to isolate the two events. These two events appear to be lagged in time between the two spacecraft, but with different durations at spacecraft 1 and 3. Taking into account the spacecraft location, these structures might be detached, spatially limited and convected towards the inner magnetosphere, but a definitive conclusion can not be made at all in the present case. As revealed through the case shown by Lockwood et al. (2001b), further multi-spacecraft analysis is needed to infer their spatial extent, and single event analysis is may be insufficient.

It has been suggested that PTE signatures inside the magnetosphere and FTE signatures at the magnetopause (and magnetosheath) may be subsequent to a unique process (Lundin et al., 2003). An argument that may favor the PTEs independent nature is however that they are often sampled deep inside the magnetosphere, showing fully mixed plasma (as in Figure 10), as well as near the magnetopause, showing a depletion in magnetospheric population fluxes. Moreover, Stenuit et al. (2001) and Lundin et al. (2003) found a poor correlation of their occurrence with IMF orientation. Merged flux tubes may not account for such properties, particularly under southward IMF when FTEs supposedly are quickly convected tailward. Some expected differences in the observational signatures of FTEs and PTEs were reviewed by Lui (2001). The possible occurrence of reconnection, FTEs, gyroradius effects, diffusion, Kelvin–Helmholtz instability and PTEs at the magnetopause were recently revisited by Sibeck et al. (1999).

### 4.3. Intermittent cold plasma accelerations

Thermal cold plasma accelerations were first revealed in Cluster data aside the flank magnetopause by Sauvaud et al. (2001). Lundin et al. (2003) later emphasized similar phenomena occurring near and within PTE signatures. Here we show their occurrence near the high-altitude cusp, both during the presence and absence of entering magnetosheath plasma.

Figure 11 is showing an interesting pass through the high-altitude cusp boundary layers and dayside plasma sheet on 19/02/2001. The energy-time spectrogram of panel a highlights the presence of cold ions below 100 eV during most of the interval. Most particularly, a mixture of magnetosheath like ($\sim$1000 eV) and accelerated cold ($<$ 100 eV) ions is clearly observed from 03:06 to 03:07 UT (also present is the high-energy component from the plasma sheet). A distribution function is displayed in Figure 12 at $\sim$03:06:30 UT. It shows three distinct plasma populations. A trapped

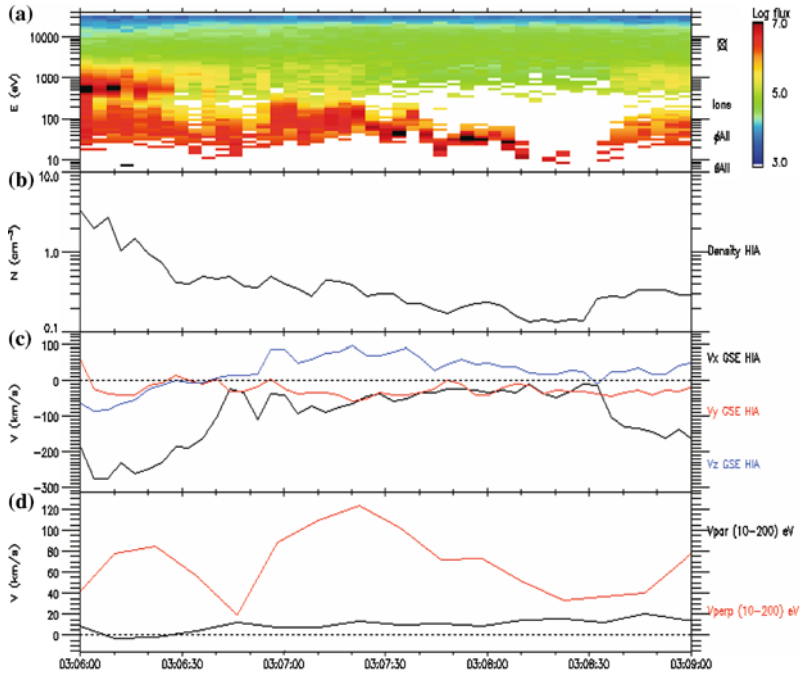


*Figure 11.* This plate presents cold ion observations near the high-altitude cusp boundary on 19/02/2001, that are sometimes mixed with magnetosheath and plasma sheet ion populations. Panel a shows the energy-time spectrogram from HIA. Panel b and c display the moments: the ions density and the ions bulk (whole energy range) velocity in GSE. The last panel shows the parallel and perpendicular to the magnetic field magnitudes of the ions velocity, computed for the range of energy (10, 200) eV only. This last panel thus highlights the cold ions population behavior more specifically.

high-energy component, that is typical for the dayside plasma sheet, is seen as the quasi-isotropic background at high energies (which extends further than the axes limits). A second, intense population flowing mainly along the magnetic field is observed. It is a typical magnetosheath plasma flow that apparently had access to magnetospheric field lines. There also appears a colder ion population, that is shown to be totally perpendicularly drifting. Lundin et al. (2003) recently showed a similar co-existence of three distinct populations, on apparently typical dayside magnetospheric field lines within the magnetopause boundary layers. Hence similar to the present case.

However, it is clearly seen in Figure 11 that cold ions are also observed without the direct presence of entering magnetosheath plasma. Such ions are detected between 03:07:30 and 03:08:30 UT. The transition from a mixture of magnetosheath like and cold plasma to uniquely cold plasma appears gradual. The cold ions are clearly accelerated in the perpendicular direction only, according to panel d. The feature shows an energy dispersion in panel a between 03:07:30 and 03:08:30 UT. While they are widely present near the

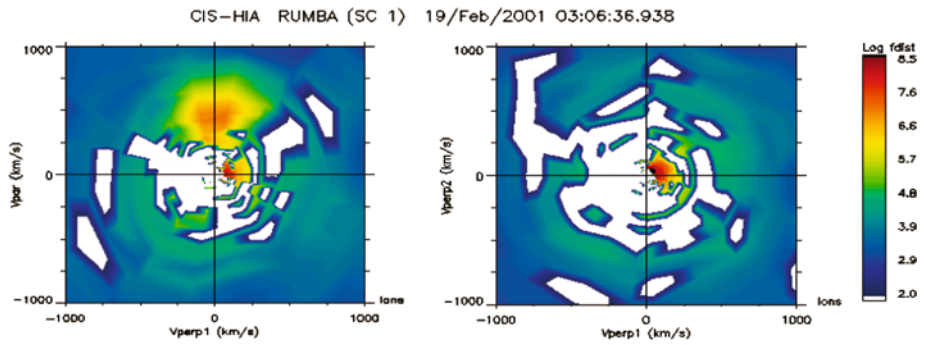


*Figure 12*. Similar ion distribution function to that of Figure 2a. It is sampled near the exterior cusp and dayside magnetopause, inside what appears to be boundary layers on 19/02/2001 at ~03:06:36 UT onboard spacecraft 1. It shows a mixture of three different populations (see text).

cusp boundary layers, their energy decreases with increasing depth within the dayside plasma sheet and they finally disappear at ~02:08:30 UT.

The intermittent nature of cold plasma acceleration is evidenced in Figure 10, between 02:31 and 02:41 UT. During this interval the ions are only detected sporadically. The cold ion population is again totally flowing perpendicular to the magnetic field (panel f, the parts surrounded in red). The perpendicular velocity is very similar in all energy ranges during the times when accelerated cold ions are observed (02:31–02:41 UT). This is evidence for the role of an electric field providing acceleration via ExB drift. This allows the cold population to become detectable to the CIS instrument.

To account for the acceleration of cold plasma near the flank magnetopause, Sauvaud et al. (2001) suggested that magnetopause current motions inwards and outwards are susceptible to induce local electric fields (Faraday''s law) that would act to accelerate the local cold plasma. On the other hand, Lundin et al. (2003)'s approach of PTEs implies the creation of an electric field resulting from depolarization after magnetosheath plasma has protruded the magnetopause. Acceleration of local cold plasma subsequent to impulsive plasma penetration, as was early envisaged by Lundin and Dubinin (1985), is thus substantially different from the former process, although not mutually exclusive.

When magnetosheath plasma is not present, we may expect the acceleration to be induced by current sheet motions. The energy-dispersed feature may thus be linked to temporal, i.e. boundary motion changes, or spatial effects, since the induced electric field strength depends on distance from the current sheet.

Both Sauvaud et al. (2001) and Lundin et al. (2003) reported the large occurrence of cold plasma detection in the Cluster data. Sauvaud et al. (2001)

gave evidence that a cold plasma component was probably existing although too cold to be detected within the CIS dynamical range during their observations. During their event, when CIS stopped detecting these ions, the Whisper instrument (Décréau et al., 2001) was still sensing nearly equal densities near the magnetopause. The cold ions thus become detectable to CIS in the presence of enhanced electric fields. This indirect sensing of cold populations should permit in the future to highlight the spatial extent and the characteristics of the source region. Although not presently shown, the cold plasma is most of the time made of $H^+$, $He^+$ and $O^+$ ions, which rules out the solar wind as a source. Possible sources are the plasmasphere or more directly the ionosphere, both from the dayside and nightside parts of the auroral oval, including the cusps (Sauvaud et al., 2001; Lundin et al., 2003).

### 4.4. Energetic ions in the exterior cusp diamagnetic cavity

The high-altitude cusp region is known to contain substantial fluxes of high-energy ions (from tens of keV to MeV), comparable to the populations observed in the dayside plasma sheet (Kremser et al., 1995; Chen and Fritz, 2001; Chang et al., 2001; Trattner et al., 2001; Fritz et al., 2003). In this paper we take advantage of the CIS CODIF composition measurements to establish the detection of a distinct high-energy ions population, from 5 keV up to 40 keV, in the cusp diamagnetic cavity. Two typical energy spectra are shown for the 04/02/2001 inside the exterior cusp cavity, for $H^+$ ions in Figure 13a and for $O^+$ ions in Figure 13b. For both $H^+$ and $O^+$ ions a clear spectral break is observed at $\sim$5 keV in the flux curves. The populations are not extensions of the magnetosheath plasma (centered at few hundreds eV). Together with the fluxes (line plots) shown in the observation section for the 19/02/2001 $H^+$ and 04/02/2001 $O^+$ events, the present data thus give evidence for the presence of a distinct high energy ion population in the exterior cusp in the range (5–40) keV.

High-energy ions ($>5$ keV), mixed with plasma of magnetosheath origin are present during those two events. In the exterior cusp itself (low magnetic field region), their fluxes are lower than in the adjacent dayside plasma sheet. They are also lower than in the adjacent boundary layers, if they exist, as for the 19/02/2001 event. During the various passage through the plasma sheet-boundary layers-exterior cusp boundaries described in the observation section, a consistent gradual transition in these fluxes is always observed. All these ions are however absent when the spacecraft are sufficiently far out in the magnetosheath proper. They are also absent in the tenuous lobes for both events.

To account for the presence of energetic ions above 40 keV (and up to MeV) in the cusp region, several sources have been proposed: the solar wind (Chang et al., 2001; Trattner et al., 2001), the ionosphere (via an energization process) (Chen and Fritz, 2001; Fritz et al., 2003) and the dayside plasma

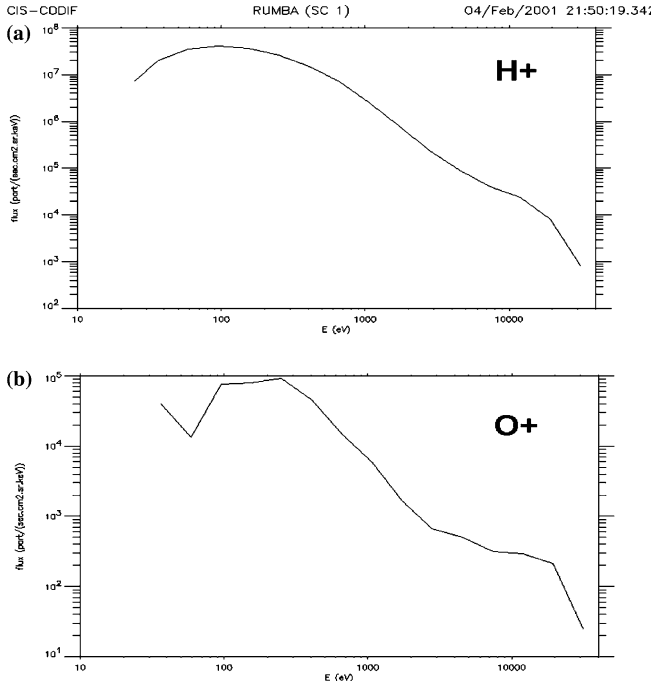


*Figure 13.* Energy spectra of the $H^+$ and $O^+$ fluxes in the exterior cusp diamagnetic cavity on 04/02/2001 around 21:50 UT. It clearly reveals the presence of a high-energy population above 5 keV for both ions.

sheet (Kremser et al., 1995; Delcourt and Sauvaud, 1998, 1999). We deal here with their possible role in the context of the 5–40 keV ions detected by the Cluster CIS CODIF instrument.

First, very few $O^+$ ions are *a priori* present in the solar wind. Substantial amounts of $O^+$ ions in the exterior cusp thus reject the solar wind as the source. Concerning the $H^+$ ions, the solar wind source appears unlikely in these particular cases because of the very low fluxes observed slightly later when Cluster sampled the magnetosheath. Some link with IMF orientation in the magnetosheath, however, may not be excluded (Trattner et al., 2001). Secondly, the constant gradual decrease of the fluxes between the dayside plasma sheet and the exterior cusp may not be expected if the ions where coming from the magnetosheath. The ions would be susceptible to enter all way long through the exterior cusp–magnetosheath boundary and therefore should not present such peculiar distributions.

An ionospheric source could explain the $O^+$ population. To account for the tens of keV $O^+$ (and up to MeV) detected by the Polar spacecraft, Chen and Fritz (2001) proposed a local energization process for ionospheric ions that would involve low frequency magnetic turbulence. On 04/02/2001 some

low frequency turbulence is observed throughout the cusp in the magnetic field data (Figure 4g). It is weaker, however, in the most distant part of the exterior cusp (low field region). These $O^+$ therefore may not be energized in this distant exterior cusp (i.e. Stagnant Exterior Cusp (Lavraud et al., 2002)). Acceleration process may however occur at lower altitudes. For instance, Bogdanova et al. (2004) recently showed the probable occurrence of cusp ion outflow heating via low-frequency electric field waves, permitting $O^+$ accelerations up to $\sim$1 keV at most. Several studies have shown observations of low frequency electromagnetic waves in the mid and high-altitude cusp (Angelopoulos et al., 2001; Le et al., 2001; Pickett et al., 2001). But how some wave particle interactions could energize ions to tens or hundreds of keV (Chen and Fritz, 2001; Fritz et al., 2003) is still to be determined (Angelopoulos et al., 2001). Finally, the gradual behavior of the flux decrease at the exterior cusp boundaries also is incompatible with a unique ionospheric source interpretation.

The similar behavior of both species throughout the cusp passes suggests a common origin for the two species. Also, the presence of high energy $O^+$ strongly favors that the magnetosphere (or ionosphere) may be the source of the cusp energetic ions in the present cases. But how magnetospheric ions gain access to the cusp needs to be explained.

During roughly southward IMF (19/02/2001), reconnection could possibly result in their access to the cusp since the dayside closed magnetospheric field lines contain such a high energy plasma. However, during northward IMF, reconnection may take place poleward of the cusp, as expected for the 04/02/2001 case. But the absence of energetic ions in the lobes rules out the nightside magnetosphere as a source. We may not rule out, nevertheless, the occurrence of reconnection equatorward (or sideways) of the cusp (and possible component merging process) which would also allow dayside magnetospheric ions to enter the exterior cusp via open field lines. However, Lavraud et al. (2002), as well as the present observations, rather favor long-term ongoing lobe reconnection during the 04/02/2001 event. The possible implication of a merging process needs further investigations.

The gradual decrease of the energetic ion fluxes away from the peak in the plasma sheet during both events tend to suggest a simple leakage across the dayside plasma sheet-exterior cusp boundary, possibly due to their large gyroradii. The presence of high-energy ions of magnetospheric origin at high latitudes was recently investigated via simulations by Delcourt and Sauvaud, 1998, 1999). They showed that the combined effect of convection, gradient/curvature drifts and the off-equator magnetic field minimum (due to the solar wind pressure at the sub-solar magnetopause) may allow high-energy ions (tens to hundreds keV) to escape into the high-latitude cusp region. In fact the observations during both events have shown the presence of high-energy ions of plasma sheet origin on the dayside magnetospheric field lines, and

within the possible boundary layers, just adjacent to the cusp diamagnetic cavity. This population is thus simply separated from the exterior cusp by a sharp boundary (for instance a TD). Leakage towards the cavity may then occur, owing to their large gyroradii. Using the Viking ion data, Kremser et al. (1995) showed an equivalent high-energy ion gradual behavior at the cusp-dayside plasma sheet transition at lower altitudes. They proposed that most of the high-energy $H^+$ fluxes (up to 50 keV) is of plasma sheet origin.

Nevertheless, none of the above hypothesis may be ruled out to explain the presence of high energy (5–40 keV) ion populations in the cusp. This high-energy plasma may have several origins, and that probably depend on the energy range as suggested by Trattner et al. (2001).

### 4.5. The exterior cusp structure and its interface with the magnetosheath

The 04/02/2001, 19/02/2001 and 18/05/2001 events represent good cases in order to highlight the global structure of the exterior cusp and its surrounding. Under steady northward IMF on 04/02/2001 the exterior cusp was bounded on its poleward edge by large flows. The sunward convection was well evidenced and the $V_y$ component of the flows has an opposite sign to the IMF $B_y$ (Figure 4e and h). No plasma mantle was present. This picture thus appears compatible with expectations for lobe reconnection. On the other hand, the 19/02/2001 event was characterized by an energy dispersion suggestive of a weak convection directed tailward (and as observed in the flows). This is consistent with the presence of a plasma mantle at the poleward edge of the cusp. Although the IMF $B_z$ component varied around 0 nT during most of the interval (Figure 2h), the positive IMF $B_x$ component suggests that the draped magnetosheath field at the dayside of the magnetosphere has a downward orientation. Hence, we may expect the magnetosheath and magnetospheric field to be anti-parallel at the dayside magnetopause, possibly allowing sub-solar reconnection.

On 04/02/2001, the large flows on the poleward side of the high-altitude cusp were followed by an exterior cusp pass, showing depressed magnetic field and stagnant plasma. The dynamics of the cusp allowed the Cluster spacecraft to make a quick exit into the dayside plasma sheet. It shows that the diamagnetic cavity (exterior cusp) was separated from the dayside plasma sheet by a sharp boundary. A similar boundary was present on 19/02/2001 between the exterior cusp and the dayside plasma sheet (or rather boundary layer) during the quick exit seen around 03:00 UT. The boundaries had a tangential nature in both events. Boundary layers were observed at the equatorward edge of the diamagnetic cavity on 19/02/2001, for instance between 02:45 and 02:55 UT. The magnetic field had a typical magnetospheric orientation and strength there, and a field aligned flow was observed (see

Figure 2b, e and g). These may be called the LLBL. Contrarily, no such boundary layers were observed at the dayside plasma sheet-exterior cusp interface on 04/02/2001. These observations appear to be compatible with a plasma entry process through the dayside magnetopause for southward IMF, which would not take place (at least at the dayside magnetopause) under northward IMF conditions. This process may be reconnection.

According to Vasyliunas (1995) the exterior cusp cannot be stagnant. He invoked subsolar reconnection and the probable subsequent tailward convection to account for the global cusp topology and characteristics. Under this context, the magnetosheath plasma gets access to the exterior cusp through the RD (an Alfvén wave) created in the subsolar region and propagating tailward over the cusps. The exterior cusp is thus filled with magnetosheath plasma, convecting at a speed attaining a non-negligible fraction of the external magnetosheath flow. However, this interpretation does not take into account the possibility of lobe reconnection under northward IMF. This could lead to the presence of a discontinuity, possibly then a counter-streaming (relative to the magnetosheath) Alfvén wave, moving very slowly sunward and downward. The downstream plasma may then be much more stagnant, as observed on 04/02/2001. The very low perpendicular velocity (not shown) in the (stagnant) exterior cusp on 04/02/2001 is on average oriented towards the dayside and the external boundary de Hoffmann–Teller frame is consistently found to be moving slowly sunward and downward (see Lavraud et al., 2002).

On the other hand, although a southward like orientation of the magnetosheath field is expected, and a global tendency of tailward convection in the cusp and plasma mantle that has previously be noted, stagnant plasma was also observed in the exterior cusp on 19/02/2001. This shows that plasma stagnation may occur in the exterior cusp even under conditions of such apparent global tailward convection. A plausible interpretation is that the exterior cusp is more stagnant because permanently made of co-existing up and down-flowing magnetosheath plasma. Part of the plasma is pre-existent. The plasma located within this very low magnetic field region appears thermalized, a heating process seems to occur at the boundary (Lavraud et al., 2002). It is unclear whether the possible occurrence of reconnection is relevant to explain these characteristics. Such a "stagnation region" had early been predicted by Spreiter and Summers (1967) and observed by HEOS 2 (Haerendel et al., 1976). It was interpreted in terms of aerodynamic behavior. Yamauchi and Lundin (1997) further emphasized the possible role of plasma inertia and escaping ions for the presence of stagnant plasma. The intriguing appearance of stagnant plasma on 19/02/2001 thus may be an argument against the role of reconnection in structuring the cusp, which may be an over-simplified view. The occurrence of plasma stagnation in the

exterior cusp as a function of solar wind conditions therefore deserves much interest.

In Figure 14 we display the plasma, magnetic and total pressures during the interval 21:35–22:05 UT in panel a. The time series of the magnetic field magnitude for the four spacecraft are shown in panel b. The nested nature of the dayside magnetospheric encounter at 21:41–21:45 UT is evidenced in panel b. The magnetic pressure increases in this region while the plasma pressure decreases. On average, the total pressure is conserved. This highlights an equilibrium between the two regions.

Cargill (1999) and Taylor and Cargill (2001) investigated the theoretical possible occurrence of shocks in the near cusp magnetosheath flow. This was first investigated by Walters (1966). However only possible intermediate and slow shock-like signatures have been reported near the cusp and magnetopause (but not established) in the literature so far (Song et al., 1992; Whaltour et al., 1995; Dubinin et al., 2002; Lavraud et al, 2002). On 04/02/2001, the exterior cusp–magnetosheath boundary may be the result of reconnection in the lobes as emphasized by Lavraud et al. (2002). The boundary would possibly be a RD originating from a reconnection site located above the

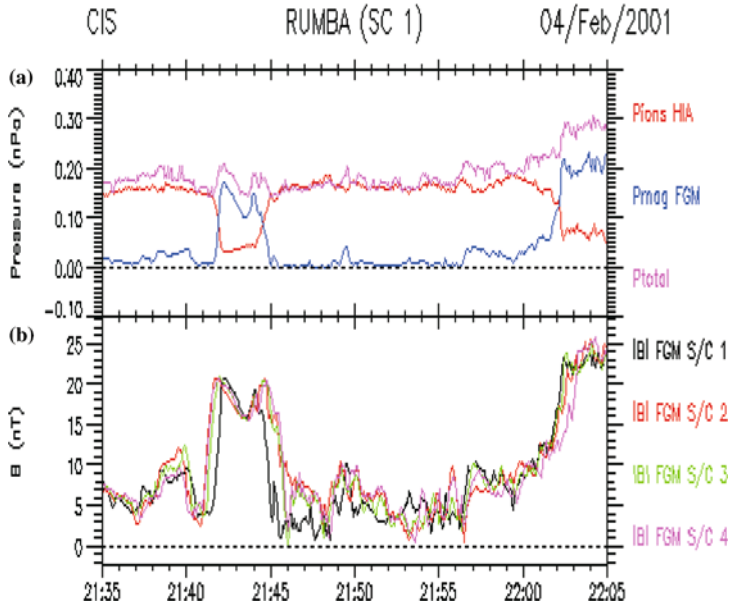


*Figure 14*. Pressures and four spacecraft magnetic field time series for an interval including the main magnetic boundaries crossed on 04/02/2001. The nested feature observed at 21:41–21:45 UT is the dayside plasma sheet encounter. The boundary observed at 22:02 UT is the external current sheet between the exterior cusp and the magnetosheath. The ion pressure from HIA ($Nk_BT$), the magnetic pressure (from FGM) and the total pressure are displayed in panel a. The magnetic field strength from FGM is presented in panel b for the four spacecraft.

spacecraft (Fuselier et al., 2000; Russell et al., 2000; Onsager et al., 2001). This boundary is indeed shown to be a sharp boundary, rotational in nature and it allows plasma entry into the cusp and subsequently the magnetosphere. But the magnetosheath plasma appears heated right at the boundary, what should not be expected at usual MHD RDs. Because of the pre-existence of out-going hot exterior cusp plasma that mixes with the entering magnetosheath plasma, the distribution functions sampled on the inside of the boundary appear quickly isotropic. This also reveals that the boundary is very complex. More comprehensive analysis will be devoted to understanding the physics of this key boundary in future papers.

Because the exact origin and nature of the discontinuity are unclear, it may be more cautious to define the magnetopause as the boundary delimiting the exterior cusp from the dayside plasma sheet (see Figure 1b). This is the definition given by Russell et al. (2000). Note that if reconnection plays a crucial role in structuring the cusp at large scale and that the external boundary is the result of this process, it may be reasonable calling the exterior cusp–magnetosheath boundary the magnetopause, which is the definition of Onsager et al. (2001). And subsequently, the "exterior" cusp we dealt within this paper would be located "interior" to the magnetopause.

## 5. Conclusions

We presented in Figure 1b a schematic of the Cluster path for all three events: 19/02/2001, 04/02/2001 and 18/05/2001. Their different actual paths through the various regions of the high-altitude magnetosphere in the cusp region have allowed a global investigation of the high-altitude cusp and its surrounding in a complementary way. We presented and analyzed the overview of typical Cluster observations in the region for different solar wind conditions. From this study, we may conclude the following.

We have described in details the high-altitude cusp precipitation region properties. The large-scale energy dispersion features and the associated large-scale convection appear to be dependent on the IMF orientation. The short time-scale plasma flows showing a pitch angle evolution in accordance with mirroring at low-altitude highlight the time-dependent nature of plasma injections in the cusp region. The current spatial-temporal ambiguity concerning "cusp ion step" like structures was pointed out and further illustrated through the analysis of the 18/05/2001 event. While such features were previously recorded with dual satellites at low or mid-altitudes, we have shown the probable occurrence of such spatial structure in the high-altitude plasma mantle. The multi-spacecraft Cluster data can play a significant role in trying to fix their spatial and temporal characteristics as well as to infer their origin.

The possible occurrence of steady reconnection in the lobes was pointed out. However, a current space physics controversy was discussed in terms of the exact characterization of the processes allowing for plasma entry into the magnetosphere. The FTE and PTE observations are possibly due to the same, unique process. These two different interpretations might reveal a certain duality in plasma physics (Lui, 2001). Anyhow, the clear transient nature of plasma penetration into the magnetosphere (and cusp) implies dynamical processes, that steady state interpretations may not support.

We have shown observations of accelerated cold plasma at locations where dynamical, kinetic effects are susceptible to generate electric fields. They were shown to be observed intermittently in this region, and both during the presence and absence of entering magnetosheath plasma. The processes susceptible to generate these electric fields (induced by magnetopause motions or following a depolarization generated by protruding plasma), as well as the origin of the cold ions (plasmasphere or ionosphere), are still unclear. The combined use of the different, complementary instruments onboard the multi-spacecraft Cluster mission will probably allow a better comprehension of these phenomena in the near future. The density of this cold plasma is often large, as pointed out by Sauvaud et al. (2001). Because these are not always detectable within classical particle detector energy ranges, the investigation of their possible permanent presence is crucial for the physics of the whole magnetosphere. In low density regions, the spacecraft potential is too high to permit the detection of this thermal population that is only of a few eV most of the time. Finding a way to limit the spacecraft potential is a major issue.

The presence of distinct populations (both $H^+$ and $O^+$ components) of high energy ions (5–40 keV) inside the exterior cusp has been evidenced by use of the Cluster CIS CODIF instrument. As presented here, several reasons for their presence may be found in the literature. The ionosphere (provided some acceleration process exists) and the bow shock have been proposed as possible source regions. The present observations, however rather favor the dayside plasma sheet as a seed population for $H^+$ and $O^+$ ions at these energies. How leakage may occur would also need be addressed. Single event studies may not permit to understand the actual origin of these ions. More surveys are needed to try to discriminate between those alternate views, or at least between their relative importance.

We finally gave an overview of the cusp large-scale picture. The global cusp convection is linked to the interplanetary conditions and there are evidence for its implication in structuring the cusp and its surrounding regions (presence or absence of boundary layers). The exterior cusp is surrounded by clear boundaries, with the lobes, the dayside plasma sheet and the magnetosheath. This distant region is always characterized by a strong magnetic depletion, which is partially the result of diamagnetic effect. The further out the space-

craft are, the more stagnant the plasma appears on 04/02/2001. In addition to a presumably low field at the null point of the Chapman Ferraro model (Chapman and Ferraro, 1931) the magnetosheath population that fills the region provides an excess plasma pressure. It is balanced by substantial diamagnetic effect and the cavity is formed, in apparent equilibrium with its surrounding. Whether reconnection occurs and can explain part of the cusp structure needs to be fixed in the future. For matter of caution, it may be preferable to define the magnetopause as the indented boundary between the exterior cusp and the magnetosphere itself. But if reconnection drives the large-scale cusp structure and topology, the exterior cusp–magnetosheath boundary depicted here may rather be called the magnetopause, implying that the so-called ''exterior cusp'' is inside the magnetopause.

The global structure, the magnetic field topology and the dynamics of the high-altitude cusp region and its surrounding boundaries are keys to understanding how solar wind plasma enters the magnetosphere. The Cluster data have showed an unprecedented potential for the characterization of the different boundaries surrounding the cusp. This paper presented multi-spacecraft observations of the magnetospheric cusps where much of the solar wind–magnetosphere interaction maps. The observations from the Cluster mission already provide new insights into the physics of the magnetosphere. It must be noted that the Cluster fleet inter-spacecraft distance will be enlarged up to $\sim$1 $R_E$ for the 2003 cusp period. Exploring the exterior cusp structure at large scale, which will also allow direct monitoring of the magnetosheath conditions, should soon give rise to interesting studies.

## Acknowledgements

We are grateful to A. Barthe and E. Penou for their incomparable work in CIS data processing and visualization. This overview of Cluster observations in the cusp is a synthesis of the many topics discussed during the recent Cluster workshops. Many thanks to the Cluster community.

## References

Angelopoulos, V., Mozer, F. S., Bonnell, J., Temerin, M., Somoza, M., Peterson, W. K., Collin, H. L., and Giles, B.: 2001. 'Wave Power Studies of Cusp Crossings with the Polar Satellite', *J. Geophys. Res.* **106**, 5987.

Balogh, A., Carr, C. M., Acuña, M. H., Dunlop, M. W., Beek, T. J., Brown, P., Fornaçon, K.-H., Georgescu, E., Glassmeier, K.-H., Harris, J., Musmann, G., Oddy, T., and Schwingenschuh, K.: 2001. 'The Cluster Magnetic Field Investigation: Overview of in-flight Performance and Initial Results', *Ann. Geo.* **19**, 1207.

Belmont, G., and Rézeau, L.: 2001. 'Magnetopause Reconnection Induced by Magnetosheath Hall-MHD Fluctuations', *J. Geophys. Res.* **106**, 10751.

Bogdanova, R., Klecker, G., Paschmann, L. M., Kistler, C., Mouikis, E., Moebius, H., Reme, J. M., Bosqued, I., Dandouras, J. A., Sauvaud, N., Cornilleau-Wehrlin, H., Laakso, A., Korth, M. B., Bavassano-Cattaneo, T., Phan, C., Carlson, G., Parks, J. P., McFadden, M., McCarthy, R., and Lundin, R., 'Investigation of the source region of inospheric oxygen outflow in the cusp using multi-spacecraft observations by CIS onboard Cluster, Advances in Space Research' 2004 (accepted).

Bosqued, J. M., Phan, T. D., Dandouras, I., Escoubet, C. P., Réme, H., Balogh, A., Dunlop, M. W., Alcaydé, D., Amata, E., Bavassano-Cattaneo, M.-B., Bruno, R., Carlson, C., DiLellis, A. M., Eliasson, L., Formisano, V., Kistler, L. M., Klecker, B., Korth, A., Kucharek, H., Lundin, R., McCarthy, M., McFadden, J. P., Moebius, E., Parks, G. K., and Sauvaud, J.-A.: 2001. 'CLUSTER Observation of the High-Latitude Magnetopause and Cusp: First Results from the CIS Ion Instruments', *Ann. Geophys.* **19**, 1545.

Cargill, P. J.: 1999. 'A Model for Plasma Flows and Shocks in the High-altitude Cusp', *J. Geophys. Res.* **104**, 14647.

Carlson, C. W., and Torbert, R.: 1980. 'Solar Wind Ion Injections in the Morning Auroral Oval', *J. Geophys. Res.* **85**, 2903.

Chang, S.-W., Scudder, J. D., Fennell, J. F., Friedl, R., Lepping, R. P., Russell, C. T., Trattner, K. J., Fuselier, S. A., Peterson, W. K., and Spence, H. E.: 2000. 'Energetic Magnetosheath Ions Connected to the Earth's Bow Shock: Possible Source of Cusp Energetic Ions', *J. Geophys. Res.* **105**, 5471.

Chapman, S., and Ferraro, V. C.: 1931. 'A New Theory of Magnetic Storms', *Terr. Magn. Atmosph. Elec.* **36**, 171.

Chen, J., and Fritz, T. A.: 2001. 'Energetic Oxygen Ions of Ionospheric Origin Observed in the Cusp', *Geophys. Res. Lett.* **28**, 1459.

Décréau, P. M. E., Fergeau, P., Krasnoselskikh, V., Le Guirriec, E., Lévêque, M., Martin, Ph., Randriamboarison, O., Rauch, J. L., Sené, F. X., Séran, H. C., Trotignon, J. G., Canu, P., Cornilleau, N., de Féraudy, H., Alleyne, H., Yearby, K., Mögensen, P. B., Gustafsson, G., André, M., Gurnett, D. C., Darrouzet, F., Lemaire, J., Harvey, C. C., and Travnicek, P., Whisper experimenters.: 2001. 'Early Results from the Whisper Instrument on Cluster: An Overview', *Ann. Geophys.* **19**, 1241.

Delcourt, D. C., and Sauvaud, J.-A.: 1998. 'Recirculation of Plasma Sheet Particles into the High-latitude Boundary Layer', *J. Geophys. Res.* **103**, 26521.

Delcourt, D. C., and Sauvaud, J.-A.: 1999. 'Populating of the Cusp and Boundary Layers by Energetic (hundreds of keV) Equatorial Particles', *J. Geophys. Res.* **104**, 22635.

Dubinin, E. et al.: 2002, ''Polar – Interball Co-ordinated Observations of Plasma and Magnetic Field Characteristics in the Regions of the Northern and Southern Distant Cusps'', *J. Geophys. Res.* **107**, N A5, SMP 2.

Dungey, J. W.: 1961. 'Interplanetary Magnetic Field and the Auroral Zones', *Phys. Rev. Lett.* **6**, 47 .

Dunlop, M. W., Woodward, T. I., Southwood, D. J., Glassmeier, K.-H., and Elphic, R. C.: 1997. 'Merging 4 Spacecraft Data: Concepts used for Analysing Discontinuities', *Adv. Space Res.* **20**, 1101.

Escoubet, C. P., Smith, M. F., Fung, S. F., Anderson, P. C., Hoffman, R. A., Basinska, E. M., and Bosqued, J.-M.: 1992, ''Staircase Ion Signature in the Polar Cusp – A Case Study'', *Geophys. Res. Lett.* **19**, 1735.

Fedorov, A., Dubinin, E., Song, P., Budnick, E., Larson, P., and Sauvaud, J. A.: 2000. 'Characteristics of the Exterior Cusp for Steady Southward Interplanetary Magnetic Field: Interball Observations', *J. Geophys. Res.* **105**, 15945.

Frank, L. A.: 1971. 'Plasma in the Earth''s Polar Magnetosphere', *J. Geophys. Res.* **76**, 5202.

Fritz, T. A., Chen , J., and Siscoe, G. L.: 2003, ''Energetic Ions, Large Diamagnetic Cavities, and Chapman-Ferraro Cusp'', *J. Geophys. Res.* **108**, SMP 17.

Fuselier, S. A., Trattner, K. J., and Petrinec, S. M.: 2000. 'Cusp Observations of High and Low-laltitude Reconnection for Northward IMF', *J. Geophys. Res.* **105**, 27509.

Haerendel, G.: 1978. 'Microscopic Plasma Processes Related to Reconnection', *J. Atmos. Terr. Phys.* **40**, 343.

Haerendel, G., Paschmann, G., Sckopke, N., Rosenbauer, H., and Hedgecock, P. C.: 1978. 'The Frontside Boundary Layer of the Magnetosphere and the Problem of Reconnection', *J. Geophys. Res.* **83**, 3195.

Harvey, C. C.: 1998, ''Spatial Gradients and the Volumetric Tensor, Analysis Methods for Multi-spacecraft Data'', *Int. Space Sci. Inst. Scientific Report Book*, 307.

Heikkila, W. J., and Winningham, J. D.: 1971. 'Penetration of Magnetosheath Plasma to Low Altitudes through the Dayside Magnetospheric Cusps', *J. Geophys. Res.* **76**, 883.

Kremser, G., Woch, J., Mursula, K., Tanskanen, P., Wilken, B., and Lundin, R.: 1995. 'Origin of Energetic Ions in the Polar Cusp Inferred from Ion Composition MeasuRèments by the Viking satellite', *Ann. Geophys.* **13**, 595.

Kuznetsova, M. M. and Zelenyi, L. M.: 1990, ''The Theory of FTE : Stochastic Percolation Model'', in C. T. Russell, E. R. Priest, and L. C. Lee (eds.), *Physics of Magnetic Flux Ropes*, AGU.

Lavraud, B., Dunlop, M. W., Phan, T. D., Réme, H., Bosqued, J.-M., Dandouras, I., Sauvaud, J.-A., Lundin, R., Taylor, M. G. G. T., Cargill, P. J., Mazelle, C., Escoubet, C. P., Carlson, C. W., McFadden, J. P., Parks, G. K., Moebius, E., Kistler, L. M., Bavassano-Cattaneo, M.-B., Korth, A., Klecker, B., and Balogh A.: 2002, ''Cluster Observations of the Exterior Cusp and its Surrounding Boundaries Under Northward IMF'', *Geophys. Res. Lett.* **29**, N. 20, 56.

Le, G., Blanco-Cano, X., Russell, C. T., Zhou, X.-W., Mozer, F., Trattner, K. J., Fuselier, S. A., and Anderson, B. J.: 2001. 'Electromagnetic Ion Cyclotron Waves in the High Altitude Cusp: Polar Observations', *J. Geophys. Res.* **106**, 19067.

Lemaire, J., and Roth, M.: 1978. 'Penetration of Solar Wind Plasma Elements into the Magnetosphere', *J. Atmos. Terr. Phys.* **40**, 331.

Lockwood, M., and Davis, C. J.: 1995. 'Occurrence probability, width and number of step of cusp precipitation for fully pulsed reconnection at the dayside magnetopause', *J. Geophys. Res.* **100**, 7627.

Lockwood, M., and Smith, M. F.: 1992. 'The Variation of Reconnection Rate at the Dayside Magnetopause and Cusp Ion Precipitation', *J. Geophys. Res.* **97**, 14841.

Lockwood, M., Opgenoorth, H., van Eyken, A. P., Fazakerley, A., Bosqued, J.-M., Denig, W., Wild, J. A., Cully, C., Greenwald, R., Lu, G., Amm, O., Frey, H., Strømme, A., Prikryl, P., Hapgood, M. A., Wild, M. N., Stamper, R., Taylor, M., McCrea, I., Kauristie, K., Pulkkinen, T., Pitout, F., Balogh, A., Dunlop, M., Réme, H., Behlke, R., Hansen, T., Provan, G., Eglitis, P., Morley, S. K., Alcaydé, D., Blelly, P.-L., Moen, J., Donovan, E., Engebretson, M., Lester, M., Watermann, J., and Marcucci, M. F.: 2001a. 'Coordinated Cluster, Ground-based Instrumentation and Low-altitude Satellite Observations of Transient Poleward-moving Events in the Ionosphere and in the Tail Lobe', *Ann. Geophys.* **19**, 1589.

Lockwood, M., Fazakerley, A., Opgenoorth, H., Moen, J., van Eyken, A. P., Dunlop, M., Bosqued, J.-M., Lu, G., Cully, C., Eglitis, P., McCrea, I. W., Hapgood, M. A., Wild, M. N., Stamper, R., Denig, W., Taylor, M., Wild, J. A., Provan, G., Amm, O., Kauristie, K., Pulkkinen, T., Strømme, A., Prikryl, P., Pitout, F., Balogh, A., Réme, H., Behlke, R.,

Hansen, T., Greenwald, R., Frey, H., Morley, S. K., Alcaydé, D., Blelly, P.-L., Donovan, E., Engebretson, M., Lester, M., Watermann, J.., and Marcucci, M. F.: 2001b. 'Coordinated Cluster and Ground-based Instrument Observations of Transient Changes in the Magnetopause Boundary Layer during an Interval of Predominantly Northward IMF: Relation to Reconnection Pulses and FTE Signatures', *Ann. Geophys.* **19**, 1613.

Lui, A. T. Y.: 2001. 'Current Controversies in Magnetospheric Physics', *Rev. Geophys.* **39**, 535.

Lundin, R., and Dubinin, E.: 1985. 'Solar Wind Energy Transfer Regions Inside the Dayside Magnetopause – II: Accelerated Heavy Ions as Tracers for MHD Processes in the Dayside Boundary Layer', *Planet. Space Sci.* **33**, 891.

Lundin, R., Sauvaud, J.-A., Réme, H., Balogh, A., Dandouras, I., Bosqued, J. M., Carlson, C., Parks, G. K., Moebius, E., Kistler, L. M., Klecker, B., Amata, E., Formisano, V., Dunlop, M. W., Eliasson, L., Korth, A., Lavraud, B.., and McCarthy, M.: 2003. 'Evidence for Impulsive Solar Wind Plasma Penetration through the Dayside Magnetopause', *Ann. Geophys.* **21**, 457.

Merka, J., Safrankova, J., Nemecek Z., et al.: 2000, ''High-altitude Cusp: INTERBALL Observations'', *Adv. Space Res.* **25**, No. 7/8, 1425.

Newell, P. T., and Meng, C. I.: 1988. 'The Cusp and the Cleft/LLBL: Low Altitude Identification and Statistical Local Time Variation', *J. Geophys. Res.* **93**, 14549.

Newell, P. T., Meng, C. I., Sibeck, D. G., and Lepping, P.: 1989. 'Some Low-altitude Cusp Dependencies on the Interplanetary Magnetic Field', *J. Geophys. Res.* **94**, 8921.

Newell, P. T., and Meng, C. I.: 1991. 'Ion Acceleration at the Equatorward Edge of the Cusp: Low Altitude Observations of Patchy Merging', *Geophys. Res. Lett* **18**, 1829.

Newell, P. T., and Meng, C. I.: 1994. 'Ionospheric Projections of Magnetospheric Regions under Low and High Solar Wind Pressure Conditions', *J. Geophys. Res.* **99**, 273.

Ohtani, S., Potemra, T. A., Newell, P. T., Zanetti, L. J., Iijima, T., Watanabe, M., Blomberg, L. G., Elphinstone, R. D., Murphree, J. S., Yamauchi, M., and Woch, J.: 1995. 'Four Large-scale Field-aligned Current Systems in the Dayside High-latitude Region', *J. Geophys. Res.* **100**, 137–153.

Onsager, T. G., scudder, J. D., Lockwood, M., and Russell, C. T.: 2001. 'Reconnection at the High Latitude Magnetopause during Northward Interplanetary Magnetic Field Conditions', *J. Geophys. Res.* **106**, 25467.

Paschmann, G., Haerendel, G., Sckopke, N., Rosenbauer, H.., and Hedgecock, P. C.: 1976. 'Plasma and Magnetic Field Characteristics of the Distant Polar Cusp Near Local Noon: The Entry Layer', *J. Geophys. Res.* **81**, 2883.

Pickett, J. S., Franz, J. R., Scudder, J. D., Menietti, J. D., Gurnett, D. A., Hospodarsky, G. B., Braunger, R. M., Kintner, P. M., and Kurth, W. S.: 2001. 'Plasma Waves Observed in the Cusp Turbulent Boundary Layer: An Analysis of High Time Resolution Wave and Particle MeasuRèments from the Polar Spacecraft', *J. Geophys. Res.* **106**, 19081.

Reiff, P. H., Hill, T. W., and Burch, J. L.: 1977. 'Solar Wind Plasma Injection at the Dayside Magnetospheric Cusp', *J. Geophys. Res.* **82**, 479.

Réme, H., Aoustin, C., Bosqued, J. M., Dandouras, I., Lavraud, B., Sauvaud, J.-A., Barthe, A., Bouyssou, J., Camus, Th., Cur-Joly, O., Cros, A., Cuvilo, J., Ducay, F., Garbarowitz, Y., Médale, J. L., Penou, E., Perrier, H., Romefort, D., Rouzaud, J., Vallat, C., Alcaydé, D., Jacquey, C., Mazelle, C., and d''Uston, C., : 2001. 'First Multispacecraft Ion MeasuRèments in and Near the Earth's Magnetosphere with the Identical CLUSTER Ion Spectrometry (CIS) Experiment', *Ann. Geophys.* **19**, 1303.

Roth, M.: 1992. 'On Impulsive Penetration of Solar Wind Plasmoids into the Geomagnetic Field', *Planet. Space Sci.* **40**, 193.

Russell, C. T., and Elphic, R. C.: 1978. 'Initial ISEE Magnetometer Results – Magnetopause Observations', *Space Sci. Rev.* **22**, 681–715.

Russell, C. T.: 2000. 'POLAR Eyes the Cusp, Proc. of the Cluster II Workshop: Multiscale/Multipoint Plasma Measurèments', *ESA* **SP-449**, 47.

Russell, C. T., Le, G., and Petrinec, S. M.: 2000. 'Cusp Observations of High and Low Latitude Reconnection under Northward IMF: and Alternate View', *J. Geophys. Res.* **105**, 5489.

Sauvaud, J.-A., Lundin, R., Réme, H., McFadden, J. P., Carlson, C., Parks, G. K., Moebius, E., Kistler, L. M., Klecker, B., Amata, E., DiLellis, A. M., Formisano, V., Bosqued, J. M., Dandouras, I., Décréau, P., Dunlop, M. W., Eliasson, L., Korth, A., Lavraud, B.., and McCarthy, M.: 2001. 'Intermittent Thermal Plasma Acceleration Linked to Sporadic Motions of the Magnetopause, First Cluster Results', *Ann. Geophys.* **19**, 1523.

Savin, S. P., : 1998. 'The Cusp/magnetosheath Interface on May 29, 1996 : Interball 1 and Polar Observations', *Geophys. Res. Lett.* **25**, 2963.

Sckopke, N., Paschmann, G., Rosenbauer, H., and Fairfield, D. H.: 1976. 'Influence of the Interplanetary Magnetic Field on the Occurrence and Thickness of the Plasma Mantle', *J. Geophys. Res.* **81**, 2687–2691.

Sibeck, D. G., Paschmann, G., Treumann, R. A., Fuselier, S. A., Lennartsson, W., Lockwood, M., Lundin, R., Ogilvie, K. W., Onsager, T. G., and Phan, T. D., : 1999. 'Chapter 5-Plasma Transfer Processes at the Magnetopause', *Space Sci. Rev.* **88**, 207.

Song, P., Russell, C. T., and Thomsen, M. F.: 1992. 'Slow Mode Transition in the Front Side Magnetosheath', *J. Geophys. Res.* **97**, 8295.

Sonnerup, B. U. O., and Cahill, L. J.: 1967. 'Magnetopause Structure and Attitude from Explorer 12 Observations', *J. Geophys. Res.* **72**, 171.

Stenuit, H., Sauvaud, J.-A., Delcourt, D. C., Mukai, T., Kokubun, S., Fujimoto, M., Buzulukova, N. Y., Kovrazhkin, R. A., Lin, R. P., and Lepping, R. P.: 2001. 'A Study of Ion Injections at the Dawn and Dusk Polar Edges of the Auroral Oval', *J. Geophys. Res.* **106**, 29619.

Taylor, M. G. G. T. and Cargill, P. J.: 2001, ''A Agnetohydrodynamic Model of Plasma Flow in the High Altitude Cusp'', *J. Geophys. Res.* **107**, N. A6, SMP 13.

Trattner, K. J., Fuselier, S. A., Peterson, W. K., Sauvaud, J. A., Stenuit, H., Dubouloz, N., and Kovrazhkin, R. A.: 1999. 'On Spatial and Temporal Structures in the Cusp', *J. Geophys. Res.* **104**, 28411.

Trattner, K. J., Fuselier, S. A., Peterson, W. K., Chang, S.-W., Friedel, R., and Aellig, M. R.: 2001. 'Origins of Energetic Ions in the Cusp', *J. Geophys. Res.* **106**, 5967.

Tsyganenko, N. A.: 1989. 'A Magnetospheric Magnetic Field Model with a Warped Tail Current Sheet', *Planet. Space Sci.* **37**, 5.

Vasyliunas, V. M., Skopke, N., and Rosenbauer, H.: 1977. 'Structure of the Polar Magnetosheath as Observed by HEOS 2', *EOS Transac. AGU* **58**, 1206.

Vasyliunas, V. M.: 1995. 'Multi-branch Model of the Open Magnetopause', *Geophys. Res. Lett.* **22**, 1245.

Vontrat-Reberac, A., Bosqued, J. M., Taylor, M. G., Lavraud, B., Fontaine, D., Dunlop, M. W., Laakso, H., Cornilleau-Werhlin, N., Canu, P. and Fazarkerley, A.: 2003, ''Cluster Observations of the High-Altitude Cusp for Northward Interplanetary Magnetic Field: A Case Study'', *J. Geophys. Res.* accepted.

Walters, G. K.: 1966. 'On the Existence of a Second Standing Shock Wave Attached to the Magnetosphere', *J. Geophys. Res.* **71**, 1341.

Whalthour, D. W., Sonnerup, B. U. O., and Russell, C. T.: 1995. 'Observation of a Slow-mode Shock in the Dayside Magnetopause Reconnection Layer', *Adv. Space Res.* **15**, 501.

Woch, J., and Lundin, R.: 1992. 'Magnetosheath Plasma Precipitation in the Polar Cusp and its Control by the Interplanetary Magnetic Field', *J. Geophys. Res.* **97**, 1421.

Yamauchi, M., and Lundin, R.: 1994. 'Classification of Large-scale and Meso-scale Ion Dispersion Patterns Observed by Viking over the Cusp-mantle Region', in J. A. Holtet, and A.. Egeland (eds.), *Physical Signatures of Magnetospheric Boundary Layer Process*, Kluwer Academic Publishers, Dordrecht Netherlands, pp. 99–109.

Yamauchi, M., Nilsson, H., Eliasson, L., Norberg, O., Boehm, M., Clemmons, J. H., Lepping, R. P., Blomberg, L., Ohtani, S.-I., Yamamoto, T., Mukai, T., Terasawa, T., and Kokubun, S.: 1996. 'Dynamic Response of the Cusp Morphology to the Solar Wind: A Case Study during Passage of the Solar Wind Plasma Cloud on February 21, 1994', *J. Geophys. Res.* **101**, 24675–24687.

Yamauchi, M., and Lundin, R.: 1997. 'The Wave-assisted Cusp Model: Comparison to Low-altitude Observations', *Phys. Chem. Earth* **22**, 729–734.

Surveys in Geophysics (2005) 26: 177–191
DOI 10.1007/s10712-005-1876-2 © Springer 2005

# LOW-FREQUENCY PLASMA WAVES IN THE OUTER POLAR CUSP: A REVIEW OF OBSERVATIONS FROM PROGNOZ 8, INTERBALL 1, MAGION 4, AND CLUSTER

J. BLECKI[1], R. WRONOWSKI[1], S. SAVIN[2], N. CORNILLEAU-WEHRLIN[3], M. PARROT[4], Z. NEMECEK[5], J. SAFRANKOVA[5], O. SANTOLIK[5], K. KUDELA[6] and J-A. SAUVAUD[7]

[1]*Space Research Centre PAS, Bartycka 18A, Warsaw, 00716 Poland*
*E-mail: jblecki@cbk.waw.pl;*
[2]*Space Research Institute RAS, Moscow, Russia;*
[3]*CETP/CNRS, Velizy, France;*
[4]*LPCE/CNRS, Orleans, France;*
[5]*Charles University, Prague, Czech Republic;*
[6]*Institute of Experimental Physics of Kosice, SAS, Slovak Republic;*
[7]*CESR/CNRS, Toulouse, France*

(Received 22 March 2003; Accepted 30 April 2004)

**Abstract.** This paper presents a review of the most interesting observations of low-frequency plasma waves together with plasma particles which were made by the Interball 1, Magion 4 and Prognoz 8 satellites in the outer polar cusp. Accelerated plasma particles, hot electron populations and very strong wave activity, particularly at low frequencies, are observed. A detailed study of the wave spectra together with the distribution function for electrons indicate the correlation between the presence of lower-hybrid waves and the population of the particles with higher energy than in the surrounding space. These experimental facts suggest that strong coupling between waves and particles is responsible for plasma heating. During polar cusp crossings by Interball 1 and Prognoz 8, FFT analysis of the wave form indicates many bursts of ULF emissions in both electric and magnetic components. These waves have highly non-stationary characteristics. To study the dynamics of changes in the spectral characteristics of the waves wavelet analysis has been used. Nonlinear interactions are studied using bispectral methods of analysis. This presentation gives the results of such an analysis for selected cusp crossings at different altitudes. An example of wave activity registered by the STAFF instrument onboard the CLUSTER spacecraft in the polar cusp is also presented.

**Keywords:** bispectral methods, cusp, FFT, plasma waves, wavelet analysis

**Abbreviations:** ISEE – International Sun–Earth Explorers; GSE – Geocentric Solar Ecliptic; GSM – Geocentric Solar Magnetic; HEOS – Highly Eccentric Orbiting Satellite; DMSP – Defense Meterological Satellite Program; ASPI – Analysis of Spectra of Plasma waves and Instabilities; DOC-S – Detektor Ochlazhdaemyj Kremnievyj (Cooled Silicic Detector)

## 1. Introduction

The polar cusp is a region of the Earth's plasma environment where intense conversion of energy takes place. Low-frequency plasma waves, which can control the dynamics of the ions in collision free plasmas, play a very important role in the formation and behaviour of this region. The fluxes of accelerated plasma particles, electron and ion populations with higher temperatures than the ambient plasma and very strong wave activity, particularly at the low frequencies, can be observed in the polar cusp. The earlier observations of waves in the polar cusp made by Hawkeye in the outer cusp, Viking in the middle cusp, and Freja and DE-1 in the lower cusp indicate the presence of Alfven, lower hybrid, electron and ion cyclotron waves as the most typical modes in this region of the magnetosphere (Pottelette et al., 1990; Blecki et al., 1998, 1999; Savin et al., 1999; Menietti et al., 2002; Savin et al., 2004). This situation indicates that the polar cusp is an ideal laboratory for studies of nonlinear plasma processes important for understanding the basic plasma physics, as well as the magnetospheric and astrophysical application of these processes.

The goal of this paper is to document some highlights of the observations made by Prognoz 8, Interball 1 and Interball's companion subsatellite Magion 4 in the polar cusp. The description of the wave instrument SAS (Spectrum Analyzer for Subsatellite) on Magion 4 has been presented by Blecki et al. (1997) and ASPI on Interball 1 by Klimov et al. (1997). Additionally, an example of multipoint wave measurements made by the Cluster satellites and other examples from the much earlier Prognoz 8 single satellite in the polar cusp are presented.

## 2. Plasma heating in the cusp

Plasma heating in the collisionless plasma in the polar cusp can be performed by wave-particle interactions. The cusp crossing on 8 February, 1996, by Interball 1 and Magion 4 presents one example of this process. The cusp identification is done using the time-energy spectrogram from the Electron instrument shown in Figure 1. Two cusp crossings are seen: the first is at 22:45–23:40 UT and the second one hour later (23:45–00:15 UT) at a distance of about 7 $R_E$. Parameters of the electron component of plasma shown in Figure 2 confirm this interpretation.

A small enhancement of the mean value of electron energy appears at 23:45 UT. This was also registered on Magion 4, 42 min ahead of Interball 1, by its MPS (Magion Plasma Spectrometer) instrument. The upper panel in Figure 3 shows a broadening of the electron energy spectra around 23:00 UT indicating an increase of the electron temperature. Thus, there is a stable region of the mechanism which leads to the heating of the electrons. This

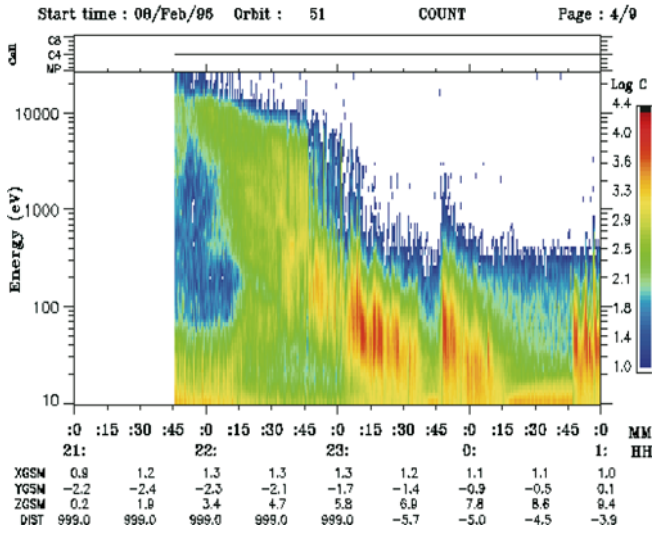


*Figure 1.* Time–energy spectrogram of the electrons registered by the Electron instrument on the Interball-tail probe on 8 February 1996. The cusp crossing is seen at 22:35–23:40 UT. The second encounter with the cusp can be observed at 23:45–00:15 UT.

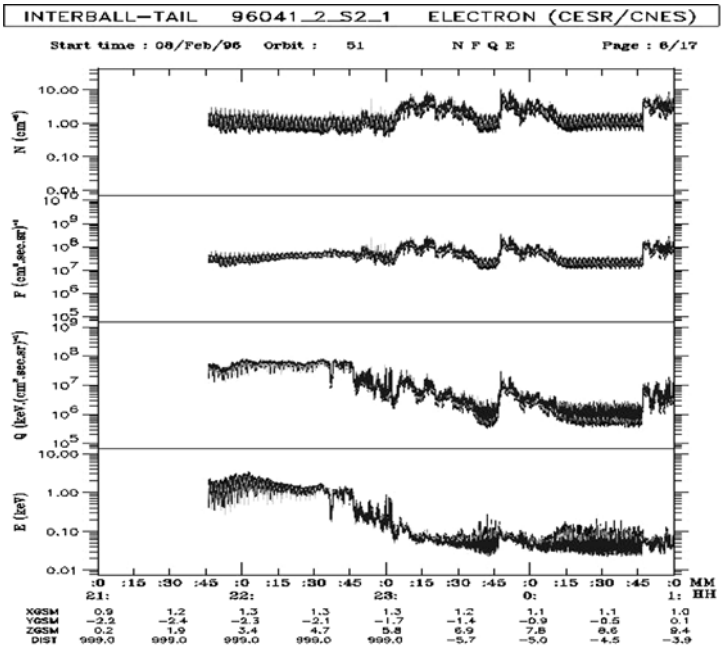


*Figure 2.* Electron parameters evaluated from the spectra of energy shown in Figure 1. A small enhancement of the mean energy (temperature) is seen (bottom panel) at 23:45 UT.

region is likely to be the edge of the cusp, where the strong waves (lower hybrid, electron cyclotron) are generated and can interact with electrons leading to their heating.

In Figure 4 the dynamic spectra of the magnetic fluctuations in the frequency range from 10 Hz up to 2 kHz are shown. The increase in the spectral density at the frequency corresponding to the electron cyclotron frequency (around 600 Hz) is seen at about 21:51 UT when Magion 4 entered the polar cusp (not shown). During the entire crossing strong wave activity was registered in the lowest part of the spectra, corresponding to the lower hybrid frequency. Comparing Figures 3 and 4, one can see the correlation of these low-frequency waves with the increase of the plasma temperature. At the moment of the increase of the electron temperature (23:00 UT), the intensity of the electron cyclotron waves rises.

A similar effect is present during the cusp crossing on 2 March, 1996. Interball 1 sees the cusp electrons at 16:25–17:15 UT at a distance of 5.5 $R_E$ (Figure 5). The broadening of the spectra indicates the increase in the electron temperature seen at the edge of the cusp. Figure 6 shows the energy–time spectrogram for the same cusp crossing by Magion 4. The time separation between both satellites was 30 min on this day; Magion was again ahead of Interball 1. Magion 4 entered into the cusp before 15:55 UT (not

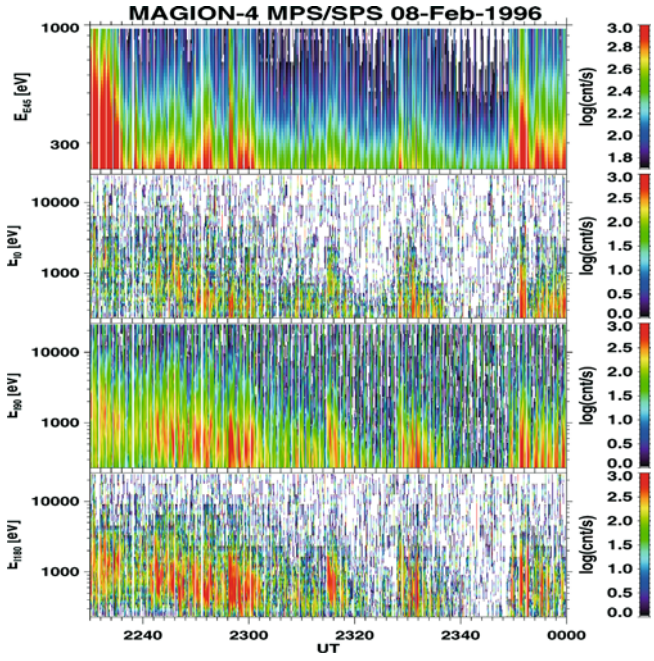


*Figure 3*. Time–energy spectrogram of electrons (upper panel) and ions of different pitch angles (3 next panels) from the MPS instrument taken during cusp crossing on 8 February, 1996.

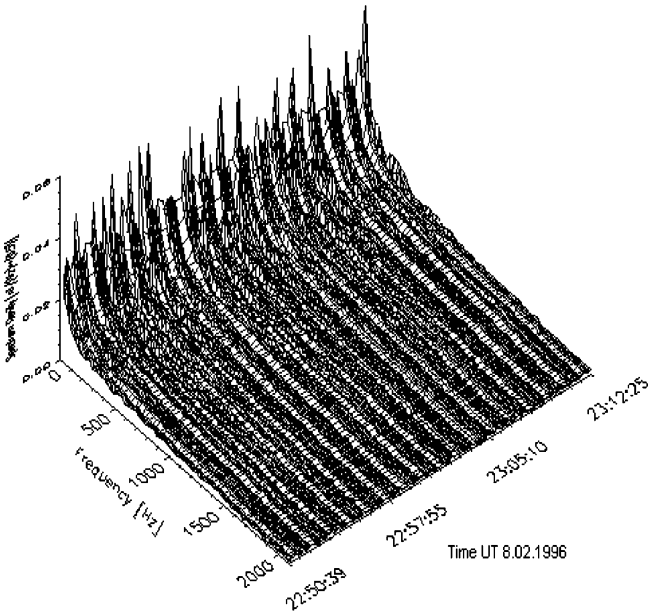


*Figure 4*. Spectra of the magnetic field fluctuations measured by the SAS instrument onboard Magion-4 in the outer polar cusp on 8 February, 1996. The vertical axis is the spectral density in $nT/Hz^{1/2}$. The lower hybrid and electron cyclotron frequencies are in the ranges 15–20 Hz and 600–800 Hz, respectively.

seen in the figure). Some broadenings of the spectra during the cusp crossing are seen in Figure 6. The broadening of the electron spectra corresponds to the presence of the ion beams (second panel in Figure 6).

Figure 7 shows the plasma wave spectra during this cusp crossing. The characteristic emissions one can see at frequencies in the lowest part of the spectra correspond to the lower hybrid frequency and in the higher part of spectra, around 300–500 Hz, to the electron cyclotron frequency. The modulation of the spectra is due to technical problems with the telemetry. A comparison of Figures 6 and 7 shows that lower hybrid waves may correlate with the heating of the electrons, which can generate higher frequencies (electron cyclotron). This case can be interpreted as the cascade of energy from lower frequency waves (lower hybrid) to higher frequency waves (electron cyclotron) through plasma heating. A discussion of cascading is given in the last Section of this paper and in Savin et al. (2004).

## 3. Waves registered at the reconnection site

The reconnection of magnetic field lines in the magnetospheric plasma produces plasma jets which can generate the low-frequency plasma waves.

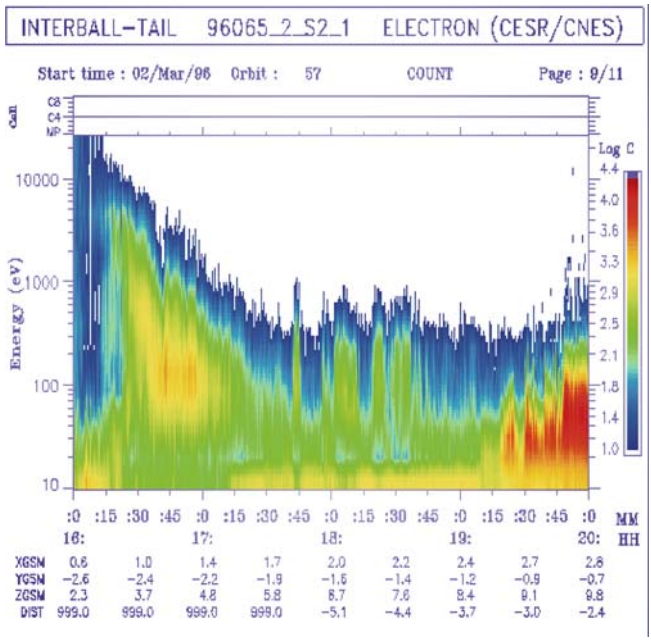


*Figure 5*. Time–energy spectrogram of the electrons registered by the instrument on the Interball-tail probe on 2 March, 1996. The cusp crossing is seen at 16:25–17:15 UT.

Figure 8 shows the spectra of the magnetic field fluctuations taken in the outer polar cusp by Magion 4 satellite in the vicinity of the reconnection site, observed by the Polar satellite on 29 May, 1996. The conjunction of the orbits of the Polar, Interball 1 and Magion 4 satellites during this event allows us to study processes occurring in the reconnection site and its vicinity simultaneously. This case was described in detail by Savin et al. (1998a, b, 2003) and Scudder et al. (1998). The very high level of wave intensity occurs in the frequency range corresponding to the lower hybrid frequency. These waves are a source of anomalous resistivity and diffusion (Haerendel, 1978, and Treumann, 1995). The enhancement of wave intensity is also seen at the electron cyclotron frequency. Magion 4 was outside the reconnection site but close to it, and observed waves generated by high energy electrons produced by reconnection. The DOC- S experiment was switched off during this event. Thus, we are not able to correlate our wave observations with registration of the high energy electrons, but a very high level of wave intensity can suggest this correlation.

## 4. Energetic electrons in the polar cusp

One of the recent discoveries made by the Polar, Interball 1 and Magion 4 satellites in the polar cusp is the presence of high energy ions and elec-

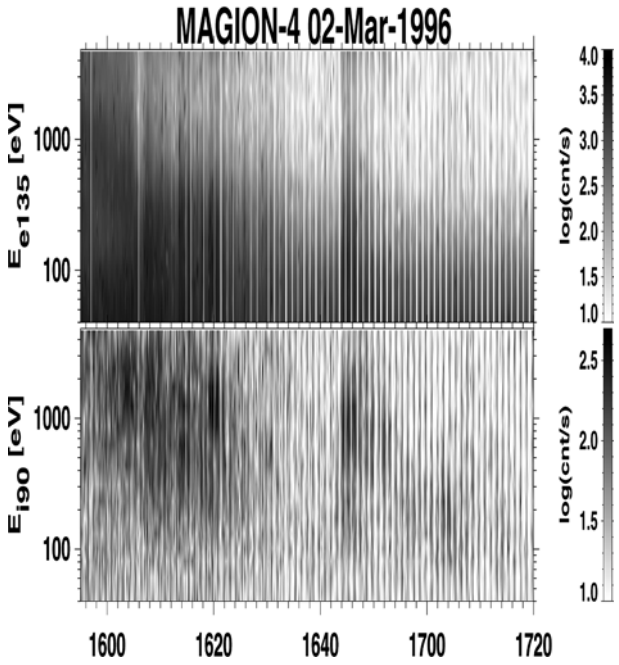


*Figure 6*. Energy–time spectrogram of electrons (135° pitch angle) and ions (90° pitch angle) from the MPS instrument taken during the cusp crossing on 2 March, 1996.

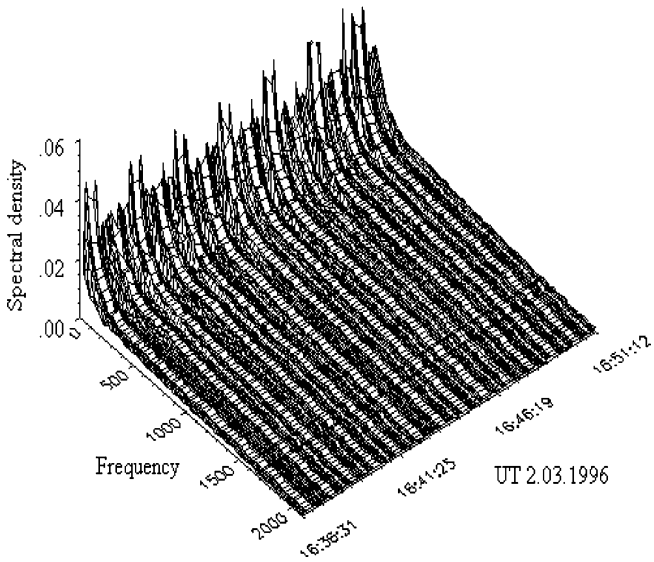


*Figure 7*. Spectra of the magnetic field taken during a pass of Magion-4 through the cusp crossing on 2 March, 1996. Lower-hybrid and electron cyclotron frequencies are in the ranges 12–20 Hz and 500–800 Hz, respectively. The spectral density is measured in $nT/Hz^{1/2}$.

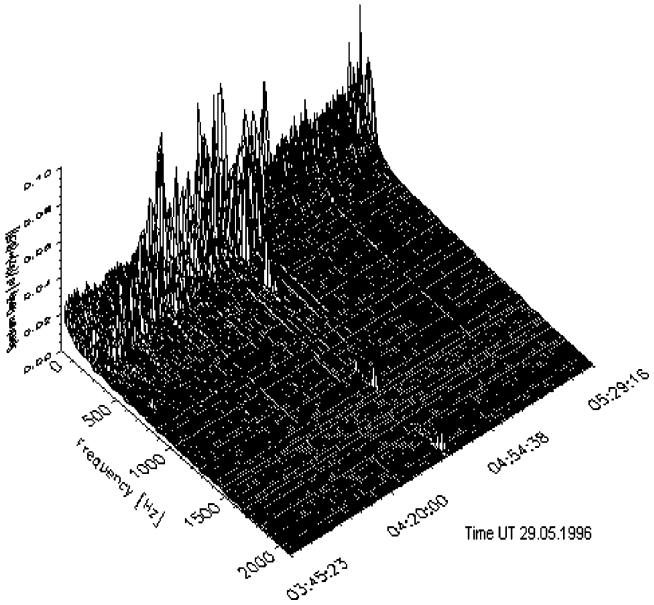


*Figure 8*. Spectra of plasma waves registered by Magion 4 on 29 May, 1996 in the vicinity of the reconnection site. The maxima of the wave intensity seen around 4:10 UT and 4:25 UT correspond to lower-hybrid waves (lower-hybrid frequency ~60–80 Hz). The spectral density is measured in $nT/Hz^{1/2}$.

trons in this region (Chen et al., 1998; Pisarenko et al., 2001). Strong plasma wave emissions are associated with these particles (Blecki et al., 1999; Pickett et al., 1999). Figure 9 shows the wave spectra taken by the SAS instrument taken during an encounter of Magion 4 with the flux of high energetic electrons (see Figure 10) on 17 January, 1996. The magnetopause was crossed around 3:50 UT when the flux of energetic electrons (20–180 keV) decreased dramatically. About 10 min later this flux increased again. Magion 4 entered into the cusp region. At 4:02 UT level of the plasma wave intensity increased to the highest level ever registered by Magion 4. The spectra shown in Figure 9 have the maxima at low frequencies corresponding to the lower hybrid mode as well as at the electron cyclotron frequency and its harmonics (up to third order). The correlation of these particles with emissions at the electron cyclotron frequency and its harmonics could suggest that a relativistic electron maser mechanism could be involved in the generation of these waves.

The temporal separation between Magion 4 and Interball 1 was 45 min. Figure 11 shows the time–energy spectrogram of the electrons; the time when Interball 1 met polar cusp was just 45 min later at 4:40 UT. This again shows the stable position of the edge of the cusp.

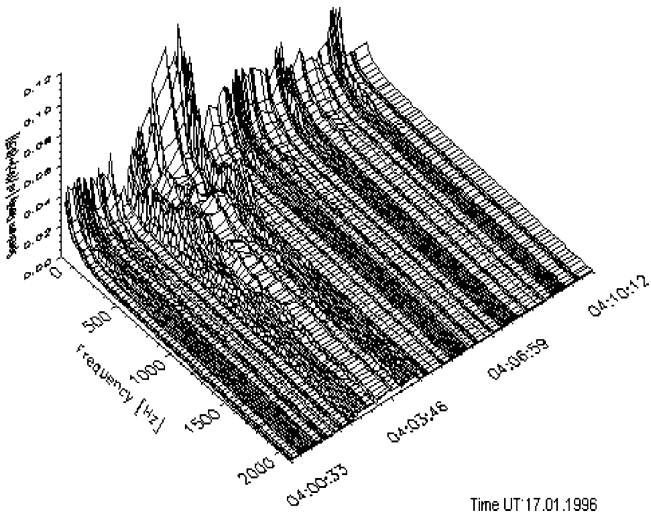


*Figure 9*. Spectra of plasma waves registered by Magion 4 on January 17, 1996 during encounter with the flux of high energy electrons. Spectral density is given in $nT/Hz^{1/2}$. The harmonics of the electron cyclotron frequency are seen at around 380 Hz, 750 Hz and 1400 Hz.

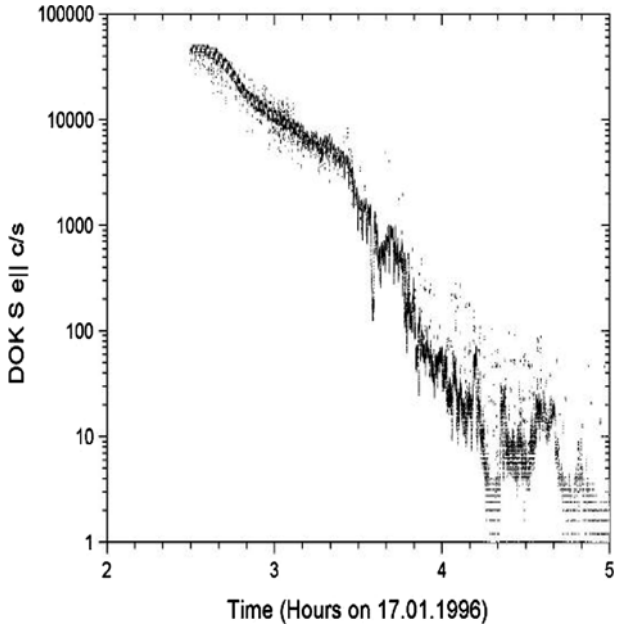


*Figure 10*. The total flux of the energetic electrons in the energy range 20–180 keV registered in the magnetosphere, at the magnetopause the drop of flux can be noted and again increase of flux in the polar cusp.

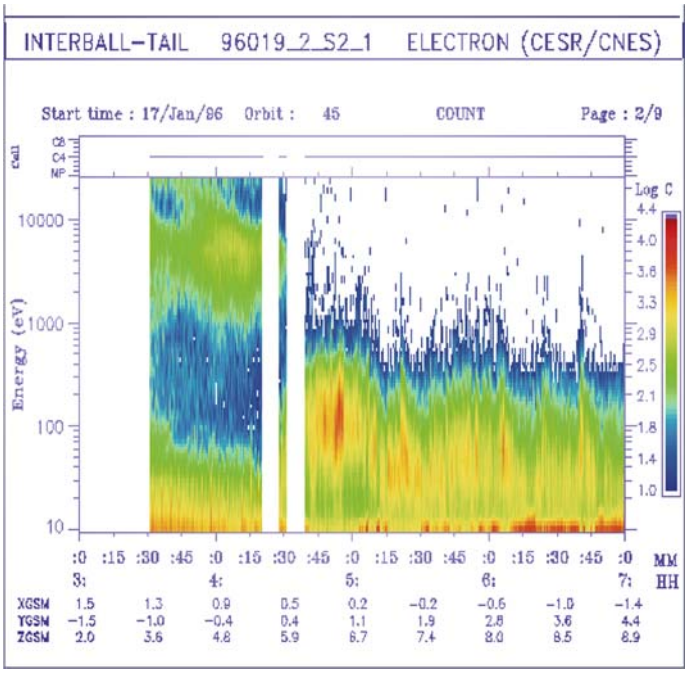


*Figure 11.* Time–energy spectrogram of the electrons registered by the ELECTRON instrument onboard Interball-tail probe on January 17, 1996. The entrance of the Interball l into the cusp is seen at 4:45 UT. The delay in relation to the observations of Magion 4 is 45 min – just the delay of the orbital movement.

## 5. Analysis of waveforms from Prognoz 8, Interball and Cluster

One of the most important problems with wave measurements made in dynamic regions of the magnetosphere is the nonstationarity of the processes occurring there. Wave spectra derived from satellite instruments usually use the Fourier analysis method. The wave spectra taken during the cusp crossing by the Cluster spacecraft on 25 September, 2001 (shown in Figure 12) indicate very strong variability from one spectrum to another. It also indicates the nonstationarity of the wave processes and strong variations in the sources of the waves within the polar cusp. The application of wavelet analysis allows us to avoid this problem. Moreover, this analysis gives a much higher spatio-temporal resolution; it can also help to find the nonlinear evolution of waves and the cascading of energy between different wave modes. The wavelet used in this analysis is based on the Morlet wavelet. An additional method used to study the wave form transmitted from the Cluster satellites is bispectral analysis, which is useful to study wave–wave interactions and find the wave modes interacting nonlinearly via three-wave

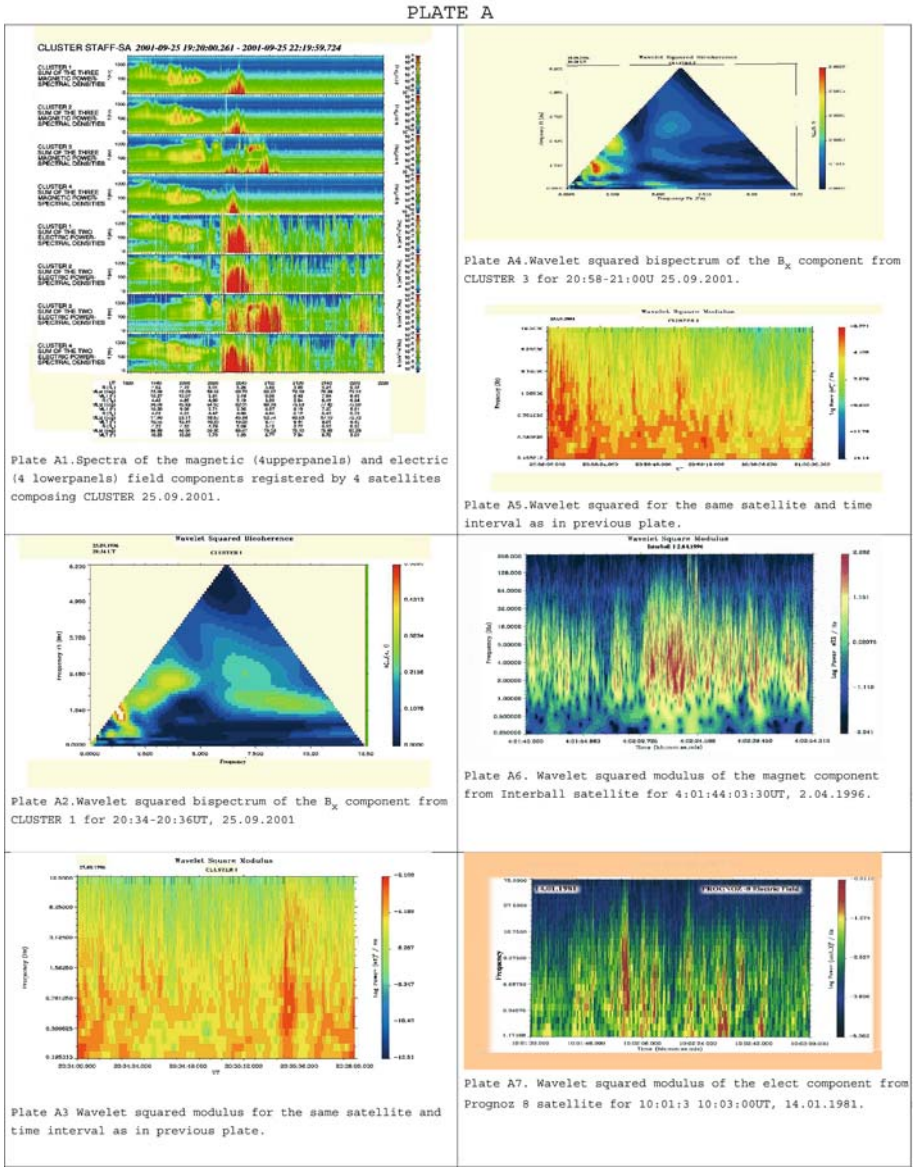


*Figure 12.* The wave activity in the polar cusp.

processes (Kim and Powers, 1978). The resonance conditions for these processes are:

$$\omega_1 + \omega_2 = \omega_3$$

$$k_1 + k_2 = k_3$$

Verification of these conditions is possible by computing the bispectrum for the three wave modes $k$, $l$ and $k+l$, defined as:

$$B(k,\ l) = E[X_k X_l X^*_{k+l}]$$

where $X$ are the spectral components of signals $k$, $l$ and $k+l$ respectively. Bispectral analysis uses the wavelet spectra. The asterisk denotes the conjugate value of the complex spectral component at $X$. The brackets denote an averaging over the analyzed time interval. A quantitive measure of the phase coherency may be made by computing the bicoherence spectrum which is defined, in terms of the bispectrum, as:

$$b^2(k,\ l) = \lim \frac{1}{T}\ \frac{|B(k,\ l)|^2}{P(k)P(l)P(k+l)}$$

where $P(k)$, $P(l)$ and $P(k+l)$ are auto power spectra. Both methods are implemented in the SWAN software developed by Lagoutte et al. (1999).

Figure 12 shows one of the most interesting cusp crossings made by the Cluster satellites on 25 September, 2001. Satellites 1, 2 and 4 entered the cusp at almost the same time (20:25 UT), satellite 3 about 20 min later. The electric wave component has a broader spectrum than the magnetic one. The electron cyclotron frequency is around 10 kHz, the lower hybrid frequency around 250 Hz and the proton cyclotron frequency around 6 Hz. The Whisper instrument (data not shown here) registered strong electron cyclotron waves during the entire cusp crossing. The analysis of the waveform of the magnetic component for two different time intervals with 2 min duration from Cluster 1 are shown in Figure 12A 3 and from Cluster 3 in Figure 12A 5. Figure 12A 2 illustrates a strong three-wave interaction at around the frequency 1.5 Hz and in the frequency range 2.5–5 Hz. Some bicoherence maxima are seen in these frequency ranges, both of which are below the ion cyclotron frequency and correspond to Alfven waves. In Figure 12A 3, wavelet spectra around 20:34 UT (corresponding to the bispectrum time interval) indicate cascading from around 0.5 Hz up to 1.5 Hz. Figure 12A 4 shows the bispectrum from Cluster 3 for the time interval 20:58–21:00 just 25 min later (the time delay from the relative position of the satellites). One can see a very similar characteristic interaction around 1.5 Hz. The wavelet spectra in Figure 12A 5 also contain information about the cascade around 0.5–1.5 Hz. The coincidence of the presence of strong nonlinear processes in the same region of space, at the edge of the cusp, suggests the existence of long-lived active structures. Figure 12A 6 shows the wavelet spectra of the magnetic wave component exactly at the cusp edge observed by Interball 1 on 2 April, 1996. The cut-off of the waves is seen at the lowest frequency, 0.5–1 Hz, which corresponds to the ion cyclotron frequency for protons and at the highest frequency, about 35 Hz, corresponding to the lower hybrid fre-

quency. The characteristic feature of the wavelet spectra is their subtle temporal structure, suggesting subtle structure in the source of these waves. Figure 12A 7 shows the wavelet spectra of the electric wave component taken by the Prognoz 8 satellite in the outer polar cusp on 14 January, 1981. This confirms the broadband character of the wave activity in the polar cusp and the subtle structure of these spectra.

## 6. Conclusions

The results presented in this paper on wave measurements in the polar cusp show that waves are a good indicator of the dynamic processes occurring there. The characteristic features of the wave spectra most frequently observed are broadband emissions, maxima at the lower hybrid frequency, the electron cyclotron frequency and sometimes its harmonics, and below the ion cyclotron frequency. In other cusp crossings such strong waves were not always present. It seems that the most intense waves in the cusp are associated with its edge and with the presence of high energy charged particles.

The waves observed in the cusp region together with the energetic particles can be discussed either in the context of plasma instabilities triggered by these particles or as a cause of the acceleration and energization of these particles. The subtle structure of the wave spectra reflects the fine structure of the cusp, and two possibilities can be discussed. One is a filamentation of the currents flowing there, and the other is a wavy structure of the cusp generated by nonlinear kinetic Alfven waves (Galperin et al., 1986; Yamauchi and Lundin, 1997; Bigham et al., 2001, more details are given in Blecki et al., 2004). Wave–particle interaction processes can be assumed as the mechanism for the energy cascade from low-frequency waves to high-frequency waves via heating and acceleration of the plasma particles in the polar cusp. The strong intensity of the waves is associated with nonlinear processes initiated by wave–wave and wave–particle interactions.

## Acknowledgements

This work has been supported by grants 8T12E 016 28 and RFFR 98-02-17402 and INTAS 03-50-4872.

## References

Bingham, R., Cairns,R. A., Dendy,R. O., Shapiro,V. D., Shukla,P. K., and Stenflo,L.: 2001, 'Auroral Particle Acceleration by Waves', *Phys. Chem. Earth* **26**, 133–144.

Blecki, J., Gadomski,S., Juchniewicz,J., Korepanov,V., Krawczyk,Z., Savin,S., Slominski,J., Vojta, J., and Wronowski,R.: 1997, 'SAS wave Experiment on Board Magion 4', *Ann. Geophys.* **15**, 528 .

Blecki, J., Rothkaehl,H., Kossacki,K., Wronowski,R., Klos,Z., Juchniewicz,J., Savin,S., Romanov, S., Klimov,S., Triska,P., Smilauer,J., Simunek,J., Kudela,K., and Forster,M.: 1998, 'ULF-ELF-VLF-HF Plasma Wave Observations in the Polar Cusp Onboard High and Low Altitude Satellites', *Phys. Scripta* **75**, 259–263.

Blecki, J., Kossacki,K., Wronowski,R., Nemecek,Z., Safrankowa,J., Savin,S., Sauvaud,J. A., Romanov, S., Juchniewicz,J., Klimov,S., Triska,P., Smilauer,J., and Simunek,J.: 1999, 'Low-Frequency Plasma Waves Observed In The Outer Polar Cusp', *Adv. Space. Res.* **23**, 1765 .

Blecki, J., Savin, S., Cornilleau-Wehrlin, N., Kossacki, K., Parrot, M., Rothkaehl, H., Stasiewicz, K., Wronowski, R., Santolik, O. and Sauvaud, J.-A.: 2003, 'Fine Structure Of The Polar Cusp As Deduced From The Plasma Wave And Plasma Measurements', *Adv. Space Res.*, in press.

Chen, J., Fritz,T. A., Sheldon,R. B., Spence,H. E., Spjeldvik,W. N., Fennell,J. F., Livi,S., Russell, C. T., Pickett,J. S., and Gurnett,D. A.: 1998, 'Cusp Energetic Particle Events: Implications for a Major Acceleration Region in Magnetosphere', *J. Geophys. Res.* **103**, 69–78.

Farrell, W. M., Gurnett,D. A., Manietti,J. D., Wong,H. K., Lin,C. S., and Burch,J. L.: 1990, 'Wave Intensifications near the Electron Cyclotron Frequency Within the Polar Cusp', *J. Geophys. Res.* **95**, 6493–6504.

Galperin, Yu, Zelenyi,L., and Kuznetsova,M.: 1986, 'Pinching of the Field-Aligned Currents as a Possible Mechanism of the Aurora Ray Structures Formation', *Cosm. Res.* **XXIV**, 865–874.

Haerendel, G.: 1978, 'Microscopic Plasma Processes Related to Reconnection', *J. Atmos. Terr. Phys.* **40**, 343–353.

Kim, Y. C., and Powers,E. J.: 1978, 'Digital Bispectral Analysis of Self-excited Fluctuaction Spectra', *Phys. Fluids* **21**, 1452–1453.

Klimov, S., Romanov,S., Amata,E., Blecki,J., Buchner,J., Juchniewicz,J., Rustenbach,J., Triska, P., Woolliscroft,L. J. C., Savin,S., Afanas'yev,Yu., de. Angelis, U., Auster,U., Bellucci, G., Best,A., Farnik,F., Formisano,V., Gough,P., Grard,R., Grushin,V., Haerendel, G., Ivchenko,V., Korepanov,V., Lehmann,H., Nikutowski,B., Nozdrachev,M., Orsini, S., Parrot,M., Petrukovich,A., Rauch,J. L., Sauer,K., Skalsky,A., Slominski,J., Trotignon, J. G., Vojta,J., and Wronowski,R.: 1997, 'ASPI Experiment: Measurements of Fields and Waves Onboard the INTERBALL-1 Spacecraft', *Ann. Geophys.* **15**, 514–527.

Lagoutte, D., Brochot, J. Y. and Latremoliere, P.:1999, 'SWAN Software for Waveform Analysis, Users Guide version 2.3', *LPCE/NI/003.D*.

Menietti, J. D., Santolik,O., Scudder,J. D., Pickett,J. S., and Gurnett,D. A.: 2002, 'Electrostatic Electron Cyclotron Waves Generated by Low-Energy Electron Beams', *J. Geophys. Res.* **107**, 8–1812.

Pickett, J. S., Gurnett,D. A., Menietti,J. D., LeDocq,M. J., Scudder,J. D., Frank,L. A., Sigwarth, J. B., Ackerson,K. L., Morgan,D. D., Franz,J. R., Kintner,P. M., Tsurutani,B. T., Ho,C. M., Chen,J., Fritz,T. A., Russell,C. T., Peterson,W. K., Kasahara,Y., Kimura, I., Watanabe,S., Arkos,G. G., Rostoker,G., Kokubun,S., Fukunishi,H., Pfaff,R. F., Mozer,F. S., Hsieh,S. -Y., Mukai,T., and Chandler,M. O.: 1999, 'Plasma Waves Observed during Cusp Energetic Particle Events', *Adv. Space Res.* **24**, 23 .

Pickett, J. S., Franz,J. R., Scudder,J. D., Menietti,J. D., Gurnett,D. A., Hospodarsky,G. B., Braunger, R. M., Kintner,P. M., and Kurth,W. S.: 2001, 'Plasma Waves Observed in the

Cusp Turbulent Layer: An Analysis of High Time Resolution Wave and Particle Measurements from the Polar Spacecraft', *J. Geophys. Res.* **106**, 19081 .

Pottelette, R., Malingre,M., Dulouloz,N., and Aparicio,B.: 1990, 'High-frequency Waves in the Cusp/Cleft Regions', *J. Geophys. Res.* **95**, 5957 .

Pisarenko, N. F., Kirpichev,I., Lutsenko,V., and Savin,S.: 2001, 'Cusp Energetic Particles, Observed by Interball Tail Probe in 1996', *Phys. Chem. Earth* **26**, 241–245.

Romanov, V., Savin, S., Klimov, S., Romanov, S., Yu. Yermolaev, Blecki J. and Wronowski R.: 1999, 'Magnetic Turbulence At The Magnetopause, Plasma Penetration', *J. Tech. Phys.* **XL**, No 1, Supplement, 329 .

Savin, S. P., Romanov,S. A., Fedorov,A. O., Zelenyi,L., and Klimov,S. I.: 1998a, 'The Cusp/Magnetosheath Interface on May 29, 1996: Interball-1 and Polar Observations', *J. Geophys. Res.* **25**, 2963–2966.

Savin, S. P., Borodkova,N. L., YuBudnik, E., Fedorov,A. O., Klimov,S. I., Nozdrachev,M. N., Morozova,E. I., Nikolaeva,N. S., Petrukovich,A. A., Pissarenko,N. F., Prokhorenko, V. I., Romanov,S. A., Skalsky,A. A., Yermolaev, I. Yu, Zastenker,G. N., Zelenyi, L. M., Triska,P., Amata,E., Blecki,J., Juchniewicz,J., Buechner,J., Ciobanu,M., Grard, R., Haerendel,G., Korepanov,V. E., Lundin,R., Sandahl,I., Eklund,U., Nemecek, Z., Safrankova,J., Sauvaud,J. A., Rustenbach,J., and Rauch,J. L..: 1998b. Interball Tail Probe Measurements in Outer Cusp and Boundary Layers, in J. L. Horwitz, D. L. Gallagher, and W. K. Peterson (eds.), *Geospace Mass and Energy Flow: From the International Solar-Terrestrial Physics Program*. Geophysical Monograph 104, *American Geophysical Union, Washington D.C., pp. 25–44*.

Savin, S., Budnik,E., Nozdrachev,M., Romanov,V., Yermolaev,Y., Zelenyi,L., Blecki,J., Buchner, J., and Nikutowski,B.: 1999, 'On the Plasma Turbulence and Transport at the Polar Cusp Outer Border', *Czech. J. Phys.* **49**, 679–693.

Savin, S., Maynard, N. C., Sandahl, I., Kawano, H., Russell, C. T., et al.: 2003, 'Interface between the Cusp and the Magnetosheath: IACG Campaign 2 First Results', submitted to *Ann. Geophys.* this volume.

Scudder, J. D., Puhl-Quinn,P. A., Mozer,F. S., Maynard,N. C., and Russell,C. T.: 1998, 'Signatures of Collisionless Reconnection within the Diffusion Region at the Magnetopause', *EOS, Trans. Am. Geophys. Union* **79**, F730 .

Smith, M. F., and Lockwood,M.: 1996, 'Earth's Magnetospheric Cusps', *Rev. Geophys.* **34**, 233 .

Treumann, R. A., Labelle,J., and Bauer,T. M..: 1995. Diffusion Processes: An Observational Perspective, in P. Song, B. U. O. Sonnerup, and M. F. Thomsen (eds.), *Physics of the Magnetopause*, American Geophysical Union, , pp. 331–341.

Woch, J., and Lundin,R.: 1992, 'Magnetosheath Plasma Precipitation in the Polar Cusp and its Control by the Interplanetary Magnetic Field', *J. Geophys. Res.* **97**, 1421–1430.

Yamauchi, M., and Lundin,R.: 1997, 'The Wave-Assisted Cups Model: Comparison to Low-Latitude Observations', *Phys. Chem. Earth* **22**, 729–734.

Surveys in Geophysics (2005) 26: 193–214
DOI 10.1007/s10712-005-1878-0 © Springer 2005

# MULTIPLE FLUX ROPE EVENTS AT THE HIGH-LATITUDE MAGNETOPAUSE: CLUSTER/RAPID OBSERVATION ON 26 JANUARY, 2001

Z. Y. PU[1], Q.-G. ZONG[2], T. A. FRITZ[2], C. J. XIAO[1], Z. Y. HUANG[1], S. Y. FU[1], Q. Q. SHI[1], M. W. DUNLOP[3], K.-H. GLASSMEIER[4], A. BALOGH[5], P. DALY[6], H. REME[7], J. DANDOURAS[7], J. B. CAO[8], Z. X. LIU[8], C. SHEN[8] and J. K. SHI[8]

[1]*School of Earth and Space Sciences, Peking University, Beijing, 100871, China*
*E-mail: zypu@pku.edu.cn;*
[2]*Center for Space Physics, Boston University, Boston, MA, 02215, USA;*
[3]*Space Sciences Division, Rutherford Appleton laboratory, Chilton, DIDCOT, Oxfordshire, OX11 0QX, UK;*
[4]*Institut für Geophysik und Meteorologie, TU Braunschweig, Mendelssohnstr. 3, Braunschweig, 38106, Germany;*
[5]*Space and Atmospheric Physics Group, The Blackett Laboratory, Imperial College, Prince Consort Road, London, SW7 2BZ, UK;*
[6]*Max-Planck-Institut für Aeronomie, Max-Planck-Str. 2, 37191, Katlenburg-Lindau, Germany;*
[7]*CESR, BP 4346, 31028, Toulouse Cedex 4, France;*
[8]*Center for Space Science and application Research, Chinese Academy of Science, Beijing, 100080, China*

(Received 30 December 2002; Accepted 30 April 2004)

**Abstract.** Cluster measurements of the cusp and high latitude magnetopause boundary on 26 January, 2001 confirm that the cusp is a dynamic region full of energetic charged particles and turbulence. An energetic ion layer at high-latitudes beyond and adjacent to the duskside magnetopause exists when the Interplanetary Magnetic Field (IMF) has a southward orientation. Multiple energetic ion flux bursts were observed in the energetic ion layer. Each energetic ion flux burst was closely related to a magnetic flux rope. The axes of the flux ropes lie in the direction pointing duskward/tailward and somewhat upward. An intense axis-aligned current flows inside the ropes, with the current density reaching ~$10^{-8}$ A/m$^2$. The main components of the energetic ions are protons, helium and CNO ions, which originate from the magnetosphere, flowing out into the magnetosheath along the axis of the flux ropes. The velocity of the magnetosheath thermal plasma relative to the deHoffman-Teller (DHT) frame is found to be basically along the axis of the flux ropes also, but towards the magnetosphere. These flux ropes seem to be produced somewhere away via magnetic reconnection and move at similar DHT velocities passing over the spacecraft. These observations further confirm that the high-latitude magnetopause boundary region plays an important role in the solar wind-magnetopause coupling.

**Keywords:** cusp, energetic particle flux, flux transfer events, high-latitude magnetopause boundary layer, magnetic flux rope, magnetic reconnection, magnetopause, magnetosheath boundary layer

**Abbreviations:** ACE – Advanced Composition Explorer; IMF – Interplanetary Magnetic Field

## 1. Introduction

The cusp region and high-latitude boundary layers are generally recognized as being key regions for the solar wind-magnetosphere interaction. The cusp is described as a funnel-shaped region where the field lines from the magnetopause boundary on the day and night sides converge towards low altitudes. Early studies suggested that the cusp was a narrow region centered near the local noon. However, from measurements at higher altitudes by Interball 1, Prognoz 7 and 8, Polar, Image and recently Cluster II, the cusp no longer is believed to be confined to be near local noon but appears to encompass a large portion of the dayside high-latitude magnetosphere. The cusp is generally identified by a decrease in the total magnetic field strength together with enhancements in plasma density and temperature. High altitude observations have further revealed that the cusp appears to be a region characterized by the presence of energetic charged particles and magnetic field turbulence as well (Fritz, 2001; Zong et al., 2002; Fritz et al., 2003). The power of turbulent waves is substantially higher there than that in the magnetosheath. The fluctuations are found to have a spiky character. Significant fluxes of energetic particles are continuously present, and energetic particle bursts are frequently registered (Chen et al., 1998; Zong et al., 2003). The sources of these particles and their role in the overall dynamics of the magnetosphere remain hot topics of scientific discussion. Nevertheless, they must be closely related to energization and transport processes occurring locally and nearby.

In the 'open' model of the magnetosphere, magnetic field lines merging on the dayside magnetopause are convected across the cusp into the mantle (Dungey, 1961). The opened field lines in the cusp map to the high-latitude ionosphere poleward of the last closed field line on the Earth's dayside. These field lines experience essentially stochastic behavior, but on average they provide topological connection between the cusp and magnetosheath and thus allow the shocked solar wind plasma to enter the magnetosphere. For southward Interplanetary Magnetic Field (IMF), reconnection tends to occur equatorward of the cusp at the subsolar region, or at higher latitudes and away from noon, depending on the IMF clock angle. For northward IMF, reconnection is expected to take place tail-ward of the cusp. Some cusp field lines can participate in anti-parallel merging for any orientation of the IMF (Crooker, 1979; Luhmann et al., 1984). With a predominant $Y$-component of the IMF reconnection occurs near and even in the cusp region. By examining an event of bursty enhanced energetic electron flux observed by Cluster II in the Cusp, Zong et al. (2003) propose that flux ropes are probably formed in the dawn (dusk) side of the northern cusp during northward IMF with a significant positive (negative) $B_y$ component. We shall refer to this as cusp

reconnection. Reconnection in the cusp region will certainly attract more and more attention in the near future.

The existence of boundary layers inside and adjacent to the magnetopause is pronounced evidence for the entry of magnetosheath plasma into the magnetosphere. Two high-latitude magnetopause boundary layers next to the exterior cusp have been identified (Sibeck et al., 1999): The entry layer (Paschmann et al., 1976), which is a region of direct, turbulent entry of magnetosheath plasma onto field lines that map to the low-altitude cusp, and the plasma mantle (Rosenbauer et al., 1975), which is located on field lines where injected magnetosheath plasma continues tailward. While the magnetopause is commonly regarded as a source region for magnetospheric plasmas, observations show that it is a loss region as well (Sibeck et al., 1999). Energetic magnetospheric particles are a common feature outside the magnetopause (West and Buck, 1976; Meng et al., 1981). The layer of magnetospheric particles outside the magnetopause is often referred to as the magnetosheath boundary layer (MSBL) (Sibeck et al., 1999). The electron layers are observed most often on the dawnside of the plasma sheet and protons on the duskside (Meng et al., 1981). Recently, Zong et al. (2002) reported that an energetic ion layer was observed by Cluster 4 spacecraft in the high-latitude magnetosheath adjacent to the afternoon magnetopause. These ions are found to be highly anisotropic and to exhibit a clear anti-sunward flow. Among all processes, which have been proposed to account for the transfer of solar wind mass into the magnetosphere and the escape of magnetospheric particles into the magnetosheath, magnetic reconnection is widely believed to be the primary mechanism. Many transient reconnection events have been observed at the dayside high-latitude magnetopause. However, it is not quite clear yet where, why and how they are initiated. Improving our knowledge of detailed reconnection signatures, the associated structures and the global consequences near high-latitude magnetopause remains one of the major tasks of magnetospheric research.

The Cluster mission is designed to study the small-scale structures and multi-scale dynamics in key regions of the magnetosphere. The scientific objectives are achieved by having the four identical spacecraft in a polar orbit of $4 \times 19.6$ Earth radii. The spacecraft trajectory crosses the cusp and dayside high-latitude magnetopause when the cluster apogee is in the solar wind. The traversals on these occasions provide unique opportunities to study the dynamical structures and processes in the cusp and high-latitude magnetopause (Balogh et al., 2001; Dunlop et al., 2001). Both magnetospheric and magnetosheath flux transfer events (FTEs) in the magnetopause boundary regions adjacent to the cusp have been measured and investigated (Wild et al., 2001). The form of the field perturbations observed in these events is found to be consistent with the formation of open flux tubes through time-dependent reconnection at the magnetopause. On January 26, 2001 from

10:30 to about 11:23 UT, after passing over the high-altitude cusp region, the Cluster constellation was traversing the high-latitude boundary regions. In the first part of this time interval, four spacecraft saw several times of Alfvenic accelerated flows and D-shaped ion distributions which were convincing signatures of magnetic reconnection initiated equatorward of the Cluster satellites (Bosqued et al., 2001). Between 11:10 and 11:23 UT, Cluster was staying in the MSBL outside, but adjacent to, the magnetopause. Four spacecraft observed an event of multiple bursty enhancements of energetic ion flux. Later, around 11:30–11:33 in the magnetosheath, the constellation encountered pronounced FTEs. The 26 January events have attracted much attention in the Cluster community, the magnetic reconnection signatures before 11:10 UT being extensively investigated by Bosqued et al. (2001). The present work is devoted to the multiple bursty enhancements of energetic ion fluxes, together with the magnetosheath FTEs.

Our paper is organized as follows. In Section 2 we briefly give useful information on RAPID imaging energetic particle spectrometer aboard Cluster by which the bursty enhancements of energetic ions were detected. In Section 3 we describe observations of energetic particles, magnetic field and thermal ions of the events. A principal axis analysis of the magnetic field data and deHoffmann-Teller (DHT) analysis are performed in Section 4. It will be shown that each enhancement of energetic ion flux is closely related to the appearance of a flux rope. In Section 5 a rigorous curlometer calculation is presented based on multi-point magnetic field measurements to evaluate the current density within the spacecraft tetrahedron. It will be seen that each flux rope corresponds to a current tube in which the magnitude of the axis-aligned current can be as high as $\sim 10^{-8}$ A/m$^2$. A brief summary is given in Section 6.

## 2. Instrumentation

The particle spectrometer RAPID on board Cluster measures the vector velocity and energy of energetic ions and electrons. It comprises two independent instruments – the IIMS for detecting ions and IES for electrons. The IIMS consists of 3 sensor heads, which can sort the incoming ions into 12 polar angle segments and 16 azimuthal sectors. With a time-of flight telescope it can identifies ion species in 3 mass ranges: 30–1500 keV for protons, 100–1500 keV for helium ions and 105–1500 keV for CNO ions. The IES is also arranged into 3 units and can sort the electron fluxes with an energy range of 20–400 keV into 9 polar segments and 16 azimuthal sectors. For more information about this advanced particle detector, readers are referred to Wilken et al. (2001) and the RAPID instrument paper (Wilken et al., 1997).

Accurate magnetic field measurements are provided by the Cluster Flux Gate Magnetometer (FGM) on board four spacecraft. Plasma measurements

are performed by the Cluster Ion Spectrometry (CIS) experiment. The experiment consists of two different instrument – a Composition and Distribution Function Analyzer (CIS1/CODIF) and a Hot Ion Analyzer (CIS2/HIA). The energy ranges of HIA and CODIF have ~5–32 keV/e and ~0–38 keV/e, respectively. For more information about these instruments, please see the relevant articles (Balogh et al., 2001; Reme et al., 2001).

## 3. Observations

In this section we present a set of data measured by RAPID, FGM and CIS for the event studied. Since the four spacecraft measurements generally have no distinguishable differences, data from only one spacecraft (CS3) are used except the cases specially mentioned.

On 26 January, 2001, the four Cluster spacecraft were traveling outbound in northern high-latitudes from the magnetosphere to the magnetosheath. Figure la shows the location of Cluster in the magnetopause boundary normal coordinate system (Russell and Elphic, 1978) at the time of interest (~11:10 UT). In the Geocentric Solar Magnetospheric (GSM) coordinate system, CS3 is at $X = 5.4R_E$, $Y = 7.6R_E$ and $Z = 9.7R_E$ (or at $X = 5.4\ R_E$, $Y = 8.0R_E$ and $Z = 9.3R_E$ in Geocentric Solar Ecliptic (GSE) coordinate system). The separation distance between the different spacecraft of the constellation is less than 700 km. Figure 1b is a dawn-dusk cut (looking from

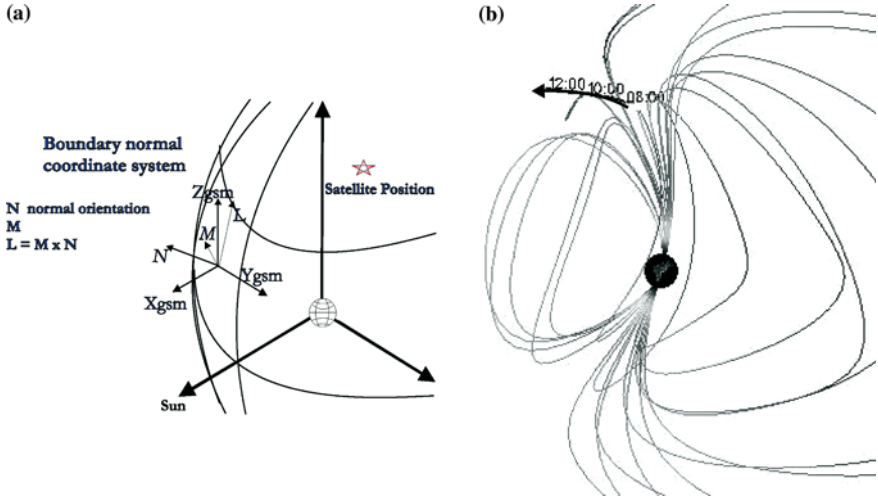


*Figure 1.* (a) Cluster location in GSM coordinate system at 11:10 UT on 26 January, 2001. (b) Cluster orbit from 08:00–12:00 UT, looking from 15:00 PM Local Time on this day, and model magnetic field lines.

15:00 Local Time) of the Cluster trajectory from 06 to 18 UT projected onto the Tsyganenko magnetic field model (Tsyganenko and Stern, 1996). It is seen that spacecraft was moving out of the plasma mantle, crossing the cusp and high-latitude magnetopause boundary regions, and entering the magnetosheath. Advanced Composition Explorer (ACE) measurements (not shown here) indicate that during the time interval of interest, IMF $B_z < 0$, $B_y$ is the dominant component and directed eastward ($< 0$); the solar wind speed is around 350 km/s.

Figure 2 gives an overview of RAPID, CIS and FGM measurements on this day from 8:00 to 12:00 UT. The six panels from the top to the bottom show, respectively, the energy-integrated flux of energetic protons and electrons, the number density of thermal ions, the thermal plasma velocity component $v_x$ and $v_y$, the total magnetic field $B_t$, and the magnetic field components $B_x$, $B_y$ and $B_z$ versus time. The GSE coordinate system is used. Four vertical lines mark the sharp boundaries between five different regions.

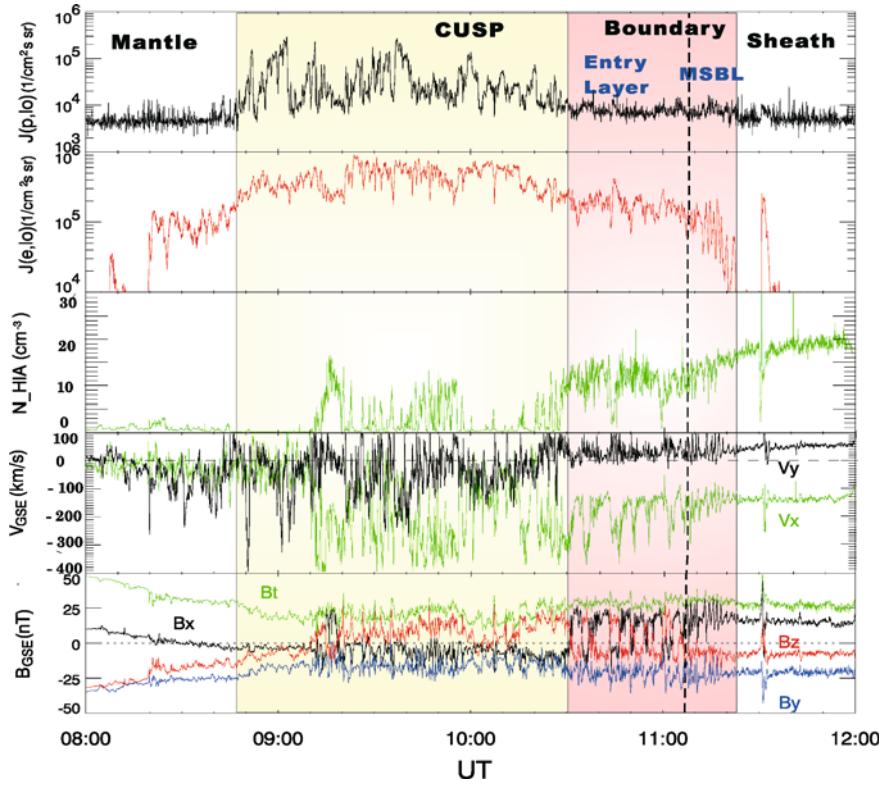


*Figure 2.* An overview of energetic proton and electron fluxes, thermal ion plasma number density and velocity, and magnetic field from the Cluster/spacecraft 3 (CS3) during 08:00–12:00 UT on 26 January, 2001.

It is seen that the cusp region is characterized by enhanced energetic particle fluxes and a depressed, but highly turbulent, magnetic field. In the magnetopause boundary regions the energetic ion flux remains high, whereas the electron flux reduces. The magnetopause separating the entry layer and the MSBL is shown by the dashed line where the $B_z$ component changes its sign. In the energetic ion layer beyond and adjacent to the magnetopause the ion flux decreases with increasing distance from the Earth. However, several noticeable spikes are seen before the spacecraft left the layer.

Later in the magnetosheath, sudden enhanced energetic ion fluxes are recorded, together with notable variations of the plasma velocity and magnetic field.

Figure 3 plots the integral fluxes of energetic ions versus time. The length of the abscissa is chosen to be from 11:06 to 11:36 UT, covering mainly the period when Cluster was moving in the energetic ion layer and in the magnetosheath adjacent to the magnetopause. The first, second and third panels show, respectively, protons ($J_p$) and electrons ($J_e$), helium ions, and CNO ions which mainly consist of oxygen ions. As has been mentioned before, while the energetic electron flux remains at a very low (background) level, eight ion bursts were found during the period from 11:10 to 11:23 UT when Cluster was crossing the energetic ion layer, the average separate time being 72 s. The sharp increases in fluxes of the three ion components occur almost simultaneously. The final huge enhancements were seen between 11:30:30 and 11:32:30 UT when the four spacecraft had entered into the magnetosheath. It is of interest to note that for the flux ratios of $J(\mathrm{CNO})/J(\mathrm{p}) \approx 10\%$ and $J(\mathrm{He})/J(\mathrm{p}) \approx 20\%$. These typical values imply that these energetic ion species have a magnetospheric origin (Zong and Wilken, 1998).

Figure 4 presents the number density, velocity, and temperature (parallel and perpendicular to the magnetic field) of the thermal plasma compared with the energetic proton flux. It is seen that, in the most energetic ion burst events, the thermal ions of solar wind origin have reduced fluxes, but somewhat raised temperature. In previous studies (such as Bosqued et al., 2001) the final burst seen in the magnetosheath was regarded as one FTE. However, by a careful inspection of each panel in Figure 4, we can see that it actually consists of two overlapping events. We will come to this point later in the paper.

Figure 5 illustrates the magnetic field variations compared with that of the energetic proton flux. The three components of the magnetic field $B_{L^*}$, $B_{M^*}$ and $B_{N^*}$ in the boundary normal coordinate system are shown in the panel. The relevant minimum variance analysis (Son-nerup and Scheible, 1998) is performed based on FGM data from 10:10 to 11:40 UT. The boundary normal coordinates ($L^*$, $M^*$, $N^*$) obtained are $L^* = (-0.76, 0.09, 0.64)$, $M^* = (0.15, -0.94, 0.31)$, and $N^* = (0.63, 0.33, 0.70)$, which are similar to those found by Bosqued et al. (2001). They can be considered to

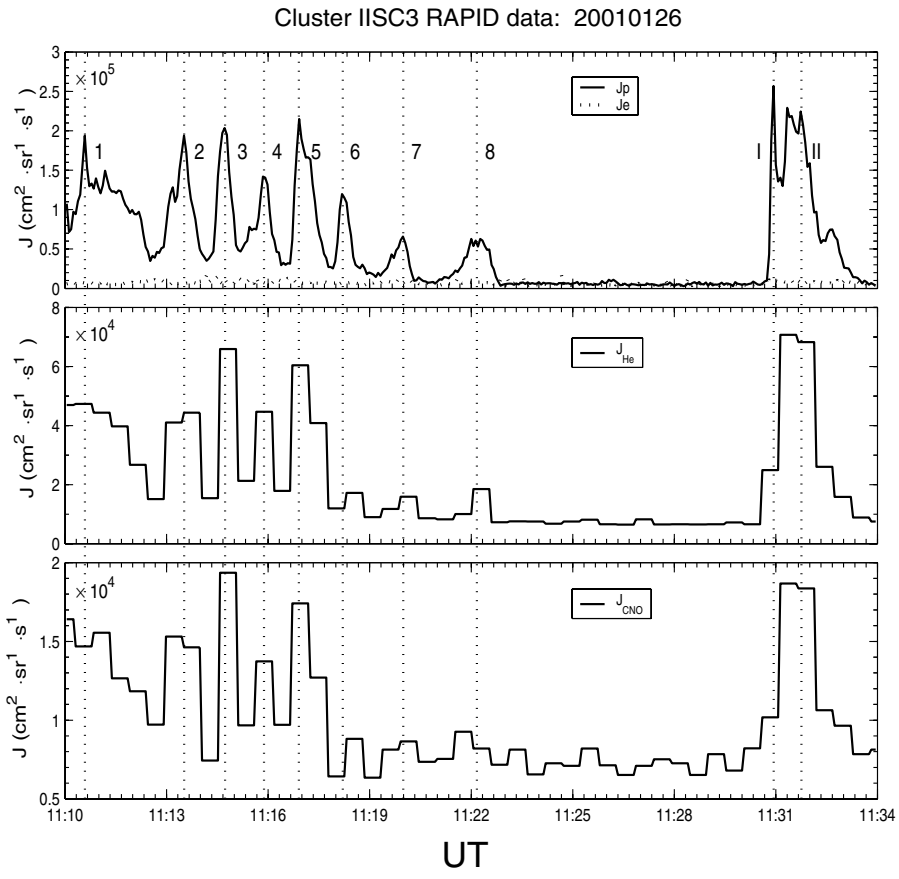


*Figure 3*. The integral fluxes of energetic protons, electrons, helium ions, and CNO ions observed by RAPID onboard CS3 for 30 min on 26 January, 2001.

be representative for the average geometry of the magnetopause boundary during this period of time. We find that each enhancement of energetic ion flux appears to be in close association with a magnetic field structure, which has a bi-polar variation in the $B_{N^*}$-component, the typical signature of a flux rope-like event. Moreover, it can be seen that the peak of each energetic ion burst almost precisely corresponds to the center of the bi-polar $B_{N^*}$. This indicates that the burst of energetic ions occurs in the center of a flux tube. We shall show later in the paper that for each flux rope-like event there exists a DHT frame (Khrabrov and Sonnerup, 1998) in which the convection electric field nearly vanishes.

The color plot of Figure 6 shows the direction of motion of the energetic ion bulk flow in the spacecraft coordinate system. $\theta$ and $\phi$ denote the polar angle and azimuthal angle, respectively. Sunward, duskward, tailward. and

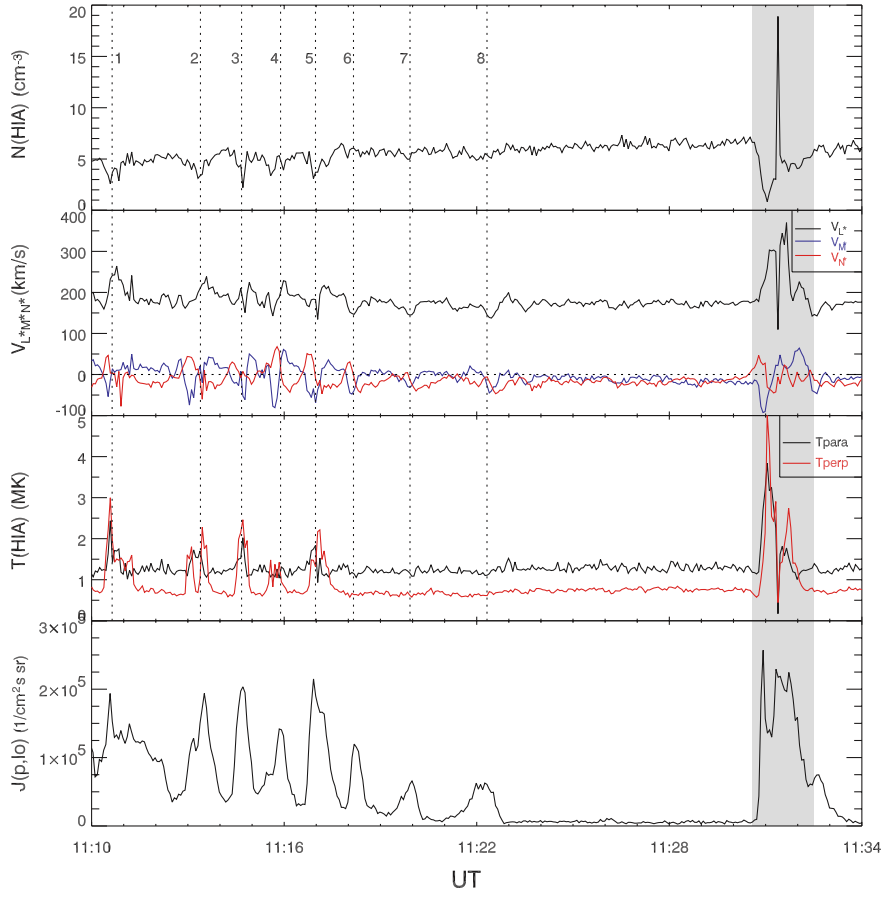


*Figure 4*. The number density, velocity and temperature of the thermal plasma by CIS/CS3, compared with the energetic proton flux by RAPID/CS3.

dawnward directions are indicated in the figure. It is seen from Figure 6 that, during the first eight events, energetic ions were moving basically duskward and tailward. For the later FTEs, the ion flow was essentially duskward. Furthermore, in first eight events the overall direction with respect to the polar angle was upward, while in the later FTEs it was nearly parallel to the ecliptic plane.

## 4. Principal axis analysis

We have shown in the previous Section that each enhancement of energetic ion flux is associated with a flux rope-like structure and that the burst of energetic ions appears to occur in the center of the flux rope. In this Section

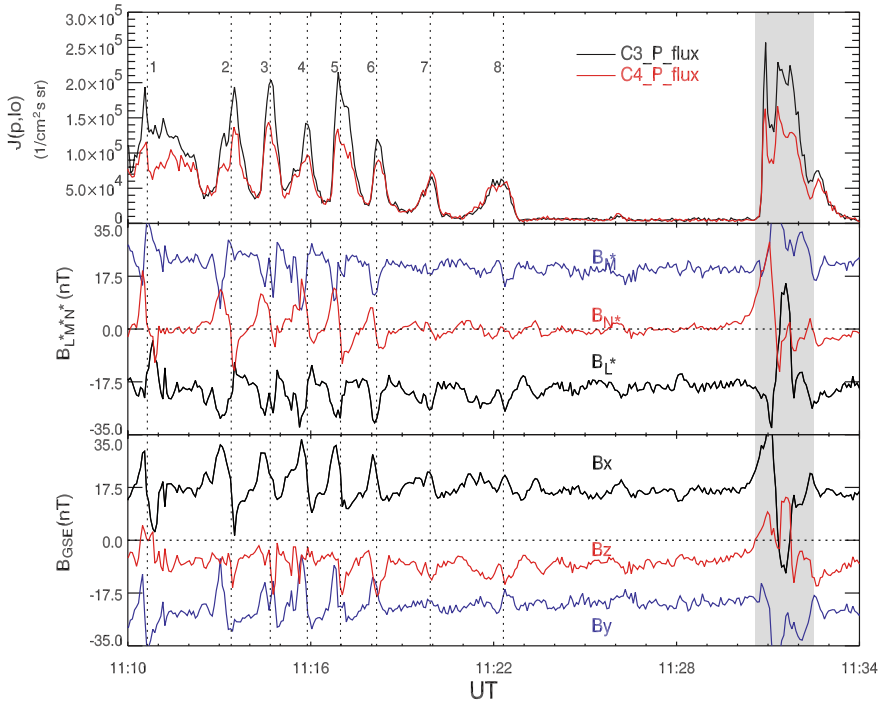


*Figure 5*. The magnetic field observed by FGM/CS3 compared with the energetic proton flux (top panel) measured by CS3 (thin) and CS4 (thick).

we perform the principal axis analysis (PAA) for each event to determine the orientation of the flux rope by using the minimum variance analysis (MVA) technique (Sonnerup and Cahill, 1968; Sonnerup and Scheible, 1998). The DHT Analysis (Khrabrov and Sonnerup, 1998) is also performed along with the PAA to show that all flux rope-like structures have a definable DHT frame so that they are quasi-stationary structures.

The original purpose of the MVA was to find from the spacecraft data the direction normal to a transition layer in the space plasma. The MVA can provide a natural coordinate system in which to display and analyze the data. We apply this technique as a PAA means to determine the axis direction of the flux ropes. Hereafter we refer to this procedure as 'magnetic field PAA.' The MVA presents the directions of maximum, intermediate and minimum variance of the magnetic field, which are denoted by $L$, $M$, and $N$, respectively. For details of the technique, readers are referred to the original papers by Sonnerup and Cahill (1968) and Sonnerup and Scheible (1998).

There have been two magnetic field PAA models for determination of the flux rope orientation: these are the Farrugia-Elphic-Southwood (FES) model (Elphic and Southwood, 1987; Farrugia et al., 1987) and the Russell and

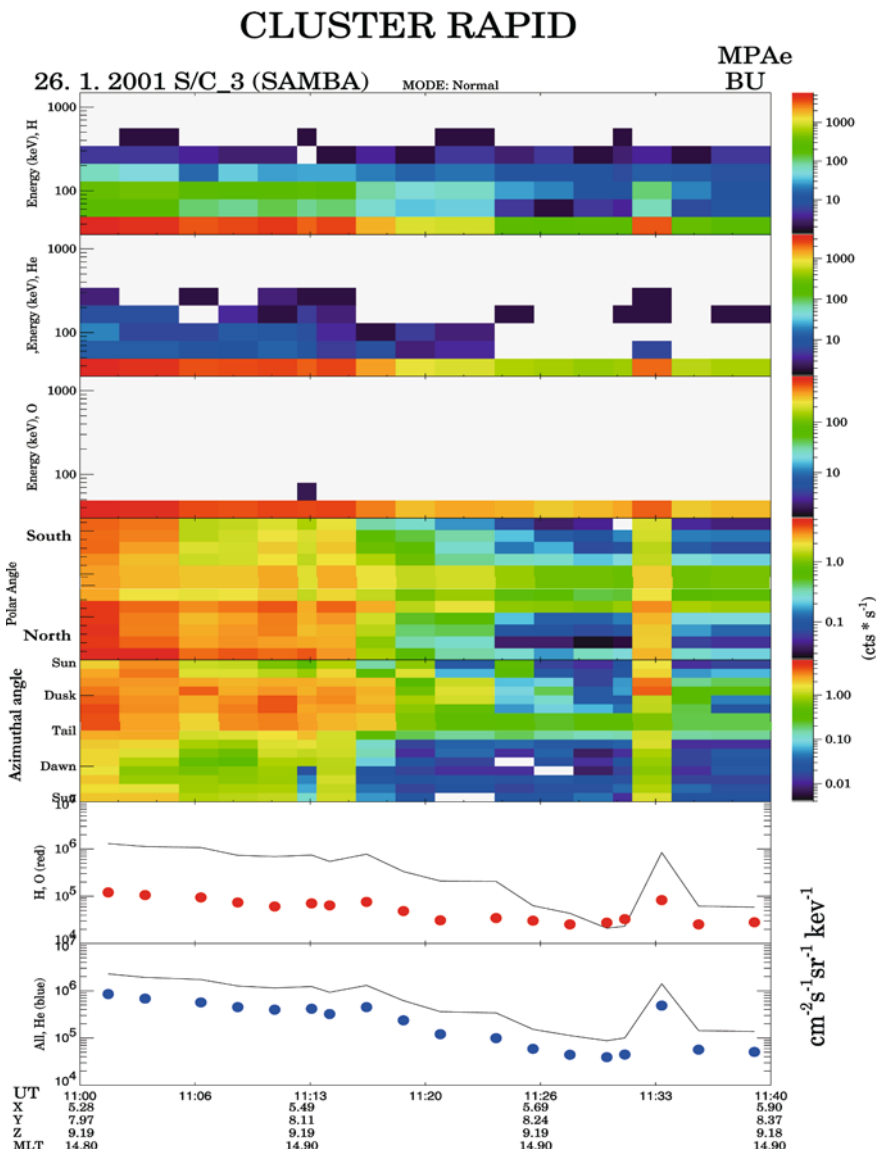


*Figure 6*. The spectrogram and direction of motion of energetic ions observed by RAPID/CS3. The panels show, from the top to the bottom: Energy spectrograms of protons, helium ions, heavy ions ($m > 4$), the polar distribution of total flux in the spacecraft coordinate system, the azimuthal distribution of total flux, the flux of protons (black line) and heavy ions (red dots), the flux of total ions (black line) and helium ions (blue dots).

Elphic (RE) model (Russell and Elphic, 1979). The FES model applies to the events of 'grazing pass' in which the spacecraft does not directly pass through the magnetic flux rope. The magnetic field and velocity variations in these cases are roughly consistent with disturbances around an impenetrable

obstacle, and the flux rope axis direction manifests the minimum variation direction (Elphic and Southwood, 1987; Papamastorakis et al., 1989). On the other hand, the RE model deals with the so-called 'crater' events in which the spacecraft trajectory does pass through the flux rope. By assuming that the flux rope is in a force-free equilibrium situation, Russell and Elphic (1979) showed that the intermediate variation direction basically represents the orientation of the flux rope and that the magnetic field component in the minimum variation direction is almost zero.

Table I presents the magnetic field PAA results for events studied in which $\lambda_i$ denotes the eigenvalue, $i = 1,2$ and 3 refer to the maximum, intermediate and minimum, respectively. The values of the ratios $\lambda_2/\lambda_3$ and $\lambda_1/\lambda_3$ of all events indicate the reasonable application of MVA (Sonnerup and Scheible, 1998). Later in this Section we show that there exists a definable $V_{\mathrm{DHT}}$ for each event (see Table II) so that all magnetic structures related to the energetic ion bursts are probably flux ropes (Khrabrov and Sonnerup, 1998).

The magnetic field PAA shows that seven of the first eight quasi-periodic events in the energetic ion layer appear to be 'grazing' ones for which the minimum variance direction is nearly parallel to the axis of the flux ropes. For these events three components of the unit vector **N** are given in Table I. Meanwhile, the event at ~11:31 UT seen in the magnetosheath manifests a typical FTE. The flux tube axis of this FTE lies in the intermediate variation direction, for which the unit vector **M** is also listed in the table. The orientation of the first (~11:10 UT) and the last (~11:32 UT) events may not be simply determined by the magnetic field PAA (see the reasons below). Nevertheless, the unit vector **N** of the first event and **M** of the last event are still put in the Table, but with a question mark, respectively.

TABLE I
Principal Axis Analysis for 10 events

| Events | *Time* (UT) | $\phi$ | $\theta$ | *Axis orientation* (*GSE*) | $\lambda_2/\lambda_3$ |
|---|---|---|---|---|---|
| 1 | ~11:10 | 134° | 42° | −0.47, 0.48, 0.74 (*N*?) | 1.9 |
| 2 | ~11:13 | 139° | 20° | −0.26, 0.25, 0.95 (*N*) | 2.5 |
| 3 | ~11:14 | 126° | 65° | −0.53, 0.73, 0.43 (*N*) | 39.0 |
| 4 | ~11:15 | 157° | 83° | −0.91, 0.38, 0.11 (*N*) | 13.4 |
| 5 | ~11:17 | 132° | 70° | −0.60, 0.67, 0.43 (*N*) | 6.7 |
| 6 | ~11:18 | 125° | 88° | −0.58, 0.81, 0.03 (*N*) | 50.7 |
| 7 | ~11:19 | 119° | 68° | −0.45, 0.81, 0.37 (*N*) | 4.7 |
| 8 | ~11:22 | 120° | 58° | −0.40, 0.69, 0.61 (*N*) | 8.3 |
| *I* | ~11:31 | 123° | 92° | −0.55, 0.84, −0.03 (*N*) | 19.2 |
| *II* | ~11:32 | 94° | 78° | −0.07, 0.98, 0.21 (*M*?) | 1.1 |

TABLE II
DeHoffmann-Teller Analysis for 10 events

| Events | *Time* (UT) | $\phi$ | $\theta$ | $V_{DHT\ (x)}$ | $V_{DHT(y)}$ | $V_{DHT(z)}$ |
|---|---|---|---|---|---|---|
| 1 | ~11:10 | 150° | 57° | −211.6 | 122.3 | 141.2 |
| 2 | ~11:13 | 149° | 58° | −224.3 | 133.3 | 151.2 |
| 3 | ~11:14 | 151° | 56° | −206.7 | 115.2 | 136.5 |
| 4 | ~11:15 | 148° | 60° | −230.3 | 145.9 | 156.8 |
| 5 | ~11:17 | 147° | 59° | −221.4 | 143.8 | 152.4 |
| 6 | ~11:18 | 149° | 57° | −210.6 | 127.5 | 141.5 |
| 7 | ~11:19 | 145° | 61° | −239.6 | 166.7 | 138.0 |
| 8 | ~11:22 | 145° | 61° | −235.7 | 163.7 | 136.2 |
| *I* | ~11:31 | 150° | 58° | −220.7 | 127.2 | 139.8 |
| *II* | ~11:32 | 155° | 54° | −201.8 | 95.7 | 160.5 |

Hodogram pairs of ($B_L$, $B_M$) and ($B_L$, $B_N$) for events at ~11:16 and ~11:31 are shown in Figures 7a and b, as representatives of the 'grazing' and the 'crater' flux ropes, respectively. Figure 7c draws the hodograms for the second overlapping (i.e. the last) event at ~11:32. It is seen that $B_M$ and $B_N$ are well comparable. Besides, the ratio of $\lambda_2/\lambda_3$ is only about 1.1, too small to distinguish the intermediate and minimum variations. Therefore MVA, and hence the two conventional models of magnetic field PAA, do not work for this event. A similar thing happens for the event at ~11:10. We try to determine the orientation of the flux rope in these events by developing a supplementary approach in the next Section.

It is worthwhile to note from Table I that, in all the events observed, the directions of the flux ropes have a negative $X$-component and a positive $Y$-component. As to the $Z$-component, it is either positive or almost zero. We can then draw an important conclusion by comparing Table I with Figure 6 that in all energetic ion burst events the bulk flow of the ions is essentially along the axis of the associated flux rope. It is likely that these ions originate from the magnetosphere (entry layer/low-altitude cusp) and escape into the magnetosheath across the high-latitude duskside magnetopause boundary.

We have also made the DHT analysis for all the events studied. The results are listed in Table II. It is clearly seen in Table II that the vectors $\mathbf{V_{HT}}$ of all events are not too different in magnitude, while their directions are quite similar. This implies that all flux ropes may come from the same direction. Moreover, in all events the velocity of magnetosheath thermal plasma relative the DHT frame is found to be basically along the axis of the flux ropes, but opposite to the main direction of the energetic ions (not shown in the Table). These flux ropes are probably produced via magnetic reconnection somewhere away from the spacecraft location. The eight flux ropes

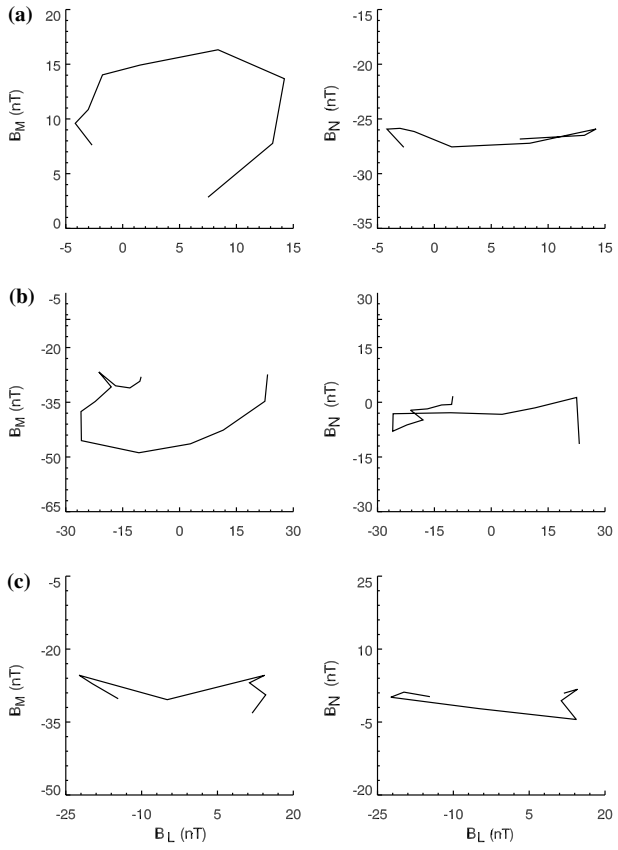


*Figure 7.* Hodogram pairs of ($B_L$, $B_M$) and ($B_L$, $B_N$) for events at: (a)~11:16, (b) ~11:31, and (c) ~11:32 UT on 26 January 2001 observed by CS3.

observed in the energetic ion layer do not necessarily have the same origin as that of the two FTEs seen in the magnetosheath. The formation mechanism of these flux ropes is left for another paper. Anti-parallel reconnection (Crooker, 1979; Luhmann et al., 1984), high-latitude unifying reconnection (Boudouridis et al., 2002) and cusp reconnection such as that by Zong et al. (2003) may shed light on this subject.

## 5. Current density determination

One of principal objectives of the four-spacecraft Cluster mission is the direct measurement of the spatial gradients of the magnetic field in the key boundary regions of the magnetosphere. In the linear approximation we can use the simultaneous measurements at the vertices of the tetrahedron to

estimate the current density within the tetrahedron. Methods which have been proposed for doing such an analysis include the 'curlometer' technique (Dunlop et al., 1988; Robert et al., 1998), the linear interpolation approach (Khurana et al., 1996), and the finite difference method on barycentric coordinates (Chanter, 1998). We have independently developed the linear interpolation approach like that of Khurana et al. (1996), and analytically and numerically demonstrated that, within the linear approximation, all the aforementioned methods lead to the exactly the same results.

We have applied the linear interpolation approach to calculate the current density **J** for all events studied. Figure 8 presents an overall view for the time period of interest compared with the energetic proton flux (bottom panel). The top panel shows the $x$, $y$, and $z$ components of **J** in the GSE coordinate system. The middle panel plots the ratios $\nabla \cdot \mathbf{B}/|\nabla \times \mathbf{B}|$ which has been regarded as the estimation of the relative error $\delta J/J$ (Robert et al., 1998). It is seen that in a number of circumstances the relative error is close to $\pm 1$. However, by careful inspection we can see that these happen mostly in the interval between two succeeding events, and that $\nabla \cdot \mathbf{B}/|\nabla \times \mathbf{B}|$ is within $\pm 0.4$ in the center of the events. Figures 9a and b show, respectively, three components of **J** in the GSE system and the relative error for the event at ~11:17 UT. It is shown that, in the center of the flux rope, the relative error is small enough, while it increases largely close to the boundary of the flux rope. In addition, the maximum **J** reaches $\sim 4 \times 10^{-8}$ A/m$^2$. Almost all events possess similar features.

Furthermore, the magnetic field PAA of this event indicates that the axis of the flux rope lies in the $N$-direction. We have projected **J** onto the $L$, $M$ and $N$ directions to obtain the components $J_L$, $J_M$ and $J_N$ and plotted them in Figure 9c. It is clear that **J** flows mainly along the axis of the flux tube. We have made a further PAA for the calculated data of **J** (hereafter we call this analysis the 'current PAA') and projected **J** onto the three eigen-directions obtained (denoted by $l$, $m$ and $n$, respectively). Figure 9d plots the corresponding three components of the current density $J_l$, $J_m$ and $J_n$. It is of special interest to see that the direction of the maximum current component is precisely coincident with the maximum variation direction. In other words, the current is preferentially flowing along the axis of the flux tube. In this sense, a flux rope is regarded as a current tube.

Figures 10a and b show the $x$, $y$, and $z$ components of **J** in GSE during the time period of 11:30–11:33. We see $J_y$ ($>0$) is the dominant component for the two events at ~11:31 and ~11:32 UT. Within the time interval between these two events, the magnitude of $\nabla \cdot \mathbf{B}/|\nabla \times \mathbf{B}|$ reaches ~1. Therefore the calculated negative $J_y$ value has a great uncertainty. The spatial scale length of the magnetic field variation is considerably smaller in this region, hence it should be regarded as the border between two flux ropes, but not a part of a larger flux tube as the previous study suggested (Bosqued et al., 2001). We

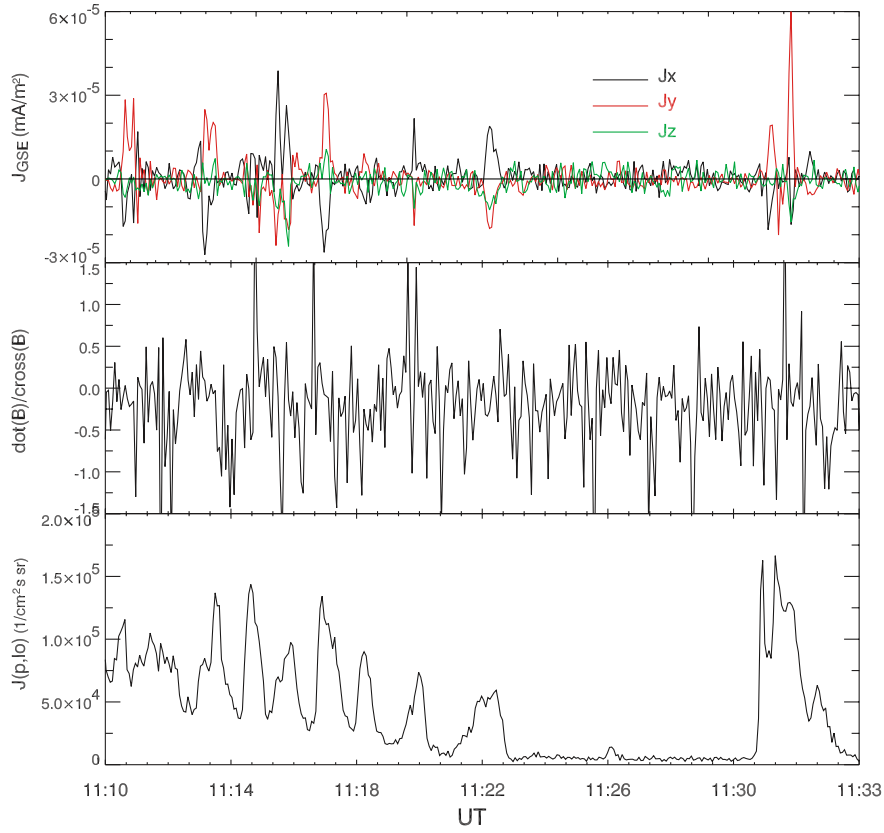


*Figure 8*. Overview of the electric current compared with the energetic proton flux (the bottom panel). The first and second panels show, respectively, the three components of current density in GSE and the ratio of $\nabla \cdot \mathbf{B}/|\nabla \times \mathbf{B}|$, which is essentially identical to the relative error of the current evaluation $\delta J/J$.

have applied both the magnetic field PAA and current PAA for these two events, and the results are illustrated in Figures 10c–f. At ~11:31 UT, the current is flowing mostly along the axis of the flux rope and the flux rope is identical to a current tube. For the second FTE at ~11:32 UT, we failed to determine the orientation of its flux rope by using the magnetic field PAA explained in the last Section. Nevertheless, Figures 10e and f show that JM is the dominant component of the electric current. Therefore, it is expected that the axis of the flux rope and current tube should be along the *M*-direction, which, according to Table I, is basically parallel to the + *Y*-axis in GSE. We have also carried out the same procedures for the event at ~11:10 UT and found that the axes of its flux rope and current tube both lie in the *N*-direction. Since the conventional magnetic field PAA is not applicable to

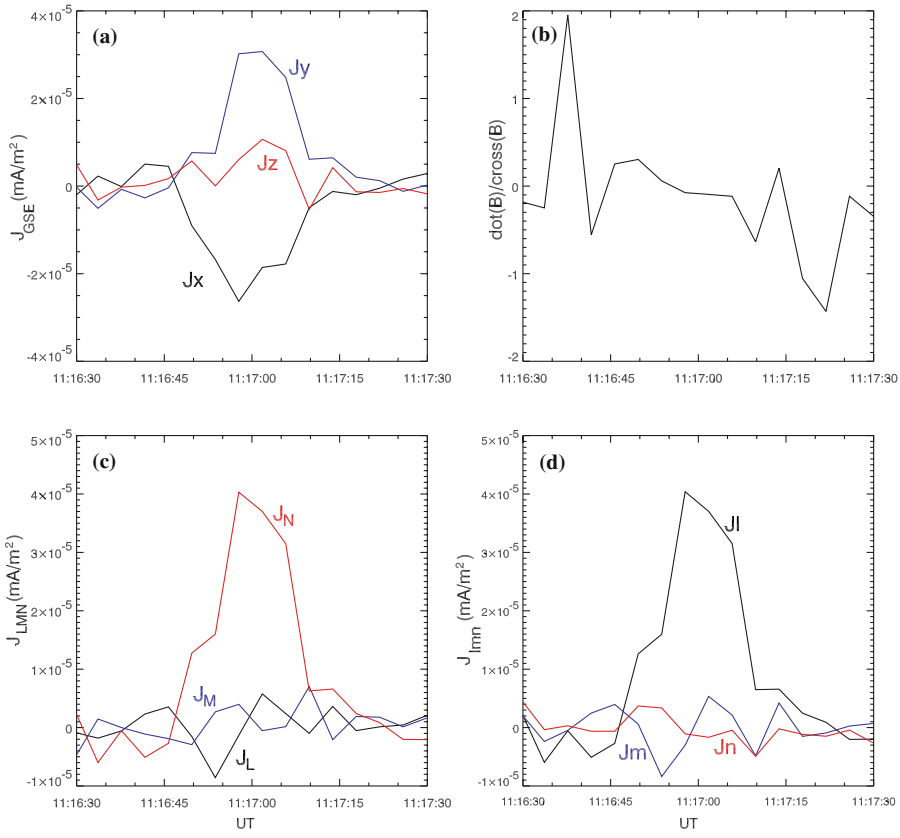


*Figure 9.* Evaluation of the current density for the event at 11:17 UT: (a) Three components of **J** in the GSE system. (b) The relative error of the current evaluation expressed by $\nabla \cdot \mathbf{B}/|\nabla \times \mathbf{B}|$. (c) Three components of **J** projected onto the magnetic field principal axis analysis coordinate system ($L$, $M$, $N$). (d) Three components of **J** projected onto the current principal axis analysis coordinate system ($l$, $m$, $n$).

these events, the current PAA then provides a supplementary approach for determination of the flux rope orientation.

We mentioned in the previous Section that in all events studied, the bulk flow of the ions is essentially along the axis of the flux rope towards the magnetosheath. How much do these ions with energies above 30 keV contribute to the total current? The largest ion flux is ~$10 \times 10^5$ s$^{-1}$ m$^{-2}$ sr$^{-1}$, and so the current density of these ions would yield ~$2 \times 10^{-9}$ A/m$^2$ if their pitch angle distribution were isotropic over a hemisphere, which is less than the largest current $10^{-8}$ A/m$^2$. It is straightforward to derive that the real distribution of energetic ions implicated in the color plot of Figure 6 leads to less intense current. Hence there must be other current carriers which make major contributions to the total current.

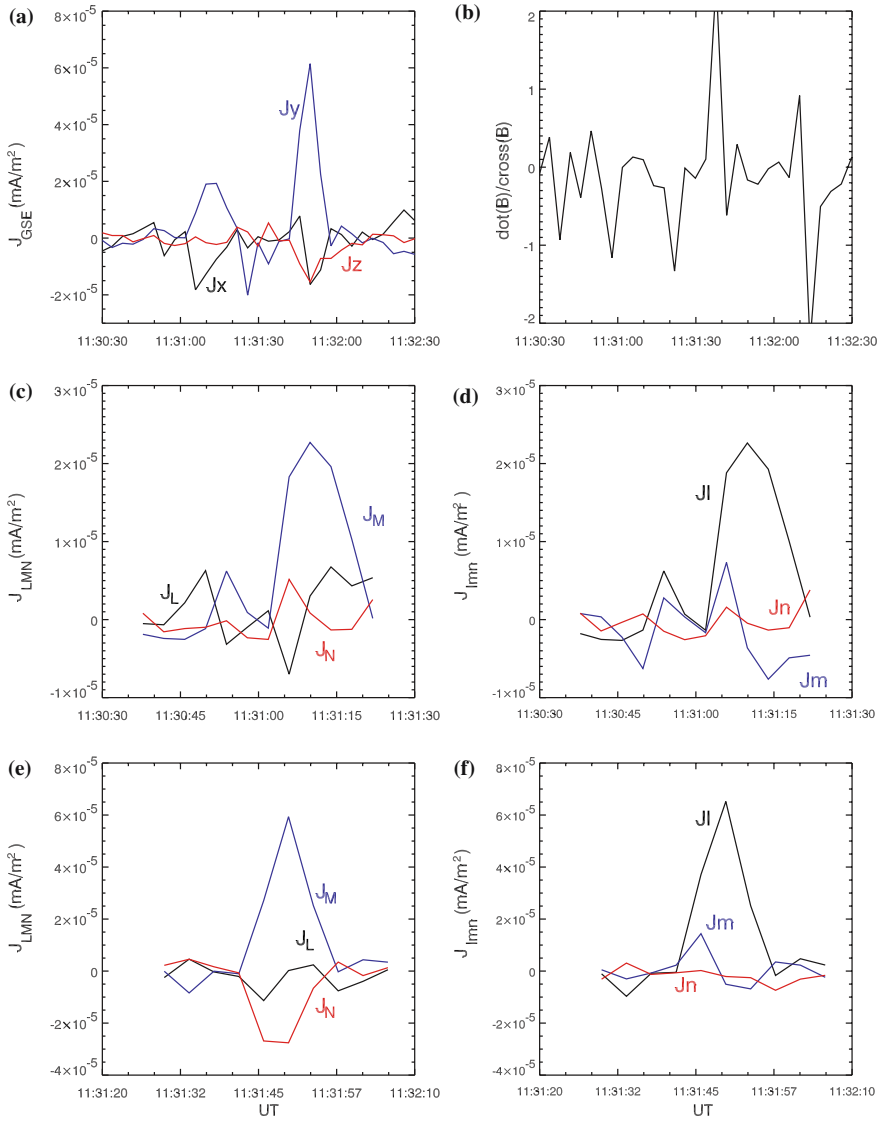


*Figure 10*. Evaluation of the current density for the time period of 11:30 to 11:33 UT: (a) Three components of **J** in the GSE system. (b) The relative error of the current evaluation expressed by $\nabla \cdot \mathbf{B}/|\nabla \times \mathbf{B}|$. (c) Three components of **J** projected onto the magnetic field principal axis analysis coordinate system ($L$, $M$, $N$) for event at ~11:31 UT. (d) Three components of **J** projected onto the current principal axis analysis coordinate system ($l$, $m$, $n$) for the event at ~11:31UT. (e) Three components of **J** projected onto the magnetic field principal axis analysis coordinate system ($L$, $M$, $N$) for the event at ~11:32 UT. (f) Three components of **J** projected onto the current principal axis analysis coordinate system ($l$, $m$, $n$) for the event at ~11:32 UT.

## 6. Summary

The present analysis of Cluster measurements of the cusp and high latitude magnetopause boundary on 26 January, 2001 lead to the following conclusions:

1. The cusp is a dynamic region full of energetic charged particles and turbulence. An energetic ion layer at high-latitudes beyond and adjacent to the duskside magnetopause exists when the IMF has a southward orientation.
2. Multiple energetic ion flux bursts were observed in the energetic ion layer. These bursts occurred quasi-periodically with a repeated period being approximately 72 s. Intense energetic ion bursts were recorded later on the same pass when the spacecraft encountered two FTEs in the magnetosheath.
3. Each energetic ion flux burst was closely related to a magnetic field structure and coincident with a decrease of the thermal plasma density. The ion burst-associated magnetic field structures appear to be flux ropes, with a strong guide field along the axes in the direction pointing duskward/tailward and upward or nearly parallel to the ecliptic plane. An intense axis-aligned current flows inside the ropes, with the current density reaching as high as $\sim 10^{-8}$ A/m$^2$. These flux ropes seem to be produced somewhere away from the spacecraft via magnetic reconnection, and move at similar HT velocities passing over the spacecraft.
4. The main components of the energetic ions are protons, helium and CNO ions. These ions have a magnetospheric origin, flow out to the magnetosheath along the axis of the flux ropes, and make a considerable contribution to the current. However, other current carriers make the major contribution to the total current. The velocity of the magnetosheath thermal plasma relative to the HT frame is found to be basically along the axis of the flux ropes, but flowing towards the magnetosphere. These observations further indicate that the high-latitude magnetopause is a source region, as well as a loss region, for the magnetospheric plasmas and that the reconnected open flux ropes provide a mechanism for the plasma entry and escape across the magnetopause.
5. The present curlometer techniques provide an effective means for estimation of the current density inside flux ropes when the scale size of the tetrahedron of four Cluster spacecraft is considerably smaller than the scale length of the flux ropes and the tetrahedron has a normal geometry.
6. The formation mechanism of the flux ropes observed remains an outstanding problem for future studies.

## Acknowledgements

This work is supported by the CNSF key Project 'Multiple Scale Processes in Geospace Storms' (40390150), the CNSS project of 49834040 ind Chinese Key Research Project G200000784. The major part of the work was accomplished while one of the authors (Z. Y. Pu) was in residence at the Center for Space Physics, Boston University where support was provided by NASA grant NAG5-10108.

## References

Balogh, A., Carr, C. M., Acuna, M. H., Dunlop, M. W., Beek, T. J., Brown, P., Fronacon, K.H., Georgescu, E., Glassmeiei, K.-H., Harris, J., Musmann, G., Oddy, T., and Schwingenschuh, K.: 2001. 'The Cluster Magnetic Field Investigation: Overview of In-flight Performance and Initial Results', *Ann. Geophys.* **19**, 1207–1217.

Bosqued, J. M., Phan, T. D., Dandouras, I., Escoubet, C. P., Reme, H., Balogh, A., Dunlop, M. W., Alcayd, D., Amata, E., Bavassano-Cattaneo, M.-B., Bruno, R., Carlson, C., DiLellis, A. M., Eliasson, L., Formisano, V., Kistler, L. M., Klecker, B., Korth, A., Kucharek, H., Lundin, R., McCarthy, M., McFadden, J. P., Mobius, E., Parks, G. K., and Sauvaud, J.-A.: 2001. 'Cluster Observations of the High-latitude Magnetopause and Cusp: Initial Results From the CIS Ion Instruments', *Ann. Geophys.* **19**, 1545–1556.

Boudouridis, A., Spence, H. E., and Onsager, T. G.: 2002, 'Formation of the LLBL in the Context of a Unifying Magnetopause Reconnection Mechanism', in P. T. Newell, and T. G. Onsager (eds.), *Earth's Low-Latitude Boundary Layer, and Its Dynamic Interaction with the Solar Wind and Magnetosphere, Geophys. Monogr.*, AGU, Washington DC, Vol. 122, 131–136.

Chanter, G.: 1998. 'Spatial Interpolation for Four Spacecraft: Theory', in G. Paschmann, and P. W. Daly (eds.), *Analysis Methods for Multi-Spacecraft Data*, International Space Science Insitute, The Netherlands, pp. 349–369.

Chen, J., Fritz, T. A., Sheldon, R. B., Spence, H. E., Spjeldvik, W. N., Fennell, J. F., Livis, S., Russell, C. T., Pickett, J. S., and Gurnett, D. A.: 1998. 'Cusp Energetic Particle Events: Implication for a Major Acceleration Region of the Magnetosphere', *J. Geophys. Res.* **103**, 69–78.

Crooker, N. U.: 1979. 'Dayside Merging and Cusp Geometry', *J. Geophys. Res.* **84**, 951–959.

Dunlop, M. W., Southwood, D. J., Glassmeier, K.-H., and Neubauer, F. M.: 1988. 'Analysis of Multipoint Magnetometer Data', *Adv. Space Res.* **8**, 273–277.

Dunlop, M. W., Balogh, A., Cargill, P., Elphic, R. C., Fornacon, K.-H., Georgescu, E., and Sedgemore-Schulthess, F., the FGM team.: 2001. 'Cluster Observes the Earth's Magnetopause: Coordinated Four-point Magnetic Field Measurements', *Ann. Geophys.* **19**, 1449–1480.

Dungey, J. W.: 1961. 'Interplanetary Magnetic Field and the Aurora Zones', *Phys. Rev. Lett.* **6**, 47–48.

Elphic, R. C., and Southwood, D. J.: 1987. 'Simultaneous Measurements of the Magnetopause and Flux Transfer Events at Widely Separeted Sites by AMPTE UKS and ISEE 1 and 2', *J. Geophys. Res.* **92**, 13,666–13,672.

Fritz, T. A.: 2001. 'The Cusp as a Sourcs of Magnetospheric Energetic Particles, Currents, and Electric Fields: A New Paradigm', *Space Sci. Rev.* **95**, 469–488.

Fritz, T. A., Zurbuchen, T. H., Gloeckler, G., Hefti, S., and Chen J.: 2003, 'The Use Of Iron Charge State Changes As A Tracer For Solar Wind Entry And Energization Within The Magnetosphere', *Ann. Geophys.* 2155–2164.

Farrugia, C. J., Elphic, R. C., Southwood, D. J., and Cowley, S. W. H.: 1987. 'Field and Flow Perturbations Outside the Open Field Region in Flux Transfer Events, 1, Theory', *Planet. Space Sci.* **35**, 277–240.

Khrabrov, A. V., and Sonnerup, B. U. O.: 1998. 'DeHoffmann-Teller Analysis', in G. Paschmann, and P. W. Daly (eds.), *Analysis Methods for Multi-Spacecraft Data*, International Space Science Insitute, Kluwer Academic Publishers, The Netherlands, pp. 221–248.

Khurana, K. K., Keplo, E. L., Kivelson, M. G., and Elphic, R. C.: 1996. 'Accurate Determination of Magnetic Field Gradients From Four-point Vector Measurements-II: Use of Natural Constraints on Vector Data Obtained From Four Spinning Spacecraft', *IEEE Trans. Magn.* **32**, 5193–5205.

Luhmann, J. G., Walker, R. J., Russell, C. T., Crooker, N. U., Spreiter, J. R., and Stahara, S. S.: 1984. 'Patterns of Potential Magnetic Field Merging Sites on the Dayside Magnetopause', *J. Geophys. Res.* **89**, 1739–1742.

Meng, C.-I, Lui, A. T. Y., Krimigis, S. M., Ismail, S., and Williams, D. J.: 1981. 'Spatial Distribution of Energetic Particles in the Distant Magnetotail', *J. Geophys. Res.* **86**, 5682–5700.

Papamastorakis, I, Paschmann, G., Baurnjohann, W., Sonnerup, B. O. U., and Luhr, H.: 1989. 'Orientation, Motion and Other Properties of Flux Transfer Event Structures on 4 September 1984', *J. Geophys. Res.* **94**, 8852–8866.

Paschmann, G., Haerendel, G., Sckopke, N., Rosenbauer, H., and Hedgecock, P. C.: 1976. 'Plasma and Magnetic Field Characteristics of the Distant Polar Cusp Near Local Noon: The Entry Layer', *J. Geophys. Res.* **81**, 2883–2899.

Reme, H., Aoustin, C., and Bosqued, J. M., : 2001. 'First Multispacecraft Ion Measurement in and Near the Earth's Magnetosphere with the Identical Cluster Ion Spectrometry (CIS) Experiment', *Ann. Geophys.* **19**, 1303–1354.

Robert, P., Dunlop, M. W., Roux, A., and Chanteur, G.: 1998. 'Accuracy of Current Determination', in G. Paschmann, and P. W. Daly (eds.), *Analysis Methods for Multi-Spacecraft Data*, International Space Science Insitute, Kluwer Academic Publishers, The Netherlands, pp. 395–418.

Rosenbauer, H. H., Grunwald, M., Montgomery, D., Paschmann, G., and Sckopke, N.: 1975. 'Heos 2 Plasma Observations in the Distant Polar Magnetosphere: The Plasma Mantle', *J. Geophys. Res.* **80**, 2723–2737.

Russell, C. T., and Elphic, R. C.: 1978. 'Initial ISEE Magnetometer Results', *Space Sci. Rev.* **22**, 681–715.

Russell, C. T., and Elphic, R. C.: 1979. 'Observation of Magnetic Flux Ropes in the Venus Ionosphere', *Nature* **279**, 618 .

Sibeck, D. G., Pachmann, G., Treumann, R. A., Fuselier, S. A., Lennartsson, W., Lockwood, M., Lundin, R., Ogilvie, K. W., Onsager, T. G., Phan, T.-D., Roth, M., Scholer, M., Scopke, N., Stasiewicz, K., and Yamauchi, M.: 1999, 'Plasma Transfer Processes at the Magnetopause', in B. Hultqvist, M. Oieroset, G. Paschmann, and R. Treumann (eds.), *Magnmetospheric Plasma Sources and Losses, Space Sci. Rev.* Vol. 88, 207–283..

Sonnerup, B. U. O., and Cahill, L. J. Jr.: 1968. 'Explorer 12 Observations of the Magnetopause Current Layer', *J. Geophys. Res.* **73**, 1757–1770.

Sonnerup, B. U. O., and Scheible, M.: 1998. 'Minimum Variation Analysis', in G. Paschmann, and P. W. Daly (eds.), *Analysis Methods for Multi-Spacecraft Data*,

International Space Science Insitute, Kluwer Academic Publishers, The Netherlands, pp. 185–220.

Tsyganenko, N. A., and Stern, D. P.: 1996. 'Modeling the Global Magnetic Field of the Large-scale Birkeland Current System', *J. Geophys. Res.* **101**, 27,187–27,195.

West, H. I. Jr., and Buck, R. M.: 1976. 'Observations of >100 keV Protons in the Eaxth's Magnetosheath', *J. Geophys. Res.* **81**, 569–584.

Wild, J. A., Cowley, S. W., Davies, J. A., Khan, H., Lester, M., Milan, S. E., Provan, G., Yeoman, T. K., Balogh, A., Dunlop, M. W., Fornacon, K.-H., and Georgescu, E.: 2001. 'First Simultaneous Observations of Flux Transfer Events at the High- latitude Magnetopause by the Cluster Spacecraft and Pulsed Radar Signatures in the Conjugate Ionosphere by the CUTLASS and EISCAT Radars', *Ann. Geophys.* **19**, 1491–1508.

Wilken, B., Axford, W. I., Daglis, I., Daly, P. W., Guttler, W., Ip, Korth, A., Kremser, G., Livi, S., Vasyliunas, V. M., Woch, J., Baker, D., Belian, R. D., Blake, J. B., Fennell, J. F., Lyons, L. R., Borg, H., Fritz, T. A., Gliem, F., Rathje, R., Grande, M., Hall, D., Kecskemety, K., McKenna-Lawlor, S., Mursula, K., Tanskanen, P., Pu, Z. Y., Sandahl, I., Sarris, E. T., Scholer, M., Sorass, F., and Ullaland, S./RAPID: 1997. 'The Imaging Energetic Particle Spectrometer on Cluster', in C. P. Escoubet, C. T. Russell, and R. Schmide (eds.), *The Cluster and Phoenix Missions*, Kluwer Academic Publishers, The Netherlands, pp. 399–473.

Wilken, B., Daly, P. W., Mall, U., Aarsnes, K., Baker, D. N., Belian, R. D., Blake, J. B., Borg, H., Buchner, J., Carter, M., Fennell, J. F., Friedel, R., Fritz, T. A., Gliem, F., Grande, M., Kecskemety, K., Kettmann, G., Korth, A., Livi, S., McKenna-Lawlor, S., Mursula, K., Nikutowski, B., Perry, C. H., Pu, Z. Y., Roeder, J., Reeves, G. D., Sarris, E. T., Sandahl, I., Sorass, F., Woch, J., and Zong, Q.-G.: 2001. 'First Results From the RAPID Imaging Energetic Particle Spectrometer on Board Cluster', *Ann. Geophys.* **19**, 1355–1366.

Zong, Q.-G., and Wilken, B.: 1998. 'Layered Structure of Energetic Oxygen Ions in the Magnetosheath', *Geophys. Res. Lett.* **25**, 4121–4124.

Zong, Q.-G., Fritz, T. A., Wilken, B., and Daly, P.: 2002. 'Energetic Ions in the High Latitude Boundary Layer of the Magnetosphere RAPID/CLUSTER Observations', *Geophys. Monograph* **122**, 101–106.

Zong, Q.-G., Fritz, T. A., Spence, H., Dunlop, M., Pu, Y. Z., Korth, A., Daly, W., Balogh, A., and Reme, H.: 2003. 'Bursty Energetic Electrons Confined in Flux Ropes in the Cusp Region', *Planet. Space Sci.* **51**, 821–830.

Surveys in Geophysics (2005) 26: 215–240
DOI 10.1007/s10712-005-1879-z © Springer 2005

# ENERGETIC ELECTRONS AS A FIELD LINE TOPOLOGY TRACER IN THE HIGH LATITUDE BOUNDARY/CUSP REGION: CLUSTER RAPID OBSERVATIONS

Q. G. ZONG[1], T. A. FRITZ[1], A. KORTH[2], P. W. DALY[2], M. DUNLOP[3], A. BALOGH[3], J. F. FENNELL[4], J. D. SULLIVAN[5], R. W. H. FRIEDEL[6] and H. REME[7]

[1]*Center For Space Physics, Boston University, Boston, MA, 02215, USA*
*E-mail: zong@bu.edu;*
[2]*Max-Planck-Institut für Aeronomie, Katlenburg-Lindau, Germany;*
[3]*Space and Atmospheric Physics Group, Imperial College, London, UK;*
[4]*Aerospace Corporation, Los Angeles, LA;*
[5]*Department of Aerospace and Mechanical Engineering, Boston University, Boston, MA, 02215, USA;*
[6]*Los Alamos National Laboratory, Los Alamos, NM;*
[7]*CESR, Toulouse, France*

(Received 1 January 2003; Accepted 30 April 2004)

**Abstract.** Energetic electrons (e.g., 50 keV) travel along field lines with a high speed of around 20 $R_E s^{-1}$. These swift electrons trace out field lines in the magnetosphere in a rather short time, and therefore can provide nearly instantaneous information about the changes in the field configuration in regions of geospace. The energetic electrons in the high latitude boundary regions (including the cusp) have been examined in detail by using Cluster/RAPID data for four consecutive high latitude/cusp crossings between 16 March and 19 March 2001. Energetic electrons with high and stable fluxes were observed in the time interval when the IMF had a predominately positive $B_z$ component. These electrons appeared to be associated with a lower plasma density exhibiting no obvious tailward plasma flow ( < 20 keV). On the other hand, no electrons or only spike-like electron events have been observed in the cusp region during southward IMF. At that time, the plasma density was as high as that in the magnetosheath and was associated with a clear tailward flow. The fact that no stable energetic electron fluxes were observed during southward IMF indicates that the cusp has an open field line geometry. The observations indicate that both the South and North high latitude magnetospheric boundary regions (including both North and South cusp) can be energetic particle trapping regions. The energetic electron observations provide new ways to investigate the dynamic cusp processes. Finally, trajectory tracing of test particles has been performed using the Tsyganenko 96 model; this demonstrates that energetic particles (both ions and electrons) may be indeed trapped in the high latitude magnetosphere.

**Keywords:** boundary, cusp, electron, energetic ions, magnetosphere, reconnection

**Abbreviations:** ISEE – international sun–earth explorers; HEOS – highly eccentric orbiting satellite; ACE – advanced composition explorer; IMF – interplanetary magnetic field; IMP –

interplanetary monitoring platform; MHD – magnetohydrodynamics; MLT – magnetic local time; RAPID – Research with Adaptive Particle Imaging Detectors; SOHO – Solar and Heliospheric Observatory

## 1. Introduction

The boundaries of the magnetosphere, including the polar cusp, are key regions for the transfer of mass, momentum and energy from the solar wind into the magnetosphere when the IMF is southward or northward.

The first identification of a thin layer of magnetosheath plasma located immediately inside the magnetopause was made by Hones et al. (1972) who introduced the term "Boundary Layer". Since then, the morphological characteristics as well as plasma properties of the magnetospheric boundary layer have been studied rather intensively (Rosenbauer, 1975; Eastman, 1976; Haerendel, 1978; Lundin, 1985; Lundin and Dubinin, 1985; Newell and Meng, 1988; Newell and Meng, 1998). The term "Low-latitude boundary layer (LLBL)", was apparently introduced by Haerendel (1978) to distinguish the very different properties observed at latitudes below about 50–60° on the magnetopause surface. In addition, there are three more boundary regions (in the high latitude) that are assumed to connect directly to the magnetosheath: the plasma mantle, the entry layer, and the exterior cusp or stagnation region (seen in Figure 1).

The plasma mantle which was first reported by Rosenbauer (1975) is located on the opened field lines where the injected magnetosheath plasma continues tailward. The plasma density in this region is less than (but comparable to) the sheath density level and has $\beta << 1$. The entry layer (Paschmann et al., 1976) is located on the magnetospheric field lines just equatorward of the cusp.

It has been so termed because it appears to be the region of dominant plasma entry into the magnetosphere. The transport mechanism is likely to be achieved through eddy convection which manifests itself in the irregular, low speed plasma flow, and may be excited by turbulence in the adjacent exterior cusp (Haerendel, 1978). Localized reconnection has been proposed by Haerendel (1978), who envisioned it as an intermittent, small scale process related to eddy turbulence in the entry layer. This intermittent small-scale reconnection could be occurring in the cusp region for both northward and southward IMF. In the entry layer, the plasma density is as high as or even higher than that in the magnetosheath, the temperature is very similar to that of the exterior cusp, and the plasma beta $\beta \approx 1$.

The exterior cusp/stagnation region is bounded on the inside by the cusp-like indentation of the magnetopause, and outside by the free-flow stream

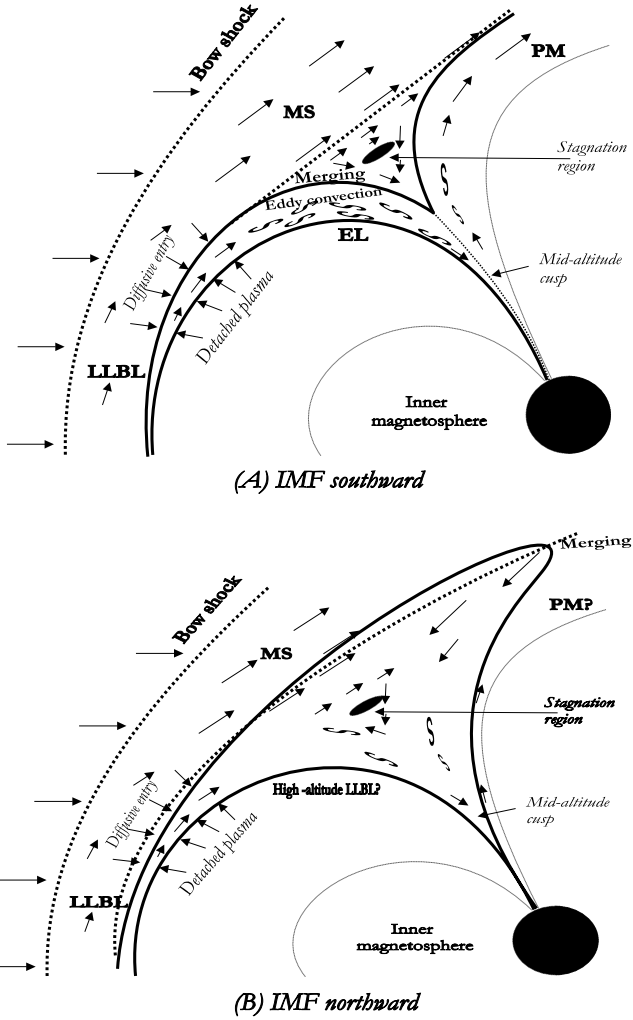


*Figure 1.* Sketch of the dayside boundary regions related to the polar cusp field lines during southward (after Haerendel, 1978) and northward IMF. MS – magnetosheath; PM – plasma mantle; LLBL – low latitude boundary layer; EL – entry layer; S – flow eddy.

lines of the magnetosheath flow (Sckopke et al., 1976, 1981) which constitutes a pocket of hot and 'stagnant', possibly turbulent, plasma. In fact, as early as the 1960s the stagnation region was already predicted by gas dynamic models (Spreiter and Summers, 1967; Spreiter and Stahara, 1980). Furthermore, this picture has been corroborated by HEOS 2 measurements (Sckopke et al., 1976, 1981). The stagnation region cannot be linked to the plasma mantle or LLBL in a simple way. A qualitative explanation was given by Haerendel (1978) who noted the similarity of the situation near the cusp to hydrodynamic flow around a corner, in which vortex formation and separation are

known to occur and to initiate some level of turbulence (Figure 1). The exterior cusp region appears to be a steady high pressure center of "stagnant" magnetosheath plasma; the flow in this region is rather turbulent, both in magnitude and direction.

The mantle is generally thicker for southward than northward IMF $B_z$ (Sckopke et al., 1976, 1981). These researchers believed that the plasma mantle was on open field lines, and the LLBL on closed. It has been indicated that in the HLBL (Entry Layer) the plasma density is almost as high as in the magnetosheath but generally lacking the strong antisunward plasma flow. In fact sunward flow has even been reported by Paschmann et al. (1976). Lundin (1985) suggested that a characteristic feature of the entry layer is a strong variability of magnetosheath plasma entry, with frequent plasma injection. On the basis of the Defense Meteorological Satellite Program (DMSP) F2 data, Newell and Meng (1987) indeed observed that the cusp low-altitude latitudinal extent is narrower when $B_z$ is southward than when $B_z$ is northward. This result has been interpreted that the enhanced convection flow is too rapid to allow the plasma to reach low altitudes. Furthermore, Newell and Meng (1987) indicate that there may not be simply slower tailward convection within the boundary layer but rather no tailward or even sunward convection when IMF $B_z$ is northward. In non-reconnection models the cusp position and extent are less sensitive to the IMF, but more strongly dependent on the solar wind ram pressure (Yamauchi and Lundin, 1998).

It should be pointed out that indications of the existence of a boundary layer from energetic particle measurements were provided even earlier. Energetic ($>25$ keV) dusk-side particles are very often present on magnetosheath field lines just outside the magnetosphere (Anderson et al., 1965; Haskell, 1969; West and Buck, 1976; Eccles and Fritz, 2002). Recently, observations by Geotail showed that the energetic ions of terrestrial origin (e.g., singly charged oxygen ions) leak out of the magnetosphere and can form layers in the equatorial magnetosheath (in the vicinity of the magnetopause) during intense storm activities. Energetic singly charged oxygen ion enhancements are frequently detected in the magnetosheath and occasionally show a total duration of about 150 min (Zong and Wilken, 1998; Zong et al., 2001). In the high latitude region, layer-like energetic ions have been observed adjacent to the magnetopause outside the magnetosphere (in the magnetosheath) during southward IMF, whereas layer-like energetic ions have been observed inside the magnetosphere during northward IMF. The energetic particles in this region are also highly anisotropic, exhibiting a clear sunward flow or bidirectional flow (sunward and anti-sunward) even if geomagnetic activity is very quiet (Zong et al., 2002).

Energetic ions with energies from tens of keV up to MeV have been observed near the magnetopause at high latitudes and in the cusp region (Aparcio et al., 1991; Kremser et al., 1995; Chen et al., 1997; Fritz et al., 1999;

Chang et al., 2000; Fritz, 2000, 2001; Trattner et al., 2001), although Roederer (1970) showed that the drift paths of energetic particles in the outer magnetosphere intersect the magnetopause, which implies that there are no energetic particles stably trapped in the high latitude cusp region. The origin of energetic particles in the cusp region has been a subject of controversy. Chen et al. (1997) and Fritz (2000) argued that the particles observed in the cusp region are the result of a localized acceleration mechanism and should be one of the sources for magnetospheric energetic particles. On the other hand, Chang et al. (1998) and Trattner et al. (2001) suggested that the energetic particles in the cusp region originate from either the bow shock or magnetosphere itself. In this case no local acceleration is needed. Delcourt and Sauvaud (1999) proposed a third interpretation in which the energetic particles in the high latitude region could be generated from the de-trapping of equatorial ions. A possible clue for the solution to this puzzle has been suggested by Sheldon et al. (1998) and Delcourt and Sauvaud (1998). They pointed out that a particle will drift on a closed path around the front of the magnetosphere and suggested that a possible stable trapping region may exist in the outer cusp. This kind of particle motion has been further explored by Fritz (2000) and has been applied to explain the origin of energetic particles in the high latitude boundary during very quiet geomagnetic conditions for both northward and southward IMF conditions (Zong et al., 2002). Further measurements of energetic electrons are therefore essential in the search for answers to these questions.

A layer of energetic electrons ($>40$ keV) lying primarily outside the magnetopause is found at high latitudes near the dusk-dawn meridional plane from the dayside to the distant magnetotail (Meng and Anderson, 1970, 1975), although the formation mechanism is still unclear. The IMP-8 spacecraft had on-board sensors of large geometric factors that provided very sensitive measurements of 200 keV electrons at 35 $R_E$ geocentric distance. With these nearly continuous measurements, Baker and Stone (1977a–c) have shown that the energetic electron magnetopause layer is persistently present along the distant magnetotail at essentially all latitudes and that the $\geq$200 keV electrons within the layer are streaming tailward along the local magnetic field. Energetic electron layers were discovered carrying significant energy flows outside the magnetopause, and this energy flux was seen to vary with the nature of the solar wind–magnetosphere interactivity. Furthermore, energetic electron layers are observed most often in the dawn-side of the plasma sheet and protons in the dusk-side (Meng et al., 1981). The acceleration of ionospheric electrons to energies up to about 10 keV in the boundary region adjacent to the cusp was also reported by Kremser and Lundin (1990).

Bursts of energetic electrons (from $>40$ to 2000 keV) were observed in the magnetosheath and in the solar wind. A statistical study (Formisano, 1979) demonstrated that those electrons are of cusp origin; the flux intensity is

highest in the exterior cusp region and decreases away from it. With increasing distance from this place the energy spectrum becomes harder since only energetic particles are able to "get away". The measured electron anisotropy and magnetic field indicate that these particles were propagating away from the exterior cusp along the magnetic field lines (Formisano, 1979). However, these studies may mix both solar energetic electrons (Lin, 1985; Klassen et al., 2002) and electrons of magnetospheric origin because these studies were based on single satellite measurements. At that time there was no solar energetic electron monitor, like the ACE, Wind, or SOHO spacecraft in the upstream interplanetary medium.

By using energetic electron observations, early work clearly delineated regions of open and closed magnetic field lines in the midtail region and thus contributed crucially to understanding the substorm dynamics. Subsequent work using the IMP-8 electron sensors (Bieber et al., 1982) demonstrated in a clear way that energetic electrons, and only energetic electrons, can be used to assess magnetic-field-line topology fully and thus distinguish between competing magnetotail dynamic models. Similar methods were used extensively on ISEE-1 and -2 (Fritz et al., 1984) to assess where, when and how acceleration and transport processes occur in and around the magnetosphere. Bursty energetic electron events (20–400 keV) have been found in the cusp region by the Cluster spacecraft (Zong et al., 2003). These electrons are found to be embedded in flux rope structures which are suggested to be generated in the cusp stagnation region. In this paper, the energetic electron behavior in the high latitude magnetospheric regions has been examined in detail by using Cluster/RAPID data for four consecutive high latitude/ cusp crossings between 16 March and 19 March 2001 (two orbits). Both spike-like and stably trapped electrons were observed during different solar wind/IMF and geomagnetic activity conditions. Energetic electrons are able to trace magnetic-field-line topology and thus distinguish between open and closed field lines in the high latitude boundary/cusp region.

## 2. Observations

The data to be presented here were obtained by the RAPID instrument on board the Cluster spacecraft (Wilken et al., 1997). The energetic particle spectrometer RAPID in the Cluster payload features novel detection principles both for ions and electrons: for either species the instrument measures the vector velocity ($V$) and the energy ($E$). Each of the ion detector heads (IIMS) is composed of a time-of-flight (TOF)/energy ($E$) telescope with a solid state detector (SSD) as the back element. Species identification comes from the function $ET^2 = A$, with $E$ and $T$ denoting the measured quantities of energy and time-of-flight (equivalent to the particle velocity), and $A$ the

atomic mass of the particle. The energy range extends from 30 to 4000 keV. The advanced design of the telescope as a projection camera also returns information on the particle direction of incidence within 12 angular intervals over a 180° field-of-view. A second detector system, the imaging electron spectrometer (IES), is dedicated to electrons between 20 and 400 keV. The IES head uses the optical principle of a pinhole camera with nine angular intervals over 180°. Together with a sectored spin plane of the spacecraft, both systems cover the unit sphere in velocity space in a contiguous manner. Detailed information about the RAPID instrument has been given by Wilken et al. (1997). Furthermore, we use magnetometer measurements from the fluxgate magnetometer (FGM) on board Cluster, which makes high resolution vector field measurements (Balogh et al., 1997) and plasma data from the Cluster Ion Spectrometer (CIS) experiment (Reme et al., 1997). The criteria for region identification in this paper is mainly based on the plasma data together with the energetic particle behavior and magnetic field data.

From 16 to 19 March 2001, the four Cluster satellites crossed the high latitude boundary and/or cusp regions four times (two in the southern hemisphere and the other two in the northern hemisphere) during two consecutive orbits (see Figure 2).

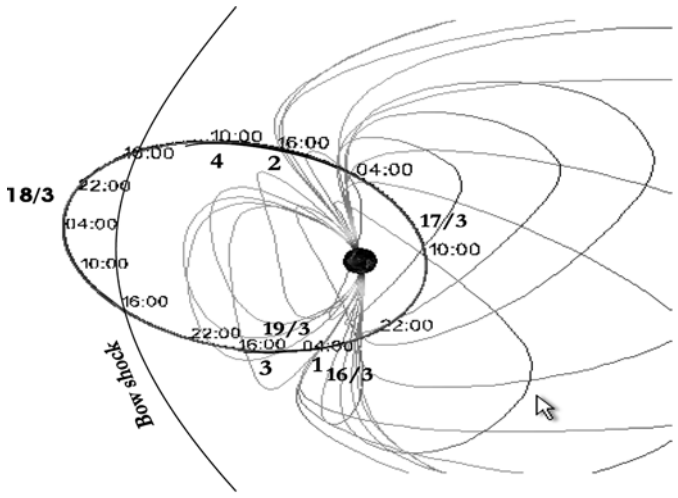


| | | | | |
|---|---|---|---|---|
| 1 | 16/3 | 17h00-19h10m | South HLBL/Cusp | quiet |
| 2 | 17/3 | 06h00-09h20m | North HLBL/Cusp | quiet |
| 3 | 19/3 | 01h00-02h30m | South HLBL/Cusp | activity |
| 4 | 19/3 | 14h50-19h00m | North HLBL/Cusp | activity |

*Figure 2.* The Cluster trajectories through the Tsyganenko magnetic field model (Tsyganenko, 1996) for 16–19 March 2001. Only one Cluster satellite is shown since the separation is too small to be resolved. The Cluster satellites trajectory and the Tsyganenko magnetic field lines have been projected onto the GSE – *XZ* plane.

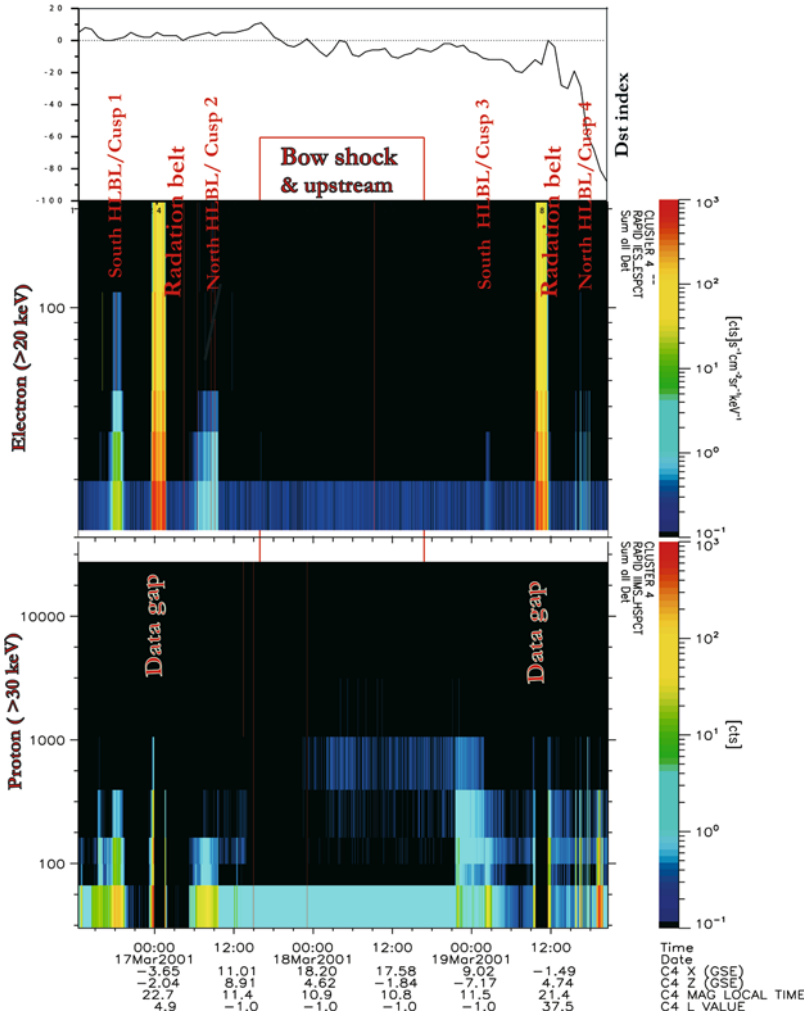


*Figure 3.* An overview of RAPID from 09:00 UT, 16 March to 21:00 UT, 19 March 2001, together with geomagnetic activity Dst index. From the top the panels show: Dst index; electron spectra from 20 to 400 keV; proton spectra from 30 to 2000 keV. The marks indicate the different regions – South HLBL/cusp, radiation belt and the North HLBL/cusp which Cluster experienced during its two consecutive orbits. The 'HLBL/Cusp' here refers to all of the high latitude magnetospheric regions, the 'radiation belt' here refers all inner magnetospheric regions; two ion data gaps are indicated.

Figure 3 shows the different regions – South cusp, radiation belt and North cusp as obtained by Cluster/RAPID during these two consecutive orbits. The geoactivity Dst index is shown in the top panel. The first two cusp crossings (1 and 2) happened during a rather quiet time period; the Dst indices were small and positive. The later two crossings (3 and 4) occurred in

the main phase of a strong magnetic storm. As we can see from Figure 3, the high latitude magnetosphere (both North and South cusp) regions are two of three locations that energetic particle are encountered. Both South and North high latitude boundary and/or cusp regions can be distinguished easily by the fact that (1) the ion flux increased sharply in all energy channels from 30 to 400 keV , whereas (2) the energetic electron flux which appeared in the quiet time was not present in the disturbed time.

### 2.1. High latitude boundary/cusp: quiet time crossings (IMF northward)

In order to inspect energetic electron events in the high latitude boundary/cusp region in more detail, the fluxes of energetic electrons and ions together with plasma parameters and the local magnetic fields for two consecutive quiet time crossings are given in Figure 4.

At about 17:06UT, 16 March 2001, the Cluster spacecrafts crossed the magnetopause from the magnetosheath into the high latitude boundary/cusp region and at around 19:07 entered the cusp region in the southern hemisphere (see Figure 4 Left). As shown in Figure 4 Right, on 17 March 2001, the Cluster spacecraft were travelling outbound from the northern hemisphere. Starting in the northern lobe, the Cluster spacecraft crossed through the cusp from 04:48 UT to 06:00 UT into the high latitude boundary region and finally entered the magnetosheath at about 09:20 UT.

The top panels (left and right) in Figure 4 show energy-integrated ion and electron flux versus time profiles. The second panel shows the plasma density variation. The third and fourth panels show plasma velocity, $V_x$, $V_y$ and $V_z$. The last three panels in Figure 4 show the components of the magnetic field obtained by the Cluster FGM instrument. Both South (Figure 4 Left) and North (Figure 4 Right) high latitude boundary/cusp regions can be distinguished from just entry into a high flux region of energetic electrons and ions by the fact that:

(1) the associated plasma velocity $V_x$ decreased sharply to around 0, whereas $V_z$ showed surprisingly a significant enhancement at around −75 km/s (Figure 4),
(2) the magnetic field $B_x$ is large and stable, around 25 nT in the southern hemisphere (Figure 4 Left) and −25 nT in the northern hemisphere (Figure 4 Right). Both $B_y$ and $B_z$ changed their polarity during the spacecraft crossing of the high latitude boundary/cusp region. $B_y$ changed its polarity first, and then $B_z$ (Figure 4),
(3) the plasma density in the high latitude boundary region was higher than that in the lobe but lower than that in the sheath,

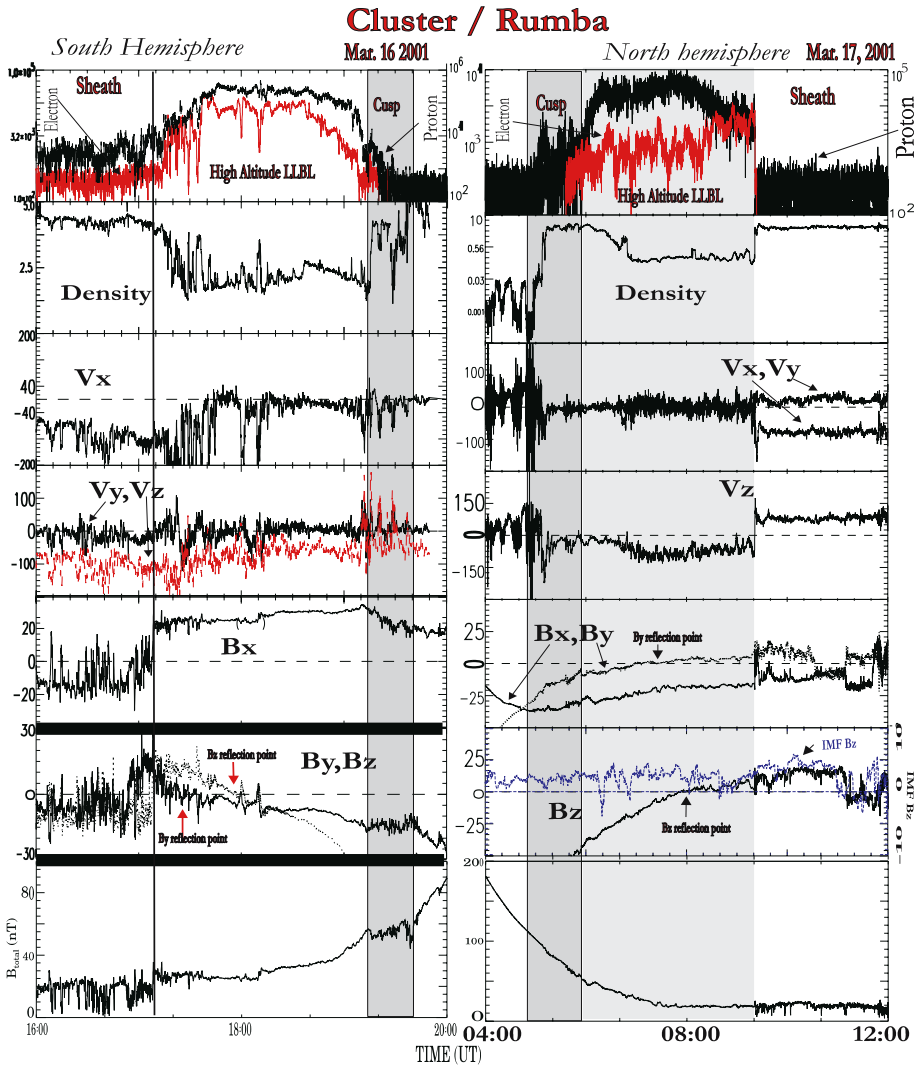


*Figure 4*. Overview plots of RAPID, CIS and FGM data from 16:00 to 20:00 UT, March 16, 2001 (Left) and from 04:00 to 12:00 UT, March 17, 2001 (Right) during northward IMF. From the top the panels show: integral electron and proton flux (in $cm^{-2} \bullet s^{-1} \bullet sr^{-1}$); plasma density (in ions/cm$^{-3}$); plasma velocity ($V_x$, $V_y$ and $V_z$ in km/s) and magnetic field GSE components and magnitude (in nT). IMF $B_z$ for 17 March 2001 is over-plotted in panel 6, the time lag is adjusted suitably. The vertical lines mark the different regions – sheath, cusp, and mantle – which Cluster experienced.

(4) the total magnetic field intensity was 25 nT with less fluctuation in Figure 4,
(5) these regions had clear interfaces with the magnetosheath.

During the above two quiet time high latitude boundary/cusp crossings, there were pronounced fluxes of electrons in the high latitude boundary/cusp region, indicating either a closed field line geometry in the cusp region, a special open field line configuration that could trap electrons very efficiently for a long time or a long-lived source supplying these electrons to open field lines. These electrons lasted about 2 h (from 17:06 to 19:07 UT, 16 March 2001) and 3 h 20 min (from 06:00 to 09:20 UT, 17 March 2001), respectively. Furthermore, no obvious substorm injections were observed by the Los Almos satellites for both of the above quiet time high latitude boundary /cusp crossings (not shown here). Further, there were no energetic electron events observed by ACE in the upstream interplanetary space during 16–19 March 2001 as documented in Figure 5. Thus, these observed electrons should not be solar energetic electrons as described by Lin (1985) and Klassen et al. (2002). The lack of substorm activity and high fluxes of electrons upstream at ACE indicates that the observed electrons are locally trapped electrons rather than substorm injected electrons drifting to the high latitude region or solar flare related electrons.

### 2.2. High latitude boundary/cusp: disturbed time crossings (IMF southward)

In contrast with Figure 4, two consecutive HLBL/cusp crossings during geomagnetically disturbed times are shown in Figure 6. There were no

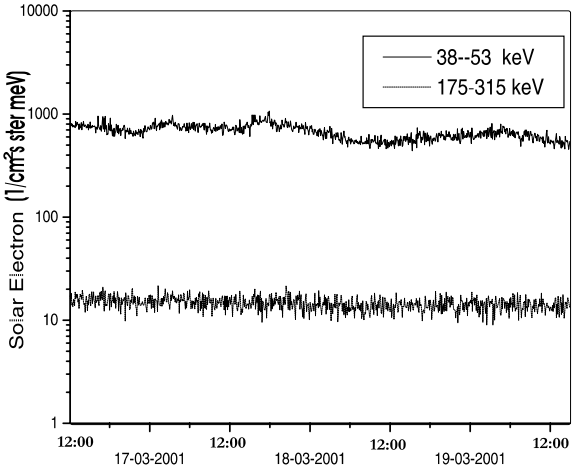


*Figure 5*. Differential energetic electron fluxes obtained by the ACE spacecraft at the first Lagrange point upstream from the Earth, for two energy ranges (38–53 and 175–315 keV).

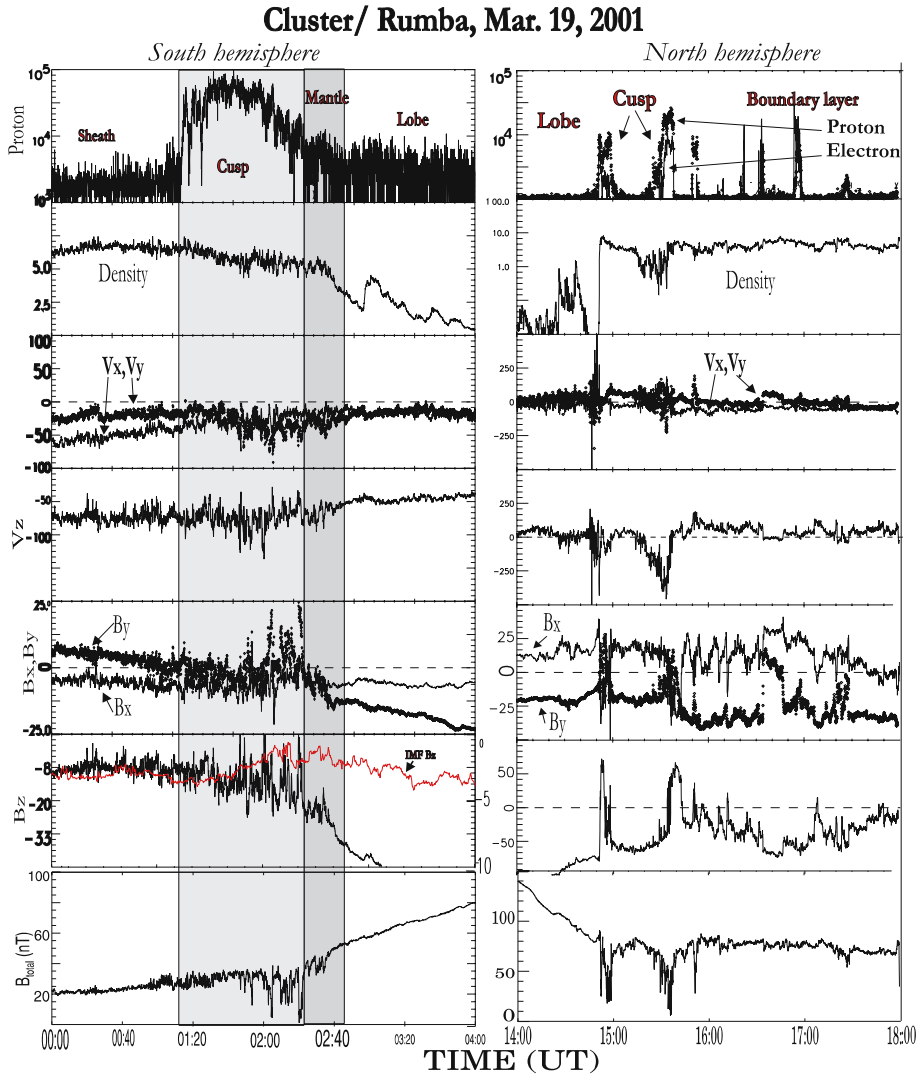


*Figure 6*. RAPID, CIS and FGM summary plots from 00:00 to 04:00 UT, 19 March 2001 (Left) and from 07:00 to 10:30 UT, 19 March 2001 (Right) during southward IMF. > From the top the panels show: integral electron flux; proton flux; plasma density; and GSE components and magnitude of the magnetic field (in nT). IMF $B_z$ between 00:00 and 04:00 UT 19 March 2001 is over-plotted in panel 6; the time lag is adjusted. The vertical lines mark the different regions – lobe, mantle, cusp, and sheath – which Cluster experienced on 19 March 2001.

significant electrons in the same place as in the previous Cluster orbit (see Figure 2) during the geomagnetically quiet time. The magnetic field data and the plasma density show no clear evidence to indicate where the magnetopause is located (Figure 6 Left), although within the cusp and the

boundary region there existed a lot of structure during the storm time (for Figure 6 Right, Dst was around −40 nT). Only the energetic ions seem to provide some indication of the interface between the cusp and the magnetosheath.

Both the southern cusp (Figure 6 Left) and the northern cusp (Figure 6 Right) can be distinguished by the fact that

(1) The plasma density in the cusp is comparable with that in the magnetosheath,
(2) The magnetic field becomes more turbulent in the region labeled cusp than that in the magnetosheath as seen in the bottom panel of Figure 6,
(3) The energetic proton flux increases dramatically, but there are no pronounced fluxes of energetic electrons present, indicating a probable open field line geometry in the cusp region during IMF southward or a lack of a source of these electrons,
(4) Not only the magnetic field, but also the plasma density and velocity, are fluctuating.

Table I provides a synoptic view of these four cusp crossings during different geomagnetic activities and IMF orientation.

TABLE I
HLBL/Cusps property

| Events | South Cusp 1 | North Cusp 2 | South Cusp 3 | South Cusp 4 |
|---|---|---|---|---|
| Time | 17:00–19:10 16 March 2001 | 06:00–09:20 17 March 2001 | 01:00–02:30 19 March 2001 | 14:50–16:00 19 March 2001 |
| Location | 11.3 MLT | 11.4 MLT | 11.5 MLT | 11.7 MLT |
| Electron ($cm^2$ $ssr^{-1}$) | $10^4$, stable | $10^3$, stable | None | Pulse |
| Proton ($cm^2$ $ssr^{-1}$) | $5 \times 10^5$, stable | $10^5$, stable | $10^5$, stable | $5 \times 10^5$, pulse |
| Plasma $V_x$ | No obvious | No obvious | Significant $-V_x$ | Significant $-V_x$ |
| Interface M (to the Mantle) | Clear | Clear | Clear | Clear |
| Interface S (to the sheath) | Clear | Clear | Not clear | Not clear |
| IMF $B_z$ | 0.5 nT | 3.3 nT | −4.4 nT | −9.3 nT |
| Ram pressure | 1.15 nPa | 1.01 nPa | 1.06 nPa | 5.03 nPa |
| Geoactivity | Quiet | Quiet | Activity | Storm |
| $K_p$ | $1^+$ | $0^+$ | 2 | 6 |
| Dst | 1 nT | 4 nT | −10 nT | −40 nT |

## 3. Interpretation and discussion

### 3.1. The interface to the magnetosheath

The variation of the energetic electron and ion fluxes for the boundary crossing observed by all Cluster spacecraft from 09:19 to 09:23 UT, 17 March 2001 are given in Figure 7 Left. As a reference, the plasma parameters and the magnetic field are also shown. A discontinuity between 09:21 and 09:22 UT can be seen in all panels of Figure 7 Left. This occurred during the northward IMF (Figure 4). After 09:22 UT, when the Cluster satellites crossed the magnetopause into the magnetosheath, the flux of energetic particle decreased quickly to the background level. This may indicate that the Cluster satellites moved far away from the magnetopause or that no particles escaped from the magnetosphere during conditions of northward IMF.

The spacecraft crossed the magnetopause at different times although the time difference is quite small. The numbers Cl, C2, C3, and C4 represent the different Cluster spacecraft – Rumba (1), Salsa (2), Samba (3), and Tango (4). The arrows indicate the time when the magnetopause was encountered. The encounter time of the proton and electron flux detected by four different satellites is slightly different. The maximum time difference between C3 (Samba, the earliest satellite to encounter the magnetopause) and C2 (Salsa, the last) is 20 s for protons and 10 s for electrons. Using a technique described by Dunlop and Woodward (1998), the thickness of the magnetopause could be estimated to be $d = 200$ km.

In order to determine whether the magnetic field in this boundary layer is categorized as some MHD discontinuity, the magnetic field data was analyzed by a minimum variance analysis (MVA) method (Sonnerup and Cahill, 1967; Sonnerup, 1976; Elphic and Russell, 1983; Hapgood, 1992). The analysis concentrated on variations involving a large and rapid change in both the magnetic field and energetic particle flux. This method is based on determining the directions of maximum and minimum variation for a given magnetic field vector data set. Choose a direction unit vector $\vec{n}$, to let the value of

$$\sum_{i=1}^{m}[(B_i - < B >) \bullet \mathbf{n}]^2 \tag{1}$$

be the minimum and maximum. Here $B_i$ is the $i$th vector, $< B >$ is the average field, $\sum$ denotes the sum over $i$. The minimization and maximization of Equation 1 are accomplished by the method of Lagrange multipliers, and this in turn can be set up as a matrix diagonalization (or eigenvalue) problem. The solutions of the matrix **M** are associated with the directions of maximum and minimum variance of the vector field $\vec{B}_i$. The minimum variance vector defines the boundary normal direction **n**. A third eigenvalue and eigenvector together with the maximum and minimum variance vectors completes the right-handed coordinate system.

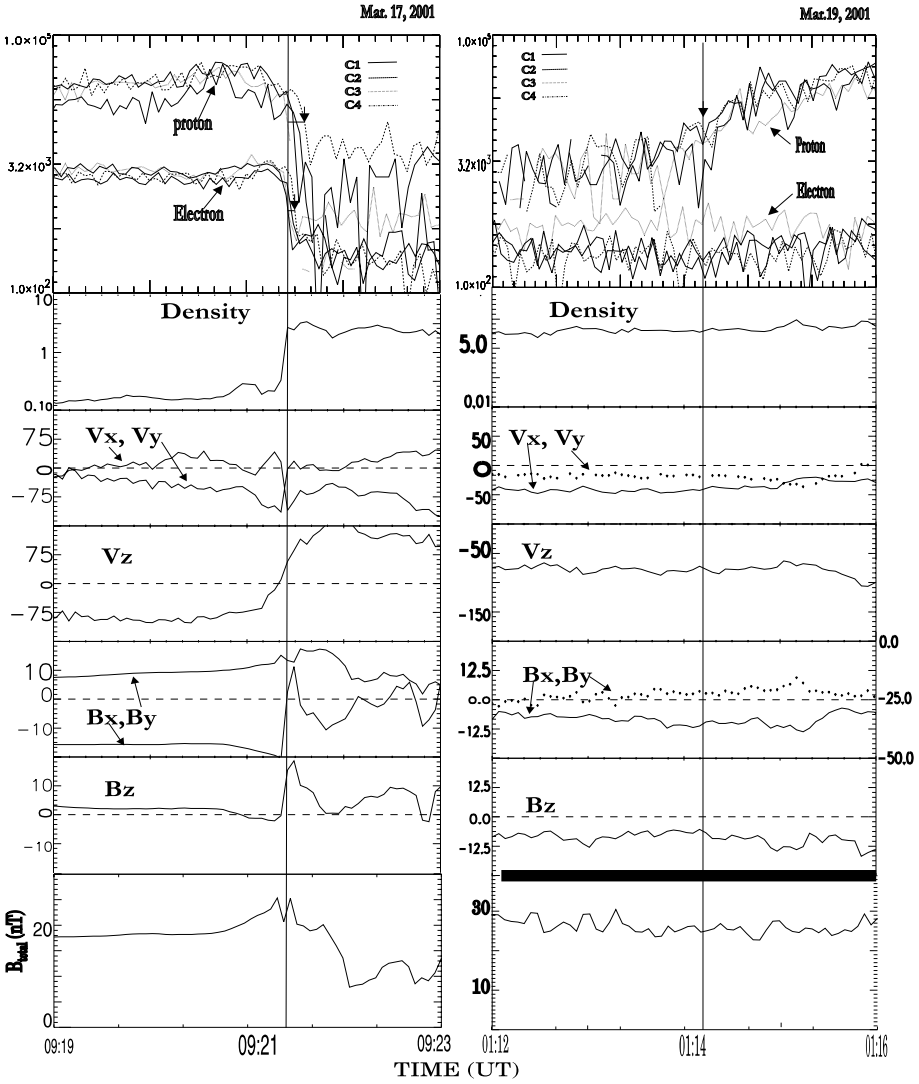


*Figure 7.* Interface crossings from the cusp region to the magnetosheath between 09:19 and 09:23 UT on 17 March 2001 during northward IMF (Left) and between 00:00 and 01:00 UT on 19 March 2001 during southward IMF (Right). From the top, the panels indicate integral electron and proton fluxes; plasma ion density, plasma ion velocity – $V_x$, $V_y$ and $V_z$ (in km/s), and superposed magnetic field $B_x$, $B_y$ and $B_z$ components for spacecraft 1 (Rumba).

The boundary crossings occurred starting from 09:21:20 UT to 09:22:30 UT. The value of the normal component is −1.8 nT. The directions of the boundary normal coordinates system (i.e., the eigenvectors) in GSE are given as follows: (1) the minimum variation direction ($B_x^*$) = (0.669 0.352

−0.654); (2) the intermediate variation direction $(B_y^*)$ = (−0.019 0.888 0.459); (3) the maximum variation direction $(B_z^*)$ = (0.743 −0.295 0.601). The ratio of the intermediate to minimum eigenvalue is 14.1; and $\frac{|B_z^*|}{B} = 0.12$. This indicates that the normal component for the boundary is well established (Sonnerup and Cahill, 1967; Lepping and Behannon, 1980). The magnetopause boundaries with $B_n \neq 0$ are referred to as rotational discontinuities (Landau and Lifshitz, 1960; Sonnerup and Ledley, 1979a). Thus, the magnetopause was a rotational discontinuity, indicating that high latitude reconnection was ongoing. For a rotational discontinuity, a non-vanishing normal magnetic field component, $B_n$, is allowed in a current sheet, which changes the physics of the current sheet dramatically. In a nonisotropic plasma, the pressure $P_{\parallel} \neq P_{\perp}$ and a change in the field magnitude on both sides of the discontinuity can occur as a result of changes in the pressure anisotropy factor (Hudson, 1970, 1971, 1973; Sonnerup and Ledley, 1979b ).

The variations of the energetic electron and ion fluxes for the boundary crossing recorded by all Cluster spacecraft from 01:12 to 01:16 UT, 19 March 2001 are given in Figure 7 Right. This boundary crossing was made in the southern hemisphere during southward IMF (see Figure 2). From Figure 7 Right, it can be seen that the flux of energetic ions increased after around 01:14 UT. After 01:14 UT, the Cluster satellites crossed from the magnetosheath into the cusp region. This energetic particle layer was observed simultaneously by all Cluster satellites. In this event, the plasma and magnetic field data show no significant difference, and there is no clear boundary layer that can be identified.

### 3.2. Energetic electrons and ions trapped in the cusp

The Cluster separation distances were around 600 km during the times of interest (16–19 March 2001). The remote-sensing ranges of the four spacecrafts for energetic ions overlap and the ion performance of the tetrahedron may be reduced to that of a single platform. However, the 30 keV electron gyroradii (even 100 keV) are always small compared with the size of the tetrahedron. The electron measurements obtained by the four different satellites can provide nearly instantaneous information about changes in the field configuration. The existing energetic electrons in the cusp region are vital in order to investigate the reconnection process because they are a rather reliable indicator for closed and open field line topology in the cusp region, and to where the flux tube is connected.

A 25 keV electron travels along field lines with a speed of nearly 14 $R_E$/s, so these swift electrons trace out field lines in a rather short time (a few seconds) in an open field line region. If an electron event exists for a few minutes, which is much longer than their bounce time (about 1.5 s for 25 keV electrons at $L = 8$), a resupply process must exist. If no stable energetic

electron fluxes are observed, this would indicate that the cusp has a general open field line geometry during southward IMF.

The observed energetic electrons cannot be accelerated by the reconnection process in the adjacent magnetopause. The magnetic tension at the magnetopause applied by reconnection can only add a velocity on the order of the Alfvén velocity, associated with the change in $\vec{B}$ across the magnetopause. For a 50 nT field rotated by 180°, $\Delta B$ is 100 nT. Assuming a typical hydrogen plasma density of 20 $cm^{-3}$, the Alfvén velocity is ≈490 km/s. For electrons this amounts to an energy gain of about 1 eV. However, the observed electrons have energies above 25 keV, which means that acceleration due to reconnection is negligible. Also, although it is claimed that the Fermi mechanism in the quasi-parallel bow shock region could accelerate incident solar wind ions to energies up to about 200 keV, it cannot accelerate electrons efficiently (Lee, 1982).

Further, during the period from 16 to 19 March 2001, there are no solar energetic electron events (Lin, 1985; Klassen et al., 2002) observed by the ACE satellite at the Lagrangian 1 point in interplanetary space (see Figure 5).

The possible mechanism is that the existence of an off-equatorial B-minimum in the outer cusp allows energetic particles starting from the equator region to be trapped in the high latitude magnetospheric region during quiet times. Energetic plasma sheet particles initially mirroring near the equator are expelled from low latitudes and subsequently swept into the boundary layer at high latitudes. Further, a particle will drift on a closed path around the front of the magnetosphere (cusp region). The importance of the existence of a minimum off equator in the outer cusp has been neglected or underestimated for a long period although it could be extreme importance for understanding the energetic particle in the magnetosphere.

According to the traditional dipole field model, the dayside high latitude or cusp region cannot trap particles (Roederer, 1970, 1977). The cusp region of the ideal dipole field is not an "excluded region" in the Störmer theory (Störmer, 1911). This means that, in the high latitude region, the particles cannot be trapped for much longer than the bounce time; the $E \times B$ drift will take the particles away. However, the dipole field can be modified fundamentally by interaction with the solar wind. The outer cusp regions where the magnetic field lines either close in the dayside sector or extend into the night side sector over the polar cap could be caused by reconnection, as proposed in the previous Section. This region is a region of weak magnetic field, which directly follows from the interaction of the solar wind with the geomagnetic field predicted by Chapman and Ferraro (1931) by using a simple image dipole, as shown by the magnetic field model of Antonova and Shabansky (1968) (see Figure 8). This has also been supported by *in situ* magnetic field

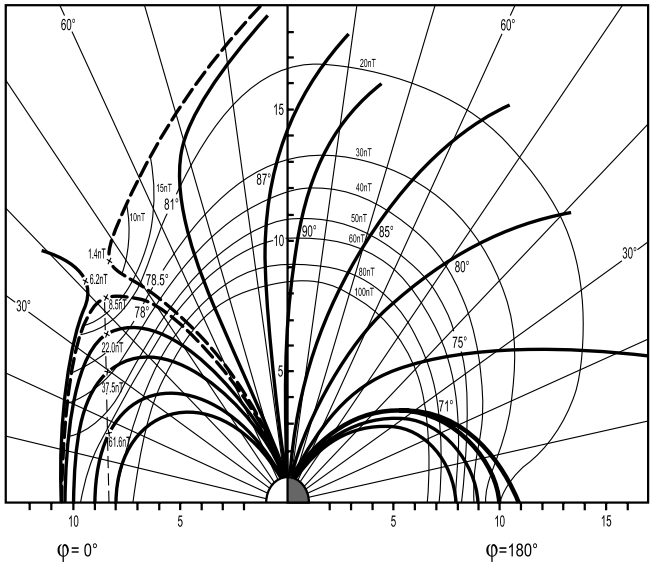


*Figure 8*. Meridional (noon-midnight) section for a modified two-dipole model (Antonova and Shabansky, 1968). The latitude $\phi$ is shown, at which the line of force with given equatorial distance crosses the Earth's surface. The narrow lines represent the lines of constant magnetic field.

measurements (Zhou et al., 1997). Instead of a dipolar field, the cusp region appears to be quadrupolar.

However, the importance of the existence of an off-equatorial B-minimum in the outer cusp has been underestimated for a long time, although it could be of extreme importance for understanding the behavior of energetic particles in the magnetosphere. Antonova and Shabansky (1968) and Shabansky (1968) noted that, with a minimum magnetic field existing off the equator in the outer cusp region (Figure 8), charged particles would not drift but rather branch off towards the magnetic field minimum at high latitudes. Shabansky (1971), Antonova and Shabansky (1975) and Antonova (1996) provided observational evidence for the trapping of energetic particles (of several tens of keV, up to a few hundreds of keV) in the high latitude region. Sheldon et al. (1998) pointed out that an energetic electron will drift on a closed path around the front of the magnetosphere, and found that electrons could be trapped in the outer cusp. In fact, a temporary trapping in the cusp field minimum was first examined by Delcourt et al. (1992). Further, Delcourt and Sauvaud (1998, 1999) pointed out that, under the effect of the cuspward mirror force near the dayside magnetopause, energetic plasma sheet particles initially mirroring near the equator are expelled from low latitudes and subsequently swept into the boundary layer at high latitudes.

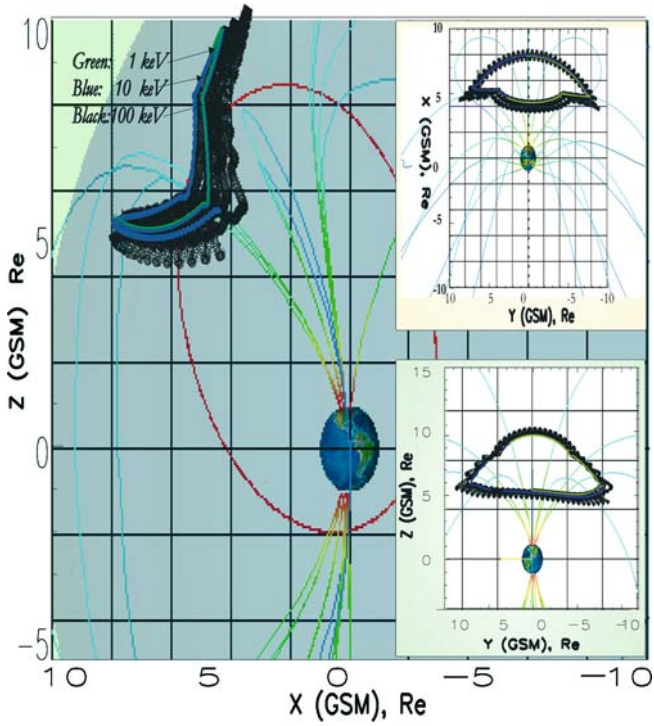


*Figure 9.* The trajectories of protons (1, 10 and 100 keV) with 90° pitch angle in the Tsyganenko 96 model magnetic field, showing trapping in the high latitude region. Magnetic fields are shown (weaker fields in blue); the Cluster orbit is shown in red.

Figure 9 shows trajectories of test protons (1, 10, 100 keV) launched with 90° pitch angle from the cusp region. The trajectory tracing was performed using the Tsyganenko 96 model. In this calculation, the full particle dynamics have been considered, not just the guding center computation (Sullivan, private communication, 2002); the calculation was performed using a fourth-order Runge–Kutta technique with a time step adjusted to some fraction of the particle gyration periods. It can be seen from Figure 9 that the test protons launched from the local minimum magnetic field region encircle the outer cusp region; all of the protons experience a pronounced bouncing motion in the high latitude region which differs from mirroring motion on either side of the equator (as ring current ions). Some selected parameters of the proton orbits are given in Figure 10.

Figure 9 shows that the ion trajectories in the outer cusp region are somewhat similar to those on L shells of a dipolar magnetic field. The limiting second invariant of these trapped orbits occurs when the mirror point $B_{\min}$ approaches the dayside equatorial field strength; in the local gradient field they drift away from the cusp. These ion trajectories exist both on the

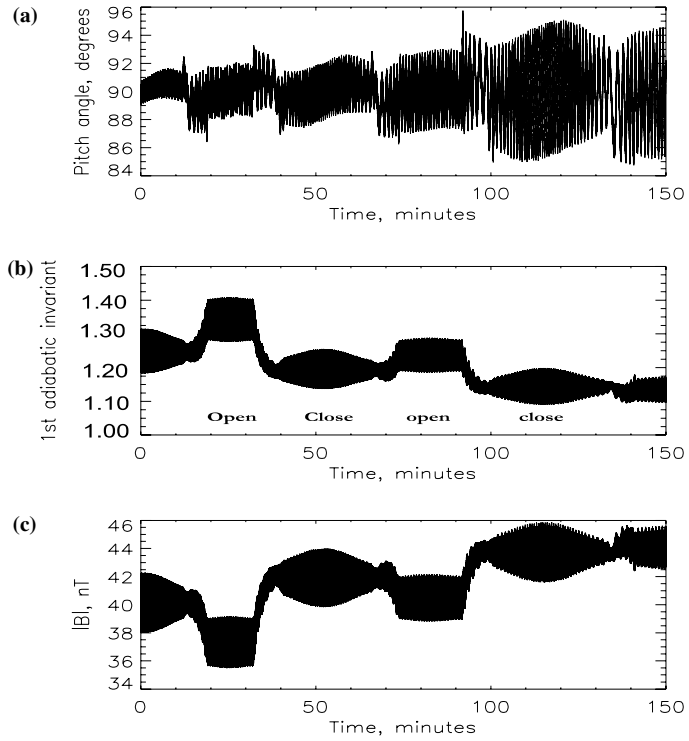


*Figure 10*. Selected parameters of 50 keV proton orbits shown in Figure 9: (a) pitch angle, (b) the first adiabatic invariant, (c) the total magnetic field experienced during its trajectory in the Tyganenko 96 model of the magnetic field. Regions of open and closed magnetic field are indicated.

dayside (equatorward, with closed magnetic field lines) and the mantel region (poleward, with open magnetic field lines). This behavior follows from the existence of a local $B_{\min}$ during the drift path from the closed field lines region to the open field line region in the frontside magnetosphere. The particles' behavior with different energies are shown in Table II.

It should be pointed out that large-scale magnetospheric convection is not accounted for in the present modeling results in the trajectory computation. If convection is accounted for, as pointed out by Delcourt and Sauvaud (1999), these closed drift paths in the outer cusp may be opened (see Figure 13 of Delcourt and Sauvaud (1999)). However, the present modeling results could apply to quiet times (northward IMF cases, as documented in Section 2.1) when magnetospheric convection is reduced and the convection electric field may be only 5% of its value during active times.

The results in this paper may offer an explanation for the presence of the electron boundary layer outside the magnetopause. The energetic electron layer ($>40$ keV) lying primarily outside the magnetopause is found at high

TABLE II
Some selected particle parameters of trapped motions near the cusp

| Energy keV | Period ($T$) min | $T_A$ (open) min | $\mu_A$ (open) keV/nT | $T_B$ (closed) min | $\mu_B$ (closed) keV/nT | Rigidity (nT Re) |
|---|---|---|---|---|---|---|
| 1 | 2580 | 1320 | 0.027 | 1260 | 0.025 | 0.72 |
| 5 | 520 | 380 | 0.14 | 140 | 0.13 | 1.60 |
| 10 | 265.2 | 160.9 | 0.27 | 104.4 | 0.25 | 2.27 |
| 25 | 107.6 | 63.6 | 0.67 | 44.0 | 0.63 | 3.59 |
| 50 | 52.2 | 32.6 | 1.35 | 19.6 | 1.25 | 5.07 |
| 100 | 26.1 | 16.3 | 2.7 | 9.8 | 2.5 | 7.17 |

latitudes near the dusk-dawn meridional plane and from the dayside to the distant magnetotail (Meng and Anderson, 1970, 1975; Baker and Stone, 1977a–c). The observed energetic electrons in the high latitude boundary region may be provided by tail plasma sheet particles because of a minimum magnetic field existing off equator in the high latitude region of the magnetosphere.

Delcourt and Sauvaud (1998, 1999) pointed out that under the effect of the cuspward mirror force near the dayside magnetopause, energetic plasma sheet particles initially mirroring near the equator are expelled from low latitudes and subsequently swept into the boundary layer at high latitudes. Both electrons and ions can be stably trapped in the high latitude region during quiet periods. This conclusion is supported by both the observations and the modeling results of the present paper. As magnetospheric convection is enhanced, the electrons initially trapped in the high latitude region could be de-trapped (Delcourt and Sauvaud, 1998, 1999). In fact, no stable trapped electrons were observed during active times (see Figure 6). These de-trapped electrons could further form an electron layer just outside the magnetopause as observed (see, e.g., Meng and Anderson, 1970 and Baker and Stone, 1977a–c).

## 4. Summary and conclusion

Energetic electrons (20–400 keV) present in the high latitude region (including the cusp) have been examined in detail by using Cluster/RAPID data for four consecutive high latitude/cusp crossings between 16 March and 19 March 2001. Energetic electrons with high fluxes were observed in the time interval when the IMF had a predominantly positive $B_z$ component. No stable energetic electron fluxes were observed during southward IMF, indicating that the cusp had an open field line geometry. High latitude magne-

tospheric (both North and South cusps) regions are able to trap energetic particles. The existence of an off-equatorial $B_{min}$ in the outer cusp allows energetic particles to be trapped in the high latitude magnetospheric region during quiet times. The main observational facts can be summarized as:

1. Energetic ions were observed in the high latitude magnetospheric region for all four crossings, no matter whether the IMF was southward or northward;
2. Stably trapped energetic electrons were observed only during northward IMF. In contrast to the ions, there were no stable electron fluxes observed in the cusp region during southward IMF. For northward IMF, the entry layer was composed of closed field lines which maintain energetic electrons. Energetic electrons found in the high latitude regions were associated with lower plasma densities and without an obvious tailward plasma flow. In the same location, during southward IMF, the electrons were not present in a region of high plasma density which was associated with a clear tailward flow.
3. There was a clear boundary between the cusp and magnetosheath during the northward IMF cases. The magnetopause has been identified as a rotational discontinuity, indicating that high latitude reconnection is ongoing. The interface between the cusp and magnetosheath during southward IMF was not very clear, with energetic ions exhibiting flux enhancements.
4. No stably trapped energetic electrons have been observed during southward IMF, indicating that the cusp has an open field line geometry.
5. The observations show that the observed electrons were locally trapped. These energetic electron observations provide new evidence to understand the dynamic nature of cusp processes.

## Acknowledgements

We acknowledge the effort of the teams which made important data sets available on web sites such as http://cdaweb.gsfc.nasa.gov/cdaweb (Dst, IMF $B_z$, and solar wind density) and http.//leadbell.lanl.govl/(geostationary electron data). One of authors (Q.-G. Z.) thanks H. Petschek and G. Siscoe for many helpful discussions.

## References

Anderson, K. A., Harris, H. K., and Paoli, R. J.: 1965, 'Energetic electron fluxes in and beyond the earth's Outer magnetosphere', *J. Geophys. Res.* **70**, 1039–1050.

Antonova, A. E.: 1996, 'High-latitude particle traps and related phenomena', *Radiat. Meas.* **26**(3), 409–411.

Antonova, A. E., and Shabansky, V. P.: 1968, 'Structure of the geomagnetic field at great distance from the Earth', *Geomagn. Aeron.* **8**, 801–811.

Antonova, A. E., and Shabansky, V. P.: 1975, 'Particles and the magnetic field in outer noon magnetosphere of the Earth', *Geomagn. Aeron.* **15**, 243–247.

Aparcio, B., Thelin, B., and Lundin, R.: 1991, 'The polar cusp from a particle point of view: A statistical study based on the Viking Data', *J. Geophys. Res.* **96**, 14023–14031.

Baker, D. N., and Stone, E. C.: 1977a, 'The Magnetopause Electron Layer along the Distant Magnetotail', *Geophys. Res. Lett.* **4**, 133–136.

Baker, D. N., and Stone, E. C.: 1977b, 'The Magnetopause Electron Layer along the Distant Magnetotail', *Geophys. Res. Lett.* **4**, 395–398.

Baker, D. N., and Stone, E. C.: 1977c, 'The Magnetopause Energetic Electron Layer 1. Observations Along the Distant Magnetotail', *Geophys. Res. Lett.* **4**, 395–398.

Balogh, A., Dunlop, M. W., Cowley, S. W. H., Southwood, D. J., Thomlinson, J. G., Glassmeier, K. H., Musmann, G., Luhr, H., Buchert, S., Acuna, M. H., Fairfield, D. H., Slavin, J. A., Riedler, W., Sachwingenschuh, K., and Kivelson, M. G.: 1997, 'The Cluster Magnetic Field Investigation', *Space Sci. Rev.* **79**, 65–91.

Bieber, J. W., Stone, E. C., Hones, E. W., Baker, D. N., and Bame, S.J.: 1982, 'Plasma behaviour during energetic electron streaming events further evidence for substorm-associated magnetic reconnection', *Geophys. Res. Lett.* **9**, 664–667.

Chang, S. W., Scudder, J. D., Fuselier, S. A., Fennell, J.F., Tratter, K. J., Pickett, J. S., Spence, H. E., Menietti, J. D., Peterson, W. K., Lepping, R. P., and Friedel, R.: 1998, 'Cusp energetic ions: A bow shock source', *Geophys. Res. Lett.* **25**, 3729–3732.

Chang, S. W., Scudder, J. D., Fuselier, S. A., Fennell, J. F., Tratter, K. J., Pickett, J. S., Spence, H. E., Menietti, J. D., Peterson, W. K., Lepping, R. P., and Friedel, R.: 2000, 'Energetic magnetosheath ions connected to the Earth's bow shock: Possibile source of CEP's', *J. Geophys. Res.* **105**, 5471–5488.

Chapman, S., and Ferraro, V. C. A.: 1931, 'A new theory of magnetic storms', *Terr. Magn. Atmos. Elect.* **36**, 171–186.

Chen, J., Fritz, T. A., Sheldon, R. B., Spence, H. E., Spjeldvik, W. N., Fennell, J. F., and Livi, S.: 1997, 'A New, temporarily confined population in the polar cap during the August 27, 1996 geomagnetic field distortion period', *Geophys. Res. Lett.* **24**, 1447–1450.

Delcourt, D. C., Moore, T. E., Sauvaud, J. A., and Chappell, C. R.: 1992, 'Nonadiabatic transport features in the outer cusp region', *J. Geophys. Res.* **97**, 16833–16842.

Delcourt, D. C., and Sauvaud, J. A.: 1998, 'Recirculation of plasma sheet particles into the high-latitude boundary layer', *J. Geophys. Res.* **103**, 26521–26532.

Delcourt, D. C., and Sauvaud, J. A.: 1999, 'Populating of Cusp and Boundary Layers by energetic (hundreds of keV) equatorial particles', *J. Geophys. Res.* **104**, 22635–22648.

Dunlop, M. W., and Woodward, T. I.: 1998, 'Multi Spacecraft Discontinuity Analysis', in G.. Paschmann, and P. W. Daly (eds.), *Analysis Methods for Multi Spacecraft Data*, ESA, Bern, Switzerland, pp. 271–305.

Eastman, T. E.: 1976, 'The Plasma Sheet Boundary Layer', *Geophys. Res. Lett.* **3**, 685–688.

Eccles, A. A., and Fritz, T. A.: 2002, 'Energetic Particle Observations at the subsolar magnetopause', *Ann. Geophys.* **20**, 445–460.

Elphic, R. C., and Russell, C. T.: 1983, 'Magnetic Flux Ropes in the Venus Ionosphere: Observations and Models', *J. Geophys. Res.* **88**, 58–72.

Formisano, V.: 1979, 'Properties of Energetic Electrons of Magnetospheric Origin in the Magnetosheath and in the Solar Wind', *Planet. Space Sci.* **27**, 867–879.

Fritz, T. A.: 2000, 'The Role of the Cusp as a Source for Magnetospheric Particles: A New Paradigm', in *Proceedings of the Cluster-II workshop on Multiscale/Multipoint Plasma Measurements* ESA, SP 449, pp. 203–209.

Fritz, T. A.: 2001, 'The Cusp as a Source of Magnetospheric Energetic Particles, Currents, and Electric Fields: New Paradigm', *Space Sci. Rev.* **95**, 469–488.

Fritz, T. A., Baker, D. N., McPherron, R. L. and Lennartsson, W.: 1984, 'Impilcation of the 11:00 UT March 22, 1979 CDAW 6 Substorm Event for the Role of Magnetic Reconnection in the Geomagnetic Tail', in E. W. Hones (ed.), *Magnetic Reconnection in Space and Laboratory Plasmas*, AGU Geophysical Monograph 30, pp. 203–207.

Fritz, T. A., Chen, J., Sheldon, R. B., Spence, H. E., and Fennell, J. F.: 1999, 'Cusp Energetic Particle Events Measured by POLAR Spacecraft', *Phys. Chem. Earth* **24**, 135–140.

Haerendel, G.: 1978, 'On the 3-Dimensional Structure of Plasmoids', *J. Geophys. Res.* **83**, 3195–3216.

Hapgood, M. A.: 1992, 'Space Physics Coordinate Transformations: A User Guide', *Planet. Space Sci.* **40**, 711–717.

Haskell, G. P.: 1969, 'Anisotropic Fluxes of Energetic Particles in the outer Magnetosphere', *Planet. Space Sci.* **74**, 1740–1748.

Hones, E. W., Akasofu, S. I., Bame, S. J., and Singer, S.: 1972, 'Outflow of Plasma from the Magnetotail into Magnetosheath', *J. Geophys. Res.* **77**, 6688–6695.

Hudson, P. D.: 1970, 'Discontinuites in an Anisotropic Plasma and Their Identification in the Solar Wind', *Planet. Space Sci.* **18**, 1611–1622.

Hudson, P. D.: 1971, 'Rotational Discontinuites in an Anisotropic Plasma', *Planet. Space Sci.* **19**, 1693–1699.

Hudson, P. D.: 1973, 'Rotational Discontinuites in an Anisotropic Plasma-II', *Planet. Space Sci.* **21**, 475–483.

Klassen, A., Bothmer, V., Mann, G., Reiner, M. J., Krucker, S., Vourlidas, A., and Kunow, H.: 2002, 'Solar Energetic Electron Events and coronal Shocks', *Astron. Astrophys.* **385**, 1078–1088.

Kremser, G., and Lundin, R.: 1990, 'Average Spatial Distributions of Energetic Particles in the Midaltitude Cusp/Cleft Region Observed by Viking', *J. Geophys. Res.* **95**, 5753–5766.

Kremser, G., Woch, J., Mursula, K., Tanskanen, P., Wilken, B., and Lundin, R.: 1995, 'Origin of Energetic Ions in the Polar Cusp Inferred from Ion Composition Measurements by the Viking Satellite', *Ann. Geophys.* **13**, 595–607.

Landau, L. D., and Lifshitz, E. M.: 1960, *Electrodynamics of Continuous Media*, Pergamon Press, Oxford.

Lee, M. A.: 1982, 'Coupled Hydromagnetic Wave Excitation and Ion Acceleration Upstream of the Earth's Bow Shock', *J. Geophys. Res.* **87**, 5063–5080.

Lepping, R. P., and Behannon, K. W.: 1980, 'Magnetic Field Directional Discontinuities, 1, Minimum Variance Errors', *J. Geophys. Res.* **85**, 4695–4703.

Lin, R. P.: 1985, 'Energetic Solar Electrons in the Interplanetary Medium', *Sol. Phys.* **100**, 537–561.

Lundin, R.: 1985, 'Plasma Composition and Flow Characteristic in the Magnetospheric Boundary Layers connected to the Polar Cusp', in J.A. Holtet, and A. Egeland (eds.), *The Polar Cusp*, Kluwer Academic Publishers, Dordrecht, The Netherlands, pp. 9–32.

Lundin, R., and Dubinin, E. M.: 1985, 'Solar Wind Energy Transfer Regions inside the Dayside Magnetopause: Accelerated Heavy Ions as Tracers for MHD-Processes in the Dayside Boundary Layer', *Planet. Space Sci.* **33**, 891–907.

Meng, C. I., and Anderson, K. A.: 1970, 'A Layer of Energetic Electrons ( > 40 keV) near the Magnetopause', *J. Geophys. Res.* **75**, 1827–1836.

Meng, C. I., and Anderson, K. A.: 1975, 'Characteristics of the Magnetopause Energetic Electrons Layer', *J. Geophys. Res.* **80**, 4237–4243.

Meng, C. I., Lui, A. T. Y., Krimigis, S. M., Ismail, S., and Williams, D. J.: 1981, 'Spatial Distribution of Energetic Particles in the Distant Magnetotail', *J. Geophys. Res.* **86**, 5682–5700.

Newell, P. T., and Meng, C. I.: 1987, 'Cusp Width and $B_z$: Observations and a Conceptual Model', *J. Geophys. Res.* **92**, 13673–13678.

Newell, P. T., and Meng, C. I.: 1988, 'The Cusp and the Cleft/Boundary Layer: Lower-Altitude Identification and Statistical Local Time Variation', *J. Geophys. Res.* **93**, 14549–14556.

Newell, P. T., and Meng, C. I.: 1998, 'Open and Closed Low Latitude Boundary Layer', in J. Moen, A. Egeland, and M. Lockwood (eds.), *Polar Cap Boundary Phenomena*, Kluwer Academic Publishers, Dordrecht, The Netherlands, pp. 91–101.

Paschmann, G., Haerendel, G., Sckopke, N., and Rosenbauer, H: 1976, 'Plasma and Field Characteristics of the Distant Polar Cusp near Local Noon: The Entry Layer', *J. Geophys. Res.* **81**, 2883–2899.

Reme, H., Bosqued, J. M., Sauvaud, J. A., Cros, A., Dandouras, J., Aoustin, C., Bouyssou, J., Camus, T., Cuvilo, J., Martz, C., Medale, J. L., Perrier, H., Romefort, D., Rouzaud, J., d'Uston, C., Mobius, E., Crocker, K., Granoff, M., Kistler, L. M., Popecki, M., Hovestadt, D., Klecker, B., Paschmann, G., Scholer, M., Carlson, C. W., Curtis, D. W., Lin, R. P., McFadden, J. P., Formisano, V., Amata, E., Bavassano-Cattaneo, M. B., Baldetti, P., Belluci, G., Bruno, R., Chionchio, G., DiLellis, A., Shelley, E. G., Ghielmetti, A. G., Lennartsson, W., Korth, A., Rosenbauer, H., Lundin, R., Olsen, S., Parks, G. K., McCarthy, M., and Balsiger, H.: 1997, 'The Cluster Ion Spectrometry(CIS) Experiment', *Space Sci. Rev.* **79**, 303–350.

Roederer, J. G.: 1970, *Dynamics of Geomagnetically Trapped Radiation*, Springer-Verlag, New York.

Roederer, J. G.: 1977, 'Global Problems in Magnetospheric Plasma Physics and Prospects for Their Solution', *Space Sci. Rev.* **21**, 23–70.

Rosenbauer, H.: 1975, 'A Boundary Layer Model for Magnetospheric Substorms', *J. Geophys. Res.* **80**, 2723–2737.

Sckopke, N., Paschmann, G., Haerendel, G., Sonnerup, B. U., Bame, S. J., Forbes, T. G., Hones, J. E. W., and Russell, C. T.: 1981, 'Structure of the Low Latitude Boundary Layer', *J. Geophys. Res.* **86**, 2099–2110.

Sckopke, N., Paschmann, G., Rosenbauer, H., and Fairfield, D. H.: 1976, 'Influence of the Interplanetary Magnetic Field on the Occurrence and the Thickness of the Plasma Mantle', *J. Geophys. Res.* **81**, 2687–2691.

Shabansky, V. P.: 1968, 'Magnetospheric Process and Related Geophysical Phenomena', *Space Sci. Rev.* **8**, 366–454.

Shabansky, V. P.: 1971, 'Some Process in the Magnetosphere', *Space Sci. Rev.* **12**, 299.

Sheldon, R. B., Spence, H. E., Sullivan, J. D., Fritz, T. A., and Chen, J.: 1998, 'The Discover of Trapped Energetic Electrons in the Outer Cusp', *Geophys. Res. Lett.* **25**, 1825–1828.

Sonnerup, B. U. O.: 1976, 'Magnetopause and Boundary Layer', in D. J. Williams (ed.), *Physics of Solar Planetary Environment*, A.G.U., Washington D.C., pp. 541–557.

Sonnerup, B. U. O., and Cahill, L. J.: 1967, 'Magnetopause Structure and Attitude from Explorer 12 Observations', *J. Geophys. Res.* **72**, 171–183.

Sonnerup, B. U. O. and Ledley B. G.: 1979a, 'Electromagnetic Structure of the Magnetopause and Boundary Layer', in *Proceedings of Magnetospheric Boundary Layers Conference*, Alpbach, ESA SP-148, pp. 401–411.

Sonnerup, B. U. O., and Ledley, B. G.: 1979b, 'Ogo 5 Magnetopause Structure and Classical Reconnection', *J. Geophys. Res.* **84**, 399–405.

Spreiter, J. R., and Stahara, S. S.: 1980, 'A New Predictive Model for Determining Solar Wind–Terrestrial Planet Interactions', *J. Geophys. Res.* **85**, 6769–6777.

Spreiter, J. R., and Summers, A.L.: 1967, 'On Conditions near the Neutral Points on the Magnetosphere Boundary', *Planet. Space Sci.* **15**, 787–798.

Störmer, C.: 1911, 'Sur les trajectories des corpuscules electrises dans L'esspace sous 1' actions des magnetisme terrestreavec appication aux auarores boreales, secondee memoire', *Arch. Sci. Phys. Nat. Ser. 4* **32**, 117–123.

Trattner, K. J., Fuselier, S. A., Peterson, W.K., Chang, S. W., Friedel, R., and Aellig, M. R.: 2001, 'Origins of energetic ions in the cusp', *J. Geophys. Res.* **106**, 5967–5976.

West, H. I., and Buck, R. M.: 1976, 'Observations of $>100$ keV protons in the Earth's Magnetosheath', *J. Geophys. Res.* **81**, 569–584.

Wilken, B., Axford, W. I., Daglis, I., Daly, P., Guttler, W., Ip, W. H., Korth, A., Kremser, G., Livi, S., Vasyliunas, V. M., Woch, J., Baker, D., Belian, R. D., Blake, J.B., Fennell, J. F., Lyons, L. R., Borg, H., Fritz, T. A., Gliem, F., Rathje, R., Grande, M., Hall, D., Kecsuemety, K., McKenna-Lawlor, S., Mursula, K., Tanskanen, P., Pu, Z., Sandahl, I., Sarris, E. T., Scholer, M., Schulz, M., Sorass, F., and Ullaland, S.: 1997, 'RAPID: The Imaging Energetic Particle Spectrometer on Cluster', *Space Sci. Rev.* **79**, 399–473.

Yamauchi, M., and Lundin, R.: 1998, 'Physical Signatures of Magnetospheric Boundary Layer Processes', in J. A. Holtet, and A. Egeland (eds.), *Physical Signatures of Magnetospheric Boundary Layer Processeses*, Kluwer Academic Publishers, Dordrecht the Netherlands, pp. 99–109.

Zhou, X.-W., Russell, C. T., Le, G., and Tsyganenko, N.: 1997, 'Comparison of Observed and Model Magnetic Fields at High Altitudes above the Polar Cap: Polar Initial Results', *Geophys. Res. Lett.* **24**, 1451–1454.

Zong, Q.-G., Fritz, T. A., Spence, H., Dunlop, M., Balogh, A., Korth, A., Daly, P. W., Pu, Z. Y., and Reme, H.: 2003, 'Bursty Energetic Electrons in the Cusp Region', *Planet. Space Sci.* **51**, 821–830.

Zong, Q.-G., Fritz, T. A., Wilken, B., and Daly, P. W.: 2002, 'Energetic Ions in the High Latitude Boundary Layer of the Magnetosphere – RAPID/Cluster Observation', in P.T. Newell, and T. G. . Onsager (eds.), *The Lower-Latitude Boundary Layer*, AGU, Washington, DC, pp. 101–110.

Zong, Q.-G., and Wilken, B.: 1998, 'Layered Structure of Energetic Oxygen Ions in the Magnetosheath', *Geophys. Res. Lett.* **25**, 4121–4124.

Zong, Q.-G., Wilken, B., Fu, S. Y., Fritz, T. A., Pu, Z. Y., Hasebe, N., and Williams, D. J: 2001, 'Ring Current Oxygen Ions in the Magnetosheath Caused by Magnetic Storm', *J. Geophys. Res.* **106**, 25541–25556.

Surveys in Geophysics (2005) 26: 241–254
DOI 10.1007/s10712-005-1881-5 © Springer 2005

# ENERGETIC PARTICLES OBSERVED IN THE CUSP REGION DURING A STORM RECOVERY PHASE

S. Y. FU[1], Q. G. ZONG[2], Z. Y. PU[1], C. J. XIAO[1], A. KORTH[3], P. DALY[3] and H. REME[4]

[1]*School of Earth and Space Sciences, Peking University, Beijing, 100871 China*
*E-mail: suiyanfu@pku.edu.cn;*
[2]*CSP, Boston University, Boston, USA;*
[3]*Max-Planck Institut fuer Aeronomie, Katlenburg-Lindau, Germany;*
[4]*CESR, BP 4346, 31028 Toulouse Cedex 4, France*

(Received 26 January 2003; Accepted 30 April 2004)

**Abstract.** In this paper we report energetic ion behavior and its composition variations observed by the Cluster/RAPID instrument when the spacecraft was travelling in the high latitude magnetospheric boundary region on the day of the 31 March, 2001, strongest magnetic storm in the past 50 years. The Dst index reached −360 nT at about 09:00 UT. During its early recovery phase, large amounts of oxygen and helium ions were observed; the ratio of oxygen to hydrogen in the RAPID energy range reached as high as 250%, which suggests that the observed energetic particles might be of magnetospheric origin. The observations further show that enhanced energetic electron fluxes are confined in a very narrow region, while protons have occupied a larger region, and heavy ions have been observed in an even larger region. The flux of energetic electrons show a slight enhancement in a region where the magnetic field magnitude is around zero. These observed energetic ions could be quasi-trapped by the current sheet in the stagnation region of the cusp.

**Keywords:** cusp, current sheet, energetic particles, ion composition, stagnation region

**Abbreviations:** CIS – Cluster Ion Spectrometer; CME – Coronal Mass Ejection; FGM – Fluxgate Magnetometer; GSE – Geocentric Solar Ecliptic; IMF – Interplanetary Magnetic Field; RAPID – Research with Adaptive Particle Imaging Detectors; S/C – Spacecraft

## 1. Introduction

The polar cusp has been a hot research topic as Polar and Cluster spacecraft produce a large amount of new data. It is now believed that the magnetospheric cusp region is not a small region, but a large and dynamic region extending in three-dimensions. It is marked by a very noticeably reduced magnetic field magnitude, with broadband electrostatic and electromagnetic waves. Very energetic electrons (up to MeV) could be trapped in the topo-

logical magnetic field minimum point around outer cusp (Sheldon et al., 1998). The origin of the energetic particles in the cusp region is still an open question. There are three different sources which could provide energetic particles in the cusp vicinity; one is the shocked solar wind (e.g., Trattner et al., 2001), another is magnetospheric leakage and the other is local acceleration (e.g., Fritz, 2000). Very little is known of the high latitude boundary layer compared with the region around the subsolar point. In the reconnection model, magnetic field lines merge at the dayside magnetopause and convect across the cusp into the mantle (Dungey, 1961; Lockwood and Smith, 1992). In such a model, the position and extension of the cusp depend strongly on the interplanetary magnetic field (IMF). When the IMF is northward, the reconnection process could happen in the vicinity of the cusp region (Dungey, 1961; Crooker, 1986; Song and Russell, 1992). During periods of extended northward IMF, the convection in the high latitude boundary-layer region is sunward and has been termed "Reverse Convection" (Crooker, 1992). Sunward convection flow has been reported by the DMSP satellites and the cusp can extend to rather low latitudes during northward IMF $B_z$ (Newell and Meng, 1987). Another important feature of high latitude reconnection is that it could open up a path for changed particles to enter the magnetosphere or escape from the magnetosphere (Zong et al., 2002). However, no matter where these energetic particles come from, there must be a mechanism which can trap or maintain them for a rather long time, or else they are being supplied continuously by a source.

As we already know, the interaction between the solar wind and the Earth's magnetosphere takes place over a narrow current sheet known as the magnetopause. Transport of mass, energy and momentum across this boundary remains one of the fundamental areas of research in space physics. The role of the current sheet in the high latitude region, including the cusp region, has been neglected or underestimated although it could be extremely important for understanding the dynamic processes occurring. Is there any difference in the current sheet for northward IMF and for southward IMF in the cusp region? What is the role of the current sheet during northward IMF? Few papers have addressed such a question to date.

The strongest storm in the past 50 years was recorded on 31 March 2001. The Dst index reached −360 nT at about 09:00 UT. This storm was triggered by a coronal mass ejection (CME), and many detailed features of this giant magnetic storm have been observed by the Cluster mission. In this paper, we focus only on its early recovery phase between 11:00–15:00 UT on 31 March 2001, when the Cluster spacecraft was travelling in the high latitude region – crossing the tail lobe, plasma mantle, the cusp region and the boundary layer. The data discussed here are obtained with the energetic particle detector RAPID onboard Cluster. The detail of the instrument can be found in the paper by Wilken et al. (1997). The Cluster spacecraft has recorded large

fluxes of high-energy particles, which are supposed to be coming out of the magnetosphere through high latitude reconnection. It is implied that the cusp current sheet might have played an important role in maintaining these energetic particles in this region.

## 2. Observations

The data to be presented here are obtained by the RAPID instrument on board the Cluster spacecraft (Wilken et al., 1997). The energetic particle spectrometer RAPID in the Cluster payload features novel detection principles both for ions and electrons. For either species the instrument measures the vector velocity ($V$) and the energy ($E$). The ion detector heads (IIMS) are composed of a time-of-flight (TOF)/energy ($E$) telescope with a solid state detector (SSD) as the back element. Species identification comes from the function $ET^2 = A$ with $E$ and $T$ denoting the measured quantities of energy and time-of-flight (equivalent to the particle velocity), $A$ is the atomic mass of the particle. The energy range extends from 30 to 4000 keV. The advanced design of the telescope as a projection camera which returns information on the particle direction of incidence, with 12 angular intervals over a 180° field-of-view. A second detector system, the imaging electron spectrometer (IES), is dedicated to electrons between 20 and 400 keV. The IES head uses the optical principle of a pinhole camera with 9 angular intervals over 180°. Together with a sectored spin plane of the spacecraft, both systems cover the unit sphere in velocity space in a contiguous manner. Furthermore, we use magnetometer measurements from the fluxgate magnetometer (FGM) on board Cluster, which makes high resolution vector field measurements (Balogh et al., 1997) and plasma data from the Cluster Ion Spectrometer (CIS) experiment (Reme et al., 1997). The time resolution of the data used in this paper is 4 s and the coordinate system is the GSE system. The criteria of the region identification in this paper is mainly based on the energetic particle behavior together with the plasma and magnetic field data.

During interval 11:00–15:00 UT, on 31 March 2001, when a CME-driven strong magnetic storm (−360 nT at 09:00 UT) was in its early recovery phase, four Cluster spacecraft were travelling through the lobe/mantle, crossing the cusp region and entering the boundary layer. Figure 1 shows the orbit of the spacecraft during this time period and also their locations relative to each other.

Figure 2 shows the event overview obtained by Cluster S/C1. The panels from top to bottom are the azimuthal angle distribution of ions, flux of protons ($>30$ keV), helium ions ($>50$ keV) and CNO group of ions ($>100$ keV). The two dashed lines indicate the time interval in which the flux of energetic particles showed an obvious enhancement. The magnetic field magnitude decreases, with strong fluctuations, in this time period.

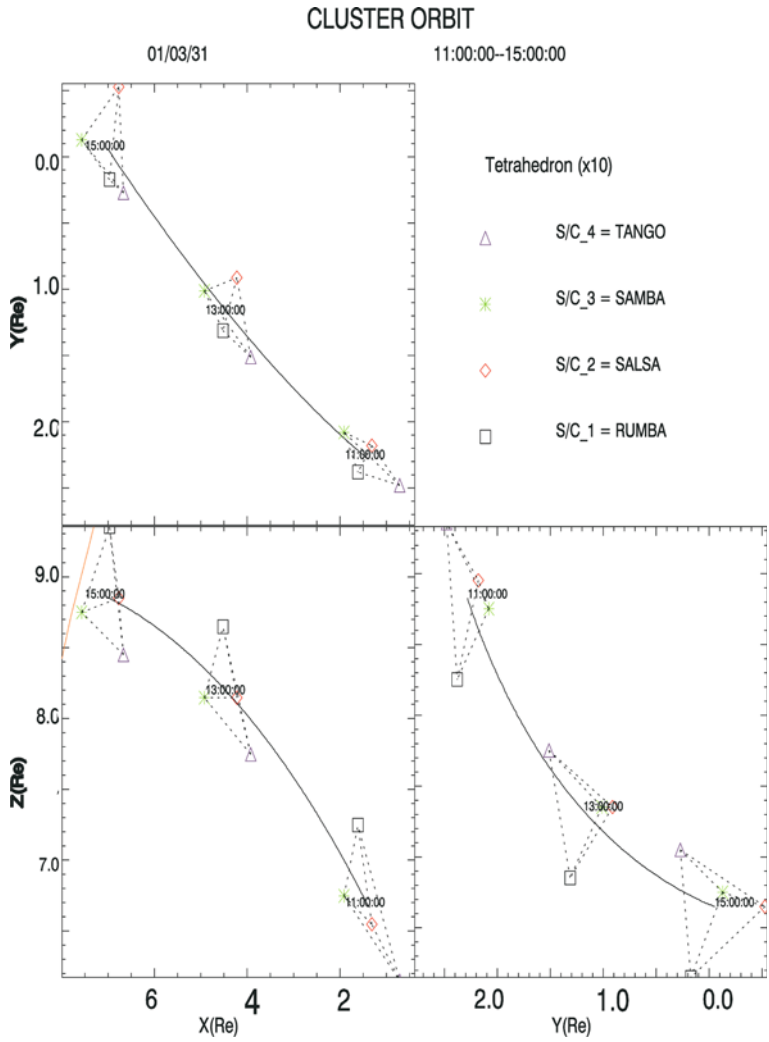


*Figure 1.* The orbit of the Cluster spacecraft in the interval from 11:00–15:00 UT, on 31 March, 2001.

As we can see from Figure 2, the proton flux increases by one order of magnitude in the central cusp region (where the magnetic field is rather weak, with $B < 60$ nT). There are many helium and heavy ions (mainly oxygen ions) after 11:38 UT. The fluxes of helium ions and heavy ions are each around $10^5$ cm$^{-2}$ s$^{-1}$ sr$^{-1}$ keV$^{-1}$ and almost reaching the flux of protons at their peak values.

As seen from the bottom four panels, the magnetic field $B_y$ and $B_z$ components detected by Cluster in the cusp region have the same variation profiles as the IMF $B_y$ and $B_z$ obtained by ACE satellite at the L1 Lagrangian

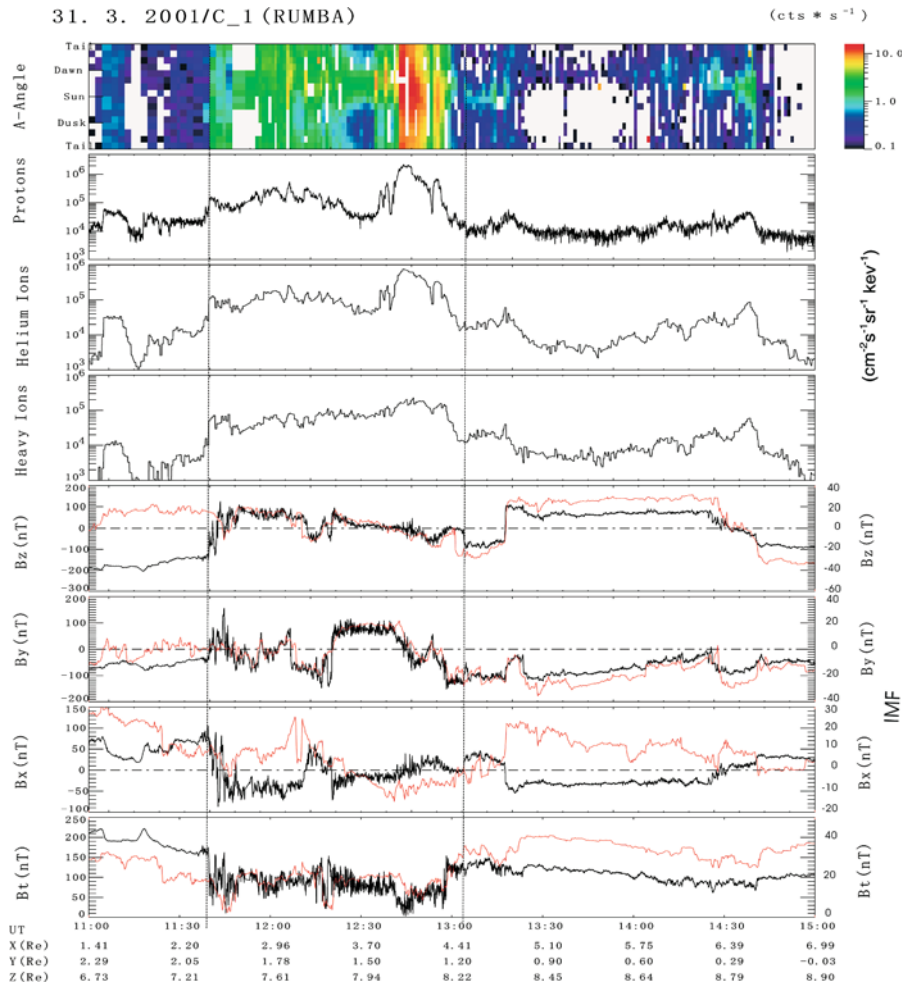


*Figure 2.* Overview of the event. The panels from top to bottom show the azimuthal angle distribution of all ions, flux of protons, helium ions and heavy ions (CNO group, m > 4), three magnetic field components and magnetic field magnitude.

point (220 $R_E$ upstream from the Earth), indicating the magnetic field $B_y$ and $B_z$ components in the cusp are mainly a result of the IMF orientation. In order to see what happens in the transition region, we show ion flow velocity, ion density from the Cluster Ion Spectrometry (CIS) experiment and magnetic field magnitude from Flux Gate Measurements (FGM) onboard S/C1 and S/C4 in Figure 3.

There are no plasma data obtained by S/C2. High speed plasma flows observed by the other three satellites begin at about 11:38 UT when they are all in the plasma mantle, and end at about 11:50 UT when they are in the

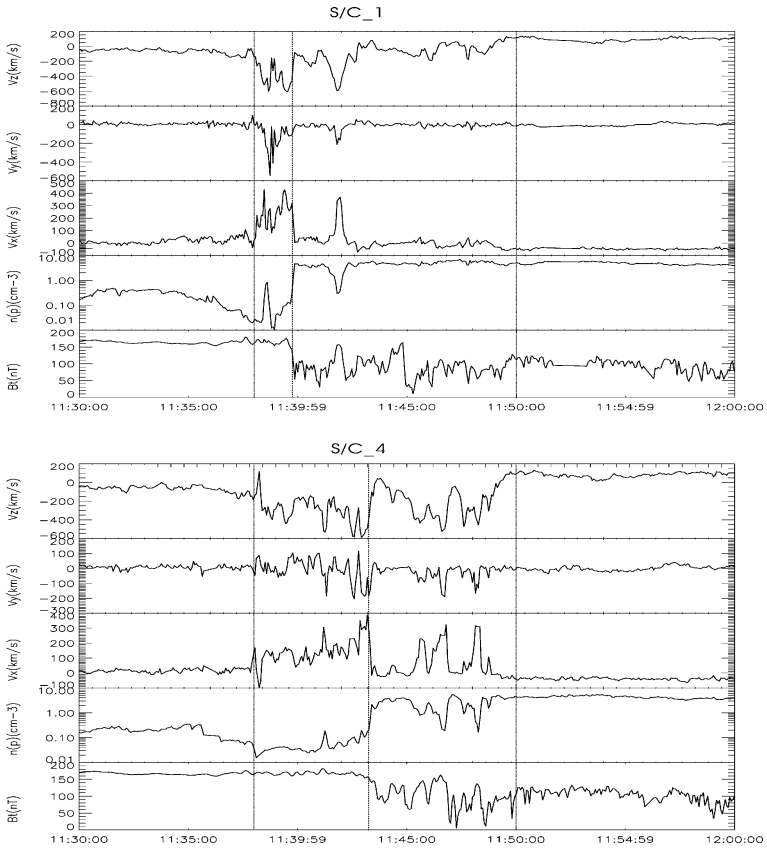


*Figure 3.* Ion flow velocity, ion density and magnetic field magnitude observed by S/C1 and S/C4. The vertical lines indicate the time interval in which strong fluctuations of the plasma flow velocity are observed. The line between them shows when the magnetic field magnitude and number density of protons change suddenly.

cusp. The time series of the number density of protons obtained by CIS (Panels 4 and 9 from the top) indicate that this transition region is the boundary between the plasma mantle and cusp.

More careful examination of the data shows that the four spacecraft, instead of observing very similar variations both in the magnetic field and the plasma flow velocity, have recorded different timings. The ion flow recorded on S/C1 lasted about 2 min until the satellite enters a very variable region at 11:40 UT with $X = 2.43\mathrm{R}_E$, $Y = 1.97\mathrm{R}_E$, $Z = 7.33\mathrm{R}_E$ in GSE coordinates. The nearby S/C3 observed similar features to those recorded by S/C1 at almost the same time (not shown here). S/C4 encountered the cusp region at about 11:43 UT and its position in GSE coordinate system is (2.43, 1.96, 7.27) at this time which is at a slightly lower altitude (GSE-Z) than S/C1 when it entered the boundary region. The four Cluster spacecraft moved out of the

cusp region at about 13:00 UT as demonstrated by the sharp increase of the magnetic field.

The ion flow directions observed by the three spacecraft are similar; $V_x$ is positive, indicating a continuous sunward flow which could be a result of the high latitude reconnection when the IMF is northward. The negative $V_z$ during this time period is also consisted with the high latitude reconnection picture. The very high speed of the flow might result from the strong magnetic field in this region because it is believed that the acceleration of the plasma during a reconnection process is closely related to the local Alfven speed (Dungey, 1961).

Figure 4 shows an expanded view of the period when the fluxes of all species show enhancements for a short time period, when the polarity of the magnetic field changes. The peaks of the fluxes of energetic particles coincide with the null point in the magnetic field. This indicates that the satellite crossed a current sheet, and that it is only in the vicinity of the current sheet that energetic electrons are observed. The region of charged electron fluxes is the narrower the shaded area when the fluxes of protons and heavy ions are both high.

We show all the RAPID observations of the four spacecraft together in Figure 5; all four spacecraft have recorded similar features. The second and third panel display the ratio of the flux of helium ions (70–1500 keV) to that of protons (30–1500 keV) and the flux of heavy ions (140–1500 keV) to that of protons, respectively. It is interesting to note that, just within the current sheet, these two ratios show a decrease, to a value around 0.5. However, the ratios on either side of the current sheet are greater than 1, and even reach 2.5. This implies that heavy ions might be "trapped" in an even wider region than that for protons. During a magnetically quiet time (e.g 5 April, 2001), these ratios in the same region are typically halved.

## 3. Discussion and summary

We show the magnetic field components in the local boundary normal coordinate system in the fourth and fifth panels of Figure 5. The $X^*$ of Figure 5, $Y^*$, $Z^*$ are defined as the maximum, intermediate and minimum variance directions (MVA) (Sonnerup and Cahill, 1967; Hapgood, 1992). The minimum variance vector defines the boundary normal direction **n**. A third eigenvalue and eigenvector together with the maximum and minimum variance vectors completes the right-handed coordinate system. The directions of the boundary normal coordinates system (i.e., the eigenvectors) in GSE are given as follows: the maximum variation direction, $X^* = (0.20\ -0.91\ -0.35)$; the intermediate variation direction, $Y^* = (-0.032\ -0.40\ 0.86)$; the minimum

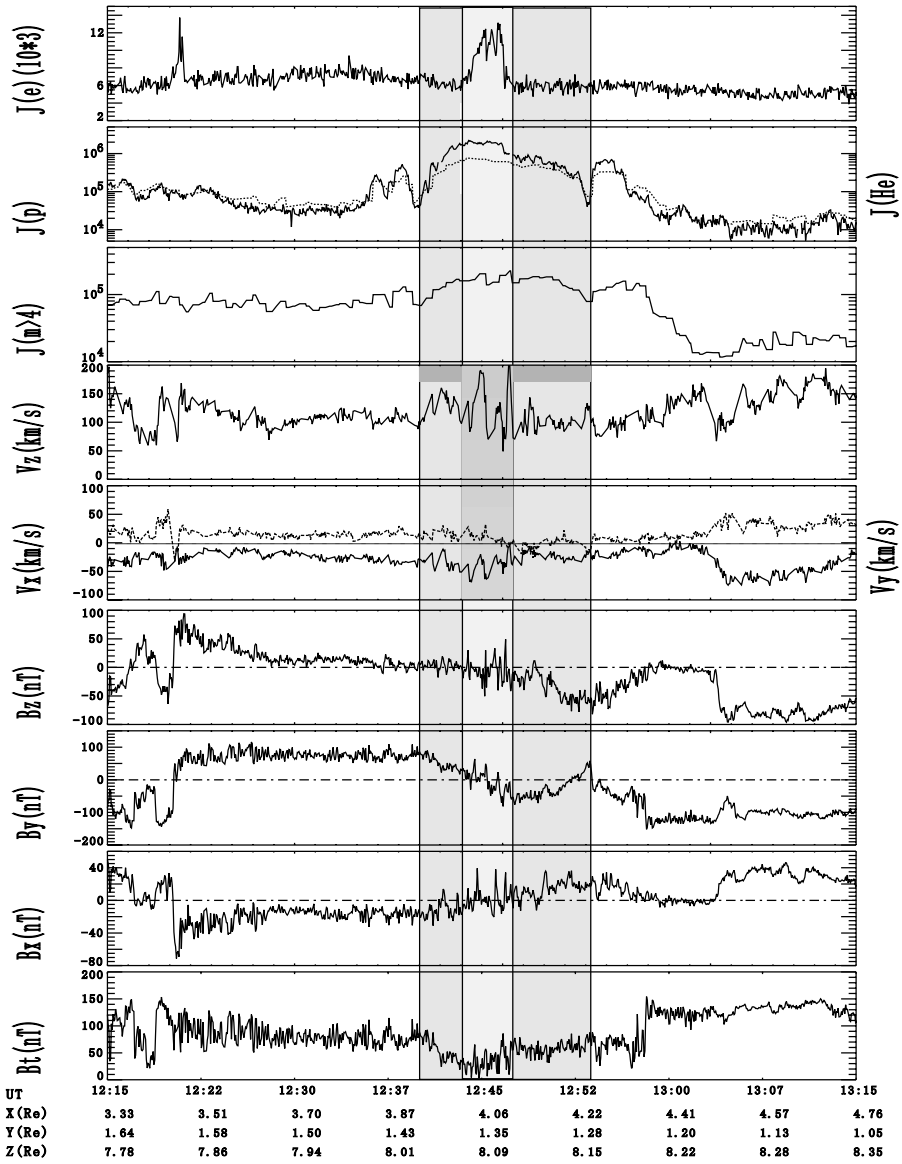


*Figure 4*. Expanded view of the different regions of energetic electrons and ions observed by S/C1. The panels from the top show the flux of high-energy electrons, protons and helium ions, heavy ions (m > 4), and three components of the plasma flow. The bottom four panels are the magnetic field components and total magnitude. The shaded area mark the flux enhancements of electrons and protons, respectively.

variation direction, $Z^* = (-0.92\ -0.064\ -0.37)$. The ratio of the intermediate to minimum eigenvalue is 14.3, and $\frac{|B_z^*|}{B}$ is 0.08. This indicates that the boundary normal system is well established (Sonnerup and Cahill, 1967;

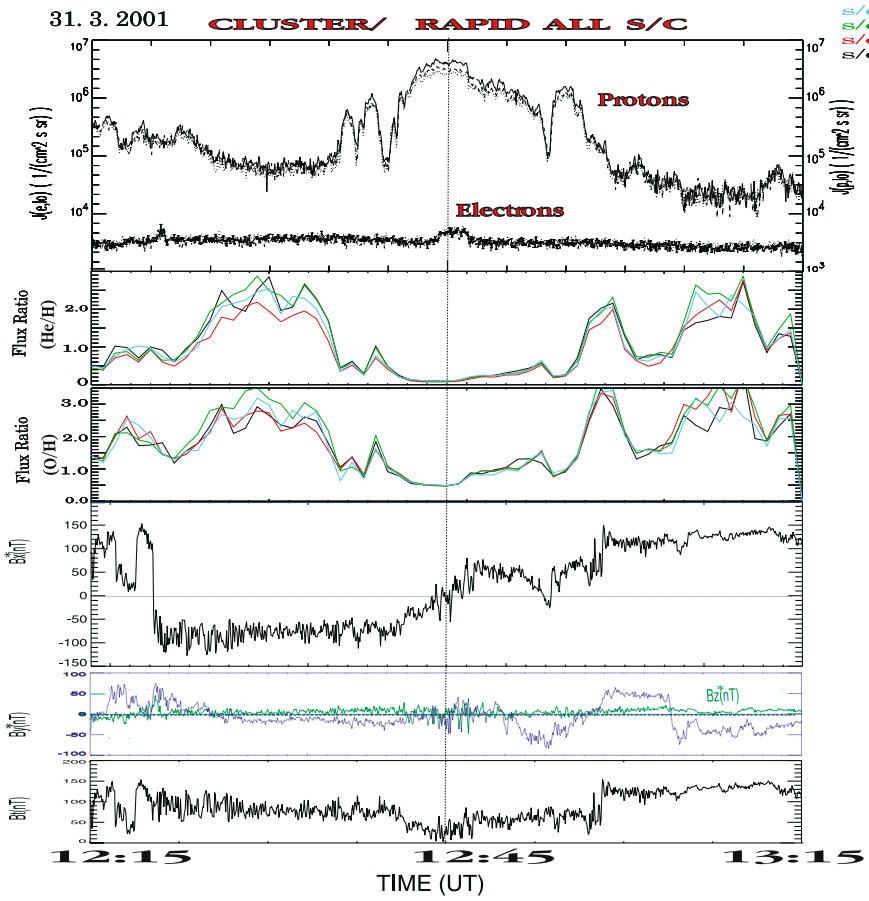


*Figure 5*. Observations made by the four Cluster spacecraft during the time period of 12:15–13:15 UT. The panels from top to bottom give the flux of energetic electrons and protons, the ratio of the flux of helium ions to that of protons and the flux of heavy ions to that of protons, the magnetic field components in the local minimum variance coordinate system, and the total magnetic field magnitude.

Lepping and Behannon, 1980). As the positive $X^*$ axis is toward dawn, this indicates that the changing of the magnetic field in the current sheet is mainly towards the local dawn. The current sheet could thus be identified by the magnetic field in its boundary normal coordinate system.

As we can see from Figure 5, this energetic particle layer has been observed simultaneously by all Cluster satellites. The only difference is in the center of the current sheet around 12:45 UT, where the ion fluxes are slightly different as observed by the different satellites; this is probably caused by the separation of the Cluster spacecraft.

The particles which are observed in the center of the current sheet have an abundance of heavy ions. Large amounts of heavy ions of ionospheric origin

in the ring current region is a typical signature for large magnetic storms (Hamilton et al., 1988; Daglis et al., 1999; Fu et al., 2001a, b). The heavy ion species can be used as an indicator of magnetospheric dynamic processes. Energetic particles observed in the polar cusp region could also come from the ring current and/or the plasma sheet (Kremser et al., 1995). The very high flux ratio of heavy ions to protons found in this event could be an indication of the energetic ions of magnetospheric origin escaping or leakage into the high latitude region during the early recovery phase of the storm. The normal ratio for the flux of oxygen to proton in the same energy range is as low as 0.1 in the solar wind (Wilken et al., 1995; Zong et al., 1998).

IMF $B_z$ observed by the ACE satellite at the L1 point was predominately positive from 10:24 to 12:00 UT (~20 nT, except for two very short periods of IMF $B_z$ negative). This indicates that IMF at the dayside magnetopause in the time period from 11:30 to 13:00 UT was essentially positive and favoured a cusp/high latitude reconnection site. High latitude reconnection often causes the so-called "reverse convection" (Crooker, 1992) which means that the plasma flow should have a sunward direction with a southward component. This is confirmed by the plasma flow velocity $V_x$ and $V_z$ observed by CIS onboard Cluster (Figure 3). Therefore, it is reasonable to believe that high latitude reconnection has opened up a path which allows energetic particles to leak out of the magnetosphere and/or escape into the cusp region.

When those high-energy particles get into the cusp region, they might be lost very quickly if there is no additional mechanism to trap them, since magnetic field lines in the cusp region are supposed to be open. The very low flux of energetic electrons is such an indicator (Zong et al., 2003). The observed current sheet provides a possible mechanism to maintain these energetic ions. By transferring to the boundary normal coordinate system, we found that the magnetic field changed mainly in the GSE $Y$ direction with the spacecraft moving mostly in the sunward direction. This implies that this current sheet is in the $Y$–$Z$ plane and the current flow probably in the $Z$ direction. Figure 6 illustrates a possible configuration of the current sheet in the cusp stagnation region, together with the orbit of the spacecraft superimposed on the T89 modelled magnetic field lines. It should be mentioned here that this current sheet may be formed by the piled up IMF against the Earth's field.

As we can see from Figure 4, during the time of interest, all three components of the magnetic field show a bipolar signature which indicates that this region is much more complex than just a simple boundary layer. The amplitude of the magnetic field is very small (probably near a magnetic null point) (see also Figure 5); the plasma velocity is also rather small. All these points suggest that the current sheet is located in the stagnation region in the cusp (Figure 6(a)). The maximum variation direction of the current is GSE (0.20 −0.91 −0.35), indicating the positive $X^*$ axis toward the dawn direction

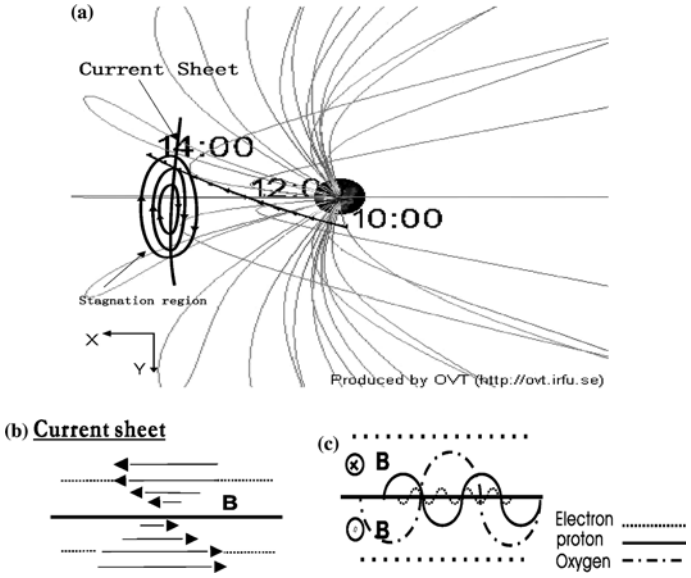


*Figure 6*. A schematic interpretation of the event on 31 March 2001. In part (a), the satellite orbit from 10:00–14:00 UT is plotted on top of magnetic field lines (T89 model). The current sheet and the magnetic field related to it are also displayed. A model current sheet with magnetic field shear is shown in (b), and charged particle motions in a current sheet and the possible trapping mechanism of the current sheet are shown in (c).

(GSE-$Y$ direction), and the change of the magnetic field in the current being mainly in the GSE $B_y$ (Figure 5). Figure 6(b) shows a simplified one-dimensional current sheet model as inferred from Figure 5. Energetic particles would have different types of motion when they are moving in such a current sheet – ''Speiser'' orbits. In the current sheet, particles could be ''trapped'' in the current sheet and also contribute some of the current. Far away from the central current (a distance larger than 2 gyro-radii), the current induced by the motion of the particles will reduce the original current.

From Figures 4 and 5, it is clear that different particles occupy different regions. Electron fluxes increase slightly in a very narrow region around the magnetic null point. This provides additional evidence for the current sheet trapping these observed energetic particles. The wider range of enhanced proton fluxes is also consistent with this assumption, since protons have a much larger gyro-radius than electrons. The ratio of the flux of helium and heavy ions to that of protons shows a decrease just near the null point of the magnetic field, while on both sides of the transition region these ratios are very high. This implies that heavy ions are ''trapped'' over a wider range than protons which is a result of their different gyro-radii (see Figure 6(c)). The same effect has been seen by GEOTAIL observations in the dayside magnetopause (Zong et al., 1999, 2001).

The observational results in this paper can be summarized as follows:

1. High fluxes of energetic protons together with heavy ions are observed in the cusp region during a giant magnetic storm.
2. The flux enhancements of different ion species occupy different regions, and are wider for heavy ions than for protons.
3. The region of flux enhancement of energetic electrons is narrower; it is only found in the central current sheet where the magnitude of the magnetic field is around zero.
4. The observed energetic particles might be of magnetospheric origin as inferred by the very high flux ratio of heavy ions to hydrogen (250%) during the early recovery phase of the large storm.
5. These energetic ions could be quasi-trapped by the current sheet in this region. This result may argue that the cusp current sheet plays a crucial role in maintaining these energetic particles in this region.

## Acknowledgements

The authors would like to thank Prof K.-H. Glaßmeier (IGM, Germany) and the FGM team members for providing the FGM data and the CIS team for the CIS data. This work is supported by the CNSF No. 40425004.

## References

Balogh, A., Dunlop, M. W., Cowley, S. W. H., Southwood, D. J., Thomlinson, J. G., Glassmeier, K. -H., Musmann, G., Luhr, H., Buchert, S., Acuna, M. H., Fairfield, D. H., Slavin, J. A., Riedler, W., Sachwingenschuh, K., and Kivelson, M. G.: 1997, 'The Cluster Magnetic Field Investigation', *Space Sci. Rev.* **79**, 65–91.

Crooker, N. U.: 1986, 'An Evolution of Antiparallel Merging', *Geophys. Res. Lett.* **13**, 1063–1066.

Crooker, N. U.: 1992, 'Reverse Convection', *J. Geophys. Res.* **97**, 19363–19372.

Daglis, I. A., Rasotakis, G., Sarris, E., Kamide, V., Livi, S., and Wilken, B.: 1999, 'Variations of the Ion Composition During a Large Magnetic Storm and their Consequences', *Phys. Chem. Earth* **24**, 229–232.

Dungey, J. W.: 1961, 'Interplanetary Magnetic Field and the Auroral Zones', *Phys. Rev. Lett.* **6**, 47–48.

Fritz, T. A.: 2000, 'The Role of the Cusp as a Source for Magnetospheric Particles: A New Paradigm,' in *Proc. Cluster-II Workshop on Multiscale/Multipoint Plasma Measurements*, ESA, SP-449, pp. 203–209.

Fu, S. Y., Wilken, B., Zong, Q. -G. and Pu, Z. Y.: 2001a, 'Ion Composition Variation in the Inner Magnetosphere-Individual and Collective Storm Effects in 1991,' *J. Geophys. Res.* **106**, 29, 683–29, 698.

Fu, S. Y., Zong, Q. G., Wilken, B., and Pu, Z. Y.: 2001b, 'Temporal and Spatial Variation of Ion Composition in the Ring Current', *Space Sci. Rev.* **95**, 539–554.

Hamilton, D. C., Gloeckler, G., Ipavich, F. M., Stüdemann, W., Wilken, B., and Kremser, G.: 1988, 'Ring Current Development During the Great Geomagnetic Storm of February 1986', *J. Geophys. Res.* **93**, 14343–14355.

Hapgood, M. A.: 1992, 'Space Physics Coordinate Transformations: A User Guide', *Planet. Space Sci.* **40**, 711–717.

Kremser, G., Woch, J., Mursula, K., Tanskanen, P., Wilken, B., and Lundin, R.: 1995, 'Origin of Energetic Ions in the Polar Cusp Inferred from Ion Composition Measurements by the Viking Satellite', *Ann. Geophys.* **13**, 595–607.

Lepping, R. P., and Behannon, K. W.: 1980, 'Magnetic Field Directional Discontinuities, 1, Minimum Variance Errors', *J. Geophys. Res.* **85**, 4695–4703.

Lockwood, M., and Smith, M. F.: 1992, 'The Variation of Reconnection Rate at the Dayside Magnetopause and Cusp Ion Precipitation', *J. Geophys. Res.* **97**, 14841–14847.

Newell, P. T., and Meng, C. I.: 1987, 'Cusp Width and $B_z$: Observations and a Conceptual Model', *J. Geophys. Res.* **92**, 13673–13678.

Reme, H., Bosqued, J. M., Sauvaud, J. A., Cros, A., Dandouras, J., Aoustin, C., Bouyssou, J., Camus, T., Cuvilo, J., Martz, C., Medale, J. L., Perrier, H., Romefort, D., d'Uston, J. R. C., Mobius, E., Crocker, K., Granoff, M., Kistler, L. M., Popecki, M., Hovestadt, D., Klecker, B., Paschmann, G., Scholer, M., Carlson, C. W., Curtis, D. W., Lin, R. P., McFadden, J. P., Formisano, V., Amata, E., Bavassano-Cattaneo, M. B., Baldetti, P., Belluci, G., Bruno, R., Chionchio, G., Dilellis, A., Shelley, E. G., Ghielmetti, A. G., Lennartsson, W., Korth, A., Rosenbauer, H., Lundin, R., Olsen, S., Parks, G. K., McCarthy, M., and Balsiger, H.: 1997, 'The Cluster Ion Spectrometry (CIS) Experiment', *Space Sci. Rev.* **79**, 303–350.

Sheldon, R. B., Spence, H. E., Sullivan, J. D., Fritz, T. A., and Chen, J.: 1998, 'The Discovery of Trapped Energetic Electrons in the Outer Cusp', *Geophys. Res. Lett.* **25**, 1825–1828.

Song, P., and Russell, C. T.: 1992, 'Model of the Formation of Low-latitude Boundary Layer for Strongly Northward Interplanetary Magnetic Field', *J. Geophys. Res.* **97**, 1411–1420.

Sonnerup, B. U. O., and Cahill, L. J.: 1967, 'Magnetopause Structure and Altitude from Explorer 12 Observations', *J. Geophys. Res.* **72**, 171–183.

Trattner, K. J., Fuselier, S. A., Peterson, W. K., Chang, S. W., Friedel, R., and Aellig, M. R.: 2001, 'Origins of Energetic Ions in the Cusp', *J. Geophys. Res.* **106**, 5967–5976.

Wilken, B., Axford, W. I., Daglis, I., Daly, P., Güttler, W., Ip, W. H., Korth, A., Kremser, G., Livi, S., Vasyliunas, V. M., Woch, J., Baker, D. N., Belian, R. D., Blake, J. B., Fennell, J. F., Lyons, L. R., Borg, H., Fritz, T. A., Gliem, F., Rathje, R., Grande, M., Hall, D., Kecscuemety, K., McKenna-Lawlor, S., Mursula, K., Tanskanen, P., Pu, Z., Sandahi, I., Sarris, E. T., Scholer, M., Schulz, M., Sorass, F., and Ullaland, S.: 1997, 'RAPID: The Imaging Energetic Particle Spectrometer on Cluster', *Space Sci. Rev.* **79**, 399–473.

Wilken, B., Zong, Q. -G., Daglis, I. A., Doke, T., Livi, S., Maezawa, K., Pu, Z. Y., Ullaland, S., and Yamamoto, T.: 1995, 'Tailward Flowing Energetic Oxygen Ion Bursts Associated with Multiple Flux Ropes in the Distant Magnetotail: GEOTAIL Observations', *Geophys. Res. Lett.* **22**, 3267–3270.

Wilken, B., Zong, Q. -G., Doke, T., Kokubun, S. and Ullaland, S.: 1998, 'Geoactivity at $X = -200$ Re in the tall – The Trailing Phase of A Solar Wind High Speed Sector,' in *Substorms–4*, Terra Scientific Publishing Company/Kluwer Academic Publishers, pp. 703–706.

Zong, Q. -G., Ritz, T. A., Spence, H., Korth, A., Daly, P. W., Dunlop, M., Balogh, A., Fennell, J., Pu, Z. Y. and Reme, H.: 2003, 'Energetic Electrons as a Field Line Topology Tracer in the High Latitude Boundary/Cusp Region: Cluster RAPID Observations,' *Surv. Geophys.* This issue.

Zong, Q. -G., Fritz, T. A., Wilken, B. and Daly, P.W.: 2002, 'Energetic Ions in the High Latitude Boundary Layer of the Magnetosphere - RAPID/CLUSTER Observation,' in *The Lower- Latitude Boundary Layer*, American Geophysical Union, Washington, D.C., pp. 101–110.

Zong, Q. -G., Wilken, B., Fu, S. -Y., Fritz, T. A., Pu, Z. -Y., Hasebe, N., and Williams, D. J.: 2001, 'Ring Current Oxygen Ions in the Magnetosheath Caused by Magnetic Storm', *J. Geophys. Res.* **106**, 25541–25556.

Zong, Q. -G., Wilken, B., Woch, J., Mukai, T., Reeves, G., Doke, T., Livi, S., Maezawa, K., Williams, D. J., Kokubun, S., Ullaland, S., and Yamamoto, T.: 1998, 'Energetic Oxygen Ion Bursts in distant Magnetotail as a Product of Intense Substorms: Three Case Studies', *J. Geophys. Res.* **103**, 20339–20363.

Zong, Q. -G., Wilken, B., Woch, J., Reeves, G., Doke, T., and Yamamoto, T.: 1999, 'Energetic particle Bursts in the near-Earth Magnetosheath During a Storm', *Phys. Chem. Earth* **24**, 293–298.

Surveys in Geophysics (2005) 26: 255–280
DOI 10.1007/s10712-005-1882-4 © Springer 2005

# COUPLING THE SOLAR-WIND/IMF TO THE IONOSPHERE THROUGH THE HIGH LATITUDE CUSPS

NELSON C. MAYNARD
*ATK Mission Research, 589 West Hollis Street, Suite 201*
*Nashua, NH 03062, USA*
*E-mail: nelson.maynard@atk.com*

(Received 7 January 2004; Accepted 30 April 2004)

**Abstract.** Magnetic merging is a primary means for coupling energy from the solar wind into the magnetosphere–ionosphere system. The location and nature of the process remain as open questions. By correlating measurements from diverse locations and using large-scale MHD models to put the measurements in context, it is possible to constrain our interpretations of the global and meso-scale dynamics of magnetic merging. Recent evidence demonstrates that merging often occurs at high latitudes in the vicinity of the cusps. The location is in part controlled by the clock angle in the interplanetary magnetic field (IMF) $Y$–$Z$ plane. In fact, $B_Y$ bifurcates the cusp relative to source regions. The newly opened field lines may couple to the ionosphere at MLT locations of as much as 3 hr away from local noon. On the other side of noon the cusp may be connected to merging sites in the opposite hemisphere. In fact, the small convection cell is generally driven by opposite hemisphere merging. $B_X$ controls the timing of the interaction and merging sites in each hemisphere, which may respond to planar features in the IMF at different times. Correlation times are variable and are controlled by the dynamics of the tilt of the interplanetary electric field phase plane. The orientation of the phase plane may change significantly on time scales of tens of minutes. Merging is temporally variable and may be occurring at multiple sites simultaneously. Accelerated electrons from the merging process excite optical signatures at the foot of the newly opened field lines. All-sky photometer observations of 557.7 nm emissions in the cusp region provide a ''television picture'' of the merging process and may be used to infer the temporal and spatial variability of merging, tied to variations in the IMF.

**Keywords:** cusp, magnetosphere, reconnection, solar wind

**Abbreviations:** ACE – Advanced Composition Explorer; DMSP – Defense Meteorological Satellite Program; MHD – magnetohydrodynamics; IMF – interplanetary magnetic field; IEF – interplanetary electric field

## 1. Introduction

The cusp and dayside boundary layer that form the magnetopause mediate how energy from the solar wind couples into the magnetosphere–ionosphere

system. The word cusp conjures up different images to different people. In a theoretically closed magnetospheric configuration, it is singularity in the ionosphere to which the whole surface of the magnetosphere maps. At high altitudes it is an indentation on the surface of the magnetopause and a region of depressed magnetic field. Chapman–Ferrero currents, whose $\mathbf{J} \times \mathbf{B}$ force balances the dynamic pressure from the solar wind at the nose, close above the cusp. This current vortex is the cause of the depression in the field in the high altitude cusp (see Siscoe et al., 2000a). In fact, the cusp is wider, in some cases extending over 4 h in magnetic local time (e.g., Maynard et al., 1997). Magnetic merging at the magnetopause between magnetic fields of opposite polarity was proposed by Dungey (1961) to interconnect the interplanetary magnetic field (IMF) with the Earth's magnetic field, breaking an IMF field line into two open field lines tied through the cusps to each ionosphere. As these open field lines are dragged anti-sunward by their tie to the solar wind, they drive convection in the northern and southern polar caps. This means that the magnetopause is open with the Earth's magnetic field lines connecting to the IMF through the cusp and through the high latitude boundary layer or mantle behind the cusp. The cusps are direct entry regions for magnetosheath particles along the open field lines. In a merging driven configuration, whether the merging location is near the nose or near the cusp, the magnetopause boundary layer below the cusp may also be open. Newly merged field lines drape over the magnetopause as they are being dragged tailward by the solar wind, forming an open boundary layer (see Maynard et al., 2002).

In this paper the cusp is defined as a region of open field lines extending poleward from the open closed boundary (which is tied to the dayside merging region on the magnetopause) to where particles no longer are able to directly enter. Subsequently, the open field lines are pulled tailward in the mantle, rotating to their solar wind orientation through currents in the mantle and the magnetosheath. In the ionosphere the cusp is several hours wide and several degrees in depth. Near the magnetopause (as well as in the ionosphere) the depressed magnetic field region of the cusp shifts in local time, depending on the IMF clock angle (see Siscoe et al., 2005 (this volume)). The quasi-circular boundary or rim of the cusp can be seen in their Figure 3. For northward IMF merging occurs at the poleward edge. At the dayside boundary between open and closed magnetic field lines the first cusp open magnetic field lines connect to the merging separatrix on the magnetopause. Magnetosheath particles, which have been accelerated by the merging process, may be observed (see also Keith et al., 2005 (this volume)). Because all newly opened magnetic field lines connect to the ionosphere through the cusp, the cusp region characteristics monitor the coupling of the magnetosphere to the solar wind.

Merging is now generally accepted as the primary mechanism for coupling. Questions remain as to (1) *where* merging takes place, (2) *when*, or on what time scale, merging is actively happening, and (3) even *how* the process is accomplished. High resolution electric and magnetic field and energetic particle measurements provide new tools for investigating these basic questions. Over the last several years, a number of new insights have been gained from combining and/or correlating remote measurements in the ionosphere (both ground- and space-based), *in situ* measurements at the magnetopause with Polar and Cluster, measurements upstream in the solar wind to monitor the input from the solar wind, and simulations using magnetohydrodynamic (MHD) models of the whole solar-wind/magnetosphere/ionosphere system. Addressing problems with simultaneous data from multiple satellites and diverse locations within the context of the large-scale picture from the simulations constrains our interpretations. In this paper we will apply these new insights to each of these basic "reporter" questions, after first providing a quick overview on methods that have been used experimentally to establish the existence and location of magnetic merging. The paper is meant to be a synopsis and a synthesis of recent results, details of which are in the referenced papers, and not a comprehensive review.

## 2. Merging primer

Magnetic merging is a local reconfiguration of the magnetic field in which fields of opposite polarity merge, resulting in a new configuration, and magnetic energy is converted to kinetic energy. At the magnetopause, interplanetary magnetic field lines connect to closed magnetospheric field lines to create two open magnetic field lines that have one foot in each hemisphere's ionosphere and extend out into the solar wind. X-type merging configurations with oppositely directed field lines (Levy et al., 1964) were generalized by Sonnerup (1974) to include merging between the antiparallel components of **B**, along a line that hinges about the subsolar point (e.g., Gonzales and Mozer, 1974). The remaining parallel component is usually referred to as a guide field.

What happens at the separator at the center of the X configuration, some times referred to as within the "black box", to provide parallel electric fields and dissipation necessary for merging is an open question. In the following we shall use the terms merging separator and X-line interchangably, while realizing that in localized features they may be closer to a point rather than a line. Both ion and electron gyrotropy must be broken. The questions revolve around "how". A recent review of the physics involved has been made by Scudder (1997). Hall and pressure gradient

terms must be considered in the generalized Ohm's law. Other terms involve anomalous resistivity and electron inertia. Simulations using both MHD and particle-in-cell (PIC) codes have been compared in the Geospace Environmental Modeling (GEM) magnetic reconnection challenge (see Birn et al., 2001 and associated papers in the same issue). Simulations which included the Hall effect, bringing the dynamics of whistler waves into the system, all produced similar rates of reconnection or merging (Birn et al., 2001). Observationally, the breaking of gyrotropy of both ions and electrons at a merging site above the cusp for northward IMF has been definitively identified by Scudder et al. (2002a).

Since most measurements are away from the merging separator, proxies in the data have been developed for identifying that merging has taken place. Minimum variance analyses (Sonnerup and Ledley, 1974) of magnetic field measurements (often combined with maximum variance of electric fields (e.g., Kawano and Higuchi, 1995)) have been employed to show that the magnetopause was a rotational discontinuity with a finite $B_{\text{normal}}$ and $E_{\text{tangential}}$, which are proportional to the merging rate. The existence of a rotational discontinuity is a necessary, but not sufficient, condition for merging. However, establishing an unambiguous finite $B_{\text{normal}}$ can be difficult. Rotational discontinuities satisfy the Walén relationship, which specifies that the change in the ion velocity is proportional to the change in the magnetic field. Often the proportionality constant found in the data is different from $\pm 1$. Scudder et al. (1999) showed that the Walén test is better done with electrons. More recently Ma et al. (2002) have shown that, depending on how the merging topology is crossed, minimum variance may provide an erroneous normal direction and even the Walén test may be compromised.

Another commonly used proxy for merging is the identification of accelerated flows of magnetosheath plasma observed near the subsolar magnetopause (Paschmann et al., 1979; Sonnerup et al., 1981). Observations of accelerated flows, often identified by "D-shaped" distributions in velocity space (Cowley, 1982), have been regarded as standard signatures of merging (e.g., Gosling et al., 1982; Paschmann et al., 1986; Sonnerup et al., 1990). This is a necessary, but not sufficient, condition for merging to have occurred. While accelerated plasmas were observed during some ISEE-1 magnetopause crossings, Aggson et al. (1984) also reported decelerated flows. Moreover, they emanated from a merging site poleward of the satellite. Scudder (1984) calculated that, as the merging site moved off the equator, the exhaust velocity from the X-line should equal the sum from the merging acceleration and the local magnetosheath velocity at the merging site. This becomes especially significant for X-lines located at high latitude where the open field lines from the backside of the separator are draped over the nose to the opposite hemisphere cusp and may have decelerated flows.

Recently, Maynard et al. (2003) have used wave Poynting flux as an additional discriminator for merging. The magnetic reconfiguration in the merging process must be communicated away from the X-line along the separatrices via Alfvén waves carrying field aligned currents (see Atkinson, 1992; Ma and Bhattachargee, 2001). These waves will have a parallel Poynting flux. Its direction, like the accelerated particles, will be away from the source. Again, this is another necessary, but not sufficient, proxy.

Crooker (1979) offered an alternative hypothesis in which merging occurs wherever magnetospheric and magnetosheath field lines are aligned antiparallel to each other. For most IMF orientations antiparallel merging proceeds at high latitudes on the magnetopause. It is of particular interest to note that on the basis of high-altitude magnetopause and cusp measurements by the HEOS-2 satellite, Haerendel et al. (1978) concluded that the merging process is intermittent, of small scale, and located predominantly in the cusp region. Sibeck and Newell (1994) have also argued for continuous and patchy, sporadic merging in the vicinity of the cusps. Both the antiparallel and component merging hypotheses locate merging at the equator for periods of southward IMF and at the poleward boundary of the dayside cusp during periods of purely northward IMF. Differences occur for the intermediate clock angles, which are the most common situations. We shall address this when we answer the question "where".

In a series of papers in the early 1990s, Cowley and Lockwood developed the concept of pulsed reconnection or merging (see Cowley and Lockwood, 1992). It was a component-merging based hypothesis that merging happened in bursts, separated by gaps when no merging was taking place at a particular location. The typical repetition rate was 8 min, similar to the typical repetition rate for flux transfer events, which were identified in the ISEE-1 and −2 data taken near the nose by Russell and Elphic (1979). In these pulses of merging, open flux was added to the dayside ionosphere, which stimulated convective flow and the ionospheric convection pattern. Earlier, Maynard and Johnstone (1974) used sounding rocket observations to identify filaments of electrons of magnetosheath character occurring on faster temporal and/or narrower spatial scales. They postulated that direct access was through multiple filamentary structures located in the broader context of the cusp. Lemaire (1977) found filamentary currents in the boundary layer at the magnetopause. Others have argued that merging was more continuous, varying in rate and location (see Newell and Sibeck, 1994). In fact, most of the theory of the process has been developed around steady state merging. Considering the variability of the magnetic field in the solar wind and the magnetosheath, the process is unlikely to be steady, although it may be occurring somewhere continuously. We shall address this when we attempt to answer the question "when".

## 3. A new perspective on solar wind coupling to the magnetosphere

Results from two sounding rockets, launched into the ionospheric extension of the cusp from Ny-Ålesund in the Svalbard archipelago, North of Norway, compelled consideration of a new view of the propagation of structures in the interplanetary magnetic field (IMF) in the solar wind and their effects on the merging process. The most startling result of Maynard et al. (2000, 2001c) was the correlation, in each case, of electric field variations seen in the ionosphere by the sounding rocket with small-scale variations in the effective interplanetary electric field nearly 200 $R_E$ upstream. In both cases the IMF had a strong $B_X$ component and $B_Y$ was stronger than $B_Z$. The variations in both data sets had scales of minutes. Remarkably, the lag time was less than the advection time (the time that a feature would take to transit the intervening distance using the measured solar wind velocity). The observed correlations indicated that surfaces of constant phase in the interplanetary electric field (IEF) must be tilted with respect to the Sun–Earth line. The sense of tilt was such that first interactions with the magnetosphere occurred on the southern hemisphere magnetopause. This forced the conclusion that the interaction with the magnetosphere that was causing the variations seen at the rocket in the northern hemisphere ionosphere had to be in the southern hemisphere. This means that part of the northern hemisphere cusp must have an open field line region with its merging source in the southern hemisphere, and a separate region with its merging source in the northern hemisphere. The cusp is thereby longitudinally bifurcated relative to source regions from the effects of $B_Y$.

Two additional assumptions were made by Maynard et al. (2001c) to harmonize these observed correlations of interplanetary and ionospheric dynamics. First, merging locations are determined using the antiparallel criterion of Crooker (1979). The antiparallel criterion in $B_Y$-dominated situations results in a separator that is split between high-latitude northern and southern hemisphere sources, causing longitudinal bifurcation. The data are insufficient to specify whether field lines at the merging site are exactly antiparallel or have a small guide field; however, the results are more easily explained if merging proceeds near the two cusps rather than at low magnetospheric latitudes. Second, an optical signal in the ionosphere marks every merging event. In the dayside cusp, poleward moving 630.0 nm auroral forms associated with flux transfer events (Sandholt et al., 1986) reflect prolonged access of magnetosheath plasma to the ionosphere. We suggest that prompt optical responses also occur in the ionosphere following small-scale variations in the merging rate/location. In following effects of such small-scale IEF variations, it is necessary to examine variations of 557.7 nm, rather than 630.0 nm, auroral emissions, because of the long lifetime of the $O(^1D)$ state.

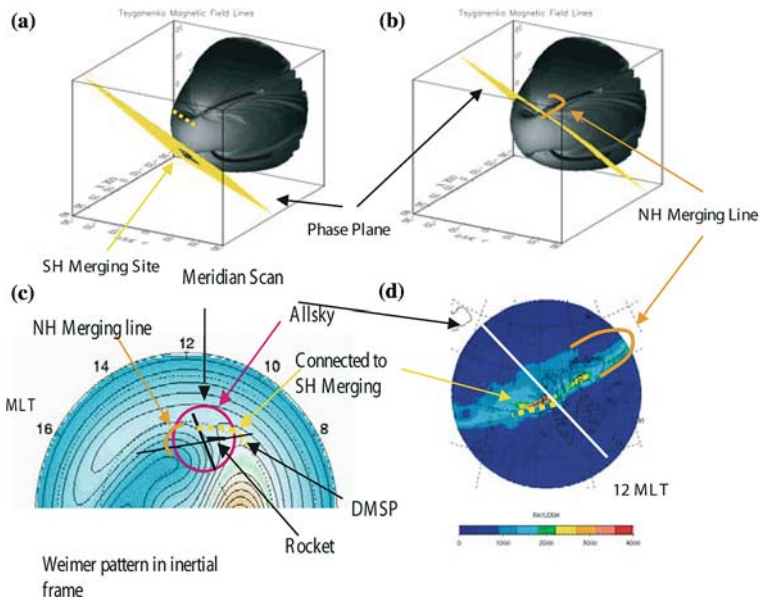


*Figure 1.* Diagram illustrating the various merging sites in the magnetosphere and ionosphere and their relationship to the aurora (Maynard et al., 2001c). The top two plots show a 3-D representation of the magnetopause defined by the last closed field line surface from the Tsyganenko 96 model with mantle field lines added. The yellow IEF phase plane is shown abutting the southern hemisphere merging site in the left plot and encountering the northern hemisphere cusp region in the right plot. Newly opened field lines in the southern hemisphere would pass by the dotted yellow region in the northern hemisphere in the top left. The orange line in the top right schematically delineates possible northern hemisphere merging sites, applying the antiparallel criterion. The bottom two plots depict the ionospheric configuration. Mapped onto a W2K convection pattern (Weimer, 2001) and an all-sky image are the field of view of the optics, the approximate rocket and DMSP trajectories, and the projections of the merging sites color coded for comparison with the top plots. Note that the all-sky image is inverted from the potential pattern, with both shown in their most commonly displayed orientation. (see text) (from Maynard et al., 2001b, 2002).

To illustrate some of the concepts involved when tilted phase planes in the solar wind interact with the magnetosphere ionosphere system, we use the diagram of Maynard et al. (2001c, 2002) for conditions when the IMF was dominated by $B_Y > 0$ and $B_X < 0$ (with slightly negative $B_Z$). The two top plots of Figure 1 show the last closed field line surface generated by the T96 magnetic field model (Tsyganenko and Stern, 1996). To give the magnetosphere its normal shape, mantle field lines were added poleward of the cusp. The basic indentation of the cusp with emanating field lines is shown along with the connected sash (White et al., 1998; Maynard et al., 2001a). For $B_Y > 0$ the separator passes through the dawn (dusk) side of the cusp in the southern (northern) hemisphere. The yellow planes in the top two plots of

Figure 1 represent surfaces of constant IEF phase. The tilt angle is comparable with estimated values during the two rocket studies. The upper left plot shows the phase plane impacting the separator first on the southern hemisphere dawn side, equatorward of the cusp. The yellow dashed line represents a conceptual mapping of recently opened field lines near the northern cusp as a result of merging in the southern hemisphere. Newly merged field lines are pulled tailward and toward dawn by $\mathbf{J} \times \mathbf{B}$ (magnetic tension) forces at the magnetopause (Siscoe et al., 2000b) as the solar wind flows past the Earth. The top right plot shows the same phase plane at a later time as it interacts with the northern hemisphere antiparallel merging site. In the case of $B_Y > 0$, the northern hemisphere antiparallel merging site is located near the dusk side of the cusp for $\theta > 90°$, in the sash for $\theta \asymp 90°$, and on the poleward edge of the cusp with northward $B_Z$. The orange line designates potential northern hemisphere merging sites. Note that, when the IEF phase plane reaches the orange line, it has already passed the time and location associated with component merging.

Figure 1a and b are simplified to emphasize the timing of the interactions in each hemisphere. Phase planes that are coplanar in the solar wind are distorted by the decreasing velocity in the magnetosheath and drape over and around the magnetopause before the IMF merges with the Earth's magnetic field. For the sake of illustration, Figure 1 ignores delays and associated field-line draping occurring as the solar wind slows in the magnetosheath (Shepherd et al., 1999). Of importance here is the fact that, because of the tilt and the negative $B_X$, merging occurs *first* in the southern hemisphere and *later* in the northern hemisphere. When $B_X$ is involved, the two hemispheres may respond to the same feature at different times as a consequence of high latitude merging.

The convection pattern shown in the lower left quadrant of Figure 1 is placed on a magnetic latitude versus magnetic local time (MLT) grid. It was derived using the Weimer (2001) (W2K) convection model, represented in inertial coordinates. Maynard et al. (1995) showed that cusp potential patterns are well ordered in the inertial reference frame in which the throat between the two cells resides near noon for both polarities of $B_Y$, in agreement with the statistical position of cusp particle precipitation. Estimated projections of the northern and southern hemisphere merging lines are represented by the orange and yellow dashed lines, respectively.

For the correlations found by Maynard et al. (2000, 2001c) to exist, logic demanded consideration of phase plane tilt and high latitude locations of the merging sites. The concept of tilted phase planes was then explored extensively by Weimer et al. (2002) using simultaneous data from four satellites in the solar wind. They allowed the lag time between any two satellites to vary and found a method of calculating that lag on a minute-to-minute basis. A simple variable lag shift harmonized all three components of the IMF, cor-

relating the data where in some cases no obvious correlation existed. When the positions of the other three satellites were adjusted by the variable lags relative to ACE, all four became located in the same plane. Moreover, that plane underwent significant orientation shifts with scales of tens of minutes. The significance of this is that more phenomena, observed in the cusp, may have direct ties to the solar wind than we previously have been able to identify. It is important to get the timing for the interaction correct and to remember that the hemispheres may respond at different times, especially when $B_X$ becomes dominant.

## 4. Where?

The previous section introduced the necessity, at least in some cases, for high latitude merging, which favors the anti-parallel merging hypothesis of Crooker (1979). This is in contrast to the more prevalent view that whenever $B_Z$ is negative, component merging occurs nearer the equatorial plane along a separator passing through the nose, but tilted somewhat by $B_Y$ (following Sonnerup, 1974; Gonzalez and Mozer, 1974). However, it is consistent with the conclusions of Haerendel et al. (1978) that merging occurs predominently in the cusp region.

The high latitude location illustrated conceptually by Figure 1 would be around the rim of the cusp, with the location dependent on the strength and direction of IMF $B_Z$ relative to $B_Y$. The merging site is post-noon (pre-noon) in the northern hemisphere if $B_Y$ is positive (negative). The opposite is true for the southern hemisphere. The rim around the indentation of the cusp is in part due to the Chapman–Ferraro currents, whose closure above the cusp depresses the magnetic field inside the loop (see Siscoe et al., 2000a). Figure 3 of Siscoe et al. (2005, this volume) shows how the indentation moves post-noon as the clock angle increases through 90° and back to being centered on noon as the clock angle approaches 180°.

Maynard et al. (2003) utilized data from Polar, Cluster and SuperDARN to conclude that merging often occurs at high latitudes for clock angles less than 150°. In their featured example from 12 March 2001, Polar was skimming the magnetopause above the nose, Cluster was passing through the northern hemisphere cusp post-noon, while SuperDARN monitored the convective flow patterns in the ionosphere. Figure 2 shows the satellite locations and an expanded insert with the configuration of the four Cluster spacecraft. Spacecraft separations were of the order of 600 km at this time. At the magnetopause crossing Polar observed accelerated particles and parallel wave Poynting flux from above the spacecraft, which was poleward of the nominal component merging line, indicating that the source was at high latitude. The minimum variance normal and an electron Walén test

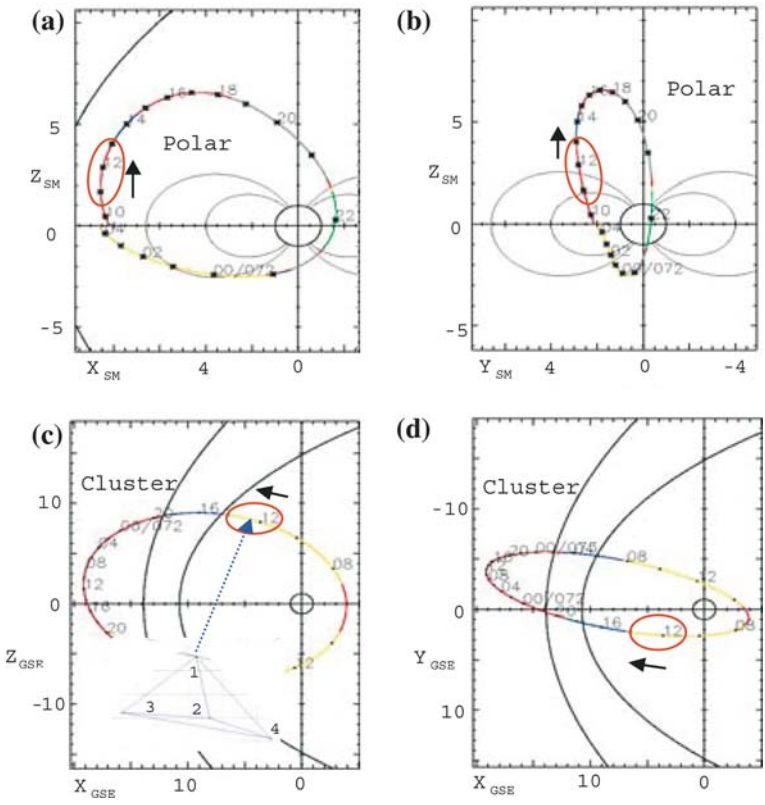


*Figure 2.* Plots of the Polar orbit in the *XZ* and *YZ* solar magnetospheric (SM) coordinate planes and of the Cluster orbit in the *XZ* and *XY* geocentric solar ecliptic (GSE) planes. The regions of interest are highlighted by the red ovals. Nominal magnetopause and bow shock configurations are indicted in panels a, c and d as appropriate. The circles at the origin represent the Earth. In panel c the insert shows the configuration of the four Cluster spacecraft with Cluster 3 leading and Cluster 4 trailing. The tetrahedron configuration is maintained quite well during the interval of interest. Spacecraft separation is of the order of 600 km (from Maynard et al., 2003).

confirmed the location above the spacecraft. None of these tests is sufficient in itself, but, as a group, the tests point to a conclusion that Polar was monitoring the back exhaust region of a high latitude merging line. Maynard et al. (2003) present evidence that SuperDARN and Cluster monitored the forward exhaust effects of the high-latitude *X*-line.

Interpretations of satellite measurements can be tested for reasonableness through comparisons with predictions of simulations using the Integrated Space Weather Model (ISM). ISM is a large-scale magneto-hydrodynamic (MHD) code developed by Mission Research Corporation to simulate the magnetosphere–ionosphere system from 40 $R_E$ upstream in the solar wind, to

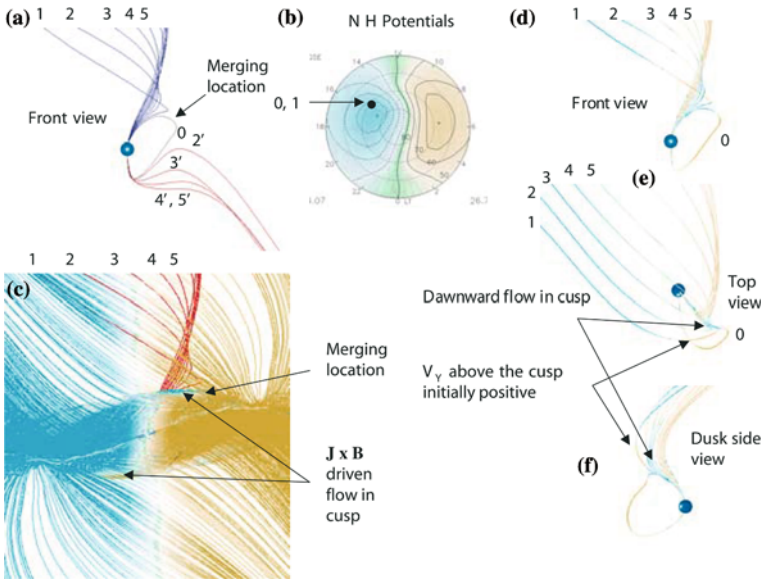


*Figure 3*. Traced magnetic field lines from a MHD simulation using the Integrated Space Weather Model (ISM). Figure 3a shows a set of field lines flowing away from a high latitude merging site. Trace 0 is closed, and its origin in the northern hemisphere is shown in Figure 3b to be between 15 and 16 MLT and 7° latitude. All others are open. Figures 3d–f show three views of these same field lines colored with the $Y$ component of the velocity. Figure 3c shows the complete set of first open field lines traced from the ionosphere in each hemisphere and also colored with $V_Y$ (see text) (from Maynard et al., 2003).

the base of the ionosphere near the Earth, and to $-300\ R_E$ in the magnetotail (see White et al., 2001). To illustrate conceptually the connectivity between diverse regions that Polar, Cluster and SuperDARN were monitoring, Figure 3 (from Maynard et al., 2003) identifies a high latitude merging site in an ISM run with an IMF input clock angle of 135°. Last closed field lines were found starting from the ionosphere in each hemisphere. By moving poleward 10 km in the ionosphere from the trace point of each closed field line, we define a set of "first" open field lines. A last-closed and first-open field line pair, traced from the northern hemisphere ionosphere, are shown in Figure 3a and labeled 0 and 1. They map from the black dot in the potential pattern in Figure 3b, near 15 MLT and 71° magnetic latitude, and pass through the post-noon cusp. Field line 0 also traverses the low latitude region of the post-noon magnetopause. This closed field line maps to near the zero equipotential line between the two convection cells in the southern hemisphere.

Several field lines have been traced from a series of points along the northern hemisphere equipotential that passes through the origin of trace 0 to understand how the field lines change after merging. The first 4 of these,

labeled 2–5 in Figure 3a, demonstrate the evolution of a field line above the separator, as it is dragged back over the magnetopause. A similar set of field lines was mapped from the equipotential contour in the southern hemisphere at the end of trace 0 and labeled 2′–5′. Although there is no way to trace the evolution of exact pairs from a merging site, these field lines illustrate the evolution below the separator and how the newly opened field lines drape over the dayside magnetopause. Line 2′ probably pairs best with 2. We infer a high-latitude merging site to be located close to where line 1 bends. The open field lines below a high latitude merging site form an open boundary layer over the dayside magnetopause (see also Maynard et al., 2002).

Figure 3c shows the complete set of first open field lines traced from each hemisphere. The field lines are colored according to $V_Y$. The northern hemisphere set of field lines in Figure 3a are colored red in Figure 3c to show their position relative to the first open field lines. Most prenoon (postnoon) field lines have a negative (positive) $V_Y$. Exceptions to this are in the cusp where $\mathbf{J} \times \mathbf{B}$ forces from the currents associated with the curvature of newly merged field lines drive flow westward (eastward) in the northern (southern) hemisphere (Siscoe et al., 2000). Figure 3d–f display the front, top, and side views of northern hemisphere closed and open field lines in Figure 3a colored with $V_Y$. Flow in the boundary layer on the closed field line (0) is toward dusk. Flow above (in) the cusp on line 1 is toward dusk (dawn), as indicated by the color change between brown and blue for positive (negative)$V_Y$ in Figure 3d and e. Subsequently the flow is toward dawn, both above and in the cusp, as the field line is dragged back through the mantle.

With this conceptual picture, Maynard et al. (2003) connected velocity enhancements measured between 1400 and 1500 MLT in the ionosphere by SuperDARN with enhancements in the merging rate measured above the nose postnoon by Polar, as it was skimming the magnetopause. Polar observed accelerated ions and wave Poynting flux originating above the satellite, which was located 10° above the component merging line of Gonzalez and Mozer (1974). Minimum variance analysis and an electron Walén test also placed the X-line above the spacecraft. They concluded that the merging was at high latitudes. Based on Figures 1 and 3, the location was probably near the postnoon side of the cusp.

Figure 4 shows the temporal response of the maximum velocity measured by SuperDARN in the 1400–1500 MLT region where the field lines in Figure 3 mapped. Three enhancements are marked with the corresponding times of enhancements at Polar. The connectivity between ground-based and satellite measurements continued as Cluster passed outward through the cusp 20 min later. The effects of temporally varying merging were observed at Cluster, which correlated with enhancements at SuperDARN shown in Figure 4. Following the conceptual picture in Figure 3, Cluster, as it crossed into the magnetosheath, would have observed effects near the outer separa-

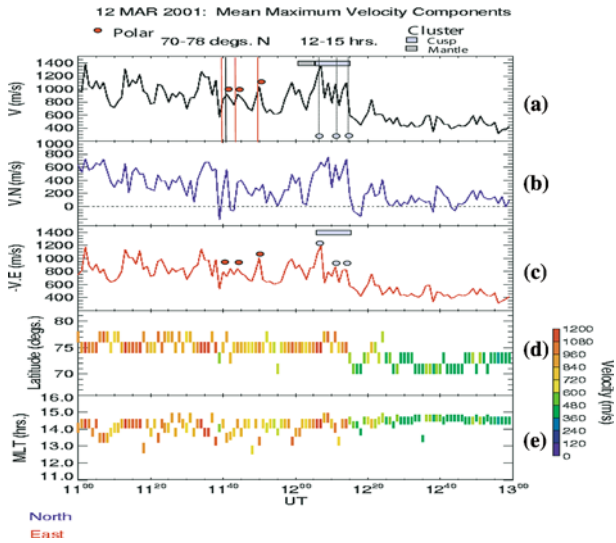


*Figure 4*. The maximum velocities of ionospheric plasma and their locations determined by SuperDARN for the interval between 1100 and 1300 UT (from Maynard et al., 2003).

trix from merging below the spacecraft, while SuperDARN measurements would be more connected to the inner separatrix, or the open-closed field line boundary.

Cluster, with the four spacecraft in an approximate tetrahedral configuration, provided additional tests on positioning. The current inside the configuration was estimated by determining curl **B** (Dunlop et al., 2002). Figure 5 displays local currents derived using a GSM coordinate system centered on Cluster 2. Also plotted are the divergence of **B** as a percentage of curl **B** and the magnitude of **B** at the locations of the four spacecraft. Since Maxwell's equations demand that $\nabla\cdot\mathbf{B}=0$, a significant calculated value of $\nabla\cdot\mathbf{B}$ implies that the result is not meaningful. Reasons for error include spatial (temporal) gradient scales of the order of the spacecraft separation (traversal time). Currents determined where the divergence-to-curl ratio exceeds 50% should be treated with caution. In general, for this configuration, the expected error in $J$ is, at a minimum, 20%. Most of the large values of the divergence occur when the currents are small, highlighting their uncertainty. However, when the currents are large, the divergence ratio is in general small, indicating where the calculated currents are reasonably valid. The curl **B** calculation integrates the currents over the scale size of the tetrahedron (600 km). The largest current was detected between 1214 and 1215 UT, as the spacecraft passed from the depressed magnetic field region of the cusp out into the magnetosheath, and is primarily in the $+Z$ and $-X$ directions, noted by the green bars. It takes the four spacecraft over a minute

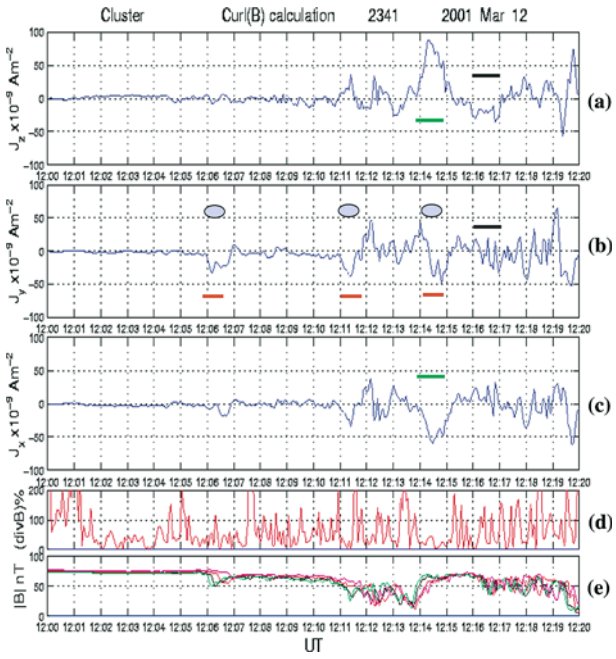


*Figure 5.* (a–c) Currents in GSM coordinates determined by the curl **B** calculation. The calculation is centered on Cluster 2. (d) The ratio of the divergence of **B** to the curl of **B** expressed in per cent. The ratio provides an indication of where the calculation is reliable (see text). The magnitude of $B$ is given in the bottom panel for context (from Maynard et al., 2003).

to cross the main current layer, indicating its temporal stability. Thus, the center of this current should be well resolved. Counterclockwise Chapman–Ferraro currents on the dusk edge of the cusp have the anticipated direction. This places Cluster near the sidewall of the cusp. The observed wave Poynting flux and particle accelerations were from below the spacecraft. This indicates that the high-latitude merging location was consistent with Figure 3 and close to the conceptual orange hook in Figure 1. Cluster was above the merging site.

When we consider that Polar and SuperDARN were showing temporally varying merging at high latitudes 20 min previously, and that the variations in the accelerated particles and Poynting flux at Cluster also connect to the SuperDARN variations, currents related to time varying merging also may be expected signatures at Cluster. $J_Y$ is the most variable component showing both polarities, although the strongest are currents in the $-Y$ direction. Some of the variability could occur if the current scale size were less than that of the Cluster configuration. Currents from structures of scale size less than 600 km may suffer from this error. Attention is directed to negative $J_Y$ excursions observed between 1206 and 1207, 1211 and 1211:40, and 1214:30 and 1215

UT marked by red bars. There is also an associated smaller $-J_X$ excursion. These correspond to times when negative velocity enhancements in the negative $Y$ direction were observed both in the particle moments and $\mathbf{E} \times \mathbf{B}$. This suggests that the variations in $J_Y$ are related to temporally varying merging.

Thus Maynard et al. (2003) have connected ionospheric signatures in the 1400–1500 MLT region with high latitude merging on the afternoon side of the cusp. Connecting merging to the 1400+ MLT region implies a wide cusp in the ionosphere. A width of the order of 4 h was in fact found by Maynard et al. (1997). The picture from the simulations provided by Siscoe et al. (2005, this volume) shows that the cusp itself is shifted toward dusk (dawn) for positive (negative) $B_Y$. The merging location may not generally be symmetric about noon. The high latitude merging location was confirmed by Polar measurements above the nose. In fact, in 13 merging events reported by Maynard et al. (2003), a high-latitude merging site was inferred whenever the IMF clock angle was less than 150°. Based on both Polar data and ISM simulation results, the merging site can move off the equator even for 180° clock angles when the dipole is tilted or there is a large IMF $B_X$. These results favor antiparallel locations, but do not exclude a small guide field. Nor can we exclude component merging at a location remote from the measurements. However, Maynard et al. (2003) pointed out that high latitude merging in the MHD simulations was remarkable in itself. The MHD code accomplishes merging through dissipation, either explicitly introduced through current dependent resistivity, or introduced by the numerics of the partial donnar method (PDM) of Hain et al. (1987) wherever large gradients need to be mediated in the code. Even in the presence of dissipation explicitly introduced to aid merging, which is keyed to where the current exceeds a threshhold (primarily located at the nose in the subsolar region and in the plasma sheet in the magnetotail), the code adds dissipation, and therefore merging, at high latitudes to satisfy the externally applied boundary conditions.

Returning to the rocket results, Maynard et al. (2001c) found that $B_X$, and the resulting tilted phase planes, forced consideration of merging in the opposite hemisphere driving a portion of the cusp in the local hemisphere near local noon. While $B_Y$ bifurcated the cusp relative to source location, $B_X$ controlled the timing of the interaction at each location. These results and recent work of Coleman et al. (2001) point toward not only high latitude merging, but also the split merging separator hypothesized in the antiparallel scenario of Crooker (1979) and further defined by Luhmann et al. (1984). Whenever $B_Y$ is dominant, the principal merging locations are at high latitudes on opposite sides of noon in the opposite hemispheres, the ends of which are loosely connected by a velocity separator across the nose at noon. Note that Wing et al. (2001) have put forward a different scenario for a

bifurcated cusp suggesting that a high latitude merging source is combined with a near equator component merging source.

Images of the cusp proton aurora from the IMAGE satellite now monitor the ionospheric response of the cusp to changes in the IMF. In northward dominated conditions the cusp aurora appears as a spot. Phan et al. (2003) have mapped an active X-line at Cluster to the vicinity of the spot in the proton aurora images. Frey et al. (2003) have statistically shown the movement of the cusp proton emissions with $B_Y$. Lockwood et al. (2003) followed the changing position of the proton aurora with changing clock angle during a southward turning. These images are sensitive to protons in the keV energy range and map the proton energy input into the cusp every 2 min, with moderate spatial resolution.

## 5. When and on what time scales does merging occur?

The influence of $B_X$ on the timing of interactions leads naturally to the next question of when and on what time scales does merging occur. The Cowley and Lockwood (1992) picture of temporally dependent merging implies that all flux transfer occurs in short episodic merging events of component merging in the near equatorial regions followed by periods where no merging takes place. The repetition time for these events is typically 6–10 min. Many have tied these episodic events to flux transfer events and ionospheric signatures such as the poleward moving auroral forms of Fasel (1995). However, these episodic events seem to have larger scales than those previously inferred from the measurements associated with flux transfer events. The merits of pulsed merging versus more continuous, but time-dependent, merging have been debated by Lockwood (1994), Sibeck and Newell (1994) and Maynard et al. (1994).

In placing merging at high latitudes Maynard et al. (2001c) also concluded that the rate was varying on time scales of 1–2 min, driven by variations in the IMF. In addition to the correlation between the solar wind electric field and the electric fields measured by the rocket, Maynard et al. (2001c) also found optical responses in all-sky images at 557.7 nm which peaked at every enhancement in the effective solar wind electric field. The variations in the green line were harmonized with the IMF measurements over more than 20 min, implying time varying, but nearly continuous, directly-driven merging. The location was closer than the location of the rocket payload to the inferred open-closed field line boundary. 557.7 nm emissions generally imply more energetic electrons than those typically found in the cusp away from the open-closed boundary, probably 500 eV or greater in energy. Maynard (2003) suggested that these could be generated during active merging, which makes localized 557.7 nm emissions a signature, in fact a

"television" record, of the spatial and temporal variability of the merging process on the magnetopause. These localized 557.7 nm emissions are separate from the larger-scale and more diffuse background aurora from higher-energy plasma-sheet electrons found in the closed field line region, and identified as "type 5" dayside aurora by Sandholt et al. (1998).

Figures 6–8 show sequences of 557.7 nm all-sky images, taken every 30 s and projected to 150 km (Maynard 2003). Referring back to the cartoon of Figure 1 for positive $B_Y$, the expected merging locations in the local hemisphere would be on the orange hook pattern on the dusk side of the high-altitude cusp and projecting down to the dusk side of the cusp in the ionosphere. The location on the hook depends on the relative strength and polarity of $B_Z$. For negative $B_Y$ the hook would be on the morning side of the cusp. In Figures 6, 7, and 8 an orange hook has been overlaid to guide the eye. We have also added yellow, pink, green and red fiducials in each image to help follow activity changes at specific locations. Magnetic North is toward Greenland in the upper left of the images. In the sequence in Figures 6 and 7 in which $B_Y$ dominates, localized emissions appear and

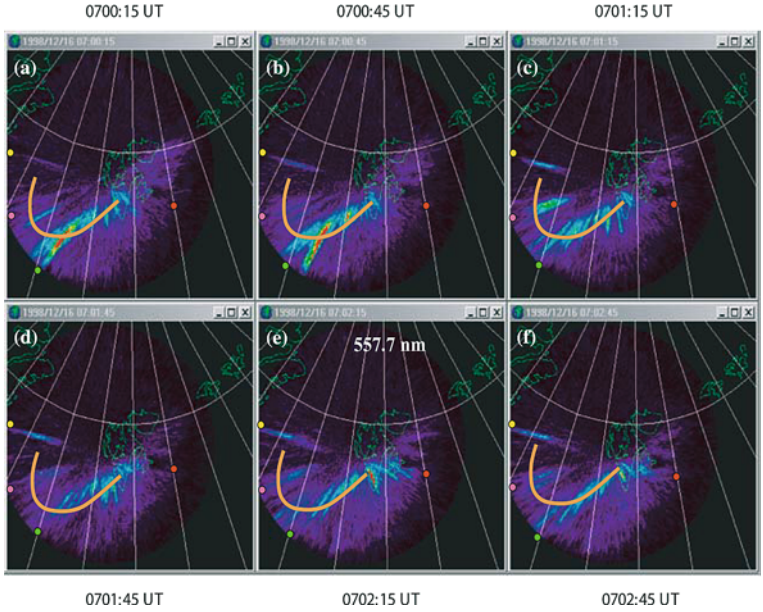


*Figure 6*. All-sky images (from Ny-Ålesund) of 557.7 nm emissions taken every 30 s, starting at 0700:15 UT on 16 December 1998. The orange hook is an approximation of the mapping locus of the northern hemisphere merging line for IMF $B_Y$ negative, following the conceptual diagram of Figure 1 (see text). Its placement is approximate and meant to guide the eye only. Note that features appear and disappear at various positions on the hook on time scales of 1–2 min. Yellow, pink, green and red fiducials are placed in the same spot in each image to help the eye follow changes (adapted from Maynard, 2003).

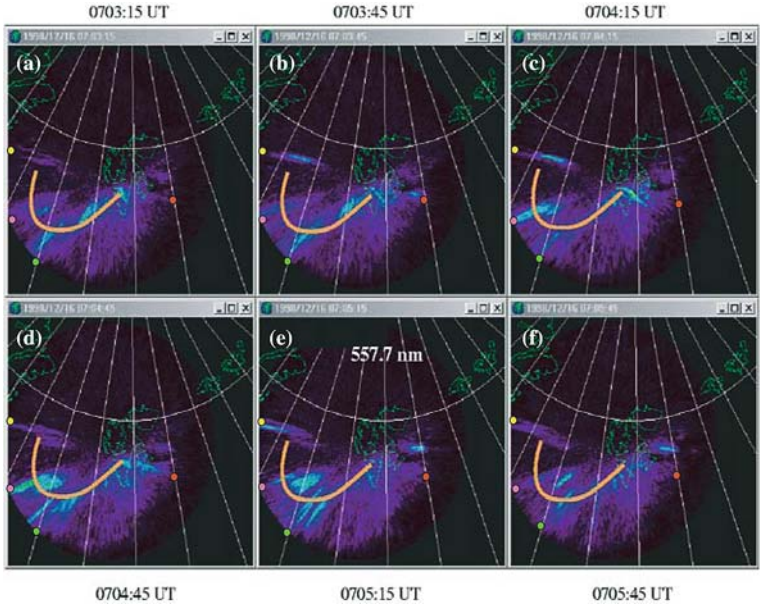


*Figure 7.* All-sky images of 557.7 nm emissions taken every 30 s, starting at 0703:15 UT on 16 December 1998. The orange hook is an approximation of the mapping locus of the northern hemisphere merging line for IMF $B_Y$ negative, following the conceptual diagram of Figure 1 (see text). Its placement is approximate and meant to guide the eye only. Note that features appear and disappear at various positions on the hook on time scales of 1–2 min. Yellow, pink, green and red fiducials are placed in the same spot in each image to help the eye follow changes.

disappear on time scales of 90 s to a few minutes. For example, follow the variations in intensity with time of the feature highlighted by the yellow fiducial. Emissions appear in Figure 6b and remain through Figure 6f. They reappear in Figure 7b and c, diminish in Figure 7d, and briefly return in Figure 7e. Multiple sites are active simultaneously, often initiating at different times. The pink fiducial marks similar behavior to that seen in the yellow, but with peaks at different times. The emissions roughly follow the hook with activity present in all images. Note that the emissions are elongated and point near the center of the image, or to magnetic zenith, which indicates that these structures are vertical rays with their length in the image tied to their vertical extent. The sequence in Figure 8 occurred 15 min later when a significant negative $B_Z$ was also present. Note that the emissions have moved to the front side of the hook as hypothesized. They are still temporally varying, but have continuity over larger spatial scales. Examples of temporal dependencies in Figure 8 are are marked by green and red fiducials. Note that emissions at the yellow and pink fiducials are no longer present.

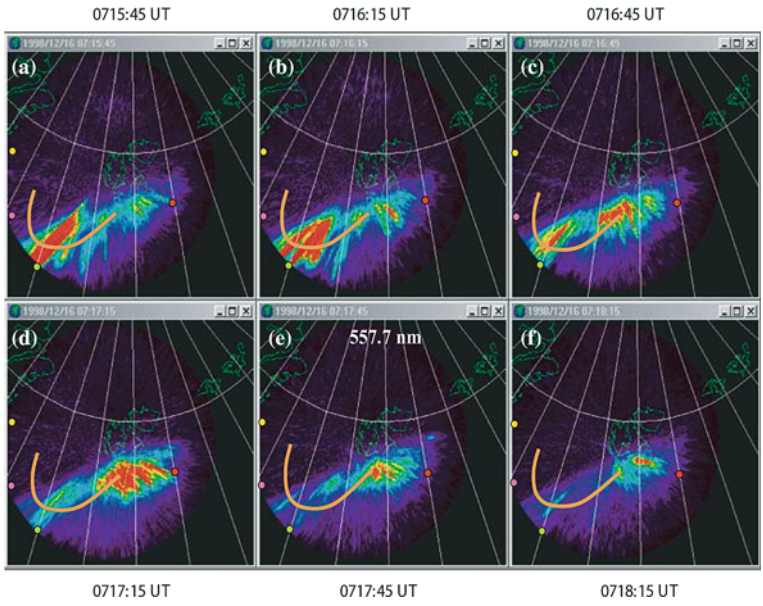


*Figure 8*. All-sky images of 557.7 nm emissions taken every 30 s, starting at 0715:45 UT on 16 December 1998. The orange hook is an approximation of the mapping locus of the northern hemisphere merging line for IMF BY negative, following the conceptual cartoon of Figure 1 (see text). Its placement is approximate and meant to guide the eye only. Note that 15 min later than the observations in Figure 6, the emissions are all on the equatorward portion of the hook. Yellow, pink, green and red fiducials are placed in the same spot in each image to help the eye follow changes (adapted from Maynard, 2003).

Placing these results back into the context of the high altitude cusp, merging would be expected to be occurring in short temporal bursts on time scales of a few minutes or less at multiple locations simultaneously on the rim of the cusp. The locations would shift from the dusk edge of the rim toward the frontside and noon as the clock angle increases, as shown in the cusp configuration from Figure 3 of Siscoe et al. (2005, this volume). This is a much different temporal response from that expected for the pulsed reconnection model of Cowley and Lockwood (1992), which is based on near equatorial component merging and which may exist under other IMF conditions. Note, however, that Lockwood et al. (2003) have more recently expanded their definition of ''low latitude'' merging to that which is occurring ''between the cusps''. The temporal variations are consistent with the observations from Maynard et al. (2003), discussed above in the context of Figures 3, 4, and 5, and the earlier conclusions of Haerendel et al. (1978). These results favor observations of small spatial-scale, temporally-variable merging at high latitudes around the cusp with time scales of a few minutes or less. High-latitude merging is expected to be more temporally variable, since

an $X$-line will not be intrinsically stable when the tangential magnetosheath flow is super-Alfvénic (Cowley and Owen, 1989; Rodger et al., 2000). The temporal variability observed by Maynard et al. (2001c) has its source in the opposite hemisphere. One may expect that temporal variations will be seen in the optical responses from both near and remote hemisphere merging sites as the cusp is bifurcated by $B_Y$.

## 6. How?

All of the above observations and conclusions have involved data taken well away from the merging separator. The question of how merging is in fact accomplished, or the microphysics of the process, can therefore not be addressed by those events. One recent experimental investigation does, however, address how and has bearing on the previous conclusions. Scudder et al. (2002a) used Polar observations above the cusp with northward IMF to discern that the spacecraft stayed in close proximity to the merging separator for over 25 min on 29 May 1996. In addition to the usual tests described above, they were able to confirm that both ion and electron gyrotropy were broken. Parallel electric fields are a necessary condition for merging. The first direct measurement of parallel electric fields at the separator was made, and it was shown that they are derived from the electron pressure gradient force, rather than from anomalous resistivity. The magnetic field reached machine zero at the separator indicating anti-parallel merging with no guide field in this northward IMF case. These results provide strong evidence that the ambipolar and Hall terms provide the necessary physics in the Ohm's Law for accomplishing merging at the separator. In fact, ambipolar electric fields may occur in other situations in addition to merging in the vicinity of the magnetopause, such as depletion layers (Scudder et al., 2002b).

The long duration of the satellite in the vicinity of the separator indicates a steady state process, albeit with possible rate variations. This is in contrast with the temporally and spatially varying properties of high latitude merging discussed above. The Scudder et al. (2002a) event was for northward IMF and was located above and behind the cusp. The other merging events described above were deduced to be located on the side and front walls of the cusp. All locations would not intrinsically support steady reconnection because of the super-Alfvénic tangential magnetosheath flow (e. g., Rodger et al., 2000). Two factors deserve consideration to resolve this issue. First, in the Scudder et al. (2002a) event the nominal magnetosheath flow would be through the X-line location. Siscoe et al. (2002a) have pointed out that in their MHD simulations an active merging site above the cusp remains stationary in the presence of fast flowing magnetosheath plasma. They refer to

this as flow-through reconnection (FTR). In the simulation a tongue of weak magnetic field extends sunward from the null point. The tongue is also characterized by strong electric current, and it has a part where the velocity is sub-Alfvénic. Whether FTR can in reality provide a means for steady state reconnection above the cusp remains to be checked experimentally. Secondly, the back wall of the cusp may serve as a barrier to mediate the flow. The interball satellite has found non-linear turbulence in a boundary layer at the indentation of the cusp (e.g., Savin et al., 2002, 2004). They postulate that the turbulence is indicative of patchy merging. The role of this turbulent boundary layer relative to merging needs further study.

## 7. Implications

These results point to commonly-occurring, high-latitude merging. The optical results and the event of 12 March 2001 depict the process also as temporally varying on scales of a few minutes or less, of small spatial scale, and may be occurring at multiple sites at any particular time. Cluster, with its ability to separate spatial from temporal effects and to measure currents is an ideal mission to verify these implications.

A consequence of high latitude merging is an open boundary layer draped over the nose (Maynard et al., 2002). Whenever $B_Y$ is comparable or greater than the other components, the cusp is bifurcated relative to its source region. The newly opened field lines on the backside of the X-line connect to the opposite hemisphere cusp. As a result, the small convection cell is in fact driven from merging in the opposite hemisphere (Maynard et al., 2001b, 2001c). Also the open boundary layer may be quite thick back along the flank of the magnetopause (Maynard et al., 2001a).

Perhaps the broadest and most far-reaching implications come from the consideration of $B_X$ and the resulting tilted phase planes (Maynard et al., 2001c; Weimer et al., 2002). The tilt can greatly change the lag time from an upstream solar wind monitor, and that lag time, as well as the phase plane tilt, can vary significantly on scales of tens of minutes. Tilted phase planes and $B_X$ lead to merging at high latitudes and timing differences between merging in each hemisphere. Maynard et al. (2001c) found a difference in interaction times of 14 min. Care must be taken in determining the variable lag to assess the possible correlation of magnetosphere and ionosphere phenomena with the IMF system inputs. The correlations found by Maynard et al. (2000, 2001c) and the coherence of small scale variations between 4 spacecraft in the solar wind found by Weimer et al. (2002) show that many small scale phenomena in the magnetosphere–ionosphere system may be directly driven.

$B_X$ serves to enhance or diminish the effective dipole tilt (Crooker, 1992). In the MHD simulations, increasing the dipole tilt can push the merging site off the equator, even for purely southward IMF (Maynard et al., 2003). We should remember that the dipole tilt varies $\pm 12°$ each day from the Earth's rotation and $\pm 23.5°$ with season. Adding to or subtracting from these changes with $B_X$ means that merging may shift to or away from the equatorial or high latitude regions with UT, season, and sector structure.

Identifying an optical response from active merging provides a new tool for understanding solar wind coupling to the magnetosphere–ionosphere system. High resolution 557.7 nm all-sky observations have been made now for the second winter at Ny-Ålesund in Svalbard (J. Moen, private communication, 2002), and their analyses should improve our understanding of the temporal and spatial behavior of magnetospheric merging, especially at high latitudes.

## Acknowledgements

I am grateful to my co-authors on the papers that this work synthesizes. Special thanks go to W. J. Burke, D. M. Ober, and D. R. Weimer, who have been the closest to these efforts, and to J. Moen for supplying the all-sky images. F. S. Mozer, J. D. Scudder and M. Dunlop contributed ideas and analysis techniques. We thank the instrument PIs on Polar and Cluster, F. S. Mozer, J. D. Scudder, C. T. Russell, M. Andre, A. Balogh, and H. Rème, and R. Pfaff, PI for one of the rockets, for access to the data. S. W. H. Cowley and G. L. Siscoe also provided helpful comments. We are grateful to C. W. Smith and D. J. McComas for use of the ACE magnetic field and plasma data, and to R. P. Lepping and K. W. Ogilvie for use of the Wind data. The work at MRC was supported by NASA contract NASW-02017, NASA grant NAG5-3182 (subcontract to the University of California, Berkeley), by the NASA Sun-Earth Connections Theory Program Grant NAG5-8135 (subcontract to Boston University) and by the Air Force Office of Scientific Research under task 2311AS. The ISM was developed under sponsorship of the Defense Threat Reduction Agency, 45045 Aviation Drive, Dulles, VA 20166-7517. Cluster is a mission of the European Space Agency and its member countries.

## References

Aggson, T. L., Maynard, N. C., Ogilvie, K. W., Scudder, J. D., and Gambardella, P. J.: 1984. Observations of Plasma Deceleration at a Rotational Magnetopause Discontinuity, *Geophys. Res. Lett.* **11**, 8.

Atkinson, G.: 1992. Mechanism by Which Merging at X-lines Causes Discrete Auroral Arcs, *J. Geophys. Res.* **97**, 1337.

Birn, J., Drake, J. F., Shay, M. A., Rogers, B. N., Denton, R. E., Hesse, M., Kuznetsova, M., Ma, Z. W., Bhattacharjee, A., Otto, A., and Pritchett, P. L.: 2001. Geospace Environmental Modeling (GEM) Magnetic Reconnection Challenge, *J. Geophys. Res.* **106**, 3715.

Coleman, I. J., Chisham, G., Pinnock, M., and Freeman, M. P.: 2001. An Ionospheric Convection Signature of Antiparallel Reconnection, *J. Geophys. Res.* **106**, 28,995.

Cowley, S. W. H.: 1982. The Causes of Convection in the Earth's Magnetosphere: A Review of Developments During the IMS, *Rev. Geophys. Space Phys.* **20**, 531.

Cowley, S. W. H., and Owen, C. J.: 1989. A Simple Illustrative Model of Open Flux Tube Motion Over the Dayside Magnetopause, *Planet. Space Sci.* **37**, 1461.

Cowley, S. W.H., and Lockwood, M.: 1992. Excitation and Decay of Solar Wind Driven Flows in the Magnetosphere–Ionosphere System, *Ann. Geophys.* **10**, 103.

Crooker, N. U.: 1979. Dayside Merging and Cusp Geometry, *J. Geophys. Res.* **84**, 951.

Dungey, J. W.: 1961. Interplanetary magnetic field and the auroral zones, *Phys. Rev. Lett.* **6**, 47.

Dunlop, M. W., Balogh, A., Glassmeier, K.-H., and Robert, P.: 2002. Four-Point Cluster Application of Magnetic Field Analysis Tools the Curlometer, *J. Geophys. Res.* **107**(A11), 1384doi10.1029/2001JA005088.

Gonzalez, W. D., and Mozer, F. S.: 1974. A Quantitative Model for the Potential Resulting from Reconnection with Arbitrary Interplanetary Magnetic Field, *J. Geophys. Res.* **79**, 4186.

Gosling, J. T., Asbridge, J. R., Bame, S. J., Feldman, W. C., Paschmann, G., Sckopke, N., and Russell, C. T.: 1982. Evidence for Quasi-Stationary Reconnection at the Dayside Magnetopause, *J. Geophys. Res.* **87**, 2147.

Fasel, G. J.: 1995. Dayside Poleward Moving Auroral Forms, A Statistical Study, *J. Geophys. Res.* **100**, 11,891.

Frey, H. U., Mende, S. B., Fuselier, S. A., Immel, T. J., and Ostgaard, N.: 2003. Proton Aurora in the Cusp During Southward IMF, *J. Geophys. Res.* **108**(A7), 1277doi10.1029/2003JA009861.

Haerendel, G., Paschmann, G., Sckopke, N., Rosenbauer, H., and Hedgecock, P. C.: 1978. The Frontside Boundary Layer of the Magnetosphere and the Problem of Reconnection, *J. Geophys. Res.* **83**, 3195.

Hain, K.: 1987. The Partial Donor Cell Method, *J. Comput. Phys.* **73**, 131.

Kawano, H., and Higuchi, T.: 1995. The Bootstrap Method in Space Physics Error Estimation for Minimum Variance Analysis, *Geophys. Res. Lett.* **22**, 307.

Keith, W. R., Winningham, J. D., Goldstein, M. L., Wilber, M., Fazakerley, A. N., Reme, H., Fritz, T. A., Balogh, A., Cornilleau-Wehrlin, N., and Maksimovic, M.: 2005, Observations of a Unique Cusp Signature at Low and Mid Altitudes, *Surveys in Geophys.*, this volume.

Lemaire, J.: 1977. Impulsive Penetration of Filamentary Plasma Elements into the Magnetospheres of Earth and Jupiter, *Planet. Space Sci.* **25**, 887.

Levy, R. H., Petschek, H. E., and Siscoe, G. L.: 1964. Aerodynamic Aspects of Magnetospheric Flow, *AIAA J.* **2**, 2065.

Lockwood, M.: 1994. Ionospheric Signatures of Pulsed Magnetopause Reconnection, in J. A. Holtet, and A. Egeland (eds.), *Physical Signatures of Magnetospheric Boundary Layer Processes*, Kluwer Academic Publishers, The Netherlands, pp. 229.

Lockwood, M., Lanchester, B. S., Frey, H. U., Thorp, K., Morley, S. K., Milan, S. E., and Lester, M.: 2003. IMF Control of Cusp Proton Emission Intensity and Dayside Convection Implications for Component and Anti-Parallel Reconnection, *Ann. Geophys.* **21**, 955.

Luhmann, J. G., Walker, R. J., Russell, C. T., Crooker, N. U., Spreiter, J. R., and Stahara, S.: 1984. Patterns of Potential Magnetic Field Merging Sites on the Dayside Magnetopause, *J. Geophys. Res.* **89**, 1739.

Ma, Z. W., and Bhattacharjee, A.: 2001. Hall Magnetohydrodynamic Reconnection the Geospace Environment Modeling Challenge, *J. Geophys. Res.* **106**, 3773.

Ma, Z. W., Scudder, J. D., and Omidi, N.: 2002, The Achilles Heel of Normal Determinations via Minimum Variance Techniques Worldline Dependencies, *EOS Trans.* AGU **83**(47), Fall Meet. Suppl., Abstract SM11B-0433.

Maynard, N. C.: 2003, Svalbard: A Window for Understanding Temporal/Spatial Aspects of Solar Wind Coupling to the Magnetosphere and Ionsphere, in J. Moen and J. A. Holtet (eds), *Egeland Symposium on Auroral and Atmospheric Research*, ISBN 82-91853-09-6, Department of Physics, University of Oslo, pp. 75.

Maynard, N. C., and Johnstone, A. D.: 1974. High-Latitude Dayside Electric Field and Particle Measurements, *J. Geophys. Res.* **79**, 3111.

Maynard, N. C., Burke, W. J., Denig, W. F., and Basinska, E. M.: 1994. Signatures and Sources of Electric Fields and Particles at Dayside High Latitudes, in J. A. Holtet, and A. Egeland (eds.), *Physical Signatures of Magnetospheric Boundary Layer Processes*, Kluwer Academic Publishers, The Netherlands, pp. 59.

Maynard, N. C., Denig, W. F., and Burke, W. J.: 1995. Mapping of Ionospheric Convection Patterns to the Magnetosphere, *J. Geophys. Res.* **100**, 1713.

Maynard, N. C., Weber, E. J., Weimer, D. R., Moen, J., Onsager, T., Heelis, R. A., and Egeland, A.: 1997. How Wide in Magnetic Local Time is the Cusp? An Event Study, *J. Geophys. Res.* **102**, 4765.

Maynard, N. C., Burke, W. J., Pfaff, R. F., Weber, E. J., Ober, D. M., Weimer, D. R., Moen, J., Milan, S., Sandholt, P. E., Egeland, A., Søraas, F., Lepping, R., Bounds, S., Acuña, M. H., Freudenreich, H., Gentile, L. C., Hardy, D. A., Holtet, J. A., Lester, M., Machuzak, J. S., Clemmons, J. H., Ning, P., Stadsnes, J., and van Eyken, T.: 2000. Driving Dayside Convection with Northward IMF Observations by a Sounding Rocket Launched from Svalbard, *J. Geophys. Res.* **105**, 5245.

Maynard, N. C., Savin, S., Erickson, G. M., Kawano, H., Nemecek, Z., Peterson, W. K., Safrànková, J., Sandahl, I., Scudder, J. D., Siscoe, G. L., Sonnerup, B. U.Ö., Weimer, D. R., White, W. W., and Wilson, G. R.: 2001a. Observation of the Magnetospheric "Sash" and Its Implications Relative to Solar-Wind/Magnetospheric Coupling: A Multisatellite Event Analysis, *J. Geophys. Res.* **106**, 6097.

Maynard, N. C., Siscoe, G. L., Sonnerup, B. U.Ö., White, W. W., Siebert, K. D., Weimer, D. R., Erickson, G. M., Schoendorf, J. A., Ober, D. M., and Wilson, G. R.: 2001b. The Response of Ionospheric Convection to Changes in the IMF: Lessons from a MHD Simulation, *J. Geophys. Res.* **106**, 21,429.

Maynard, N. C., Burke, W. J., Sandholt, P. E., Moen, J., Ober, D. M., Lester, M., Weimer, D. R., and Egeland, A.: 2001c. Observations of Simultaneous Effects of Merging in Both Hemispheres, *J. Geophys. Res.* **106**, 24,551.

Maynard, N. C., Burke, W. J., Moen, J., Sandholt, P. E., Lester, M., Ober, D. M., Weimer, D. R., and White, W. W.: 2002. Bifurcation of the Cusp: Implications for Understanding Boundary Layers, in P. T. Newell, and T. Onsager (eds.), *Earth's Low-Latitude Boundary Layer, Geophys. Mon. 133*, Am. Geophys. Union, Washington, DC, pp. 319.

Maynard, N. C., Ober, D. M., Burke, W. J., Scudder, J. D., Lester, M., Dunlop, M., Wild, J. A., Grocott, A., Farrugia, C. J., Lund, E. J., Russell, C. T., Weimer, D. R., Siebert, K. D., Balogh, A., Andre, M., and Reme, H.: 2003. Polar, Cluster and SuperDARN Evidence for High Latitude Merging During Southward IMF: Temporal/Spatial Evolution, *Annales Geophys.* **21**, 2233.

Newell, P. T., and Sibeck, D. G.: 1994. Magnetosheath Fluctuations, Ionospheric Convection and Dayside Ionospheric Transients, in J. A. Holtet, and A. Egeland (eds.), *Physical Signatures of Magnetospheric Boundary Layer Processes*, Kluwer Academic Publishers, The Netherlands, pp. 245.

Paschmann, G., Sonnerup, B. U. Ö., Papamastorakis, I., Skopke, N., Haerendel, G., Bame, S. J., Asbridge, J. R., Gosling, J. T., Russell, C. T., and Elphic, R. C.: 1979. Plasma Acceleration at the Earth's Magnetopause Evidence for Reconnection, *Nature* **282**, 243.

Paschmann, G., Papamastorakis, I., Baumjohann, W., Sckopke, N., and Lühr, H.: 1986. *J. Geophys. Res.* **91**, 11,099.

Phan, T., Frey, H. U., Frey, S., Peticolas, L., Fuselier, S., Carlson, C., Reme, H., Bosqued, J.-M., Balogh, A., Dunlop, M., Kistler, L., Moukis, C., Dandouras, I., Sauvaud, J.-A., Mende, S., McFadden, J., Parks, G., Moebius, E., Klecker, B., Paschmann, G., Fujimoto, M., Petrinec, S., Marcucci, M. F., Korth, A., and Lundin, R.: 2003. Simultaneous Cluster and IMAGE Observations of Cusp Reconnection and Auroral Proton Spot for Northward IMF, *Geophys. Res. Lett.* **30**(10), 1509doi10.1029/2003GL016885.

Rodger, A. S., Coleman, I. J., and Pinnock, M.: 2000. Some Comments on Transient and Steady-State Reconnection at the Dayside Magnetopause, *Geophys. Res. Lett.* **27**, 1359.

Russell, C. T., and Elphic, R. C.: 1979. ISEE Observations of Flux Transfer Events at the Dayside Magnetopause, *Geophys. Res. Lett.* **6**, 33.

Sandholt, P. E., Deehr, C. S., Egeland, A., Lybekk, B., Viereck, R., and Romick, G. J.: 1986. Signatures in the Dayside Aurora of Plasma Transfer from the Magnetosheath, *J. Geophys. Res.* **91**, 10063.

Sandholt, P. E., Farrugia, C. J., Moen, J., Noraberg, Ø, Lybekk, B., Sten, T., and Hansen, T.: 1998. A Classification of Dayside Auroral forms and Activities as a Function of Interplanetary Magnetic Field Orientation, *J. Geophys. Res.* **103**, 22,325.

Savin, S., Büchner, J., Consolini, G., Nikutowski, B., Zelenyi, L., Amata, E., Auster, H. U., Blecki, J., Dubinin, E., Fornacon, K. H., Kawano, H., Klimov, S., Marcucci, F., Nemecek, Z., Pedersen, A., Rauch, J. L., Romanov, S., Safrankova, J., Sauvaud, J. A., Skalsky, A., Song, P., and Yermolaev, Yu.: 2002. On the Properties of Turbulent Boundary Layer Over Polar Cusps, *Nonlinear Processes in Geophys.* **9**, 443.

Savin, S., Zelenyi, L., Romanov, S., Sandahl, I., Pickett, J., Amata, E., Avanov, L., Blecki, J., Budnik, E., Buchner, J., Cattell, C., Consolini, G., Fedder, J., Kawano, H., Klimov, S., Korepanov, V., Lagoutte, D., Marcucci, F., Mogilevsky, M., Nemecek, Z., Nikutowski, B., Nozdrachev, M., Parrot, M., Rauch, J. L., Romanov, V., Romantsova, T., Russell, C. T., Safrankova, J., Sauvaud, J. A., Skalsky, A., Smirnov, V., Stasiewicz, K., Trotignon, J. G., and Yermolaev Yu.: 2004, Magnetosheath-Cusp Interface, *Annales Geophys.* **22**, 183.

Scudder, J. D.: 1984. Fluid Signatures of Rotational Discontinuities, *J. Geophys. Res.* **89**, 7431.

Scudder, J. D.: 1997. Theoretical Approaches to the Description of Magnetic Merging the Need for Finite $\beta_e$, Anisotropic Ambipolar Hall MHD, *Space Sci. Rev.* **80**, 235.

Scudder, J. D., Puhl-Quinn, P. A., Mozer, F. S., Ogilvie, K. W., and Russell, C. T.: 1999. Generalized Walén Tests Through Alfvén Waves and Rotational Discontinuities using Electron Velocities, *J. Geophys. Res.* **104**, 19,817.

Scudder, J. D., Mozer, F. S., Maynard, N. C., and Russell, C. T.: 2002a. Fingerprints of Collisionless Reconnection at the Separator: I, Ambipolar-Hall Signatures, *J. Geophys. Res.* **107**(A10), 1294doi10.1029/2001JA000126.

Scudder, J. D., Maynard, N., Ober D., and Mozer, F.: 2002b, Ambipolar Electric Fields Parallel and Perpendicular to the Local Magnetic Field: at Magnetopause and Depletion Layers, *EOS Trans. AGU* **83**(47), Fall Meet. Suppl., Abstract SM21B-04.

Shepherd, S. G., Greenwald, R. A., and Ruohoniemi, J. M.: 1999. A Possible Explanation for Rapid, Large-Scale Ionospheric Responses to Southward Turnings of the IMF, *Geophys. Res. Lett.* **26**, 3197.

Sibeck, D. G., and Newell, P. T.: 1994. Concerning the Location of Magnetopause Merging, in J. A. Holtet, and A.. Egeland (eds.), *Physical Signatures of Magnetospheric Boundary Layer Processes*, Kluwer Academic Publishers, The Netherlands, pp. 263.

Siscoe, G. L., Crooker, N. U., Erickson, G. M., Sonnerup, B. U. Ö., Siebert, K. D., Weimer, D. R., White, W. W., and Maynard, N. C.: 2000a, Global Geometry of Magnetospheric Currents Inferred from MHD Simulations, in *Magnetospheric Current Systems, Geophysical Monograph 118*. American Geophysical Union, Washington, DC, pp 41.

Siscoe, G. L., Erickson, G. M., Sonnerup, B. U. Ö., Maynard, N. C., Siebert, K. D., Weimer, D. R., and White, W. W.: 2000b. Deflected Magnetosheath Flow at High-Latitude Magnetopause, *J. Geophys. Res.* **105**, 12,851.

Siscoe, G. L., Erickson, G. M., Sonnerup, B. U. Ö., Maynard, N. C., Schoendorf, J. A., Siebert, K. D., Weimer, D. R., White, W. W., and Wilson, G. R.: 2002a, Flow-Through Magnetic Reconnection, *Geophys. Res. Lett.* **29**(13), 10.1029/2001GL013536.

Siscoe, G. L., Erickson, G. M., Sonnerup, B. U. Ö., Maynard, N. C., Schoendorf, J. A., Siebert, K. D., Weimer, D. R., White, W. W., and Wilson, G. R.: 2002b. MHD Properties of Magnetosheath Flow, *Planet. Space Sci.* **50**, 461.

Siscoe, G. L., Siebert, K. D., Crooker, N. U., Maynard, N. C., Weimer, D. R., and White, W. W.: 2005, Cusp Geometry in MHD Simulations, *Surveys in Geophys.*, this volume.

Sonnerup, B. U. Ö.: 1974. Magnetopause Reconnection Rate, *J. Geophys. Res.* **79**, 1546.

Sonnerup, B. U. Ö., and Ledley, B. G.: 1974. Magnetopause Rotational Forms, *J. Geophys. Res.* **79**, 4309.

Sonnerup, B. U. Ö., Paschmann, G., Papamastorakis, I., Sckopke, N., Haerendel, G., Bame, S. J., Asbridge, J. R., Gosling, J. T., and Russell, C. T.: 1981. Evidence for Magnetic Reconnection at the Earth's Magnetopause, *J. Geophys. Res.* **86**, 10,049.

Sonnerup, B. U. Ö., Papamastorakis, I., Paschmann, G., and Lühr, H.: 1990. The Magnetopause for High Magnetic Shear Analysis of Convection Electric Fields from AMPTE/IRM, *J. Geophys. Res.* **95**, 10,451.

Tsyganenko, N. A., and Stern, D. P.: 1996. Modeling the Global Magnetic Field of the Large-Scale Birkeland Current Systems, *J. Geophys. Res.* **101**, 27,187.

Weimer, D. R.: 2001. An Improved Model of Ionospheric Electric Potentials Including Substorm Perturbations and Application to the GEM November 24, 1996 Event, *J. Geophys. Res.* **106**, 407.

Weimer, D. R., Ober, D., Maynard, N. C., Burke, W. J., Collier, M. R., McComas, D. J., Ness, N. F., and Smith, C. W.: 2002, Variable Time Delays in the Propagation of the Interplanetary Magnetic Field, *J. Geophys. Res.* **107**(A8), 10.1029/2001JA009102.

White, W. W., Siscoe, G. L., Erickson, G. M., Kaymaz, Z., and Maynard, N.C., Siebert, K. D., Sonnerup, B. U. Ö., and Weimer, D. R.1998The Magnetospheric Sash and Cross-Tail SGeophys. Res. Lett.251605.

White, W. W., Schoendorf, J. A., Siebert, K. D., Maynard, N. C., Weimer, D. R., Wilson, G. L., Sonnerup, B. U. Ö., Siscoe, G. L., and Erickson, G. M.: 2001. MHD Simulation of Magnetospheric Transport at the Mesoscale, in Paul Song, Howard J. Singer, and George Siscoe (eds.), *Space Weather, Geophysical Monograph Series*, Volume 125, American Geophysical Union, Washington, DC, pp. 229.

Wing, S., Newell, P. T., and Ruohoniemi, J. M.: 2001. Double Cusp Model Prediction and Observational Verification, *J. Geophys. Res.* **106**, 25,571.

Surveys in Geophysics (2005) 26: 281–305
DOI 10.1007/s10712-005-1883-3 © Springer 2005

# SPATIAL AND TEMPORAL CUSP STRUCTURES OBSERVED BY MULTIPLE SPACECRAFT AND GROUND BASED OBSERVATIONS

K. J. TRATTNER[1], S. A. FUSELIER[1], T. K. YEOMAN[2], C. CARLSON[3], W. K. PETERSON[4], A. KORTH[5], H. REME[6], J. A. SAUVAUD[6] and N. DUBOULOZ[7]

[1]*Lockheed-Martin Advanced Technology Center, Palo Alto CA 94304, USA*
*E-mail: trattner@star.spasci.com;*
[2]*Department of Physics and Astronomy, University of Leicester, Leicester LE1 7RH, England;*
[3]*University of California, Berkeley CA 94724, USA;*
[4]*Laboratory for Atmospheric and Space Physics, University of Colorado, Boulder CO 80309, USA;*
[5]*Max-Planck-Institut für Aeronomie, Katlenburg-Lindau Germany;*
[6]*CESR, Toulouse France;*
[7]*LPCE/CNES, Orleans France*

(Received 10 February 2003; Accepted 30 February 2004)

**Abstract.** Downward precipitating ions in the cusp regularly exhibit sudden changes in ion energy distributions, forming distinctive structures that can be used to study the temporal/spatial nature of reconnection at the magnetopause. When observed simultaneously with the Polar, FAST, and Interball satellites, such cusp structures revealed remarkably similar features. These similar features could be observed for up to several hours during stable solar wind conditions. Their similarities led to the conclusion that large-scale cusp structures are spatial structures related to global ionospheric convection patterns created by magnetic merging and not the result of temporal variations in reconnection parameters. The launch of the Cluster fleet allows cusp structures to be studied in great detail and during changing solar wind conditions using three spacecraft with identical plasma and field instrumentation. In addition, Cluster cusp measurements are linked with ionospheric convection cells by combining the satellite observations with SuperDARN radar observations that are used to derive the convection patterns in the ionosphere. The combination of satellite observations with ground-based observations during variable solar wind conditions shows that large-scale cusp structures can be either spatial or temporal. Cusp structures can be described as spatial features observed by satellites crossing into spatially separated flux tubes. Cusp structures can also be observed as poleward-traveling (temporal) features within the same convection cell, most probably caused by variations in the reconnection rate at the magnetopause.

**Keywords:** cusp geometry, cusp structures, precipitating ions

**Abbreviations:** APL – Applied Physics Laboratory, Johns Hopkins University; DMSP – Defense Meterological Satellite Program; ML – magnetic local time; FAST – Fast Auroral SnapshoT satellite; SC – spacecraft

## 1. Introduction

Magnetic reconnection between the interplanetary magnetic field (IMF) and the geomagnetic field is most probably the dominant process whereby mass and energy are transferred from the solar wind into the magnetosphere. The classical picture of magnetic reconnection was presented by Dungey (1961), where a purely southward IMF and the northward geomagnetic field merged at the sub-solar magnetopause. Convincing evidence about magnetic reconnection has been accumulated with the observation of magnetosheath ions in the boundary layer inside the magnetopause (e.g., Paschmann et al., 1979; Sonnerup et al., 1981) and precipitating ions in the cusp (e.g., Escoubet et al., 1997; Reiff et al., 1977). The incoming magnetosheath distribution is truncated as it crosses the magnetopause so that only a limited part of the initial magnetosheath distribution enters the magnetosphere, forming a characteristic D-shaped distribution that had been predicted by Cowley (1982) and observed by, e.g., Fuselier et al. (1991, 2001). These ions will also stream continuously into the cusp along newly opened magnetic field lines (e.g., Lockwood and Smith, 1993, 1994; Onsager et al., 1993) and exhibit distinct energy versus latitude dispersion patterns as predicted by Rosenbauer et al. (1975) and observed by Shelley et al. (1976).

The complicated structures in cusp precipitation, with variations in flux levels and sudden changes in the energy of the precipitating ions (e.g., Newell and Meng, 1991; Escoubet et al., 1992), are the basis of a debate as to whether dayside reconnection is quasi-steady or transient (e.g., Newell and Sibeck, 1993; Lockwood et al., 1994; Trattner et al., 2002a, and the references therein). All newly opened magnetic field lines convect under the joint action of magnetic tension and momentum transfer from shocked solar wind flow. Thus transient cusp steps are convected, creating an ever-changing structural profile of precipitating cusp ions for observing satellites. This interpretation is based on a model by Cowley and Lockwood (1992) (for which the existence of cusp steps was predicted by Cowley et al. (1991) and Smith et al. (1992)). In this pulsating cusp model, cusp steps are the result of changes in the reconnection rate at the magnetopause that creates neighboring flux tubes in the cusp with different time histories since reconnection (e.g., Lockwood and Smith, 1994). While single-satellite observations are unable to demonstrate that steps in the cusp ion distribution signatures are moving, observations of steps have been interpreted as temporal rather than spatial variations. The observation of poleward moving events by the EISCAT radar (see Lockwood, 1995, 1996; Lockwood et al., 1995) is a natural consequence of a temporal feature, not predicted by a spatial interpretation, and supports this view.

The appearance of temporal cusp steps also depends on the satellite velocity relative to the convection velocity of the cusp structures. Satellites

crossing the boundary from a newly opened flux tube to an older one would encounter a decrease in the ion energy dispersion, while satellites crossing from an older flux tube into a recently opened newer one would see an increase in the ion energy signature. Figure 1 illustrates how one convecting cusp structure will be observed by a slow-moving high-altitude satellite like Polar (crossing the cusp in about 3 hours) and a fast-moving low-altitude satellite like FAST (crossing the cusp in 3 minutes). The slow-moving Polar spacecraft should be overtaken by the convecting structures and move from a ''old'' flux tube to a ''newer'' flux tube with less time since reconnection. As shown in Figure 1 (bottom panel), Polar will encounter an increase in the cusp ion energy dispersion. In contrast, the rapidly moving low-altitude FAST spacecraft would overtake the convecting cusp structure. FAST would cross from a ''new'' flux tube into an ''older'' one, encountering a decrease in the cusp ion energy dispersion (Figure 1, top panel). When observed on multiple satellites with large altitude separation in the cusp, structures caused by temporal variations of the reconnection rate should not only convect with the solar wind, but should also appear differently at different satellites.

Another characteristic to be considered in the observation of temporal structures in the cusp is the number of structures encountered by satellites at different altitudes like Polar and FAST. Depending on the convection speed of the reconnection pulses, the pulse frequency, and the spacecraft velocity in the cusp, many more pulses can be expected on Polar than on FAST.

Flux tubes on open field lines with precipitating magnetosheath ions could also be spatially separated, emanating from multiple X-lines. Crossing the boundary between such spatially separated flux tubes would also appear as a step in the ion energy dispersion due to the different time history since

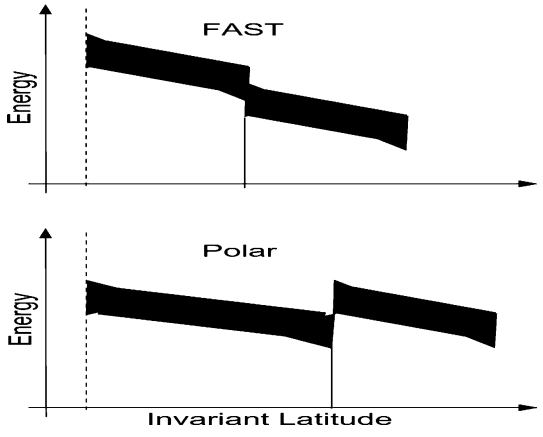


*Figure 1.* Schematic representation of one temporal step in the cusp ion energy dispersion as observed by satellites at vastly different altitudes, e.g., FAST and Polar (from Trattner et al., 2002a).

reconnection for field lines within the two flux tubes (Lockwood et al., 1995). However, this step would not be convecting with the solar wind but would appear as a standing feature in the cusp. Independent of the time delay between the cusp crossings or the satellite velocities, the satellites should encounter unchanged cusp structures at about the same latitude, observing a spatial feature. Such an observation would indicate that the reconnection rate at the magnetopause is rather stable, and not highly variable, to the point where it may even be zero for a limited period of time.

Figure 2 illustrates how two satellites encounter a spatial cusp structure (e.g., Trattner et al., 2002a). It also illustrates how this spatial feature might be encountered at slightly different latitudes by the two satellites. Spacecraft II enters flux tube I at lower latitudes than spacecraft I. The differences in the positions where the satellites enter the cusp are the simple consequence of the form of the equatorward edge of the cusp and the orbital paths of the satellites.

The latitudinal extent of individual cusp structures observed by two satellites also depends on the form of the flux tube and the orbital path intersecting it. These slight variations can, however, lead to misleading interpretations. Since temporal structures are expected to move with the convection flow, variations in the extent of structures could be interpreted as motion. The interpretation is especially difficult when spacecraft close together and at about the same altitude (e.g., Cluster) observe regular structures like the classical staircase.

The appearance of spatial structures has also been discussed by Wing et al. (2001), who modeled cusp precipitation characteristics for periods with a dominant $B_y$ IMF. For these conditions they found that a characteristic "double cusp" signature was not only predicted but also observed in DMSP

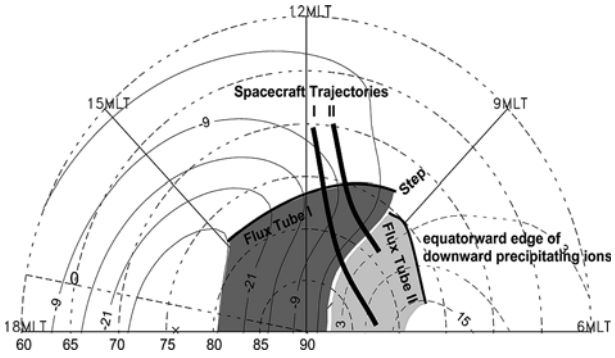


*Figure 2.* Ionospheric convection cells derived from the APL statistical model for $-B_z$ and $-B_y$ input. To illustrate how major cusp structures could be spatial instead of temporal, two flux tubes and two satellite trajectories have been superimposed on the plasma convection cells (from Trattner et al., 2002a).

satellite data. Also using multi-spacecraft observations, Onsager et al. (1995) showed two cusp crossings of the high-altitude Dynamic Explorer 1 (DE 1) and low-altitude DE 2 spacecraft separated by 20 minutes. A similar step in the ion dispersion signature at both spacecraft was interpreted as a spatial structure rather than a temporal variation of the reconnection rate. This event is especially interesting since the low-orbiting satellite encountered an upward step. A temporal convecting cusp structure would require the satellite to move along the open-closed field line boundary to allow the convecting structure to overtake the rapidly moving low-altitude satellite. However, the observing satellite was in a meridian orbit (i.e., presumably perpendicular to the open-closed field line boundary). Further evidence that cusp ion steps can be produced in steady state by spatial variations has also been discussed by, e.g., Newell and Meng (1991), Phillips et al. (1993), Lockwood and Smith (1994) and Weiss et al. (1995).

Ambiguity between spatial and temporal variations is a common problem in interpreting any sequence of data from an orbiting satellite. Multi-spacecraft observations have proven their usefulness in distinguishing between spatial and temporal phenomena. Ground-based information offers an opportunity for remote sensing of the plasma in a given region over a prolonged period. Such measurements also distinguish between temporal and spatial structures but suffer from lower resolution. In addition, transient signatures in the cusp observed from the ground by radar cannot unambiguously define the structures as being caused by precipitating ions (e.g., Lockwood et al., 1993).

In this study we review multi-spacecraft observations from Interball, FAST, Polar and three Cluster spacecraft. In addition, the Cluster observations are discussed in conjunction with SuperDARN radar observations. Among the strong evidence supporting the theory that cusp structures are spatial features, we also present evidence that structures observed within a flux tube appear to be temporal as discussed by Trattner et al. (2002a).

## 2. Mid- and high- altitude cusp observations

Trattner et al. (1999) compared cusp observations made by the toroidal imaging mass-angle spectrograph (TIMAS) on Polar (Shelley et al., 1995) with simultaneous observations made by the ION and HYPERBOLOID instruments on the Interball-AP spacecraft (Dubouloz et al., 1998; Sauvaud et al., 1998). Figure 3 shows a comparison of Polar/TIMAS proton flux data ($1/(\mathrm{cm}^2\ \mathrm{s\ sr\ keV/e})$) observed at an altitude of 5–6 $R_E$ with Interball/ION, HYP observations at 3 $R_E$ altitude for the cusp crossings on 3 May 1997, 13:30 to 15:10 UT. The data are plotted versus invariant latitude (ILAT). Both satellites crossed the cusp near local noon in opposite directions. Polar

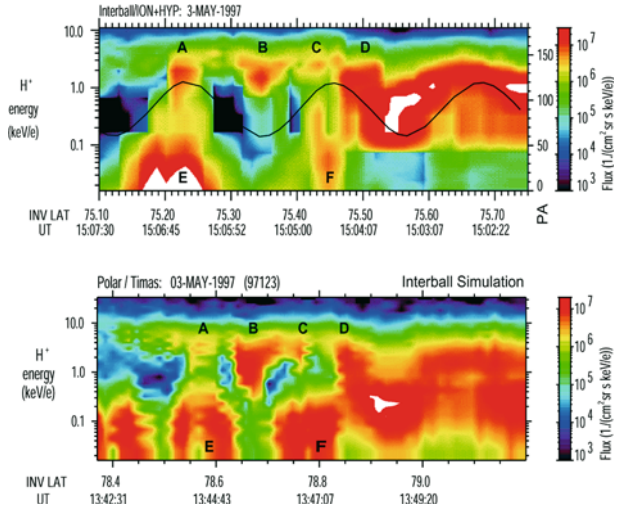


*Figure 3*. Comparison of flux measurements (1/(cm$^2$ s sr keV/e)) by Interball-AP/ION + HYP and Polar/TIMAS at the open-closed field line boundary for the 3 May 1997 cusp event. Polar/TIMAS observations were sampled to obtain a pitch angle distribution similar to Interball/ION. The cusp observations occurred at about the same local time but separated in time by 1 hour 25 minutes. The similarities in the ion dispersion signatures are interpreted as spatial structures rather than temporal variability in the reconnection rate (from Trattner et al., 1999).

was moving poleward and first encountered downward precipitating cusp ions at the equatorward edge of the cusp at about 13:40 UT, while Interball-AP was moving equatorward and left the cusp at about 15:06 UT.

The Interball-AP ION and HYPERBOLOID data are sampled during a two-minute spin period. This causes the pitch angle (PA) window to alternate between upgoing and downgoing ions within a two-minute spin (see black line in the top panel of Figure 3). The ION instrument encountered three sudden decreases in the low-energy cutoff of cusp ions close to the equatorward edge of the cusp. In Figure 3, the three steps are at 75.2° (A), 75.35° (B), and 75.45° (C) ILAT. The three downward steps are followed by a sharp drop of the ion energy at 75.5° (D) ILAT.

To compare Polar/TIMAS with Interball-AP ION and HYPERBOLOID under similar conditions, the two-minute pitch angle period was simulated with TIMAS data. The pitch angles observed at Interball during those steps and structures are transferred from Interball-AP to Polar latitudes, and only the same pitch angle ranges have been accumulated from the Polar measurements. The bottom panel in Figure 3 shows the TIMAS data as they would have been observed by ION and HYPERBOLOID on Interball-AP at the time that Polar crossed into the cusp. The data are averaged over 12 seconds (two spins) for the TIMAS energy range from 16 eV/e to 33 keV/e.

Polar encountered downward precipitating ions with energies up to 10 keV/e briefly at about 78° and 78.2° ILAT while crossing the ion open-closed field line boundary several times. It finally moved completely into the cusp and continuously measured downward precipitating ions at 13:42 UT. The energy of the downward precipitating ions remained constant until Polar reached 78.85° ILAT (13:47 UT), but included three short sudden decreases of the low-energy cutoff of cusp ions at 78.55° (A), 78.65° (B), and 78.75° (C) ILAT. At 78.85° (D) the downward precipitating cusp ion energy dropped from an average of about 5 keV/e to 200 eV/e.

The TIMAS and ION/HYPERBOLOID observations in the cusp are 1 hour 25 minutes apart but show remarkable similarities. In both observations there are three sudden drops of the low-energy cutoff (A, B and C) for ions, followed by a sharp decrease in the ion energy (D). The subsequent rise of ion energy in the ION data, caused by the slow movement of the pitch angle window, is also reproduced in the TIMAS data. The flux enhancements at lower energies (E and F) seen by both HYPERBOLOID and TIMAS are also well-reproduced. In addition, the changes in latitude between the steps are similar in both observations despite the overall latitude difference. The TIMAS and ION/HYPERBOLOID observations are close to the equatorward edge of the cusp; therefore, these observations represent flux tubes that have been recently opened. For the 3 May 1997 event, a series of distinctive features – three brief decreases in the low-energy cutoff followed by a step-down in ion energy – have moved about 3° equatorward and remained close to the equatorward edge of the cusp. These features were still observable after 1 hour 25 minutes, and appear to be spatial structures rather than temporal features caused by variations in the reconnection rate.

## 3. Low-and high-altitude observations

As outlined above, the comparison of cusp observations from satellites at different altitudes is helpful when distinguishing between temporal and spatial structures, since temporal structures would appear different at satellites at different altitudes. This technique has been successfully used by Onsager et al. (1995), Trattner et al. (2002a, b), and others. An extreme combination of cusp observations by satellites at different altitudes is achieved by combining FAST (at about 3000 km) with Polar (up to 8 $R_E$) with their associated very different cusp crossing times of 3 minutes and 3 hours, respectively. Trattner et al. (2002a) compared major steps in the ion energy dispersion of four Polar-FAST cusp crossings during quiet solar wind and IMF conditions. This restriction was chosen to avoid changes in cusp structures due to changes in the location of the X-line at the magnetopause.

Figure 4 shows solar wind observations by the Solar Wind Experiment (SWE) and the Magnetic Field Investigation (MFI) onboard the Wind spacecraft for the Polar-FAST cusp crossings on 8 May 1998. The data have been propagated by about 38 minutes to account for the travel time from the Wind spacecraft to the magnetopause. Plotted are solar wind density $N$, solar wind velocity $V_x$ and the magnetic field components $B_x$ (thick line), $B_y$ (thin line) and $B_z$ (shaded area). Black bars indicate the times when Polar and FAST crossed the cusp and illustrate the temporal separation of the spacecraft. For this 6-hour interval the solar wind conditions were stable, with the solar wind density slightly decreasing from 3.5 $cm^{-3}$ to 2.5 $cm^{-3}$ and a solar wind velocity of about 600 km/s. The IMF observations indicate that $B_z$ was southward for the entire interval, with an average of about −2 nT. $B_y$ was the weakest component, with an average of about −1 nT, while $B_x$ was the dominant component, with an average of about 4 nT.

A comparison of the flux measurements for the Polar and FAST cusp passes on 8 May 1998 is shown in Figure 5. The spacecraft crossed the cusp on field lines mapping to about 09:40 MLT (Polar) and 12:00 MLT (FAST), resulting in a temporal and spatial separation by up to 5 hours in UT and up to 3 hours in MLT. Plotted are $H^+$ flux measurements as observed by the Ion ElectroStatic Analyzer (IESA) (Carlson et al., 2001) (top) and TIMAS (bottom) instruments on FAST and Polar, respectively. White regions in the

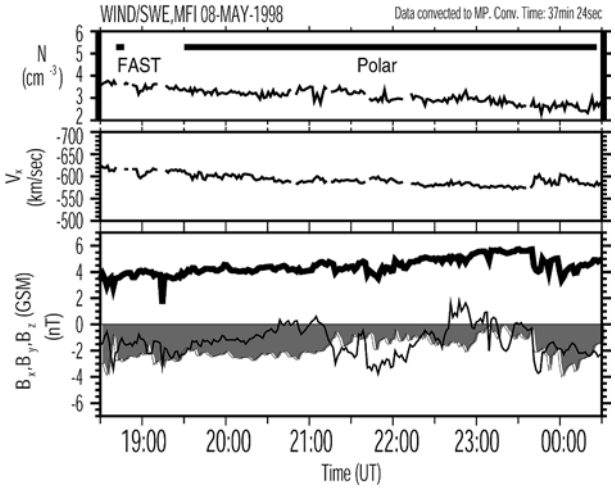


*Figure 4*. Solar wind parameter measurements by Wind/SWE, MFI upstream of the Earth's bow shock on 8 May 1998. The data have been propagated by about 38 minutes to account for the travel time from the Wind spacecraft to the magnetopause. Plotted are solar wind density $N$, solar wind velocity $V_x$ and the magnetic field components $B_x$ (thick line), $B_y$ (thin line), and $B_z$ (shaded area). Black bars indicate the times when Polar and FAST crossed the cusp to illustrate the temporal separation of the spacecraft (from Trattner et al., 2002a).

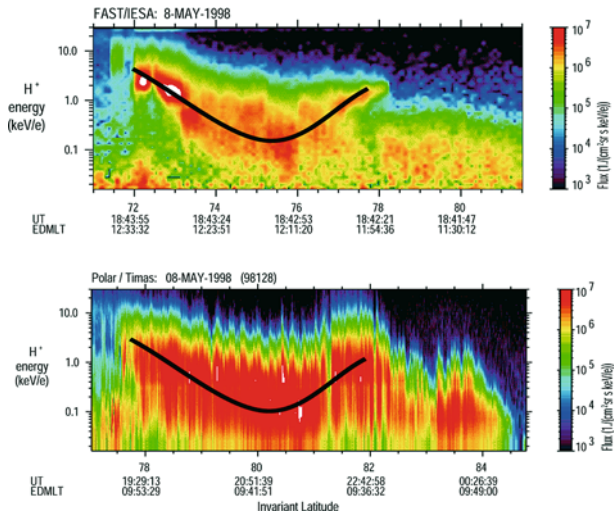


*Figure 5.* Comparison of FAST/IESA and Polar/TIMAS omnidirectional flux measurements (1/(cm$^2$ s sr keV/e)) for cusp crossings on 8 May 1998. The observations are separated by up to 3 hours in MLT and up to 5 hours in time. Even for these extreme spatial and temporal separations, there are remarkable similarities in the FAST/IESA and Polar/TIMAS cusp observations (from Trattner et al., 2002a).

color-coded plot indicate regions with flux levels above the maximum flux level indicated in the color bars. To help to guide the eye, additional lines have been overlaid which represent an average location of the maximum flux in the cusp ion energy dispersion. The FAST spacecraft, moving equatorward in this event, exited the cusp at about 18:44 UT at 72° ILAT and crossed the downward precipitating ion region in about 3 minutes. Seen from the equatorward edge of the cusp at 72° ILAT, the FAST cusp crossing is characterized by a classical velocity dispersion, with lower energy particles arriving at higher latitudes. This velocity filter effect (e.g., Rosenbauer et al., 1975; Onsager et al., 1993) is smoothly reversed at higher latitudes, where the energy of precipitating ions starts to increase again and forms a new maximum. After this second maximum at about 78° ILAT, the cusp ion energy decreases again, in agreement with the classical velocity dispersion.

The Polar spacecraft, moving poleward, encountered downward precipitating ions at about 19:15 UT at 77.5° ILAT. However, in contrast to the 3-minute snapshot of the cusp by FAST, Polar observed precipitating cusp ions for 5 hours. Nevertheless, Polar observed the same basic cusp structure seen by FAST. Cusp ion energies first decreased with increasing ILAT and smoothly reversed at about 80.5° ILAT, to form a new maximum at 82° ILAT. After the second maximum, the cusp ion energy continued to decrease again.

The Polar cusp pass also showed minor structures superimposed on the major cusp ion signature. There are periodic increases and decreases in the cusp ion energy, with a period of about 10 minutes. This feature could be the signature of surface waves at the magnetopause that push the X-line slightly in and out, thereby slightly changing the distance from the spacecraft to the X-line. This feature could also be the signature of pulsed reconnection. Lockwood (private communication, 2001) pointed out that for this specific example the ratio of Polar to FAST cusp steps encountered by the spacecraft should be about 20, which is indeed the case. The form and number of the cusp steps is in agreement with predictions from the pulsed reconnection model (e.g. Lockwood et al., 1998).

If cusp structures are spatial features, similar cusp structures should form for similar IMF conditions when observed in about the same MLT sector. This was the motivation for a subsequent study by Trattner et al. (2002b) who compared three Polar-FAST crossings observed at about the same MLT in the pre-noon sector and during very similar solar wind and IMF conditions.

Figure 6 shows solar wind observations made by Wind/SWE and Wind/MFI for the Polar and FAST cusp crossings on 22 October 1998. The data have been propagated by about 10 minutes to account for the travel time from the Wind spacecraft to the magnetopause. Plotted are solar wind

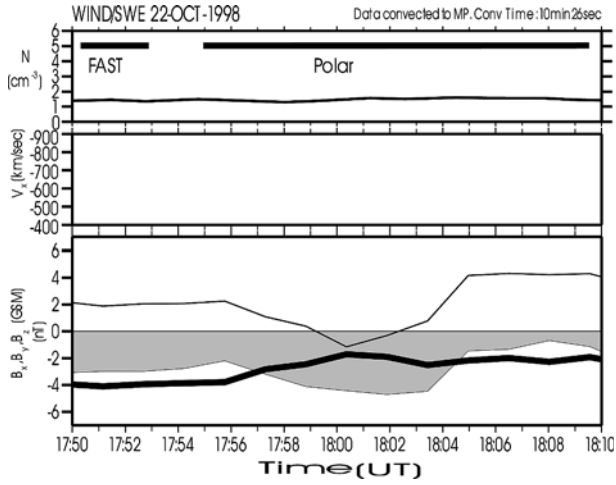


*Figure 6*. Solar wind parameter measurements by Wind/SWE, MFI upstream of the Earth's bow shock on Oct. 22, 1998. The data have been propagated by about 10 minutes to account for the travel time from the Wind spacecraft to the magnetopause. Plotted are solar wind density $N$, solar wind velocity $V_x$ and the magnetic field components $B_x$ (thick line), $B_y$ (thin line) and $B_z$ (shaded area). Black bars indicate the times when Polar and FAST crossed the cusp, illustrating the temporal separation of the spacecraft (from Trattner et al., 2002b).

density $N$, solar wind velocity $V_x$ and the magnetic field components $B_x$ (thick line), $B_y$ (thin line) and $B_z$ (shaded area). Black bars indicate the times when Polar and FAST crossed the cusp and illustrate the temporal separation of the spacecraft. The solar wind density and velocity were about 1.5 $cm^{-3}$ and 600 km/s, respectively. The IMF observations indicate that $B_z$ was southward for the entire interval, with an average value of about −3 nT, $B_y$ was at about 3 nT with a brief negative period at 18:01 UT, and $B_x$ was also negative with an average value of about −3 nT.

Polar and FAST crossed the cusp on 22 October 1998, in the morning sector at about 10:30 MLT (Polar) and 09:40 MLT (FAST), separated by up to 20 minutes in UT and by about 1 hour in MLT. The satellites again moved in opposite directions, with Polar moving equatorward and FAST moving poleward. A comparison of Polar and FAST flux measurements (1/($cm^2$ s sr keV/e)) for the cusp crossings is shown in Figure 7. Plotted are $H^+$ flux measurements as observed by the IESA (top) and TIMAS (bottom) instruments on FAST and Polar, respectively. Also indicated in the Polar and FAST flux panels are the energies where the maximum flux of the cusp ions occurred. To guide the eye, additional lines have been overlaid to emphasize structures in the ion energy distribution.

Both spacecraft observed distinct energy-latitude dispersions typical for southward IMF with the highest energy ions arriving at the lowest ILAT

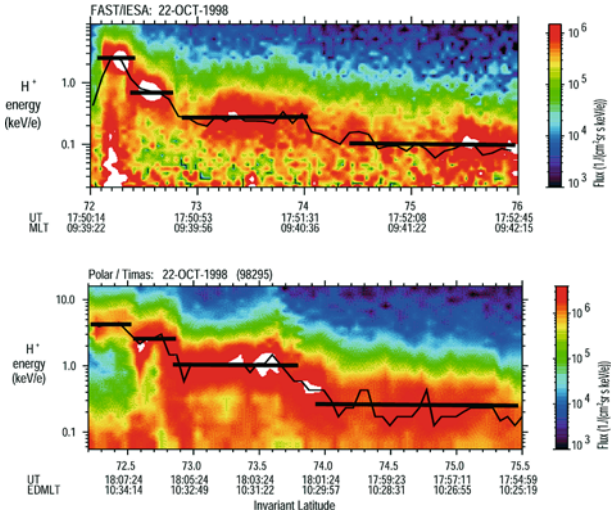


*Figure 7.* Comparison of FAST/IESA and Polar/TIMAS flux measurements (1/($cm^2$ s sr keV/e)) for cusp crossings on 22 October 1998. The observations are separated by about 1 hour in MLT and 20 minutes in UT. The cusp structures in the ion dispersion signatures are interpreted as spatial rather than temporal structures (from Trattner et al., 2002b).

and lower-energy particles arriving at successively higher ILAT. In addition, these decreasing ion energy dispersions at both spacecraft were interrupted by three distinctive cusp steps. The FAST spacecraft entered the cusp at about 17:50 UT, crossed the downward precipitating ion region in 3 minutes, and moved onto lobe field lines. The FAST cusp crossing shows three major steps in the ion energy dispersions that are located at 72.3°, 73°, and 74.2° ILAT. The cusp ion energy decreased sharply from about 3 keV to 700 eV and subsequently to 300 eV for the first two steps. These two cusp steps are followed by a smoother decrease of the cusp ion energy to about 100 eV.

The Polar spacecraft crossed the cusp in about 20 minutes and left the precipitating ion region at 18:10 UT, 20 minutes later than FAST. In agreement with the cusp structures observed by FAST, the decreasing ion energy dispersion seen by Polar is interrupted by three steps located at 72.6°, 72.9°, and 73.8° ILAT. As in the FAST cusp observations, the first two steps seen by Polar show sharp decreases of the cusp ion energy from 4 keV to about 1.5 keV and subsequently to 1 keV. These are followed by a smoother decrease to about 200 eV. Comparing the Polar observations with FAST observations, we find that, while the spacecraft encounter cusp steps at slightly different latitudes, they have not moved within the cusp. This is in agreement with a spatial interpretation of cusp structures. The differences in the cusp ion energies can be attributed to the separation in local time of the two spacecraft and the subsequent different locations where the spacecraft entered neighboring flux tubes with their independent time history since reconnection. The cusp ion energy is also influenced by the location of the X-line and the degree of acceleration of the ions as they cross the dayside magnetopause (e.g., Lockwood and Smith, 1992).

By comparing the Polar and FAST cusp crossings, there is no indication that Polar observed a different number of major cusp steps than FAST did, as we would expect for temporal structures. There is also no indication that FAST encountered a "step-down" in the ion energy dispersion signature while Polar encountered a "step-up", which is also expected for the observations of temporal structures by spacecraft with large altitude separations. Both spacecraft observed the same number and orientation of cusp structures that also have not moved (convected) relative to each other, as expected for temporal cusp features. In addition, Trattner et al. (2002b) showed that all three events observed at about the same MLT in the pre-noon sector and during similar stable solar wind and IMF conditions had the same sequence of cusp steps, two sharp drops in the ion energy dispersion followed by a smoother transition to another energy level. Cusp structures appear to be not only spatial events but seem to be organized in the same sequence for similar IMF conditions.

## 4. Spatial cusp structures observed by cluster and radar observations

Studies like Trattner et al. (2002a) have been limited to events during stable solar wind and IMF conditions to ensure that changes in the cusp ion energy dispersion are not caused by changes in the location of the X-line. In a study by Trattner et al. (2003), multi-spacecraft observations from three Cluster spacecraft are combined with SuperDARN radar observations to investigate cusp structures in unprecedented detail and under any solar wind and IMF conditions.

Figure 8 shows solar wind conditions for the Cluster cusp crossing on 25 July 2001, observed by the Wind/SWE and MFI instruments. The solar wind data have been propagated by about 8 minutes to account for the travel time from the Wind spacecraft to the magnetopause. Solar wind density $N$ and velocity $V_x$ for July 25, 2001, were about 4 $cm^{-3}$ (top panel) and about 560 km/s (middle panel), respectively. The IMF components $B_x$ (black line), $B_y$ (green line) and $B_z$ (colored area) are shown in the bottom panel. At the beginning of the Cluster cusp crossing until about 23:40 UT the IMF shows a typical Parker spiral configuration with a positive $B_x$ of about 3 nT, a negative $B_y$ of about −4 nT and a negative $B_z$ of also about −4 nT (blue colored area). Starting at about 23:35 UT the $B_z$ component rotated through zero (at 23:47 UT) and then switched northward to about 4 nT (red colored area). The $B_y$ component changed direction from negative to positive for 15 minutes at about the same time that the $B_z$ component changed from southward

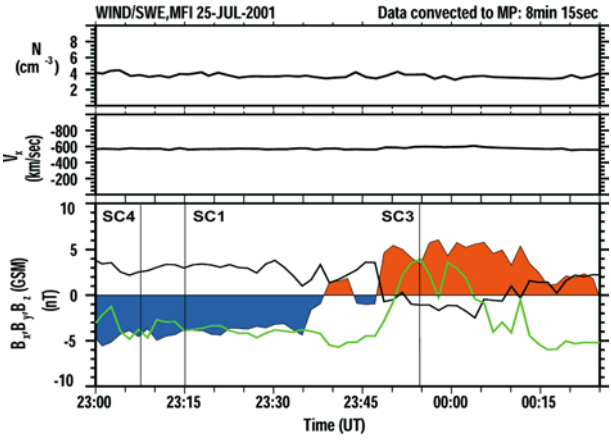


*Figure 8.* Solar wind parameter measurements by Wind/SWE, MFI on 25 July 2001. The data have been propagated by about 8 minutes to account for the travel time from the Wind spacecraft to the magnetopause. Plotted are solar wind density $N$, solar wind velocity $V_x$ and the magnetic field components $B_x$ (black line), $B_y$ (green line) and $B_z$ (shaded area). Black lines indicate the times when Cluster satellites crossed into the cusp to illustrate the temporal separation of the spacecraft (from Trattner et al., 2003).

to northward. Finally, the $B_x$ component also switched from positive to negative for about 15 minutes. Black lines indicate the times when the Cluster satellites crossed into the cusp to illustrate the temporal separation of the spacecraft. SC4 and SC1 entered the cusp at 23:09 UT and 23:15 UT, respectively, during which time the IMF was southward and stable for an extended period of time. SC3 entered the cusp at 23:54 UT, 7 minutes after the IMF switch northward.

Figure 9 shows the temporal separation of the Cluster/CIS observation for the cusp crossings on 25 July 2001. Plotted are $H^+$ omnidirectional flux measurements (1/(cm$^2$ s sr keV/e)) from SC1 (top panel), SC3 (middle panel) and SC4 (bottom panel), observed in an MLT range from 14:00 to 11:00, an ILAT range from 76.8° to 86°, and a geocentric distance from 4.8 to 6 $R_E$. White regions in the color-coded plot indicate regions with flux levels above the maximum flux level indicated in the color bars.

SC1 entered the cusp at about 23:15 UT, marked by a white line (1a), where it encountered downward precipitating magnetosheath ions. SC1 subsequently observed the typical cusp ion energy dispersion for a southward interplanetary magnetic field, with lower energy ions arriving at higher latitudes. The ion energy distribution decreases smoothly, indicating a constant magnetospheric reconnection rate at the magnetopause. At about 23:37 UT, SC1 encounters a sudden increase in the ion energy dispersion (1c), consistent with a typical step-up ion signature for crossing onto magnetic field lines that have been reconnected more recently. The ion energy of the precipitating ions again decreases until about 23:45 UT, when a new low is reached. Pitch angle

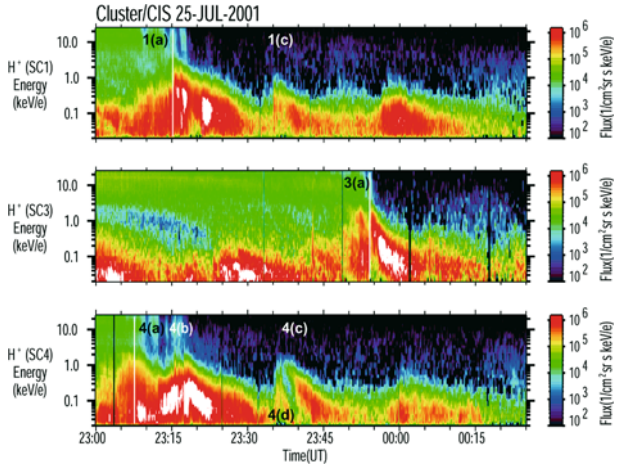


*Figure 9*. Cluster/CIS observation for cusp crossings on 25 July 2001. Plotted are $H^+$ omnidirectional flux measurements (1/(cm$^2$ s sr keV/e)) for SC1, SC3 and SC4. All satellites encounter distinctive structures, sudden jumps in the ion energy dispersion that are similar on SC1 and SC4, but different on the later arriving SC3 satellite (from Trattner et al., 2003).

analysis of this low energy distribution shows that it is solely composed of ionospheric ion outflow.

SC3 crosses into the cusp at 23:54 UT, indicated by a white line in the color spectrogram (3a). This spacecraft also observes a typical decreasing ion energy dispersion for a stable rate of reconnection with no further cusp structures later on. The fact that the observed ion dispersion at SC3 is typical for a southward IMF configuration while the IMF changed northward 6 minutes earlier is the result of a delayed response of the magnetosphere to changes in the solar wind. A delayed response to IMF changes is not unusual and is also observed in the ionospheric convection patterns that are significantly reconfigured about 10 minutes after the IMF change.

The first Cluster satellite to enter the cusp on 25 July 2001 is SC4 at 23:09 UT (4a). The cusp encounter is followed by a decreasing ion energy dispersion which is reversed at about 23:13 UT. The precipitating ion energy reaches a new maximum at 23:15 UT (4b), the same time that SC1 enters the cusp. This enhancement is explained by a change in the configuration of the convection cell which brought the ion open-closed field line boundary closer to the position of SC4, shortening the convection distance (see Trattner et al., 2003). The ion energy again starts to decrease before a second brief increase at 23:35 UT. A detailed pitch angle analysis showed that this signature was caused by ionospheric outflow and not ion precipitation from the magnetosheath. A pitch angle analysis of the proton distribution for the same time interval revealed that such a localized ion outflow distribution was also present at the position of SC1. However, this population was not as clearly separated from the immediately following downward precipitating ions as at the location of SC4. SC4 encounters this second sudden increase in ion energy at about 23:37 UT (4c), which is similar to the increase observed by SC1 at the same time. This step-up structure is also followed by a decrease of ion energy until about 23:45 UT, where a constant low energy flux is reached, typical for high latitude ionospheric outflow.

Figure 10 shows a combination of the temporal and spatial separations of the Cluster spacecraft. The Cluster magnetic foot points and the ionospheric convection streamlines for 25 July 2001, at 23:37 UT, are shown. The ionospheric convection streamlines, presented as contour lines, have been calculated using line-of-sight velocity data from the 8 operating northern hemisphere SuperDARN radars (Greenwald et al., 1995) together with the technique of Ruohoniemi and Baker (1998). Here the fit to the line-of-sight data is made to a sixth spherical harmonic expansion, with the fit stabilized by a statistical pattern keyed to the upstream IMF data from the Wind satellite, delayed by 8 minutes to allow for the propagation time from the spacecraft to the magnetopause (Ruohoniemi and Greenwald, 1996).

Overlaid on the magnetic foot points are 14-minute intervals of the Cluster/CIS flux measurements presented in Figure 9, which are centered on

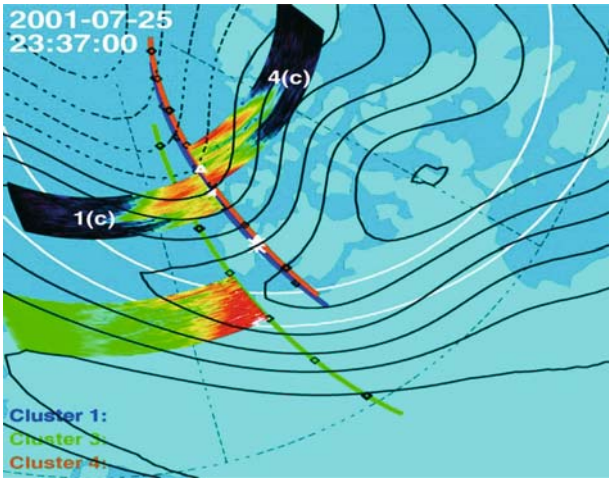


*Figure 10*. Composite plot of Cluster magnetic foot points and ionospheric convection streamlines for 25 July 2001, at 23:37 UT. Overlaid on the magnetic foot points are 14-minute intervals of the Cluster/CIS flux measurements presented in Figure 9, which are centered on the actual position of the Cluster satellites at 23:37 UT. The original entry points of SC1 and SC4 into the cusp are marked with a star and a triangle, respectively, along the tracks of their magnetic foot points. SC1 and SC4 are deep inside the cusp and have just entered the dawn convection cell (dashed lines) resulting in an almost simultaneous sudden increase of the ion energy dispersion on both satellites (also marked with symbols), as expected from a spatial interpretation of cusp structures. During that time SC3 was still on closed field lines (from Trattner et al., 2003).

the actual position of the Cluster satellites at 23:37 UT. This representation shows the actual Cluster measurements in time at the proper spatial location. White lines in Figure 10 represent the average location of the auroral oval.

SC1 and SC4 are deep inside the cusp while SC3 is still on closed field lines. The original entry point of SC1 and SC4 into the cusp are marked with a star and a triangle, respectively, along the tracks of their magnetic foot points. At 23:37 UT the IMF shows a strong decrease in the value of $B_z$, which later changes sign. An equatorward directed bulge in the convection pattern moved rapidly equatorward which in turn allowed the dawn convection cell (dashed black lines) to move equatorward as well. At 23:37 UT, SC1 and SC4 have progressed poleward far enough to be overtaken by the equatorward moving dawn convection cell. The transfer from one convection cell to another resulted in an almost simultaneous sudden increase of the ion energy dispersion (structures 1c and 4c in Figure 9) on both satellites, indicating that the ion open-closed field line boundary in the dawn cell is much closer to the SC1 and SC4 magnetic footprints than in the dusk convection cell (solid black lines). The satellite positions at 23:37 UT, which are also the positions of the sudden increase in the ion energy dispersion, are marked with star (SC1) and triangle (SC4) symbols.

The sudden increase in the ion energy dispersion coincides with a satellite moving into a neighboring spatially separated flux tube (or convection cell). This feature was discussed above, based on earlier cusp observations by Trattner et al. (2002a, 2002b) during stable solar wind conditions. Figure 10 shows not only that such a scenario can take place but that it also occurs during dynamic solar wind IMF conditions. The change in IMF conditions most probably caused a change in the location of the reconnection site, which in turn caused a shift in the positions of spatially separated flux tubes.

## 5. Temporal cusp structures observed by cluster

Figure 11 shows solar wind conditions for the Cluster cusp crossing on 23 September 2001, observed by Wind/SWE, MFI. The solar wind data have been propagated by about 18 minutes to account for the travel time from the Wind spacecraft to the magnetopause. Figure 11 has the same format as Figure 8 and shows a highly variable solar wind density $N$ covering a range between 5 and 20 $cm^{-3}$ (top panel) and a solar wind velocity $V_x$ of about 520 km/s (middle panel). The IMF components $B_x$ (black line), $B_y$ (green line) and $B_z$ (colored area) are shown in the bottom panel. For the Cluster cusp crossing from 11:00 UT to 12:30 UT, the IMF is dominated by a strong

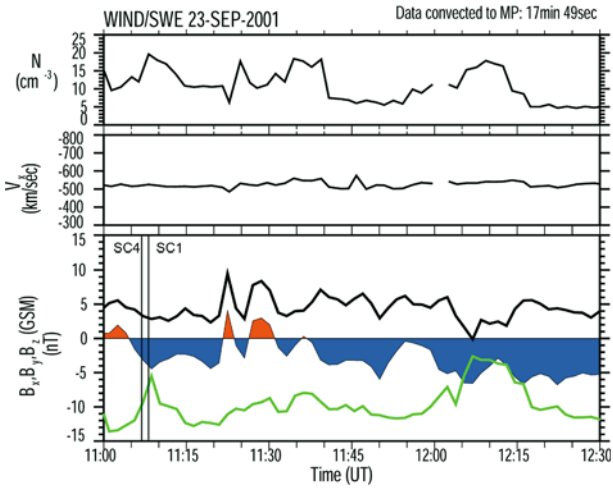


*Figure 11.* Solar wind parameter measurements by Wind/SWE, MFI on 23 September 2001. The data have been propagated by about 18 minutes to account for the travel time from the Wind spacecraft to the magnetopause. Plotted are solar wind density $N$, solar wind velocity $V_x$, and the magnetic field components $B_x$ (black line), $B_y$ (green line) and $B_z$ (shaded area). Thin vertical black lines indicate the times when Cluster SC1 and SC4 satellites crossed into the cusp.

but variable negative $B_y$ component ranging from −3 to −15 nT. The $B_x$ component is positive and centered on 5 nT, while the $B_z$ component is less then 5 nT and switches several times between northward (red) and southward (blue). This Cluster cusp event is characterized by strong variations in solar wind density and IMF directions that will introduce temporal changes in the reconnection location and, most probably, temporal changes in the reconnection rate. Black vertical lines indicate the times when the Cluster SC1 and SC4 satellites crossed into the cusp.

Figure 12 shows $H^+$ omnidirectional flux measurements (1/(cm$^2$ s sr keV/e)) from SC1 (top panel) and SC4 (bottom panel) for this cusp crossing. These measurements were observed in an MLT range from 11:30 to 13:00, an ILAT range from 75° to 83° and a geocentric distance from 4.5 $R_E$ to 5.4 $R_E$.

SC1 enters the cusp at about 11:08 UT, marked by a black vertical line. SC1 subsequently observes two typical step-up cusp structures in the ion energy dispersion at about 11:18 UT (1a) and 11:25 UT (1b). Cluster spacecraft SC4 enters the cusp about 1 minute before SC1 at 11:07 UT, also indicated by a black vertical line. Like SC1, SC4 encounters two step-up cusp structures at about 11:19 (4a) and 11:27 UT (4b). The two cusp steps at SC1 and SC4 are very similar to the spatial structures discussed before. However, their projection into the ionosphere revealed the temporal nature of these structures.

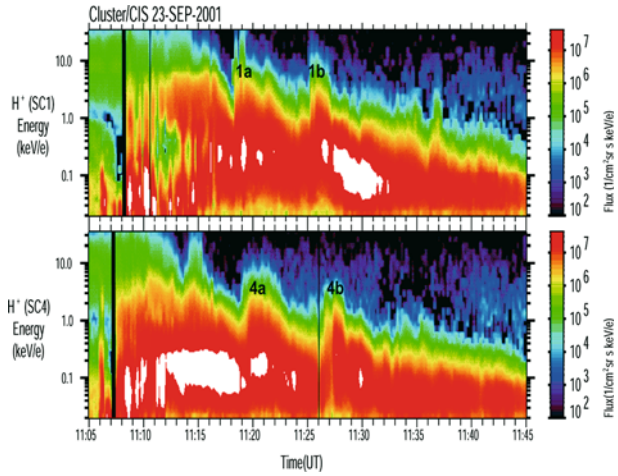


*Figure 12.* Cluster/CIS observation for a cusp crossing on 23 September 2001. Plotted are $H^+$ omnidirectional flux measurements (1/(cm$^2$ s sr keV/e)) for SC1 and SC4. The satellites encounter distinctive "step-up" structures in the ion energy dispersion that are similar on the two Cluster spacecraft. After comparing the satellite observations with simultaneous SuperDARN radar observations, these structures have been identified as temporal structures that are convecting poleward with the convecting magnetic field lines.

Figure 13 shows a composite plot to combine the temporal and spatial separations of the Cluster observations. Shown are the Cluster magnetic foot points and the ionospheric convection streamlines for 23 September 2001, at about 11:18 UT. Overlaid on the magnetic foot points are 14-minute intervals of the Cluster/CIS flux measurements presented in Figure 12, which are centered on the actual position of the Cluster satellites at 11:18 UT. The spacecraft are located at the intersection of the magnetic foot points with the white lines in the overlaid color spectrograms. Poleward (top) of the white lines, the "future" spectra to be observed by SC1 and SC4 are shown, while equatorward (bottom) of the white lines the spectra from the "past" are plotted.

SC1 and SC4 are deep inside the cusp and moving obliquely to the ionospheric convection direction while SC3 is still on closed field lines. The original entry points of SC1 and SC4 into the cusp are marked with a star and a triangle along the tracks of their magnetic foot points. In addition, a black dashed line marks the likely location of the ion open-closed field line boundary that intersects the cusp entry points. At 11:18 UT, SC1 encountered the first step-up cusp structure (1a). SC4, positioned just downstream and poleward of SC1

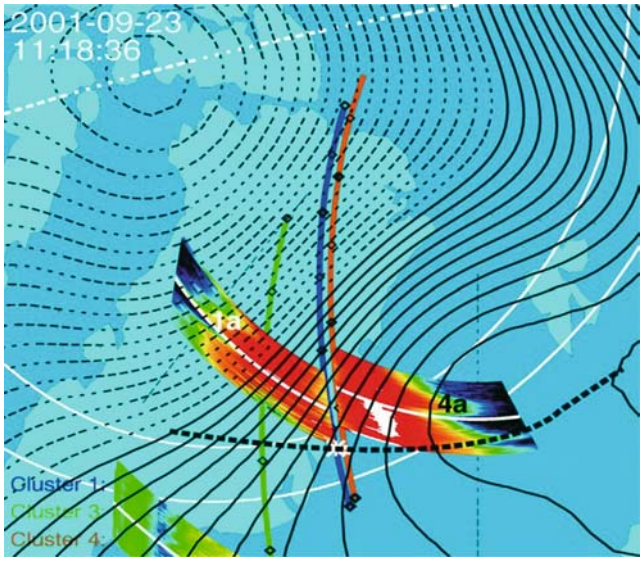


*Figure 13*. Composite plot of Cluster magnetic foot points and ionospheric convection streamlines for 23 September 23 2001, at 11:18 UT. Overlaid on the magnetic foot points are 14-minute intervals of the Cluster/CIS flux measurements presented in Figure 12, which are centered on the actual position of the Cluster satellites at 11:18 UT (indicated by white lines in the spectra). The original entry points of SC1 and SC4 into the cusp are marked with a star and a triangle, respectively, along the tracks of their magnetic foot points. Passing through this location is a thick dashed line representing the most likely position of the ion open-closed field line boundary. SC1 has just encountered a step-up cusp structure while along the convection path about 1° poleward of SC1, SC4 will encounter a similar step about 1 minute later.

along the convection path, will encounter a similar step marked (4a) in about 1 minute. Observing a similar step feature about 1° higher in latitude and about 1 minute later than the low latitude satellite is consistent with a temporal moving structure as predicted by the pulsed reconnection line.

The scenario repeats itself for the second step-up structure. Figure 14 shows the same composite plot as Figure 13 but 7 minutes later. At that time, SC1 encountered the second step-up cusp structure (1b), while again SC4, positioned just downstream and poleward of SC1, will encounter a similar step marked (4b) in about 1 minute and 1° higher in latitude. Also still visible in the 14-minute overlaid spectra for SC4 is the first step-up (4a). Both step structures observed by one spacecraft seem to have convected 1° poleward in the direction of the convection path within about 1 minute, which represents a convection velocity of about 1.5 km/s, in agreement with observed convection speed in the ionosphere of about 1.2 km/s, as measured by the SuperDARN radars (see also Lockwood et al., 1990, Pinnock et al., 1993). These poleward moving structures are consistent with temporal moving structures and could be an indication of a variation of the reconnection rate.

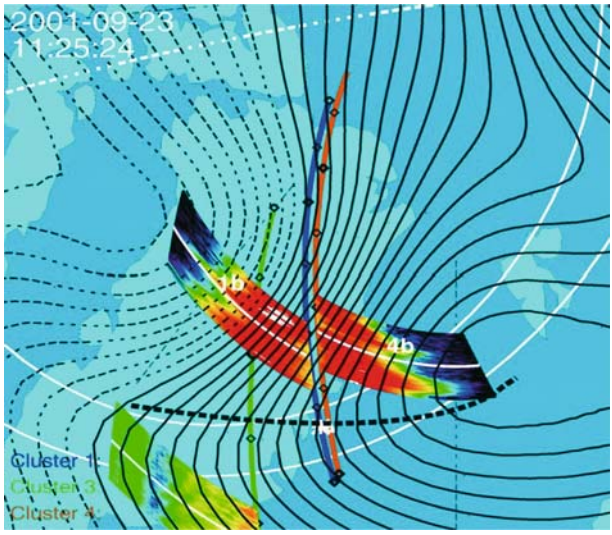


*Figure 14*. Composite plot of Cluster magnetic foot points and ionospheric convection streamlines for 23 September 2001, at 11:25 UT. Overlaid on the magnetic foot points are 14-minute intervals of the Cluster/CIS flux measurements presented in Figure 12, which are centered on the actual position of the Cluster satellites at 11:25 UT (indicated by white lines in the spectra). The original entry point of SC1 and SC4 into the cusp are marked with a star and a triangle, respectively, along the tracks of their magnetic foot points. Passing through this location is a thick dashed line representing the most likely position of the ion open-closed field line boundary. SC1 again encountered a step-up cusp structure while along the convection path about 1° poleward of SC1, SC4 will encounter a similar step about 1 minute later. The previous step-up structure is also still visible in the overlaid spectrogram of SC4.

## 6. Summary and conclusions

The spatial and temporal variations of the cusp reflect the spatial and temporal variations in dayside reconnection location and rate. Early on, sudden changes (steps) in the ion energy spectra were observed by various satellites. The nature of these steps in cusp ion energy dispersion has been discussed for more than a decade and evidence has been accumulated for two different mechanisms – temporal variations in the reconnection rate (i.e., pulsed reconnections) and spatial variations in the reconnection location.

In the pulsed cusp model, steps are described as periods of little or no reconnection at the magnetopause (e.g., Lockwood and Smith, 1989, 1990, 1994; Lockwood et al., 1998). These variations in the reconnection rate create a series of poleward convecting magnetic flux tubes (pulses) with different time histories since reconnection.

Spatial cusp structures have been studied by Onsager et al. (1995), Trattner et al. (2002a) and others, using observations from multiple satellites. These studies revealed that, while individual cusp crossings for different solar wind conditions are very dissimilar, cusp crossings by two satellites during stable solar wind conditions are remarkably similar over extended time periods (up to 5 hours) and spatial separations (about 2 hours in MLT) of the satellites. If this conclusion is correct, then reconnection at the magnetopause would be a rather constant process with only minor variations. Smaller cusp structures embedded in major steps most probably caused by such minor reconnection rate variations have been reported (Trattner et al., 2002a). Even changes in the IMF conditions, which move reconnection lines to different positions at the magnetopause and also move flux tubes emanating from these reconnection lines, exhibit spatial cusp structures (Trattner et al., 2003). While flux tubes would change their positions, cusp steps will still be encountered by crossing the boundary between the flux tubes, crossing onto open field lines with a different time since reconnection.

Recent observations made by the three Cluster spacecraft combined with simultaneous observations made by the SuperDARN radar network have allowed cusp structures to be investigated in unprecedented detail. This study revealed that, indeed, both spatial and temporal structures occur in the cusp. Our conclusions about the mechanisms to create temporal and spatial structures are:

(1) Cusp structures are the result of temporal changes in the location of convection pattern that either drastically shorten or lengthen the convection length of magnetic field lines from the ion open-closed field line boundary to the position where they are intercepted by the satellites. The change can be a smooth reversal of a previous ion energy dispersion or a sudden step.

(2) Cusp structures are caused by the entry into a different convection cell or flux tube where the location of the ion open-closed field line boundary was significantly different from that in the old cell. This can result in a step-up or step-down ion energy dispersion. The observed cusp structure is a spatial structure and will appear unchanged for satellites at every altitude (Trattner et al., 2002a, 2002b).
(3) Cusp structures are caused by a variation of the reconnection rate at the reconnection location. This temporal cusp structure will be convected with the open geomagnetic field lines and travel along the ionospheric convection direction. In agreement with the pulsating cusp model (e.g., Lockwood and Smith, 1989), fast low-altitude satellites overtakimg the convecting structure encounter a step-down ion energy dispersion while slow high-altitude satellites are overtaken by the convecting cusp structure and encounter a step-up dispersion profile.

While spatial and temporal processes have been observed, the combination of multi-spacecraft observations with large scale ground observations will allow new insight into pulse frequency, convection velocity, the magnitude of cusp steps, and the conditions necessary to observe either spatial or temporal cusp structures.

## Acknowledgements

We acknowledge the use of ISTP $K_p$ database. Solar wind observations were provided by K. Ogilvie at NASA/GSFC (Wind/SWE) and D.J. McComas (ACE/SWE). Observations of the interplanetary magnetic field were provided by R. Lepping at NASA/GSFC (Wind/MFI) and N. Ness (ACE/MFI). The work at Lockheed Martin was supported by NASA contracts NAS5-30302, NAG5-3596 and NAG5-13218. The work at the Max-Planck-Institut fuer Aeronomie was supported by DLR under contract 50 OC 8904 0 (Cluster-CIS). We would like to thank the SyperDARN PIs (W. A. Bristow, P. Dyson, R. A. Greenwald, T. Kikuchi, M. Lester, M. Pinnock, N. Sato, G. Sofko, J.-P. Villain, and A. D. M. Walker) for providing the coordinated cluster support radar modes which were running during the Cluster-SuperDARN spacecraft conjunctions.

## References

Carlson, C. W., McFadden, J. P., Turin, P., Curtis, D. W., and Magoncelli, A.: 2001. 'The Electron and Ion Plasma Experiments for FAST', *Space Sci. Rev.* **98**, 1.

Cowley, S. W. H.: 1982. 'The Cause of Convection in the Earth's Magnetosphere: A Review of Developments During the IMS', *em Rev. Geophys. Res.* **20**, 531.

Cowley, S. W. H., Freeman, M.P., Lockwood, M., and Smith, M.F..: 1991. 'The Ionospheric Signatures of Flux Transfer Events', in C.I. Barron (ed.), *CLUSTER: Dayside Polar Cusp*, European Space Agency Spec. Publ., ESA, pp. 105SP-330.

Cowley, S. W. H., and Lockwood, M.: 1992. 'Excitation and Decay of Solar Driven Flows in the Magnetosphere–Ionosphere System', *Ann. Geophys.* **10**, 103.

Dubouloz, N., Berthelier, J. -J., Malingre, M., Girard, L., Galperin, Y., Covinhes, J., Chugunin, D., Godefroy, M., Gogly, G., Guérin, C., Illiano, J. -M., Kossa, P., Leblanc, F., Legoff, F., Mularchik, T., Paris, J., Stzepourginski, W., Vivat, F., and Zinin, L.: 1998. 'Thermal Ion Measurements on Board Interball Aurora Probe by the Hyperboloid Experiment', *Ann. Geophys.* **16**, 1070.

Dungey, J. W.: 1961. 'Interplanetary Magnetic Field and Auroral Zones', *Phys. Rev. Lett.* **6**, 47.

Escoubet, C. P., Smith, M. F., Fung, S. F., Anderson, P. C., Hoffman, R. A., Baasinska, E. M., and Bosqued, J. M.: 1992. 'Staircase Ion Signature in the Polar Cusp: A Case Study', *Geophys. Res. Lett.* **19**, 1735.

Escoubet, C. P., Bosqued, J. M., Hoffman, R. A., Berthelier, A., and Anderson, P. C.: 1997. 'Opposite Ion Dispersions Observed Quasi-simultaneously in the Polar Cusp by the DE-2 and Aureol-3 Satellites', *Geophys. Res. Lett.* **24**, 2487.

Fuselier, S. A., Klumpar, D. M., and Shelley, E. G.: 1991. 'Ion Reflection and Transmissions During Reconnection at the Earth's Subsolar Magnetopause', *Geophys. Res. Lett.* **18**, 139.

Fuselier, S.A., Waite, J.H., Avanov, L.A., Smirnov, V.M., Vaisberg, O.L., Siscoe, G. and Russell, C.T.: (2001). Characteristics of Magnetosheath Plasma in the Vicinity of the High Latitude Cusp. *J. Geophys. Res.*, submitted.

Greenwald, R. A., Hunsuker, R. D., Sofko, G., Koehler, J., Nielsen, E., Pellinen, R., Walker, A. D. M., Sato, N., and Yamagishi, H.: 1995 'DARN/SUPERDARN A Global View of the Dynamics of High-latitude ConvectionSpace Sci. Rev. **71,** 761.

Lockwood, M.: 1995. Ground-based and Satellite Observations of the Cusp: Evidence for Pulsed Magnetopause Reconnection, in P. Song, B. U. O. Sonnerup, and M. F. Thomsen (eds.), *Physics of the Magnetopause*, Geophys. Monogr. Ser., 90 AGU, Washington, D.C., pp. 417.

Lockwood, M.: 1996. 'The Case for Transient Magnetopause Reconnection', *EOS Trans. AGU* **77**, 246.

Lockwood, M., Cowley, S. W. H., Sandholt, P. E., and Lepping, R. P.: 1990. 'The ionospheric signatures of flux transfer events and solar wind dynamic pressure changes', *J. Geophys. Res.* **95**, 17113.

Lockwood, M., Cowley, S. W. H., and Smith, M. F.: 1994. 'Comment on: 'By Fluctuations in the Magnetosheath and Azimuthal Flow Velocity Transient in the Dayside Ionosphere' by Newell and Sibeck', *Geophys. Res. Lett.* **21**, 1819.

Lockwood, M., Davis, C. J., Smith, M. F., Onsager, T. G., and Denig, W. F.: 1995. 'Location and Characteristics of the Reconnection X-line Deduced from Low-altitude Satellite and Ground-based Observations, Defense Meteorological Satellite Program and European Incoherent Scatter data', *J. Geophys. Res.* **100**, 21803.

Lockwood, M., Davis, C. J., Onsager, T. G., and Scudder, J. D.: 1998. 'Modeling Signatures of Pulsed Magnetopause Reconnection in Cusp Ion Dispersion Signatures Seen at Middle Altitudes', *Geophys. Res. Lett.* **25**, 591.

Lockwood, M., Dening, W. F., Farmer, A. D., Davda, V. N., Cowley, S. W. H., and Lühr, H.: 1993. 'Ionospheric Signatures of Pulsed Reconnection at the Earth's Magnetopause', *Nature* **361**, 424.

Lockwood, M. and Smith, M. F.: 1989. 'Low-altitude Signatures of the Cusp and Flux Transfer Events', *Geophys. Res. Lett.* **16**, 879.

Lockwood, M., and Smith, M. F.: 1990. 'Reply to Comment by P.T. Newell on 'Low-altitude Signatures of the Cusp and Flux Transfer Events' by M. Lockwood and M.F. Smith', *Geophys. Res. Lett.* **17**, 305.

Lockwood, M., and Smith, M. F.: 1992. 'The Variation of Reconnection Rate at the Dayside Magnetopause and Cusp Ion Precipitation', *J. Geophys. Res.* **97**, 14841.

Lockwood, M., and Smith, M. F.: 1993. 'Comment on "Mapping the Dayside Ionosphere to the Magnetosphere According to Particle Precipitation Characteristics" by P.T. Newell and C.-I. Meng', *Geophys. Res. Lett.* **20**, 1739.

Lockwood, M., and Smith, M. F.: 1994. 'Low- and Mid-altitude Cusp Particle Signatures for General Magnetopause Reconnection Rate Variations I Theory', *J. Geophys. Res.* **99**, 8531.

Newell, P. T., and Meng, C.-I.: 1991. 'Ion Acceleration at the Equatorward Edge of the Cusp: Low-altitude Observations of Patchy Merging', *Geophys. Res. Lett.* **18**, 1829.

Newell, P. T., and Sibeck, D. G.: 1993. 'Upper Limits on the Contribution of FTE's to Ionospheric Convection', *Geophys. Res. Lett.* **20**, 2829.

Onsager, T. G., Kletzing, C. A., Austin, J. B., and MacKiernan, H.: 1993. 'Model of Magnetosheath Plasma in the Magnetosphere: Cusp and Mantle Particles at Low Altitudes', *Geophys. Res. Lett.* **20**, 479.

Onsager, T. G., Chang, S.-W., Perez, J. D., Austin, J. B., and Jano, L. X.: 1995. 'Low-altitude Observations and Modeling of Quasi-steady Magnetopause Reconnection', *J. Geophys. Res.* **100**, 11831.

Paschmann, G., Sonnerup, B.U.Ö., Papamastorakis, I., Sckopke, N., Haerendel, G., Bame, S. J., Asbridge, J. R., Gosling, J. T., Russell, C. T., and Elphic, R. C.: 1979. 'Plasma Acceleration at the Earth's magnetopause: Evidence for Magnetic Field Reconnection', *Nature* **282**, 243.

Phillips, J. L., Bame, S. J., Elphic, R. C., Gosling, J. T., Thomson, M. F., and Onsager, T. G.: 1993. 'Well-resolved Observations by ISEE 2 of Ion Dispersion in the Magnetospheric Cusp', *J. Geophys. Res.* **98**, 13429.

Pinnock, M., Rodger, A. S., Dudeney, J. R., Baker, K. B., Newell, P. T., Greenwald, R. A., and Greenspan, M. E.: 1993. 'Observations of an Enhanced Convection Channel in the Cusp Ionosphere', *J. Geophys. Res.* **98**, 3767.

Reiff, P. H., Hill, T. W., and Burch, J. L.: 1977. 'Solar Wind Plasma Injections at the Dayside Magnetospheric Cusp', *J. Geophys. Res.* **82**, 479.

Rosenbauer, H., Grünwaldt, H., Montgomery, M. D., Paschmann, G., and Sckopke, N.: 1975. 'Heos 2 Plasma Observations in the Distant Polar Magnetosphere: The Plasma Mantle', *J. Geophys. Res.* **80**, 2723.

Ruohoniemi, J.M. Greenwald, R. A.: 1996. 'Statistical Patterns of High Latitude Convection Obtained from Goose Bay HF Radar Observations', *J. Geophys. Res.* **101**, 21743.

Ruohoniemi, J. M., and Baker, K. B.: 1998. 'Large-scale Imaging of High Latitude Convection with Super Dual Auroral Radar Network HF Radar Observations', *J. Geophys. Res.* **103**, 20797.

Sauvaud, J.-A., Barthe, H., Aoustin, C., Thocaven, J. J., Rouzaud, J., Penou, E., Popescu, D., Kovrazhkin, R. A., and Afanasiev, K. G.: 1998. 'The ION Experiment Onboard the Interball-Aurora Satellite: Initial Results on Velocity-dispersed Structures in the Cleft and Inside the Aurora Oval', *Ann. Geophys.* **16**, 1056.

Shelley, E. G., Sharp, R. D., and Johnson, R. G.: 1976. 'He$^{++}$ and H$^{+}$ Flux Measurements in the Day Side Cusp: Estimates of Convection Electric Field', *J. Geophys. Res.* **81**, 2363.

Shelley, E. G., Ghielmetti, A. G., Balsiger, H., Black, R. K., Bowles, J. A., Bowman, R. P., Bratschi, O., Burch, J. L., Carlson, C. W., Coker, A. J., Drake, J. F., Fischer, J., Geiss, J., Johnstone, A., Kloza, D. L., Lennartsson, O. W., Magoncelli, A. L., Paschmann, G.,

Peterson, W. K., Rosenbauer, H., Sanders, T. C., Steinacher, M., Walton, D. M., Whalen, B. A., and Young, D. T. : 1995. 'The Toroidal Imaging Mass-angle Spectrograph (TIMAS) for the Polar Mission', *Space Sci. Rev.* **71**, 497.

Smith, E. J., Lockwood, M., and Cowley, S. W. H.: 1992. 'The Statistical Cusp: The Flux Transfer Event Model', *Planet. Space Sci.* **40**, 1251.

Sonnerup, B.U.Ö, Paschmann, G., Papamastorakis, I., Sckopke, N., Haerendel, G., Bame, S. J., Asbridge, J. R., Gosling, J. T., and Russell, C. T.: 1981. 'Evidence for Magnetic Field Reconnection at the Earth's Magnetopause', *J. Geophys. Res.* **86**, 10049.

Trattner, K. J., Fuselier, S. A., Peterson, W. K., Sauvaud, J.-A., Stenuit, H., and Dubouloz, N.: 1999. 'On Spatial and Temporal Structures in the Cusp', *J. Geophys. Res.* **104**, 28411.

Trattner, K. J., Fuselier, S. A., Peterson, W. K., Boehm, M., Klumpar, D., Carlson, C. W., and Yeoman, T. K.: 2002a. 'Temporal Versus Spatial Interpretation of Cusp Ion Structures Observed by Two Spacecraft', *J. Geophys. Res.* **107**(A10), 1287doi: 10.1029/2001JA000181.

Trattner, K. J., Fuselier, S. A., Peterson, W. K., and Carlson, C. W.: 2002b. 'Spatial Features Observed in the Cusp Under Steady Solar Wind Conditions', *J. Geophys. Res.* **107**(A10), 128810.1029/2001JA000262.

Trattner, K. J., Fuselier, S. A., Yeoman, T. K., Korth, A., Fraenz, M., Mouikis, C., Kucharek, H., Kistler, L. M., Escoubet, C. P., R' eme, H., Dandouras, I., Sauvaud, J. A., Bosqued, J. M., Klecker, B., Carlson, C., Phan, T., McFadden, J. P., Amata, E., and Eliasson, L.: 2003. 'Cusp Structures: Combining Multi-spacecraft Observations with Ground Based Observations', *Ann. Geophys.* **21**, 2031.

Weiss, L. A., Reiff, P. H., Carlson, H. C., Weber, E. J., and Lockwood, M.: 1995. 'Flow-alignment Jets in the Magnetospheric Cusp: Results from the Geospace Environment Modeling Pilot program', *J. Geophys. Res.* **100**, 7649.

Wing, S., Newell, P. T., and Rouhoniemi, J. M.: 2001. 'Douple Cusp: Model Prediction and Observational Verification', *J. Geophys. Res.* **106**, 25571.

Surveys in Geophysics (2005) 26: 307–339
DOI 10.1007/s10712-005-1885-1 © Springer 2005

# OBSERVATIONS OF A UNIQUE CUSP SIGNATURE AT LOW AND MID ALTITUDES

W. R. KEITH[1,2], J. D. WINNINGHAM[1], M. L. GOLDSTEIN[2], M. WILBER[3], A. N. FAZAKERLEY[4], H. RÈME[5], T. A. FRITZ[6], A. BALOGH[7], N. CORNILLEAU-WEHRLIN[8] and M. MAKSIMOVIC[9]

[1]*Southwest Research Institute, P. O. Drawer 28510, San Antonio, TX 78228-0510, USA*
*E-mail: wayne.keith@gsfc.nasa.gov;*
[2]*NASA Goddard Space Flight Center, Code 612.2, Greenbelt, MD 20771, USA;*
[3]*University of California, Space Science Laboratory 7450, Berkeley, CA 94720, USA;*
[4]*Mullard Space Science Laboratory, Holmbury St Mary, Dorking, Surrey RH5 6NT, UK;*
[5]*CESR, BP 4346, 9 Ave Colonel Roche, Cedex, Toulouse 31029, France;*
[6]*Boston University, Center for Space Physics, 725 Commonwealth Ave, Boston, MA 02215, USA;*
[7]*Imperial College Space and Atmospheric Physics group, The Blackett Laboratory, London, UK;*
[8]*CETP, 10-12 Ave de Europe, Velizy, 78140, France;*
[9]*LESIA and CNRS, Paris Observatory, 61 Ave de l'Observatoire, France*

(Received 20 January 2003; Accepted 30 April 2004)

**Abstract.** Observations of a unique cusp feature at low and mid altitudes are reported. This feature has a consistent double-peaked or "V"-shaped structure at the equatorward edge of high-latitude particle precipitation flux, and is predominantly present for high IMF $B_y$ conditions. The observations are consistent with the Crooker ('A split separator line merging model of the dayside magnetopause', *J. Geophys. Res.* 90 (1985) 12104, 'Mapping the merging potential from the magnetopause to the ionosphere through the dayside cusp', *J. Geophys. Res.* (1988) 93 7338.) antiparallel merging model, which predicts a narrow wedge-shaped cusp whose geometry depends greatly on the dawn/dusk component of the IMF. Various observations are presented at low altitudes (DE-2, Astrid-2, Munin, UARS, DMSP) and at mid altitudes (DE-1, Cluster) that suggest a highly coherent cusp feature that is consistent with the narrow, wedge-shaped cusp of Crooker (1988), and contains persistent wave signatures that are compatible with previously reported high-altitude measurements. A statistical survey of Astrid-2 and DMSP satellite data is also presented, which shows this feature to be persistent and dependent on the IMF angle at the magnetopause, as expected. Thus, the cusp signatures observed at a wide range of altitudes present a coherent picture that may be interpreted in terms of a footprint of the magnetopause current layer.

**Keywords:** cusp, true cusp, magnetosphere

**Abbreviations:** ISEE: International Sun–Earth Explorers; GSE: Geocentric Solar Ecliptic; GSM: Geocentric Solar Magnetic; ACE: Advanced Composition Explorer; CODIF: Composition and Distribution Function Analyzer; DMSP: Defense Meteorological Satellite

Program; FFT: Fast Fourier Transform; ESA: European Space Agency; HIA: Hot Ion Analyzer; MHD: Magnetohydrodynamics; UT: Universal Time; RAPID: Research with Adaptive Particle Imaging Detectors; VEFI: Vector Electric Field Instrument; SSJ: Special Sensor Aurora Particle; STAFF: Spatio-Temporal Analysis of Field Fluctuations; DE: Dynamics Explorer; HEPS: High-Energy Particle Spectrometer; MEPS: Medium-Energy Particle Spectrometer

## 1. Introduction

Ever since Chapman and Ferraro (1931) first induced the basic nature of the Earth's magnetosphere, its 2-D and 3-D topology has indicated the existence of a dayside magnetic cusp. In the past, however, understanding the geometry and dynamics of the cusps has been limited by the simple 2-D cut planes used to describe them. The term "cusp" itself demonstrates the historical bias towards 2-D representations, since only in a 2-D cut plane does this region fit the mathematical definition of a point of reversal on a curve. This cusp, or weak magnetic field region, is invariably near magnetic local noon at the latitude where magnetic field lines switch from closing on the dayside to being mapped back into the tail. This geometry was thought to allow for more or less direct penetration of magnetosheath particle fluxes to low altitudes. Early observations (Heikkila and Winningham, 1971) showed a high-latitude band of low-energy particle precipitation with magnetosheath-like properties on the dayside at low altitudes. They interpreted this feature as the long sought for evidence of direct solar wind entry via a magnetic cusp. This general region of particle penetration was later separated into a "cusp proper" and a "Cleft/Boundary Layer", representing separate particle entry processes (i.e., direct and indirect) (Newell and Meng, 1988). This terminology builds upon the "cusp" versus "cleft" distinction of Heikkila (1972) and Reiff (1979), who argued that the "cusp" represented direct entry whereas the "cleft" was the low-altitude signature of the Low Latitude Boundary Layer.

Newell and Meng (1988) defined the low-altitude cusp proper as the subregion of plasma flux that more closely resembles magnetosheath plasma spectral characteristics, indicating "more direct" entry than that associated with low altitude access via the Low Latitude Boundary Layer (LLBL), the plasma region just equatorward of the cusp representing plasma near the magnetopause but inside the magnetosphere. This definition results in a cusp of much narrower extent in Magnetic Local Time (MLT) and Invariant Latitude (IL), and is limited to fairly direct plasma entry processes (i.e., little or no acceleration of the magnetosheath population). This smaller, more directly connected region is continuously present with a density that remains consistent with solar wind density variations (Aparicio et al., 1991).

The cusp proper averages approximately 2 to 3 h in longitude centered at noon, and about 1° to 5° in IL centered at about 78° IL (1° $\approx$ 100 km at

100 km altitude) (Newell and Meng, 1988; Lundin 1998; Aparicio et al., 1991). Its location and size vary with changes in the IMF direction and solar wind dynamic pressure, but it is always present (Newell and Meng, 1988). The above size and location represent statistical averages and are quite large. At low altitude ( < 1000 km polar circular orbit), a feature of this size will be traversed on average in about 15 s to a minute. Trajectories not cutting through the center of the cusp would have even shorter traversal times, on the order of a few seconds. Orbits with more equatorward inclinations may spend more time in the cusp, depending on how much local time is covered while inside the appropriate latitude range. A theoretical maximum for a cusp traversal (3 h of local time at about 77° latitude) would be on the order of 8 min. It is important to note that while the quick traversals of the cusp at low altitude may have limited the detail seen in the past, they have the advantage of being more of a "snapshot", with the data less likely to be contaminated with temporal changes during the traversal. The faster sample times of recent instruments (described in the Appendix A) allows the detail to be seen without the need to rely on higher altitudes and slower traversals, with the concomitant intermixing of populations due to horizontal transport. That is, mid-altitude measurements, while showing many similar particle characteristics, may contain bounced and tailward convected populations that may have histories different from the downcoming particles.

Extending the concept of antiparallel merging (Crooker, 1985) to the low altitude cusp, Crooker (1988) proposed a mapping of the potential drop along the merging line at the magnetopause down to the ionosphere via the cusps. The antiparallel model predicts a stretched cusp radiating away from the classical cusp point (i.e., where the cusp would be without interconnection of the fields), with the potential drop across an increasingly shorter distance along the magnetopause mapping to points further from this classical location. In order to maintain a realistic distance across which this potential is applied, the cusp must be wedge-shaped, with its base at the classical cusp point and the full potential drop applied across it (Figure 1). The edges of the wedge would map to the innermost regions of the magnetopause along the neutral line, moving to the outer surface as one moves towards the center of the wedge (Stasiewicz, 1991).

Another result of this topology of interconnected field lines is that this distended cusp rotates about its base with variations in the $y$-$z$ plane (in GSM coordinates) of the Interplanetary Magnetic Field (Figure 2). For a purely southward IMF the wedge is wide with the point facing towards lower latitudes, and resembles the more generally conceived large ovoid cusp. As $B_y$ increases, though, the tip begins to swing in the direction of the $B_y$ component, until for a purely $B_y$ case the point of the wedge faces duskwards perpendicular to its southward orientation. As $B_z$ becomes more positive, this cusp wedge continues to rotate and become thinner (since the total potential

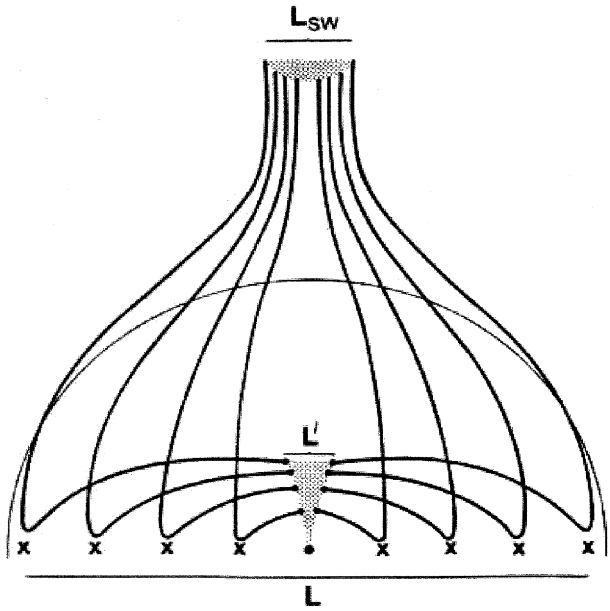


*Figure 1.* View from the Sun towards the Earth of southward Interplanetary Magnetic Field lines mapping the solar wind potential drop through the magnetopause down to the cusp. X's represent the places where the field lines cross the X-line. The geomagnetic (curved) field lines are shown near the magnetopause surface until they turn Earthward towards the cusp (shaded). The footprint of these 'first open' field lines thus is a wedge in the ionosphere. (Adapted from Crooker, 1988).

drop across it becomes less), until it becomes a very narrow poleward directed wedge for a pure positive IMF $B_z$. This type of narrow, IMF-dependent cusp wedge is consistent with the observations in the next section, in which a double-sided or "V" energy dispersion signature is seen for high IMF $B_y$ cusp crossings. The simple three-dimensional image of the cusp as a "funnel" thus becomes a much more complex structure, depending on $B_y$ and $B_z$ in shape as well as location. A single satellite track can encounter very complex spatial structures in the cusp, although until recently it has been very difficult to distinguish them from temporal features. The ESA/NASA Cluster multi-satellite mission has begun to clarify such long-standing ambiguities.

Recent studies of the high-altitude, exterior cusp region have shown there to be a highly turbulent layer (labeled Turbulent Boundary Layer in Figure 3) containing large amplitude, low frequency waves. Savin et al. (1998) and Dubinin et al. (2002) have shown this region to be a permanent feature. Using Interball and Prognoz data, the following features of the exterior cusp shown in Figure 3 have been defined. The stagnation region (previously defined by Paschmann et al. (1976)) is broken down into the Turbulent Boundary Layer outside the magnetopause, and the Outer Cusp inside the magnetopause. The magnetopause boundary is defined as the

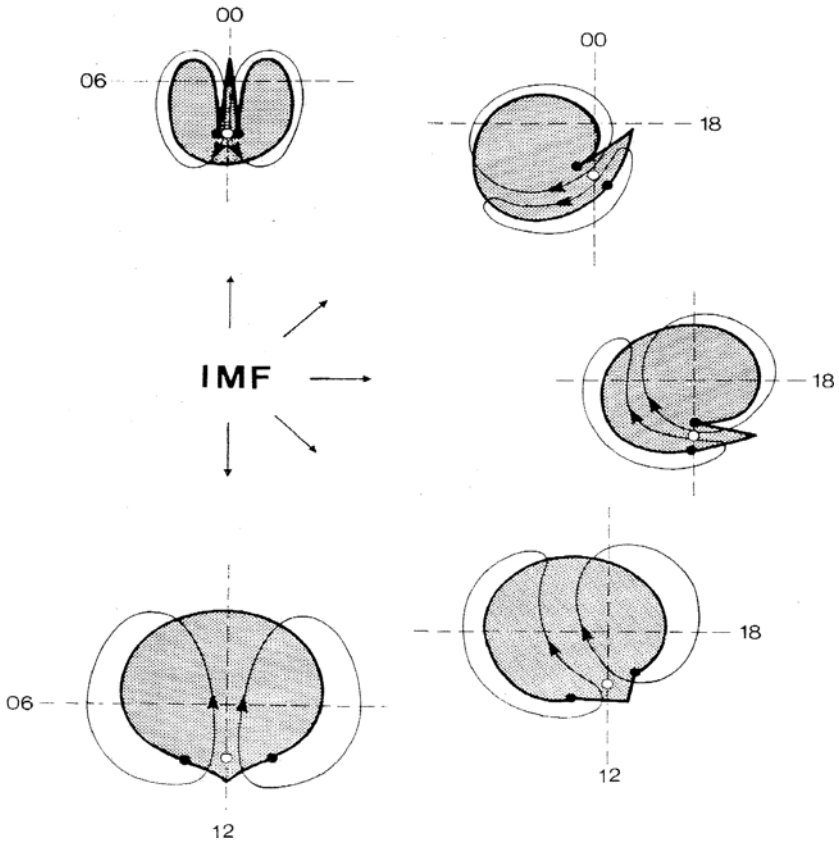


*Figure 2.* Schematic of the relationship between IMF angle and northern polar cap convection and cusp geometry. The Sun is towards the bottom and the view is from above the North pole. The 'wedge cusp' (where the lighter flow lines cross the heavier polar cap boundary) can be seen to narrow and rotate with changes in the IMF direction from southward (bottom) to duskward (middle) and finally northward (top). (From Crooker, 1988).

separatrix between the geomagnetic field and the IMF. The boundary is shown dashed in the exterior cusp region since the dynamic properties of the cusp often prevent an unambiguous determination of the magnetopause location. The Inner Cusp extends below these regions to low altitudes. Since the magnetopause boundary passing through this stagnation region can frequently not be identified, the distinction between the boundaries and characteristics of the sub-regions in Figure 3 may become blurred. This empirical exterior cusp model is based primarily on data from spacecraft heading outwards from the tail lobe of the magnetosphere, through the cusp, and out into the magnetosheath. Thus the extent and structure of this model in mid-altitude regions is not well defined. Multi-spacecraft mid-altitude cusp passages are now starting to facilitate refining the lower end of this exterior cusp model and its 3D, dynamic geometry.

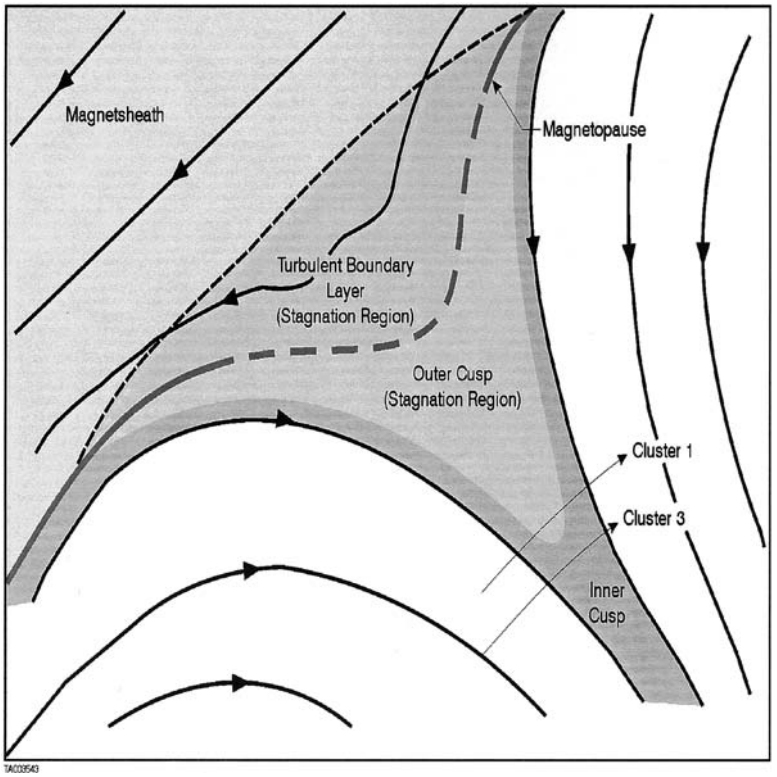


*Figure 3*. The regions of the exterior cusp as proposed by Savin, including external and internal field geometry. Two Cluster spacecraft trajectories are also shown (see Observations section). (Adapted from Savin et al., 1998).

## 2. Observations

We present data from several satellites, all of which show similar cusp signatures. Due to the large number of individual measurements involved with the observations, details of the instrumentation used are not given here. A brief description of the instruments used can be found in the Appendix A. In this section examples of data from the various satellites will be presented in order to establish the characteristics of this new signature, and to demonstrate its independence of any particular instrument, measurement or altitude. These examples are representative of the larger set of cusp passes surveyed.

### 2.1. DE DATA

The first example of this cusp feature comes from a pass of the DE-2 satellite on September 6, 1982 (Figure 4). LAPI particle spectrograms are from the

electron sensor with a look angle of 19° from the magnetic field (top panel) and from the ion sensor with a look direction 64° from the magnetic field. The data were taken on a southern hemisphere equatorward pass, the cusp being located at an IL of −63° and a pre-noon MLT of 10:13. A clear dispersion signature can be seen in the ion data (Figure 4, second panel), moving from lower (poleward) energies to higher (equatorward) energies,

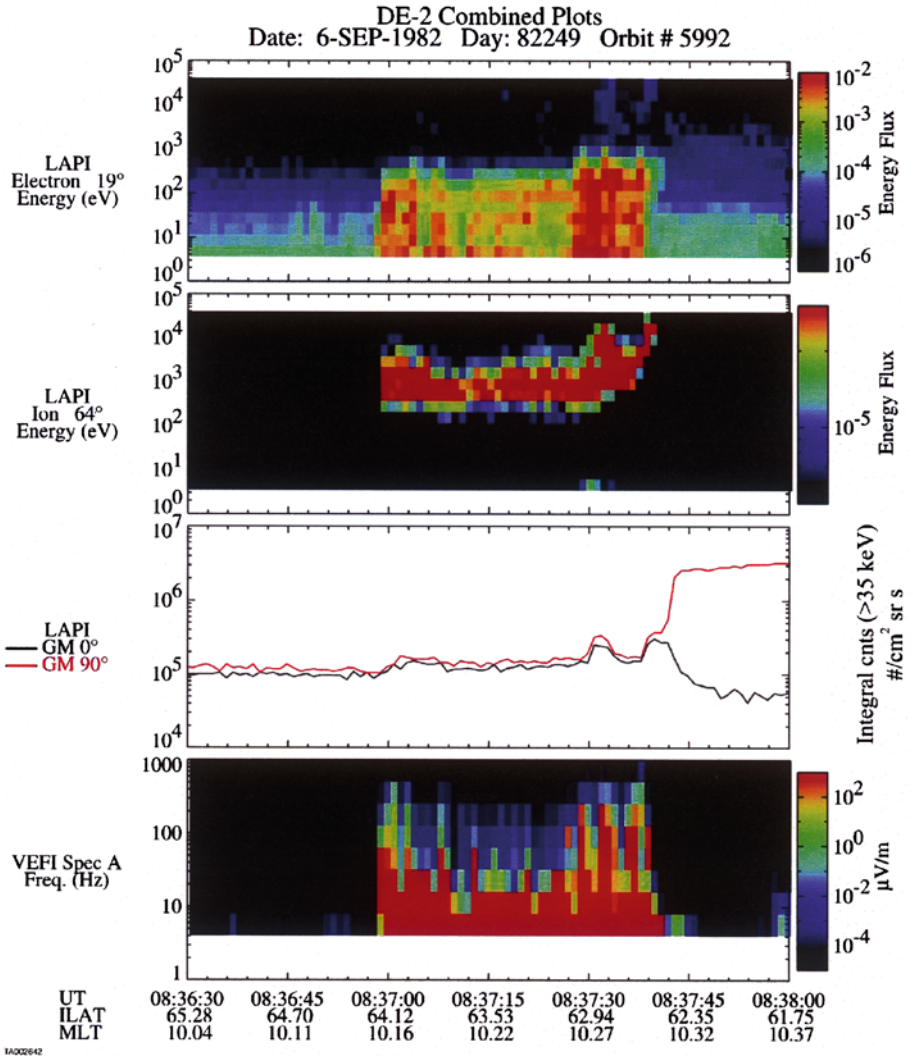


*Figure 4.* DE-2 data from September 6, 1982. Data were taken during an equatorward cusp pass in the southern hemisphere. The top spectrogram is for electrons measured at a 19° pitch angle. The second is for ions measured at a pitch angle of 64°. The third plot shows high energy electrons integrated for energies greater than 35 keV and 0° and 90° pitch angle, and the bottom spectrogram presents the measured square root of the electric wave power.

although the spectrogram appears to be flat at about 1 keV from 8:37:00 to 8:37:30 (all times given in UT). The feature of interest, however, is the higher-energy piece at the right-hand end of the ion spectrogram. This "V" shaped signature can be clearly seen beginning at the equatorward edge from 8:37:30 to 8:37:40. This example is at unusually high energies, with peaks at around 20 keV down to 2 keV at the center. The feature is consistent with the narrow wedge cusp of the Crooker model, with the highest energies being found towards the outer edges. The electrons (Figure 4, top panel) clearly show enhancement during this same time period, from 30 keV down to the lowest energies. Above 1 keV the fluxes vary spatially the same as the G-M data in panel 3. Below 1 keV there is a different morphology, though, remaining steady throughout the feature. The third panel of Figure 4 is Geiger–Mueller data and the parallel (black) and perpendicular (red) lines both indicate clear enhancements over their already elevated levels at the two edges of the feature and are colocated with the ion V edges. At the equatorward edge the 90° pitch angle G–M data jump to much higher fluxes, indicating trapped particles on closed field lines.

The bottom panel of Figure 4 is the square root of AC electric wave power from the VEFI instrument displayed from 4 to 1000 Hz. This spectrogram shows strong waves at 400 Hz and lower during the V. This is consistent with the turbulence seen at the magnetopause (Gurnett, 1979) and exterior cusp regions, indicating that these field lines may be connected with those regions while passing through the ion V cusp feature. The V covers about 0.4° in IL and about 18 min of MLT, which corresponds to a very narrow feature of approximately 76 km. For purposes of inter-comparison, we will also give an approximate size when projected down to 100 km. In this case, the projected width in this dimension is approximately 69 km. Examples of this type of feature are by no means unique, but can be hard to spot due to their small size, and the fact that they are very localized in IL and MLT, being found within about an hour of noon in MLT (depending on the IMF) at cusp latitudes. The ISEE 1 and 2 satellites measured the IMF during this time period to be steady and primarily duskward, with significant southward and tailward ($B_x$) components. Duskward IMF is consistent with a pre-noon located cusp in the southern hemisphere. Strong $B_y$ and weakly southward IMF is also consistent with a passage across a narrow wedge cusp as described above.

The DE-1 spacecraft traversed the mid-altitude cusp on October 1, 1981 (Figure 5). In this case the particle data were recorded by HAPI. This is an example of a mid-altitude crossing of the cusp, about 18,850 km in altitude (3.96 $R_E$ geocentric distance). The top spectrogram is of electrons, and the second ions, both measured in the spin plane of the satellite. The line overplot on the top panel shows the flux of electrons integrated between 2 and 25 keV, and highlights the morphology of the higher-energy electrons. The third and

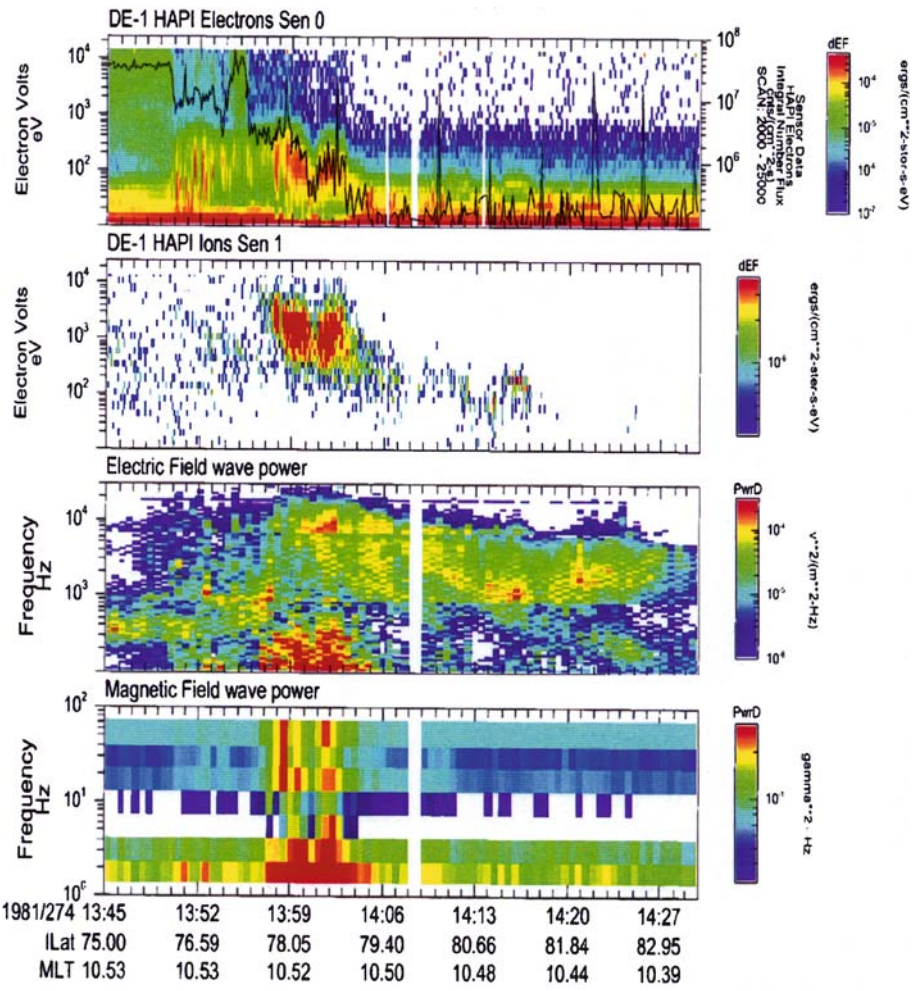


*Figure 5.* DE-1 data from October 1, 1981. Data were taken during an equatorward cusp pass in the northern hemisphere. The top two spectrograms are for electrons and ions measured in the spin plane. The third and fourth give electric and magnetic field wave power.

fourth panels are proportional to the electric and magnetic wave power, respectively. The data were taken in the pre-noon sector, on a poleward pass in the northern hemisphere. The feature is seen in the ions (second panel) beginning at 13:59 at about 2 keV. The ion flux decreases in energy and intensity to about 500 eV a minute and a half later, only to return to the original values at 14:03. This morphology is typical and very much like the lower-altitude pass described. The electron intensities peak as well during the time of the ion V, with the highest energy particles showing the transition from closed to open field lines. The electric and magnetic field wave power shown in the bottom two spectrograms show a typical increase, especially at

the lowest frequencies, during the passage through the feature. The width of the satellite track through this cusp sub-region is about 1125 km, which translates to a 100 km footprint of about 148 km. This is very consistent with the size range seen at other altitudes. The IMF during this time was strongly positive in $B_x$, with equally weaker positive $B_y$ and negative $B_z$.

## 2.2. DMSP DATA

Particle data from the SSJ/4 instrument of the DMSP-F10 satellite can be seen in Figure 6. The data presented are from March 28, 1992, when the satellite was passing equatorward over the cusp at an IL of 73° and a MLT just post noon (12:20). The ion data (lower panel) again exhibit the energy-latitude dispersion as it passes from higher to lower latitudes, and also clearly show a "V" structure beginning at 10:10:55 UT which lasted just under 25 s. The peak energy of the poleward edge of the structure is slightly less in this case, about 1 keV; however, the middle and equatorward edge are peaked at

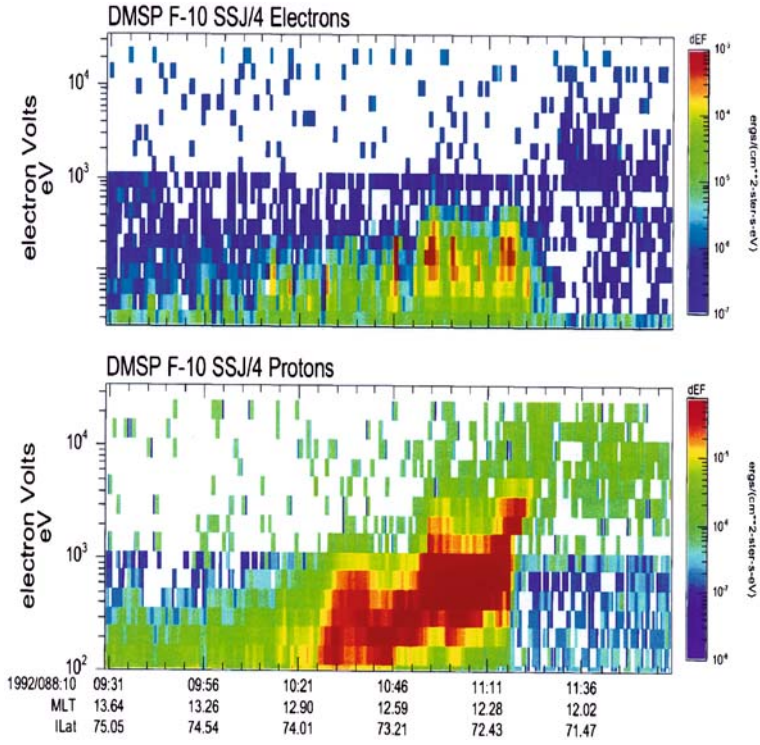


*Figure 6*. DMSP F-10 data from March 28, 1992. Data were taken during an equatorward cusp pass in the northern hemisphere. The upper spectrogram is for electrons, and the lower spectrogram ions.

500 eV and 2 keV, respectively. This is typical for many of the examples we have studied. The corresponding electron (upper panel) enhancements at the edges are also typical, being mostly in the 100 to 200 eV range. The satellite altitude at the time of the pass was 770 km, and the feature spanned 0.77° of Invariant Latitude, giving it a latitudinal width of about 96 km (84 km at 100 km) and an orbital track of just over 178 km (156 km at 100 km). As for other cases this is very small, on the order of a proton gyroradius at the magnetopause. IMF data for this time period are not available.

A second DMSP-F10 passage can be seen in Figure 7. The plot format is the same as in the previous example. These data were taken on September 25, 1991, during another equatorward northern cusp pass. The IL is 70.5° at a pre-noon MLT (11:20) at the time of the V signature in the ion data from 8:15:40 to 8:16:10. This pass is fairly typical, except that the low energy tail poleward of the feature of interest is slightly separated. This may represent a temporal change, or a particularly unusual crossing geometry. The crossing geometry is probably also the reason why the poleward edge of the V appears to be compressed and has a lower peak energy than the equatorward side,

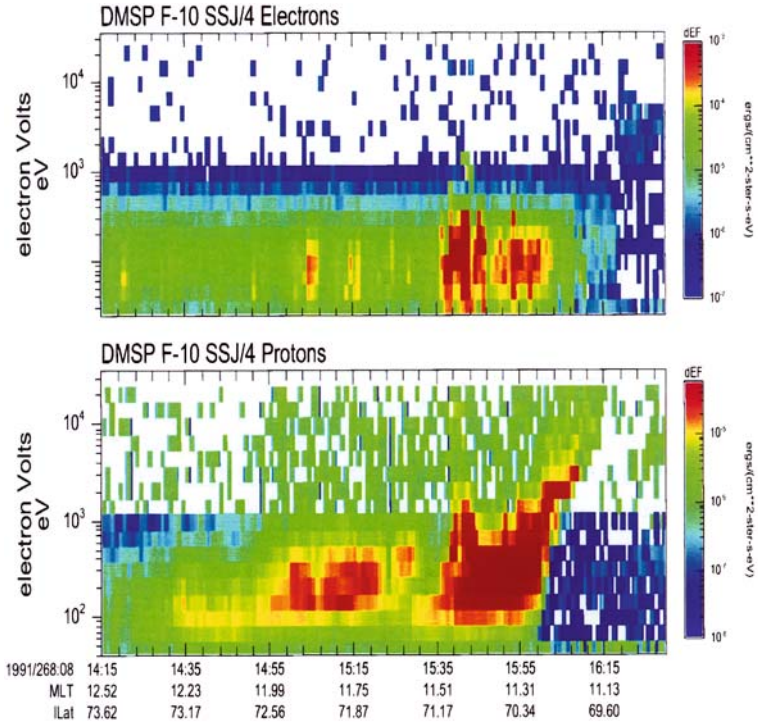


*Figure 7.* DMSP F-10 data from September 25, 1991. Data were taken during an equatorward cusp pass in the northern hemisphere. Upper spectrogram is for electrons, and the lower spectrogram ions.

giving a lopsided or "J" shaped appearance to the feature. This is similar to the other DMSP example shown in Figure 6. The total size of this feature is slightly larger, though, covering 1° of Invariant Latitude at an altitude of 815 km. This equates to a latitudinal width of 125 km (108 km at 100 km) with an orbital track distance of 213 km (185 km at 100 km), similar to the other cases. The IMF at this time was over 10 nT in $B_y$ and almost −5 nT in $B_z$.

### 2.3. Astrid-2 data

Data from the MEDUSA and EMMA instruments aboard Astrid-2 are shown in Figure 8. The data were taken on January 13, 1999, during a pass over the southern auroral zone. The spacecraft was traveling equatorward at an altitude of 1029 km. In the antiparallel (downward moving) ion spectrogram (Figure 8, bottom panel), a typical dispersion signature can be seen, with a long section that is nearly flat at about 300 eV from 20:12:49 to 20:13:13. The region of interest, however, is less than a third of this dispersion pattern, at the equatorward edge from 20:13:16.5 to 20:13:28. It stands out as a sudden increase of about 1.5 keV (from 500 eV to 2 keV) in the peak energy of the ions. The peak energy of the feature then dips to about 1 keV at 20:13:21.5 and becomes weaker in intensity. From this point until 20:13:28 the energy steadily increases back to 2 keV. This 10-second interval clearly has the V shaped ion structure, with higher energies on the edges and lower energies towards the center. Many of the older-style instruments discussed in this paper have sweep resolutions of 1 to 8 s, which would hardly be enough to identify this feature. MEDUSA, however, has an ion sweep resolution of 0.125 s, so it can easily distinguish this crossing. The ions cut off abruptly on the equatorward edge of the cusp at 20:13:30. The same feature is present in the mirroring perpendicular pitch-angle ions, and the 2 keV "wings" appear in the parallel (upwards) ions, however, the lower energy central portion is not present. In these latter two spectrograms (Figure 8, second and third from the bottom), low-energy enhancements (3–100 eV) can also be seen at the beginning (20:13:18) and end (20:13:25) of the feature moving up the field line. The middle three spectrograms contain the medium energy electron data. The antiparallel (downwards) electrons (sixth panel from the top) and to a lesser extent the other pitch-angle electrons, also show $< 300$ eV enhancements at 20:13:18 and 20:13:25.

EMMA electric and magnetic field data are shown in the fourth through seventh panels of Figure 8 (line plots). For the data presented here, the electric field along the direction of the magnetic field has been assumed to be zero, and the two perpendicular components in the eastward and equatorward directions have been calculated. (This assumption is consistent with other low-altitude spacecraft results (Bonnell et al., 1999).) The magnetic field

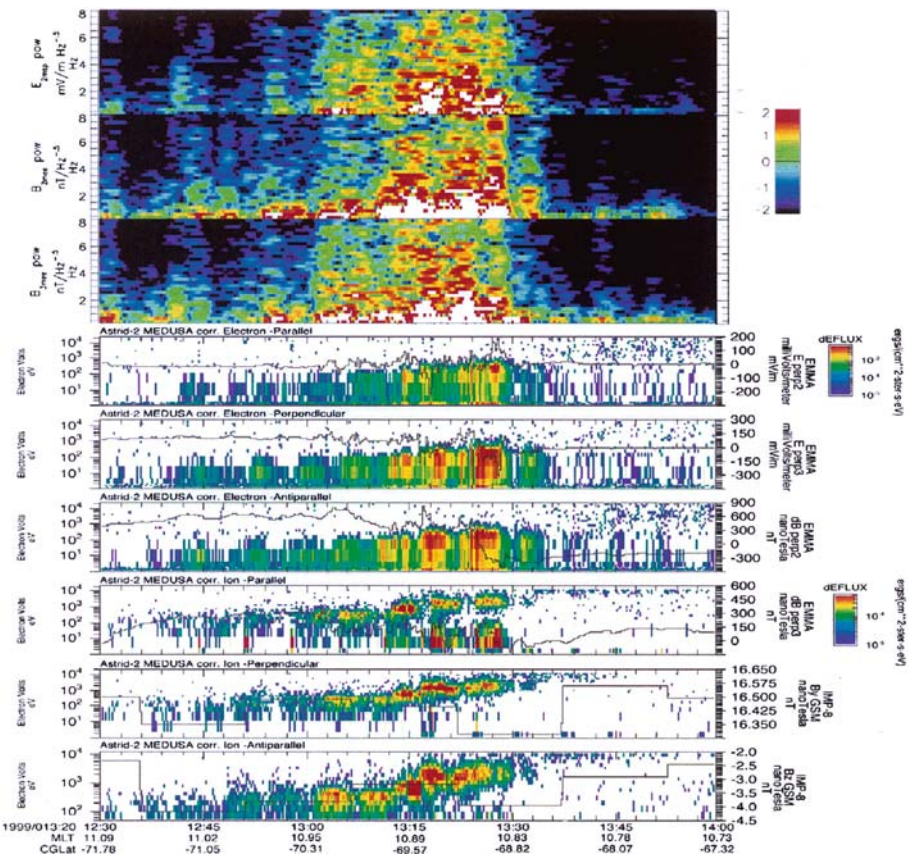


*Figure 8.* Astrid-2 data from January 13, 1999. The data were taken during an equatorward pass through the southern cusp region. The top three panels contain frequency–time spectrograms of electric (top) and magnetic (second two) waves up to 8 Hz. The middle three panels show electron fluxes and the bottom three panels ion fluxes. For both the electrons and ions, the top panel is for particles at 'zero' pitch angle (flowing up the field line), the middle for trapped particles (90° pitch angle) and the bottom for downcoming particles (180° pitch angle). The fourth and fifth panels also contain line plots of the two perpendicular electric field components (with a scale on the right). Panels six and seven display residual magnetic field intensity (after subtracting a model field) for the same two perpendicular directions as the electric field. The bottom two line plots are the y and z components of the IMF as measured by IMP-8.

direction makes an angle of −23° with the spacecraft spin-plane at the time of this cusp crossing. Linear scales for the electric and magnetic field data are shown on the right hand side of the bottom six panels, and are in units of mV/m and nT, respectively. The electric field in the fourth (eastward) panel fluctuates about −10 mV/m outside of the cusp, but begins to gain amplitude going into the high-latitude end of the dispersion feature at about 20:13:00. The field peaks to −225 mV/m at the poleward edge of the ion feature at

20:13:16.5. After this, it increases steadily to 200 mV/m at the equatorward end of the feature (20:13:28), and afterwards settles to 0. The equatorward (North, in this case) pointing perpendicular electric field in the fifth panel begins at a potential of 100 mV/m before dropping by 250 mV/m at the poleward edge of the V. It then returns to its original value of 100 mV/m in the center before plunging to −300 mV/m at the far edge of the feature. It then settles to approximately zero as well. The electric field is V shaped about the centerline and does not reverse direction along the line of the satellite track, which is approximately in the North/South direction (i.e., the equatorward electric field always shows a negative deflection from its equilibrium value). The integrated potential is the order of 50–70 kV. This does not represent the maximum of potential difference, as the satellite does not cross the maximum contours. This is consistent with Crooker's (1988) idea of a concentrated electric field in the throat.

The detrended (delta) magnetic field data are shown on the fourth and third from the bottom panels of Figure 8 for the same two directions as the electric field data. The upper (eastward) component goes from 600 nT before the V, down to −150 nT at the end, revealing a significant current system in that one limited region. Northward data in the lower (equatorward) panel also show a net drop of about 200 nT over the feature, although the trend is much less obvious in this case. The bottom two panels contain line plots of the GSM y and z components of the Interplanetary Magnetic Field, as measured by IMP-8. These values have not been time-shifted to account for the solar wind; however, they are representative of the delayed values for this pass (weakly southward and strongly duskward). The top three panels of Figure 8 contain values proportional to the square root of the wave power for the electric (top panel) and magnetic (second and third panels) fields. The vertical axis is in Hertz, and the color bar indicates the log of the intensity. The spectrograms for the magnetic field fluctuations are calculated by an FFT from the detrended magnetometer data perpendicular to the main field in the eastward (second panel) and equatorward (third panel) directions, and shown in $nT/Hz^{0.5}$. The square root of the electric field wave power is calculated in the same manner, and is shown at the top of Figure 8 with a color bar in units of log mV/m $Hz^{-0.5}$. The sonograms show frequencies up to 8 Hz, calculated with a four second sliding window. The time period of the ion feature, from 20:13:16 to 20:13:28, coincides with a dramatic increase of over two orders of magnitude in the wave power at all displayed frequencies.

The Magnetic Local Time of the ion V event was about 10:52, and the Invariant Latitude range covered only 0.57°, from −69.54° to −68.97°. The length of the satellite track as it crossed this feature is only 86 km (69 at 100 km) (only about 10 of the old one-second sweeps), which makes this a very small feature indeed, even in terms of the cusp proper.

## 2.4. Munin data

MEDUSA-2 particle data from December 20, 2000 are shown in Figure 9. The electron sector closest to antiparallel to the field (i.e. particles coming down to the Earth along the field) is shown on top, while the ions from the same look angle are shown on the bottom. The satellite was near apogee at 1826 km heading poleward over the South polar region. The structure in this case begins at 21:10:44 UT at the equatorward edge of the cusp dispersion pattern with an initial peak in the ions of about 2 keV. The ion energy quickly falls after this to about 500 eV before quickly spiking back to nearly 2 keV, about 2 s after the first peak. The feature stands out as usual in the electron data, although the intensification at the edges is hard to see due to the strong electron fluxes throughout this pass. This very small feature is visible due to the relatively high sample rate of MEDUSA-2 of two complete sweeps per second for ions and 4 sweeps per second for electrons. Similar instruments with sample intervals of 1 or more seconds would not be able to resolve such a small feature. The feature took place over an Invariant Latitude range of 0.08° centered at −82.98°. The

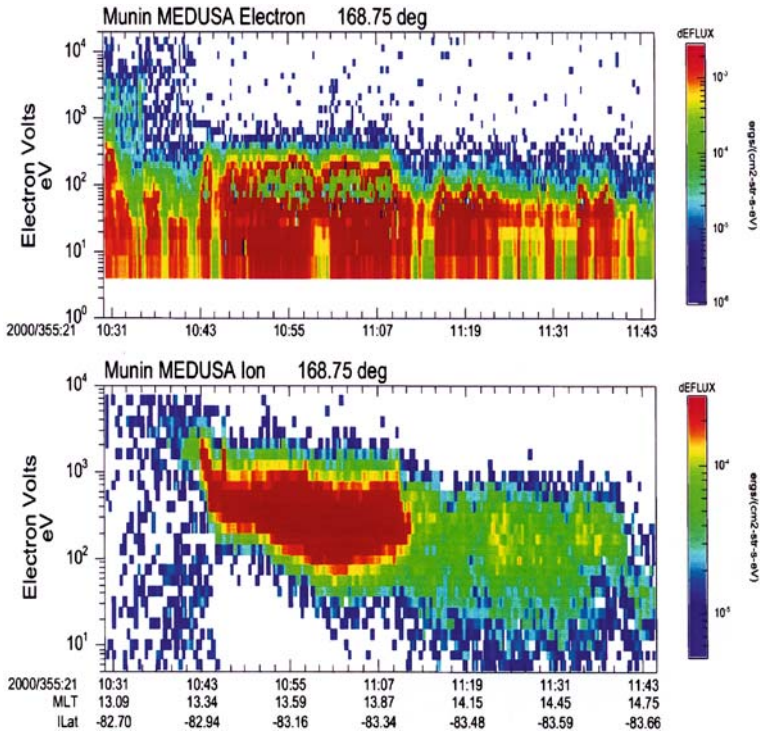


*Figure 9.* Munin data from December 20, 2000. Data are from a poleward cusp pass in the southern hemisphere. The upper spectrogram is for precipitating electrons, and the lower spectrogram shows the ions for the same look direction. A very small V feature can be seen at the equatorward (left) edge of the ion flux in the lower panel, near 21:10:43 UT.

Magnetic Local Time was in the afternoon sector, centered at 13:38 h. The size of the feature along the satellite track was an astonishing 12 km (8 at 100 km), by far the smallest such feature yet seen in the data. The IMF during this time, as measured by the ACE spacecraft, was weakly northward and strongly duskward. Since the cusp wedge is expected to narrow for northward IMF, this small size is consistent with theory.

### 2.5. UARS DATA

HEPS data presented here (Figure 10, lower two spectrograms) show electrons from one of the near-zenith pointing detectors, and protons from one of the LEP detectors. The MEPS data here (upper two spectrograms) are electrons and ions from the detector that has a look direction of 36.6° with respect to the spacecraft zenith (Winningham et al., 1993). The time resolution is 2 s for MEPS, and 4 and 8 s for HEPS electrons and protons, respectively. Data from a cusp pass are presented in Figure 10, and were taken on November 9, 1991, while UARS was heading poleward at an altitude of about 600 km. The feature of interest is located in the afternoon (13:30) sector in MLT and about −67° IL. A V-shaped feature can be distinguished which lasts about 40 s in the MEPS ion data (second panel). It begins at 05:40:40 at about 2 keV, decreases to 500 eV in the center (05:40:56) and increases back to 2 keV at 05:41:17. In contrast to many of the other examples, no ions are seen poleward of the V structure. The MEPS electron data (top panel) over this same time period show enhancements centered on about 40 eV at the beginning and end, with a strong flux of 100 eV electrons throughout the event. Notice the softening of the electrons at the ends, where the density is the highest. HEPS high-energy particle data (lower two spectrograms) also show significant enhancements at the edges of the feature at all energies up to the maximum plotted, about 300 keV. Equatorward of the feature, both electrons and ions show very large fluxes, which indicates that the particles are trapped on closed field lines. From 05:40:26 to 05:40:43, the HEPS electrons (second from the bottom) falls off steadily, corresponding to the beginning of the MEPS ion feature. There is also a significant increase in the flux of electrons at the poleward edge of the feature at 05:41:16, which peaks at or below the low-energy cutoff of 40 keV. The flux of LEP protons (bottom panel) decreases at the onset of the feature in a similar way to the HEPS electron flux, and also shows an increase at all energies at the opposite end (05:41:16).

The $B_y$ magnetic field (line plot in third from top panel of Figure 10), which is fairly constant before and after the feature, is very disturbed during the period from 05:40:33 to 05:41:19, increasing sharply and then decreasing steadily during this time period, with a sharp rise at the end. This implies field-aligned currents directed upwards at the edges and downwards in the

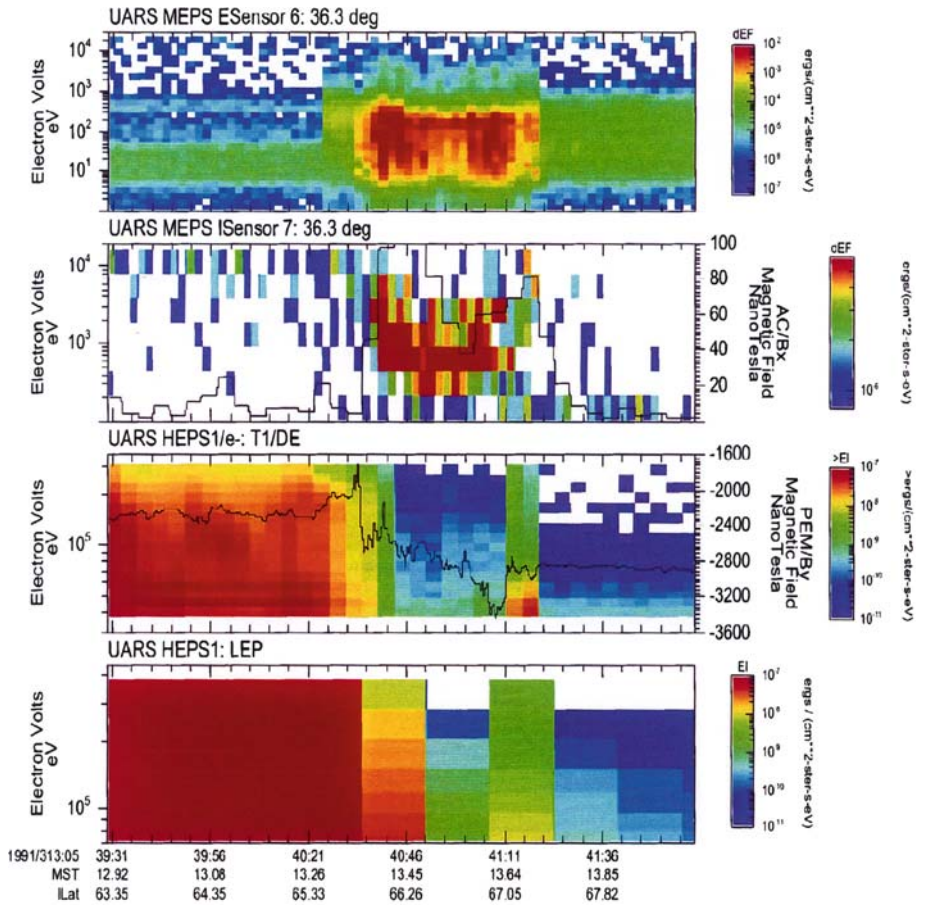


*Figure 10*. UARS data from November 9, 1991. The top two spectrograms are for medium energy electrons and ions, while the lower two are for high energy electrons and ions. The upper line plot is the integrated square root of magnetic wave power, while the lower line plot is magnetic field perpendicular to the spacecraft.

center. The square root of magnetic wave power data, integrated from 0 to 100 Hz and labeled AC/$B_x$ (the scale is on the right of the second panel), increases by over an order of magnitude to 100 nT at the onset of the ion feature, dips down to about 40 nT near the center at 05:41:01, and then peaks again at 80 nT at the end of the structure before returning to low (below 10 nT) values. The invariant latitude covered during this time, though, is only 1.2°, which is about 143 km in the North/South direction, or 127 km projected to 100 km altitude. This pass, however, also had a significant East/West velocity component, which gives an orbital distance of almost 280 km (248 at 100 km), mostly in MLT. This is at the high end of sizes for this type of feature at low altitudes, a factor of 3 larger than the Astrid-2 feature, but

still at the very bottom of the range of normal cusp sizes. The IMP-8 satellite measured the IMF at this time to be weakly southward and very strongly duskward.

### 2.6. Cluster data

Data from August 16, 2001 mid-altitude cusp pass of the four Cluster spacecraft are shown in Figures 11–14. The data were taken during a poleward pass over the northern cusp at a geocentric distance of about 5.4 $R_E$ (distances range for the four Cluster spacecraft in order from 5.63 $R_E$ at Cluster-1 to 5.3 $R_E$ at Cluster-4). The invariant latitude for all spacecraft at the cusp passage was about 78°, and the MLT was just after 14:00. This is consistent with an afternoon-shifted cusp, which is expected from the dominant IMF $+B_y$ seen by ACE at this time (with the appropriate propagation delay from ACE to Cluster).

Figure 11 shows data from all four spacecraft, two panels each; the time axis is common to all observations. RAPID $>30$ keV ions (black) and a detrended magnetic field (green) are shown in the upper plots, and STAFF magnetic wave power spectrograms from 8 Hz up to 4 kHz and plasma pressure derived from the PEACE electrons (red) in the lower plots. A time shift indicating when each successive spacecraft was on approximately the same given field line is indicated by the blue vertical bars. This location was set for the lead spacecraft Cluster-4 at the time that the internal magnetospheric ion flux drops off (black line in panel 7). Times when the invariant latitude and magnetic local times of the other spacecraft most closely matched those of the Cluster-4 time were subsequently marked (panels 1, 3, and 5). These marks agree remarkably well with the time that the internal source ion cuts off. The periods of enhanced wave power correspond to the periods of intensified medium energy ions and electrons shown below.

Figure 12 shows a view from the Orbit Visualization Tool (OVT) of the four satellite tracks from 9:30 to 10:30 UT as projected onto the *x*-*z* GSE plane. The actual tracks fall nearly in this plane, and are separated almost exclusively by altitude. The spacecraft markers (and associated field lines) are for the times listed next to each marker, which correspond approximately to the times of the blue vertical bars of Figure 11. The positions agree with the equatorward edge of the model cusp used in the OVT software (T87).

Figures 13 and 14 show ion and electron spectra at 0°, 90°, and 180° pitch angles for spacecraft 1 and 3, respectively. CIS/HIA (ion) data are unavailable for 2 and 4, however, the PEACE electron data (not shown) suggest that the morphology of the plasma at Cluster-2 is similar to that at 1, while the plasma at Cluster-4 is much like that at 3. The data in Figure 14 (Cluster-3) show a signature consistent with the previous low altitude cases. At the equatorward edge of the cusp, the downward (0° pitch angle) ion flux intensifies at about

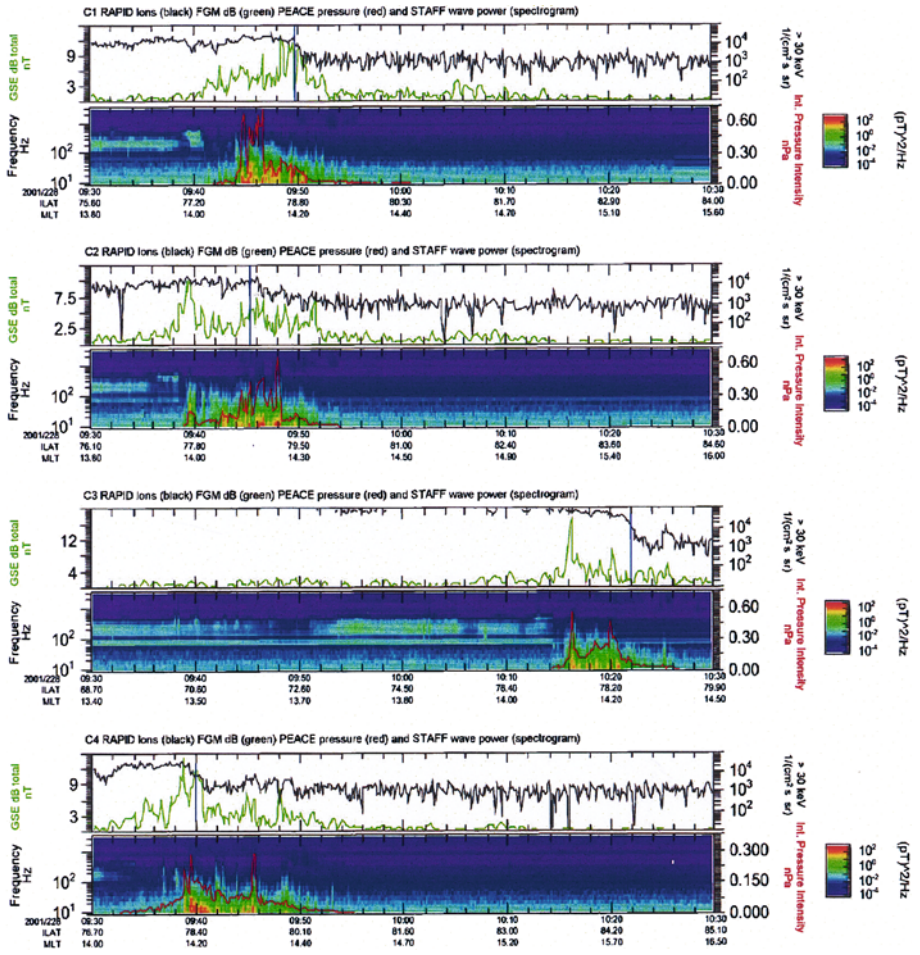


*Figure 11.* Cluster data from August 16, 2001. Each pair of panels corresponds to one of the four spacecraft, ordered 1 to 4 from top to bottom. Line plots on panels 1,3,5, and 7, are high energy ions (black) from RAPID and delta B (green). Spectrograms are wave power from STAFF data, while line plots over the spectrograms are electron pressure.

1 keV at 10:15:30, then drops to about 300 eV in the center at 10:17:30 before returning to over 800 eV at 10:20. The electrons also show a morphology similar to the low-altitude data, with large enhancements at the edges of the feature and elevated fluxes in between. In Figure 13 (Cluster-1), however, the dominant flow direction of the plasma changes directions many times as seen in the peak fluxes of the parallel and anti-parallel panels (first and fourth panels). These reversals are also evident in the moments data (not shown). They disrupt the cusp feature under study, although some properties such as its size and energy range remain intact. The magnetic wave properties at this spacecraft also indicate fully developed turbulence as seen in the external cusp (turbulent

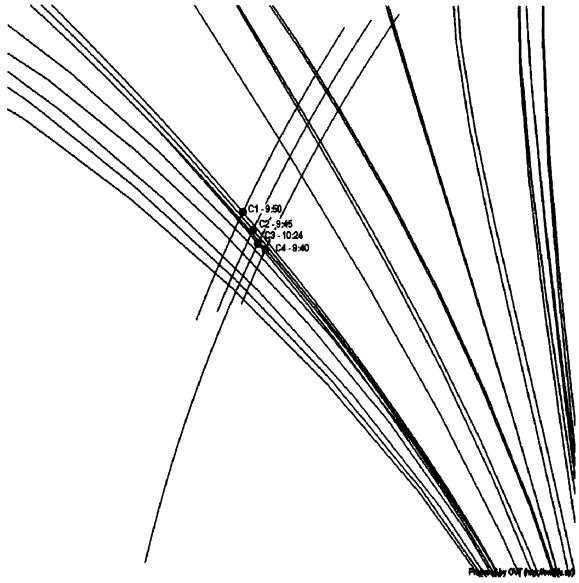


*Figure 12.* Cluster spacecraft satellite tracks in the GSE $x$–$z$ plane from 9:30 to 10:30 UT. The Sun is to the left and the spacecraft are traveling towards the North ($+z$). The curved lines originating in the lower right corner are magnetic field lines connecting to the Earth (not shown). The spacecraft markers are displayed at the times shown for each, corresponding to their entry into the cusp field region. See Figure 3 for context. (Adapted from OVT output images).

boundary layer) region. Comparing the available data at all spacecraft and ordering by their similarities to the low-altitude V cusp crossings or the high-altitude turbulent cusp crossings, the order is the same as the spacecraft altitudes, with Cluster-4 being the most similar to low altitude data and Cluster-1 the most similar to high altitude data. Cluster-4 is also the only one to show the high-energy ion cutoff at the beginning of the feature, as the low altitude crossings show. This is despite the fact that three of the spacecraft (1, 2 and 4) traverse this feature at approximately the same time, while Cluster 3 follows about half an hour later. This would imply that the differences in the plasma characteristics are due more to the spatial separation in altitude rather than in the timing of the crossings (see satellite tracks in Figure 3). The cusp feature crossings are all of similar size, averaging about 1170 km across, which corresponds to a 100 km footprint of 98 km.

## 3. Statistical survey

In order to understand this unique feature in more detail, and its correlation with factors such as the interplanetary magnetic field (IMF), a statistical

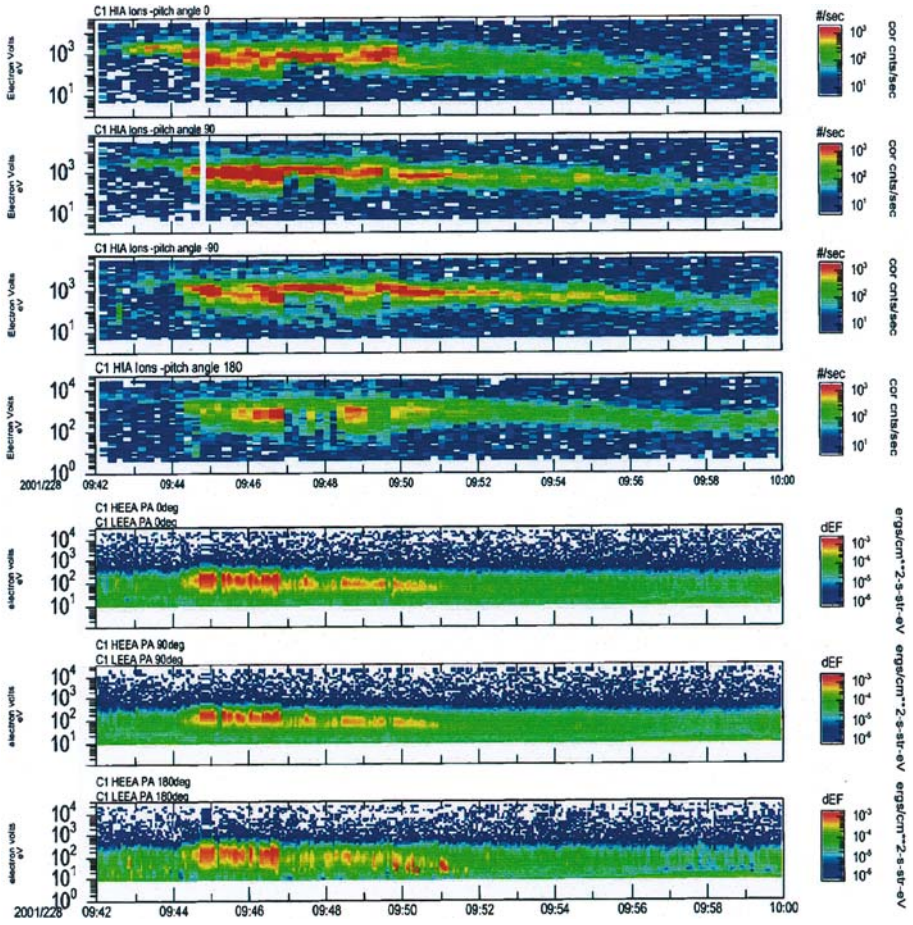


*Figure 13.* Cluster-1 data from August 16, 2001. The top four panels are for HIA ions in the parallel, perpendicular, and antiparallel directions. The bottom three panels are for PEACE electrons, for the same pitch angle directions.

survey was undertaken. The survey produced a set of time-tagged cusp passes for 4 of the DMSP satellites (F8, F9, F10, and F11) and Astrid-2, with the time-delayed IMF given as a clock-angle sector. This allowed a large number of passes ($>3700$) to be evaluated quickly, taking into account the prevailing IMF for the pass. The primary goal of this survey is to determine the consistency of the "V" feature and to correlate it with position and IMF. Also, a rough frequency estimate may be made, keeping in mind that the feature and the satellite tracks are both very narrow, and so will not necessarily intersect even when all other conditions are favorable.

Although this study of a large number of cusp passes highlighted the almost infinite variety of particle signatures that may be encountered, for this study it was necessary to limit the scope of the survey to finding those events

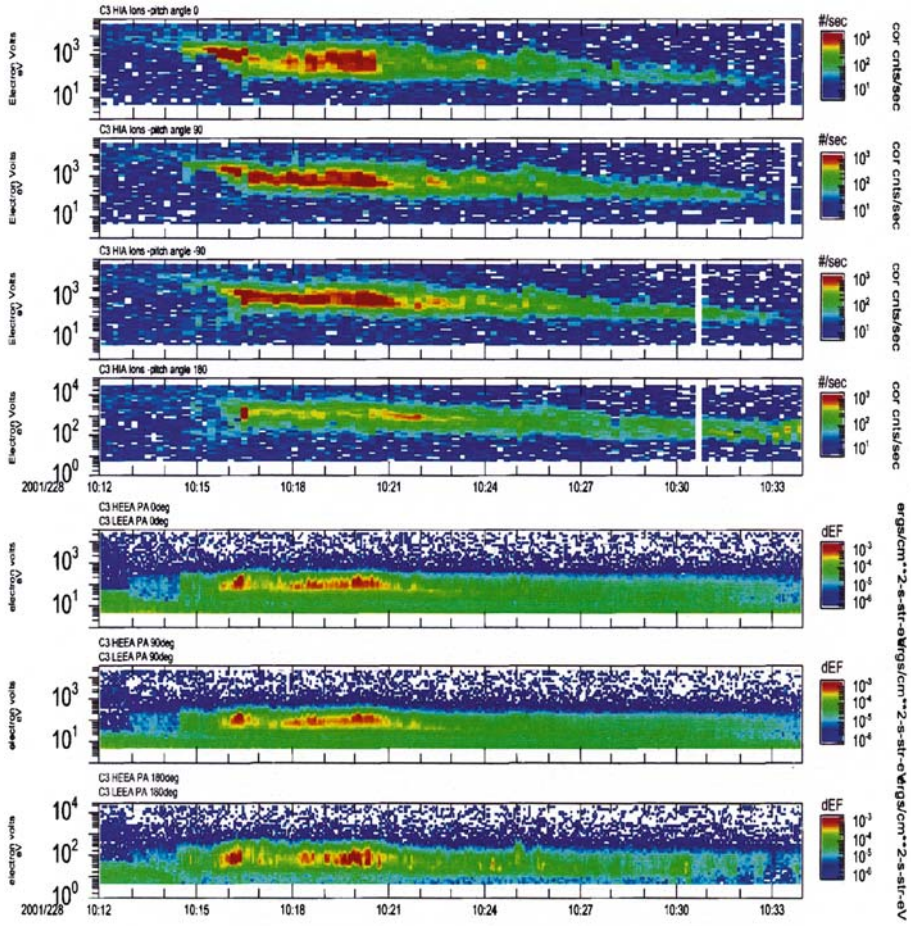


*Figure 14*. Cluster-3 data from August 16, 2001. The top four panels are for HIA ions in the parallel, perpendicular, and antiparallel directions. The bottom three panels are for PEACE electrons, for the same pitch angle directions.

that clearly show the defined "V" morphology. From initial observations and theoretical considerations such as the Crooker (1988) model, we expect to see these distinctive features at the equatorward end of cusp passes, and depending on the cut angle and IMF orientation, a narrow V shape in the down-going ion flux at around 1–2 keV and a scale-size on the order of 100 km. Since the size, location, and orientation of the cusp for a given set of IMF conditions is not known a priori, the relative orientation of the satellite track through the feature tends to obscure and complicate the identification for many of the passes. For example, for a given wedge cusp configuration (pure $+B_y$ in Figure 15a or pure $-B_y$ in Figure 15b) a satellite passing through the cusp may or may not cross both sides of the wedge and therefore

will not always have the expected V morphology. In both images of Figure 15, the gray satellite track would see a V, while the black satellite track would not. This orbital track bias does have an effect on the statistical analysis, as described in the Results section. The apparent continuum of V sizes in the data studied also tends to blur the distinction between the small cusp signature of interest here and larger-scale V's, which are discussed in more detail in the Discussion section. For our purposes, however, we have chosen a maximum size of 300 km for the V's, corresponding to a 40 s passage for the DMSP and Astrid-2 satellites, which have similar low-altitude circular orbits (800 and 1000 km, respectively). The majority, however, are below 100 km (about 10 s) in width.

### 3.1. Setup and parameters

The first step in the survey was to build a database of cusp passes for the satellites to be studied. The satellites were chosen due to the large amount of data to work from (in the case of the DMSP satellites), and their favorable orbits and instrument suites. Although the cusp is quite limited in spatial extent for a given low-altitude pass, it moves around significantly, so a fairly large "cusp box" had to be defined in the North and South directions in order to catch the majority of candidate passes. The boxes were defined as being between 10:30 and 13:30 in MLT, and the northern (southern) box at an Invariant Latitude of between 60° and 80° (−60° and −80°). The entry and

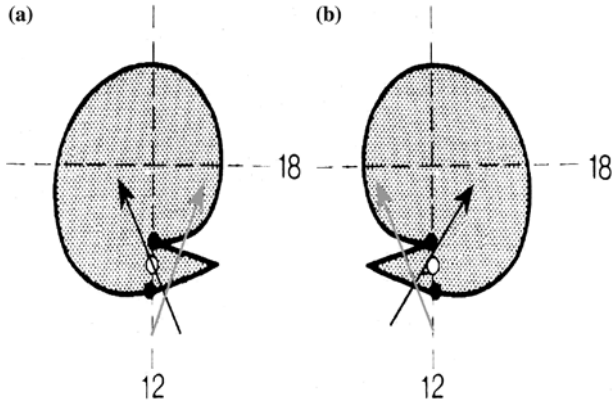


*Figure 15*. Diagram showing possible cusp wedge traversals in high $B_y$ cases: the Sun is towards the bottom of the figure marked by a 12, (a) The northern polar cap for duskward IMF (or southern polar cap for dawnward IMF), (b) The northern polar cap for dawnward IMF (or southern polar cap for duskward IMF). In each case, a satellite track represented by the gray arrow would see a V structure, while a satellite track, marked as black, would not. (Adapted from Crooker, 1988).

exit times of each passage through the boxes were compiled without regard to IMF direction.

Once the cusp crossing times had been compiled, each time was used to calculate a time-shift for IMF data taken by the IMP-8 satellite (when available). This time shift was subsequently used to calculate an average IMF for each pass, which was converted into one of 8 clock angle sectors in the GSM *y-z* plane. Once all of these data had been collected, the crossing times were used to create spectrogram images for each cusp crossing. The filenames were time tagged with the beginning time, and included codes for which hemisphere the spacecraft was in, as well as the IMF clock angle during the pass. These image files were then manually sorted by content. First, a list of "successful" cusp passes was compiled, success being defined as having a clear cusp signature in the ion and electron spectrogram data. Next, possibly relevant passes were noted for closer examination. A more detailed look was then taken of the candidate passes so that they could be correctly categorized. This process was repeated for all of the satellites examined, and the results compiled together.

### 3.2. Survey results

After examining over 3700 cusp passes from the Astrid-2 and four DMSP satellites, it became clear that these small-scale V's are not equally likely at all orientations of the IMF. Figure 16 is a histogram of occurrences vs. the eight IMF bins showing the combined data for all of the satellites in the study. The number of observed passes from each satellite has been weighted relative to the percentage of passes occurring during each of the eight IMF clock angles. This general morphology occurs, however, within each individual satellite data set both weighted and unweighted. This robust statistical trend clearly shows a preference for strong IMF $B_y$, with a lesser preference towards southward IMF. It is interesting to note that the data also show a strong preference for duskward over dawnward IMF, the occurrence of the duskward peak being 2.4 times the dawnward peak value. This is probably due to the available angles with which the various spacecraft passed through the cusp region. In the orbits used in the study, the angle between the satellite tracks and noon MLT is such that, in the North, a wedge pointing duskward (for duskward IMF) would be traversed more perpendicularly, while a dawnward pointing wedge would be crossed less perpendicularly, making the double signature visible less often (as in the black tracks of Figure 15). A similar argument holds for the southern hemisphere, keeping in mind that in the South the wedge moves in the direction opposite the IMF, rather than with it. A "V" signature is expected only if the spacecraft crosses both arms of the wedge. Given the traversal direction of the passes, this is much more likely in the South for dusk-pointing fields than for dawn-pointing fields.

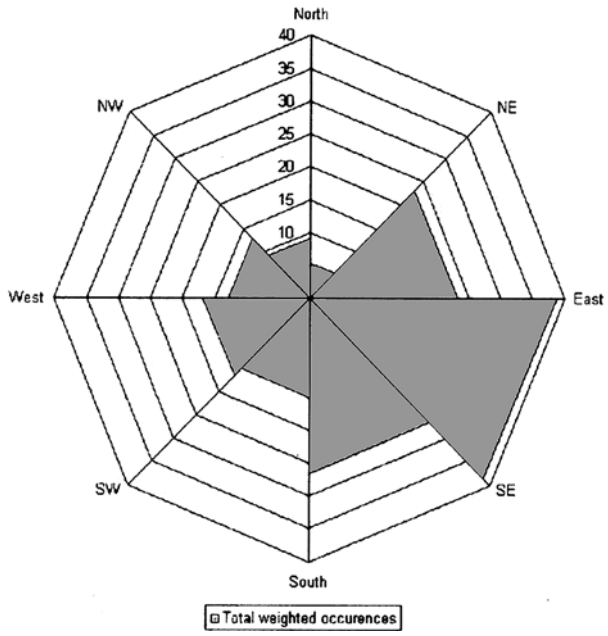


*Figure 16*. Histogram of weighted "V" Occurrences vs. IMF clock angle. A strong duskward and weaker dawnward peak can be seen, as expected from theoretical considerations.

Overall, some sort of cusp was seen in the particle data for about 40% of the passes studied. Of those, about 10% contained a V signature. This is a very reasonable percentage for a persistent feature with an average size of about 0.75° in Invariant Latitude and only 0.28 h of Magnetic Local Time (at the cut angles available in this study). The uneven sampling of the box by the satellites used in the study limits the conclusions that can be drawn about the cusp's overall movements within the box; clearly it moves around a great deal, and its shape and position are strongly influenced by the IMF at the magnetopause. The picture that emerges from this statistical survey is of a consistently present limited region within the cusp that is governed by the IMF direction and tends to stretch longitudinally with increasing $B_y$, making it more likely to be encountered by polar-orbiting satellites.

## 4. Discussion

We have presented cusp-related data from several different satellites, instruments and altitudes, representing various sensor types and technologies. The fact that the narrow "V" feature is consistent throughout all of the data sets indicates that it is not a characteristic of the instruments taking the data, but must be considered to be a real structure. Also, the fact that the

energetic particle and field instruments see a feature at the same time with a comparable scale-size also points to it being something physical. The feature is also persistent, as the statistical survey of Astrid-2 and DMSP data has shown.

Reiff et al. (1977) discuss convective dispersion, an injection model which they called for northward IMF – "diffusive injection"; it assumes a dependence on energy for the rate of diffusion from a central "injection field line." This results in an energy dispersion in which the highest energy particles are towards the edges of the cusp (since they can random walk farther from their injection point than the lower energy particles). Later works (Reiff et al., 1980; Burch et al., 1980; Woch and Lundin, 1992; Weiss et al., 1995) confirmed that these features are seen, usually during northward IMF conditions, and offered other explanations for these "large scale V's". Possible explanations such as tail reconnection, changes in the IMF $B_z$, and lobe reconnection have been offered. The features presented here, however, are of a scale size much smaller than the large V dispersion features studied by these authors, and appear to be very localized to the equatorward edge of the precipitating particle region. For this work, we have defined 300 km to be the break in scale size (at low altitudes) between the two types of features. It is clear that in the complex 3-D geometry of the cusp there are multiple ways to cut through in order to create a "V" in the ion spectrograms, so this distinction should be viewed simply as one more step towards fully parsing the features of the cusp into understandable components. It should also be noted that, while the large-scale V's have been found to occur predominantly during northward IMF conditions, the small V's have been shown here to have a minimum at that orientation. While some characteristics and possible causes of these two structures no doubt overlap, we believe that they are not equivalent.

The scale size, plasma characteristics, shape and location of this feature are all consistent with the Crooker model (1985, 1988) of the narrow wedge cusp presented in the Introduction. This feature should always be present, but its size and variable orientation naturally limit the extent to which it can be observed. A spacecraft trajectory is unlikely to cross the full potential difference across the V, so that only for relatively lucky crossings when the V structure is lying significantly across the trajectory would the feature be visible. This wedge cusp can be defined in terms of the magnetopause current layer, which contains the outermost layer of magnetic field lines of the magnetosphere. This very thin layer is the site of the interconnection between the Earth's magnetic field and the interplanetary magnetic field and produces other interesting processes, not all of which are understood. The low-altitude regions to which these outermost field lines map are the magnetic cusps (i.e., defined by field geometry rather than particle population), which we believe are associated with this small sub-region of the particle-defined cusp, called

the "true cusp" by Keith et al. (2001). Thus, this "true cusp" can represent a unique window into the large-scale workings of the magnetosphere and the magnetopause current layer. Newell and Meng (1991) noted a spatially distinct region of accelerated plasma at the equatorward edge of the cusp very similar to these observations, although with a less favorable geometry for seeing the structure clearly. They also argue against temporal variations as a cause, due to the fact that the accelerated region is always at the equatorward edge of the cusp.

The primary difference between this definition and that of the cusp proper is that the particles are expected to be more energetic, reflecting the populations accelerated through non-MHD processes in the magnetopause current layer and seen by *in situ* measurements (Gosling et al., 1986; Song et al., 1990) and simulations (Nakamura and Scholer, 2000). It is also possible for drifting energetic particles to become temporarily trapped in the outer cusp region from low latitudes (Sheldon et al., 1998; Delcourt and Sauvaud, 1999). Particles with pitch angles initially near 90° drift from the near-tail to the dayside magnetosphere (Figure 17, trajectories labeled 1, 2, and 3). Particles along 1, the innermost track, circulate in a well-behaved (ring-current) manner. The outermost third track reaches the equatorial dusk flank. Particles following the second (center) track, however, encounter a non-equatorial mirror force in the vicinity of the cusp where they are drawn to high latitudes and can become trapped temporarily in the local magnetic field minimum surrounding the cusp funnel. A portion of this population precipitates around the perimeter of the cusp funnel. Locally penetrating, unaccelerated magnetosheath plasma from the magnetopause boundary layer is also seen near the boundary (Lundin, 1988), and should propagate in the cusp proper to low-altitudes poleward (and occasionally equatorward) of the accelerated plasma population of the true cusp.

Mid-altitude data from Cluster, although preliminary, point to a temporally stable feature with a great deal of structure at the transition region between the turbulence-dominated exterior cusp region described by Savin et al. (1998) and the more stable, Crooker (1985, 1988)-like wedge cusp seen at lower altitudes. The correlation of the data between the four Cluster spacecraft is most easily explained by their varying altitudes, even though the spacecraft were relatively close. The data from the lower satellites looked more similar to those expected for the Crooker cusp, while the higher ones contained characteristics found in the Savin et al. (1998) exterior cusp. This observation must be investigated further to help establish the existence of such a transition region at mid altitudes.

A survey of over 3700 cusp passes taken from five different satellite platforms confirms the strong preference of IMF direction expected from the Crooker (1988) model of the cusp. The movements of the cusp and the angle through which it is traversed by the spacecraft all influence the shape of the

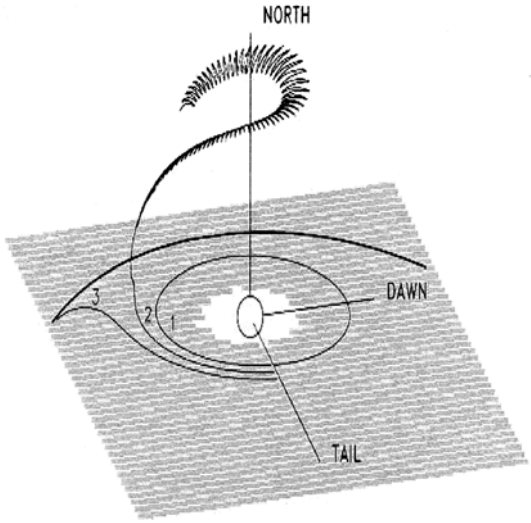


*Figure 17.* Equatorial ring current particles drift from the plasma sheet to the dayside magnetopause region and are deflected into a cusp-orbiting trajectory. From here they may be lost along the edges of the cusp to low altitudes. (From Delcourt and Sauvaud, 1999).

spectrogram that is seen; however, the experimental evidence points to a cusp that swings from side to side with the IMF, and is very limited in size. The evidence from the survey is, therefore, supportive of the existence of a true cusp region in the form of a wedge that responds to the Interplanetary Magnetic Field by rotating and extending in Magnetic Local Time.

## 5. Conclusions

An important, yet small-scale feature has been presented here; it is consistent with the wedge cusp of Crooker (1988), and with the turbulent exterior cusp. The location and energization of these features fits our expectation of a mapping of the magnetopause current layer, which has been previously reported in Keith et al. (2001). It is hoped that, as more high-resolution, low and mid altitude data become available, new information about the cusp and the associated particle entry processes may be derived.

Although more work is certainly needed in order to fully understand this unique feature, it is clear from these initial investigations that a window to the larger workings of the magnetosphere exists at low-altitudes, perhaps even more so than previously thought (Newell and Meng, 1995). The data studied indicate a unique feature in the cusp, distinct from the remaining cusp precipitation, which we believe to be the low altitude mapping of the magnetopause current layer, i.e., the true cusp. As more detailed work is

conducted, it is hoped that this model may be integrated to a further degree with the overall mainstream picture of the cusp and its dynamics.

The data presented here are consistent with a measurable low altitude image of the magnetopause current layer. These field lines are those on which ions are accelerated above magnetosheath energies and which form the classical magnetic cusp (i.e., *not* a plasma cusp). The mapping topology at low and mid altitudes appears to "swing" with $B_y$ as expected from the Crooker (1988) model and has an enhanced electric field, as predicted. The wave data in the ELF/ULF region are consistent with the observations of a turbulent, noisy magnetopause. Energetic particles seen at the edges of the V feature are consistent with drifting particles that see a non-equatorial mirror force (Sheldon et al., 1998; Delcourt and Sauvaud, 1999) near the magnetopause and drift up into the magnetic cusp where they circulate and can be lost. The transition region from the turbulent exterior cusp has been sampled by the set of Cluster spacecraft, indicating a continuum between the morphologies seen at high altitudes and those seen at low altitudes.

Future work will focus on understanding in greater detail the connections between the IMF, magnetopause current layer and the cusp. This includes the addition of new data, especially from the Cluster mission, which has already begun to revolutionize our understanding of these regions. Recent DMSP data can hopefully be used along with Cluster to study concurrent mid and low altitude passages. It is hoped that this work may lead to a consensus on the methods of charged particle entry in the magnetopause and on the relationship of the magnetopause current layer to the cusp.

## Acknowledgements

This work is supported by NASA grant NAG510863. We would like to acknowledge Nelson Maynard for the use of DE-2 VEFI data, Donald Gurnett for DE-1 PWI data, and the NSSDC OMNIWeb and participating investigators for solar wind and IMF data.

## Appendix A

The earliest observations presented are from the High Altitude Plasma Instrument (HAPI) and the Low Altitude Plasma Instrument (LAPI) on the DE-1 and −2 satellites. HAPI uses five parabolic electrostatic analyzers at fixed viewing angles of $\pm 45°$, $\pm 12°$, and 0 (relative to the spin axis (Burch et al., 1981). LAPI consists of 15 parabolic electrostatic analyzers covering

180° for ions and electrons from 5 eV to 32 keV and two Geiger–Mueller (G–M) counters that measure >35 keV electrons at 0° and 90° pitch angles relative to the magnetic field. The spectrometers take one 32-step spectrum each second from each sensor (Winningham et al., 1981).

The U.S. Air Force's SSJ/4 particle instruments on the DMSP satellites comprise the highest volume of data studied, thanks to multiple satellite platforms covering many years of operations. SSJ/4 is a set of four cylindrical electrostatic analyzers, two sensors each (high and low energies) for both electrons and ions. Together they cover an energy range from 30 eV to 30 keV, completing a spectrum once per second. The DMSP satellites are non-spinning, and the SSJ/4 detectors are mounted such that they are always pointed radially outwards from the Earth. Near the northern (southern) polar cusp, this zenith direction will be close to the (anti)parallel magnetic field direction. Further information about the DMSP program and the SSJ/4 instruments can be found in Hardy et al. (1984).

Data have also been presented from the MEDUSA-1 and −2 instruments flown aboard the Swedish Astrid-2 and Munin spacecraft, respectively. The Miniaturized Electrostatic DUal-top-hat Spherical Analyzer (MEDUSA) was first flown aboard the Swedish Astrid-2 microsatellite (Marklund, 2001). The instrument is composed of two spherical top-hat analyzers placed top-to-top with a common 360° field of view. Each detector is divided into 16 azimuthal sectors of 22.5°, with an elevation acceptance of about 5°. They have an energy per charge range of about 1 eV to 20 keV for electrons and positive ions. A second, almost identical unit, MEDUSA-2, was flown aboard the Munin nanosatellite. The Munin spacecraft was locked to the Earth's magnetic field such that the 16 MEDUSA-2 input sectors looked in constant pitch angle directions. MEDUSA-1 has a sample rate for ions of 8 sweeps per second, and 16 sweeps per second for electrons. The sample rates for MEDUSA-2 are one quarter those of MEDUSA-1 due to telemetry limitations. More information on the MEDUSA instruments can be found in Keith (1999) and Norberg et al. (2001). Astrid-2 also had a fields experiment named Electric and Magnetic field Measurements for Astrid-2 (EMMA). EMMA (Blomberg, 2001) measures two spin-plane components of the electric field and all three components of the magnetic field.

The HEPS instrument on the UARS satellite studying high-energy electrons and ions (from 30 keV to 5 MeV and 150 MeV, respectively) consists of four electron/proton detectors, two electron detectors, and two Low Energy Proton (LEP) detectors. The MEPS spectrometer is made up of eight parabolic plate electrostatic analyzers and looks at electrons and ions in the 1 eV to 32 keV range. Each detector is situated on the spacecraft so as to have a different look direction angle with respect to the spacecraft (Winningham et al., 1993).

Recent Cluster data complete the list. Particle detection for this mission is spread over several experiments on each spacecraft. We are primarily interested in electron data from the Plasma Electron and Current Experiment (PEACE) and ion data from the Cluster Ion Spectrometry (CIS) experiment. PEACE consists of two sensors with hemispherical electrostatic analyzers, each with a 180° field of view radially outwards and perpendicular to the spin plane. Together, the sensors cover an energy range from 0.6 eV up to 26 keV over twelve polar sectors (Johnstone et al., 1997). CIS also consists of two sensors, one with ion mass resolution and the other without. Both have spherical electrostatic energy analyzers, the mass resolving instrument CODIF covers four ion species from 20 eV to 40 keV/charge, while the non-mass-resolving unit HIA has an energy range from 5 eV to 32 keV. Each instrument is divided into two 180° fields of view tangential to the spin axis with different sensitivities. The high sensitivity sides face spinward and cover all polar angles, while the low sensitivity sides face anti-spinward (Rème et al., 1997). The STAFF Spectrum Analyzer computes the electric and magnetic waves fluctuations at 27 frequencies distributed logarithmically in the frequency range from 8 Hz to 4 kHz (Cornilleau-Wehrlin et al., 1997). Detailed information on all of the instruments for the Cluster mission can be found in Escoubet et al., (1997).

## References

Aparicio, B., Thelin, B., and Lundin, R.: 1991, 'The Polar Cusp From a Particle Point of View: A Statistical Study Based on Viking Data', *J. Geophys. Res.* **96**, 14023–14031.

Bonnell, J., Elphic, R. C., Palfrey, S., Strangeway, R. J., Peterson, W. K., Klumpar, D., Carlson, C. W., Ergun, R. E., and McFadden, J. P.: 1999, 'Observations of polar cap arcs on FAST', *J. Geophys. Res.* **104**, 12669–12681.

Burch, J. L., Reiff, P. H., Heelis, R. A., Spiro, R. W., and Fields, S. A.: 1980, ''Cusp region particle precipitation and ion convection for northward interplanetary magnetic field'', *Geophys. Res. Lett.* **7**, 393–396.

Burch, J. L., Winningham, J. D., Eaker, N., Blevins, V. A., and Hoffman, R. A.: 1981, 'The High Altitude Plasma Instrument (HAPI)', *Space Sci. Inst.* **5**, 455–463.

Chapman, S., and Ferraro, V.C.A.: 1931, 'A new theory of magnetic storms', *Terr. Magn. Atmos. Electr.* **36**, 171–186.

Cornilleau-Wehrlin, N., Chauveau, P., Louis, S., Meyer, A., Nappa, J. M., Perraut, S., Rezeau, L., Robert, P., Roux, A., Villedary, C.de, Conchy, Y.de, Friel, L., Harvey, C. C., Hubert, D., Lacombe, C., Manning, R., Wouters, F., Lefeuvre, F., Parrot, M., Pincon, J. L., Poirier, B., Kofman, W., and Louarn, P.: 1997, 'The CLUSTER Spatio-Temporal Analysis of Field Fluctuations (STAFF) Experiment', *Space Sci. Rev.* **79**, 107–136.

Crooker, N. U.: 1985, 'A Split Separator Line Merging Model of the Dayside Magnetopause', *J. Geophys. Res.* **90**, 12104–12110.

Crooker, N. U.: 1988, 'Mapping the Merging Potential From the Magnetopause to the Ionosphere Through the Dayside Cusp', *J. Geophys. Res.* **93**, 7338–7344.

Delcourt, D. C., and Sauvaud, J.-A.: 1999, 'Populating of the Cusp and Boundary Layers by Energetic (Hundreds of keV) Equatorial Particles'', *J. Geophys. Res.* **104**, 22635–22648.

Dubinin, E., Skalsky, A., Song, P., Savin, S., Kozyra, J., Moore, T. E., Russell, C. T., Chandler, M. O., Fedorov, A., Avanov, L., Sauvaud, J.-A., and Friedel, R. H.W.: 2002, 'Polar-Interball coordinated observations of plasma and magnetic field characteristics in the regions of the northern and southern distant cusps', *J. Geophys. Res.* **107**, SMP 2-1.

Escoubet, C. P., Russell, C. T., and Schmidt, R. (eds.): 1997, '*The Cluster and Phoenix Missions*', Kluwer Academic Publishers.

Gosling, J. T., Thomsen, M. F., Bame, S. J., and Russell, C. T.: 1986, 'Accelerated Plasma Flows at the Near-Tail Magnetopause', *J. Geophys. Res.* **91**, 3029.

Gurnett, D. A., Anderson, R. R., Tsurutani, B. T., Smith, E. J., Paschmann, G., Haerendel, G., Bame, S. J., and Russell, C. T.: 1979, 'Plasma Wave Turbulence at the Magnetopause: Observations From ISEE 1 and 2', *J. Geophys. Res.* **84**, 7043–7058.

Hardy, D. A., Schmitt, L. K., Gussenhoven, M. S., Marshall, F. J., Yeh, H. C., Schumaker, T. L., Huber, A., and Pantazis, J.: 1984, *'Precipitating electron and ion detectors (SSJ/4) for the block 5D/flight 6-10 DMSP satellites: Calibration and data presentation', Rep. AFGL-TR-84-0314.*, Air Force Geophys. Lab, Hanscom Air Force Base, Mass.

Heikkila, W. J., and Winningham, J. D.: 1971, 'Penetration of Magnetosheath Plasma to Low Altitudes Through the Dayside Magnetospheric Cusps', *J. Geophys. Res.* **76**, 883–891.

Heikkila, W. J.: 1972. '*The Morphology of Auroral Particle Precipitation*.' Space Res. XII, Akademie-Verlag, Berlin, pp. 1343.

Johnstone, A. D., Alsop, C., Burge, S., Carter, P. J., Coates, A. J., Coker, A. J., Fazakerley, A. N., Grande, M., Gowen, R. A., Gurgiolo, C., Hancock, B. K., Narheim, B., Preece, A., Sheather, P. H., Winningham, J. D., and Woodliffe, R. D.: 1997, 'PEACE: A Plasma Electron and Current Experiment', *Space Sci. Rev.* **79**, 351–398.

Keith, W. R.: 1999, 'Development of an Ion/Electron Plasma Spectrometer,' Master of Science Thesis, Rice University, Houston, Texas.

Keith, W. R., Winningham, J. D., and Norberg, O.: 2001, 'A New, Unique Signature of the True Cusp', *Ann. Geophys.* **19**, 611–619.

Lundin, R.: 1998, 'On the Magnetospheric Boundary Layer and Solar Wind Energy Transfer into the Magnetosphere', *Space Sci. Rev.* **48**, 263–320.

Marklund, G. T., Blomberg, L. G., and Persson, S.: 2001, 'Astrid-2, an Advanced Microsatellite for Auroral Research', *Ann. Geophys.* **19**, 589–592.

Nakamura, M., and Scholer, M.: 2000, 'Structure of the magnetopause reconnection layer and of flux transfer events: Ion kinetic effects', *J. Geophys. Res.* **105**, 23179–23191.

Newell, P. T., and Meng, C.-I.: 1988, 'The Cusp and Cleft/Boundary Layer: Low Altitude Identification and Statistical Local Time Variation', *J. Geophys. Res.* **93**, 14549–14556.

Newell, P. T., and Meng, C.-I.: 1991, 'Ion Acceleration at the Equatorward Edge of the Cusp: Low altitude Observations of Patchy Merging', *Geophys. Res. Lett.* **18**, 1829–1832.

Newell, P. T., and Meng, C.-I.: 1995, 'Magnetopause Dynamics as Inferred from Plasma Observations on Low-Altitude Satellites', *AGU Geophys. Monogr.* **90**, 407–416.

Norberg, O., Winningham, J. D., Lauche, H., Keith, W., Puccio, W., Olsen, J., Lundin, K., and Scherrer, J.: 2001, 'The MEDUSA electron- and ion spectrometer and the PIA photometers on Astrid-2', *Ann. Geophys.* **19**, 593–600.

Paschmann, G., Haerendel, G., Sckopke, N., Rosenbauer, H., and Hedgecock, P. C.: 1976, 'Plasma and Magnetic Field Characteristics of the Distant Polar Cusp near Local Noon: The Entry Layer', *J. Geophys. Res.* **81**, 2883–2889.

Reiff, P. H.: 1979, Low Altitude Signatures of the Boundary Layers. In: Battrick, B, Proceedings of Magnetospheric Boundary Layers, Alpbach, 11–15 June 1979, ESA SP-148, Noordwijk, Netherlands, pp. 167–173.

Reiff, P. H., Hill, T. W., and Burch, J. L.: 1977, 'Solar Wind Plasma Injection at the Dayside Magnetospheric Cusp', *J. Geophys. Res.* **82**, 479–491.

Reiff, P. H., Burch, J. L., and Spiro, R. W.: 1980, 'Cusp Proton Signatures and the Interplanetary Magnetic Field', *J. Geophys. Res.* **85**, 5997–6005.

Rème, H., Bosqued, J. M., Sauvaud, J. A., Cros, A., Dandouras, J., Aoustin, C., Bouyssou, J., Camus, Th., Cuvilo, J., Martz, C., Médale, J. L., Perrier, H., Romefort, D., Rouzaud, J., D'Uston, C., Möbius, E., Crocker, K., Granoff, M., Kistler, L. M., Popecki, M., Hovestadt, D., Klecker, B., Paschmann, G., Scholer, M., Carlson, C. W., Curtis, D. W., Lin, R. P., McFadden, J. P., Formisano, V., Amata, E., Bavassano-Cattaneo, M. B., Baldetti, P., Belluci, G., Bruno, R., Chionchio, G., Di Lellis, A., Shelley, E. G., Ghielmetti, A. G., Lennartsson, W., Korth, A., Rosenbauer, H., Lundin, R., Olsen, S., Parks, G. K., McCarthy, M., and Balsiger, H.: 1997, 'The cluster ion spectrometry (CIS) Experiment', *Space Sci. Rev.* **79**, 303–350.

Savin, S. P., Borodkova, N. L., Budnik, E.Yu., Fedorov, A. O., S. I., Klimov, Nozdrachev, M. N., Morozova, I. E., Nikolaeva, N. S., Petrukovich, A. A., Pissarenko, N. F., Prokhorenko, V. I., Romanov, S. A., Skalsky, A. A., Yermolaev, Yu.I., Zastenker, G. N., Zelenyi, L. M., Triska, P., Amata, E., Blecki, J., Juchniewicz, J., Buechner, J., Ciobanu, M., Grard, R., Haerendel, G., Korepanov, V. E., Lundin, R., Sandahl, I., Eklund, U., Nemecek, Z., Safrankova, J., Sauvaud, J. A., Rustenbah, J., and Rauch, J. L.: 1998, 'Interball Tail Probe Measurements in Outer Cusp and Boundary Layers', *AGU Geophys. Monogr.* **104**, 25–44.

Sheldon, R. B., Spence, H. E., Sullivan, J. D., Fritz, T. A., and Chen, J.: 1998, 'The discovery of trapped energetic electrons in the outer cusp', *Geophys. Res. Lett.* **25**, 1825–1828.

Song, P., Elphic, R. C., Russell, C. T., Gosling, J. T., and Cattell, C. A.: 1990, 'Structure and Properties of the Subsolar Magnetopause for Northward IMF: ISEE Observations', *J. Geophys. Res.* **95**, 6375–6387.

Stasiewicz, K.: 1991, 'Polar Cusp Topology and Position as a Function of Interplanetary Magnetic Field and Magnetic Activity: Comparison of a Model With Viking and Other Observations', *J. Geophys. Res.* **96**, 15789–15800.

Weiss, L. A., Reiff, P. H., Webber, E. J., Carlson, H. C., Lockwood, M., and Peterson, W. K.: 1995, 'Flow-Aligned Jets in the Magnetospheric Cusp: Results From the Geospace Environment Modeling Pilot program', *J. Geophys. Res.* **100**, 7649–7659.

Winningham, J. D., Burch, J. L., Eaker, N., Blevins, V. A., and Hoffman, R. A.: 1981, 'The Low Altitude Plasma Instrument (LAPI)', *Space Sci. Inst.* **5**, 465–475.

Winningham, J. D., Sharber, J. R., Frahm, R. A., Burch, J. L., Eaker, N., Black, R. K., Blevins, V. A., Andrews, J. P., Rudski, J., Sablik, M. J., Chenette, L. D., Datlowe, D. W., Gaines, E. E., Imhof, W. I., Nightingale, R. W., Reagan, J. B., Robinson, R. M., Schumaker, T. L., Shelley, E. G., Vondrak, R. R., Voss, H. D., Bythrow, P. F., Anderson, B. J., Potemra, T. A., Zanetti, L. J., Holland, D. B., Rees, M. H., Lummerzheim, D., Reid, G. C., Roble, R. G., Clauer, C. R., and Banks, P. M.: 1993, 'The UARS Particle Environment Monitor', *J. Geophys. Res.* **98**, 10649–10666.

Woch, J., and Lundin, R.: 1992, 'Magnetosheath Plasma Precipitation in the Polar Cusp and Its Control by the Interplanetary Magnetic Field', *J. Geophys. Res.* **97**, 1421–1430.

Surveys in Geophysics (2005) 26: 341–367
DOI 10.1007/s10712-005-1886-0 © Springer 2005

# CUSP MODELING AND OBSERVATIONS AT LOW ALTITUDE

S. WING, P. T. NEWELL and C.-I. MENG
*Applied Physics Laboratory, The Johns Hopkins University, Laurel, MD, 20723-6099, USA*
*E-mail: simon.wing@jhuapl.edu*

(Received 15 October 2002; Accepted 30 April 2004)

**Abstract.** Cusp properties have been investigated with an open-field line particle precipitation model and Defense Meteorological Satellite Program (DMSP) satellite observations. Particular emphasis is placed on the effects of IMF $B_y$, since previous studies focus mostly on IMF $B_z$. The model-data comparisons for various IMF configurations show that the model captures the large-scale features of the particle precipitation very well, not only in the cusp region, but also in other open-field line regions such as the mantle, polar rain, and open-field line low-altitude boundary layer (LLBL). When the IMF is strongly duskward/dawnward and weakly southward, the model predicts the occurrence of double cusp near noon: one cusp at lower latitude and one at higher latitude. The lower latitude cusp ions originate from the low-latitude magnetosheath whereas the higher latitude ions originate from the high-latitude magnetosheath. The lower latitude cusp is located in the region of weak azimuthal $\mathbf{E} \times \mathbf{B}$ drift, resulting in a dispersionless cusp. The higher latitude cusp is located in the region of strong azimuthal and poleward $\mathbf{E} \times \mathbf{B}$ drift. Because of a significant poleward drift, the higher latitude cusp dispersion has some resemblance to that of the typical southward IMF cusp. Occasionally, the two parts of the double cusp have such narrow latitudinal separation that they give the appearance of just one cusp with extended latitudinal width. From the 40 DMSP passes selected during periods of large (positive or negative) IMF $B_y$ and small negative IMF $B_z$, 30 (75%) of the passes exhibit double cusps or cusps with extended latitudinal width. The double cusp result is consistent with the following statistical results: (1) the cusp's latitudinal width increases with |IMF $B_y$| and (2) the cusp's equatorward boundary moves to lower latitude with increasing |IMF $B_y$|.

**Keywords:** cusp, double magnetopause, reconnection

**Abbreviations:** AACGM: altitude adjusted corrected geo-magnetic coordinates; APL: Applied Physics Laboratory; DMSP: Defense Meterological Satellite Program; FTE: flux transfer event; IMF: interplanetary magnetic field; IMP: interplanetary monitoring platform; MHD: magnetohydrodynamic; NSSDC: National Space Science Data Center; SSJ/4: Precipitating Electron and Ion Spectrometer; TIMAS: Toroidal Imaging Mass-Angle Spectrograph

## 1. Introduction

An important part of the dayside solar wind–magnetosphere interaction is magnetic merging or reconnection. A classic picture of this model was presented by Dungey (1961) where a purely southward interplanetary mag-

netic field (IMF) and a northward magnetospheric magnetic field near the subsolar magnetopause merge. As a result, the shocked solar wind ions and electrons, can and do enter the magnetosphere and some precipitate into the ionosphere. Although these particles originate in the solar wind, once they have entered the magnetosphere and ionosphere they exhibit distinctly different characteristics in energy, density, and temperature at different local times and latitudes. Observations at low altitude show that the resulting particle precipitation associated with open-field lines can generally be classified into four regions (ordered from low to high latitude for a typical southward IMF case): open-field low-latitude boundary layer (LLBL), cusp, mantle, and polar rain (e.g., Newell et al., 1991b; Newell and Meng, 1995; Onsager and Lockwood, 1997). Of these four regions, the cusp was discovered first (Eather and Mende, 1971; Frank, 1971; Heikkila and Winningham, 1971), partly because of its higher flux and energy and partly because of its theoretical importance, and has attracted the most attention ever since.

Over the three decades since their discoveries, researchers have been able to gather enough evidence to infer some of the main physical processes that give rise to the four particle precipitation regions. However, self-consistent global models are not yet advanced enough to permit precise quantitative comparisons with the observations. For example, single-fluid MHD simulations cannot capture parallel electric fields arising from the charge-quasi-neutrality constraints on the open-field lines in the magnetosphere. The suprathermal electrons, which populate much of polar rain, are absent in the MHD simulations.

Efforts to produce a model that can withstand detailed comparisons to low-altitude or mid-altitude cusp data advanced significantly with the work of Onsager et al. (1993). Instead of developing a global model self-consistently for the entire magnetosheath-magnetosphere-ionosphere system, Onsager et al. (1993) used an assimilative approach that combines good quality empirical models for different regions. In their model, for a given southward IMF orientation, solar wind temperature and density, ionospheric convection speed, and dipole tilt angle, the model computes the phase space density of the precipitating ions and electrons in three steps. In the first step, which assumes the magnetic moment is conserved, the ionospheric particles are traced back along the guiding centers to the magnetopause entry point using the Stern (1985) magnetic field model modified by uniform IMF penetration (cf. Cowley et al., 1991; Wing et al., 1995; Wing and Sibeck, 1997) and a simple dawn-dusk electric field. The second step is to compute the acceleration ($\mathbf{j} \bullet \mathbf{E} > 0$) or deceleration ($\mathbf{j} \bullet \mathbf{E} < 0$) imparted on the particles when they cross the magnetopause current layers from the magnetosheath to the magnetosphere. This computation is done with the aid of the de Hoffman–Teller reference frame in which $\mathbf{E} = 0$ (e.g., Hill and Reiff, 1977; Cowley and Owen, 1989). From this calculation, the model obtains the velocity that

the particle originally had in the magnetosheath. Finally, it computes the phase space density of particles with that velocity using the gas-dynamics calculations of Spreiter and Stahara (1985) with the assumption that all the particles, ions and electrons, have Maxwellian distributions. Assuming conservation of phase space density along particle trajectories, the model can be used to compute the differential energy flux at the location where the particle was "detected" in the ionosphere. The original model result and Defense Meteorological Satellite Program (DMSP) data comparison shows that the southward IMF cusp can be modeled fairly well but the model electrons have a much more latitudinally extended entry and a much higher temperature in the mantle and polar rain regions (Onsager et al., 1993; Wing et al., 1996). Other problems include the cusp latitude being several degrees too high (mainly a problem with the magnetic field model) and ionospheric convection velocity (100 $ms^{-1}$) being several times too low.

This paper focuses on the extent to which observational low-altitude cusp properties are well modeled and hence well understood. There have been many studies on IMF control of particle cusp properties, e.g., locations, energy–latitude dispersions and longitudinal widths (e.g., Burch, 1972; Hill and Reiff, 1977; Carbary and Meng, 1986; Newell et al., 1989; Aparicio et al., 1991; Woch and Lundin, 1992; Zhou et al., 2000). Most of these studies examine IMF $B_z$ effects on the cusp. As a result, the relationships between the cusp and IMF $B_y$ are not well known. This paper highlights and reviews (1) the observed cusp properties under various IMF conditions, including IMF $B_y$, (2) APL particle precipitation model calculations, which provide insights into the observations, e.g., locations of particle entries, convection electric field, energy–latitude dispersion, etc. The present paper uses the standard low-altitude particle definitions for the open-field LLBL, cusp, mantle, and polar rain (e.g., Newell et al., 1991a; 1991c). The cusp, sometimes known as "cusp proper", is characterized by very high-fluxes of ions and electrons. Typically, the ions have a spectral peak of $>10^8$ eV/$cm^2$ s eV sr. The typical average electron and ion energies, $<E_e>$ and $<E_i>$ are: $<E_e><200$ eV and 300 eV $<<E_i><3$ keV. The cusp ions frequently, but not always, exhibit energy–latitude dispersion, especially during periods of southward IMF (see Section 4 for cusp ions that do not show dispersions). The open-field line LLBL is the region closest to the open-closed field line boundary. In this region, the ions and electrons have higher energies and lower fluxes than in the cusp because the bulk of the ions have not yet arrived and the electron entries are limited by the charge quasi-neutrality (see section 3). In this region, typically only ions with energies $>1$ keV are present. In the mantle, the ions and electrons have lower energies and lower fluxes than those in the cusp. The typical mantle energies range from a few tens to 100 eV, but there are considerable variabilities. The fluxes are lower by a factor of 3–10 from those in the cusp. The mantle ions generally exhibit energy–latitude disper-

sions. The polar rain electrons have typical energies < a few hundred eVs and have little structures. There is a noticeable absence of ions in the polar rain.

## 2. APL open-field line particle precipitation model

The Johns Hopkins University Applied Physics Laboratory (APL) open-field line particle precipitation model basically uses the same approach as Onsager et al. (1993). However, we have introduced more realistic processes into the model and, as a result, we can model not just the cusp, but the entire open-field line particle precipitation region, namely open-field LLBL, cusp, mantle, and polar rain (Wing et al., 1996, 2001; Newell and Wing, 1998). This is summarized below.

Electrons have thermal speeds far exceeding the magnetosheath flow speed and therefore can enter the magnetosphere along the open field lines across the polar cap. In contrast, ions have slower thermal speeds and therefore can only enter the magnetosphere from the regions in the magnetopause where the magnetosheath flow is subsonic (Reiff et al., 1977). Several researchers have noted that there has to be a mechanism that limits the entry of the electrons to balance the charge carried by the ions, maintaining charge quasi-neutrality in the precipitating particle populations (e.g., Reiff et al., 1977; Burch, 1985). Solar wind electrons have been observed to have thermal and suprathermal components (e.g., Feldman et al., 1978; Fairfield and Scudder, 1985). The original Onsager model mantle ions have much lower flux than in the DMSP data, but ions in the solar wind and the magnetosphere have been observed to have $\kappa$ distributions (e.g., Feldman et al., 1974; Christon et al., 1989). A $\kappa$ distribution resembles a Maxwellian at low energies, but approaches a power law distribution at high energies. For a given characteristic energy, a $\kappa$ distribution produces a higher total flux in the ionosphere, owing to its high-energy tail. Magnetic field models have been steadily improved in the recent years, e.g., with the inclusion of Birkeland currents etc. (e.g., Tsyganenko and Stern, 1996). Finally, in much of the polar cap, the electric field frequently deviates from the dawn-dusk direction, especially when the IMF $y$-component dominates.

Motivated by these results, we extended the original Onsager et al. (1993) model as follows (Wing et al., 1996, 2001; Newell and Wing, 1998): (1) imposed charge-quasi-neutrality with a self-adjusting parallel electric field; (2) included suprathermal electrons; (3) used a $\kappa$ distribution for ions; (4) replaced the Stern (1985) magnetic field model with the T96 model (Tsyganenko and Stern, 1996); and (5) used the convective electric field obtained from the statistical APL convection patterns (Ruohoniemi and Greenwald, 1996). Although the APL convection pattern provides an accurate electric field, it is not consistent with the T96 magnetic field model. The T96 model

itself has its own deficiencies, e.g., it does not take into account the effects of IMF on the magnetopause shape and size, which in turn can affect the cusp footprint (e.g., Shue et al., 1997). The Spreiter and Stahara (1985) magnetosheath model is a single-fluid gas-dynamic model that does not take into account the magnetic field. In addition, the model has not taken all the particle precipitation processes into account such as wave-particle interactions, non-adiabatic motions, particle diffusion across the magnetopause, etc.

## 3. Southward IMF cusp

### 3.1. Strongly southward IMF cusp

The result of the model calculation for the strongly southward IMF is presented in Figure 1a (from Plate 2 in Wing et al., 2001). Note that the $y$-axis of the ion panel displays the lowest energy at the top, the opposite from the way the electron is displayed. The input parameters to the model are: IMF ($B_x$, $B_y$, $B_z$) = (−3.4, −0.5, −12.3) nT, solar wind thermal $n = 11$ cm$^{-3}$, $T_i = 1 \times 10^5$ K, $T_e = 3 \times 10^4$ K, suprathermal (halo) electron $n_s = 0.2$ cm$^{-3}$, $T_s = 1 \times 10^6$ K, $\kappa = 7$, and the altitude of "detected" particle $= 1.13 R_E$, which corresponds to the DMSP spacecraft altitude. DMSP observations under similar solar wind and IMF conditions are shown in Figure 1b. DMSP are sun-synchronous satellites in a nearly circular polar orbit at an altitude of roughly 835 km and period of approximately 101 min per orbit. The Precipitating Electron and Ion Spectrometer (SSJ/4) instrumental package included on all recent DMSP flights uses curved plate electrostatic analyzers to measure ions and electrons from 32 eV to 30 keV in 19 logarithmically spaced steps. One complete 19-point electron and ion spectrum is obtained each second. The magnetic coordinates used in our studies are the Altitude Adjusted Corrected Geomagnetic coordinates (AACGM) (Baker and Wing, 1989). The solar wind thermal electron temperature is taken to be somewhat lower than that of the ions to compensate for excessive heating in the model magnetosheath. This is because the Spreiter and Stahara (1985) model is a single fluid model, which overestimates the amount of electron heating in the magnetosheath. Since the ions carry most of the kinetic energy, upon encountering the magnetopause they are thermalized to a higher temperature than are electrons.

Many large-scale features that are seen in the model can also be seen in a typical DMSP pass such as the one shown in Figure 1b. Figure 1 clearly shows that the model can successfully calculate the precipitating ion and electron fluxes for the cusp, mantle, and the open-field LLBL, which is located equatorward of the cusp (in order to focus more on the cusp, comparisons with the polar rain are not shown here, but they have been shown to compare well (Wing et al., 1996). The model cusp equatorward boundary is located at 71° invariant magnetic latitude ($\lambda$), which is very close to the

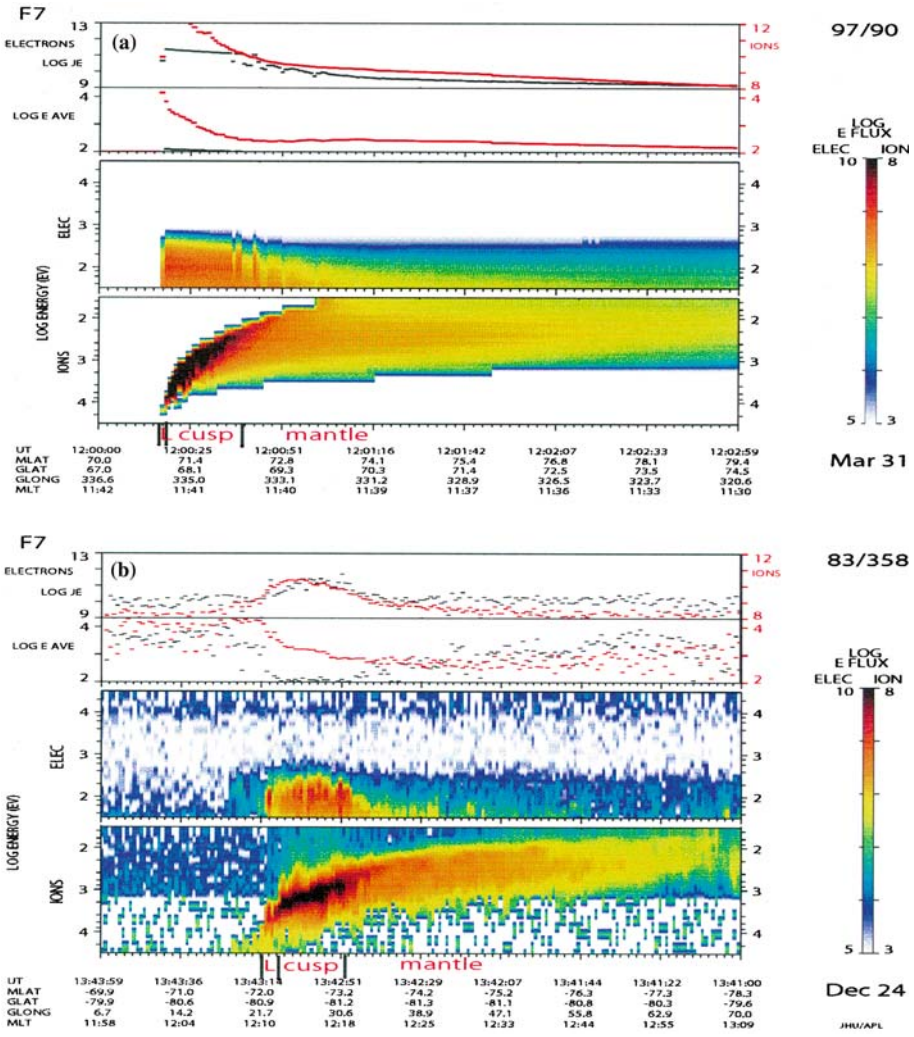


*Figure 1.* (a) The results of the model calculations for strongly southward IMF case and (b) a DMSP observation under similar IMF conditions. The spectrogram shows log differential energy flux, un units of eV/cm$^2$ s sr eV, from 32 eV to 30 keV, with the ion energy scale inverted. The lower of the two line plots shows the average energy in eV for the electrons (black) and ions (orange), and the top line plot is of integral energy flux in units eV/cm$^2$ s sr. The red labels beneath the *x*-axis indicate the region types. L indicates the open-field LLBL, which is located equatorward of the cusp.

statistical cusp boundary for the same IMF condition presented later in this paper as well as in previous studies (e.g., Carbary and Meng, 1986; Newell and Meng, 1989; Zhou et al., 2000).

The southward IMF cusp exhibits an energy–latitude dispersion, in which the characteristic energy decreases with increasing latitude. The low energy cut off decreases with increasing latitude, which is mainly due to the time of flight effect. The higher-energy ions arrive in the ionosphere closer to the point of injection and within each field line, the lower-energy particle comes from a lower latitude (e.g., Onsager et al., 1993). The high energy cutoff also decreases with increasing latitude in the model results as well as in satellite observations. In the model, this primarily results from the decreasing magnetosheath temperature and decreasing acceleration at the magnetopause crossing at the higher latitude entry points.

The model cusp ions originate from the low-latitude magnetopause, within $7R_E$ from the subsolar point. This result is in agreement with the previous observational cusp studies during the period of southward IMF (e.g., Reiff et al., 1977). In the present paper, "low-latitude magnetopause" refers to the magnetopause locations where $|z| < \sim 5R_E$, "mid-latitude" refers to the region $5R_E < |z| < 10R_E$ and "high-latitude" refers to regions where $|z| > \sim 10R_E$.

The success of the open-field line particle precipitation model strongly suggests that the same large-scale processes govern all four particle precipitation regions in the open-field line domain, namely, open field-line LLBL, cusp, mantle, and polar rain (Wing and Newell, 1996). Open-field LLBL is the region closest to the open/closed boundary. When the field line first becomes open, electrons having higher speeds than ions flow into the magnetosphere ahead of the ions. Charge quasi-neutrality and the resulting parallel electric field, however, limit the number of electrons that can enter. Thus, in this region, few electrons and ions are present. In the cusp, the ions have reached the ionosphere and intense fluxes of ions and electrons are usually observed. In this region, the electrons and ions can enter the magnetosphere relatively freely because the numbers of magnetosheath ions and electrons are already balanced, resulting in little or no parallel electric field. In the mantle region, fewer ions can enter as the magnetosheath flow becomes increasingly tailward and larger, whereas the magnetospheric magnetic field (and hence precipitating particle velocity) becomes more sunward, a condition which is less favorable for particle entries. In this region, $\mathbf{j} \bullet \mathbf{E} < 0$, which means that the magnetic stress at the magnetopause is directed to decelerate the plasma (e.g., Hill and Reiff, 1977; Cowley and Owen, 1989). Some of the solar wind thermal or core electron entries are limited by the ensuing parallel electric field that arises to maintain charge quasi-neutrality. Finally, in the polar rain region, no significant amount of ions enter the magnetosphere and the parallel electric field rises to the level where only higher-energy tail end of the core electrons and the suprathermal electrons can enter the magnetosphere, by the virtue of having higher energy that can overcome the parallel electric potential.

An example of the typical parallel electric potential for these four regions for one of our model calculations (not for Figure 1) is shown in Figure 2 (from Figure 1 of Newell and Wing 1998). This shows the parallel electric potential needed to maintain charge-quasi-neutrality and is obtained in the model using a binary search algorithm. Using observations from POLAR satellite, Krauklis et al. (2001) recently obtained a parallel electric field of 9.0 μ V $m^{-1}$ in the open-field LLBL region. If the magnetic field line length from the magnetopause to ionosphere is assumed to be $12R_E$ and the parallel electric field is assumed to be constant, then this would result in a potential drop of 690 V, which is a few hundred V higher than that in our model. However, in the model, the parallel potential drop has a strong dependence on the input solar wind and IMF parameters, which differ in the events described in Newell and Wing (1998) and in Krauklis et al. (2001). The potentials in these two studies are within the same order of magnitude. The parallel electric field resulting from maintaining charge quasi-neutrality of the precipitating magnetosheath ions and electrons should have implications to the ionospheric outflows. For example, the parallel electric field that prevents magnetosheath electrons from entering the magnetosphere should help increase the electron outflow and retard ion outflow.

### 3.2. Weakly southward IMF cusp

In the second case, the IMF is weakly southward. The input parameters to the model remain the same as before except for the IMF, which has been

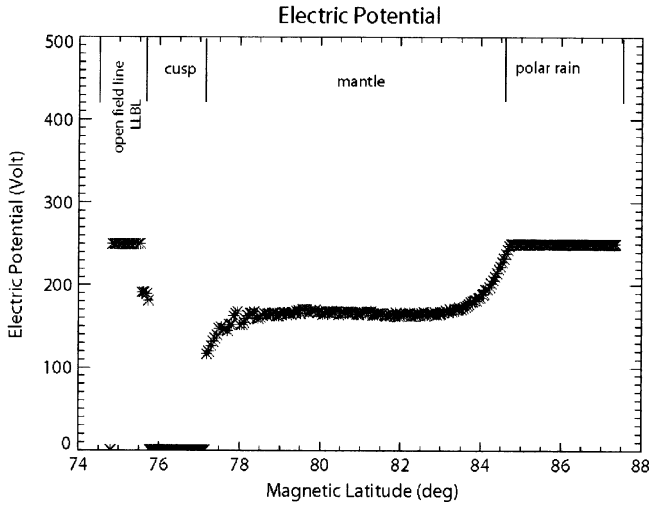


*Figure 2.* The model parallel electric potential between the Earth and the magnetosheath needed to retard electron entry enough to satisfy charge quasi-neutrality as a function of magnetic latitude.

changed to IMF ($B_x$, $B_y$, $B_z$) = (−0.5, −0.5, −3) nT. The model output and DMSP observations under similar IMF conditions are shown in Figures 3a and 3b, respectively (from Plate 3 in Wing et al. 2001). Figure 3 shows that again the model seems to be able to capture the macro-scale features that are seen in the observations. The location of the cusp equatorward boundary at 76.5° λ is very close to the statistical cusp boundary for similar IMF periods (e.g., Carbary and Meng, 1986; Newell et al., 1989; Zhou et al., 2000). However, these studies also show that the locations of this boundary exhibit large scatters. The DMSP cusp in Figure 3b was obtained not under the same exact solar wind and IMF conditions as in Figure 3a. (To facilitate comparisons between the model results, the solar wind input parameters are kept

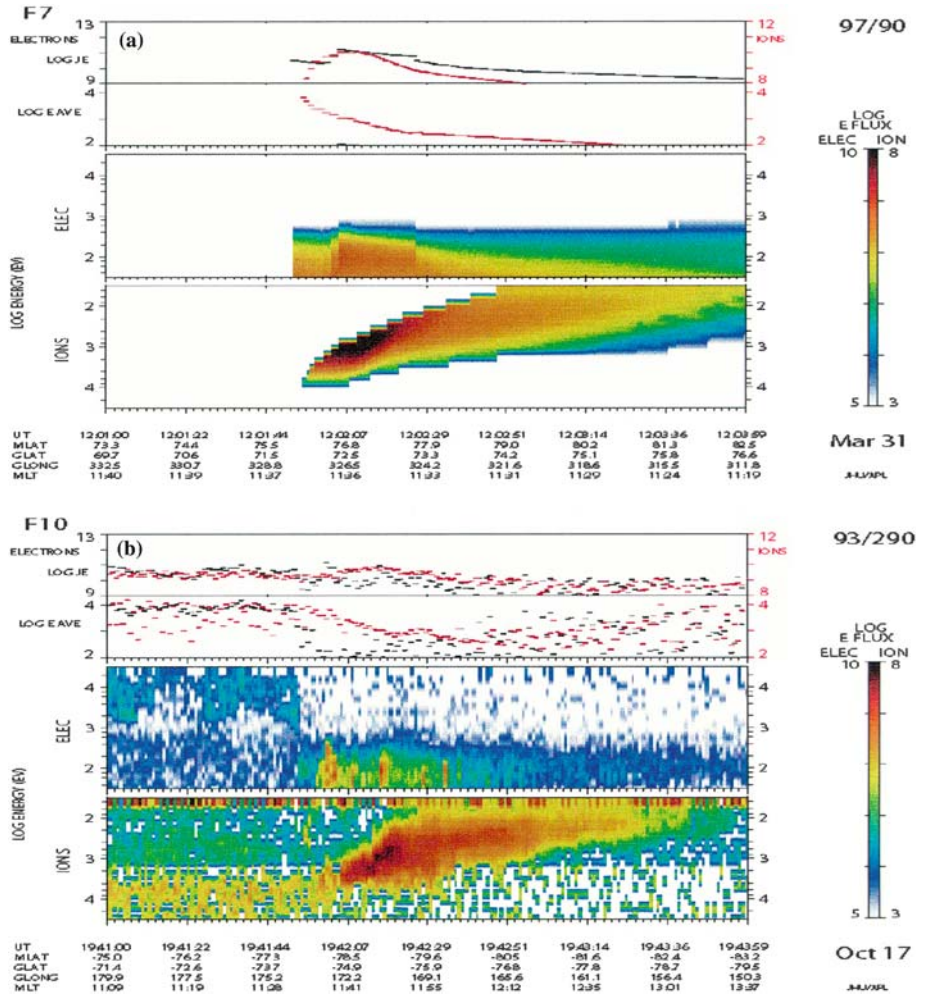


*Figure 3*. The same as Figure 1, except for weakly southward IMF case. See caption of Figure 1 for description of units, scales, etc. From Plate 2 of Wing et al. (2001).

the same and only the IMFs change in Figures 1a and 3a). These two factors contribute to the discrepancy of the location of this boundary in the model results and the DMSP example in Figure 3.

One of the main differences between this and the previous IMF case is that the cusp location moves to higher latitude as IMF $B_z$ increases, a well-documented phenomenon in many observational studies (e.g., Carbary and Meng, 1986; Newell et al., 1989; Zhou et al., 2000). The movement of the cusp location has been interpreted in terms of merging and the flux erosion on the dayside when IMF $B_z$ turns more southward (e.g., Zhou et al., 2000). Our model does not have explicit merging, but most of this effect is captured by the magnetic cusp location in T96 (geometrical effect). In addition, the model magnetopause increases in size with increasing IMF $B_z$, resulting in longer field lines between the ionosphere and the magnetopause shape (Roelof and Sibeck, 1993). The longer field increases the duration of the particles undergoing $\mathbf{E} \times \mathbf{B}$ drift (time of flight effect). As a result, the particle cusp location is shifted more poleward of the open-close field line separatrix compared to that in the strongly southward IMF cusp. Thus, the model predicts a wider open-field line LLBL for weakly southward IMF than that for strongly southward IMF.

The model cusp ions in the weakly southward IMF case originate in the low- to mid-latitude magnetopause/magnetosheath, z $\sim$2–10$R_E$. The higher-energy cusp ions enter from mid-latitude magnetopause, z$\sim$5–10$R_E$. The entry points are at higher latitude compared to those for the strongly southward IMF case.

In both southward IMF cases, the near-noon magnetospheric magnetic field line and the $\mathbf{E} \times \mathbf{B}$ convection have little IMF $y$-component. So, the precipitating cusp ions at noon originate approximately from the noon meridian magnetopause at low latitude. Once they enter the magnetosphere, they undergo strong $\mathbf{E} \times \mathbf{B}$ poleward drift, resulting in the classical cusp dispersion in which the ion characteristic energy decreases with increasing latitude, as shown in Figures 1 and 3.

## 4. Cusp for large IMF $B_y$ and small IMF $B_z$

For the third case, the IMF $B_z$ is weakly negative and $B_y$ is strongly positive. The input parameters are the same as before, except that now IMF ($B_x$, $B_y$, $B_z$) = (−3.4, 12.3, −0.5) nT. This IMF configuration amounts to −90° rotation in the $y$–$z$ plane from the strongly southward IMF case while the magnitude remains unchanged. The model result is shown in Figure 4 (from Plate 4 in Wing et al., 2001). The model predicts two cusps (double cusp) that are latitudinally separated. The lower latitude cusp has little or no dispersion (stagnant) and the higher latitude cusp exhibits dispersion that has some

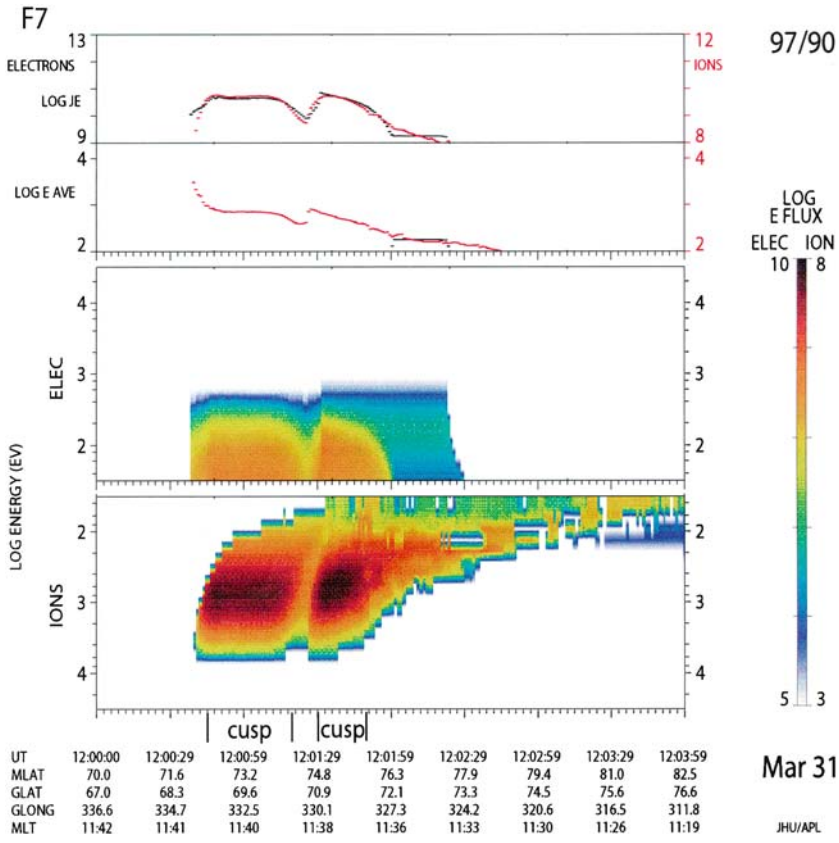


*Figure 4*. The same as Figure 1, except for strongly duskward and weakly southward IMF case. The calculation result shows two cusp regions that are latitudinally separated (double cusp). The model stops tracing at $x < -50R_E$, which explains the sudden cutoff of the polar rain electron spectra. See caption of Figure 1 for descriptions of the units, scales, etc. From Plate 4 of Wing et al. (2001).

resemblance to the classical southward IMF dispersion. The model stops tracing whenever the particle reaches $x < -50R_E$. This explains the sudden cutoff of the polar rain electrons in Figure 4. However, the polar rain in this region is fairly homogeneous and featureless. Had the model continued tracing tailward of $x = -50R_E$, the resulting polar rain spectra would look just like the ones immediately preceding the cutoff.

Examples of DMSP observations when IMF $B_z$ is small and $B_y$ is large are shown in Figure 5 (from Plate 5 in Wing et al., 2001). In the DMSP observations, sometimes the separation between the two cusps narrow to give the impression of just one cusp with an extended latitudinal width. However, the dispersion signatures remain the same: the lower-latitude cusp has little or no dispersion and the higher-latitude cusp has dispersion that has some resemblance to that of the southward IMF cusp.

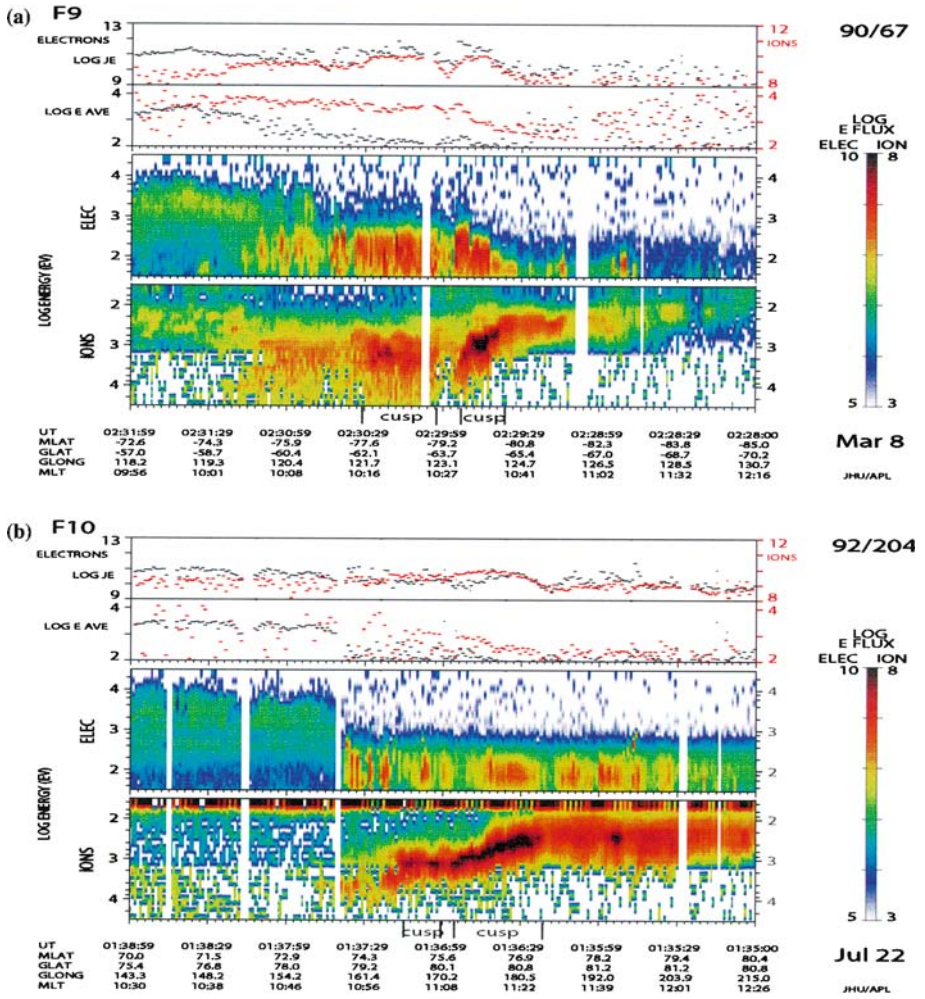


*Figure 5.* DMSP double cusp events (a, b) during periods of strongly duskward IMF. In (b) the lower latitude and the higher latitude cusp appear to form one cusp with extended latitudinal width. See caption of Figure 1 for descriptions of the units, scales, etc. From Plate 5 of Wing et al. (2001).

In the model, the lower-latitude cusp ions originate from low latitude magnetopause ($-5 < z < 5R_E$) and the higher-latitude cusp ions originate from high latitude magnetopause ($7 < z < 13R_E$). In the APL convection pattern, the $\mathbf{E} \times \mathbf{B}$ convection in the lower latitude cusp region is weak and directed dawnward, whereas in the higher latitude cusp region, it is strong and directed dawnward and poleward (see Figure 2 of Wing et al., 2001). Thus, the model satellite traveling in the meridional direction near noon encounters ions from two magnetosheath sources. The first population is associated with the ions that enter from the low-latitude magnetopause near noon meridian and then

undergo little $\mathbf{E} \times \mathbf{B}$ dawnward convection, nearly perpendicular to the satellite path. This results in the dispersionless ion signature in the lower-latitude cusp in Figures 4 and 5. The second population is associated with ions that enter at the high-latitude magnetopause eastward of the satellite location. Upon entering the magnetopause, the ions $\mathbf{E} \times \mathbf{B}$ convect strongly westward and poleward. Because of a significant poleward convection, the model satellite "observes" dispersion that is similar to the classical southward IMF dispersion. Our model does not have explicitly merging processes. If all magnetosheath ion entries are the result of merging, then the result here suggests that merging simultaneously occurs at the high- and low-latitude magnetopause. This scenario is depicted in Figure 6, which is adapted from Figure 5 in Weiss et al. (1995).

Recently several observational studies with Polar, Fast, and DMSP satellites report the discontinuous cusp as a spatial feature rather than temporal feature (e.g., Trattner et al., 1999, 2002; Su et al., 2001; Pitout et al., 2002). Our model can provide the framework to interpret these results (as is done in Pitout et al., 2002). Trattner et al. (1999, 2002) report observations of multiple cusps (more than 2) under steady solar wind and IMF. However, in their study, they do not distinguish among the cusp, the mantle, and the open-field line LLBL regions, but rather all these three regions are lumped together as cusp. In our classification scheme (Wing et al., 1998, 2001), some of their cusps would be labeled as mantle or open-field line LLBL.

As an example, Figure 7 shows a Polar TIMAS observation for an event discussed in Trattner et al. (2002). During this period, the IMF was southward and duskward, with the $z$-component comparable to the $y$-component, averaging $(B_x, B_y, B_z) = \sim(-3, 3.5, -3.5)$ nT. They identified four cusp regions as indicated by the solid horizontal lines. Not only is the double cusp featured

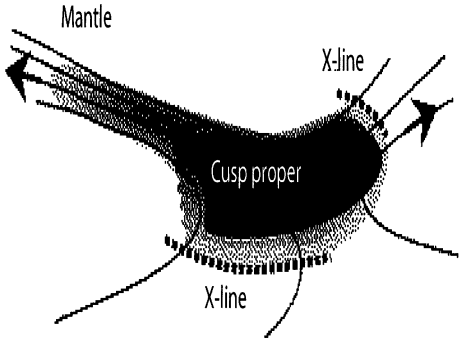


*Figure 6*. With two simultaneous merging sites, an ionospheric satellite traveling in a meridional trajectory near noon (dashed line) could encounter discontinuous cusp ion dispersions and two sources of ion population. The lower latitude cusp ions are associated with the field lines that have recently merged at low-latitude near noon magnetopause. The higher latitude cusp ions are associated with the field lines that have recently merged at high-latitude postnoon and then convect westward to pre-noon magnetopause. The schematic diagram is for a steady, large and positive IMF $B_y$ (adapted from Figure 5 in Weiss et al., 1995).

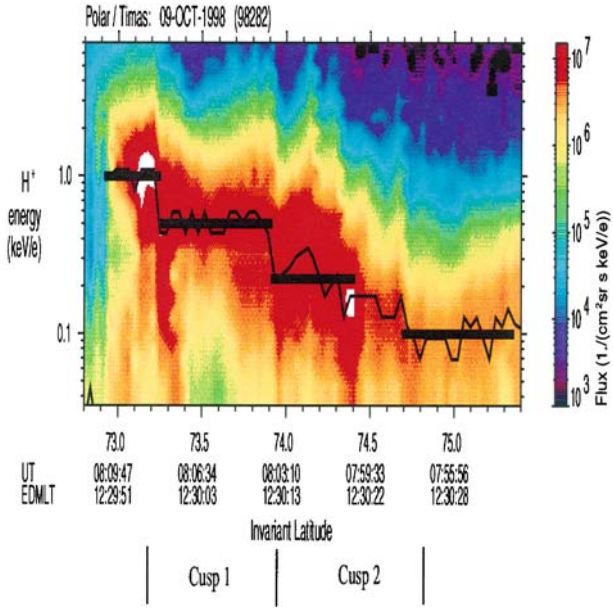


*Figure 7.* An example of double cusp in Polar TIMAS flux measurements (1./(cm$^2$ s sr keV/e)). Consistent with the model prediction, the lower latitude cusp (cusp 1) has little or no dispersion whereas the higher latitude cusp (cusp 2) shows the classical southward IMF dispersion. The region poleward of cusp 2 has lower fluxes and energies, which would be classified as mantle. The region equatorward of cusp 1, which has higher energies, may be the open-field line LLBL, although this is hard to ascertain without the accompanying electron spectrogram. From Plate 2 of Trattner et al. (2002).

prominently in this event, but it has the same dispersion signature predicted by our model, namely the lower-latitude cusp has little or no dispersion and the higher-latitude cusp has some dispersion. The lower and higher latitude cusps are labeled cusp 1 and 2, respectively, in Figure 7. The region poleward of cusp 2, which has lower fluxes and energies, would be called the mantle in our classification scheme (Wing et al., 1998, 2001). The region equatorward of cusp 1, which has slightly higher energy, may be the open-field line LLBL, although this is hard to ascertain without the accompanying electron spectrogram.

We would also like to distinguish our double cusp events from the event presented in Coleman et al. (2001). Their event shows a discontinuity in the mantle (not cusp) region, which they attribute to merging locations in the northern and southern hemisphere that is consistent with the anti-parallel merging. The discussion in this paper pertains only to the cusp.

Not all the features in the DMSP observations match the model results because the model still needs to incorporate a number of processes, as mentioned in Section 2. Nonetheless, the model seems to be able to capture the large-scale features in the observations.

## 5. The frequency of double cusp occurrence in the DMSP data set

The DMSP database for the period of 1985–1995 was searched for cusp events when the IMF has a large $y$-component and a small negative $z$-component. The automated algorithm that identifies auroral oval boundaries and structures based on DMSP particle precipitation data developed by Newell et al. (1991a, 1991b) was used to search for these events. IMF was obtained from the IMP-8 15-s database provided by the NASA NSSDC website. The solar wind propagation delay from IMP8 to the ionosphere is estimated rather crudely as (t = ballistic propagation of solar wind to the magnetopause standoff distance ($x = 10R_E$) + 5 min propagation in the magnetosheath (e.g., Lockwood et al., 1989; Ridley et al., 1998) + 3.5 min for 1 keV ions to travel along the field line from the magnetopause to the ionosphere ($15R_E$) (e.g., Carlson and Torbert, 1980). The database was divided into two classes: IMF $B_y < 0$ (toward sector) and IMF $B_y > 0$ (away sector).

The criteria for selecting IMF $B_y > 0$ events are: (a) IMF $-4$ nT $\leq B_z \leq 0$ nT and $B_y \geq 8$ nT; and (b) the IMF has been relatively stable so that (a) is satisfied for at least 15 min. The latter requirement attempts to restrict events to those in a quasi-steady state. The search returns a total of 22 cusp events. From these 22 events, 16 events or 73% of the total events show double cusps or latitudinally extended cusps while six events do not.

The criteria for selecting IMF $B_y < 0$ events are the same as above except that the IMF $B_y$ condition is reversed: (a) IMF $-4$ nT $\leq B_z \leq 0$ nT and $B_y \leq -8$ nT; and (b) the IMF has been relatively stable so that (a) is satisfied for at least 15 min. There are 18 cusp events that satisfy the IMF criteria. Of these 18 events, 14 events show double cusps or latitudinally extended cusps and four do not. This amounts to 77% of the total events with double cusps or latitudinally extended cusps.

In all, it appears that double cusps or latitudinally extended cusps appear fairly frequently, approximately 75% of the time, when IMF has a large (positive or negative) $y$-component and a small negative $z$-component.

## 6. IMF control of the cusp location and latitudinal width

There have been many statistical studies of the IMF and solar wind control of cusp properties e.g., locations, boundaries etc. (e.g., Carbary and Meng, 1986; Newell et al., 1989; Aparicio et al., 1991; Zhou et al., 2000). However, none of these studies has examined the IMF $B_y$ control of the latitudinal cusp width or the cusp's equatorward boundary. As discussed above, IMF $B_y$

should have some influence on these two cusp properties. For example, the cusp latitudinal width increases for the type of double cusp events shown in Figure 5b, e.g., when the latitudinal separation between the two cusps is very narrow. With years of DMSP data available, these two cusp properties can now be determined statistically.

For selecting the cusp events, we used the same DMSP automated cusp identification algorithm in the case study above to search cusp events in the DMSP data for the period of one solar cycle, 1985–1995 (Newell et al., 1991a; 1991b). Upon inspection of several double cusp events, it is found that this automated algorithm works reasonably well most of the time. However, it sometimes identifies cusps with low energy flux as LLBL. Although this inevitably introduces noise into the data set, there has been no perfect automated cusp identification algorithm. NASA NSSDC provides the IMP-8 simultaneous hourly averaged solar wind and IMF data. With this method and database, 2259 cusp events were identified. The cusp's equatorward boundary and latitudinal width are correlated with the IMF $B_y$ and $B_z$. In each case, the data are divided according to the sign of the IMF components. Thus, there are four cases to be considered.

### 6.1. Cusp's equatorward boundary

It is well established that the cusp latitudinal location correlates well with IMF $B_z$. The same result holds with our data and methodology, which uses computer algorithms to search the DMSP data for cusp events for the period of one solar cycle. The result can be seen in Figure 8a, which includes 2177 data points. The results of the linear least square fits are: cusp equatorward boundary (ceb)invariant latitude in degrees = $(0.78 \pm 0.03)$ IMF $B_z + (77.3 \pm 0.1°)$ for southward IMF, with $B_z$ in nT, and ceb = $(6 \times 10^{-4} \pm 0.04)$ IMF $B_z + (77.9 \pm 0.1°)$ for northward IMF.

The sign of IMF $B_z$ is already included in the equations. The correlation coefficients are 0.55 and $5 \times 10^{-4}$ for southward and northward IMF, respectively. The near-zero correlation coefficient of the latter simply reflects the nearly constant locations of the cusp's equatorward boundary latitude during periods of northward IMF, as can also be seen in the scatter plot in Figure 8a. These results are in very good agreement with the previous result ceb = 0.76 IMF $B_z + 77.0°$ for southward IMF, and ceb = 0.11 IMF $B_z + 77.2°$ for nortthward IMF, given by Newell et al., 1989.

They are comparable with ceb = 0.86 IMF $B_z + 79.5°$, and ceb = 0.07 IMF $B_z + 79.2°$, respectively, given by Zhou et al., 2000.

The latter results were obtained with mid-altitude Polar satellite observations, which may explain the slight location shift. The decrease of the cusp latitude with decreasing IMF $B_z$ during periods of southward IMF $B_z$ has been interpreted as the effect of merging and flux erosion on the dayside (e.g.,

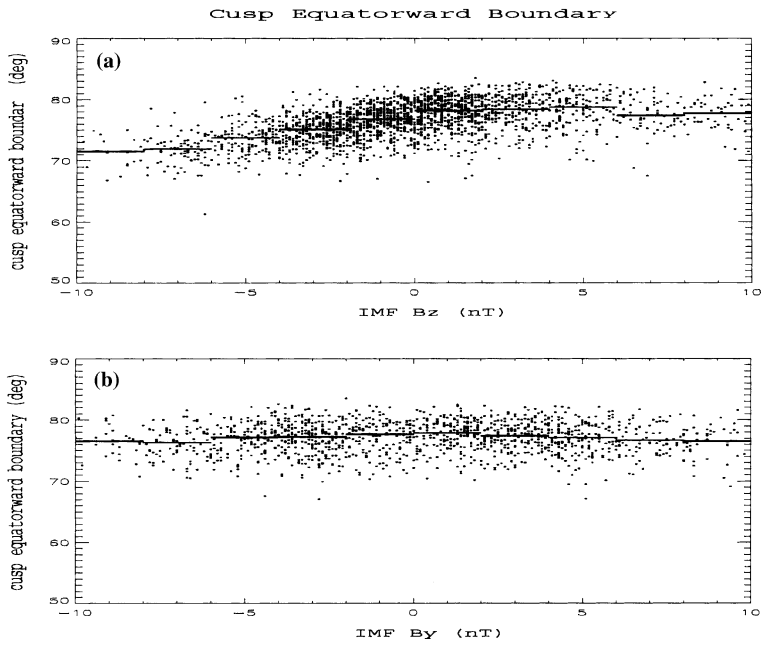


*Figure 8*. Cusp equatorward boundary as a function of (a) IMF $B_z$ and (b) IMF $B_y$. The medians in (a) 2 nT IMF $B_z$ and (b) IMF $B_y$ bins are indicated by horizontal bars. From Figure 5 of Wing et al. (2001).

Aubry et al., 1970; Zhou et al., 2000). In contrast, IMF $B_z$ does not control much of the cusp's equatorward boundary during periods of northward IMF.

The above relationship between IMF $B_z$ and the cusp's equatorward boundary is obtained when all cusp events are included. If the cusp events with large— $|IMFB_y|$—are removed from the data, then the cusp equatorward boundary moves to higher latitude. There are 798 such cusp events which were chosen with the IMF $B_y$ criterion: $-3$ nT $\leq$ IMF $B_y$ $\leq$ 3 nT. The result of the linear least square fits are then

$$\text{ceb} = (0.81 \pm 0.05)\ \text{IMF}\ B_z + (77.7 \pm 0.2^\circ), \text{and}$$
$$\text{ceb} = (0.04 \pm 0.06)\ \text{IMF}\ B_z + (78.1 \pm 0.2^\circ)$$

forsouthward and northward IMF respectively. Their correlation coefficients are 0.54 and 0.04 respectively. This difference is statistically significant, e.g., for IMF $B_z = 0$, the difference of the cebs (77.7°–77.3°) is larger than the uncertainty ($\sqrt{0.1^2 + 0.2^2} \pm 0.2$). The poleward shift, resulting from the removal of large |IMF $B_y$| events, ranges from 0.1° to 0.4° as IMF $B_z$ increases from $-10$ to 0 nT. Thus, the poleward shift is greater for weakly southward IMF than for strongly southward IMF. This shift is consistent

with the removal of the double cusp events. However, there could be other factors at work simultaneously, such as the effect of merging and flux removal (discussed next).

Merging also occurs during periods of large IMF $B_y$ and the ensuing flux erosion is expected to move the cusp's latitudinal location equatorward as in the case for southward IMF. We selected 1337 cusp events with small IMF $B_z$, $-3$ nT $<$ IMF $B_z < 3$ nT. The results of the linear least square fits of IMF $B_y$ versus the equatorward boundary of the cusp are shown in Figure 8b. The linear least square fit results are

$$\text{ceb} = (0.12 \pm 0.05)\ \text{IMF}\ B_y + (77.3 \pm 0.2°) \text{ and}$$
$$\text{ceb} = (-0.14 \pm 0.04)\ \text{IMF}\ B_y + (77.7 \pm 0.2°)$$

for negative and positive IMF $B_y$ respectively. The correlation coefficient is 0.10 and $-0.13$ for IMF $B_y < 0$ and IMF $B_y > 0$ respectively. The slopes are much smaller than that for southward IMF case. The cusp equatorward boundary moves slightly equatorward when IMF $B_y$ increases in magnitude but this effect is much weaker than the southward IMF effect. The small correlation coefficients indicate the presence of rather large scatter in the data distribution but they are statistically significant considering the size of the data set, namely 635 and 696 points for IMF $B_y < 0$ and IMF $B_y > 0$ respectively. A $t$-test indicates that the probability that IMF $B_y$ and ceb are uncorrelated is $< 1\%$ (e.g., Pugh and Winslow, 1966). Furthermore, this result is consistent with the poleward shift of ceb in Figure 8a when large |IMF $B_y$| events are removed, as discussed in the previous paragraph.

The relationships between IMF and ceb can be illustrated more easily by the plots of their medians. The median values of ceb in 2 nT IMF $B_z$ and $B_y$ bins are indicated by horizontal bars in Figure 8a and b respectively. The correlation coefficients of these medians are 0.99, $-0.57$, 0.93, $-0.98$ for IMF $B_z < 0$, IMF $B_z > 0$, IMF $B_y < 0$, IMF $B_y > 0$, respectively. The cusp's equatorward boundary is clearly more affected by IMF $B_z$ than IMF $B_y$. The larger effect of IMF $B_z$ over IMF $B_y$ is typical for many cusp properties.

### 6.2. Cusp's latitudinal width

In contrast to the cusp equatorward latitude, the effect of IMF $B_y$ is at least as strong as that of IMF $B_z$ on the cusp's latitudinal width near noon meridian, $11 \leq \text{MLT} \leq 13$. Figure 9 shows that the cusp latitudinal width increases with |IMF $B_y$| and |IMF $B_z$|. In this study, the cusp's latitudinal width is obtained within $\sim$1–2 min from an individual cusp observation made by a DMSP pass that reaches 81° $\lambda$ or higher. This requirement helps

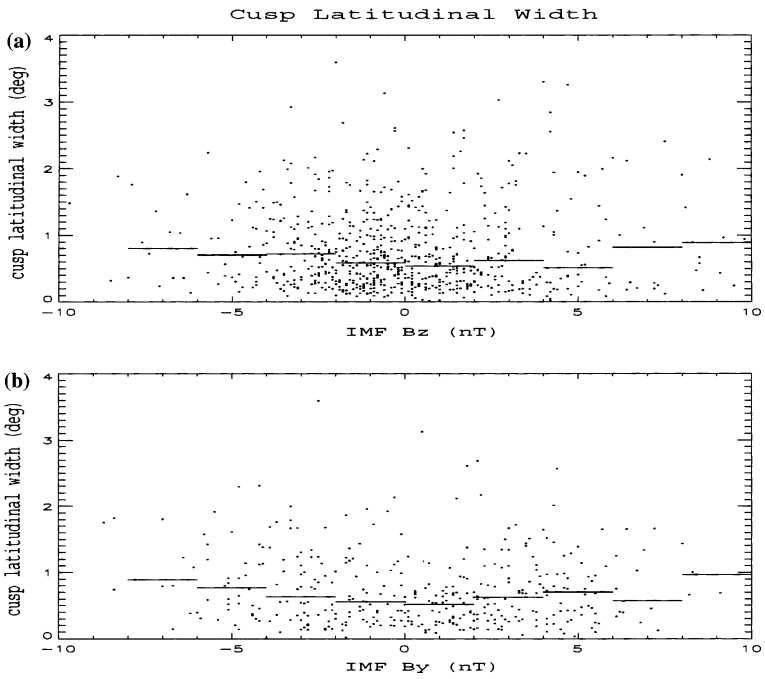


*Figure 9.* Cusp latitudinal width as a function of (a) IMF $B_z$ and (b) IMF $B_y$. The medians in 2 nT bins are indicated by horizontal bars. From Figure 6 of Wing et al. (2001).

eliminate passes that just graze the cusp; e.g., the statistical location of the cusp is well below 81° λ (e.g., Newell et al., 1989).

In Figure 9b, all the events have been selected so that they have weakly southward IMF component, $-3$ nT $\leq$ IMF $B_z \leq 0$ nT which restricts the number of events to 396. The medians of the cusp's latitudinal width (clw) in 2 nT IMF $B_y$ bins are plotted as horizontal lines in Figure 9b. The medians are computed only for bins that contain five data points or more. The least square fits of the medians are

$$\text{clw} = (-0.06 \pm 0.004)\text{IMF } B_y + (\text{in nT}) + (0.5 \pm 0.02)^\circ \text{ for IMF } B_y < 0$$

and

$$\text{clw} = (0.04 \pm 0.02)\text{IMF } B_y + (0.5 \pm 0.1)^\circ \text{ for IMF } B_y > 0$$

The correlation coefficients are $-0.99$ and 0.76, respectively. This result is consistent with our case study above which shows that at times the double cusp, associated with large |IMF $B_y$|, forms a single cusp with extended latitudinal width, e.g., Figure 5b.

Figure 9a shows that the effect of IMF $B_z$ on the cusp latitudinal width. The results of the least squares fir of the medians are

clw = (−0.03 ± 0.01) IMF $B_z$ (in nT) + (0.6 ± 0.05)° for southward IMF and,
clw = (0.04 ± 0.02) IMF $B_z$ + (0.4 ± 0.1)° for northward IMF

Their correlation coefficients are −0.91 and 0.84 for southward and northward IMF, respectively. Again, only bins containing five or more data points are included in the mdedian calculations. Figure 9a shows a similar trend as Figure 5 of Zhou et al. (2000), especially if their extremely small (IMF $B_z < -8$ nT) and large IMF $B_z$ (IMF $B_z > 5$ nT) bins, which contain much fewer points, are excluded from their figure. In any case, the scatter is very large in both studies. In this study, the large scatter may be partly due to the misclassification of cusps having low energy flux as open-field line LLBL as well as other factors such as dipole tilt etc. Also, the usage of the hourly averaged IMF may contribute to the noise.

## 7. Seasonal effects on cusp

From simple geometrical considerations, it can easily be seen that the cusp field lines emanating from the summer hemisphere, tilted toward the solar wind flow, would have access to the magnetosheath plasma at a lower latitude than those from the winter cusp. This is shown in Figure 10. The magnetosheath plasma has lower density and higher tailward velocity with increasing latitude, as it moves around the magnetopause obstacle. The higher tailward velocity results in fewer particle entries. Both of these

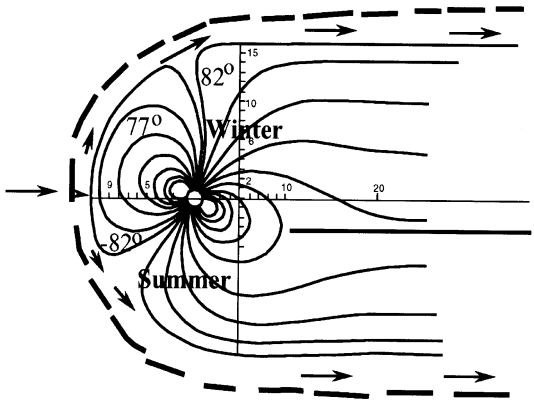


*Figure 10.* Summer (southern) hemisphere cusp field lines access the magnetosheath region at lower latitude, where plasma has higher density and lower velocity, compared to the magnetosheath region where the winter (northern) hemisphere cusp field lines connect. The length of the arrows indicates the relative velocities of the magnetosheath plasma. Also, the location of the summer hemisphere cusp is at higher latitude than that of the winter hemisphere cusp. Adapted from Newell and Meng (1989) and Voight (1974).

properties of the magnetosheath plasma as a function of latitude result in higher fluxes of ions and electrons in the summer cusp compared to the winter cusp. Indeed, Newell and Meng (1988) show that precipitating energy fluxes of both ions and electrons are about 50–60% higher in the summer cusp than the winter cusp. The same geometric considerations can explain the observed higher-latitude location of the summer cusp compared to that of the winter cusp (e.g., hypothetically consider what would happen to the cusp latitude if the dipole tilte = 90°). Newell and Meng (1989) report that for every degree of dipole tilt, the cusp position shifts by 0.06°.

Although our model has not been run to show seasonal effects, these effects on the cusp ions at mid-altitude have been successfully modeled by Xue et al. (1997). Their model uses a similar approach as ours, but it uses different magnetic and electric fields and it does not take into account parallel electric field and suprathermal electrons. The last two affect mostly the electrons in the open-field line region, not their model cusp ions, which look realistic.

## 8. Summary

The processes creating the particle cusp are complex, even for those that occur in quasi-steady state conditions. However, this paper demonstrates that the APL particle precipitation model can produce not just most of the large-scale observational features found in the cusp, but also in other open-field line regions, namely, the open-field line LLBL, mantle, and polar rain. For example, the locations, dispersions, flux levels (densities), and energies of the ions and electrons in these four regions in the model results compare well with the DMSP observations. These are all spatial features that occur under steady solar wind and IMF conditions. The results collectively strongly suggest that the four regions are governed by a single set of physical processes (Wing et al., 1996, 2001; Newell and Wing, 1998). The main processes and parameters that govern the large-scale features are merging sites, shocked solar wind evolution along the magnetopause entry points, IMF, magnetopause acceleration/deceleration, $\mathbf{E} \times \mathbf{B}$ drift, field line distance from the magnetopause to the ionosphere (time of flight), observational point (spacecraft trajectory), charge-quasi-neutrality, and parallel electric field.

For example, the spacecraft trajectory and $\mathbf{E} \times \mathbf{B}$ are important for determining the observed ion dispersions. The ion and electron fluxes depend on the solar wind (magnetosheath) density and velocity, merging sites (hence IMF), and acceleration/deceleration at the magnetopause. In addition, the magnetosheath electron entries are limited by the parallel electric field resulting from maintaining the charge-quasi-neutrality. Good understanding of how these processes/parameters interact can help unravel the mystery of the spatially discontinuous cusps, one of the most exciting and more recently

discovered cusp phenomena. Before discussing this, it should be noted that the model does not yet include the physical processes that generate the micro- and meso-scale features in the cusp.

In addition to the spatial features, the cusp sometimes exhibits temporal features, including discontinuous cusp structures. The discontinuous cusp ion signature has long been associated with the discontinuity in the IMF, solar wind, and/or merging rate (e.g., FTE, pulsed or bursty or intermittent injections, etc.) (e.g., Lockwood and Smith, 1989, 1992; Escoubet et al., 1992; Smith et al., 1992; Lockwood et al., 1995; Boudouris et al., 2001).

However, Trattner et al. (1999) present discontinuous cusps events in which two satellites crossed the same open flux tubes at different times and yet observed similar discontinuous cusp structures. These observations led them to conclude that (1) the discontinuous cusps can be a stable spatial feature that can persist up to 1.5 h and (2) the presence of the discontinuous cusp does not necessarily indicate the temporal nature of the merging parameters.

It turns out that some of these spatial discontinuous cusps favor certain IMF orientations (Wing et al., 2001). During periods of stable and $B_y$ dominant IMF, two cusps (double cusp) are frequently observed by DMSP satellites with the following properties:

1. The two cusps are separated latitudinally.

2. The lower latitude cusp ion exhibits little or no energy–latitude dispersion (stagnant plasma) whereas the higher latitude cusp ion exhibits the classical southward IMF dispersion (see Figure 5). Sometimes the latitudinal separation of the two cusps in the double cusp narrows to the point of giving the impression of just one cusp with extended latitudinal width. This may result from several factors, e.g., the seasonal variation which changes the latitudinal locations of the northern and southern merging sites, satellite trajectories etc. (e.g., Weiss et al., 1995; Rodger et al., 2000).

3. In the DMSP data, the double cusp is observed in 30 out of 40 events (75% of the events) during periods of $B_y$ dominant IMF.

The formation of the double cusp was actually predicted by APL open-field line particle precipitation model (Wing et al., 2001). In the model:

1. The lower-latitude cusp ions originate from the low-latitude magnetopause, $z \sim -5$–$5R_E$. In this region, the ions undergo a moderate $\mathbf{E} \times \mathbf{B}$ azimuthal drift during their flight from the magnetopause to the ionosphere. This results in a dispersionless or stagnant cusp.

2. The higher-latitude cusp ions originate from higher-latitude magnetosheath regions ($z \sim 7$–$13R_E$) eastward/westward of the satellite, depending on the orientation of the IMF $B_y$. Once the ions enter the magnetosphere, they undergo strong $\mathbf{E} \times \mathbf{B}$ azimuthal and poleward drift, resulting in the classical dispersion. The lower-latitude dispersionless cusp perhaps corresponds to the "stagnant" or "weak IMF $B_z$" cusp in the cusp

classification scheme developed by Yamauchi and Lundin (1994). In their study, stagnant cusps occur most frequently during periods of weak IMF $B_z$. With a weak $z$-component, the IMF orientation may be dominated by the $y$-component. If this is the case, then their results can be explained in terms of merging locations and $\mathbf{E} \times \mathbf{B}$, as discussed here. The results here strongly suggest that in addition to IMF $B_z$, IMF $B_y$ plays an equally important role in determining cusp morphology.

Both the statistical widening of the cusp's latitudinal width and shifting of equatorward boundary to a lower latitude during periods of large IMF $B_y$ are consistent with the formation of double cusps (separation between the two cusp can sometimes narrow to give the impression of just one cusp with an extended latitudinal width).

The model does not explicitly include merging processes. However, if the magnetosheath ion entries are assumed to result from merging, then the result here suggests that merging simultaneously occurs at low- and high-latitude magnetopause during periods of large–|IMF $B_y$|–and small IMF $B_z$. Merging at low-latitudes during periods of non-southward IMF orientation has been previously reported. For example, observations in the vicinity of the magnetopause indicated that in the vicinity of the subsolar region merging occurs at modest magnetic shear, ranging from 60° to 180°, but at high-latitudes merging occurs when the magnetic shear is larger, $>135°$ (e.g., Gosling et al., 1990, 1991). A recent cusp study reports simultaneous merging at both low- and high-latitudes during periods of northward IMF (e.g., Fuselier et al., 2000).

## Acknowledgements

The DMSP SSJ4 instrument was designed and built by Dave Hardy and colleagues at the AFRL. Fred Rich has been helpful in our acquiring this data, as has the World Data Center in Boulder, Colorado. Simon Wing was supported by NASA Grant NAG5-10971 and NSF Grant ATM-9819705.

## References

Aparicio, B., Thelin, B., and Lundin, R.: 1991, 'The Polar Cusp from a Particle Point of View: A Statistical Study based on Viking Data', *J. Geophys. Res.* **98**, 14023–14031.

Aubry, M. P., Russell, C. T., and Kivelson, M. G.: 1970, 'Inward Motion of the Magnetopause before a Substorm', *J. Geophys. Res.* **75**, 7018–71031.

Baker, K. B., and Wing, S.: 1989, 'A New Magnetic Coordinate System for Conjugate Studies at High Latitudes', *J. Geophys. Res.* **94**, 9139–9143.

Boudouridis, A., Spence, H. E., and Onsager, T. G.: 1992, 'Investigation of Magnetopause Reconnection Models using Two Colocated, Low-altitude Satellites: A Unifying Reconnection Geometry', *J. Geophys. Res.* **106**, 29451–29466.

Burch, J. L.: 1972, 'Precipitation of Low Energy Electrons at High Latitudes: Effects of Interplanetary Magnetic Field and Dipole Tilt Angle', *J. Geophys. Res.* **77**, 6696–6707.

Burch, J. L.: 1985, 'Quasi-Neutrality in the Polar Cusp', *Geophys. Res. Lett.* **12**, 469–472.

Carbary, J. F., and Meng, C.-I.: 1986, 'Relations between the Interplanetary Magnetic Field $B_z$, AE Index, and Cusp Latitude', *J. Geophys. Res.* **91**, 1549–1556.

Carlson, C. W., and Torbert, R. B.: 1980, 'Solar Wind Ion Injection in the Morning Auroral Oval', *J. Geophys. Res.* **85**, 2903–2908.

Christon, S. P., Williams, D. J., Mitchell, D. G., Frank, L. A., and Huang, C. Y.: 1989, 'Spectral Characteristics of Plasma Sheet Ion and Electron Populations during Undisturbed Geomagnetic Conditions', *J. Geophys. Res.* **94**, 13409–13424.

Coleman, I. J., Chisham, G., Pinnock, M., and Freeman, M.: 2001, 'An Ionospheric Convection Signature of Antiparallel Reconnection', *J. Geophys. Res.* **106**, 28995–29007.

Cowley, S. W. H., and Owen, C. J.: 1989, 'A Simple Illustrative Model of Open Flux Tube Motion Over the Dayside Magnetopause', *Planet. Space Sci.* **37**, 1461–1475.

Cowley, S. W. H., Morelli, J. P., and Lockwood, M.: 1991, 'Dependence of Convective Flows and Particle Precipitation in the High-latitude Dayside Ionosphere on the x and y Components of the Interplanetary Magnetic Field', *J. Geophys. Res.* **96**, 5557–5564.

Dungey, J. W.: 1961, 'Interplanetary Magnetic Field and the Auroral Zone', *Phys. Rev. Lett.* **6**, 47–48.

Eather, R. H., and Mende, S. B.: 1971, 'Airborne Observations of Auroral Precipitation Patterns', *J. Geophys. Res.* **76**, 1746–1752.

Escoubet, C. P., Smith, M. F., Fung, S. F., Anderson, P. C., Hoffman, R. A., Baasinska, E. M., and Bosqued, J.-M.: 1992, 'Staircase Ion Signature on the Polar Cusp: A Case Study', *Geophys. Res. Lett.* **19**, 1735–1738.

Fairfield, D. H., and Scudder, J. D.: 1985, 'Polar Rain: Solar Coronal Electrons in the Earth's Magnetosphere', *J. Geophys. Res.* **90**, 4055–4068.

Feldman, W. C., Asbridge, J. R., Bame, S. J., and Montgomery, M. D.: 1974, 'Interplanetary Solar Wind Streams', *Rev. Geophys. Space Phys.* **12**, 715–723.

Feldman, W. C., Asbridge, J. R., Bame, S. J., Gosling, J. T., and Lemons, D. S.: 1978, 'Characteristic Electron Variations across Simple High-speed Solar Wind Streams', *J. Geophys. Res.* **83**, 5285–5295.

Frank, L. A.: 1971, 'Plasma in the Earth's Polar Magnetosphere', *J. Geophys. Res.* **76**, 5202–5219.

Fuselier, S. A., Trattner, K. J., and Petrinec, S. M.: 2000, 'Cusp Observations of High- and Low-latitude Reconnection for Northward Interplanetary Magnetic Field', *J. Geophys. Res.* **105**, 253–266.

Gosling, J. T., Thomsen, M. F., Bame, S. J., and Elphic, R. C.: 1990, 'Plasma Flow Reversals at the Dayside Magnetopause and the Origin of Asymmetric Polar Cap Convection', *J. Geophys. Res.* **95**, 8073–8084.

Gosling, J. T., Thomsen, M. F., Bame, S. J., and Elphic, R. C.: 1991, 'Observations of Reconnection of Interplanetary and Lobe Magnetic Field Lines at High-latitude Magnetopause', *J. Geophys. Res.* **96**, 14097–14106.

Heikkila, W. J., and Winningham, J. D.: 1971, 'Penetration of Magnetosheath Plasma to Low Altitudes through the Dayside Magnetospheric Cusps', *J. Geophys. Res.* **76**, 833–891.

Hill, T. W., and Reiff, P. H.: 1977, 'Evidence of Magnotospheric Cusp Proton Acceleration by Magnetic Merging at the Dayside Magnetopause', *J. Geophys. Res.* **82**, 3623–3628.

Krauklis, I., Johnstone, A. D., and Peterson, W. K.: 2001, 'Acceleration of Ionospheric O+ Ions on Open Field Lines in the Low-latitude Boundary Layer and the Cusp Region', *J. Geophys. Res.* **106**, 29611–29618.

Lockwood, M., Sandholt, P. E., Cowley, S. W. H., and Oguti, T.: 1989, 'Interplanetary Magnetic Field Control of Dayside Auroral Activity and the Transfer of Momentum across the Dayside Auroral Magnetopause', *Planet. Space Sci.* **37**, 1347–1365.

Lockwood, M., and Smith, M. F.: 1989, 'Low-altitude Signatures of the Cusp and Flux Transfer Events', *Geophys. Res. Lett.* **16m**, 879–882.

Lockwood, M., and Smith, M. F.: 1992, 'The Variation of Reconnection Rate at the Dayside Magnetopause and Cusp Ion Precipitation', *J. Geophys. Res.* **97**, 14841–14847.

Lockwood, M., Davis, C. J., Smith, M. F., Onsager, T. G., and Denig, W. F.: 1995, 'Location and Characteristics of the Reconnection X-line Deduced from low-altitude Satellite and Ground Observations, Defense Meteorological Satellite Program and European Incoherent Scatter Data', *J. Geophys. Res.* **100**, 21803–21813.

Menietti, J. D., and Burch, J. L.: 1988, 'Spatial Extent of the Plasma Injection Region in the Cusp–Magnetosheath Interface', *J. Geophys. Res.* **93**, 105–113.

Maynard, N. C., Denig, W. F., and Burke, W. J.: 1995, 'Mapping Ionospheric Convection Patterns to the Magnetosphere', *J. Geophys. Res.* **100**, 1713–1721.

Newell, P. T., and Meng, C.-I.: 1988, 'Hemispherical Asymmetry in Cusp Precipitation Near Solstices', *J. Geophys. Res.* **93**, 2643–2648.

Newell, P. T., Meng, C.-I., Sibeck, D. G., and Lepping, R.: 1989, 'Some Low-altitude Dependencies on the Interplanetary Magnetic Field', *J. Geophys. Res.* **94**, 8921–8927.

Newell, P. T., and Meng, C.-I.: 1989, 'Dipole Tilt Angle Effects on the Latitude of the Cusp and the Cleft/LLBL', *J. Geophys. Res.* **94**, 6949–6953.

Newell, P. T., Burke, W. J., Meng, C.-I., Sanchez, E. R., and Greenspan, M. E.: 1991, 'Identification and Observations of the Plasma Mantle at Low Altitude', *J. Geophys. Res.* **96**, 35–45.

Newell, P. T., Wing, S., Meng, C.-I., and Sigilito, V.: 1991, 'The Auroral Oval Position, Structure, and Intensity of Precipitation from 1984 Onward: An Automated on-line Data Base', *J. Geophys. Res.* **96**, 5877–5882.

Newell, P. T., Burke, W. J., Sanchez, E. R., Meng, C.-I., Greenspan, M. E., and Clauer, C. R.: 1991, 'The Low-latitude Boundary Layer and the Boundary Plasma Sheet at Low-altitude: Prenoon Precipitation Regions and Convection Reversal Boundaries', *J. Geophys. Res.* **96**, 21013–21023.

Newell, P. T. and Meng, C. -I.: 1995, 'Magnetopause Dynamics as Inferred from Plasma Observations on Low-altitude Satellites' in P. Song, B. U. ö. Sonnerup, and M. F. Thomsen (eds.), *Physics of Magnetopause, Geophys. Monogr. Ser*, Vol. 90, pp. 407–416.

Newell, P. T. and Wing, S.: 1998, 'Entry of Solar Wind Plasma into the Magnetosphere: Observations Encounter Simulation, in L. Horwitz D. L. Gallagher, and W. K. Peterson (eds.), Geospace Mass and Energy Flow: Results from the International Solar-Terrestrial Physics Program', *Geophys. Monogr. Ser*, Vol. 104, pp. 73–84.

Onsager, T. G., Kletzing, C. A., Austin, J. B., and MacKiernan, H.: 1993, 'Model of Magnetosheath Plasma in the Magnetosphere: Cusp and Mangle Particles at Low-altitudes', *Geophys. Res. Lett.* **20**, 479–482.

Onsager, T. G., and Lockwood, M.: 1997, 'High-latitude Particle Precipitation and its Relationship to Magnetospheric Source Regions', *Space Sci. Rev.* **80**, 77–107.

Pitout, F., Newell, P. and Buchert, S.: 2002, 'Simultaneous High- and Low-latitude Reconnection: ESR and DMSP Observations', *Ann. Geophys.* in press.

Pugh, E. M., and Winslow, G. H.: 1966, *High-latitude Particle Precipitation and its Relationship to Magnetospheric Source Regions*, Addison-Wesley, Reading 188–199.

Reiff, P. H., Hill, T. W., and Burch, J. L.: 1977, 'Solar Wind Plasma Injection at the Dayside Magnetospheric Cusp', *J. Geophys. Res.* **82**, 479–491.

Ridley, A. J., Lu, G., Clauer, C. R., and Papitashvili, V. O.: 1998, 'A Statistical Study of the Ionospheric Convection Response to Changing Interplanetary Magnetic Field Conditions using the Assimilative Mapping of Ionospheric Electrodynamics Technique', *J. Geophys. Res* **103**, 4023–4039.

Roelof, E. C. and Sibeck, D. G.: 1993, 'Magnetopause Shape as a Bivariate Function of Interplanetary Magnetic Field $B_z$ and Solar Wind Dynamic Pressure', *J. Geophys. Res* 98, 421–450.

Rodger, A. S., Coleman, I. J., and Pinnock, M.: 2000, 'Some Comments on Transient and Steady-state Reconnection at the Dayside Magnetopause', *Geophys. Res. Lett* **27**, 1359–1362.

Ruohoniemi, J. M., and Greenwald, R. A.: 1996, 'Statistical Patterns of High-latitude Convection Obtained from Goose Bay HF Radar Observations', *Geophys. Res. Lett* **101**, 21743–21763.

Shue, J.-H., Chao, J. K., Fu, H. C., Russell, C. T., Song, P., Khurana, K. K., and Singer, H. J.: 1997, 'A New Functional form to Study the Solar Wind Control of the Magnetopause Size and Shape', *J. Geophys. Res* **102**, 9497–9511.

Spreiter, J. R. and Stahara, S. S.: 1995, 'Magnetohydrodynamic and Gasdynamic Theories for Planetary Bow Waves', in B. T. Tsurutani and R. G. Stone (eds.), *Collisionless Shocks in the Heliosphere: Reviews of Current Research, Geophys. Monogr. Ser.*, Vol. 35, pp. 85–107.

Stern, D. P.: 1985, 'Parabolic Harmonics in Magnatospheric Modeling: The Main and the Ring Current', *J Geophys. Res.* **90**, 10851–10863.

Su, Y.-J., Ergun, R. E., Peterson, W. K., Onsager, T. G., Pfaff, R., Carlson, C. W., and Strangeway, R. J.: 2001, 'FAST Auroral Snapshot Observations of Cusp Electron and Ion Structures', *J. Geophys. Res.* **106**, 25595–25600.

Trattner, K. J., Fuselier, S. A., Peterson, W. K., Sauvaud, J.-A., Stenuit, H., and Dubouloz, N.: 1999, 'On Spatial and Temporal Structures in the Cusp', *J. Geophys. Res* **104**, 28411–28421.

Trattner, K. J., Fuselier, S. A., Peterson, W. K. and Carlson, C. W.: 2002, 'Spatial Features Observed in the Cusp under Steady Solar wind Conditions', *J. Geophys. Res* 107(A0), 10.1029/2001JA000262.

Tsyganenko, N. A., and Stern, D. P.: 1996, 'Modeling the Global Magnetic Field of the Large-scale Birkeland Current Systems', *J. Geophys. Res* **101**, 27187–27198.

Voigt, G.-H.: 1974, 'Calculation of the Shape and Position of the Last closed Field Line Boundary and the Coordinates of the Magnetopause Neutral Points in a Theoritical Magnetospheric Field Model', *J. Geophys.* **40**, 213–228.

Weiss, L. A., Reiff, P. H., Weber, E. J., Carlson, H. C., Lockwood, M., and Peterson, W. K.: 1995, 'Flow-aligned Jets in the Magnetospheric Cusp: Results from the Geospace Environment Modeling Pilot Program', *J. Geophys. Res.* **100**, 7649–7659.

Wing, S., Newell, P. T., Sibeck, D. G., and Baker, K. B.: 1995, 'A Large Statistical Study of the Entry of Interplanetary Magnetic Field *y*-Component into the Magnetosphere', *Geophys. Res. Lett* **22**, 2083–2086.

Wing, S., Newell, P. T., and Onsager, T. G.: 1996, 'Modeling the Entry of Magnetosheath Electrons into the Dayside Ionosphere', *J. Geophys. Res.* **101**, 13155–13167.

Wing, S., and Sibeck, D. G.: 1997, 'Effects of Interplanetary Magnetic Field z Component and the Solar wind Dynamic Pressure on the Geosynchronous Magnetic Field', *J. Geophys. Lett* **102**, 7207–7216.

Wing, S., Newell, P. T., and Ruohoniemi, J. M.: 2001, 'Double Cusp: Model prediction and Observational Verification', *J. Geophys. Res.* **106**, 25571–25593.

Woch, J., and Lundin, R.: 1992, 'Magnetosheath Plasma Precipitation in the Polar Cusp and its Control by the Interplanetary Magnetic Field', *J. Geophys. Res.* **97**, 1421–1430.

Xue, S., Reiff, P. H., and Onsager, T. G.: 1997, 'Mid-altitude Modeling of Cusp ion Injections under Steady and Varying Conditions', *Geophys. Res. Lett.* **24**, 2275–2278.

Yamauchi, M. and Lundin, R.: 1994, 'Classification of Large-scale and Meso-scale Ion Dispersion Patterns Observed by Viking over the Cusp-mantle Region', in J. A. Holtet and A. Egeland (eds.), *Physical Signatures of Magnetospheric Boundary Layer Processes*, pp. 99–109.

Zhou, X. W., Russell, C. T., Le, G., Fuselier, S. A., and Scudder, J. D.: 2000, 'Solar wind control of the polar cusp at high-altitude', *J. Geophys. Res.,* **105,** 245–251.

Surveys in Geophysics (2005) 26: 369–386
DOI 10.1007/s10712-005-1900-6 © Springer 2005

# SIMULATION STUDIES OF HIGH-LATITUDE MAGNETOSPHERIC BOUNDARY DYNAMICS

Q. Q. SHI[1], Z. Y. PU[1], H. ZHANG[1], S. Y. FU[1], C. J. XIAO[1], Q. -G. ZONG[2], T. A. FRITZ[2] and Z. X. LIU[3]

[1]*School of Earth and Space Sciences, Peking University, Beijing, 100871, China*
*E-mail: sqq@pku.edu.cn;*
[2]*Center for Space Physics, Boston University, 725 Commonwealth Avenue, Boston, MA, 02215, USA;*
[3]*Space Weather Laboratory, Center for Space Science and Application Research, Chinese Academy of Science, Mail Box 8701, Beijing, 100080, China*

(Received 31 December 2002; Accepted 30 April 2004)

**Abstract.** Magnetic reconnection at the high-latitude magnetopause is studied using 2–1/2-dimensional (2−1/2-D) Hall-MHD simulation. Concentric flow vortices and magnetic islands appear when both Hall effect and sheared flow are considered. Plasma mixing across the magnetopause occurs in the presence of the flow vortices. Reconnected structure generated in the vicinity of the subsolar point changes its geometry with increasing flow shear while moving to high latitudes. In the presence of flow shear, with the Hall-MHD reconnection a higher reconnection rate than with the traditional MHD is obtained. The out-of-plane components of flow and magnetic field produced by the Hall current are redistributed under the action of the flow shear, which makes the plasma transport across the boundaries more complicated. The simulation results provide some help in understanding the dynamic processes at the high-latitude magnetopause.

**Keywords:** entry layer, flow shear, hall effect, magnetic reconnection, magnetopause, vortex reconnection

**Abbreviations:** GEM – Geospace Environmental Modeling; GSE – Geocentric Solar Ecliptic

## 1. Introduction

The existence of magnetopause boundary layers (MBLs) adjacent to the magnetopause current sheet is an important signature of the solar wind-magnetosphere interaction. MBLs extend over all known portions of the magnetopause. So far in the literature three distinct regions have been recognized: the low-latitude boundary layer, the plasma mantle, and the high-latitude cusp (or, alternatively, the entry layer) (Haerendel and Paschmann, 1982; Hughes, 1995). The entry layer is found on the dayside of the exterior cusp (which is identified by some authors as the fourth MBL region), extending about 3 h on either side of local noon.

It connects to the low-latitude cusp along the field lines and borders on the ring current. As the high-latitude boundary layer near local noon, the entry layer shows significantly different features from the plasma mantle and the low-latitude boundary layer. Density and temperature do not exhibit any considerable change at the magnetopause and reach their magnetosheath levels right at the inner edge of the entry layer. The plasma $\beta$, the ratio of plasma thermal pressure to the magnetic field pressure, is larger than 1. The flows are low-speed and turbulent, with substantial cross-field components (Paschmann et al., 1976). Recent Cluster II measurements have confirmed these observations (Zong et al., 2002). The characteristics of the entry layer suggest that solar wind plasma and energy directly enter the region across the magnetopause. The transfer processes which have been suggested comprise anomalous diffusion, impulsive penetration of solar wind plasma blobs, direct influx along open field lines, as well as eddy transport (Haerendel and Paschmann, 1982; and references therein). Up to now there is no consensus regarding the essence of the direct transport process, although it is generally thought that this process is closely connected with transient magnetic reconnection (Haerendel and Paschmann, 1982) at the magnetopause.

Magnetic reconnection (MR) at the dayside magnetopause is of vital importance for the solar wind-magnetosphere interaction. MR generates a bulge or flux rope near the leading edge of the diffusion region when the reconnection rate is intensified. These flux tubes move along the magnetopause and hence represent transient events (Otto, 1995) termed flux transfer events (FTEs) (Russell and Elphic, 1978). In the last two decades, a variety of transient MR models have been developed (Scholer, 1995, and references therein). Most of these models (for instance, the multiple X-line reconnection (MXR) model by Lee and Fu (1985) and the bursty single line reconnection model (BSXR) by Scholer (1988) and Southwood et al. (1988) were devoted to explain the formation of FTEs near the nose of the magnetopause where the flow shear between the magnetosheath and the magnetosphere is negligible. However, at the high latitude magnetopause, flow shear due to magnetosheath plasma flow is larger than that at low latitudes; the presence of the sheared flow may also lead to the formation of transient reconnection (Liu and Hu, 1988). Early studies (Liu and Hu, 1988; Pu et al., 1990a, b; Pu and Fu, 1997, and references therein) showed with two-dimensional (2-D) incompressible MHD simulation that the magnetic islands thus formed are concentric with flow vortices, and that plasmas in the magnetosheath and magnetosphere move across the magnetopause and mix with each other. They named this reconnection process vortex-induced reconnection (VIR). Shen and Liu (1999) found that in compressible plasmas VIR takes place within a limited sheared velocity range. Chen et al. (1997) showed that, in contrast to the incompressible case where the reconnection rate increases

with increasing flow shear when the latter is greater than a certain critical value, the presence of flow shear reduces the reconnection rate.

All these VIR works did not include the Hall effect. However, the width of the magnetic reversal layer $L$ in the dayside magnetopause is comparable to the ion inertia scale length $\lambda_i$ (Berchem and Russell, 1982) below which the motion of electrons and ions decouple and the Hall current effect plays a role in reconnection (Sonnerup, 1979). Recent simulation results of the GEM Reconnection Challenge project have illustrated that the Hall effect is a critical factor which must be included to model collisionless reconnection (Birn et al., 2001; Shay et al., 2001). Detailed analysis of Polar observations (Scudder et al., 2002) provides clear evidence of hall physics at the magnetopause. Once the Hall effect is included, a quadrupole $B_y(B_M)$ structure is generated even in the case when the initial $B_{y0}(B_{M0}) = 0$ (Sonnerup, 1979; Terasawa, 1983; Wang et al., 2000; Birn et al., 2001; Ma and Bhattacharjee, 2001). Based on Geotail measurements, Deng and Matsumoto (2001) found that the Hall current generated a core field in the dayside magnetopause. Karimabadi et al. (1999) found a modified quadrupole $B_y$ in FTEs using a three-dimensional (3-D) hybrid simulation. In addition, the existence of the Hall effect increases the reconnection rate (Birn et al., 2001). Studies of MR in the presence of both Hall effect and velocity shear are required, and are of importance for a better understanding of high-latitude solar wind-magnetosphere interaction.

The present work performs 2–1/2-D compressional Hall-MHD simulations of MR at the magnetopause considering both the Hall currents and sheared flows. Our key goal is to reveal the characteristics of transient reconnection at the dayside high-latitude magnetopause and the role which it may play in plasma and energy transport at the dayside high-latitude magnetopause. Our simulation shows that the magnetic field and flow structures produced by the transient MR in the presence of a flow shear are similar to those of the original VIR type. The terminology of vortex reconnection (VR) is used to identify this MR process. It is found that VR effectively leads to plasma mixing across the magnetopause. The Hall effect increases the reconnection rate. The conventional Hall-generated $B_y$ structure is considerably modified by the sheared flow.

## 2. Simulation method

The compressible dimensionless Hall-MHD equations in 2–1/2-D are given in SI Units by

$$\frac{d\rho}{dt} = -\rho\nabla \cdot \vec{V} \tag{1}$$

$$\rho \frac{d\vec{V}}{dt} = \nabla \cdot \overleftrightarrow{P} + \vec{J} \times \vec{B} \tag{2}$$

$$\frac{\partial B_y}{\partial t} = -(\nabla \times \vec{E})_y \tag{3}$$

$$\frac{\partial A_y}{\partial t} = -E_y \tag{4}$$

$$\frac{\partial p}{\partial t} = -\vec{V} \cdot \nabla p - \gamma p \nabla \cdot \vec{V} + (\gamma - 1)(\vec{J} \cdot \vec{E}_R + (\overleftrightarrow{\tau} \cdot \nabla)\vec{V}) \tag{5}$$

$$\vec{E}_R = R_m^{-1}\vec{J} + \frac{h}{\rho}\left(\vec{J} \times \vec{B} - \frac{1}{2}\nabla p\right) \tag{6}$$

together with $\vec{J} = \nabla \times \vec{B}, \vec{E}_R = \vec{E} + \vec{V} \times \vec{B}$ and $\overleftrightarrow{P} = -P\overleftrightarrow{I} + \overleftrightarrow{\tau}$, where $\rho, \vec{V}, \vec{B}$ and $p$ are the plasma mass density, velocity, magnetic field and thermal pressure, respectively. They are normalized by characteristic values of the system $\rho_{\text{msh}}, V_A = B_{\text{msh}}/\sqrt{\mu_0 \rho_{\text{msh}}}, B_{\text{msh}}$ and $p_0 = B_{\text{msh}}^2/\mu_0$, respectively, where $\rho_{\text{msh}}$ and $B_{\text{msh}}$ represent the density and magnetic field in the magnetosheath refers to the viscous stress tensor. The length scale is normalized to the half scale width of the current sheet $L_0$. The time $t$ is normalized to a characteristic Alfvén transit time $\tau_A = L_0/V_A$. Dimensionless parameters $R_v = \rho_0 V_A L_0/\mu$ and $R_m = \mu_0 V_A L_0/\eta$ denote the Reynolds number and the magnetic Reynolds number, respectively. The Hall coefficient is defined by the ratio of the ion inertia length to the half width of the current sheet, i.e., $h = \lambda_i/L_0$.

We solve Equations (1)–(6) in a rectangular domain of $-L_x < X < L_x$ and $L_{z1}$ with an assumption of $\partial/\partial_y = 0$ for all variables, where $\hat{Z}$ is normal to the magnetopause, $\hat{Z}$ is along the magnetopause and $\hat{Y} = -\hat{X} \times \hat{Z}$. The mesh system is $160 \times 128$. Free boundary conditions are applied in the $X$ direction, while the periodic condition is used in the $Z$ direction. The Runge–Kutta scheme in time and centered differences scheme in space are adopted in the calculations.

The initial plasma density is given by

$$\rho = 0.5(\rho_{\text{msh}} + \rho_{\text{msh}}) + 0.5(\rho_{\text{msh}} - \rho_{\text{msh}})\tanh(x/L_0) \tag{7}$$

where $\rho_{\text{msp}}, \rho_{\text{msh}}$ are the mass density at the magnetosphere and magnetosheath, respectively. The initial sheared velocity is given by

$$\vec{V}(X) = V_0 \tanh(x/L_0)\vec{e}_z \tag{8}$$

which implies that in the magnetospheric frame of reference, the reference frame used is moving at half the velocity of the magnetosheath flow. The magnetic field is expressed by

$$\vec{B} = 0.5(B_{\mathrm{zmsp}} + B_{\mathrm{zmsp}})\vec{e}_z + 0.5(B_{\mathrm{zmsp}} - B_{\mathrm{zmsp}})\tanh(x/L_0)\vec{e}_z + 0.5(B_{\mathrm{zmsp}} + B_{\mathrm{zmsp}})\vec{e}_y + 0.5(B_{\mathrm{zmsp}} - B_{\mathrm{zmsp}})\tanh(x/L_0)\vec{e}_y \quad (9)$$

The initial thermal pressure $p$ is determined by the total pressure balance condition.

We assume a local enhancement of anomalous resistivity which takes the form (Scholer, 1989):

$$R_m^{-1} = R_{m0}^{-1} + R_{m0}^{-1}\alpha\{\exp[(x - x_1)^2] - (z - z_1)^2 + \exp[-(x - x_2)^2 - (z - z_2)^2]\}\exp(-t/t_0) \quad (10)$$

where $\alpha$ indicates the enhancement coefficient, and $t_0 = 30$ is the decay time. In all our simulations in this paper we adopt $x_1 = x_2 = 0.0, z_1 = 0.0, z_2 = 36, R_v^{-1} = R_m^{-1} = 0.005, \alpha = 3.0; \beta = 1.6$ (Paschmann et al., 1976; Zong et al., 2002).

## 3. Simulation results

### 3.1. Magnetic field and flow configuration of the VR

At the dayside magnetopause the width of the current sheet is about 400–1200 km, which is 4–10 times $\lambda_i$ (Berchem and Russell, 1982). We take $h = 0.4$ in our calculations.

Figure 1a and b plot the magnetic field lines (solid lines) and the streamlines (dashed lines) for the modified tearing mode (without flow shear) and the transient MR in the presence of sheared flow, respectively. The Hall effect is considered in both cases. It is seen in Figure 1a that there are four symmetric vortices around the magnetic island when the initial flow is set to be zero ($V_0 = 0.0$). This is consistent with the field and flow geometry obtained in the simulations of Birn et al. (2001). On the other hand, when the sheared flow is taken into account, the configuration of the reconnected structure is quite different. Figure 1b shows an example in which $V_0 = 0.6$ is assumed. It is seen that the flow vortex is concentric with magnetic island. This configuration is similar to the VIR result in incompressible MHD simulation for $V_0 > 0.4$ with no Hall effect (Pu et al., 1990a). Our simulations indicate that, when $\beta \approx 1$, the coexistence of a vortex and a magnetic island appears for $0.1 \leq V_0 < 1.0$. Hereafter we call this reconnection process vortex reconnection (VR).

### 3.2. Plasma mixing across the magnetopause

The Hall-MHD equations which we presented in the previous Section adopt the Eulerian description in which the thermal pressure, velocity, and all other

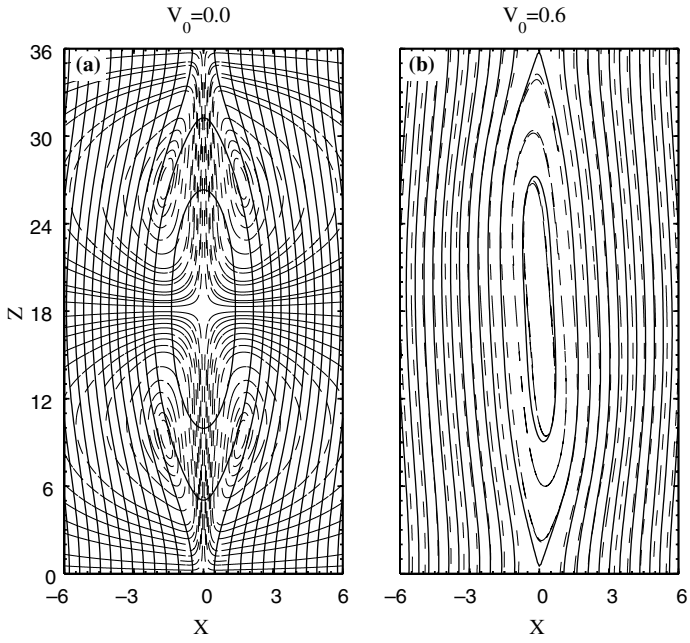


*Figure 1.* Magnetic field lines (solid lines) and streamlines (dashed lines) for (a) the modified tearing mode with the Hall effect and (b) the vortex reconnection (VR).

plasma properties are described as fields within the control volume. In the Eulerian description, one can only find out the velocity, acceleration, etc., of whatever plasma element happens to be at a particular location at a particular time, but not the location or velocity of any particular plasma element, which is inconvenient in the knowledge of plasma motion across the magnetopause. If the velocity field of every location at every time is known, one can easily obtain the trajectories of any plasma element by transferring the Eulerian to the Lagrangian description, solving

$$\frac{dx}{dt} = u(x, y, z, t) \tag{11}$$

$$\frac{dx}{dt} = v(x, y, z, t) \tag{12}$$

$$\frac{dx}{dt} = w(x, y, z, t) \tag{13}$$

where $(x, y, z)$ presents the location of one particular plasma element at every time. Figure 2a shows the motions of the plasma elements in the modified tearing mode which includes the Hall effect but not the sheared flow. We select some

plasma elements on both sides of the neutral line at $t = 30$, then trace their locations for $t > 30$, see Figure 2a. Figure 2b shows that, as time goes on, the plasmas on each side of the boundary are still on that side, not penetrating into the opposite region, though upward and downward accelerated outflows are formed on either side of the central current sheet. No plasma transport across the magnetopause is directly seen in this 2–1/2-D simulation with the Lagrangian description. In fact, the magnetic field and flow field distribution in classical (2-D) fast reconnection models are consistent with this picture (Vasyliunas, 1975, and the references therein).

Figure 3a and b present a similar simulation study for the VR, and with the same number of plasma elements at the same locations as those in Figure 2a at the start. Figure 3b indicates that, along with the development of VR, some plasma elements initially on one side of the current sheet move across the magnetopause into the other region.

For a realistic magnetopause boundary system, the density in the magnetosheath is larger than that in the magnetosphere. We take $\rho_{msh}$ : $\rho_{msh} = 1{:}0.5$ to model an asymmetric magnetopause in a simulation run with the Eulerian description. Figure 4a and b plot the magnetic field (lines), flow field (arrows) and density distribution (color scale) at $t = 0$ and $t = 180$, respectively. We can easily show that the density which is initially lower (higher) in the magnetosphere (magnetosheath) turns to be higher (lower) at

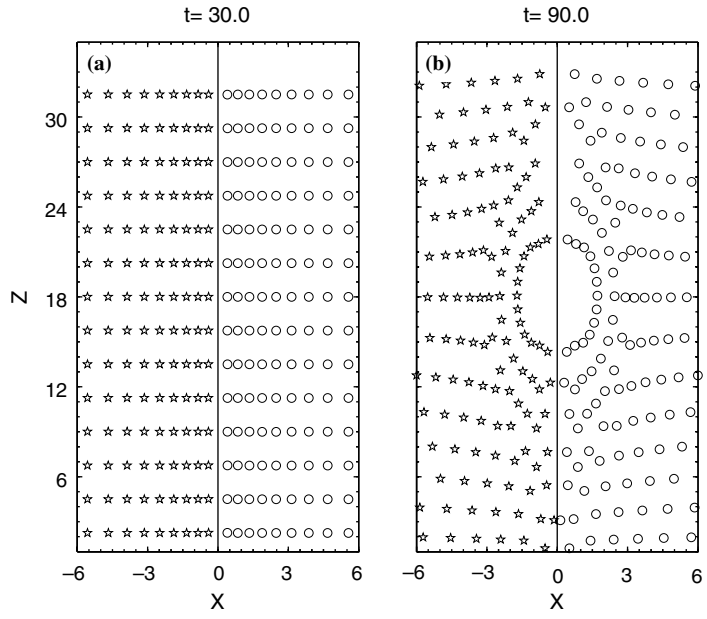


*Figure 2.* Locations of plasma elements at (a) $t = 30$ and (b) $t = 90$ for the modified tearing mode. Pentagrams represent the plasma elements initially on the magnetosheath side, while circles represent the plasma elements initially on the magnetospheric side.

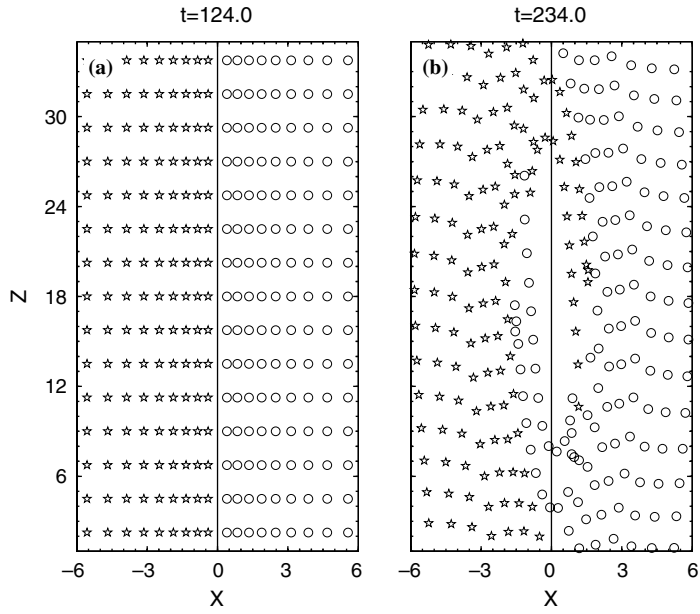


*Figure 3.* Locations of plasma elements at (a) $t = 124$ and (b) $t = 234$ for the VR. Pentagrams represent the plasma elements initially on the magnetosheath side, while circles represent the plasma elements initially on the magnetospheric side.

$t = 180$ inside the island. The initial density jump is thus smoothed out and becomes unclear. A similar situation happens to the temperature distribution (not shown here). The 'mixture' of mass and of temperature appears in close association with the vertical motion.

These simulation results suggest that VR provides a mechanism that leads to an effective mixing of plasma across the magnetopause boundary. The cross-field components of the flow velocity inside the magnetosphere can also be caused by the VR.

### 3.3. The evolution of the moving reconnected structure

The BSXR and MXR models suggest that MR generates bulges or flux ropes in the dayside equatorial region where sheared flows are negligible. The 2-D view of the magnetic field and flow configuration has been shown in Figure 1a. These reconnected structures move to higher latitudes along the magnetopause (Russell, 1995). Along with the motion of the structures, the magnetosheath flow becomes faster. How do the field and flow patterns of these structures vary when the sheared flows become stronger and not negligible? To find out the answer to this question we perform a two step simulation study (Pu et al., 1990b): first we run the code by setting $V_0 = 0$ and obtain the results similar to those shown in Figure la, then we take the obtained island and vortex as initial

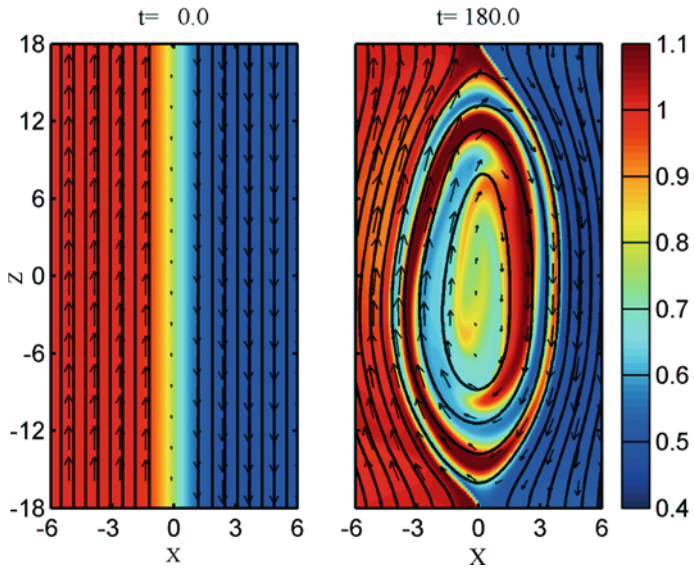


*Figure 4*. Magnetic field lines, flow vectors and color-coded density with initial density jump 1:0.5 at (a) $t = 0$ and (b) $t = 180$.

perturbations to run the VR code with a flow shear which increases linearly with time during $0 < t < 40$, reaching $\Delta V$ at $t = 40$, and then stop increasing after $t = 40$. It is found that, as the flow shear enhances, magnetic field lines tend to be parallel to the streamlines rather quickly; meanwhile, the magnetic island and vortex gradually become concentric. The interaction of the magnetic field with the flow field causes MR to proceed all the time. This process should also be referred to as VR.

Figure 5a illustrates a corresponding field and flow configuration when $\Delta V = 0.6$. The reconnected structures maintain the VR-like type for a wide range of $\Delta V$ until reaching a certain critical value ($\Delta V \sim 1.0$) when they start to split into smaller-scale ones, then the concentric structure disappears, see Figure 5b. This two step simulation implies that the field and flow structures of transient MR observed at the high-latitude magnetopause may differ significantly from those seen at low-latitudes.

### 3.4. New feature of the VR with the Hall effect: higher reconnection rate

Previous studies have shown that Hall currents increase the reconnection rate for the collisionless tearing mode (Sonnerup, 1979; Birn et al., 2001). If the flow shear is involved, does the Hall effect also reinforce the efficiency of transient MR?

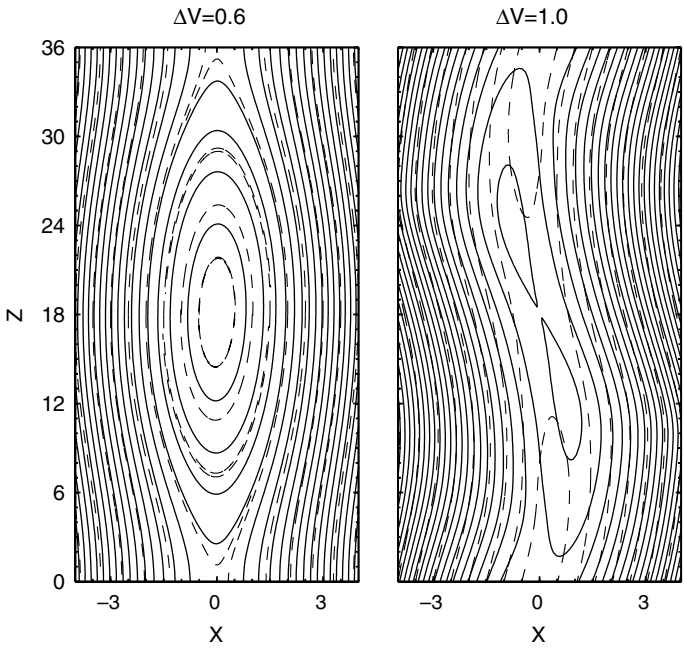


*Figure 5.* Magnetic field lines (solid lines) and streamlines (dashed lines) for a increasing flow shear (a) $\Delta V = 0.6$, and (b) $\Delta V = 1.0$.

We define the reconnection rate as the ratio of the reconnected flux to the total flux, i.e., $R_s = (A_{\max} - A_{\min})/F$ (Matthaeus and Lamkin, 1985), where $A_{\max}$. and $A_{\min}$ represent the maximum and minimum value of the magnetic potential, respectively, and $F$ denotes the total magnetic flux. Figure 6 plots how $R_s$ varies with $t$ for different Hall coefficients $h$ when $V_A = 0.6$. It is seen that the larger the $h$, the greater the $R_s$. This indicates that though the presence of flow shear reduces the reconnection efficiency somewhat (Chen et al., 1997), Hall currents can compensate for the reduction of the reconnection rate, especially for larger values of $h$.

### 3.5. New feature of the VR with the Hall effect: generation of modified $B_y$ and $V_y$ distributions

In addition to introducing whistler and kinetic Alfvén wave dynamics in transient MR, the Hall effect produces an out-of-plane magnetic field. The Hall generated $B_y$ has a quadrupole structure "center-symmetric" with respect to the reconnection point for the collisionless tearing mode (Terasawa, 1983; Birn et al., 2001). When sheared flow is involved, the $B_y$ distribution is greatly modified. It is interesting to notice from Figure 7a and b that the polarity of $B_y$ for the case with sheared flow parallel to the magnetic

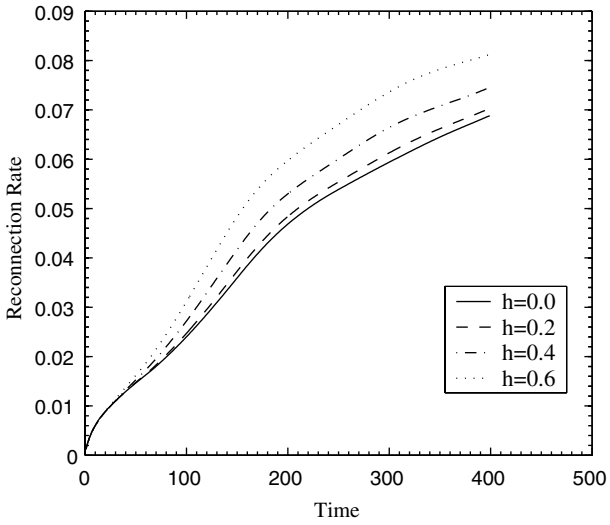


*Figure 6*. Reconnection rate vs. time for different Hall coefficients.

field (applicable to the southern hemisphere) is just opposite to the case with sheared flow anti-parallel to the magnetic field (applicable to the northern hemisphere).

Concomitant with the Hall-generated $B_y$ is the production of the out-of-plane flow $V_y$, which has not been much studied before. Figure 8a and b show that the Hall-generated $V_y$ has similar polarity for both the "anti-parallel" and "parallel" cases.

The Hall generation of $B_y$ and $V_y$ in VR might be of interest for transport processes in the high-latitude magnetopause. Once $B_y$ and $V_y$ are produced and redistributed, plasma elements move not only in the $x$–$z$ plane, but also in the $y$-direction, which makes the transport of mass, energy and momentum more complex than that without the $B_y$ and $V_y$ generation.

## 4. Comparisons with observations

In previous Sections we have made 2–1/2 Hall MHD simulations of transient MR at the dayside high-latitude magnetopause with sheared flow being taken into account. A great effort was devoted to study the configuration of the magnetic islands and vortices, the evolution of convecting reconnected structures, the influence of the Hall current on the reconnection rate, the redistribution of Hall-generated $B_y$ and $V_y$ under the action of flow shear, and plasma mixing across the magnetopause. The key goal of these studies is

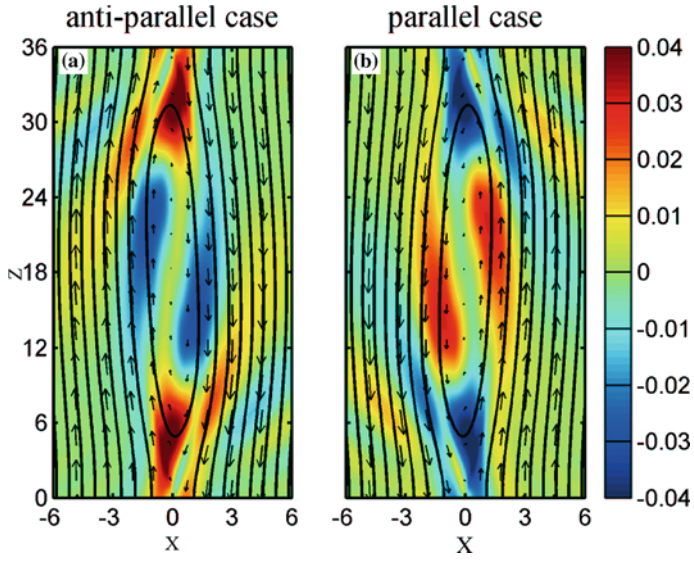


*Figure 7*. Magnetic field lines, flow vectors and color-coded $B_y$ for (a) velocity shear anti-parallel to the magnetic field shear, and (b) velocity shear parallel to the magnetic field shear.

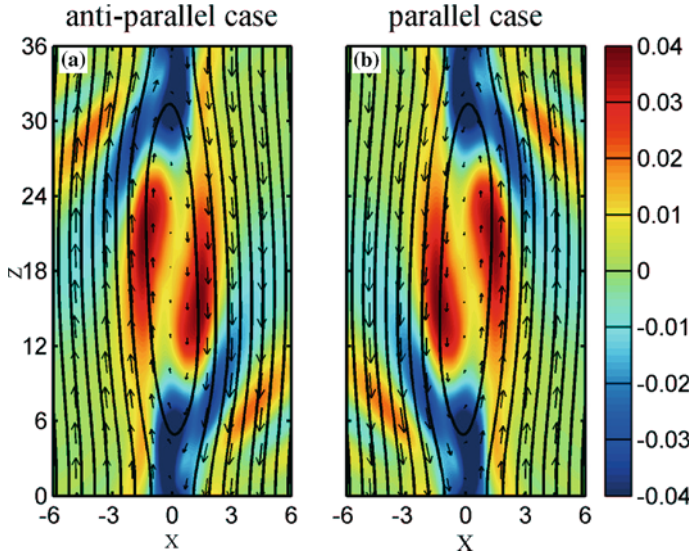


*Figure 8*. Magnetic field lines, flow vectors and color-coded $V_y$ for (a) velocity shear anti-parallel to the magnetic field shear, and (b) velocity shear parallel to the magnetic field shear.

to reveal the characteristics of transient reconnection at the dayside high-latitude magnetopause and the role which it possibly plays in plasma and energy transport at the dayside high-latitude magnetopause. In this section

we try to compare the simulation results with HEOS 2 and Cluster II observations.

The HEOS 2 and Cluster II measurements (Paschmann et al., 1976; Zong et al., 2002, 2003a, b; Pu et al., 2003) indicate that the plasma temperature in the magnetosheath adjacent to the entry layer is about $T \approx 5 \times 10^6 - 10^7 K$, the bulk speed ranges from about 200 to 300 km/s, and plasma $\beta$ is greater than 1. By taking $\beta = 1.6$, we obtain $V_A \approx 230$–$320$ km/s and hence $V_0 \approx 0.30$–$0.65$. VR develops in the cases of $1.0 \geq V_0 \leq 0.1$. Therefore the VR condition seems to be fulfilled at the dayside high latitude magnetopause boundary region.

Paschmann et al. (1976) applied the asymmetric model of a magnetospheric boundary flow published by Levy et al. (1964) to the measurements of HEOS 2 and found that this model appears to fit the data. In the meantime there remains one difficulty: the model (Levy et al., 1964) predicts that one should expect invariably to see higher flow velocities tangent to the magnetopause inside the boundary layer than outside it, which is in contrast to the observations. One of the characteristics of the entry layer is the lack of order in the bulk speed, and existence of even sunward-directed and cross-field components of the flow. The magnitude of the flow is usually substantially lower than the values just outside the magnetopause. These features are consistent with the VR process and our simulation.

Recently, Cluster II measurements provided us with more detailed features of the region just dayside of the exterior cusp (Pu et al., 2003; Zong et al., 2003a, b). On January 26, 2001, the four Cluster spacecraft were travelling inbound in north high-latitudes from the cusp into the magnetosheath across the high-latitude magnetopause at about 11:00 UT. Figure 9 illustrates an overview of the RAPID, CIS and FGM measurements on this day from 00:00 to 04:00 UT (Pu et al., 2003). Five panels from the top to the bottom show, respectively, the energy-integrated flux of energetic electrons, protons, the number density of thermal plasma, the $V_x$ and $V_y$ components of the plasma velocity, the $B_x$, $B_y$ and $B_z$ components of the magnetic field, and the total magnetic field $B_t$ . The GSE coordinate system was used, and the dotted vertical line marks the magnetopause. The magnetic field data and the plasma density show no clear evidence of magnetopause location. Only the energetic ions and $B_z$ seem to provide some indication of the interface between the cusp and the magnetosheath (Pu et al., 2003). We see that the plasma density in the entry layer is comparable with that in the magnetosheath. In contrast to the quiet time cusp, the plasma velocity components $V_x$ and $V_y$ are significant. The electron flux is rather low in Figure 9, indicating an open field line geometry in the near cusp region during southward IMF. The magnetic field become more turbulent than that in the magnetosheath, the plasma density and velocity are rather turbulent as well. All these features are consistent with the prediction of our simulations. For instance, the lack of

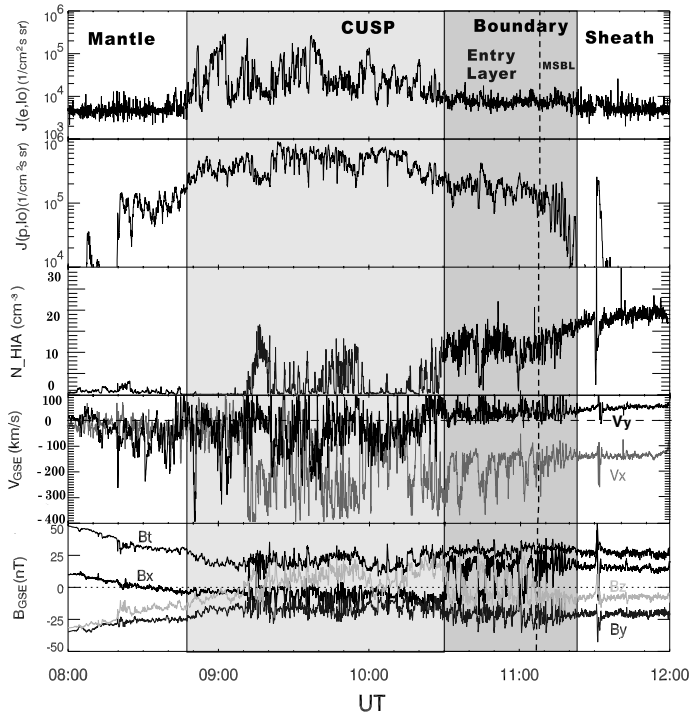


*Figure 9.* An overview of energetic electron and proton fluxes, thermal ion plasma number density and velocity, and magnetic field from the Cluster/spacecraft 3 (CS3) from 08:00 to 12:00 UT on 26 January, 2001. (adapted from Pu et. al., 2003, this volume).

a change of the plasma density from magnetosheath to magaetosphere may be explained in terms of the plasma mixing presented in Section 3.2; the presence of $V_x$ and $V_y$ can be seen from the results shown in Sections 3.1 and 3.5. In the previous section we fixed the simulation system in a 2–1/2-D domain. However, in the real 3-D situation, flux ropes will form instead of magnetic islands (especially in those cases where there is a preexisting or Hall-modified $B_y$). Liu and Hu (1988) and Fu et al. (1995) drew a 3-D structure of this type of flux tube based on the VIR model. The energetic electrons will soon escape along the open field lines when transient reconnection occurs.

In the VR simulation shown in the previous sections with periodic boundary conditions along the $Z$ direction, only one concentric magnetic island and flow vortex appear in the simulation domain. In reality, a number of reconnection structures are present at the high-latitude magnetopause. Figure 10 illustrates a further simulation with the free boundary condition along the $Z$ direction and the half-length of the current layer being $L_z = 100$, while other conditions are the same as those in the previous studies. It is seen

that more than one magnetic island are generated. These magnetic islands interact with each other, with the flow shear, and with the reconnected structures convecting from low latitudes (see Section 3.3), making the situation much more complicated. This could account for the highly turbulent magnetic field and highly disordered flow velocity observed in the cusp and entry layer. In summary, most of the observed characteristics of the dayside high-latitude magnetopause boundary region axe compatible with the concept of transient MR in the presence of sheared flow.

However, there are at least two shortcomings with the present VR model. First, it neglects the existence of the exterior cusp, which presents an obstacle to both the magnetosheath flow and the anti-sunward boundary flow (Paschmann et al., 1976). Second, it ignores the drag force exerted by reconnected field lines and omits the curvature force resulting from the sharp bends in reconnected field lines. These two forces can only be considered in 3-D global simulation and models. These are far beyond the present study.

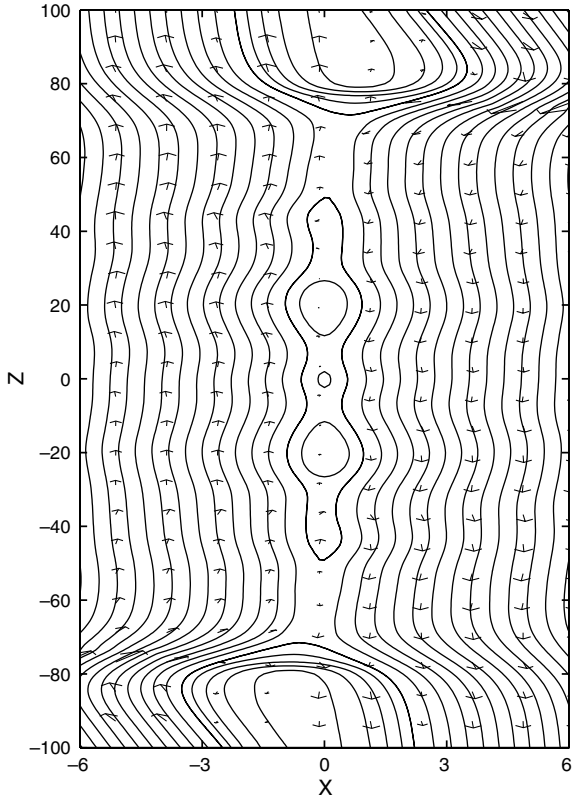


*Figure 10*. Magnetic field lines, flow vectors for the vortex reconnection with free boundary conditions in the $Z$ direction.

## 7. Conclusions

The Hall-MHD simulation results presented in this paper reveal the characteristics of transient reconnection at the dayside high-latitude magnetopause, which can help us to gain insight into *in situ* observations in the entry layer, such as the substantial cross-field components of the flow velocity, lack of density and temperature changes at the magnetopause, and 3-D phenomena of the flow and magnetic field.

The configuration of the reconnected structure is similar to that of VIR in the incompressible and compressible plasmas studied before and different from that without flow shear. In the presence of flow shear the consideration of the Hall effect provides a higher reconnection rate than without it.

When transferred to a Lagrangian description, the system shows obvious plasma mixing across the current sheet. The initial jumps in density and temperature tend to be smoothed out across at the magnetopause.

The reconnected structure formed near the subsolar point changes to the VR type with increasing flow shear while moving to high latitudes. Plasma mixing is expected to occur because of the existence of the flow vortex.

An out-of-plane magnetic field $B_y$ and velocity component $V_y$ appear when the Hall effect and flow shear are involved. The conventional quadrupole distribution of the Hall-generated $B_y$ is significantly modified by the flow shear, and so is the Hall generated $V_y$. These make the transport of mass, energy and momentum more complex.

The present work is a first step in an attempt to reveal the characteristics of transient MR in the high-latitude magnetopause using a 2–1/2-D Hall MHD simulation. Three-dimensional analytical and simulation studies are necessary in order to have a better understanding of MR dynamics, the geometry of the flow and magnetic field structure, as well as transport processes occurring at high-latitudes.

## Acknowledgements

This work is supported by the CNSF key Project "Multiple Scale Processes in Geospace Storms" (40390150), and project of 49834040 and Chinese Key Research Project G200000784. We thank Zhiwei Ma and Xiaogang Wang for their great assistance.

## References

Berchem, J., and Russell, C. T.: 1982, 'The Thickness of the Magnetopause Current Layer: ISEE 1 and 2 Observations', *J. Geophys. Res.* **87**, 2108–2114.

Birn, J., Drake, J. F., Shay, M. A., Rogers, B. N., Denton, R. E., Hesse, M., Kuznetsova, M., Ma, Z. W., Bhattacharjee, A., Otto, A., and Pritchett, P. L.: 2001, 'Geospace

Environmental Modeling (GEM) Magnetic Reconnection Challenge', *J. Geophys. Res.* **106**, 3715–3719.

Chen, Q., Otto, A., and Lee, L. C.: 1997, 'Tearing Instability, Kelvin–Helmholtz Instability, and Magnetic Reconnection', *J. Geophys. Res.* **102**, 151–161.

Deng, X. H., and Matsumoto, H.: 2001, 'Rapid Magnetic Reconnection in the Earth's Magnetosphere Mediated by Whistler Waves', *Nature* **410**, 557–560.

Fu, S. Y., Pu, Z. Y., and Liu, Z. X.: 1995, 'Vortex-induced Magnetic Reconnection and Single X line Reconnection at the Magnetopause', *J. Geophys. Res.* **100**, 5657–5663.

Haerendel, G., and Paschmann, G.: 1982, 'Interaction of the Solar Wind with the Dayside Magnetopause', in A. Nishida (ed.), *Magnetospheric Plasma Physics*, Center for Academic Pub., Japan, pp. 81–122 .

Hughes, W. J.: 1995, 'The Magnetopause, Magnetotail and Magnetic Reconnection', in M. G. Kivelson, and C. T. Russell (eds.), *Introduction to Space Physics*, Cambridge University Press, pp. 259–287.

Karimabadi, H., Krauss-Varban, D., Omidi, N., and Vu, H. X.: 1999, 'Magnetic Structure of the Reconnection Layer and Core Field Generation in Plasmoids', *J. Geophys. Res.* **104**, 12,313–12,316.

Lee, L. C., and Fu, Z. F.: 1985, 'A Theory of Magnetic Flux Transfer at the Earth's Magnetopause', *Geophys. Res. Lett.* **12**, 105–108.

Levy, R. H., Petschek, H. E., and Siscoe, G. L.: 1964, 'Aerodynamic Aspects of the Magnetospheric Flow', *AIAA J.* **2**, 2065–2076.

Liu, Z. X., and Hu, Y. D.: 1988, 'Local Magnetic Reconnection Caused by Vortices in the Flow Field', *Geophys. Res. Lett.* **15**, 752–755.

Ma, Z. W., Otto, A., and Lee, L. C.: 1994, 'Core Magnetic Field Enhancements in Single X line, Multiple X line and Patchy Reconnection', *J. Geophys. Res.* **99**, 6125–6136.

Ma, Z. W., and Bhattacharjee, A.: 2001, 'Hall Magnetohydrodynamic Reconnection: The Geospace Environmental Modeling Challenge', *J. Geophys. Res.* **106**, 3773–3782.

Matthaeus, W. H., and Lamkin, S. L.: 1985, 'Rapid Magnetic Reconnection Caused by Finite Amplitude fluctuations', *Phys. Fluids* **28**, 303.

Otto, A.: 1995, 'Magnetic Reconnection at the Magnetopause: A Fundamental Process and Manifold Properties', *Rev. Geophys.* **33**(Supplement), 657.

Paschmann, G., Haerendel, G., Sckopke, N., Rosenbauer, H., and Hedgecock, P. C.: 1976, 'Plasma and Magnetic Field Characteristics of the Distant Polar Cusp Near Local Noon: The Entry Layer', *J. Geophys. Res.* **81**, 2883–2899.

Paschmann, G., Haerendel, G., Paparnastorakis, I., Sckopke, N., Bame, S. J., Gosling, J. T., and Russell, C. T.: 1982, 'Plasma and Magnetic Field Characteristics of Magnetic Flux Transfer Events', *J. Geophys. Res.* **87**, 2159–2168.

Pu, Z. Y., Yei, M., and Liu, Z. X.: 1990a, 'Generation of Vortex-Induced Tearing Mode Instability at the Magnetopause', *J. Geophys. Res.* **95**, 10,559–10,566.

Pu, Z. Y., Hou, P. T., and Liu, Z. X.: 1990b, 'Vortex-induced Tearing Mode Instability as a Source of Flux Transfer Events', *J. Geophys. Res.* **95**, 18,861–18,869.

Pu, Z. Y., and Fu, S. Y.: 1997, 'Transient Magnetic Reconnection at the Magnetopause in the Presence of a Velocity Shear', *Plasma Phys. Control. Fusion* **39**, A251–A260.

Pu, Z. Y., Zong, Q. G., Fritz, T., Xiao, C. J., Huang, Z. Y., Fu, S. Y., Shi, Q. Q., Dunlop, M. W., Glassmeier, K. -H., Balogh, A., Daly, P., Cao, J. B., Liu, Z. X., Shen, C., Shi, J. K., Reme, H. and Dandouras, J.: 2003, 'Multiple Flux Rope Events at the High-latitude Magnetopause: Cluster/Rapid Observation on January 26, 2001', Surveys Geophys. **64**, this volume.

Russell, C. T., and Elphic, R. C.: 1978, 'Initial ISEE Magnetometer Results: Magnetopause Observations', *Space Sci. Rev.* **22**, 681–715.

Russell, C. T.: 1995, 'The Structure of the Magnetopause', in P. Song, B. U. O. Sonnerup, and M. F. Thomsen (eds.), *Physics of the magnetopause, Geophysical Monograph 90*, American Geophysical Union, Washington D.C, pp. 81–98.

Scholer, M.: 1988, 'Magnetic Flux Transfer at the Magnetopause Based on Single X line Bursty Reconnection', *Geophys. Res. Lett.* **15**, 291–294.

Scholer, M.: 1989, 'Asymmetric Time-dependent and Stationary Magnetic Reconnection at the Dayside Magnetopause', *J. Geophys. Res.* **94**, 15,099–15,011.

Scholer, M.: 1995, 'Models of Flux Transfer Events', in P. Song, B. U. O. Sonnerup, and M. F. Thomsen (eds.), *Physics of the magnetopause Geophysical Monograph 90*, American Geophysical Union, Washington D.C, pp. 235–245.

Scudder, J. D., Mozer, F. S., Maynard, N. C., and Russell, C. T.: 2002, 'Fingerprints of Collisionless Reconnection at the Separator: I, Ambipolar-Hall Signatures', *J. Geophys. Res.* **107**, 1294, doi:10.1029/2001JA000126.

Shay, M. A., Drake, J. F., Rogers, B. N., and Denton, R. E.: 2001, 'Alfvénic Collisionless Magnetic Reconnection and the Hall Term', *J. Geophys. Res.* **106**, 3759–3772.

Shen, C., and Liu, Z. X.: 1999, 'The Coupling Mode Between Kelvin–Helmholtz and Resistive Instabilities in Compressible Plasmas', *Phys. Plasmas* **6**, 2883–2886.

Sonnerup, B. U. O.: 1979, 'Magnetic field reconnection', in L. J. Lanzerotti, C. F. Kennel, and E. N. Parker (eds.), *Solar System Plasma Physics 3*, North Holland Pub., Amsterdam, pp. 46–108.

Southwood, D. J., Farrugia, C. J., and Saunders, M. A.: 1988, 'What are Flux Transfer Events?', *Planet. Space Sci.* **36**, 503–508.

Vasyliunas, V. M.: 1975, 'Theoretical Models of Magnetic Field Line Merging, 1', *Rev. Geophys. Space Phys.* **13**, 303–336.

Bhattacharjee, A., and Ma, Z. W.: 2000, 'Collisionless Reconnection: Effects of Hall Current and Electron Pressure Gradient', *J. Geophys. Res.* **105**, 27,633–27,648.

Zong, Q.-G., Fritz, T. A., Wilken, B., and Daly, P.: 2002, 'Energetic Ions in the High-latitude Boundary Layer of the Magnetopause RAPID/CLUSTER Observation', *Geophys. Monograph* **122**, 101–110.

Zong, Q.-G., Fritz, T. A., Spence, H., Dunlop, M., Pu, Z. Y., Korth, A., Daly, P. W., Balogh, A., and Reme, H.: 2003a, 'Bursty Energetic Electrons Confined in Flux Ropes in the Cusp Region', *Planet. Space Sci.* **51**, 821–830.

Zong, Q.-G., Fritz, T. A., Spence, H., Korth A., Daly, P. W., Dunlop, M., Balogh, A., Fennell, J., Pu, Z. Y. and Reme, H.: 2003b, 'Energetic Electrons as a Field Line Topology Tracer in the High-Latitude Boundary/Cusp Region: Cluster RAPID Observations', Surveys Geophys. **26**, this volume.

Surveys in Geophysics (2005) 26: 387–407
DOI 10.1007/s10712-005-1902-4 © Springer 2005

# CUSP GEOMETRY IN MHD SIMULATIONS

GEORGE SISCOE[1], NANCY CROOKER[1], KEITH SIEBERT[2], NELSON MAYNARD[2], DANIEL WEIMER[2] and WILLARD WHITE[2]
[1]*Center for Space Physics, Boston University, Boston, MA, 02215, USA*
*E-mail: siscoe@bu.edu;*
[2]*Mission Research Corporation, Nashua, NH, 03062, USA*

(Received 13 August 2003; Accepted 30 April 2004)

**Abstract.** The MHD simulations described here show that the latitude of the high-altitude cusp decreases as the IMF swings from North to South, that there is a pronounced dawn–dusk asymmetry at high-altitude associated with a dawn–dusk component of the IMF, and that at the same time there is also a pronounced dawn–dusk asymmetry at low-altitude. The simulations generate a feature that represents what has been called the cleft. It appears as a tail (when the IMF has a $B_y$ component) attached to the cusp, extending either toward the dawn flank or the dusk flank depending on the dawn–dusk orientation of the IMF. This one-sided cleft connects the cusp to the magnetospheric sash. We compare cusp geometry predicted by MHD simulations against published observations based on Hawkeye and DMSP data. Regarding the high-altitude predictions, the comparisons are not definitive, mainly because the observations are incomplete or mutually inconsistent. Regarding the low-altitude prediction of a strong dawn–dusk asymmetry, the observations are unambiguous and are in good qualitative agreement with the prediction.

**Keywords:** cusp geometry, MHD, simulation

**Abbreviations:** DMSP – Defense Meteorological Satellite Program; GSE – Geocentric Solar Ecliptic; GSM – Geocentric Solar Magnetic; HEOS – Highly Eccentric Orbiting Satellite; IMF – Interplanetary Magnetic Field; IMP – Interplanetary Monitoring Platform; ISEE – International Sun–Earth Explorers; MHD – Magnetohydro-dynamic

## 1. Introduction

To speak of the geometry of the dayside cusp one must differentiate between the cusp viewed as a dimple in the surface of the magnetopause and the cusp sensed as a weakening of the magnetic field or, equivalently, as a pool of magneto-sheath plasma within the magnetosphere. The first of these two ways to speak of the cusp refers to its surface geometry and the second to its volume geometry. In both cases the question of interest is how does cusp geometry – that is, its position and shape either as a surface expression or as a 3-D volume – change with variations in solar wind flow and magnetic field

parameters and with dipole tilt. Both surface geometry and volume geometry have been the subject of studies of measurements taken by the relatively few high-latitude, high-altitude (and, so, cusp-traversing) spacecraft (e.g., IMP 5, Hawkeye, HEOS 2, Prognoz 7, Magion 4, Polar, and Cluster II). As determined from statistical compilations of data thus accumulated, resolution of cusp geometry has gradually increased from representations based on a few cusp traversals, which characterized the discovery stage of cusp studies (Frank, 1971), to images now that can distinguish the change with season in the position and shape of the cusp dimple (Boardsen et al., 2000) and the cusp volume (Tsyganenko and Russell, 1999). Despite the increased resolution in images of the cusp now possible through statistical processing of accumulated measurements, some aspects of cusp geometry are still not represented. An example of such a missing aspect is a clear representation of how the dawn–dusk asymmetry of the cusp shape associated with the dawn–dusk component of the interplanetary magnetic field (IMF) changes with IMF clock angle. According to MHD simulations presented here, this dawn–dusk asymmetry in cusp shape is pronounced. It possibly clarifies the relation between the polar cusp and the polar cleft, which up to now has been unclear. In addition to filling in aspects of cusp geometry covered in few or no studies published up to now, we present here a series of images that illustrate how the volumetric geometry of the cusp and its ionospheric image change with IMF orientation. Thus this paper focuses on the volume aspect of cusp geometry (as opposed to the surface aspect). The results presented here are based on outputs of numerical simulations performed by a global MHD code called ISM (which stands for Integrated Space Weather Prediction Model), described in the next section.

## 2. The ISM code

As mentioned, the results presented here are based on numerical simulations performed by the Integrated Space Weather Prediction Model (ISM), which is a global-magnetospheric MHD numerical code, details of which are contained in White et al. (2001) and Sonnerup et al. (1990). Here we repeat a few of ISM's essential features. The code integrates the standard MHD equations over a volume that extends from 40 $R_E$ upwind from the Earth to 300 downwind, and 60 $R_E$ radially from an axis through the Earth parallel to the solar wind flow direction. Pertinent to the present application is ISM's treatment of the coupling between the magnetosphere and the ionosphere, which is unique among global MHD codes. Other codes project MHD parameters from some inner boundary down to the ionosphere where a separate code then computes the ionosphere response to the magnetospheric input and feeds the result back to the MHD code. ISM, on the other hand,

treats the magnetosphere and the ionosphere together as a single domain governed by a single set of equations. This single set of equations moves continuously from the ionosphere to the solar wind in the form of continuum mechanics equations appropriate to each domain. The advantage that this approach has in the present application is that whereas other codes can project cusp plasma parameters only down to the inner boundary of the MHD grid (usually an Earth-centered spherical surface with a radius between 3 and 4 $R_E$) ISM can project them continuously down to the ionosphere. This allows the cusp's image to be mapped at the ionospheric level.

The resolution of ISM's finite-difference grid varies from a few hundred kilometers in the ionosphere to several Earth radii at the outer boundary of the computational domain. At the magnetopause, resolution ranges from 0.2 to 0.8 $R_E$ ISM's numerical algorithm consists of a second order finite difference, scheme with partial donor cell method (PDM) terms (Hain, 1987) to provide numerical stability in regions containing large gradients. The Earth does not rotate in these simulations, Pedersen conductance is uniform and set to 6 S (except where otherwise stated), and Hall conductance is set to zero. Other parameters vary from run to run and are specified as needed.

## 3. Cusp geometry in the noon meridian plane

Figure 1 shows the cusp in the noon meridian plane as rendered in contours of electric current flowing into (solid contours) and out of (dashed contours) the figure plane. The solar wind and IMF parameters in this case are 350 km/s, 5 protons/cm$^3$, $2.2 \times 10^5$ K, and 5 nT straight South. Also shown is a projection onto the figure plane of a narrow strip of the last-closed-field-line surface. (Hereafter we refer to the last closed field line surface as the CFS, closed-field surface.) The CFS in this instance happens to contain an island shed by reconnection at the subsolar point. This feature is incidental to the discussion of cusp geometry given here. The CFS separates the volume of closed field lines (the volume embraced by its arch) from the volume of open field lines (above it in the figure) and the volume of IMF field lines that are not attached to the Earth (to the right of it).

Figure 1 illustrates basic aspects of cusp geometry such as the cusp as outlined by current contours. This is equivalent to the definition of the cusp given above – a weakening of the magnetic field owing to a pool of magnetosheath plasma within the magnetosphere – since the current is the plasma's diamagnetic current associated with the field weakening. Defined by the currents, the cusp has the shape of a funnel in a meridian plane. The geometrical core of the cusp, marked by an imaginary line that threads the "hole" through the funnel, lies within the volume of open field lines. A part of the cusp also lies within the volume of closed field lines, which in an MHD

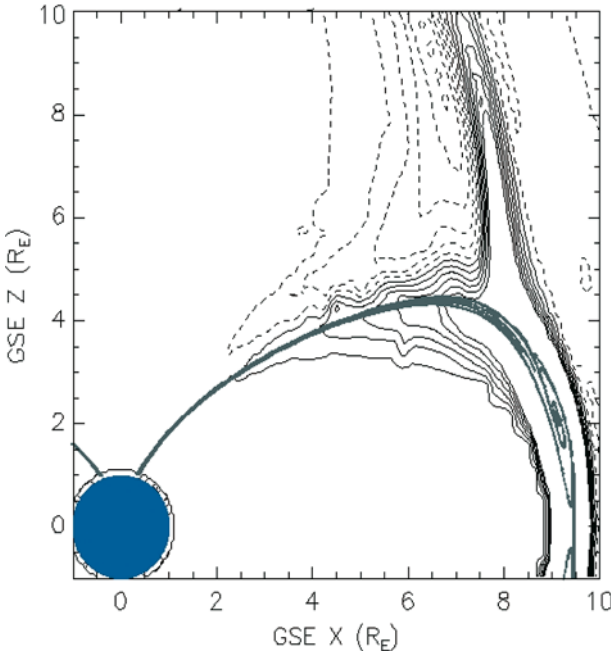


*Figure 1.* Contours in the noon meridian plane of the dawn (dashed lines) – to dusk (solid lines) component of electric current. Contour levels separated by 0.2 $nA/m^2$, starting at this level. Also shown are magnetic field lines on the last closed field line surface.

code probably reflects numerical diffusion. A third basic geometrical aspect that the figure illustrates is that the funnel of current that outlines the cusp is both deep at its tip and broad at its rim. That is, as defined by electrical current the cusp occupies a relatively large volume. Because the current that defines the cusp generates a magnetic field that weakens the field that would otherwise be there (i.e., it is a diamagnetic current), this aspect implies that the field within the cusp is in general weaker than that predicted by vacuum models of the magnetopause. (This statement is false, of course, near the topologically mandated null point or points in vacuum models where the field strength vanishes.) Tsyganenko and Russell (1999) called attention to the weak-field aspect of the cusp.

The presence of current within the cusp implies that there is also pressure-bearing plasma within the cusp. This pressure is seen in Figure 2 which uses contours of plasma pressure to compare the location and shape of the cusp as a function of IMF clock angle. The figure plane of the panels is the noon meridian plane. The solar wind speed, density, and temperature are the same as in Figure 1. A zero-IMF case is also shown. (Zero IMF is not the same as a vacuum magnetosphere since both cusp currents and tail currents are present.) A property to note that is common to all panels in Figure 2 is that

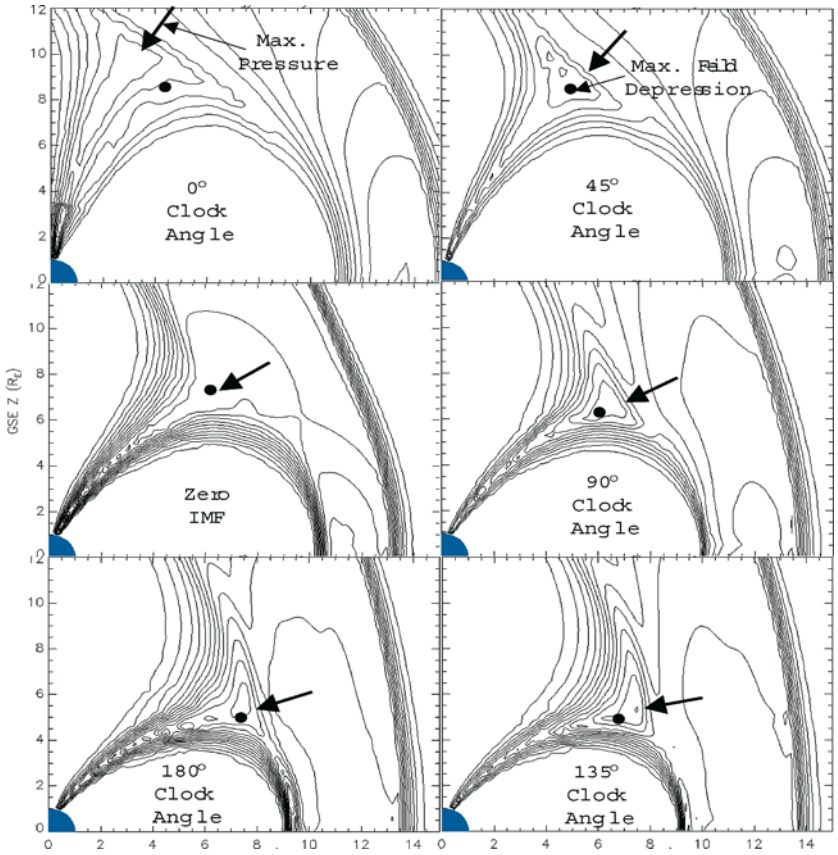


*Figure 2.* Contours in the noon meridian plane of the plasma pressure for the five cardinal IMF clock angles and zero IMF cases. Contour levels separated by 0.067 nP, starting at this level. Arrows point to the approximate location of the throat of the cusp. Black dots mark the point of maximum field strength depression in this plane.

the pressure contours extend down to the ionosphere, which illustrates the unique feature of the ISM code mentioned earlier; i.e., the absence of an inner boundary within which codes other than ISM do not compute plasma parameters. We use this feature later (Section 5) to mark the location and shape of the cusp in the ionosphere. Here it serves the purpose of producing realistic (i.e., non-truncated) contours. The black dot in each panel (labeled ''Max Field Depression'' in the 45° clock angle panel) shows where in the figure plane the difference between the dipole field strength and the computed magnetic field strength is maximum. This point marks the core of the cusp as far as the magnetic field is concerned. It lies very close to the maximum in plasma pressure (shown by the arrow) except for the 0° clock angle (northward IMF) case. One expects the maximum field strength depression to lie close to the maximum in plasma pressure so that the total pressure remains

locally roughly uniform. The offset between the maximum field strength depression and the maximum plasma pressure in the northward IMF case is curious but is perhaps related to the contours of field strength depression being quite broad in this case. That is the maximum depression is not very marked, so that the offset between the pressure maximum and the black dot appears more remarkable than the real difference in the depth of the depression at the two places perhaps warrants.

Figure 2 shows that the latitude of the mouth of the cusp decreases as the IMF rotates from straight North to straight South, illustrated here by rotations in 45° increments. (Ignore the zero IMF case for now.) This behavior is, of course, expected and has been inferred from analyses of data taken at high, low, and middle altitudes (see a review and new results on this topic from Magion 4 contained in Merka et al., 2002). Figure 2 shows the expected behavior explicitly in a full geometrical setting. The latitude of the center of the mouth of the cusp roughly doubles from about 35° to about 70° between straight South and straight North IMF directions. The northward IMF case has the weakest plasma pressure, 0.4 nPa versus 0.8 nPa in the southward IMF case. This difference in pressure is consistent with the cusp in the northward IMF case being farthest from the stagnation point (that is, it lies at the highest latitude). For comparison we note that in all these cases the solar wind ram pressure ($\rho V^2$, where $\rho$ and $V$ are mass density and flow speed, respectively) is very close to 1 nPa. (As an aside apropos of pressure, note that pressure has a secondary maximum in the cusp, the primary maximum being at the stagnation point as expected. The secondary maximum is a consequence of the cusp being a region of locally weak magnetic field. The plasma pressure must therefore have a local maximum so that the total pressure in the cusp (plasma plus magnetic) balance the adjacent total magneto-sheath pressure the magnetic part of which has no local minimum at the cusp. In this connection, note the absence of a local maximum of plasma pressure in the zero IMF case. Here the magnetic pressure in the magneto-sheath is zero, and it is also very weak in the cusp; therefore plasma pressure is approximately continuous across the cusp-magneto-sheath transition).

As previously mentioned the latitude of the mouth of the computed cusp shown in Figure 2 ranges from about 70° to 35°. How does this range compare with observations? In a statistical study of cusp traverses, identified by field-strength depressions seen in magnetometer data taken by the Hawkeye satellite, Farrell and Van Allen (1990) have given us what would appear to be an appropriate data set for comparison. Taking field-strength depressions greater than 30 nT to represent the heart of the cusp, Farrell and Van Allen (1990) found that the latitude of the cusp is lower when the IMF points southward than when it points northward (their Figure 17), in qualitative agreement with our Figure 2. They found that Hawkeye encountered the cusp over a latitude range from about 70° to about 45°.

(This statement refers to latitude relative to the magnetic equator, which is the appropriate latitude for comparison with Figure 2.) The comparison suggests that the high-latitude end of the computed range (70°) is about right but that, if the data are taken at face value, the low-latitude end might be too low (35° versus 45°). The authors note, however, that "Because of the geometric character of the Hawkeye orbit and consequent lack of coverage, the low-latitude edge of this [cusp] region is not defined, and thus may extend to latitudes even lower than those indicated." (Farrell and Van Allen, 1990, p. 20,951). The question therefore remains open regarding whether or not high-altitude cusp traversals might occur be low 45° latitude for southward IMF under typical solar wind conditions as Figure 2 predicts.

The issue of the latitudinal location of the high-altitude cusp under southward IMF is important to those who, approach magnetospheric studies through global MHD simulations. One other such study that has been published based on the Lyon–Fedder–Mobarry (LFM) code indicates that for southward IMF the high-altitude cusp resides above 50° latitude (Russell, 2000, Figure 11), considerably poleward of the cusp that the ISM code computes. Here is an opportunity for observers to help guide the development of global MHD codes by launching a project aimed at mapping the latitudinal position of the high-altitude cusp for southward IMF.

The issue goes beyond assessing the ability of MHD codes to get the latitude of the cusp right. Already there are indications that nature produces greater field-strength depressions in the cusp than MHD simulation predicts. Farrell and Van Allen found that among 70 cusp traversals in which the field-strength depression exceeded 30 nT (their criterion for identifying *bona fide* cusp traversals) there were 21 cases (30%) in which field-strength depression exceeded 60 nT. As we show in the next section, none of Figure 2's simulation runs produce field-strength depressions that exceed 60 nT. This comparison is, of course, merely statistical and so might be discounted as a fluke resulting from Hawkeye having encountered the cusp perhaps more than the statistically expected number of times when the solar wind was registering extreme conditions. During such times the maximum field-strength depressions found in the ISM runs illustrated in Figure 2 might not apply to the observations, and so it cannot be said that Hawkeye's having frequently observed bigger-than-predicted field-strength depressions necessarily disagrees with the simulations. But there is a case study based on Polar data in which the field in the cusp was substantially weaker than MHD simulation predicted for the position of Polar under appropriate solar wind conditions (Fritz et al., 2003). We have more to say about this observation in the next Section. We mention it here because it supports a straightforward (no statistical fluke) comparison with the Hawkeye data and so adds to an emerging impression that non-MHD

processes might be producing macroscale modifications of cusp geometry compared with MHD simulation.

## 4. Cusp geometry perpendicular to the sun–earth line

Figure 3 compares the shape of the cusp for different IMF clock angles in planes perpendicular to the solar wind flow direction, which for convenience we call the Sun–Earth line although in reality it is only approximately that. The distance along the Sun–Earth line that these planes lie from the Earth is not the same in each case. The distance has been chosen so that the plane contains the deepest field-strength depression. The contours in Figure 3 show field-strength perturbation, which is defined as the field strength computed by the MHD code minus the dipole field strength. Negative perturbations

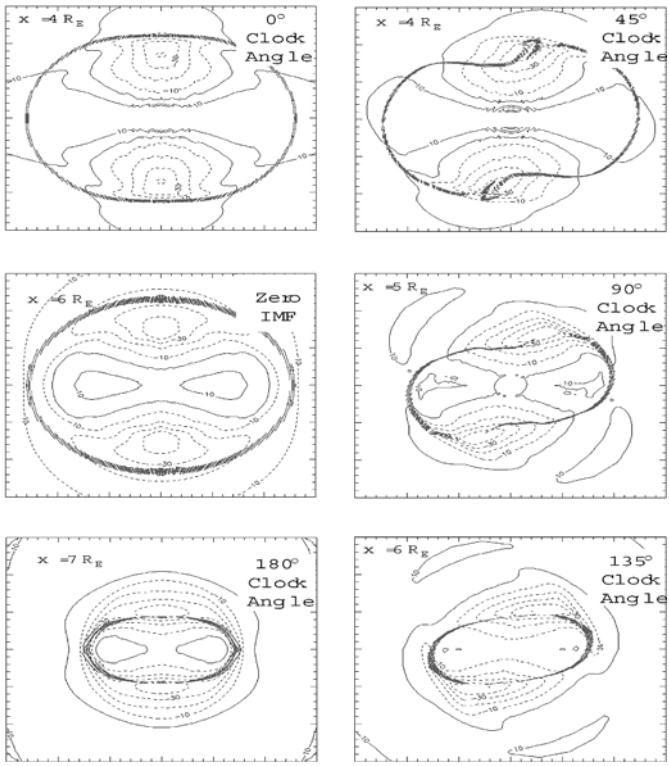


*Figure 3.* Contours of magnetic field strength perturbation (computed field strength minus dipole field strength) for the five cardinal IMF clock angles and zero IMF cases as seen from the Sun. Figure planes cut through the point of maximum field strength depression in each case. A ''picket fence'' of short field line stubs in each panel marks the intersection of the last closed field line surface with the figure plane.

(indicated with dashed contours) therefore correspond to field-strength depressions. Besides contours of field-strength perturbations, Figure 3 also shows where the CFS (last-closed-field-line surface) penetrates the figure planes. The CFS is marked by short segments of field lines that are centered on the plane and are seen projected onto it. Magnetic field lines that cut the planes within the areas that the CFS circumscribes are closed; outside these area they are either open or IMF field lines that are unattached to the Earth. Figure 3 contains perhaps this paper's main contribution to the study of cusp geometry in the form of images that show explicit dawn–dusk asymmetries as seen in the right-hand panels.

Before considering these asymmetries, however, we point out a few more general aspects of cusp geometry that can be seen in the symmetrical, left-hand panels. Note first of all that positive perturbations dominate the equatorial latitudes and negative perturbations the high latitudes. We see here the trademark signature of the Chapman–Ferraro current system; it strengthens the field at low latitudes and weakens it at high latitudes. Although the Chapman–Ferraro model applies strictly to a vacuum magnetosphere and the case of zero IMF (see Siscoe, 1988 for a review of this and related models), its influence continues to dominate the pattern of field-strength perturbations even in the presence of plasma and a non-zero IMF. (In MHD simulation when the IMF becomes strongly southward, however, the Chapman–Ferraro pattern is replaced by one in which the field-strength perturbation is negative everywhere on the dayside, that is, there is no equatorial band of positive perturbation, Siscoe et al., 2002b). The high latitude band of negative perturbations in each hemisphere is, of course, the domain of the cusp.

The width of the cusp as measured by the dawn–dusk extent of the −30 nT contour (i.e., a field strength depression of 30 nT) increases as the IMF swings from North to South. It is about 3 $R_E$ wide for the northward case and about 10 $R_E$ wide for the southward case. In terms of longitudes, however (which takes account of the different distances of the figure planes from the Earth) these dawn–dusk widths correspond to 48° and 78°, respectively. The North–South extent of the cusp does not vary as much with IMF orientation (from about 3 $R_E$ to 4 $R_E$). The fraction of the cusp that is on closed field lines varies from essentially 100% for the northward IMF case to virtually nil for the southward IMF case. Conversely the fraction that is plasma mantle goes from virtually nil to essentially 100% over the same 180° rotation of IMF clock angles. In qualitative terms, these properties concerning the relative amounts of plasma in the plasma mantle agree with observations (Paschmann et al., 1976). In the respects just mentioned, the zero IMF case unsurprisingly resembles the northward IMF case. We should also note that the panels in Figure 3 refer to idealized situations in which the IMF has no Sun–Earth component and the

geomagnetic dipole is perpendicular to the solar wind flow direction. Departures from these idealizations would probably change the fractions of the cusp on open and closed field lines quantitatively but not qualitatively.

We may usefully compare these general properties, which are independent of the dawn–dusk component of the IMF, against the statistical study of Hawkeye magnetometer data that Farrell and Van Allen (1990) carried out and to which we referred in the previous Section. Farrell and Van Allen (1990) did not sort their data into separate positive clock angle (duskward IMF) and negative clock angle (dawnward IMF) bins, which has the following important impact on comparing the MHD results with the Hawkeye data. Assuming that the IMF was about equally likely to be dawnward or duskward when Hawkeye traversed the cusp, the mixing of dawnward and duskward cases mentioned earlier means that Figure 3's asymmetries in the right hand panels would be symmetrized in the data by reflection in the noon meridian plane. The Hawkeye orbit had good longitudinal coverage (unlike its latitudinal coverage at the altitude of the magnetopause), so there should be no artificial cutoffs in the dawn–dusk direction (which Figure 3 addresses). Farrell and Van Allen (1990) found that, as Hawkeye swept from dusk to dawn through noon, it encountered cusp-like magnetic field depressions throughout most of this range, but the depressions were deepest around the noon meridian, a property which Figure 3's left hand panels also display. Hawkeye encountered the cusp most often around the noon meridian, as one would naturally expect. The longitude sector within which Hawkeye was more likely than not to intercept the cusp was about 100° wide, approximately centered on noon (but not exactly). This topic comes up again in more detail below.

Turning now to Figure 3's right-hand panels and their dawn–dusk asymmetries, we consider first the shape of the CFS and its relation to the cusp. We have already mentioned that the cusp crosses the CFS from the domain of closed field lines to the domain of open field lines as the IMF swings from North to South. Figure 3's right hand panels show intermediate stages of this migration. When the IMF has a northward and a duskward component (exemplified by the 45° clock angle case), the CFS is marked by an interesting convolution where the field is weakest. In fact the CFS passes directly through the point of weakest field (4 nT). The convolution of the CFS just noted for the 45° clock angle case is absent in the 90° and 135° clock angle cases (though there is a vestige of it in the 90° case). Yet in these cases the CFS still passes very near the point of weakest field, notwithstanding the fact that most of the cusp lies outside the CFS.

We consider next the very marked asymmetries in the geometry of the perturbation contours in Figure 3's right hand panels. The asymmetry that is most obvious is the dawn–dusk shift away from noon of the "centers" of the

contours-duskward in the northern hemisphere and dawnward in the southern hemisphere. These shifts amount to about 1.5 $R_E$, 2.5 $R_E$, and 3.0 $R_E$ for the 45°, 90°, and 135° clock angle cases, respectively. Besides dawn–dusk shifts, the contours have acquired "tails" on their terminator sides (i.e., the side opposite the noon meridian). These tails carry the cusp's field-strength depression toward the flanks of the magnetosphere.

The tail-like character of the extension of the field-strength depressions toward the flanks is better seen in Figure 4, which shows field-strength perturbation contours for the 90° clock angle case in a plane that lies parallel to the equatorial plane but 7 $R_E$ North of it. The contours resemble tadpoles with their distinctive tadpole tails. The tails' one-sided extensions toward the flanks at high latitudes that one sees in Figures 3 and 4 suggests that they are interior expressions of the magnetospheric sash (White et al., 1998). The magnetospheric sash is a weak-field feature that is usually discussed as a surface feature of the CFS or as a product of anti-parallel merging, which again stresses its surficial character (Siscoe et al., 2002a). Here we see its relation to the entire, three-dimensional weak field volume associated with the cusp. The tails that we have been discussing possess an

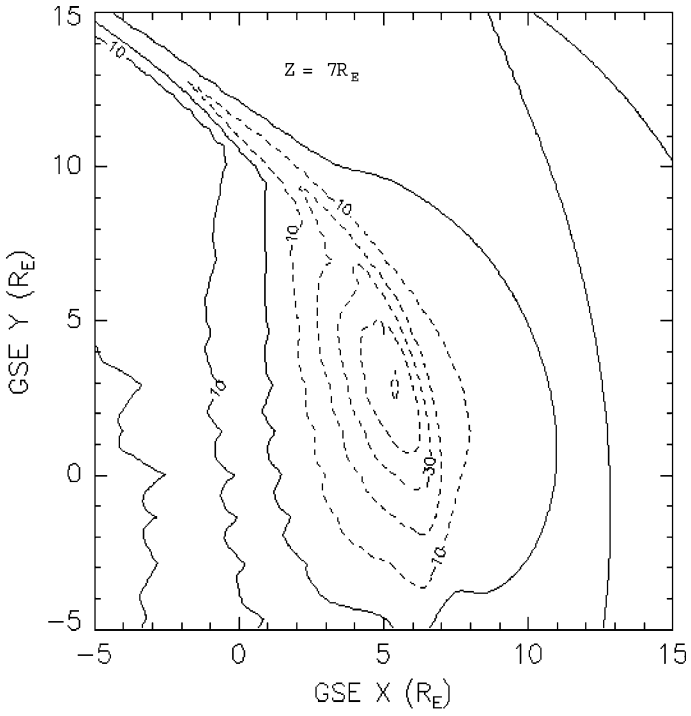


*Figure 4.* Contours of field strength perturbation for the 90° clock angle case. The figure plane is parallel to the equatorial plane and 7 $R_E$ North of it.

aspect that we associate with the cleft. (We use the words "cusp" and "cleft" in a non-formal way. Cusp to us means that part of the feature that has a roughly conical shape (that is, the body of the aforementioned tadpole) and cleft refers to its tail-like extension toward the flanks. This distinction does not work well for the 180° clock angle case where the tail of the tadpole in Figure 3 is as thick its body.) An important difference between the tails of Figures 3 and 4 and the cleft as usually conceived is that the cleft is assumed to extend about equally dawnward and duskward from the cusp in each hemisphere, whereas the tails in the figures are one sided, that is, either they extend toward the dawn flank or the dusk flank, but not in both directions in the same hemisphere. The northern cusp (to pick one) has a duskward tail when the IMF points duskward (clock angle lying between 0° and 180°) and a dawnward tail when the IMF points dawnward (clock angle lying between 180° and 360°). To summarize this discussion, Figure 4 displays for the first time the geometrical relations between the cusp, the cleft, and the sash.

The sash turns out to be a one-sided cleft, which itself turns out to be a tail-like appendage of the cusp. Said differently, the sash and the cusp are attached by the cleft, which is an interior, one-sided (and, so, tail-like) extension of the cusp.

Let us attempt to become quantitative by comparing the MHD results against statistical results based on Hawkeye data pertaining, to the longitudinal width of the cusp. We do this over procedural objections that might be raised against MHD results referring to steady solar wind conditions unlike Hawkeye results. We get around this mismatch of conditions by bracketing the Hawkeye results between two extreme ways of statistically representing the MHD results. To proceed. If we take the −30 nT contour in Figure 4 to represent the outline of the cusp, as before, we find that for this 90° clock angle case the longitude of the cusp relative to the noon meridian extends asymmetrically over about 64° from 4° dawnward to 60° duskward. This is a remarkably pronounced asymmetry also apparent in the LFM code (Russell, 2000, Figure 13).

For the purpose of comparing the MHD results against Hawkeye data, it is useful to perform the same measurements of longitudinal limits of the −30 nT contour relative to noon for the other clock angle cases. Table I shows the result. The column labeled "Clock Angle" combines situations in which the IMF points dawnward and duskward. The row labeled "45° and 315°", for example, refers to the upper-right panel of Figure 3, which gives the geometry for the 45° clock angle IMF orientation and its mirror-symmetric image. The columns in Table I labeled "Minimum longitude" and "Maximum longitude" give the longitudes to which the −30 nT contours extend relative to noon. (The limits for the 90° clock angle case differ slightly from the ones that we gave above that pertain to Figure 4 (that is, 4° and 60°)

TABLE I

| Clock angle | Minimum longitude | Maximum longitude | Percentage occurrence |
|---|---|---|---|
| 0° | 24°24′ | 17°48′ | 5.2% |
| 45° | 315° | 380° | 22.7% |
| 90° | 270° | 9°65′ | 45.5% |
| 135° | 225° | 13°62′ | 21.9% |
| 180° | 39° | 39°2.7′ | 5.1% |

As determined with MHD simulations, longitudes relative to noon of the dawnward and duskward extents of the 30 nT field-strength depression contours (representing the borders of the cusp) for the clock angles listed in column 1. The last column gives the percentage of time determined from ISEE 3 data that the IMF points within/pm 22.5° of the listed clock angles.

which were illustrative only. To construct Table I we searched a range of planes to find the absolute limits in each case.) The 0° and 180° clock angle cases are symmetric relative to noon, so the minimum and maximum limits are the same.

The last column in Table I gives the percentage of time that the direction toward which the IMF points lies within 45° sectors centered on the clock angles listed in the first column. To compute these percentages we used hourly averages of ISEE 3 IMF data available from the National Space Science Data Center (covering August 1978 through the end of 1981). We see the influence of the Parker spiral to coil the IMF in the dawn–dusk direction, thereby giving the IMF a strong tendency to lie in the dawn–dusk direction and so in the 45° and 135° sectors in Table I. These percentages refer to clock angles in the GSE coordinate system instead of the GSM coordinate system, which might be more appropriate for this study. The effect of using GSM coordinates instead of GSE coordinates would be to reduce somewhat the percentage in the 45° and 135° row and increase it somewhat in the other rows, that is, to reduce the peak and increase the wings in the percentage distribution. Still the correction would not change the general conclusion reached by comparing the numbers in Table I against Hawkeye data, which we now proceed to do.

Figure 5 compares statistics derived from Table I against corresponding statistics compiled from Hawkeye data. The thick line in the figure labeled "Hawkeye Data" records the percentage of Hawkeye orbits in 10° longitude sectors that intercepted the cusp (from Farrell and Van Allen, 1990, Figure 14). The thin line labeled "MHD Simulation: Fixed IMF$B_y$" gives the probability (as a percentage) of encountering the cusp as determined from the angles and percentages listed in Table I. This line gives the percentage assuming that the IMF is equally likely to be pointing dawnward or duskward when a satellite encounters the cusp, but that it stays fixed in that

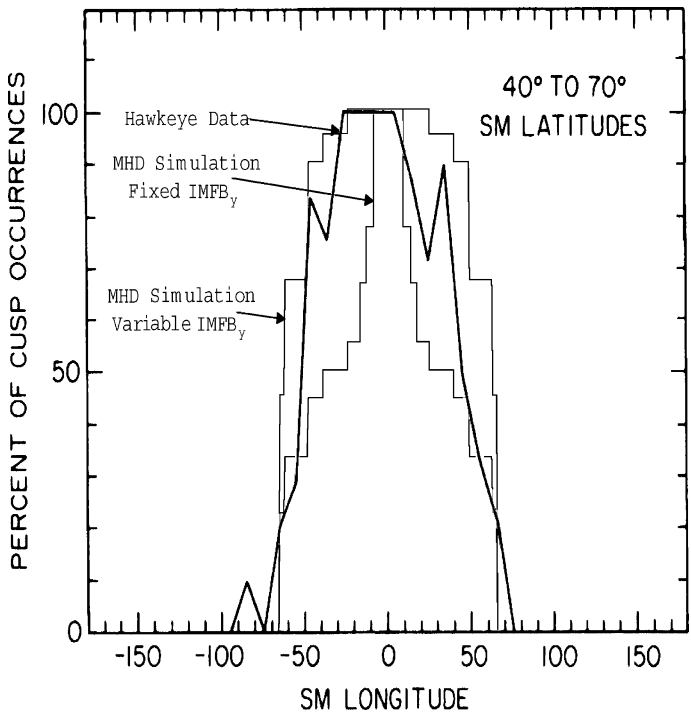


*Figure 5.* Probability of encountering the cusp (defined as a field-strength depression of 30 nT or more) as a function of longitude relative to noon. Thick line (from Farrell and Van Allen, 1990) is based on Hawkeye data. Thin lines give maximum and minimum probabilities based on MHD simulations and statistics of IMF pointing directions.

orientation throughout the satellite's passage through the cusp region. Formally, this line is a plot of the function

$$P(\phi) = p(0)\phi(0) + p(45)[\phi_{\min}(45) + \phi_{\max}(45)]/2 + p(90)[\phi_{\min}(90) + \phi_{\max}(90)]/2 + p(135)[\phi_{\min}(135) + \phi_{\max}(135)]/2 + p(180)\phi(180) \quad (1)$$

where $P$ is the probability of a cusp encounter at longitude $\phi$; $p(0)$, $p(45)$, etc. are the numbers listed in the "Percentage occurrence" column for 0°, 45°, etc., clock angles; and $\phi(0)$, $\phi(45)$, etc., are the corresponding numbers listed in the two longitude columns of Table I. The factor 12 in such terms as $[\phi_{\min}(45) + \phi_{\max}(45)]/2$ indicates that the minimum and maximum longitudinal extents of the cusp contribute equally in an "either-or" sense to the total probability. The "either-or" condition corresponds to the IMF being dawnward or duskward throughout the satellite's traversal of the cusp region. This is an extreme assumption since the IMF can change from pointing dawnward to pointing duskward, or vice versa, while the satellite is

in the region of the cusp. Then the appropriate longitudinal width of the cusp to use in Table I is the maximum angle (column 3) as we now do. The thin line labeled "MHD Simulation: Variable IMF$B_y$" represents the opposite extreme assumption, that is, that the IMF changes its dawn–dusk orientation during every satellite pass through the cusp region. This is probably closer to the real situation for Hawkeye, since on average (based on the same ISEE 3 data used to compile Table I) the IMF changed its dawn–dusk orientation about every 8 h, and Hawkeye typically spent more than 10 h traversing the cusp region. Formally then, the "Variable IMF$B_y$" line is a plot of the function.

$$P(\phi) = p(0)\phi(0) + p(45)\phi_{\max}(45) + p(90)\phi_{\max}(90) + p(135)\phi_{\max} + p(180)\phi(180) \quad (1)$$

The "Variable IMF$B_y$" line fits the Hawkeye line better than the "Fixed IMF$B_y$" line. We could probably make the fit arbitrarily close by combining the two MHD-derived lines with appropriate weighting factors that favor the "Variable IMF$B_y$" line. We would go beyond what the comparison allows, however, to conclude that the apparent agreement just noted strongly confirms the MHD results. The problem is that the agreement is statistical instead of a one-to-one matching of actual events.

An alternative reading of Figure 5, for example, is simply that the cusp is about 100° wide in longitude nearly all of the time (80%), but that its width is weakly modulated by the North–South component of the IMF. This reading contradicts the marked dawn–dusk asymmetry seen here in Figures 3 and 4. In support of this alternative reading, there is a case study based on Polar magnetometer data that exhibits an interval of strong field-strength depression on the side relative to noon opposite to where it ought to be according to Figure 3 (Fritz et al., 2003). Citing this and other similar cases, these authors assert that the cusp is typically quite broad in longitude and by and large independent of the IMF dawn–dusk orientation. The relation between observations and MHD simulation results remains ambiguous, however, if we consider a report by Zhou et al. (2000). This paper concludes from a statistical study also based on Polar measurements that the center of the cusp as identified in magnetometer data at high altitude shifts dawnward and duskward relative to noon in response to the dawn–dusk component of the IMF in the sense of Figure 3.

Russell (2000) repeats this result and notes that the shifts can exceed 1 h of local time when the dawn–dusk component of the IMF is 6 nT or greater. Crooker et al. (1987) arrived at virtually the same result from an analysis of data obtained by the ISEE 1 and 2 and HEOS satellites as they crossed the magnetopause. Eastman et al. (2000), on the other hand, failed to detect such

shifts in a statistical analysis of Hawkeye data. The reason for these disparate results is unclear, but it might be related to different authors using different criteria to identify the cusp. In the following section we make a similar comparison between the results of MHD simulation and data taken at low altitude. Here, unlike the high-altitude comparison just considered, there is unambiguous agreement between the asymmetry seen in the model and in the data.

There is another aspect of Figure 5 that can be compared with MHD results: the noticeable dawnward shift away from noon of the center of the "Hawkeye Data" line. The MHD-derived lines show no such shift as their manner of construction, which is in itself dawn–dusk symmetric, precludes it. Adding a component of the IMF parallel to the Sun–Earth line in the MHD simulation, however, produces a shift like the one observed, as Figure 6 illustrates. This figure shows a situation corresponding to the 90° clock angle panel in Figure 3, except that a Sun–Earth component has been added to give the IMF a 45° orientation relative to the Sun–Earth line in the sense predicted by the Parker spiral. The IMF strength remains 5 nT, however. The

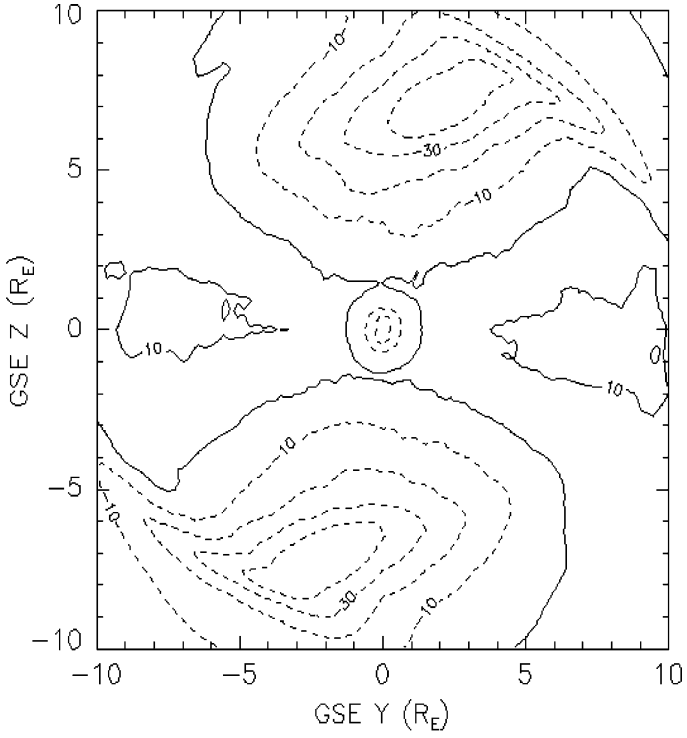


*Figure 6*. Same as the 90° clock angle panel in Figure 3 except here there is a solar-wind aligned component of the IMF to give it a Parker spiral orientation.

pattern of the perturbation contours is very similar in Figures 3 and 6, except that in Figure 6 they are extended dawnward relative to noon.

We see this in Figure 6 itself by comparing the tails of the contours in the northern hemisphere against corresponding ones in the southern hemisphere. The shift is greatest for the weak-perturbation contours (note, for example, the −10 nT contour), but the effect is evident also in the tails of the two −30 nT contours, which define the cusp in the construction of Figure 5. Thus the shift in the Hawkeye data seen in Figure 5 probably has its origin in a dawn–dusk asymmetry, of the magnetosphere that is induced by the solar-wind aligned component of the IMF in its dominantly Parker spiral configuration.

To conclude this section, although MHD simulations reveal striking dawn–dusk asymmetries in cusp geometry at high altitudes, it remains unclear whether such simulations capture this geometry correctly. Regarding a dawn–dusk asymmetry at high altitudes, the few directly relevant observations can be (and have been) interpreted as favoring a longitudinally wide cusp whose width is mostly independent of the dawn–dusk orientation of the IMF. The lack of certainty regarding whether cusp geometry is sensitive to the dawn–dusk component of the IMF should be short lived, we optimistically predict, as more case studies are made that compare high-altitude cusp encounters against each other with the same definition of the cusp, and as more case studies are made that compare high-altitude cusp encounters against corresponding MHD simulations. Case studies should be supplemented with statistical studies of the longitudinal extent of cusp-like field-strength depressions at high altitudes. In such studies encounters should be separated into bins for dawnward and duskward pointing IMF. This statistical approach would seem to be the most direct way to test the prediction of MHD simulation that the cleft is one sided, extending either dawnward or duskward away from the cusp depending on the dawn–dusk orientation of the IMF.

## 5. Cusp geometry at ionospheric altitude

As previously mentioned, a novel feature of the ISM MHD code is its ability to compute plasma parameters continuously from the solar wind to the ionosphere. This ability was illustrated in Figure 2 by the plasma pressure contours that extend from the magneto-sheath through the cusp down to the Earth without a break. Thus we are able to map the geometry of the cusp at ionospheric altitude. Figure 7 shows such a map for the 90° clock angle case. This is the most interesting of the five clock angle cases in Figure 3 on account of its being the most lopsided. The lines in Figure 7 are contours of constant number density of protons that have entered the magnetosphere through the cusp from the solar wind. (Besides its ability to compute plasma

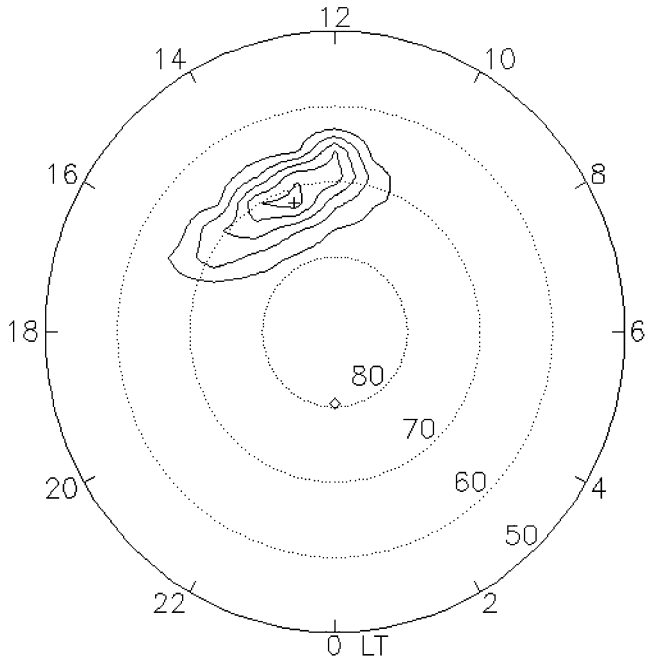


*Figure 7.* Contours of cusp ion density just above the ionospheric "plane" at 2000 km altitude (representing the low-altitude cusp) for the 90° clock angle case. Contour levels separated by 0.5 ions/cm$^3$, starting at this level.

parameters down to the Earth, the ISM code also has the ability to track plasma from various origins. Here we use this ability to isolate plasma of solar wind origin that has reached low altitude.) The altitude of the contours in this figure is 2000 km, which is above the ionosphere since at much lower altitudes the solar wind density goes to zero, being stopped by the ionosphere. The contour levels run from a minimum of 0.5 ions/cm$^3$ to a maximum of 2.5 ions/cm$^3$ (the peak density value is 2.75 ions/cm$^3$). Thus this island of contours can be taken to represent the cusp geometry at low altitudes. The number density contours of cusp ions in Figure 7 display the same marked dawn–dusk asymmetry seen in the right hand panels of Figures 3 and in Figure 4, which pertain to the high-altitude cusp. The asymmetry is therefore seen to be as strong at low altitude as at high altitude. The cusp contours extend about 5 h of local time in the East–West direction, from about 1 h before noon to about 4 h after noon. The peak of the density lies about 1.5 h duskward of noon.

With respect to observations against which to compare the MHD simulation results, the situation is better at low altitude than at high altitude, as particle data from the DMSP satellites (with which to identify cusp features) are plentiful. A compilation of data relevant for comparison (in that the data

are sorted into separate bins for dawnward and duskward pointing IMF) appears in Newell et al. (1989). From a statistical analysis of about 1000 DMSP passes through the cusp region when the IMF was pointing in the duskward direction (the proper direction for comparing with Figure 7), these authors have found that the probability of encountering the cusp is highly asymmetric relative to noon in the sense that agrees with Figure 7. In their data, the probability of encountering the cusp shows two, roughly equal local maxima, one at noon and the other about 1.5 h after noon. The probability falls off rapidly dawnward of the noon peak but more slowly duskward of the local afternoon peak. Their findings are in qualitative agreement with the geometry of the cusp contours shown in Figure 7. Certainly the gross asymmetry is the same in terms of its magnitude and its direction.

A published event study also provides a data comparison with Figure 7 (Maynard et al., 2002). During the study event the IMF pointed dawnward, and thus MHD simulation would predict that the northern cusp should shift dawnward. The study indeed found a dawnward shift of nearly 1 h local time of the low-altitude cusp and an East–West extent of the cusp of around 4 h. Both the shift and the width of the cusp in this case agree with Figure 7 as well as we could expect (after a requisite reflection in the noon meridian plane). The Maynard et al. (1997) study combined particle data from DMSP 11 (which threaded the East–West width of the cusp) with optical measurements from Svalbard. Thus the geometry of the cusp was well revealed in the data. The agreement between the MHD result (Figure 7) and the observations in both the statistical study (Newell et al., 1989) and the event study (Maynard et al., 1997) are unambiguously good (in contrast to the high-altitude comparisons). Since the low-altitude situation is a reflection of the high-altitude situation, we expect that further analyses of high-altitude data will eventually uncover a strong dawn–dusk asymmetry coordinate with that found at low-altitude.

## 6. Summary

This paper has presented "images" obtained from MHD simulations which reveal aspects of macroscale cusp geometry that MHD simulation is particularly well suited to investigate. We have focused on the geometry of the volume of the cusp (marked by the presence of magneto-sheath plasma and associated field-strength depression) as distinct from the geometry of its surface (marked by a dimple in the magnetopause). We have concentrated mainly on how the following aspects of macroscale cusp geometry vary with IMF orientation:

- the latitude of the high-altitude cusp (it decreases as the IMF swings from North to South, Figure 2),

- a high-altitude dawn–dusk asymmetry associated with a dawn–dusk component of the IMF (it is very pronounced, Figures 3 and 4), and
- a low-altitude dawn–dusk asymmetry associated with a dawn–dusk component of the IMF (it, too, is very pronounced, Figure 7).

We have compared the MHD simulation results presented here with observations with mixed results. Regarding results pertaining to the high-altitude latitude of the cusp, the observed latitude is smaller on average when the IMF has a southward component than when it has a northward component, in qualitative agreement with the MHD simulations. But observations have not yet been processed to tell whether the equatorward shift of the cusp for southward IMF is as great as MHD simulation predicts (Figure 2). Moreover, comparisons made in connection with this part of the work suggest that the cusp is more pronounced (in the sense of possessing greater field-strength depressions) than MHD simulations predict. Regarding results pertaining to a high-altitude dawn–dusk asymmetry associated with a dawn–dusk component of the IMF, observations are ambiguous, some reporting such an asymmetry and some not.

On the modeling side, the results are interesting in that they reveal the relation between the cusp, the cleft and the magnetospheric sash. The geometrical relation between these features has been previously unclear. Perhaps the result of greatest significance in this part of the work is the prediction that the cleft is one sided. Either it extends duskward from the cusp (as in Figure 4) or it extends dawnward from the cusp, but not in both directions at once as in the usual conception of the cleft. Which direction it extends (dawnward or duskward) depends on whether the IMF points dawnward or duskward. Regarding results pertaining to a low-altitude dawn–dusk asymmetry associated with a dawn–dusk component of the IMF, here the observations are unambiguous and in reasonable agreement with the MHD predictions.

## Acknowledgements

The work was supported by grants from NSF's Upper Atmospheric Section of the Atmospheric Sciences Division and NASA's SR&T and Sun–Earth Connections Theory Programs. The Integrated Space Weather Model was developed by Mission Research Corporation under contract from the Defense Threat Reduction Agency.

## References

Boardsen, S. A., Eastman, T. E., Sotirelis, T., and Green, J. L: 2000. An Empirical Model of the High Latitude Magnetopause, *J. Geophys. Res.* **105**, 23,193–23,219.

Eastman, T. E., Boardsen, S. A., Chen, S.-H., Fung, S. F., and Kessel, R. L: 2000. Configuration of High-latitude and High-altitude Boundary Layers, *J. Geophys. Res.* **105**, 23, 221–23, 238.

Farrell, W. M., and Van Allen, J. A: 1990. Observation of the Earth's Polar Cleft at Large Radial Distances with the Hawkeye 1 Magnetometer, *J. Geophys. Res.* **95**, 20, 945–20, 958.

Frank, L. A: 1971. Plasma in Earth's Polar Magnetosphere, *J. Geophys. Res.* **76**, 5202–5219.

Fritz, T. A., Chen, J. and Siscoe, G. L.: 2003, 'Energetic Ions, Large Diamagnetic Cavities, and Chapman–Ferraro Cusp', *J. Geophys. Res.* **108**(A1), 1028, doi: 10.1029/2002JA009476.

Hain, K: 1987. The Partial Donor Cell Method, *J. Comp. Phys.* **73**, 131 .

Merka, J., Afrnkov, J. and Nemecek, Z.: 2002, 'Cusp-like Plasma in High Altitudes: A Statistical Study of the Width and Location of the Cusp from Magion-4', *Ann. Geophys.* **20**, 311–320.

Crooker, N. U., Berchem, J., and Russell, C. T: 1987. Cusp Displacement at the Magnetopause for Large IMF Y Component, *J. Geophys. Res.* **92**, 13,467–13,471.

Siebert, K. D., Weimer, D. R., Wilson, G. R., and White, W. W: 2002. How Wide in Magnetic Local Time is the Cusp? An Event Study, *Planet. Space Sci.* **50**, 461–471.

Newell, P. T., Meng, C.-I., Sibeck, D. G., and Lepping, R: 1989. Some Low Altitude Cusp Dependencies on the Interplanetary Magnetic Field, *J. Geophys. Res.* **94**, 8921–8927.

Newell, P. T., and Meng, C.-I: 1992. Mapping the Dayside Ionosphere to the Magnetosphere According to Particle Precipitation Characteristics, *Geophys. Res. Lett.* **19**, 609–612 .

Paschmann, G., Sckopke, N. and Grnwaldt, H.: 1976, 'Plasma in the Polar Cusp and Plasma Mantle', in B. M. McCormac (ed.), *Magnetospheric Particles and Fields*, D. Reidel Publishing Company, pp. 37–53.

Russell, C. T: 2000. The Polar Cusp, *Adv. Space Res.* **25**(7/8 6), 1413–1424.

Siscoe, G. L.: 1988, 'The Magnetospheric Boundary, in T. Chang, G. B. Crew and J. R. Jasperse (eds.), *Physics of Space Plasmas* (1987), Scientific Publishers, Inc.

Siscoe, G. L., Crooker, N. U., Erickson, G. M., Sonnerup, B. U. Ö., Siebert, K. D., Weimer, D. R., White, W. W. and Maynard N. C.: 2000a, 'Transpolar Potential Saturation: Roles of Region 1 Current System and Solar Wind Ram Pressure, *J. Geophys. Res.* **107**(A10), 1321, doi:10.1029/2001JA009176, 2002.

Sonnerup, B. U., Siebert, K. D., White, W. W., Weimer, D. R., Maynard, N. C., Schoendorf, J. A., Wilson, G. R., Siscoe, G. L., and Erickson, G. M: 1990. Simulations of the Magnetosphere for Zero IMF: The Groundstate, *J. Geophys. Res.* **106**, 29,419–29,434.

Tsyganenko, N. A., and Russell, C. T: 1999. Magnetic Signatures of the Distant Polar Cusps: Observations by Polar and Quantitative Modeling, *J. Geophys. Res.* **104**, 24,939–24,955.

White, W. W., Siscoe, G. L., Erickson, G. M., Kaymaz, Z., Maynard, N. C., Siebert, K. D., Sonnerup, B. U. Ö., and Weimer, D. R: 1998. The Magnetospheric Sash and Cross-tail S, *Geophys. Res. Lett.* **25**, 1605–1608.

White, W. W., Schoendorf, J. A., Siebert, K. D., Maynard, N. C., Weimer, D. R., Wilson, G. L., Sonnerup, B. U.Ö., Siscoe, G. L., and Erickson, G. M.: 2001. MHD Simulation of Magnetospheric Transport at the Mesoscale, in Song. Paul, Singer. Howard J., and L. G. Siscoe (eds.), *Space Weather, Geophysical Monograph Series, Vol. 125*, American Geophys Union, Washington, DC, pp. 229–240.

Zhou, X. W., Russell, C. T., Le, G., Fuselier, S. A., and Scudder, J. D: 2000. Solar wind control of the cusp at high altitude, *J. Geophys. Res.* **105**, 245–251.

Surveys in Geophysics (2005) 26: 409–414
DOI 10.1007/s10712-005-1904-2 © Springer 2005

# THE MAGNETOSPHERIC CUSPS: A SUMMARY

T. A. FRITZ and Q. G. ZONG
*Center For Space Physics, Boston University, Boston, MA, 02215, USA*
*E-mail: fritz@bu.edu*

(Received 1 January 2004; Accepted 30 April 2004)

**Abstract.** The polar cusps of the magnetosphere are key regions for the transfer of mass, momentum, and energy from the solar wind into the magnetosphere. Understaning these key regions and the dynamical interactions that occur there are fundamentally important to determining the physical nature of the magnetosphere. In this paper we try to summarize many of the conclusions reached in the papers of this special issue emphasizing the present concepts and definition of the cusp, what variations could be temporal structures and what could be spatial structures. We address the need for further measurements and the role of present and planned projects to address these needs.

**Keywords:** boundary, cusp, electron, energetic ions, magnetosphere, reconnection

**Abbreviations:** DMSP – Defense Meteorological Satellite Program; LLBL – Low Latitude Boundary Layer; TBL – Turbulent Boundary Layer; IMF – Interplanetary Magnetic Field; FTE – Flux Transfer Event; MHD – Magnetohydrodynamics; MLT – Magnetic Local Time; RAPID – Research with Adaptive Particle Imaging Detectors

## 1. Cusp definition

This special issue on the magnetospheric cusps has attempted to present a collection of papers to focus on the question ''What is the cusp?'' In particular these papers have addressed the structure and dynamics of the cusp using a variety of satellite data sets and theoretical approaches. An unstated question in the Introduction concerned the role of the northern and southern cusps in the functioning of the magnetosphere: ''Do we really understand the role of these two regions on the dayside where the solar wind plasma is able to penetrate well inside the magnetosphere?'' The cusps have been shown in these papers to be regions of turbulent magnetic fields filled with shocked solar wind plasma and, occasionally, with plasma of ionospheric origin. This paper is intended as a coherent summary of the results covered in this special issue on the magnetospheric cusp, summarizing some of details presented in the papers found in this volume.

The definition of the cusp used by MHD simulation (Siscoe et al.) is "a weakening of the magnetic field owing to a pool of magnetosheath plasma within the magnetosphere – since the current is the plasma's diamagnetic current associated with the field weakening" or in concept as "a region of open field lines extending poleward from the open/closed boundary (which is tied to the dayside merging region on the magnetopause) to where particles no longer are able to directly enter" (Maynard). However, there is not always a clear distinction between such a conceptual definition, some observational identifications, and actual determinations of when the cusp is really being observed by a given spacecraft. The primary and the most widely used method of identifying the cusp is by means of a combination of plasma and magnetic field observations, although just plasma or magnetic field measurements have been used in the past in some cases. Using both sets of observational data the cusp has been defined as a high latitude region with a population of particles of shocked solar wind energies and density somewhere within or near the local noon sector together with turbulent or depressed local magnetic fields (Dunlop et al.; Pu et al.; Lavraud et al.; Zong et al.).

On the terminology of the region in question, the "cusp" versus "cleft" argument seems to be solved. The "cusp" represents direct entry whereas the "cleft" is the high-altitude signature of the Low Latitude Boundary Layer (the region between closed field lines and the first open field line) (Keith et al.).

Where is the cusp? There are several conclusive results about the position of the cusp reported herein (Wing et al.; Merka et al.). The IMF influence on the cusp position has been known for some time. The cusp latitudinal width appears to increase with |IMF $B_z$| (Wing et al.). The cusp latitudinal width increases with |IMF $B_y$| and the equatorward boundary moves to lower latitude with increasing |IMF $B_y$| (Trattner et al.). The cusp moves toward dawn or dusk, away from noon, depending on the sign of $B_y$. The high altitude cusp may be wider than that proposed by Chapman and Ferraro (1931); that is discussed in more detail later. Statistically, the cusp has been observed over an extended region of local time on the dayside, being observed four or more hours away from local noon (Maynard, Chen and Fritz, Merka et al.). Those observations seem to be consistent with MHD simulations in the framework discussed by Siscoe et al. but they also provide challenges for the MHD simulations as discussed by Chen and Fritz.

## 2. Temporal structures

Temporally formed cusp diamagnetic cavities (CDC, or "plasma balls") appear in the region indented in accordance with the funnel shaped magnetic

field topology of Chapman and Ferraro (1931). This region is subject to interaction with the interplanetary medium through the exterior cusp-magnetosheath boundary (Lavraud et al.). Multiple FTEs (ten in total) associated with energetic ion flux bursts were observed by Pu et al. These FTEs occurred quasiperiodically, with a repetition period approximately 72 s. This is substantially different from that for the FTEs in the subsolar region, which are believed to be generated every 8 min on average.

The existence of a bifurcated cusp geometry, or "double cusp", during extreme conditions has been suggested by the low altitude DMSP satellite observations (Wing et al.). The double cusp has been suggested to be the result of merging simultaneously occurring at the low- and high-latitude magnetopause during periods of large |IMF $B_y$| and small IMF $B_z$. In this way, a satellite travelling in the meridional direction near noon can observe two different ion populations caused by the low- and high-latitude reconnection.

Turbulence seems to be a very common phenomenon in the cusp region. The coherent waves control the spectral shape, and result in non-Gaussian statistical characteristics of the disturbances that conform to the fluctuation intermittency (Savin et al.). Wave-particle interaction processes can be assumed as the mechanism for the energy cascade from low-frequency waves to high-frequency waves, via heating and acceleration of the plasma particles in the polar cusp (Blecki et al.; Chen and Fritz).

The cusp current sheet has been addressed by Fu et al. where the energetic particles observed by RAPID onboard Cluster are shown to be well organized by the current sheet. However, the high latitude current sheet does not always seems to be stable, as pointed out by Shi et al.

## 3. Spatial substructures

The substructures in the cusp region outlined by Haerendel (1978) seems to be accepted widely (Dunlop et al.; Lavraud et al.; Savin et al.; Zong et al.). Haerendel (1978) noted the similarity of the situation near the cusp to hydrodynamic flow around a corner, in which vortex formation and separation are known to occur and to initiate some level of turbulence. The term "low-latitude boundary layer (LLBL)" was introduced to distinguish the very different properties observed at latitudes below about 50°–60° on the magnetopause surface. In addition, there are three more boundary regions (in the high latitude) that are assumed to connect directly to the magnetosheath: the plasma mantle, the entry layer, and the exterior cusp or stagnation region.

These terms have been widely used in this special issue. In the entry layer, the plasma density is as high as, or even higher than, that in the magnetosheath, the temperature is very similar to that of the exterior cusp, and the

ratio of particle pressure to the magnetic field pressure in the plasma $\beta \approx 1$. The exterior cusp/stagnation region bounded on the inside by the cusp-like indentation of the magnetopause, and outside by the free-flow stream lines of the magnetosheath flow, constitutes a pocket of hot and stagnant, possibly turbulent, plasma. In addition, the turbulent boundary layer, TBL (Savin et al.), has been described to be a region dominated by irregular magnetic fields and plasma flows. It is located just outside and/or at the near cusp magnetopause. However, such a layer is not always present, at least during northward IMF conditions. The interface between cusp and the magnetosheath is in most cases not obvious, but in some cases during northward IMF conditions it can be well defined (Zong et al.).

Another type of cusp substructure is a step-like energy dispersion signature that is thought to be caused by particle entry into different convection cells (or flux tubes) where the location of the ion open-closed field line boundary in the new cell is significantly different from that in the old cell. This can result in either a step-up or a step-down in the ion energy dispersion signature. Trattner et al. showed that these observed cusp structures are a spatial structure whose appearance is the same for satellites at every altitude.

## 4. Energetic electrons and ions trapped in the cusp

According to the traditional geomagnetic field model, the dayside high latitude or cusp region cannot trap particles (Roederer, 1970). The cusp region of the ideal dipole field is not an "excluded region" in the theory of Störmer (1911). This means that, in the high latitude region, the particles cannot be trapped for much longer than their bounce time; the $\mathbf{E} \times \mathbf{B}$ drift will take the particles away as well. However, energetic particles are a consistent and commonly observed feature of the high altitude dayside cusp. The origin of energetic particles observed in the cusp region has been a subject of controversy. Chen and Fritz argued that the particles observed in the cusp region are the result of a localized acceleration mechanism, and should be a source for magnetospheric energetic particles. On the other hand, Chang (1998) and Trattner et al. (1999) suggested that the energetic ions – but not electrons – in the cusp region originate from the bow shock, and Blake (1999) has argued that they originate within the magnetosphere itself. In these cases no local acceleration would be needed. The implications of this controversy have been discussed in a series of comments (Trattner et al. 1999; Chen et al. 2003; Sheldon et al. 2003) and their companion replies (Fritz and Chen, 1999; Chang et al. 2003; Trattner et al. 2003) to which the interested reader is referred. Energetic electron observations at the cusp described by Zong et al. provide some new evidence since they cannot be accelerated either by the reconnection process in the adjacent magnetopause (for electrons this

amounts to an energy gain of about 1 eV) or by the Fermi mechanism in the quasi-parallel bow shock region. Yet as shown by Zong et al. energetic electrons are observed on the magnetopause in association with the cusp. This suggests that at least some of the energetic particles observed in the cusp do not come from either of the two mechanisms just noted.

The dipole geomagnetic field is modified fundamentally by interaction with the solar wind. The outer cusp region magnetic field lines either close in the dayside sector or extend into the night side sector over the polar cap. This region is a region of weak magnetic field, which directly follows from the interaction of the solar wind with the geomagnetic field predicted by Chapman and Ferraro (1931). Instead of being dipolar, the cusp region field appears to be quadrupolar. With a minimum magnetic field existing off the equator in the outer cusp region, charged particles drifting in longitude would not drift through the subsolar equatorial region but would rather branch off towards the magnetic field minimum at high latitudes as described by Shabansky (1968). Following the work of Sheldon et al. (1998), Zong et al. pointed out that an energetic ion will drift on a closed path around the front of the magnetosphere, and they found that ions could be efficiently trapped in the outer cusp.

The importance of the existence of a region of minimum magnetic field off the equator in the outer cusp has been either neglected or underestimated for a long period, although it could be of extreme importance for understanding both the source and the dynamics energetic particles in the magnetosphere.

## 5. Conclusion

Did these papers answer the more fundamental questions of the role of the cusps in the functioning of the magnetosphere and the possible acceleration of the plasma in these regions? The answer is probably not in any definitive manner but they have provided a forum for further discussion of the issues. What does come out from these papers is the importance of the cusp to the physics of the magnetosphere and the topology of the front side high-latitude magnetopause. However, the full impact of the cusp is going to be evident only when we have multiple satellites displaced from one another by large distances (from a large fraction of an Earth's radius to a few Earth radii), as well as satellites located within 100 km of one another and observing using interferometric techniques. These papers have posed a number of questions that now need to be investigated in detail:

Is the cusp really as broad a region as the statistical studies presented in this collection of papers indicate?

Are there multiple cusps active at a given time?

Or does a single region move around more and faster than its low altitude counterpart?

Only with measurements at larger separations and more coordination of multiple satellite measurements for particular cusp crossings will it become evident what the true nature of the cusp is and what roles the cusps play. Understanding the polar cusps is essential for a thorough understanding of the entire physics of the magnetosphere, and of the dynamical interaction between the solar wind and any planetary magnetosphere.

## References

Blake, B.: 1999, Comment on 'Cusp: A New Acceleration Region of the Magnetosphere', by J. Chen et al. *Czech. J. Phys.* **49**, 675.

Chang, S.-W., Scudder, J. D., Fuselier, S. A., Fennell, J. F., Trattner, K. J., Pickett, J. S., Spence, H. E., Menietti, J. D., Peterson, W. K., Lepping, R. P., and Friedel, R.: 1998, Cusp energetic ions: A bow shock source, *Geophys. Res. Lett.*, **25**(19), 3729–3732, 10.1029/98GL52808.

Chang, S.-W., Scudder, J. D., Kudela, K., Spence, H. E., Fennell, J. F., Lepping, R. P., Lin, B. P., and Russell, C. T.: 2003, Reply to comment on 'MeV Magnetosheath Ions Energized at the Bow Shock', by J. Chen, T. A. Fritz, and R. B. Sheldon, *J. Geophys. Res.* **108**(A8), 1312.

Chapman, S., and Ferraro, V. C. A.: 1931, A New Theory of Magnetic Storms, *Terr. Magn. Atmos. Elect.* **36**, 171–186.

Chen, J., Fritz, T. A., and Sheldon, R. B.: 2003, Comment on 'MeV Magnetosheath Ions Energized at the Bow Shock', by S.-W. Chang et al. *J. Geophys. Res.* **108**(A8), 1311.

Fritz, T. A., and Chen, J.: 1999, Reply, *Geophys. Res. Lett.* **26**, 1363–1364.

Haerendel, G.: 1978, On the 3-dimensional Structure of Plasmoids, *J. Geophys. Res.* **83**, 3195–3216.

Roederer, J. G.: 1970, *Dynamics of Geomagnetically Trapped Radiation*, Springer-Verlag, New York.

Shabansky, V. P.: 1968, Magnetospheric Processes and Related Geophysical Phenomena, *Space Sci. Rev.* **8**, 366–454.

Sheldon, R. B., Spence, H. E., Sullivan, J. D., Fritz, T. A., and Chen, J.: 1998, The Discovery of Trapped Energetic Electrons in the Outer Cusp, *Geophys. Res. Lett.* **25**, 1825–1828.

Sheldon, R. B., Chen, J., and Fritz, T. A.: 2003, Comment on 'Origins of Energetic Ions in the Cusp', in K. J. Trattner et al. *J. Geophys. Res.* **108**(A7), 1302.

Störmer, C.: 1911, Sur les trajectories des corpuscules electrises dans l'espace sous l'actions des magnetisme terrestre avec application aux auarores boreales, secondee memoire., *Arch. Sci. Phys. Nat. Ser. 4* **32**, 117–123.

Trattner, K. J., Fuselier, S. A., Peterson, W. K., and Chang, S.-W.: 1999, Comment on 'Correlation of Cusp MeV Helium with Turbulent ULF Power Spectra and Its Implications', by J. Chen and T. A. Fritz *Geophys. Res. Lett.* **26**, 1361.

Trattner, K. J., Fuselier, S. A., Peterson, W. K., Chang, S.-W., Friedel, R. W., and Aellig, M. R.: 2003, Reply to comment on 'Origins of Energetic Ions in the Cusp', by R. Sheldon, J. Chen, and T. A. Fritz, *J. Geophys. Res.* **108**(A7), 1303.